ALTERNATE SLIDING FRICTION FORMULATIONS OF ELASTO - HYDRODYNAMIC OF SPUR GEARS

Dr. Abbas F. Abbas Al-Zubaidi
Dept. of Mech. Eng./ Baghdad University

ABSTRACT

In this paper, several sliding friction formulations used in spur gear dynamics are examined and compared in terms of the predictions of interfacial friction forces and off-line-of-action. Computing friction formulations include Coulomb models with time-varying friction coefficients and empirical expressions based on elasto - hydrodynamic and/or boundary lubrication regime principles. Predicted results compare well with friction force measurements and appeared completely conformed with specific objectives of this paper are established as follows: (1) propose an improved MDOF spur gear pair model with time-varying coefficient of' friction, μ(t), given realistic mesh stiffness profiles.(2) comparatively evaluate alternate sliding friction models and predict the interfacial friction forces and motions in the off-line-of-action (OLOA) direction: and (3) validate one particular model (III) by comparing predictions to the benchmark gear friction force measurements

الخلاصة:

في هذا البحث فأن هنالك العديد من معادلات الاحتكاك الانزلاقي المستخدمة في ديناميكية التروس الاسطوانية العدلة تم اختبارها ومقارنتها مع الظروف المتوقعة في قوى الاحتكاك السطحية البينية و خط التأثير .أن معادلات الاحتكاك هذه تتضمن نماذج كولوم مع معادلات الاحتكاك باختلاف الزمن وكذلك علاقات تجريبية تعتمد على علم الديناميكا المائعية المرنة وعلى مبادئ التوازن لحد التزييت . ان النتائج المتوقعة في هذا البحث تم مقارنتها جيدا مع قياسات قوى الاحتكاك وظهرت متوافقة تماما معها .ان الاهداف الاساسية لهذا البحث مبنية على مايلي ؛

1- تطوير وتحسين MDOF لنموذج زوج من التروس الاسطوانية العدله مع تغير الزمن ومعامل الاحتكاك

2- للمقارنة مع نماذج التروس المقدرة ذات الاحتكاك الانزلاقي المتبادل وقوى الاحتكاك الداخلية الناتجة واتجاه الحركات عند خط التاثير OLOA

3- اختبار صلاحية نموذج عملي واحد (III) ومقارنته مع قياسات قوى الاحتكاك للنموذج المنتج لترس بينجمارك .

KEYWORDS :
spur gear interfacial, friction forces, line action of motion, coulomb models, boundary lubrication.

INTRODUCTION

Gear dynamic researchers have typically modeled sliding friction phenomenon by assuming Coulomb formulation with a constant coefficient (μ) of friction (it is designated as Model I in this paper). In reality, tribological conditions change continuously due to varying mesh properties and

lubricant film thickness as the gears roll through a full cycle . Thus, μ varies instantaneously with the spatial position of each tooth and the direction of friction force changes at the pitch point. Alternative tribological theories, such as elasto-hydrodynamtc lubrication (EHL), boundary lubrication or mixed regime, have been employed to explain the interfacial friction in gears. For instance, **(Benedict,G.H.and Kelley,B.W.,1961)** proposed an empirical dynamic friction coefficient (designated as Model II) under mixed lubrication regime based on measurements on a roller test machine**.(Xu,E.A.,1972)** recently proposed yet another friction formula (designated as Model III) that is obtained by using a non-Newtonian, thermal EHL formulation. Duan and Singh, developed a smoothened Coulomb model for dry friction in tornsional dampers; it could be applied to gears to obtain a smooth transition at the pitch point and designate this as Model IV**.(Hamrock,B.J. and Dawson,D.1977)** suggested an empirical equation to predict the minimum film thickness for two disks in line contact. They calculated the film parameter A. which could lead to a composite, mixed lubrication model for gears (designated as Model V). Overall, no prior work has incorporated either the time-varying $\mu(t)$ or Models II to V, into multi-degree-of-freedom (MDOF) gear dynamics. To overcome this void in the literature.

MIDOF SPUR GEAR MODEL

Transitions in key meshing events within a mesh cycle are determined from the undeformed gear geometry. **Fig. 1(a)** is a snapshot for the example gear set (with a contact ratio σ of about 1.6) at the beginning (t = 0) of the mesh cycle (t_c). At that time, pair #1 (defined as the tooth pair rolling along line AC) just comes into mesh at point A and pair #0 (defined as the tooth pair rolling along line CD), is in contact at point C, which is the highest point of single tooth contact (HPSTC). When pair #1 approaches the lowest point of single tooth contact (LPSTC) at point B, pair #0 leaves contact. Further, when pair #1 passes through the pitch point P, the relative sliding velocity of the pinion with respect to the gear is reversed, resulting in a reversal of the friction force. Beyond point C, pair #1 will be re-defined as pair #0 and the incoming meshing tooth pair at point A will be re-defined as pair #1. resulting in a linear time-varying (LTV) formulation. The spur gear system model is shown in **Fig. 1(b)** and key assumptions for the dynamic analysis include the following: (i) pinion and gear are rigid disks; (ii) shaft-bearing stiffness elements in the line-of-action (LOA) and OLOA directions are modeled as lumped springs which are connected to a rigid casing; (iii) vibratory angular motions are small in comparison to the kinematic motion. Overall, obtain a linear time-varying system formulation with a constant μ. Refinements to the multi-degree-of-freedom model of **Fig.1** with time-varying sliding frictionμ(t) are proposed as follows. The governing equations for the torsional motions θ_p(t) and θ_g(t) are as follows **(Lundvall,O.and .Stomberg , N.,2004)**

$$J_p\ddot{\theta}_p(t) = T_p + \sum_{i=0}^{n=floor(\sigma)} x_{pi}(t)F_{pfi}(t) - \sum_{i=o}^{n=floor(\sigma)} r_{bp}N_{pi}(t) \quad \textbf{(1)}$$

$$J_g\ddot{\theta}_g(t) = -T_g + \sum_{i=0}^{n=floor(\sigma)} x_{gi}(t)F_{gfi}(t) - \sum_{i=o}^{n=floor(\sigma)} r_{bg}N_{gi}(t) \quad (2)$$

Here, the "floor" function rounds off the contact ratio σ to the nearest integer (towards a lower value); J_p and J_g are the polar moments of inertia for the pinion and gear; T_p and T_g are the external and braking torques;N_{pi}(t) and $N_{gi}(t)$ *are* the normal loads defined as follows:

$$N_{pi}(t) = N_{gi}(t)$$
$$= K_i(t)\left[r_{bp}\theta_p(t) - r_{bg}\theta_g(t) + x_p(t) - x_g(t)\right]$$
$$+ c(t)\left[r_{bp}\dot{\theta}_p(t) - r_{bg}\dot{\theta}_g(t) + \dot{x}_p(t) - \dot{x}_g(t)\right] = floor(\sigma), \quad i = 0,1..n \qquad (3)$$

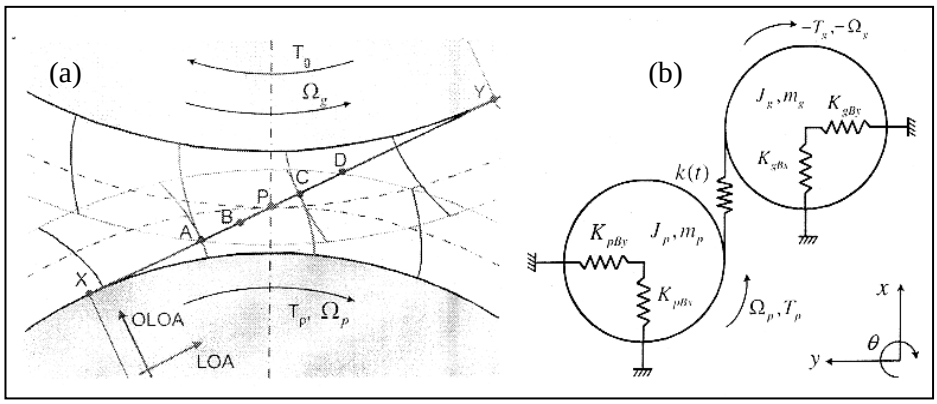

Fig.1.(a) Snap shot of contact pattern(at t=0) in the gear pair:(b)MDOF spur gear pair system; here K(t) is in the LOA direction.

Where $k_i(t)$ and $c_i(t)$ are the time-varying realistic mesh stiffness and viscous damping profiles; r_{bp} and r_{bg} are the base radii of the pinion and gear; and $x_p(t)$ and $x_g(t)$ denote the translational displacements (in the LOA direction) at the bearings I the sliding (interfacial) friction forces $F_{pfi}(t)$ and $F_{gfi}(t)$ of the ith meshing pair are derived as follows; note that five alternate $\mu(t)$ models

$$F_{pfi}(t) = \mu(t)N_{ri}(t), \quad F_{gfi}(t) = \mu(t)N_{gi}(t), \quad i = 0,....a. \qquad (4a,b)$$

The frictional moment arms $x_{pi}(t)$ and $x_{gi}(t)$ acting on the ith tooth pair are:

$$x_{pi}(t) = L_{xA} + (n - i)\lambda + mod(\Omega_g, r_{bp}\, t, \lambda), \quad i = 0,...n. \qquad (5a)$$

$$X_{gi}(t) = L_{yc} + i\,\lambda - mod((\Omega_g r_{bg} t\,\lambda), \quad i=0,.... n. \qquad (5b)$$

Where "mod" is the modulus function defined as: mod(x, r) = $x - y$ floor(x,y), if $y \neq 0$; "sgn" is the sign function: Ω_p, and Ω_g are the nominal operational speeds (in rad/s); and λ. is the base pitch. Refer to. **Fig. 1(a)** for length L.. The governing equations for the translational motions $x_p(t)$ and $x_g(t)$ in the LOA direction are:

$$m_p\ddot{x}_p(t) + 2\zeta_{pBx}\sqrt{K_{pBx}m_p}\,\dot{x}_p(t) + K_{pBx}x_p(t) + \sum_{i=0}^{n=floor(\sigma)} N_{pi}(t) = 0, \qquad (6)$$

$$m_g\ddot{x}_g(t) + 2\zeta_{gBy}\sqrt{K_{gBy}m_g}\,\dot{x}_g(t) + K_{gBy}x_g(t) + \sum_{i=0}^{n=floor(\sigma)} N_{gi}(t) = 0, \qquad (7)$$

Here, m_p and $m_g$are the masses of the pinion and gear; K_{pBx}, and K_{gBx}, are the ffective shaft-bearing stiffness values in the LOA direction, andζ_{pBx} andζ_{gBx} are their damping ratios. Likewise, the governing equations for the translational motions $y_p(t)$ and y_g (t) in the OLOA direction are written as:

$$m_p\ddot{x}_p(t) + 2\zeta_{pBy}\sqrt{K_{pBy}m_p}\dot{y}_p(t) + K_{pBx}y_p(t) - \sum_{i=0}^{n=floor(\sigma)} F_{pfi}(t) = 0, \quad (8)$$

$$m_g\ddot{y}_g(t) + 2\zeta_{gBy}\sqrt{K_{gBy}m_g}\dot{y}_g(t) + K_{gBy}y_g(t) - \sum_{i=0}^{n=floor(\sigma)} F_{gfi}(t) = 0, \quad (9)$$

ALTERNATE SLIDING FRICTION MODELS

Model 1: Coulomb Model With μ(t)

The Coulomb friction model with time-varying (periodic) coefficient of friction $\mu_{ci}(t)$ for the ith meshing tooth pair is derived as follows, where$\mu_{avg}$is the magnitude of the time-average:

$$\mu_{Ci} = \mu_{avg}\, sgn\left[mod(\Omega_p r_{bp}t, \lambda) + (n-i)\lambda - L_{Ap}\right], i = 0, \dots, n \quad (10)$$

Model 11: Benedict and Kelley Model

The instantaneous profile radii of curvature (mm) ρ(i) of ith meshing tooth are:

$$\rho_{pi}(t) = L_{xA} + (n-i)\lambda + mod(\Omega_p r_{bp}t, \lambda), \rho_{gi}(t) = L_{xy} - \rho_{pi}(t),\ i = 0, \dots, n \quad (11a,b)$$

The rolling (tangential) velocities v_r (t) (m/s) of ith meshing tooth pair are:

$$v_{rpi}(t) = \frac{\Omega_p\rho_{pi}(t)}{1000}, \quad v_{rgi}(t) = \frac{\Omega_g\rho_{gi}(t)}{1000}, \qquad i = 0, .., n \quad (12a,b)$$

The sliding velocity v_s(t) and the entraining velocity v_e (i) (m/s) of ith meshing tooth pair are:

$$v_{ei}(t) = \left|v_{rpi}(t) - v_{rgi}(t)\right|, \quad v_{si}(t)\left|v_{rpi}(t) + v_{rgi}(t)\right|, i = 0, \dots, n \quad (13a,b)$$

The unit normal load (N/mm) is $w_n = T_{p/}$(Zr$_{wp}$, cos α.), where α is the pressure angle, Z is the face width (mm), T_p is the torque (N mm) and r_{wp} is the operating pitch radius of pinion (mm). Our *μ(t)* prediction for the ith meshing tooth pair is based on the Benedict and Kelley model, though it is modified to incorporate a reversal in the direction of friction force at the pitch point. Here, $s_{avg} = 0.5(s_{ap} + s_{ag})$ is the averaged surface roughness (μm), and η_M is the

dynamic viscosity of the oil entering the gear contact:

$$\mu_{Bi}(t) = \frac{0.0127 \times 1.13}{1.13 - S_{avg}} log_{10}\left[\frac{29700 w_n}{n_M v_{si0}(t) v_{ei}^2(t)}\right] sgn\left[mod\left(\Omega_p r_{bp} t, \lambda\right) + (n-i)\lambda - L_{Ap}\right] \quad (14)$$

Model III Formulation Suggested by Xu et al. and Kahraman

The composite relative radius of curvature $\rho_r(t)$(mm) of ith meshing tooth pair is

$$\rho_{ri}(t) = \frac{\rho_{pi}(t)\rho_{gi}(t)}{\rho_{pi}(t)+\rho_{gi}(t)} \qquad i=0,\ldots.n \quad \textbf{(15)}$$

The effective modulus of elasticity (GPa) of mating surfaces is E = 2/[(1 — v_p^2/ E_p) + (1 — v_g^2/ E_g)], where E and v are the Young's modulus and Poisson's ratio, respectively. The maximum Hertzian pressure (GPa) for the ith meshing tooth pair is:

$$\rho_{hi}(t) = \sqrt{\frac{W_n E}{2000\pi\rho_{ri}(t)}} \quad \textbf{(16)}$$

Define the dimensionless slide-to-roll ratio *SR(t)* and oil entraining velocity V_e(t) (m/s) of ith meshing tooth pair as

$$SR_i(t) = \frac{2v_{si}(t)}{v_{ei}(t)}, \qquad V_{ei}(t) = \frac{v_{ei}(t)}{2}, \; i = 0, \ldots. n. \quad \textbf{(17a,b)}$$

The empirical sliding friction expression (for the ith meshing tooth pair), as proposed by H. Xu et al.and Kahraman based on non-Newtonian, thermal EHL theory, is modified in this work to incorporate a reversal in the direction of the friction force at the pitch point as

$$\mu_{xi}(t) = e^{f\left(sR_i(t)p_{hi}(t)\eta_M S_{avg}\right)} p_{hi}^{b2} |SR_i(t)|^{b3} V_{ei}^{b6}(t) \eta_M^{b7} R_i^{b8}(t) sgn\left[mod\left(\Omega_p r_{bp} t, \lambda\right) + (n-i)\lambda - L_{Ap}\right], f\left(SR_i(t)\rho_{hi}(t), \eta_M, S_{avg}\right) = b_1 + b_4|SR_i(t)|p_{hi}(t) log_{10}(\eta_M) + b_5 e^{-|SR_i(t)|p_{hi}(t) log_{10}(\eta_M)} + b_9 e^{S_{avg}}, \quad i = 0, \ldots. n$$

(18a,b)

Xu suggests the fallowing empirical coefficients (in consistent units) for the above formula: b_1 = -8.916465, b_2 = 1.0 3303, b_3= 1.036077, b_4 = -0.354068, b_5= 2.812084, b_6= -0.100601, b_7 = 0.752755, b_8 = -0.390958 and b_9 = 0.620305.

Model IV: Smoothened Coulomb Model

Xu and Kahraman,conducted a series of friction measurements on a ball-on-disk test machine and measured the *μ(t)*values as a function of SR: these results resemble the smoothening function reported by Duan and Singh near the pitch point (SR = 0) especially at very low speeds (boundary lubrication conditions). By denoting the periodic displacement of

ith meshing tooth pair as $x_i(t) = \mathrm{mod}(\Omega_p r_{bp} t, \lambda) + (n - i)\lambda - L_{Ap}$, a smoothening function could be used in place of the discontinuous Coulomb friction. The arc-tangent type function is proposed as follows though one could also use other functions

$$\mu_{Si} = \frac{2\mu_{avg}}{\pi} \arctan[\Phi_{xi}(t)] + x_i(t)\frac{2\mu_{avg}\sigma}{\pi[1+\Phi^2 x_i^2(t)]} \quad i=0,\ldots,n. \tag{19}$$

In the above, the regularizing factor Φ is adjusted to suit the need of smoothening requirement. A higher value of Φ corresponds to a steeper slope at the pitch point

Model V:Composte Friction Model

Alternate theories (Models I to IV) seem to be applicable over specific operational conditions. This necessitates a judicious selection of an appropriate lubrication regime as indicated by the film parameter, Λ,that is defined as the ratio of minimum lubrication film thickness and composite surface roughness $R_{comp}=\sqrt{R_{rms,g}^2 + R_{rms,p}^2}$ measured with a filter cutoff wave length L_x, where R_{rms} is the rms gear-tooth surface roughness. The film parameter for rotorcraft gears usually lies between 1 and 10. In the mixed lubrication regime the films are sufficiently thin to yield partial asperity contact. while m the EHL regime the lubrication film completely separates the gear surfaces. Accordingly. a composite friction model is proposed as follows:

$$\mu(t) = \begin{cases} \mu_C(t) \text{ simplified Coulomb model, computaionally coefficient(Model I)}, \\ \mu_B(t)\ 1 < \Lambda < 4, \text{mixed lubrication , (Model II)}, \\ \mu_x(t) 4 \le \Lambda < 10, \text{EHL lubrication, (ModelIII)}, \\ \mu_S(t) \text{low } \Omega_p, \text{high } T_p, \Lambda < 1, \textit{boundary lubriacation} \text{ (Model IV)}. \end{cases} \tag{20}$$

Application of Models II. III or IV would. of course, depend on the operational and tribological conditions though Model I could be easily utilized for computationally efficient dynamic simulations. Note that the magnitude μ_{avg} of Model I or IV should be determined separately. For instance. the averaged coefficient based on Moods II was used in this work. Also, the critical Λ value between different lubricating regimes must be carefully chosen. The film thickness calculation employs the following equation developed by **(Hamrock,B.J. and Dowson,D.1977)** based on a large number of numerical solutions that predict the minimum film thickness for two disks in line contact. Here, G is the dimensionless material parameter, W is the load parameter, U is the speed parameter, H is the dimensionless central film thickness and b_H is the semi-width of Hertzian contact band.

$$A_i(t) = \frac{H_{ci}(t)\rho_{ri}(t)\times 10^8}{R_{comp}}\sqrt{\frac{L_x}{2b_{Hi}(t)}}, \quad i = 0, \ldots n \tag{21a}$$

$$b_{Hi}(t) = \sqrt{\frac{8w_n\rho_{ri}(t)}{\pi E_r}}, H_{ci}(t) = 3.06\frac{G^{0.56}U_i^{0.69}}{W_i^{0.10}(t)}, G = k\eta_M^s E_r, \tag{21b,c}$$

$$U_i(t) = \frac{\eta_M v_{si}(t)}{2E_r\rho_{ri}(t)} \times 10^{-16}, \ W_i(t) = \frac{w_n}{E_r\rho_{ri}(t)} \tag{21d,e}$$

RESULTS AND DISCUSSION

Fig.2(a) shown the magnitudes of $\mu(t)$ as predicted by Models II and III for a spur gear set given T_p= 22.6 Nm (200 lb in)and Ω_p = 1000 rev/ min. The linear time- varying formulations for meshing tooth pairs # 0 , and #1 result in periodic profiles for both models. Two major differences between these two models are: (1) the averaged magnitude from Model II much higher compared with that of Model III since friction under mixed lubrication is generally higher than under EHL and (2) while Model III predicts nearly zero friction near the pitch point. Model II predicts the largest μ value due to the entraining velocity term in the denominator. As explained by **(Xu,H. and Kahraman,A.2007)** three different regions could be roughly defined on a μ versus SR curve. When the sliding velocity is zero, there is no sliding faction, and only rolling friction (though very mall) exists. Thus. the μ value .should be almost zero at the pitch point. When the SR is increased from zero, μ first increases linearly with small values of SR. This region is defined as the linear or isothermal region. When the SR is increased slightly further, μ reaches a maximum value and then decreases as the SR value is increased beyond that point. This region is referred to as nonlinear or non-Newtonian region. As the SR is increased further, the fraction decreases in an almost linear fashion; this is called as the thermal region. Model II seems to be valid only in the thermal region.

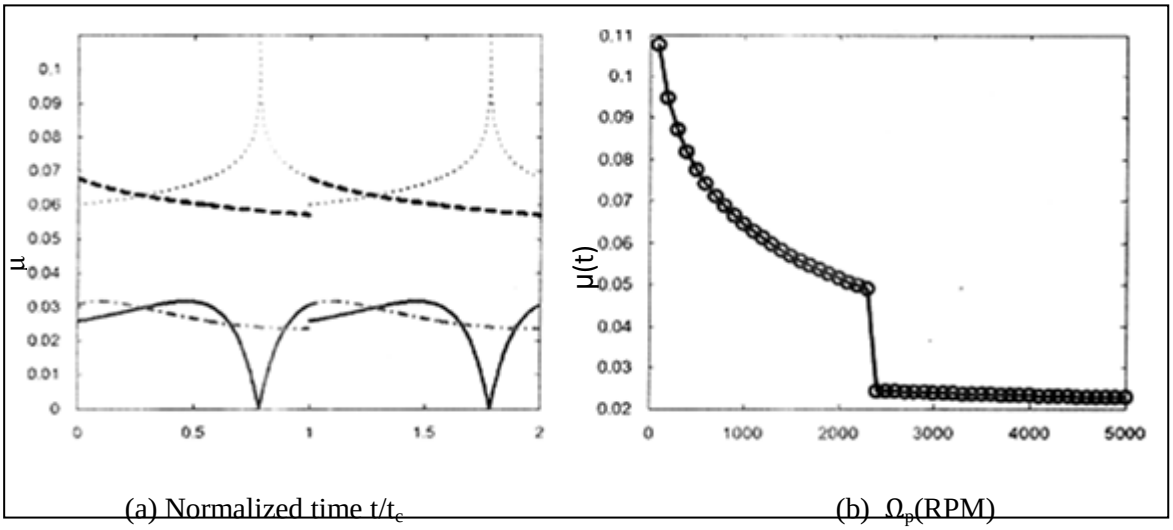

(a) Normalized time t/t_c (b) Ω_p(RPM)

Fig. 2. (a) Comparison of Model I I and Model III given T_p = 22.6 N m (200 lb in) and Ω_p = 1000 rev/min. Key; …. pair #1 with Model II;----pair #0 with model II; -·-· pair #1 with Model III; —— pair #0 with Model III; (b) Averaged magnitude of the coefficient of friction predicted as a function of speed using the composite Model V with T_p= 22.6 Nm (200lb in). Here, t_c is one mesh cycle.

Fig. 2(b) shows the averaged magnitude of μavg predicted as a function of Ωp using the composite formulation (Model V) with T_p = 22.6 Nm (200 lb in). An abrupt change in magnitude is found around 2500 rev/min corresponding to a transition from the EHL to a

mixed lubrication regime. Similar results could be obtained by plotting the composite $\mu(t)$ as a function of T_p .Though our composite model could be used to predict μ (t) over a large range of lubrication conditions, care must be exercised since the calculation of Λ itself is based on an empirical equation

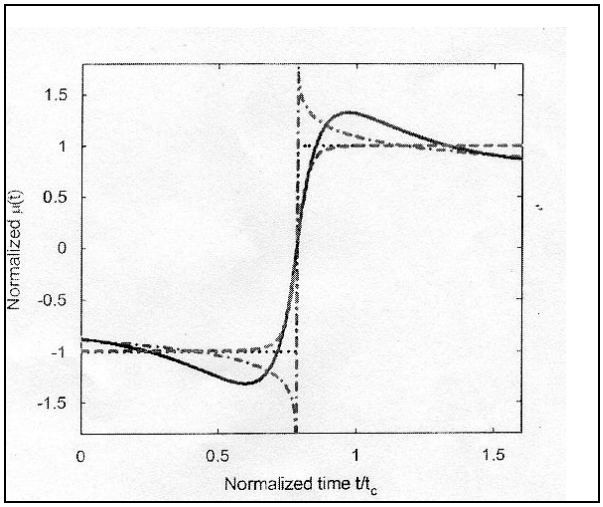

Fig.3.Comparison of normalized friction models. Key: …… Model I (Coulomb friction with discontinuity); —— Model II; -·-·- Model III:;----- Model IV (smoothened Coulomb friction) . Note that curve between $0 \leq t/t_c < 1$ is for pair #1; and the curve between $1 \leq t/t_c < \sigma_c$ is for pair #0

Fig. 3 compares four friction models on a normalized basis. The curves between $0 \leq t/t_c < 1$ are defined for pair #1 and those between $1 \leq t/t_c < \sigma$ are defined for pair #0. Discontinuities exist near the pitch point for Models I and II, and these might serve as artificial excitations to the OLOA dynamics. On the other hand, smooth transitions are observed for Models III and IV corresponding to the EHL condition. **Fig.4** compares the combined normal loads and friction force time histories as predicted by four friction models given T_p= 56.5 N m (500 lb in) and Ωp= 4875 rev/min. Note that while **Fig. 3** illustrates $\mu(t)$for each meshing tooth pair the friction forces of **Fig. 4** include the contributions from both (all) meshing tooth pairs, Though alternate friction formulations dictate the dynamic friction force profiles, they have negligible effect on the normal loads.

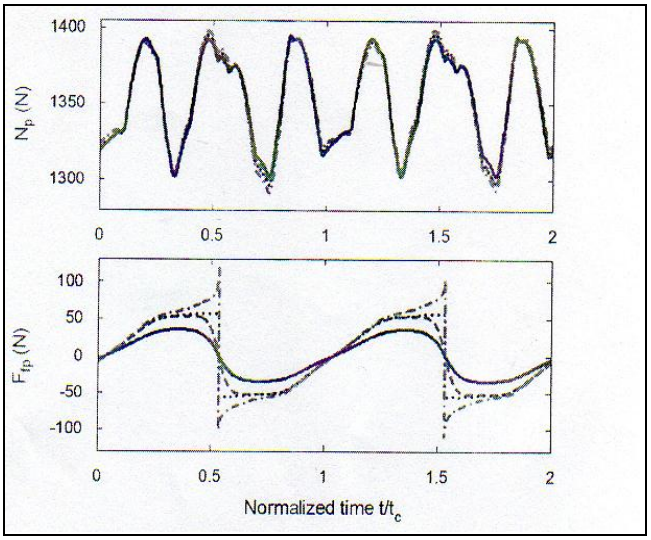

Fig. 4. Combined normal load and friction force time histories as predicted using alternate friction models given T_p= 56.5 N m (500 lb in) and Ω_p= 4875 rev/ min. Key;: ….. Model I; -·-· Model II;— Model III;----- Model IV.

Fig. 5 compares the predicted LOA and OLOA displacements with alternate friction models given T_p = 56.5 Nm (500 lb in) and Ω_p= 4875 rev/min.

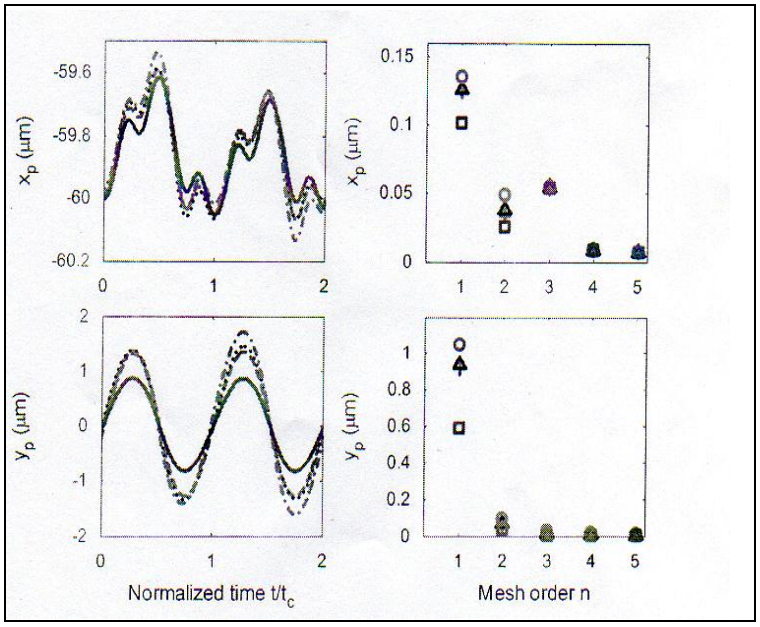

Fig. 5. Predicted line-of-action and off-line-of-action displacements using alternate friction models given T_p = 56.5 N m (500lb in) and Ωp=4875 rev/ min. Key: in time domain… Model I: -·-· Model II; — Model III; ----Model IV; in frequency (mesh order *n)* domain; ΔModel I; ◯ Model II; □ Model III;+ Model IV

The differences between predicted motions are not significant though friction formulations and friction force excitations differ. This implies that one could still employ the simplified Coulomb formulation (Model I) in place of more realistic time-varying friction

models (Models II to IV). Similar trend is observed in **Fig.6.** for the dynamic transmission errors (DTE), defined as $\delta(t)=r_{bp}\theta_p(t)—r_{bg}\ \theta_g(t)+\ x_p(t)-x_g(t)$.

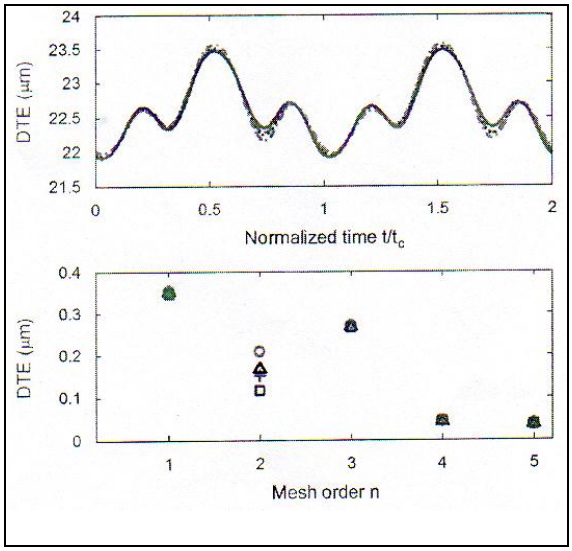

Fig.6. Predicted dynamic transmission error (DTE) using alternate friction models given T_p= 56.5Nm (500 lbin) andΩ_p= 4875rev/min Key: in time domain:------Model I:-·-· Model II; Model III;--- Model IV; in frequency (mesh order n) domain:Δ Model I:○ Model II:□ Model III:+ Model IV.

Predicted normal load and friction force time histories (with Model III) are validated using the benchmark friction measurements made by Rebbechi et al.Results are shown in **Fig. 7**..

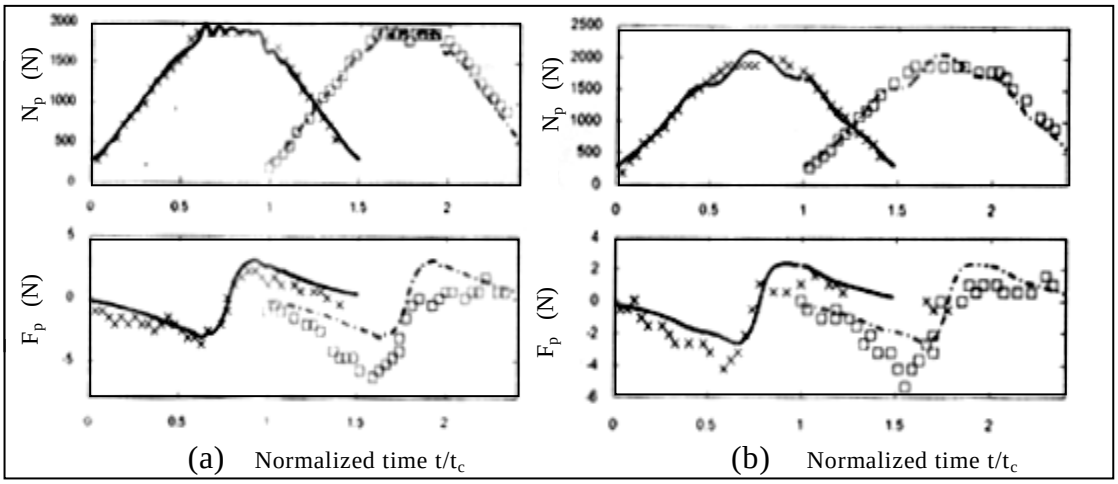

Fig. 7. Validation of the normal load and sliding friction force predictions : (a) at Tp = 79.1 Nm (700 lb in) and Ωp= 800 rev/min; (b) at Tp = 79.1 Nm (7001b in) and Ωp = 4000 rev/ min. Key: — prediction of tooth pair A with Model III:-·-· prediction of tooth pair B with Model III; X measurement of tooth pair A□ measurement of tooth pair B.

CONCLUSIONS

Following are the main conclusions drawn from this paper :

1. The most significant variation induced by friction formulation is at the second harmonic, which matches the results reported by Lundvall et al.
2. Based on the comparison, μ is found to be about 0.004 since it was not given in the experimental study
3. The periodic LTV definitions of meshing tooth pairs #0 and #1 to be consistent with those of measurements, where meshing tooth pairs A and B are labeled in a continuous manner
4. Predictions match well with measurements at both low (Ω_p= 800 rev/min) and high (Ω_p = 4000 rev/min) speeds.
5. Ongoing research focuses on the development of semi-analytical solutions given a specific μ(t) model and an examination of the interactions between tooth modifications and sliding friction
6. The mean absolute discrepancy between three curves shown in **Fig.5** is about 8%.
7. Predicted results compare well with friction force measurements and appeared completely conformed with , that the maximum error rate was about 3%

REFERENCES

- AGMA Information Sheet 925-A03. Effect of lubrication on gear surface distress. 2003.
- Rebbechi.B., Oswald, F.B Measurement of gear tooth dynamic friction. ASME Power Transmission and Gearing Conference Proceedings, San Diego. 6-9 October 1996, DE-Vol. 88. pp.355-363.
- Hamrock, B.J. Dowson , D. Isothermal elastohydrodynamic lubrication of point contacts, part III-fully flooded results. Journal of Lubrication Technology 99 (2) (1977) 264-276.
- Duan, C.. Singh, R Dynamic of a 3DOF torsional system with a dry friction controlled path. Journal of sound and Vibration 289 (4-5) (2006) 657-688.
- Benedict, G.H. Kelley, B.W. Instantaneous coefficients of gear tooth friction. Transactions of American Society of Lubrication Engineers 4 (1961) 59–70.
- Xu, H. Kahraman A.,Prediction of mechanical effieiecy of parallel-axis gear pairs. ASME Journal of Mechanical Design 129 (1)(2007) 58-68.
- Xu, H. Development of a generalized mechanical efficiency prediction methodology, PhD Dissertation (Advisor: A. Kahraman) The Ohio State University, 2005.
- Vaishya, M. Singh, R.Analysis of periodically varying gear mesh systems with Coulomb friction using Floquet theory, Journal of Sound and Vibration 243 (3) (2001) 525-545.

- Vaishya, M. Singh, R. Sliding friction-induced non-linearity and parametric effects in gear dynamics, Journal of Sound and Vibration 248 (4) (2001) 671- 694.

- Vaishya, M. Singh, R.S Strategies for modeling friction in gear dynamics, ASME Journal of Mechanical Design 125 (2003) 383-393.

- Lundvall. O. Stomberg, N, Klarbring, A. A flexible multi-body approach for frictional contact in spur gears, Journal of Sound and Vibration 278 (3) (2004) 479-499.

- Velex, P. Sainsot, P. An analytical study of tooth friction excitations in spur and helical gears, Mechanism and Machine Theory 37 (2002)641-658.

- Velex, P. Cahouet, V. Experimental and numerical investigations on the influence of tooth friction in spur and helical gear dynamics, ASME Journal of Mechanieal Design 122 (4) (2000) 515-522.

- .He.R.Gunda, S Single R., Effect of sliding friction on the dynamics of spur gear pair with realistic times- varying stiffness, Journal of Sound and Vibration 301 (3 - 5) (2007) 927–949.

- Xu ,E,A ,Non _Newtonian Thermal design of fricition formula in spur gears 2110 (4) (1972) .

THEORETICAL AND NUMERICAL ANALYSIS OF FUEL DROPLET COMBUSTION PROCESS WITH CONVENTIONAL AND TRANSIENT MODELS

BASMA ABBAS ABDULMAJEED
Iraq, Baghdad
Univ. of Baghdad, College of Eng
Chem. Eng. Dept

ALI SABRI
Iraq, Baghdad
Univ. of Baghdad, College of Eng
Chem. Eng. Dept

ABSTRACT

The study introduces a theoretical analysis and numerical solution for the combustion of a hydrocarbon fuel droplet inside the combustion chamber. The study employs two mathematical models to analyze the combustion process. Conventional (Classical) model and Transient model. The combustion process of a stagnant droplet in the steady state was analyzed in the classical model, while, In the transient model, it was assumed that there is a period of time in the stages of the droplet combustion in which the droplet is heated before combustion. The effect of change in temperature on the thermo-physical properties of the fuel was adopted through the two models. For the classical model, a convenient approximation was adopted for the heat transferred inside the droplet.

KEY WORDS

droplet, combustion, numerical, modeling, transient.

INTRODUCTION

Droplet burning has relevance to many practical combustion devises, including, rockets, and gas-turbine engines, as well as oil-fired boilers, furnaces, and process heaters. In these devices, spray combustion is the dominant feature [Turns, 2000]. The problem of droplet burning includes both the evaporation and the combustion process. Solving problems concerning droplet evaporation and combustion needs the use of mass transfer and thermodynamic laws and equations. In all the above systems, liquid fuels and/or oxidizer are usually injected into the combustion chamber as a spray of droplets, which undergoes process [Lamnna, et.al. 2004]. Research on the gasification, oxidation,

and dynamics of fuel droplet commands both practical and fundamental interest to energy and combustion science. On the practical aspect one recognizes that petroleum oil constitutes a significant share of the world energy supply [Law, 1982]. According to law, droplet combustion is a problem involving complex chemically reacting multicomponent two-phase flows with phase change, rich in physical and chemical phenomena typically to be studied. Theories and studies concerning the evaporation and combustion fuel droplets took into account a spherical droplet (motionless or moving). It is cold and is placed in a hot stagnant, gravity free environment, [Law, 1982]. No forced or natural convection is concerned. Heat is transferred from the ambience towards the cold surface of droplet, where some of it is used to gasify the droplet and the remaining is transferred to the interior of droplet to heat it up. According to Law, through the above mechanism, a liquid mass can be converted to vapor and eventually dispersed to ambience, with the rate controlling process as heat and mass diffusion the ignition of the droplet causes a reaction or oxidation of the fuel with heat generated to be transferred both outward and inward. With D^2-law [Godsave, 1953, Spalding, 1953, Goldsmith & Penner, 1954] with its simple assumptions and some inadequacies. Then different approaches were conducted to develop the D^2-law. Some included the unsteady droplet heating and combustion [Law & Sirignano, 1977]. Others included internal circulation, transient heating, multicomponent fuel, radiation, high pressure, sprays, etc., introducing modern computational models [Williams & Sirignano,1983, Abraham,2001, Dombrovsky & Sazhin,2003, Hohmann & Ranz,2003,Sazhin,et.al.,2004,Sazhin,et.al.,2005,andYan&Aggarwal,2006].

THEORIES

Classical Droplet Combustion Model:

D^2-law theory for droplet combustion established the basic fundamentals for droplet combustion model. One of the assumptions of that theory is that thermophysical properties are constant for all temperature of droplet surface and it is surrounding, so that it's more suitable to consider the dependence of thermophysical properties to a reference temperature which vary with the variation of surface and environmental temperature. This behavior will be considered later through this work to obtain its effects on the main parameters of combustion process such as mass burning rate. Mass burning rate represents the amount of fuel that is burned during the combustion process. It is dependent on the mass vaporization, rate which is the amount of fuel that evaporates from the surface of the droplet as a result of heat that is transferred to the surface (or droplet) because of the burning fuel in the process. Mass burning rate represents the combustion process and affects other parameters in the process such as flame radius, which Is the radius of flame front that is surrounding the burning fuel droplet. The flame radius can be expressed as flame standoff ratio. It is a ratio of the radius of flame to the radius of the individual liquid droplet, and that can show the position of flame front from the surface of the droplet at any time of droplet combustion process. Flame temperature is the temperature of the flame front that is surrounding the fuel droplet. Knowing this temperature can provide primary knowledge to the heat that is transferred inward and outward the fuel droplet, and that heat is dependent on the mass burning rate. In the classical model for

combustion, mathematical model will be considered and solved for mass and heat transfer for the gas-phase of droplet combustion process. The solution will provide the basic equations that relates the main characteristic parameters, which will be solved numerically to evaluate their values overall the combustion process. A suitable approach for the heat that is transferred to the droplet interior will be considered.

TRANSIENT DROPLET COMBUSTION MODEL:

The study of transient combustion process is required to understand the effects of heat up period on the combustion parameters. Heat up period is the period of time that the droplet surface is raised from its initial temperature to a steady temperature (boiling temperature) by gaining heat from its surrounding flame. In heat up period, heat that is transferred to the droplet can be divided into two parts, one part used for heating the droplet liquid to its steady temperature, and the other part for vaporizing the liquid fuel, causing dominant effects on the main parameters of combustion process such as mass burning rate. Surface temperature of the droplet varies with time until it reaches to a steady temperature. This variation can affect latent heat of vaporization that can be considered to become slowly –time varying latent heat of vaporization and can be expressed as a function of surface temperature, which, in turns, can be expressed as a function of time, and the numerical substitution can be used to simplify this dependence. Numerical computation will be used to solve the basic equations which relate the basic parameters evaluated from the solution of mass and heat transfer equations for the mathematical model.

MATHEMATICAL WORK

Classical Droplet Combustion Model: Problem Statement

Spherical fuel droplet that has the initial radius r_{so} is burning and is surrounded by thin flame sheet that has a radius r_f and is surrounded by infinite medium of oxidizing atmosphere to the radius ∞. Liquid fuel is vaporized at the droplet surface, the droplet is the source of vapor in the system, vapor is convicting and diffusing outward toward the flame. The source of convicting species at the droplet surface is the specific volume change associated with phase change at the surface, while the oxidizer diffuses inward from the ambient environment to the flame sheet [Kuo, 1986]. The fuel and the oxidizer react stoichometrically ,and the chemical kinetics are assumed to be infinitely fast, so that the fuel vapor mass fraction Y_F is maximum at the droplet surface and monotonically decrease to zero at the flame sheet, where the fuel is totally consumed . The oxidizer mass fraction Y_{ox} mirrors this, being a maximum far from the flame and decrease to zero at the flame sheet . If the fuel is burning at a medium of pure oxygen then the value of mass fraction of the oxidizer at infinity is unity. Most of combustion systems are working in air rather than in pure oxygen, so that the environment will be considered as air in the calculations and Y_{ox} will be calculated. Heat is generated at the reaction on the flame sheet causing the flame temperature T_f to be the highest temperature in the system. Heat is transported via conduction and radiation outward from the flame to infinity and inward back to the droplet surface causing vaporization. The heat deposited at the droplet surface is balanced by the evaporation process at the vapor-liquid interface.

There are three important temperatures in the system, the droplet surface temperature T_s, the flame temperature T_f, and the temperature of the medium at infinity T_∞. The combustion products have their maximum concentration at the flame sheet (unity) diffusing both inward toward the droplet and outward away from the flame [Turns, 2000].

The major assumptions of this model are [Law, 1982]:

* Spherically symmetric: forced and natural convection are neglected, this reduces the analysis to one dimension.
* No spray effects: the droplet is an isolated one, immersed in an infinite oxidizing environment.
* Isobaric process: at 1 atm.
* Flame-sheet combustion: chemical reaction rates are much faster than gas-phase diffusion rates such that the flame is of infinitesimal thickness and can be treated simply as a sink for the reactants and a source of chemical heat released.
* Gas-phase is quasi-steady.
* Simultaneous fuel gasification and consumption: this assumes that the amount of fuel gasified at the surface is instantly consumed at the flame; it neglects the accumulation of fuel vapor between the droplet and the flame.
* Single fuel species: thus it is unnecessary to analyze liquid-phase mass fraction.
* The fuel has zero solubility for gases and phase equilibrium prevails at the liquid-gas interface.
* No soret, Dufour, sooting, and radiation effects.

* Thermophysical properties are functions of temperature only.

CONSERVATION OF MASS:

With the assumption of quasi-steady burning, the mass flaw rate $\dot{m}(r)$ is constant, independent of radius; thus:

$$\dot{m} = \dot{m}_F = \rho v_r A = constant$$

For the inner region bounded between the zone (r_s < r <r_f), Fick's law of diffusion can be applied to the inner region:

$$\dot{m}_A'' = Y_F(\dot{m}_A'' + \dot{m}_B'') - \rho D_{AB} \nabla Y_A$$

This can be simplified to;

$$\frac{dY_F}{dr} = \frac{-\dot{m}_F}{4\rho\pi D} \frac{1 - Y_F}{r^2} \qquad (1)$$

With the boundary conditions;

$$Y_F(r_s) = Y_{Fs} \tag{2.a}$$

$$Y_F(r_f) = 0 \tag{2.b}$$

The outer region is that bounded by the zone (r_f < r < ∞), the important diffusing species is the oxidizer, Fick's law of diffusion can be applied to the outer region:

$$\dot{m}_{ox}'' = Y_{ox}(\dot{m}_{ox}'' + \dot{m}_{Pr}'') - \rho D_{AB} \nabla Y_{ox}$$

It can be written as:

$$\frac{dY_{ox}}{dr} = \frac{\dot{m}_F}{4\pi\rho D} \frac{(Y_{ox} + v)}{r^2} \tag{3}$$

With the boundary conditions;

$$Y_{ox}(r_f) = 0 \tag{4.a}$$

$$Y_{ox}(\infty) = Y_{ox\infty} \tag{4.b}$$

CONSERVATION OF ENERGY:

The Shvab-Zeldovich form of the energy equation is used. Since the chemical reactions occur at the boundary, i.e., the flame sheet, the reaction rate term is zero both inside the flame and outside the flame [Turns, 2000]:

$$\frac{1}{r^2}\frac{d}{dr}[r^2(\rho v r \int CpdT - \rho D \frac{d}{dr}\int CpdT)] = -\sum h^\circ f_i \dot{m}_i'$$

This equation can be re-arranged and written as:

$$\frac{d_2T}{dr^2} = \left(\frac{\dot{m}_F\, Cp_g}{4\pi\, k_g r^2} - \frac{2}{r}\right)\frac{dT}{dr} \tag{5}$$

With the boundary conditions for inner region:

$$T(r_s) = T_s \tag{6.a}$$

$$T(r_f) = T_f \tag{6.b}$$

And for outer region:

$$T(r_f) = T_f \tag{7.a}$$

$$T(\infty) = T_\infty \tag{7.b}$$

ENERGY BALANCE AT DROPLET SURFACE:

Heat is conducted from the flame through the gas-phase to the droplet surface. Some of this heat is used to vaporize the fuel, while the remaining is conducted into the droplet interior. Mathematically:

$$\dot{Q}_{g-i} = \dot{m}_F h_{fg} + \dot{Q}_{i-l} \tag{8}$$

Where:

$$\dot{Q}_{g-i} = -\left[4\pi\, r_s^{\,2}\, k_g \left.\frac{dT}{dr}\right|_{r_s}\right]$$

The droplet is assumed to be consisting of two zones, an interior zone existing uniformly at its initial temperature T_o, and then surface layer at the surface temperature T_s. For this it is called "onion-skin model ":

$$\dot{Q}_{i-l} = \dot{m}_F\, Cp_l(T_s - T_o)$$

So that, equation (8) becomes:

$$-k_g 4\pi\, r_s^{\,2} \frac{dT}{dr}\Big|_{r_s} = \dot{m}_F\big(hfg + Cp_l(T_s - T_o)\big) \tag{9}$$

ENERGY BALANCE AT FLAME SHEET:

Since the flame temperature is the highest temperature in the system, heat is conducted both toward the droplet, $\dot{Q}_{f-i}$, and away to infinity, $\dot{Q}_{f-\infty}$The chemical energy released at the flame is taken into account by using absolute enthalpy fluxes for the fuel, oxidizer, and products. A surface energy balance at the flame sheet can be written as:

$$\dot{m}_F \Delta h_c = \dot{Q}_{f-i} + \dot{Q}_{f-\infty} \tag{10}$$

Where $\dot{Q}_{f-i}$, $\dot{Q}_{f-\infty}$can be represented as:

$$\dot{Q}_{f-i} = -k_g 4\pi\, r_f^{\,2} \frac{dT}{dr}\Big|_{r_f^-}$$

$$\dot{Q}_{f-\infty} = -\,k_g 4\pi\, r_f^{\,2} \frac{dT}{dr}\Big|_{r_f^+}$$

SOLUTION:

solving equation (1) with the boundary conditions (2.a, b) for $\dot{m}_F$ gives:

$$\dot{m}_F = \frac{4\ln\left(\frac{1}{1-Y_{Fs}}\right)\pi\rho D r_s}{1-\frac{r_s}{r_f}} \tag{11}$$

Solving equation (3) with the boundary conditions (4.a, b) for r_f presents:

$$r_f = \frac{-\dot{m}_F}{4\pi\rho D\ln\left(\frac{\nu}{\nu+Y_{ox\infty}}\right)} \tag{12}$$

Solving equation (5) with the boundary conditions (6.a,b) gives the temperature distribution of inner region, which can be derived with respect to r, and the resulted equation can substituted into equation (9) which can be solved for T_s to obtain:

$$T_s = f\left(\dot{m}_F, T_f, r_s, r_f\right) \tag{13}$$

Solving equation (5) with the boundary conditions (7.a,b) gives the temperature distribution of outer region, which can be derived with respect to r, and the resulted equation can substituted into equation (10) which can be solved for T_f to obtain:

$$T_f = f\left(\dot{m}_F, T_s, r_s, r_f\right) \tag{14}$$

To estimate the relation that describe the equilibrium between the liquid and vapor-phase of the fuel at the surface, and applying Antoine equation gives :

$$Y_{Fs} = \frac{exp\left(A-\frac{B}{T_s+C}\right)Mw_F}{exp\left(A-\frac{B}{T_s+C}\right)Mw_F + \left[P-exp\left(A-\frac{B}{T_s+C}\right)\right]Mw_{Pr}} \tag{15}$$

The droplet life time was obtained using the mass balance, which states that the rate at which the mass of the droplet decreases is equal to the rate at which the liquid is vaporized [Williams, 1965]:

$$\frac{dm_d}{dt} = -\dot{m}_F \tag{16}$$

Where:

$$m_d = \rho_l V = \frac{4}{3}\pi r_s^3 \rho_l$$

And $\dot{m}_F$ can be expressed as a function of r_s :

$$\dot{m}_F = 4\,\pi\rho D r_s \ln\left(\frac{\frac{1}{1-Y_{Fs}}}{\frac{\nu}{\nu+Y_{ox\infty}}}\right)$$

Equation (16) can be written as:

$$\frac{dr_s}{dt} = \frac{-3\rho D}{r_s\rho_l}\ln\frac{\frac{1}{1-Y_{Fs}}}{\frac{\nu}{\nu+Y_{ox\infty}}} \qquad (17)$$

TRANSIENT DROPLET COMBUSTION MODEL

Problem Statement:

In order to formulate the model that describes the droplet heating and combustion, the major assumptions will be [Chigier, 1981]:

1. Constant, stagnant, unbounded atmosphere.
2. Combustion process is spherically symmetric and isobaric.
3. The combustion process is following the double-film theory.
4. Fuel and oxidizer meets in a satoichiometric ratio at the flame front.
5. The reaction kinetics is fast compared with gas-phase transfer.
6. Physical properties will be calculated at reference temperature.
7. Single component droplet with no liquid-phase flows.
8. No soot formation, negligible radiation.

The problem is analyzed as follows. At time $t = 0$, the droplet with radius $r_s = r_{so}$ and temperature $T = T_{so}$ is igniting in constant, unbounded atmosphere characterized by its temperature T_∞, pressure P_∞, and oxidizer mass fraction $Y_{ox\infty}$. The outwardly diffusing fuel vapor reacting stoichiometrically and completely with the inwardly diffusing oxidizer gas at a thin flame front located at r_f. For analyzing the inner and outer regions, mass and heat balance will be obtained considering the non-dimensional quasi-steady phase equations [Law, 1976].

CONSERVATION OF MASS:

Inner region is expressed by non-dimensional equation [Law, 1976]:

$$\hat{m}_F Y_F - \hat{r}^2\frac{dY_F}{d\hat{r}} = \hat{m}_F \qquad (18)$$

Where:

$$\hat{m} = \frac{\dot{m}}{4\pi\rho D r_s}, \hat{r} = \frac{r}{r_s}$$

With the boundary conditions:

$$Y_F(1) = Y_{Fs} \qquad (19,a)$$

$$Y_F(\hat{r}_f) = 0 \qquad (19,b)$$

Outer region is represented by the non-dimensional equation [Law, 1976]:

$$\hat{m}_F Y_{ox} - \hat{r}^2 \frac{dY_{ox}}{d\hat{r}} = -\hat{m}_F \nu \qquad (20)$$

With the boundary conditions:

$$Y_{ox}(\hat{r}_f) = 0 \qquad (21,a)$$

$$Y_{ox}(\infty) = Y_{ox\infty} \qquad (21,b)$$

CONSERVATION OF ENERGY:

for the inner region:

$$\hat{m}_F(\hat{T} - \hat{T}_s) - \hat{r}^2 \frac{d\hat{T}}{d\hat{r}} = -\hat{m}_F \hat{Q} \qquad (22)$$

Where:

$$\hat{Q} = \frac{Q}{h_{fg}}, \hat{T} = \frac{CpT}{h_{fg}}$$

With the boundary conditions:

$$\hat{T}(1) = \hat{T}_s \qquad (23,a)$$

$$\hat{T}(\hat{r}_f) = \hat{T}_f \qquad (23, b)$$

For the outer region:

$$\hat{m}_F(\hat{T} - \hat{T}_s) - \hat{r}^2 \frac{d\hat{T}}{d\hat{r}} = -\hat{m}_F(\hat{Q} - \hat{H}) \quad (24)$$

Where:

$$\hat{H} = \frac{\Delta h_c}{h_{fg}}$$

And the boundary conditions:

$$\hat{T}(\hat{r}_f) = \hat{T}_f \qquad (25,a)$$

$$\hat{T}(\infty) = \hat{T}_\infty \qquad (25,b)$$

SOLUTION:

Solving equation (18) with the boundary conditions (19.a, b) for $\hat{m}_F$ and expressing with dimensional form:

$$\dot{m}_F = \frac{4\ln(1 - Y_{Fs})\pi\rho\, Dr_s}{\frac{r_s}{r_f} - 1} \qquad (26)$$

After solving equation (20) for r_f and applying boundary conditions, equation (21, a, b), expressing with dimensional form:

$$r_f = \frac{-\dot{m}_F}{4\ln\left(\frac{\nu}{\nu + Y_{ox\infty}}\right)\pi\rho D} \qquad (27)$$

T_f Can be expressed in dimensional form after solving equation (22) with boundary conditions (23, a, b) as:

$$T_f = \frac{Cp_g\, T_s - Q + \exp\left(\frac{-m_F}{4\pi\rho D\, r_f}\right) Q\, exp\left(\frac{m_F}{4\pi\rho D\, r_s}\right)}{Cp_g} \qquad (28)$$

Where, Q expressed after solving equation (24) with the boundary conditions (25, a, b), in dimensional form:

$$Q = \frac{Cp_g(T_f - T_s) - \Delta h_c + \left(\Delta h_c + Cp_g(T_s - T_\infty)\right)\exp\left(-\frac{m_F}{4\pi\rho D\, r_f}\right)}{\exp\left(-\frac{m_F}{4\pi\rho D\, r_f}\right) - 1} \qquad (29)$$

The relation of surface temperature with droplet radius can be found using the expression of time varying latent heat of vaporization as:

$$\hat{Q} = 1 + \frac{\frac{\dot{Q}_{sen}}{m}}{h_{fg}} \qquad (30)$$

Where:

$$\frac{\dot{Q}_{sen}}{m} = \frac{\frac{4}{3}\pi r_s^{\,3}\rho_l\, Cp\frac{dT}{dt}}{-4\pi\rho_l\, r_s^{\,2}\frac{dr_s}{dt}}$$

Chain rule can be used to reduce one of the derivatives as :

$$\frac{dT_s}{dt} = \frac{dT_s}{d\sigma}\frac{d\sigma}{dr_s}\frac{dr_s}{dt}$$

Where:

$$\sigma = \frac{r_s^{\,2}}{r_{so}^{\,2}}$$

Substituting into equation (30), and simplifying:

$$\frac{d\hat{T}_s}{d\sigma} = \frac{3\left(1-\hat{Q}\right)}{2\sigma} \qquad (31)$$

In order to solve this equation to obtain $\hat{T}_s$ as function of σ (orr_s), the term $\hat{Q}$ which is function of ($\hat{T}_s$, $\hat{m}_F$, $\hat{T}_f$, and $\hat{r}_f$) must be expressed as function of $\hat{T}_s$ only, the vapor is saturated at the droplet surface, an independent relation between Y_{Fs} and $\hat{T}_s$ was given by [Law,1976]:

$$Y_{Fs}\,(T_s) = P_\infty^{\,-1}\exp\left[\frac{Cp}{R}\left(\hat{T}_b^{\,-1} - \hat{T}_s^{\,-1}\right)\right]$$

Using computational substituting is necessary obtain $\hat{Q}$ as function of$\hat{T}_s$, then substituting the resulted equation into (31) gives:

$$\frac{d\hat{T}_s}{d\sigma} = \frac{3}{2\sigma}\left(1 - f\left(\hat{T}_s\right)\right)$$

With boundary condition:

$$\hat{T}_s(1) = \hat{T}_o$$

Solving this equation presents$\hat{T}_s = f(\sigma)$, which can be expressed as dimensional form as:

$$T_s = f(r_s) \qquad (32)$$

The droplet lifetime could be evaluated as follows:

$$\hat{m}_F = \frac{m}{4\pi\rho_g\, D\, r_s}$$

This can be expressed as:

$$\hat{m}_F = -\frac{4\pi\rho_l \; r_s^{\,2} \frac{dr_s}{dt}}{4\pi\rho_g \; D \; r_s} \tag{33}$$

Where dt can be expressed as dimensionless form as:

$$\hat{t} = \frac{2\rho_g \; D}{\rho_l \; r_{so}^{\,2}} \; t$$

Differentiating:

$$dt = \frac{\rho l \; r_{so}^{\,2}}{2\rho_g \; D} d\hat{t}$$

This equation can substituting into equation (33) and r_s can be expressed as dimensional fromσ, rearranging the resulted equation gives:

$$d\hat{t} = -\frac{d\sigma}{\hat{m}_F} \tag{34}$$

CALCULATIONS

For both models, the following relations were used for calculate the terms and thermo-physical properties as; for Cp, k, and μ [Andrews & Biblarz, 1981]:

$$Cp = \sum_{1}^{7} a_i \; T^{i-1}$$

$$k = \sum_{1}^{7} b_i \; T^{i-1}$$

And:

$$k_g = 0.4k_F(\bar{T}) + 0.6k_\infty(\bar{T})$$

Where k_∞ for air, For binary diffusion coefficient [Reid, et.al. 1987] :

$$D_{AB} = \frac{3}{16} \frac{(4\pi \; k_B \; T/Mw_{AB})^{\frac{1}{2}}}{(P/RuT)\pi \; \sigma_{AB}^{\,2} \; \Omega_D} \; f_D$$

The parameters of this equation are listed in reference above, Mass fraction of the oxidizer (Oxygen) at the infinite medium (air) was suggested as followed:

$$Y_{ox\infty} = \frac{mol\ oxidizer \times Mw_{ox}}{mol\ air \times Mw_{air}}$$

The molecular weights of the fuel and the products that used in the analyses, Mw_F andMw_{pr}, were calculated as:

$$CxHy + \left(x + \frac{y}{4}\right)(O_2 + 3.76N_2) \rightarrow xCO_2 + \frac{y}{2}\ H_2O + 3.76\left(x + \frac{y}{4}\right)\ N_2$$

So:

$$Mw_F = 12x + y$$

$$Mw_{pr} = 44x + 9y + 105.28\left(x + \frac{y}{4}\right)$$

The above relations were obtained at reference temperature as[Sparrow & Gregg,1958]:

$$T_r = T_s + \frac{1}{3}\ (T_\infty - T_s)$$

NUMERICAL WORK

Computer programs were created to evaluate the required properties, solving the ordinary differential equations evaluated from heat and mass Transfer balances, then constructs systems of non-linear equations as follows; for the classical model, the program fixed the value of surface temperature as T_{boil} , This is a reasonable assumption when the droplet is burning vigorously after its initial heat-up transient.[Turns,2000, Kuo,1986, kotake & Okazaki,1969, Law, 1982]. The program substituted equation (13) into equation (14) and resolving for T_f , then used the resulted equation with equations (11)and(12) to construct system of non-linear equation, calculating the Jacobian matrix for the system, then solving the system with Newton-Raphson method using the Jacobian. The droplet lifetime was obtained by solving equation (17) using Range-Kutta 4 method with appropriate time interval. For transient model, the program solves dimensionless equations for mass and heat balances, then made numerical substitution to obtain $T_s = f(r_s)$, constructing system of non-linear equations using equations (26),(27),(28),(29),(32) and the equation that related $Y_{Fs} = f\ (T_s)$, then solving the system with Newton-Raphson method using the Jacobian. Droplet lifetime can be obtained using equation (34).

RESULTS AND DISSCUSION

The droplet size used in calculations are; d=100μm as an initial diameter, and d=0 as a final diameter. The environment conditions are taken as 1500K, and pressure 1 atm.. Figures (1) and (2), shows the behavior of mass burning rate with the size ratio of the two fuels and for both models. The droplet size changes from r_{so} to zero. It is expressed in terms of a size ratio so it changes from 1

to zero. It is evident from these figures, For the classical model, the burning rates greater than that for the transient model due to the classical theory, which assumes that all the heat gain to the droplet is used in the vaporization of the fuel droplet at the surface. This will lead to an increase in mass vaporization rate, which in turn, will increase the mass burning rate. Actually, some of the heat gained to the droplet is used for heating the droplet in early stages of its lifetime. This decreases the amount of fuel vaporized from the droplet surface, and this will lead to a decrease in the mass burning rate.

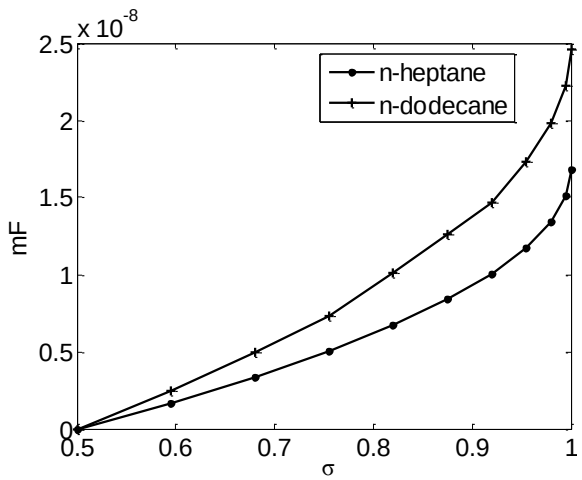

Fig.1 Burining rate vs.size ratio (Classical)

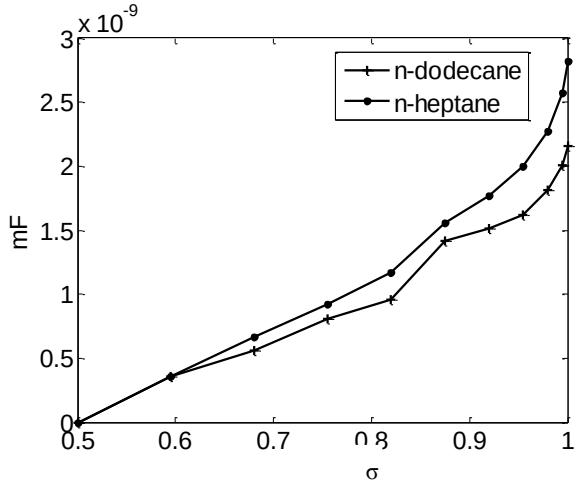

Fig.2 Burining rate vs.size ratio (Transient)

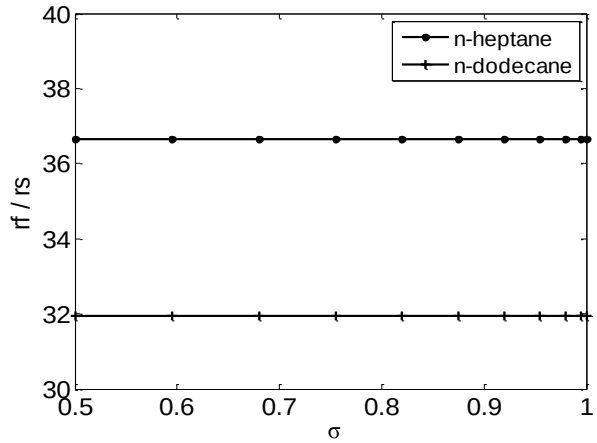

Fig.3 Stand off ratio vs.size ratio (Classical)

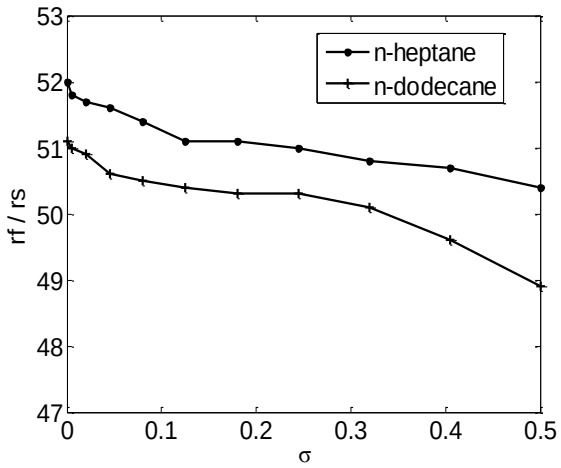

Fig.4 Stand off ratio vs.size ratio (Transient)

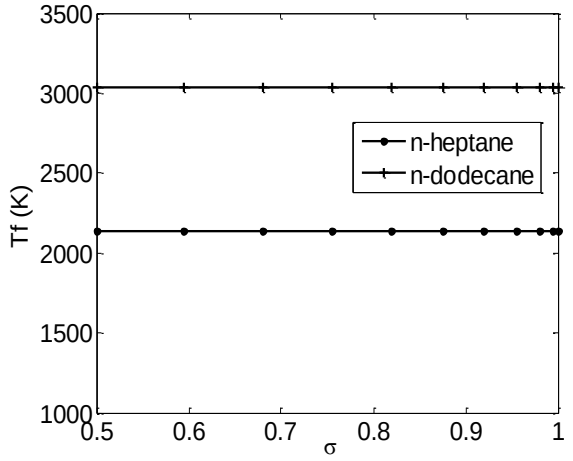

Fig.5 Flame temprature vs.size(Classical)

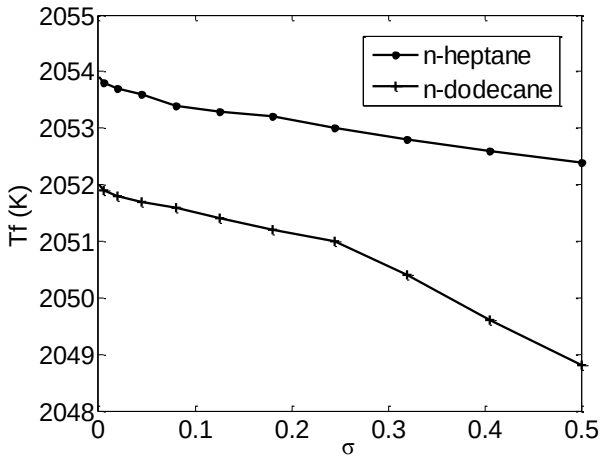

Fig.6 Flame temprature vs.size(Transient)

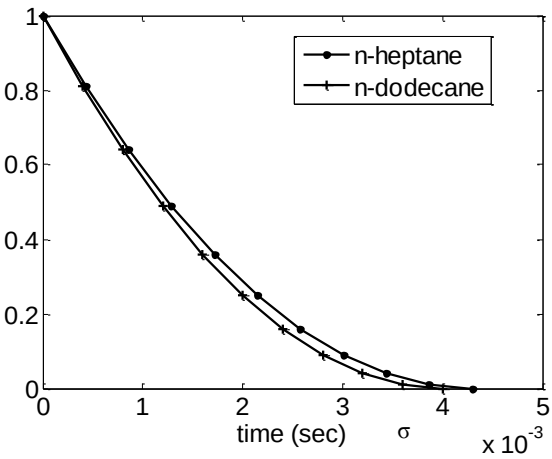

Fig.7 size ratio vs. time (Classical)

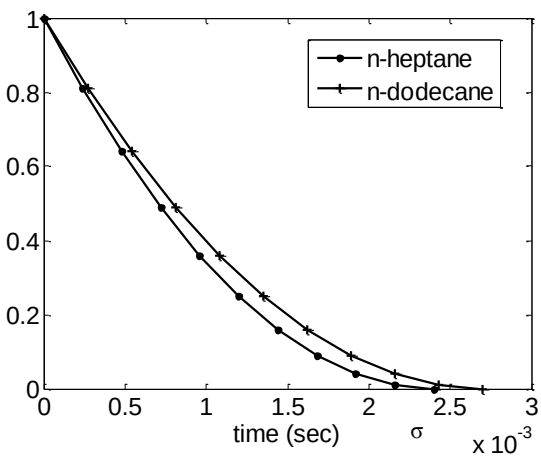

Fig.8 size ratio vs. time (Transient)

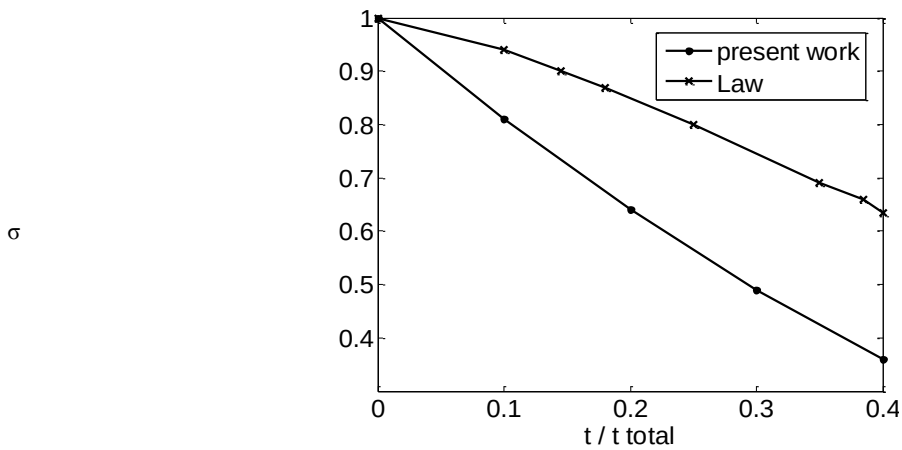

Fig.9 comparison of present Transient model

With model of Law

Figure (3) and (4) represent the variation of flame radius in terms of flame stand off ratio for the two fuels and two models as a function of size ratio. It can be seen that the values of stand off ratio

for the transient model is higher than that for the other model. The assumption of quasi-steady burning of the fuel in the stagnant case resulted in raising the values of flame stand off ratios much more than its original values.

Figures (5) and (6) show the variation of flame temperature with size ratio, the flame temperature increases with the decrease in the size of droplet for the transient model. This can be attributed to the assumption of variable surface temperature.The flame temperature values for the classical model is higher than that of the transient model for the same condition. The burning rate of this model is higher than that of the transient model. This will lead to the burning a larger amount of fuel.

Figures (7) and (8) show the relationship between the time of the combustion process with the size ratio for both models and for the same condition. From these figures, it can be seen that the droplet size decreases with the increases in time. This is attributed to the consumption of the liquid fuel during the combustion process. This behavior continues through the whole process and the complete consumption of the droplet. The final time of the process is reached when the droplet radius diminishes completely.

Regarding and referring to the results expressed in the figures, two fuels were considered, namely: n-heptane and n-dodecane. The difference encountered between the two fuels can be attributed to the fact that the two fuels have different boiling point. The boiling point for n-heptane and n-dodecane are (371.4) and (489.3) respectively. For the transient model, the amount of heat that is used to reach the boiling point of n-dodecane is larger than that for n-heptane, and the fraction of heat used to heat up the droplet for n-dodecane is larger than that of n-heptane. As a result, the heat required to complete the vaporization will be less. Consequently, the vaporization rate will be less. The reduction in the burning rate causes a reduction in the flame conditions, which are position and the temperature. The position of the flame or radius of the flame. The flame temperature may increase as the burning rate becomes larger, since large amount of fuel is burning. Referring to the figure (8), it can be seen that the fuel of the largest burning rate has the shortest lifetime. Increase the burning rate causes the fuel to consume more rapidly. For that reason the figures of transient model is exactly opposite to the arrangements of fuel in the figures of other model.

COMPARISON WITH OTHER WORK:

for the transient model, Figure (9) shows the comparison between the transient combustion models with that of Law [Law, 1976]. Figure (9) shows the droplet size ratio variation with the variation of non-dimensional time (time to final time). Good agreement between Law's model and the present model can be seen with some difference, this difference can be attributed to the more complicated and elongated model used by Law and his use of the finite difference method.

CONCLUSION

The two models show that thermophysical properties are strong functions to reference temperature even when the droplet surface temperature is assumed constant. For classical model shows that the variation of surface temperature can be neglected and this temperature can be assumed constant. For transient model shows that the period of droplet heat up is dominant in the process and caused the mass burning rate at the early stages to be less than that expected in classical theory droplet combustion.

REFERENCES

- Abraham, J., 2001***,"Improved Modeling of Drop Vaporization and Combustion in Sprays",*** Purdue University, Lafayette School of Mech. Eng.
- Andrews, J.R., Biblarz, O., 1981***," Temperature Dependence of Gas Properties in polynomial Form "***, Naval Postgraduate School, NPS67-81-001, January.
- Chigier, N. , 1981, ***" Energy, Combustion, and Environment "***, McGraw-Hill, Inc..
- Dombrovsky, L.A., Sazhin, S.S., 2003, ***"A Simplified Non-isothermal Model for Droplet Heating and Evaporation"***, Int. Comm. Heat Mass Transfer, Vol. 30, No. 6, pp. 787-796.
- Godsave, G.A.E., 1953, ***"Studies of the combustion of Drops in a Fuel Spray : The Burning of Single Drops of Fuel"*** Fourth Symposium (International) on Combustion, Williams and Wilkins, Baltimore, pp. 813-839.
- Goldsmith, M., Penner, S.S. , 1954, ***"On the Burning of Single Drops of Fuel in an Oxidizing Atmosphere"***, Jet propulsion, Vol. 24, pp. 245.
- Hohmann, S., Renz, U., 2003 ***"Numerical Simulation of Fuel Spray at High Ambient Pressure: The Influence of Real Gas Effects and Gas Solubility on Droplet Vaporization"***, Int. Journal of Heat and Mass Transfer, Vol. 46, pp. 3017-3028.
- Kotake, S., Okazaki, T. , 1969, ***"Evaporation and Combustion of Fuel Droplet"***, Int. J. Heat and Mass Transfer , Vol. 12 , pp. 595-610.
- Kuo. KK., 1986, ***"Principles of Combustion"***, John Wiley and Sons Inc..
- Lamnna, G., et.al., 2004, ***"On the Evaporation of a Monodisperse Droplet stream at High Pressure"***, XXI. ICTAM, 15-21 August, Warsaw, Poland.
- Law, C.K. , 1976, ***"Unsteady Droplet Combustion with Droplet Heating"***, Combustion and Flame, Vol. 26, pp. 17-22.
- Law, C.K. , 1982, ***"Resent Advanced in Droplet Vaporization and Combustion"***, Prog. Energy Combust. Sci., Vol. 8, pp.171-201.
- Law, C.K., Sirignano, W.A.,1977 ***"Unsteady Droplet Combustion with Droplet Heating II : Conduction Limit"***, Combustion and Flame, Vol. 28, pp.175-186.
- Ried, R.C., Prausnitz, J.M., Poling,B.E.,1987, ***"The Properties of Gases and Liquids",*** 4th edition, McGraw-Hill, Inc..
- Sazhin, S.S.,2005, ***"New Approach to Numerical Modeling of Droplet Transient Heating and Evaporation"***, Int. Journal of Heat and Mass Transfer, Vol. 48, pp. 4215-4228.

- Sazhin, SS., et. al., 2004, ***"Numerical Modeling of Droplet Transient Heating and Evaporation"***, School of Engineering, University of Brighton
- Spalding, D.B., 1953, ***"The combustion of Liquid Fuels"***, 4th Symposium on Combustion, pp. 864-874.
- Sparrow, E.M., Gregg, J.L., 1958, ***"Similar Solutions for Free convection From A Non-isothermal vertical Plate"***, Trans. Of the ASME, Vol. 80, pp. 379-386.
- Turns, S.R., 2000, ***"An Introduction to Combustion Concepts and Applications"***, Second Edition, McGraw-Hill International Editions.
- Williams, A., Sirignano, 1983, "***Fuel Droplet Vaporization and Spray Combustion Theory"***, Prog. Energy Combust. Sci. , Vol. 9, pp. 291-322.
- Williams, F.A., 1965, ***"Combustion Theory"***, Addison-Wesley Publishing Company, Inc.
- Yan, C., Aggarwal, S.K.,2006, ***"A high-Pressure Droplet Model for Spray Simulations"***, Transaction of ASME, Vol. 128, pp. 482-492.

NOMENCLATURES

A, B, C: Antoine equation constants

$Cp(\frac{J}{kgK})$: Specific heat

$D\left(\frac{m2}{s}\right)$: Binary mass Diffusivity co-efficient

$h\left(\frac{J}{kg}\right)$: Enthalpy

$h_{fg}(\frac{J}{kg})$: Latent heat of vaporization

$k(\frac{W}{mK})$: Thermal conductivity

$m(kg)$: Mass

$\dot{m}(\frac{kg}{s})$: Mass flow rate

$\dot{m}''(\frac{kg}{m^2 s})$: Mass flux

$Mw\left(\frac{kg}{kgmol}\right)$: Molecular Weight

$P(atm)$: Pressure

Pr : Prandtl number

$\dot{Q}(W)$: Heat transfer rate

$Q(\frac{J}{kg})$: Time varying latent heat of vaporization per unit mass

$r(m)$: Radius

$t(s)$: Time

$v_r(\frac{m}{s})$: Radial velocity

x : Number of carbon atoms in fuel molecule

$Y\left(\frac{kg}{kg}\right)$: Mass fraction

y : Number of hydrogen atoms in fuel molecule

GREEK SYMBOLS

$\Delta h_c(\frac{J}{kg})$: Heat of combustion

σ : Size ratio

$\nu(\frac{kg}{kg})$: Oxidizer to fuel stoicheometric ratio

SUBSCRIPTS AND ABBREVIATIONS

b: Boiling

d : Droplet

F : Fuel

f : Flame

g : Gas

$g-i$: Gas–phase to interface region

$i-l$: Interface region to liquid-phase

ox : Oxidizer

Pr : Products

ref :reference

s : Droplet surface

sen : Sensible

o : Initial

∞ : Environment

Study of Drop Size Distribution in RTL Contactor

Adil A.A. Al-Hemiri
Chemical Engineering / University of Baghdad

Yahya J. Jany
Chemical Engineering / University of Technology

ABSTRACT

The present work studied the drop size distribution in the RTL contactor using two liquid-liquid systems, xylene-acetone-water and kerosene-acetone-water. Process variables studied were: rpm (10-50 min^{-1}), continuous phase flow rate (4-12 l/h), dispersed phase flow rate (4-12 l/h), and concentration (0.1-0.5 mole/l). It was found that Sauter mean drop diameter (d_{32}) decreased with increasing rpm and continuous phase flow rate, and decreasing dispersed phase flow rate and concentration. An empirical correlation, with a correlation coefficient equal to (92.6%), relating d_{32} with process variables was developed having the form:

$$\frac{d_{32}}{R} = 9.845*10^{-3}(\Phi)^{0.0627}(We)^{-0.367}(\mathrm{Re})^{0.228}(\frac{Q_d}{Q_c})^{0.43}$$

الخلاصة

تمت دراسة التوزيع الحجمي للقطرات في جهاز الملامسة الكرايسير (RTL) باستخدام منظومتى سوائل هي: الزايلين/اسيتون/ماء و الكيروسين/ اسيتون/ماء. تمت دراسة المتغيرات التالية: سرعة المزج (10-50 دقيقة$^{-1}$ ، جريان الطور المستمر (4-12 لتر/ساعة)، جريان الطور المشتت (4-12 لتر/ساعة) و التركيز (0.1-0.5 مول/لتر).

لقد تم الحصول على ما يلي:- ان معدل قطر القطرات (d_{32}) يصغر مع زيادة سرعة المزج و جريان الطور المستمر ونقصان جريان الطور المشتت و الركيز.

تم الحصول على علاقة تربط معدل قطر القطرة مع المتغيرات المذكورة اعلاه وبنسبة معامل علاقة (Correlation Coefficient) 92.6% وهي كما يلي:

$$\frac{d_{32}}{R} = 9.845*10^{-3}(\Phi)^{0.0627}(We)^{-0.367}(\mathrm{Re})^{0.228}(\frac{Q_d}{Q_c})^{0.43}$$

KEYWORDS

Drop size distribution, RTL contactor, Liquid extraction.

INTRODUCTION

The separation of the constituents of a homogeneous liquid mixture is a problem frequently encountered in the chemical processing industry. Liquid-liquid extraction has been emerging as a very important method for separating such liquid mixtures. The addition of a solvent in this process corresponds to the addition of heat in the case of separation by distillation. The solvent used in the extraction process should be immiscible or partially miscible with one of the components of the mixture in order to facilitate the separation of liquid phases [Hartland 1970, Treybal 1981].

The case for the use of liquid-liquid extraction will depend upon its either accomplishing a separation that cannot be achieved by other operations such as: distillation, evaporation, and crystallization, or effecting the separation more economically. Liquid-liquid extraction is now being adopted as a more economic alternative to other separation processes and has found immense applications in the separation of [Benitez 2002]:

1. Solutions of components having low relative volatility, especially when vacuum distillation is expensive.
2. Solutions of close boiling and azeotrope forming components.
3. Dissolved solute when evaporation may be impractical.
4. Solutions of heat sensitive components such as antibiotics.
5. Components of differing chemical type whose boiling points may overlap as in the case of petroleum hydrocarbons.

The RTL (Formerly Graesser Raining Bucket) contactor consists of a single rotor operating on a substantially horizontal axis in a cylindrical stator. The rotor comprises a series of circular baffles, between which are mounted a number of cylindrical buckets, partly open in the direction of rotation. RTL contactor applied to many extraction processes, such as: pyrethrum refining, purification of herbicide products, and dearomatization of naphtha. Possibilities exist for the applications of the RTL contactor to systems containing a solid phases; thus apparatus has been used for

the treatment of oil bearing sands, with the use of kerosene to remove bitumen as one product, leaving clean treated sand as the under flow [Tech, et al. 1983].

RTL contactor differs in some major respects from vertical type contactors. It has the operating advantages that:

1- Density changes during extraction will not induce axial circulation since the axis is horizontal.
2- The RTL contactor recovers easily from any sudden shutdown since drainage of material from stage to stage cannot occur.

These factors in addition to its ability to handle easily emulsified systems, have contributed to its success over the past years. [Laddha and Degaleesan 1976, Tech, et al. 1983, Mark and Othmer 1998].

DROP SIZE DISTRIBUTION

The effects of drop size and size distribution on the performance of an extraction column are the most important hydrodynamic characteristics, because under steady operating conditions, drop size is related to the interfacial area by:

$$a_s = \frac{6\Phi}{d_{32}}$$

Where:

Φ = Dispersed phase holdup.

d_{32} = Sauter mean diameter = $\frac{\sum n_i d_i^3}{\sum n_i d_i^2}$

The prediction of interfacial area in agitated dispersions is of a considerable importance in heat and mass transfer operations.

Many investigators studied the effect of drop size distribution on the performance of different contactors. Drop size distribution is an important parameter as it defines the available interfacial area for mass transfer. No general correlation is available at present time to describe the drop size distribution in each contactor. Each investigator found a different distribution function suitable to describe his data [Lovick, et al. 2005]. No attempts have been done till now to study the effect of drop size distribution with mass transfer conditions on the performance of RTL contactor.

The following two tables shows some relations used to represent the drop size distribution with and without mass transfer conditions.

Table (1). Published correlation of drop size without mass transfer [Kumar and Hartland 1986].

No	Correlation	Ref.
1	$\frac{d_{32}}{\sqrt{\frac{\sigma}{\rho_c g}}} = 16.7(\frac{N^* R^2 \rho_c}{\mu_c})^{-0.3}(\frac{N^{*2} R}{g})^{-0.3} n^{-0.23}$	Kagan, et al. 1964
2	$\frac{d_{32}}{R} = 0.037(\frac{N^{*2} R^3 \rho_c}{\sigma})^{-0.6}(\frac{N^{*2} R}{g})^{-0.27}(\frac{N^* R^2 \rho_c}{\mu_c})^{0.14}$ $(\frac{\mu_d}{\mu_c})^{0.06}(\frac{D_r}{R})^{0.875}(\frac{H}{w})^{0.45}[1+\frac{3.7}{\exp(0.008N^* + 0.25n)}]$	Fischer 1971
3	$\frac{d_{32}}{D} = 0.62(\frac{N^2 D^3 \rho_c}{\sigma})^{-0.52}[1+\frac{35}{n^{1.22}(\frac{N^2 D^3 \rho_c}{\sigma})^{0.5}}](1+2\varepsilon)$	Fischer 1973
4	$\frac{d_{32}}{R} = 4.7*10^{17}(\frac{N^* R^2 \rho_c}{\mu_c})^{-3.33}(\frac{\mu_d}{\mu_c})^{0.23}(\frac{N^* R \mu_c}{\sigma})^2 \varepsilon^{0.225}\exp(0.4\frac{n}{n_t})$	Mumford and Al-Hemiri 1974
5	$\frac{d_{32}}{R} = 0.17(\frac{N^{*2} R^3 \rho_c}{\sigma})^{-1.2}(\frac{N^* R^2 \rho_c}{\mu_c})^{0.6}$	Mar, et al. 1975, 1978
6	$\frac{d_{32}}{R} = 0.3(\frac{N^{*2} R^3 \rho_c}{\sigma})^{-0.6}(\frac{N^{*2} R}{g})^{-0.27}(\frac{N^* R^2 \rho_c}{\mu_c})^{0.14}$	Mersmann 1980

Table (2). Published correlations of drop size under mass transfer conditions [Kumar and Hartland 1986].

No.	Correlation	Reference
1	$d_{32} = [1.04(\frac{R}{D_r} - 0.66) + 0.06]N^{*-2.2}$	Spathe and Weiss 1972
2	$\frac{d_{32}}{D_r} = 108*10^{-5}(\frac{N^* R^2 \rho_c}{\mu_c})^{2.15}(\frac{N^{*2} R}{g})^{1.05}(\frac{N^{*2} R^3 \rho_c}{\sigma})^{-2.7}$ $(\frac{U_d}{U_c})(\frac{\sigma}{U_c \mu_c})^{-0.27}(\frac{\mu_d}{\mu_c})^{-1.93}(\frac{\rho_d}{\rho_c})^{0.77} n^{-0.35}$	Magiera and Zadlo 1977
3	$\frac{d_{32}}{D_r} = 1.43[\frac{U_d(1-\varepsilon)}{U_c \varepsilon}]^{0.45}[\frac{N^* R(1-\varepsilon)}{U_c}]^{-0.565}[\frac{\rho_c H U_c}{\mu_c(1-\varepsilon)}]^{-0.117}$	Blazej, et al. 1978
4	$\frac{d_{32}}{R} = 1.48[\frac{U_d H \rho_c}{\varepsilon \mu_c}]^{-0.23}(\frac{N^{*2} R^3 \rho_c}{\sigma})^{-0.004}(\frac{U_d^2}{\varepsilon^2 g D_r})^{0.44}$ $(\frac{\Delta\rho}{\rho_c})^{-0.57}(\frac{H}{D_r D_s})^{-0.24}(\frac{n}{n_t})^{-0.07}$	Jeffreys, et al. 1981

5	$\frac{d_{23}}{R} = 1.26(\frac{N^{*2} R^3 \rho_c}{\sigma})^{-0.52}[\frac{36}{n^{1.22}(\frac{N^{*2} R^3 \rho_c}{\sigma})^{0.5}}]$	Hartung and Weiss 1982

Shinnar and Church [1960] investigated the predication of drop size in agitated dispersions. The average drop diameter was calculated for concentrated liquid-liquid distribution in agitated tanks for various liquids by the following empirical equation derived by Rodger, et al. [1956].

$$d_{av} = \frac{R}{k}(\frac{R^3 N^{*2} \rho_c}{\sigma})^{-0.36}[\frac{R^k}{D_r}(\frac{\nu_d}{\nu_c})^{0.2}(\frac{t}{t_o})^{\frac{1}{6}} \exp(3.6\frac{\Delta\rho}{\rho_c})0.71\exp(0.35\frac{D_r}{D_{ro}})]^{-1}$$

(1)

Hinze [1955] has proposed an equation for the maximum stable drop size, based on the assumption of an isotropic homogeneous turbulence in liquid-liquid systems with mass transfer:

$$d_{\max} = 0.725(\frac{g_c \sigma}{\rho_c})^{\frac{3}{5}} \varepsilon^{-\frac{2}{5}} \quad (2)$$

Strand, et al. [1962] studied the performance of rotating disc contactors under mass transfer conditions. Some attempts to measure (d_{max}) have been made. The authors couldn't obtain enough information to generalize, but it can be said that such data will be more difficult to interpret, especially if rates of drop breakup or coalescence are sensitively affected by solute concentration or by the direction of transfer. They suggested that a mechanism for predicting (d) or (d_{max}) during mass transfer will be difficult to devise.

Olney [1964] investigated the prediction of drop size distribution in a counter-current rotating disc contactor for five liquid-liquid systems. The study presented an interpretation of drop size distribution data in a contactor for which a fairly complete analysis of drop dynamics and mass transfer processes were obtained based on the simplified (average drop) concept. Olney showed that rotor speed have a marked effect on the average or characteristic drop size but not much effect on the parameters of the size distributions. For example, the data for white oil dispersed in water showed that the volume median drop size (d_{50}) decreased from (3.1-0.8 mm) as rotor speed is increased from (650-1100 rev/min) but the width of the size distribution changed only from (4.5 to 4.2).

Effect of holdup on the size distribution at a given rotor speed, as the holdup increased the increase in drop sizes over the whole spectrum may be caused solely by higher drop interaction rates due to smaller inter particle distances.

Olney showed that all his experimental data of the five systems were obeying the upper-limit distribution proposed by Mugele and Evans (1951).

Coulaloglou and Tavlarides [1976] studied the drop size distributions and coalescence frequencies of liquid-liquid distributions in flow vessels. Drop size distribution measurements in the circulation and impeller regions and dispersed phase coalescence frequencies measurements were made co-currently for the turbulently agitated dispersion of kerosene – dichlorobenzene (d) - in water (c), in a 12 liter flow vessel. The ranges of operating conditions studied were dispersed phase holdup (0.025-0.15), impeller speed (190-310 rev\min) and nominal residence time of (10min). The Sauter mean diameter was correlated by the following relation:

$$\frac{d_{32}}{R} = 0.081(1 + 4.47\Phi)(We_{crit})^{-0.6} \tag{3}$$

Magiera, et al. [1976] investigate the hydrodynamics of rotating disc contactor. They showed that Sauter mean diameter is calculated from:

$$d_{32} = [1.045(\frac{R}{D_r} - 0.66) + 0.06]N^{*2.2} \tag{4}$$

Many studies have been done on the bubble size distribution in different contactors [Alves, et al. 2002, Mouza, et al. 2005, and Lage 1999]. Martinez, et al. [1999] studied the breakup frequency of air bubble in a fully turbulent flow. They found that the diameter for which breakup frequency will be a maximum depends on:

$$d_{\max} = 1.63(\frac{12\sigma}{8.2\rho})^{\frac{3}{5}} \varepsilon^{-\frac{2}{5}} \tag{5}$$

EXPERIMENTAL WORK:

Liquid-Liquid Systems: -

Physical properties of the liquid-liquid systems employed are summarized in table (3). The selection of these two systems is based in general on:

1. Availability and cost.
2. Selectivity.

3. Difference in physical properties.
4. Corrosivity.

The systems used were:

1. Water (c)-acetone (s)-xylene (d).
2. Water (c)-acetone (s)-kerosene (d).

Table (3) Physical properties of the studied systems.

System	Temp	Density g/cm^3		Viscosity g/cm.sec		Diffusivity cm^2/sec		Interfacial tension dyne/cm	Distribution coefficient
		Disp.	Cont.	Disp.	Cont.	Disp.	Cont		
xylene-acetone-water	25	0.860	0.997	0.610	1.020	0.389	0.109	28.01	0.438
kerosene-acetone-water	21	0.795	0.998	1.123	1.050	0.227	0.109	39.9	0.905

Description of Equipment: -

A (0.1 m) diameter, (1 m) long Graesser raining bucket contactor supplied by Corning Ltd., England, was employed. The contactor consists of a horizontal cylindrical shell with a compartment rotor which is made up of a number of circular plates which have "C-shape" buckets mounted near the outer edge between each pair of plates.

The contactor is capable of handling a total phase throughput of (12 l/h) and it consist of (36) compartments, each of (0.025 m) long and consists of (6) buckets, each bucket is (0.025 m) in diameter.

The two phases flow counter-currently along the shell from compartment to another through a peripheral gap between the rotor and the shell. A short disengaging zone is provided at each end of the unit to ensure complete separation of the phase. The heavy phase, which was aqueous phase, enters and leaves the contactor at points just below the rotor shaft, while the light (organic) phase enters and leaves at points above the rotor shaft. A (1/3 hp) AC motor drives the rotor shaft. The drive shaft of the motor was coupled to the contactor shaft via a gear box to select the required rpm (0-50).

Six (0.01 m^3) QVF glass spherical vessels were used as storage reservoirs and were mounted on a special vessel support. Two Stuart-Turner centrifugal pumps, type

number 12, capable of handling (720-750 gph) against (10-45 ft) head of water were used to transfer the liquids.

The pumps were made of stainless steel and the pump glands were especially adapted for use with solvents.

Flow rates were measured by independently calibrated rotameters. The range of flow of each rotameter is (2.4-30 L/h) of water at 20 ^{0}C.

MEASUREMENTS OF SOLUTE CONCENTRATION: -

Concentrations of solute in organic phase and aqueous phase were measured by UV-visible spectrophotometer (Shimadzu UV-160).

EXPERIMENTAL PROCEDURE: -

The dispersed phase solution was made up to the required concentration. The contactor filled with the continuous phase, and then the dispersed phase was introduced into the contactor. Flow rates were adjusted to the required value until the dispersed phase made up to (50%) holdup. The continuous phase flow and the agitator were adjusted to the required values.

Pictures were taken at several compartments of the contactor, namely compartment [6, 11, 16, 21, 26, and 31]. After steady state was reached, pictures were taken.

LG web camera, version LG Lic-100, connected to P4 computer, which have the ability for recording video or pictures, used for picturing. The camera has the ability to record (33 frames per second).

Lighting was provided by two (1000, 250 watt) photoflood lamps placed directly behind the contactor.

Pictures were taken through the glass shell of the contactor, and the area pictured was (0.025 m) in width, bracketing one compartment, and (0.03 m) in length. And since the object is very close to the contactor wall distortion due to curvature is therefore negligible.

(800) to (1500) pictures were taken for each experiment (130 to 250 pictures in each compartment). Drop size measurements were taken from pictures using picasa programmed in P4 computer to calculate the drop size, (15-35) picture were analyzed

for each compartment. Finally, samples from liquid vessels were taken and analyzed by UV-spectrophotometer to obtain the concentrations of solute.

PROCESS VARIABLES: -

Table (5) shows the range of operating conditions studied in the present research: -

Table (5) operating conditions studied

	Variable	Range
X_1	Rotation of speed	10-50 rpm
X_2	Continuous phase flow rate	4-12 l/h
X_3	Dispersed phase flow rate	4-12 l/h
X_4	Concentration of dispersed phase	0.1-0.5 mole/l

EMPIRICAL MODEL OF SAUTER MEAN DIAMETER: -

The effect of operating conditions, physical properties, and contactor geometry on the Sauter mean diameter of each experiment were correlated using dimensionless analysis (Buckingham theorem).

d_{32} is assumed to be a function of the following variables:

$$d_{32} = f(Q_d, Q_c, \Phi, \mu_d, \mu_c, \rho_d, \rho_c, N^*, \sigma, R) \qquad (6)$$

$$d_{32} = i * R * (\Phi)^{i_1} \left(\frac{\rho_c N^{*2} R^3}{\sigma}\right)^{i_2} \left(\frac{Q_d}{Q_c}\right)^{i_3} \left(\frac{\mu_d}{\mu_c}\right)^{i_4} \left(\frac{\Delta\rho}{\rho_c}\right)^{i_5} \left(\frac{N^* R^2 \rho_c}{\mu_c}\right)^{i_6}$$

Using STATISTICA program, the constant (i) and the powers were found to be:

$i = 9.845*10^{-3}$ $i_1 = 0.0627$ $i_2 = -0.367$ $i_3 = 0.4003$ $i_4 = 0.0723$ $i_5 = -0.00818$

$i_6 = 0.228$

Thus the final correlation obtained is:

$$\frac{d_{32}}{R} = 9.845*10^{-3} (\Phi)^{0.0627} (We)^{-0.367} (\mathrm{Re})^{0.228} \left(\frac{Q_d}{Q_c}\right)^{0.43} \qquad (7)$$

Since modified We no. $= \dfrac{\rho_c N^{*2} R^3}{\sigma}$ and modified Re no. $= \dfrac{N^* R^2 \rho_c}{\mu_c}$

This equation correlates the data with a correlation coefficient equal to (92.6%).

RESULTS AND DISCUSSIONS :

The Influence of Process Variables on Sauter Mean Drop Diameter (d_{32}): -

Variation of d_{32} along the axial distance of the contactor is shown in figures (1) for xylene-acetone-water system and (2) for kerosene-acetone-water system. The two figures showed that the d_{32} decreased with the axial distance from the dispersed phase inlet. This was because, in the inlet of the dispersed phase and due to the horizontal nature of the contactor the holdup is higher in compartment number one than that in the other compartments and decreased with the axial distance along the contactor and reached a minimum value at the inlet of the continuous phase. This was in agreement with Al-Hemiri and Kareem [1990], as the holdup increased the d_{32} increase.

EFFECT OF RPM: -

Figures (3) and (4) show the effect of rpm on d_{32} for the two systems xylene-acetone-water system and kerosene-acetone-water system respectively.

The two figures showed that increasing the rpm decreased d_{32}. This was because increasing the rpm increased drop breakup and lead to smaller drops. This was in agreement with Coulaloglou and Tavlarides [1976], Lovick, et al. [2005].

Equation (7) shows a good agreement with the experimental results as shown in the two figures.

EFFECT OF CONTINUOUS PHASE FLOW RATE: -

Figures (5) and (6) show the effect of continuous phase flow rate on the d_{32} for the two systems xylene-acetone-water system and kerosene-acetone-water system respectively.

Increasing the continuous phase flow rate decreased the d_{32} for the two systems. This was because an increase in continuous phase flow rate leads to more redispersion resulting in smaller drops. This was in contrary to the observations of Mumford [1970], who suggested that in agitated columns, the vertical contactors like the RDC, the drop size distribution was directly affected by the continuous phase flow rate, but it is in agreement with Al-Hemiri and Kaream [1990], and Kolb and Bart [2002].

Equation (7) shows a good agreement with the experimental results as shown in the two figures.

EFFECT OF DISPERSED PHASE FLOW RATE:-

Figures (7) and (8) show the effect of dispersed phase flow rate on d_{32} for the two systems xylene-acetone-water and kerosene-acetone-water respectively.

Increasing the dispersed phase flow rate increased the d_{32}, this was because a larger amount of the dispersed phase enhance coalescence and cause an increase in the drop sizes. This was in agreement with Jeffreys, et al. [1981], and Al-Hemiri and Kareem [1990].

Equation (7) shows a good agreement with the experimental results as shown in the two figures.

EFFECT OF CONCENTRATION: -

Figures (9) and (10) show the effect of concentration on d_{32} for the two systems xylene-acetone-water and kerosene-acetone-water respectively.

For both systems used increasing the concentration increased the d_{32} this is because the transfer is from the dispersed phase to the continuous phase, which enhances the drop size to be larger due to the Marangoni effect, This was in agreement with Kumar and Hartland [1986] and Bratsun and Dewitt [2004].

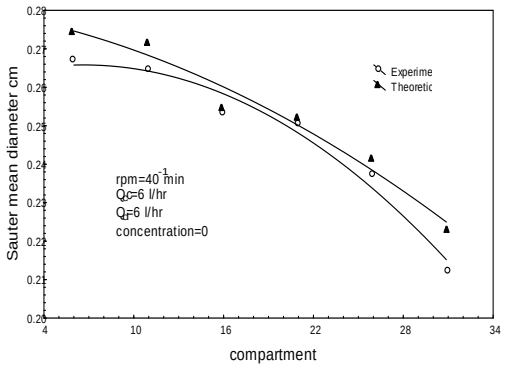

Fig. (1). Sauter mean diameter along the axial contactor length experiment (8) xylene-acetone-water system.

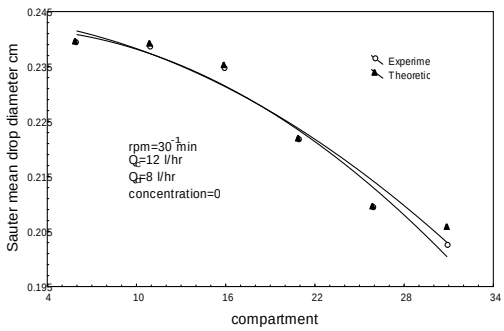

Fig. (2). Sauter mean diameter along the axial contactor length experiment (20) kerosene-acetone-water system.

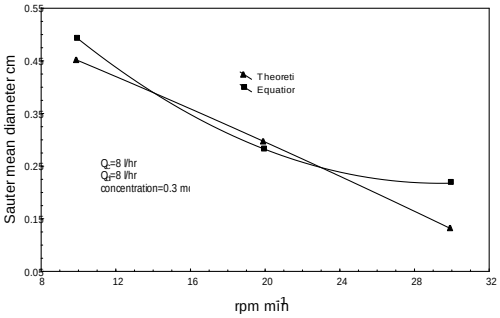

Fig. (3). Effect of rpm on the Sauter mean diameter for xylene-acetone-water system.

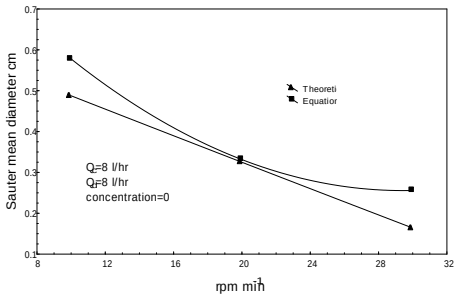

Fig. (4). Effect of rpm on the Sauter mean diameter for kerosene-acetone-water system.

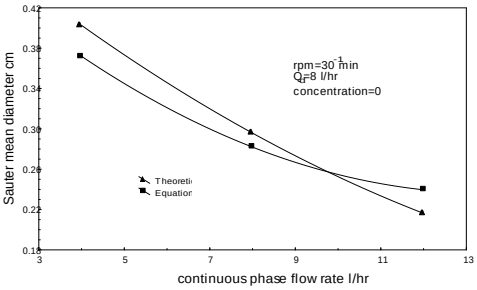

Fig. (5). Effect of continuous phase flow rate on the Sauter mean diameter for xylene-acetone-water system.

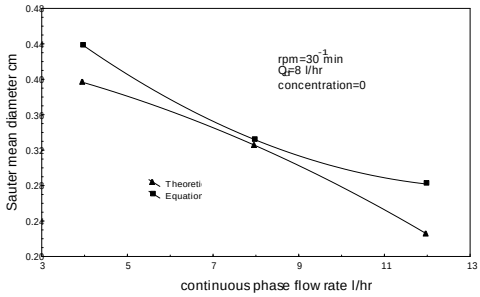

Fig. (6). Effect of continuous phase flow rate on the Sauter mean diameter for kerosene-acetone-water system.

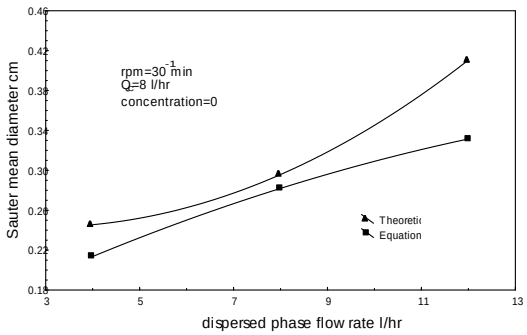

Fig. (7). Effect of dispersed phase flow rate on the Sauter mean diameter for xylene-acetone-water system.

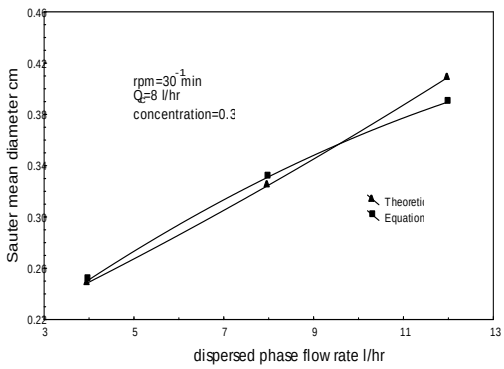

Fig. (8). Effect of dispersed phase flow rate on the Sauter mean diameter for kerosene-acetone-water system.

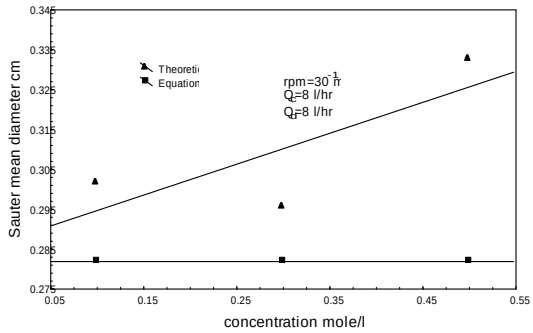

Fig. (9). Effect of concentration on the Sauter mean diameter for xylene-acetone-water system.

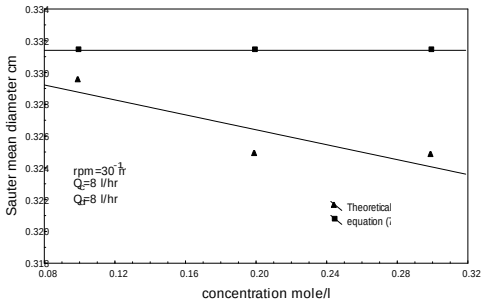

Fig. (10). Effect of concentration on the Sauter mean diameter for kerosene-acetone-water system.

CONCLUSIONS:-

* The Sauter mean drop size (d_{32}) decreased with the axial distance along the contactor from the point of the inlet of the dispersed phase.

* An empirical correlation was correlated between d_{32} and operating conditions, contactor geometry, and physical properties of the studied system, expressed as a function of dimensionless groups with a correlation coefficient of (92.6%).

* The d_{32} was found to decrease with:

- Increasing rotation of speed (rpm).
- Increasing continuous phase flow rate.
- Decreasing dispersed phase flow rate.

REFERENCES

* Al-Hemiri, A.A.A., and Kareem, A., (1990) *"Drop size distribution in a Graesser contactor"*, Can. J. Chem. Eng., 68, 569.

* Alves, S.S., C.I. Maia, J.M.T. Vasconcelos, and A.J. Serralheiro, (2002)*"Bubble size in aerated stirred tanks"*, Chem. Eng. J., 89, 109.

* Benitez, J., (2002)*"Principles and modern applications of mass transfer operations"*, John Wiley &Sons, Inc., New York,.

* Blazej, L., M. Vajda, and S. Bafrncova, (1978) Chem. Zvesti, 32, 314, [cited by Kumar and Hartland 1986].

* Bratsun, D.A., and De Wit, H., (2004)*"On Marangoni convective patterns driven by exothermic chemical reaction in two layer systems"*, Physics of fluids, 16, 1082.

* Coulaloglou, C.A., and Tavlarides, L.L., (1976)*"Drop size distribution and coalescence frequencies of liquid-liquid dispersions in flow vessels"*, AICHE.J., 22, 289.

* Fischer, A., (1971) Verfahrenstechnik, 5, 360, [cited by Kumar and Hartland 1986].

* Fischer, A., Ph.D. thesis, ETH Zurich, (1973) [cited by Kumar and Hartland 1986].

* Hartland, S., (1970)*"Counter-current extraction"*, Pergamon press Ltd., Oxford.

* Hartung, J., and Weiss, S., (1982) Chem. Tech. (Leipzig), 34, 300, [cited by Kumar and Hartland 1986].

* Hinze, J.O., (1955)*"Fundamentals of hydrodynamic mechanism of splitting in dispersion processes"*, AICHE.J., 1, 289.

* Jeffreys, G.V., K.K.M. Al-Aswad, C. Mumford, (1981)*"Drop size distribution and dispersed phase holdup in a large rotating disc contactor"*, Separation science and Technology, 16, 1217.

* Kagan, S.Z., et al., J. (1964)Appl. Chem. USSR, 37, 67, [cited by Kumar and Hartland 1986].

* Kolb, P., and Bart, H., (2002)*"Liquid-liquid miniplant extractor- A novel tool for process design"*, International solvent extraction Conference, South Africa.

* Kumar, A., and Hartland, S., (1986)*"Prediction of drop sizes in rotating disc extractors"*, Cand. J. Chem. Eng., 64, 915.

* Lage, P.L.C., (1999)*"Conservation of bubble size distribution during gas reactive absorption in bubble column reactors"*, Braz. J. Chem. Eng., 16, 290.

* Lovick, J., et al., (2005)*"Drop size distribution in highly concentrated liquid-liquid dispersions using a light back scattering method"*, J. Chem. Technol. Biotech., in press, 0268-2575/ .

* Magiera, J., B. Tal, J. Zadlo, (1976)*"Hydrodynamic and kinetic problems of mass transfer in rotating disc extraction column"*, Int. Chem. Eng., 16, 744.

* Magiera, J., and Zadlo, J., (1977) Inz. Chem., 7, 127, [cited by Kumar and Hartland 1986].

* Mar, R., G. Husung, and F. Moser, (1978) Verfahrenstechnik, 12, 139, [cited by Kumar and Hartland 1986].

* Martinez, C.B., J.L. Montanes, and J.C. Lasheras, (1999)*"On the breakup of an air bubble injected into a fully developed turbulent flow"*, J. Fluid Mech., 401, 157.

* Mersmann, A., (1980) Chem. Ing. Tech., 52, 933, [cited by Kumar and Hartland 1986].

* Mouza, A.A., G.K. Dalakoglou, and S.V. Paras, (2005)*"Effect of liquid properties on the performance of bubble column reactors with fine pore spargers"*, Chem. Eng. Sci., 60, 1465.

* Mugele, R.A., and Evans, H.D., (1951)*"Droplet size distribution in sprays"*, Ind. Eng. Chem., 43, 1317.

* Mumford, C.J., and Al-Hemiri, A.A.A., (1974)*"The effect of wetting characteristic upon the performance of rotating disc contactor"*, Proc. Int. solvent Extr. Conf., society of chemical industry, London, Vol. 2, 1591.
* Olney, R.B., (1964)*"Droplet characteristic in a counter-current contactor"*, AICHE. J., 10, 827.
* Rodger, W.A., et al., (1956)Chem. Eng. Progr., 52, 515, [cited by Shinnar and Church 1960]
* Shinnar, R., and Church, J.M., (1960)*"Prediction particle size in agitated dispersions"*, Ind. Eng. Chem., 52, 255.
* Spathe, W., and Weiss, S., (1972) Leuna-Mersburg, 14, 66, [cited by Kumar and Hartland 1986].
* Strand, C.P., R.B. Olney, and G.H. Ackerman, (1962)*"Fundamental aspects of rotating disc contactor performance"*, AICHE.J., 8, 252.
* Tech, L., H.I. Malcolm, and C. Hanson, (1983)*"Handbook of solvent extraction"*, John Wiley &Sons, New York.
* Treybal, R.E., (1981)*"Mass transfer operations"*, 2nd ed., McGraw-Hill book Comp., New York.

NOMENCLATURE:-

Symbol	Definition	Units
A	Interfacial mass transfer area	cm^2
a_s	Specific interfacial mass transfer area	cm^2/cm^3
D	diffusivity	cm^2/s
D_r	Column diameter	cm
d_{32}	Sauter mean drop diameter	cm
g	Acceleration of gravity	cm/s^2
H	Width of contactor compartment	cm
h_m	Height of mixing compartment	cm
K_o	Overall mass transfer coefficient	cm/s
k_c	Individual mass transfer coefficient of continuous phase	cm/s
K_{oc}	Overall mass transfer coefficient based on continuous phase	cm/s
K_{od}	Overall mass transfer coefficient based on dispersed phase	cm/s
k_d	Individual mass transfer coefficient of dispersed phase	cm/s
L	Length of contactor	cm
m	Distribution coefficient	
n	Compartment number	
N^*	Rotor speed	min^{-1}
Q	Volumetric phase flow rate	l/h
R	Impeller (rotor) diameter	cm
S_f	Superficial flow velocity	$cm^3/cm^2.s$
U	Superficial phase velocity	cm/s
U_k	Characteristic velocity	cm/s

U_t	Terminal velocity	cm/s
V	Volume of contactor	l
$X_{1,2,3,4}$	Process variables	

GREEK SYMBOLS:

Symbol	Definition	Units
ε	Dissipation energy per unit mass	erg/g.s
μ	viscosity	g/cm.s
ν	Kinamatic viscosity	cm^2/s
ρ	density	g/cm^3
σ	Interfacial tension	dyne/cm
Φ	Dispersed phase holdup fraction	

SUBSCRIPT:

Symbol	Definition
c	Continuous phase
d	Dispersed phase
max	Maximum
min	Minimum
crit	Critical

COMPARATIVE STUDY OF TRADITIONAL PWM INVERTERS AND MULTILEVELS INVERTERS

Dr. K. S. Krikor, Dr. Khalid I. Alnaimi, and Dr. Jamal Abdul-Kareem Mohammed*

ABSTRACT:

The need of higher powers in electrical drives has forced the researchers to develop new power source possibilities. Multilevel inverters have been presented as a cost effective solution for various high voltage and high power applications including power quality and motor drive problems.

The traditional pulse width modulated (PWM) Inverter does not completely eliminate the unwanted harmonics in the output waveform. Using the multilevel inverter as an alternative to traditional PWM inverters for electric motor drive applications is investigated.

The concept of the Optimized Harmonic Elimination Stepped-Waveform (OHESW) technique for a multilevel inverter is presented. The effectiveness of this technique in minimizing the inverter switching losses and its output voltage harmonic content which cause reducing harmonic losses and torque pulsations of an induction motor fed form is investigated analytically.

Comparison between the Selective Harmonic Eliminated PWM (SHEPWM) as a traditional PWM technique for three-level inverter and the OHESW technique for multilevel inverter with regard to the switching losses, harmonic distortion, additional harmonic losses in the motor and the pulsating torques is also presented.

الخلاصة :

أن الحاجة للقدرات العالية في المسوقات الكهربائية أجبرَت الباحثين لتطوير أمكانيات جديدة لمصدر القدرة. تمّ أبداء العواكس المتعددة المستويات كحلّ فعّال ومناسب لمختلف تطبيقات القدرة العالية والفولتية العالية ومنها مسائل سوق المحرك وجودة القدرة.

التضمين التقليدى لعرض النبضة لا يحدف التوافقيات الغير مرغوب بها من الموجة الخارجة بشكل تام. تمّ تحقيق أستخدام العاكس متعدد المستويات كبديل عن العواكس التقليدية التي تعمل بتضمين عرض النبضة في تطبيقات سوق المحرك الكهربائي.

تمّ أبداء مفهوم تقنية الموجة المثالية الخطوية لحدف التوافقيات (OHESW) لعاكس متعدد المستويات. تمّ التحقق تحليلياً من فعالية هده التقنية في تقليل خسائر التشغيل في العاكس والمحتوى التوافقي للفولتية الخارجة منه والدي يؤدي الي تقليل الخسائر التوافقية والعزوم التنبضية لمحرك حثي يغدى من دلك العاكس.

تمّ أبداء مقارنة بين تضمين عرض النبضة بحدف التوافقيات الأنتقائي (SHEPWM) كتقنية تضمين تقليدية لعاكس ثلاثي المستويات وتقنية الموجة المثالية الخطوية لحدف التوافقيات لعاكس متعدد المستويات, من حيث خسائر التشغيل والتشويه التوافقي الكلي والخسائر التوافقية الأضافية والعزوم التنبضية في المحرك.

KEYWORDS

Harmonic Elimination, PWM, Multilevel Inverter.

INTRODUCTION:

In the industry, there are two basic needs for the development of the power electronic devices. The needs are a higher power capability (over 1 MW) and a smoother output voltage. In a classical 2- or 3-level low power inverter increasing the switching frequency and modifying the modulation techniques have been executed for a smoother output voltage. In the case of the high power applications, the switching frequency cannot be increased, because of higher switching losses and electronic limitation of the power switches (turn on and off times are bigger with high voltage switches than with low voltage switches). One solution for this problem is a multilevel inverter. In the multilevel inverters the voltage rating of power switches can be lower than in 2- or 3-level inverters. Lower voltage rating of switches, decrease the switching losses and diminish the electronic limitation of the high voltage switches. Increasing the voltage levels of an inverter can solve the problems of a 2- or 3-level inverter [*M. Jokinen* 2005].

* Dept. of Electromechanical Engineering, University of Technology, Baghdad-IRAQ.

The poor quality of current and voltage fed by a classical 2- or 3-levels inverter which has been pointed out in previous works [*P. N. Enjeti* 1990, *H. S. Patel* 1973, and *J. Sun* 1992] leads to the use of multilevel inverters in the drives community, for high power adjustable speed systems.

Traditional PWM inverters have recently been found to be a major cause of motor bearing failures due to excessive bearing currents in inverter-motor drive systems [*J. M. Erdman* 1996].
One of the problems of the PWM controlled AC motors is the acoustic noise that could become unacceptable when used in silent environments [*S. Laurentiu* 2002]. Traditional PWM schemes have the inherent problems of producing Electromagnetic Interference (EMI). Rapid changes in voltages (dv/dt) are a source of EMI. The presence of a high dv can cause damage to electrical motors [*J. M. Erdman* 1996].

The Selective Harmonic Eliminated PWM (SHEPWM) technique is currently applied in conventional 2- or 3-level inverter circuits. The concept of the SHEPWM technique will be presented in this paper.

Multilevel inverters synthesize the AC voltage from several different levels of DC voltages. Each additional DC voltage level adds a step to the AC voltage waveform. Therefore, a staircase (stepped) waveform can be produced which approaches the sinusoidal waveform with minimum Total Harmonic Distortion (THD) [*J. S. Lai* 1996]. A harmonic distortion decreases when the number of voltage levels increase. This means that there is no need for such filters, which are implemented nowadays. With the multilevel inverter, also, $d\upsilon/dt$ decrease. Smaller $d\upsilon/dt$ decreases the motor failures like bearing failures and insulation breakdowns [*M. Jokinen* 2005].

The Optimized Harmonic Elimination Stepped-Waveform (OHESW) technique is very suitable for a multilevel inverter circuit. By employing this technique along with the multilevel topology, the low THD output waveform without any filter circuit is possible. Switching devices, in addition, turn on and off only one time per cycle, this can overcome the switching loss problem, as well as EMI problem [*S. Sirisukparsert* 1999].

The objective of this paper is to compare the results of the multilevel inverter using cascaded-inverters with OHESW technique to those of the traditional 3-level full-bridge inverter with SHEPWM technique to get the optimum one.

MULTILEVEL INVERTER ADVANTAGES AND DISADVANTAGES:

The most attractive features of multilevel inverters are as follows:

* They can generate output voltages with extremely low distortion and lower *dv*/*dt*.
* They draw input current with very low distortion.
* They generate smaller Common Mode (CM) voltage, thus reducing the stress in the motor bearings. In addition, using sophisticated modulation methods, CM voltages can be eliminated.
* They can operate with a lower switching frequency [*J. Rodriguez* 2002].

Compared to a full bridge inverter which can generate 2- or 3- level output voltage waveforms, a multilevel inverter has the following advantages:
* If the number of DC bus voltage levels is high, a near-sinusoidal staircase voltage can be generated with only fundamental frequency switching. Fundamental frequency switching minimizes switching losses and is particularly suitable for high power, high voltage applications such as large induction motor drives or static Volt-Ampere reactive (VAr) compensators.
* When the number of levels is sufficiently high, harmonic content will be low enough to avoid the need for filters.
* High voltages on the DC side do not have to be blocked by one switching device only, but by a number of switching devices in series. Therefore, the switching devices in a multilevel inverter can be rated at lower voltages compared to switching devices applied in a full bridge inverter.
* Some multilevel inverter topologies such as the flying capacitor and cascaded multilevel inverters provide switch combination redundancies. These redundancies for example, can be used for balancing the different voltage levels, for minimizing the switching frequency and for employing each switching device equally, hence, avoiding asymmetrical wear and asymmetrical temperature distribution within the inverter.
* Fast dynamic response of a multilevel inverter can be achieved by switching “larger” voltage steps to the output. Due to the flexibility arising from the accessibility of different DC potentials, control schemes can be tailored depending on the application of the inverter [*J. S. Lai* 1996 and *F. Z. Peng* 1996].

Disadvantages of multilevel inverters can be summarized as:
* They require more devices than traditional inverters. The system cost may increase (part of the increased cost may be offset by the fact that switches with lower ratings are being used). Using more devices also means; the probability of a system failure will increase.
* The increased number of switches will result in more complicated control.
* They have narrow range of modulation indexes [*S. Sirisukprasert* 2002].

TRADITIONAL 3-LEVEL VOLTAGE SOURCE INVERTER:

Switch-mode dc-to-ac inverters used in ac power supplies and ac motor drives where the objective is to produce a sinusoidal AC output whose magnitude and frequency can both be controlled. Practically, we use an inverter in both single-phase and three-phase ac systems. A half-bridge is the simplest topology, which is used to produce a 2-level square-wave output waveform. The full-bridge topology is used to synthesize a 3-level square-wave output waveform. The 3-level full-bridge or H-bridge configuration of the single-phase voltage source inverter is shown in Fig. 1.

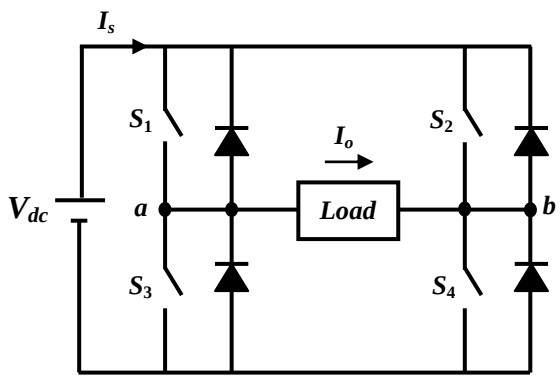

Fig. 1: H-bridge Inverter

The full bridge inverter can provide either Bipolar or Unipolar output voltage switching. The unipolar inverter is optimum for harmonic elimination more than the bipolar inverter. Therefore the unipolar scheme is the optimum technique [*K. S. Krikor* and *J. A. Mohammed* 2002] which is to be compared with the OHESW technique later. The unipolar inverter circuit consists of four main switches and four freewheeling diodes. According to four-switch combination, three output voltage levels, $+V_{dc}$, $-V_{dc}$, and 0, can be synthesized for the voltage across *a* and *b* [*J. M. Jacob* 2004]. Fig. 2 shows the unipolar waveform output from H-bridge inverter.

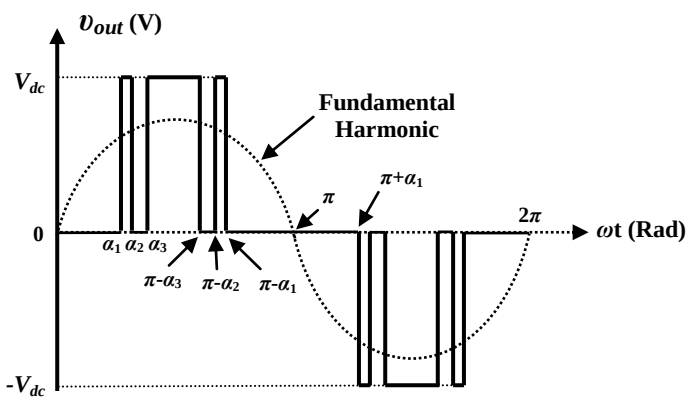

Fig. 2: Unipolar Switching Scheme

- SHEPWM TECHNIQUE:

The SHEPWM technique is currently used to synthesize an output waveform of both a half-bridge and a full-bridge inverter. In this paper, a 3-level SHEPWM generated by a full-bridge inverter is considered.

Since the advent of the family of new semiconductors, tremendous interest has been renewed in inverter technology. The ability of switching devices having turn-off times in the range of a few microseconds or sub microseconds has increased the flexibility of achieving a practically sinusoidal output by employing sophisticated switching patterns in inverter circuit. SHEPWM technique is introduced by *Patel* [*H. S. Patel* 1973]. The idea of such a method is that the basic square-wave output is “chopped” a number of times, which are obtained by proper off-line calculations.

- OPTIMIZED SHEPWM SWITCHING ANGLES:

The optimized unipolar output waveform shown in Fig. 2 is assumed to be the quarter-wave symmetric. *Patel* and *Hoft* [*H. S. Patel* 1973] presented the Fourier series of the 3-level SHEPWM as follows:

$$\upsilon_{out}(\omega t) = \sum_{n=1}^{\infty} \frac{4V_{dc}}{n\pi} \left[\sum_{k=1}^{\infty} (-1)^{(k-1)} \cos(n\alpha_k) \right] \sin(n\omega t) \tag{1}$$

where α_k is the optimized switching angles, which must satisfy the following condition: $0 \le \alpha_1 \le \alpha_2 \le ... \alpha_k \ldots \le \pi/2$. The amplitude of all odd harmonic components including fundamental one, are given by:

$$h_n = \frac{4V_{dc}}{n\pi} \sum_{k=1}^{\infty} (-1)^{(k-1)} \cos(n\alpha_k) \tag{2}$$

where n is the harmonic order. The amplitude of DC component and all even harmonics equal zero. Thus, only the odd harmonics in the quarter-wave symmetric waveform need to be eliminated. The switching angles of the waveform will be adjusted to get the lowest output voltage THD.

SOLVING SHEPWM EQUATIONS:

Eqs. 2 are nonlinear equations and transcendental in nature. As a result, many people have utilized numerical iterative techniques in order to solve these equations. For example, *Jian Sun* used the Newton-Raphson numerical technique [*J. Sun* 1992]. Another numerical technique one might use is Gauss-Seidel, although this particular numerical technique is not as robust as Newton-Raphson.
Unfortunately, numerical iterative techniques have their drawbacks:

1. These techniques require an initial guess in order to work. However, if the initial guess is not good enough, a solution will not be found.
2. They will only find one solution, if one exists.
3. They needed large time for calculation. This time increased with increasing the degree of freedom of the nonlinear equations.

The obvious drawback here is that more than one solution might exist to the problem at hand. Using the *fast recursive algorithm* derived in [*D. Czarkowski* 2002]; all solutions to these nonlinear equations can be found without the need for an initial guess.

MULTILEVEL VOLTAGE SOURCE INVERTER:

A multilevel inverter is a power electronic system that synthesizes a desired voltage output from several levels of DC voltages as input, typically obtained from capacitor voltage sources. The so-called "multilevel", starts from three levels. As the number of levels reach infinity, the output THD approaches zero. The number of the achievable voltage levels, however, is limited by voltage unbalance problems, voltage clamping requirement, circuit layout, and packaging constraints.
The multilevel voltage source inverter is recently applied in many industrial applications such as ac power supplies, static VAR compensators, drive systems, etc. One of the significant advantages of multilevel configuration is the harmonic reduction in the output waveform without increasing switching

frequency or decreasing the inverter power output [*J. S. Lai* 1996]. In this paper, three capacitor voltage synthesis-based multilevel inverters are introduced, i.e.

1. Diode-Clamped Multilevel Inverter.
2. Flying-Capacitor Multilevel Inverter.
3. Cascaded-Inverters with Separated DC Sources [*J. S. Lai* 1996 and *S. Sirisukparsert* 1999].

Implicitly, the multilevel inverter using cascaded-inverters requires the least number of components. Another advantage of cascaded-inverter is circuit layout flexibility. Modularized circuit layout and packaging is possible because each level has the same structure, and there are no extra clamping diodes or voltage balancing capacitor. The number of output voltage levels can be easily adjusted by adding or removing the full-bridge cells.

*** Cascaded H-bridges Multilevel Inverter:**

The cascaded H-bridges multilevel inverter is a relatively new inverter structure [*J. S. Lai* 1996, *T. Cunnyngham* 2001, and *S. M. Tenconi* 1995]. It is proposed here to solve all the above-mentioned problems of the multilevel inverters as well as conventional multi pulse inverters (or traditional PWM inverter). This new multilevel inverter eliminates the excessively large number of *i*) bulky transformers required by conventional multi pulse inverters, *ii*) clamping diodes required by multilevel diode-clamped inverters, and *iii*) flying capacitors required by multilevel flying-capacitor inverters [*F. Z. Peng* 1996].

A cascaded H-bridges multilevel inverter is simply a series connection of multiple H-bridge inverters. Each H-bridge inverter has the same configuration as a typical single-phase full-bridge inverter [*J. S. Lai* 1996 and *T. Cunnyngham* 2001].

The cascaded H-bridges multilevel inverter introduces the idea of using (Separate DC Sources) SDCSs to produce an AC voltage waveform. Each H-bridge inverter is connected to its own DC source V_{dc}. By cascading the AC outputs of each H-bridge inverter, an AC voltage waveform is produced. Fig. 3 provides an illustration of a single-phase cascaded H-bridges multilevel inverter using 3-SDCSs.

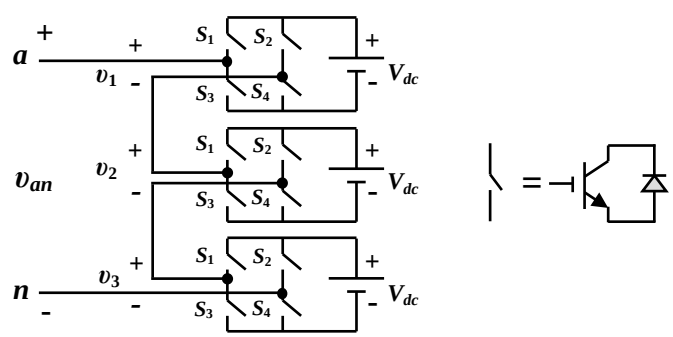

Fig. 3: Cascaded H-bridges Multilevel Inverter using 3-SDCSs

By closing the appropriate switches, each H-bridge inverter can produce three different voltages: $+V_{dc}$, 0 and $-V_{dc}$.

As mentioned earlier, each H-bridge inverter produces an AC voltage v_i, where *i* stands for one particular H-bridge inverter. Fig.3 contains three such H-bridges, one for each DC source. Therefore, to obtain the total AC voltage produced by the multilevel inverter, these three distinct AC voltages are added together.

Fig. 4 provides an illustration of these ideas, when the Multilevel Fundamental Switching (MFS) scheme is used. It also illustrates the idea of "levels" in a cascaded H-bridges multilevel inverter.
The smallest number of voltage levels for a multilevel inverter using cascaded inverter with SDCSs is three. To achieve a 3-level waveform, a single full-bridge inverter is employed.

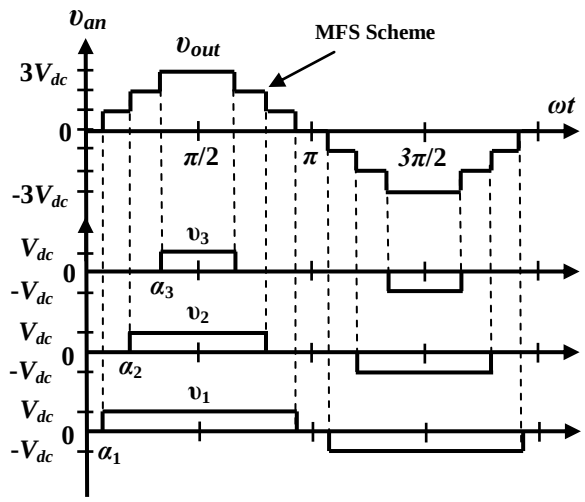

Fig. 4: Output Voltage of Cascaded H-bridges 7-level Inverter

In Fig. 4, one notices that three distinct DC sources (s = 3, where s is the number of DC sources) can produce a maximum of (l = 7 distinct levels) in the output phase voltage of the multilevel inverter. More generally, a cascaded H-bridges multilevel inverter using s-SDCSs can produce a maximum of $2s + 1$ distinct levels l in the output phase voltage [*P. M. Bhagwat* 1983].

OHESW TECHNIQUE:

Among modulation techniques being used these days, OHESW technique is very suitable for multilevel inverter topologies, and low THD output waveform without using any filter circuit is possible.

Basically, the concept of the OHESW technique is to combine the idea of the SHEPWM presented by Patel *et al* [*H. S. Patel* 1973] with the quarter-wave symmetric idea concept presented by Stefano Vic *et al* [*P. M. Bhagwat* 1983]. The concept of the harmonic reduction is presented here to eliminate the specific harmonics, which are the lowest orders.
The proposed technique is to synthesize waveform by the multilevel inverter using cascaded inverter with SDCSs, which was presented in Section A.

OPTIMIZED HARMONIC ELIMINATION SWITCHING ANGLES:

The OHESW is assumed to be the quarter-wave symmetric. Fourier series of the quarter-wave symmetric s H-bridge cell multilevel waveform is written as follows:

$$\upsilon_{out}(\omega t) = \upsilon_{an} = \sum_{n=1}^{\infty} \frac{4V_{dc}}{n\pi}\left[\sum_{k=1}^{s}\cos(n\alpha_k)\right]\sin(n\omega t) \tag{3}$$

where α_k is the optimized switching angles, which must satisfy the following condition: $\alpha_1 < \alpha_2 < ... < \alpha_s < \pi/2$. The amplitude of all odd harmonic components including fundamental one, are given by:

$$h_n = \frac{4V_{dc}}{n\pi} \sum_{k=1}^{s} \cos(n\alpha_k) \tag{4}$$

where n is the harmonic order. The amplitude of DC component and all even harmonics equal zero. Thus, only the odd harmonics in the quarter-wave symmetric multilevel waveform need to be eliminated. The switching angles of the waveform will be adjusted to get the lowest output voltage THD.

SOLVING OF OHESW EQUATIONS:

When the MFS scheme shown in Fig. 4 is implemented using s switching angles, Eq. 4 can be used to derive s different harmonic equations. In other words, s switching angles will be used to control the values of s different harmonics.

Unfortunately, these harmonic equations are transcendental equations, making them difficult to solve without making use of some sort of numerical iterative technique, such as Newton-Raphson.

Until recently, numerical iterative techniques seemed to be the only viable method to solve the aforementioned nonlinear harmonic equations [*P. N. Enjeti* 1990, *H. S. Patel* 1973, and *J. Sun* 1992]. Using Resultant method presented in [*K. S. Krikor* and *J. A. Mohammed* 2007], all solutions (if they exist) to the nonlinear equations can be found without the need for an initial guess. However, by making some simple changes of variables and simplifying, these transcendental equations can be transformed into a set of polynomial equations [*K. S. Krikor* and *J. A. Mohammed* 2007].

RESULTS AND DISCUSSION:

The object of this paper is to design a computer MATLAB program to make comparison between the traditional 3-level inverter with SHEPWM technique and multilevel inverter with OHESW technique, to assist the optimum design calculation, and to get some results such as switching angles (α) necessary for studying the optimum technique.

In the case of SHEPWM scheme, computation was done as the modulation index m increased between (0 and 1) and for K= (2-17) (K is the number switching angles per quarter cycle). The instantaneous SHEPWM, 3-level output voltage waveforms at minimized THD (THDmin) and for K=3 and 17, are shown in Fig. 5. A SHEPWM waveform consists of a series of positive and negative pulses of constant amplitude but with variable switching instants. For example, for K=3, the 3rd and 5th harmonics will be eliminated from the output voltage waveform. Increasing K causes increasing the number of odd harmonics to be eliminated.

In the case of OHESW scheme, computation was done as m increased between (0 and s) and for number of voltages levels l = (5-15). Fig. 6 shows the instantaneous output voltage OHESW for two values of voltage levels (l = 7 and 15) and with THDmin. If the number of l is higher, a near-sinusoidal staircase voltage can be generated with only fundamental frequency switching.

The optimization technique has been used to minimize the harmonics content of the inverter output voltage. The best compromise between efficiency and quality of the inverter operation is achieved by the optimal switching pattern technique [*K. S. Krikor* and *J. A. Mohammed* 2002].

The behavior of the motor drive is explained by the simulation program. By using the equivalent circuit of the motor and the corresponding performance equations, it can be easy to analyze the performance of the motor operated on an inverter under the proposed two techniques.

Fig. 7 illustrates the comparison of the proposed motor drive performance under the SHEPWM and OHESW techniques to get the optimum one. From the figure, it can be seen that the THD, switching losses Psw_{min}, additional motor power losses $\Sigma Padd_{min}$, and additional motor pulsating torque $Tpulsadd_{min}$, motor current I_{rmin} and motor input power Pin_{min} versus K are less with OHESW technique than that with SHEPWM technique. On the other hand, the optimum technique should maximize the motor power factor Pf_{max} and efficiency η_{max} for same K. These factors for OHESW scheme seem to be higher than with SHEPWM scheme.

THD curve shows that THDmin increases with K for SHEPWM technique while it decreases with K in the case of OHESW technique. On the other hand THDmax decreases with K in the two techniques [See also Table 1]. It can be seen from the figure, that the motor performance with OHESW technique is approximately constant with K or $s > 3$ ($l > 7$), and converges form that motor performance which excited from pure sinusoidal excitation while, it does not converges to that performance with increasing K, in the case of SHEPWM technique [See also Table 2]. Therefore the cascade multilevel with 7-level is suitable to get good performance of the proposed motor with less cost [All the motor parameters are listed in Table 3 in the Appendix].

From the simulation results, THDmin of the 15-level, or 7-switching ($s = K = 7$), OHESW waveform is 6.4554 % with modulation index $m_a = m/s = 0.7036$ [See Table 1], when each power switch is switching one time per cycle (50Hz) for single-phase cascade multilevel inverter, which may can meets the 5% of IEEE standard for the three-phase multilevel inverter without any filter circuits. On the other hand, THDmin of the 7-switching, SHEPWM waveform is 49.1002 %, with m_a=0.79, (which does not decrease with increasing K like OHESW does) and each power switch is switching 28 times per cycle (1.4 kHz). As a result THD in OHESW decreased by 86.85 % and the switching losses decreases 28 times with respect to SHEPWM waveform. It can also be seen that for the same output power $Pout_{min}$, the inverter under the OHESW control exhibits less switching losses than that under SHEPWM control, for example; with $Pout_{min}$= 175.1732Watt, the multilevel inverter needs 3-switching angles per quarter cycle ($K = s = 3$) while traditional 3-level inverter needs approximately 9-switching ($K = 9$).

As a result, the waveform under OHESW control for multilevel inverter is apparently closer to a sinusoidal waveform and has less harmonic content, less switching losses, reduced voltage stress on each power device, as a result, higher quality power and higher efficiency than the waveform under SHEPWM control for traditional 3-level inverter. Therefore, multilevel inverter is better than the traditional 3-level PWM inverter of improving waveform quality.

CONCLUSIONS:

The multilevel inverter topology can overcome some of the limitations of the standard 2-level or 3-level inverter. Output voltage and power increase with number of inverter levels.

Harmonics decrease as the number of levels increase. In addition, increasing multilevel output voltage does not require an increase in voltage rating of individual force commutated devices.

In OHESW multilevel inverter, not only does the line voltage THD decrease, but also the lowest exist harmonics is shifted to higher frequency. This, size of a filter circuit applied in OHESW inverter can be decreased dramatically.

Traditional Pulse Width Modulation (PWM) methods employ switching frequencies on the order of several kHz, while Multilevel Fundamental Switching (MFS) scheme employs 50Hz. Therefore, this scheme will lead to minimum switch conduction losses comparable to typical PWM schemes. However,

switching losses increase as the switching frequency increases. As a result, it is desirable to make the switching frequency as low as possible.

The comparative results show that the OHESW technique for multilevel inverter is the optimum technique for improving the quality of the motor drive. Therefore, the best compromise between efficiency and quality of operation is achieved by the multilevel inverter.

REFERENCES:

D. Czarkowski, D. V. Chudnovsky, G. V. Chudnovsky, and *I. W. Selesnick*, "**Solving the Optimal PWM Problem for Single-Phase Inverters**," IEEE Trans. on Circuits and Sys., vol. 49, no.4, pp. 465-475, April 2002.

F. Z. Peng, J. S. Lai, J. W. McKeever, and *J. VanCoevering*, "**A Multilevel Voltage-Source Inverter with Separate DC Sources for Static Var Generation**," IEEE Trans. Industry Applications, vol. 32, no. 5, Sept. / Oct. 1996, pp. 1130-1138.

H. S. Patel and *R. G. Hoft*, "**Generalized harmonic elimination and voltage control in thyristor converters: Part I –harmonic elimination**," IEEE Transactions on Ind. Applicat., vol. 9, pp. 310-317, May/June 1973.

J. M. Erdman, R. J. Kerkman, D. W. Schlegel, and *G. L. Skibinski*, "**Effect of PWM Inverters on AC Motor Bearing Currents and Shaft Voltages**," IEEE Trans. on Ind. Appl., vol. 32, no. 2, March/April 1996.

J. M. Jacob, **Power Electronics: Principles & Applications**, 2nd Edition, Vikas Publishing House Pvt. Ltd., Singapore, 2004.

José Rodriguez, Jih-Sheng Lai, and *F. Z. peng*, "**Multilevel Converters: A Survey of Topologies, Controls and Applications**," IEEE Trans. on Ind. Electronics, vol. 49, no. 4, pp. 724-738, August 2002.

J. S. Lai and *F. Z. Peng*, "**Multilevel Converters-a New Breed of Power Converters**," IEEE Trans. Ind. Applicat., vol. 32, pp. 509–517, May/June 1996.

J. Sun, H. Grotstollen, "**Solving Nonlinear Equations for Selective Harmonic Eliminated PWM Using Predicted Initial Values**," in Proc. IECON 1992, pp. 259-264.

K. S. Krikor and *Jamal A. Mohammed*, "**Optimum Design of Single-Phase Multilevel Inverter Using OHESW Technique**", to be published, Engineering & Technology, 2008.

K. S. Krikor and *Jamal A. Mohammed*, "**PWM Strategies for Inverter-Fed Induction Motors - A Comparative Study**," University of Technology, vol. 21, no. 11, 2002.

Markku Jokinen and *Anssi Lipsanen*, "**Fundamental Study of 2-level and 3-level Frequency Converters**", SMØLA, Norway. Assignment on Converter Losses, Multilevel Converter Topologies, Lappeenranta University of technology, Finland, 2005.

P. M. Bhagwat and *V. R. Stefanovic*, "**Generalized Structure of a Multilevel PWM Inverter**," IEEE Trans. on Ind. Applicat., vol. IA-19, no. 6 Nov./Dec., 1983, pp.1057-1069.

P. N. Enjeti, P. D. Ziogas, and *J. F. Lindsay*, "**Programmed PWM Techniques to Eliminate Harmonics: A Critical Evaluation**," IEEE Trans. Ind. Applicat., vol. 26, pp. 302-316, Mar./Apr. 1990.

S. Laurentiu, B. de Fornel, M. Fadel and *F. Jadot*, "**On the Acoustic Noise Radiated by PWM AC Motor Drives**", EPE-PEMC 2002 Dubrovnik & Cavtat.

S. M. Tenconi, M. Carpita, C. Bacigalupo and *R. Call*, "**Multilevel Voltage Source Converters for Medium Voltage Adjustable Speed Drives**," IEEE, Proceedings on Indus. Electronics, vol. 1, Jul, 1995, pp. 91-98.

S. Sirisukprasert, J. S. Lai, and *T. H. Liu*, "**Optimum Harmonic Reduction with a Wide Range of Modulation Indexes for Multilevel Converters**," IEEE Trans. on Industrial Electronics, vol. 49, Issue: 4, Aug. 2002, pp. 875 – 881.

S. Sirisukparsert, "**Optimized Harmonic Stepped-Waveform for Multilevel Inverter**," M.Sc. Thesis, Blacksburg, Virginia University, Sep. 1999.

T. Cunnyngham, "**Cascade Multilevel Inverters for Large Hybrid-Electric Vehicle applications with variant DC sources**," M.Sc. Thesis, University of Tennessee, Knoxville, May 2001.

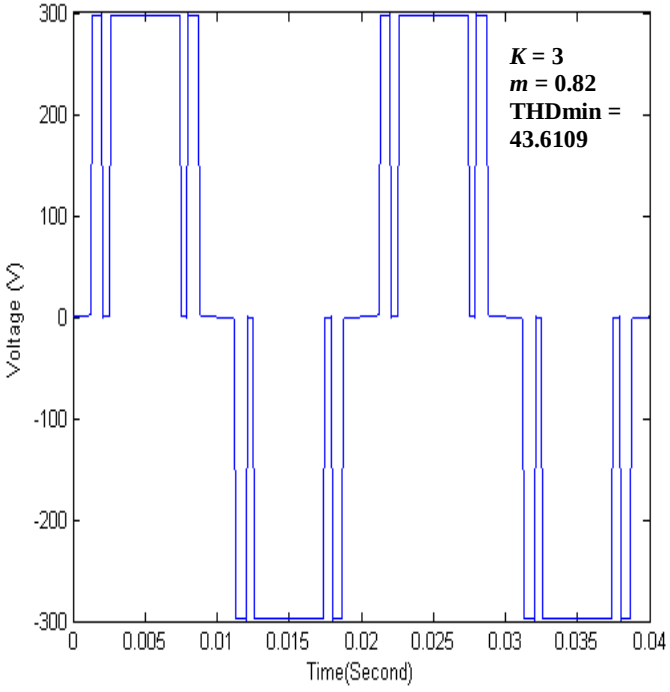

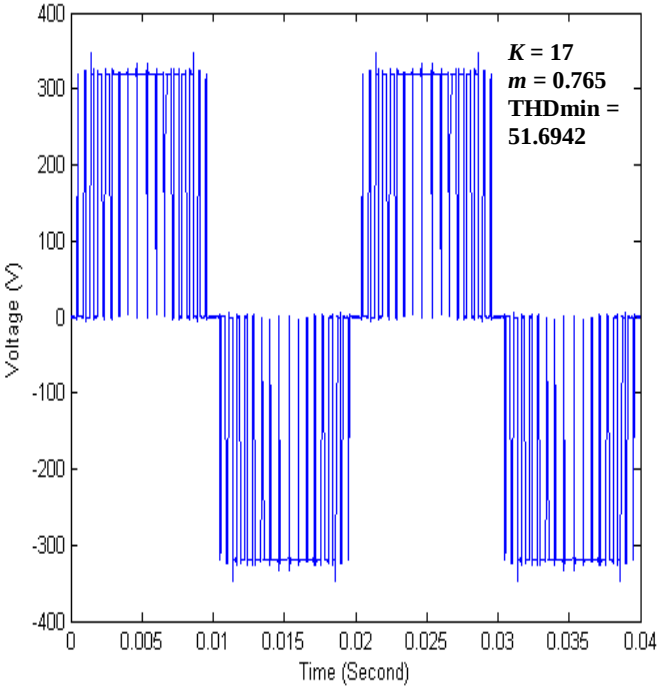

Fig. 5: the Instantinuos Voltage of SHEPWM 3-Level Inverter at THDmin with Different No. of Switching Angles (*K*)

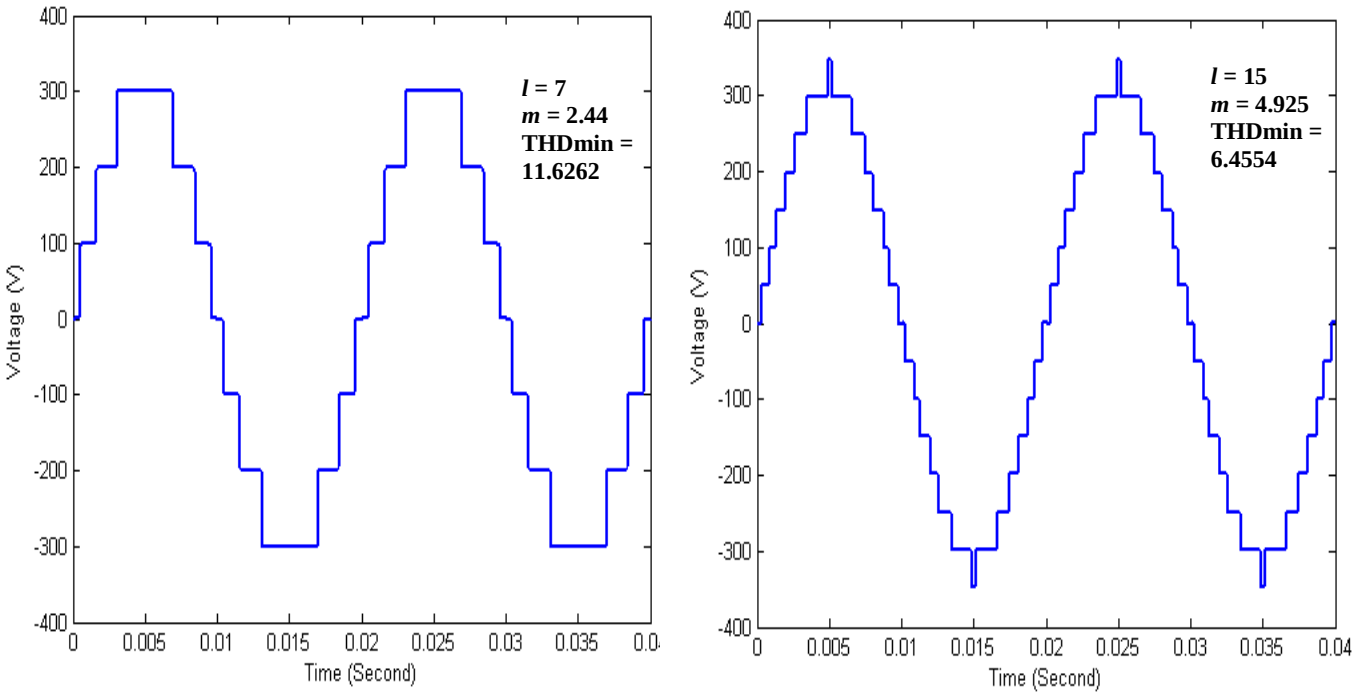

Fig. 6: The Instantaneous Voltage of OHESW Multilevel Inverter at THDmin with Different Voltage Levels (*l*)

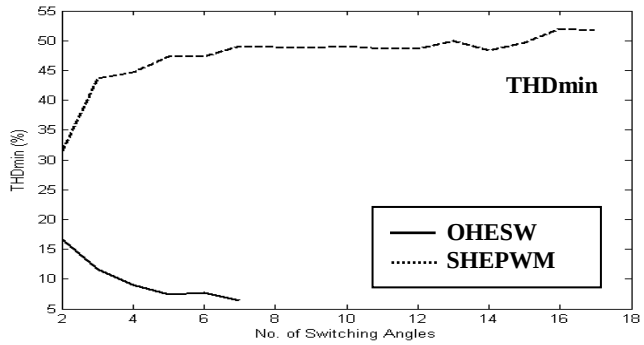
THDmin
OHESW
SHEPWM
THDmin (%)
No. of Switching Angles

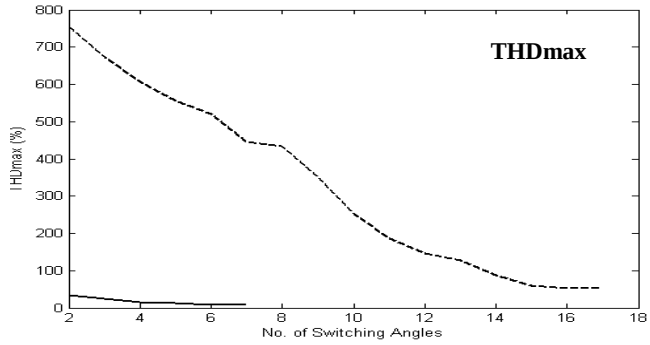
THDmax
THDmax (%)
No. of Switching Angles

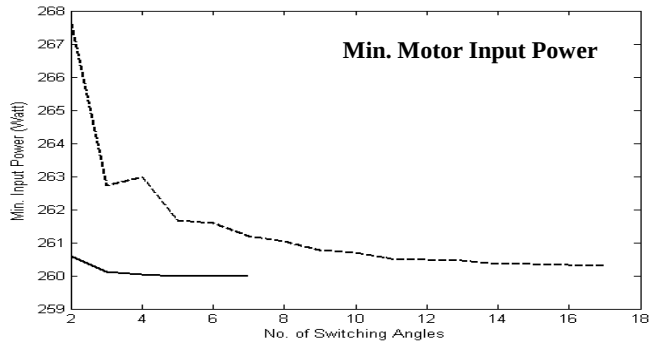
Min. Motor Input Power
Min. Input Power (Watt)
No. of Switching Angles

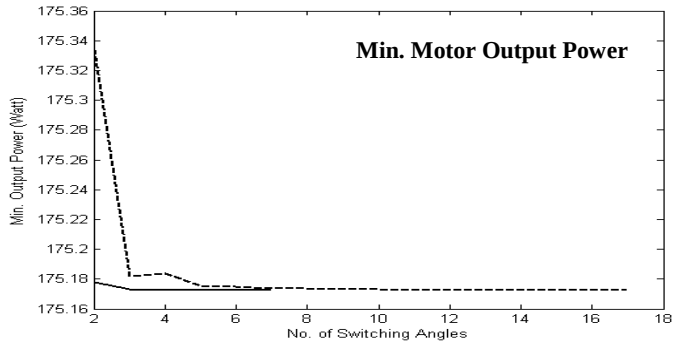
Min. Motor Output Power
Min. Output Power (Watt)
No. of Switching Angles

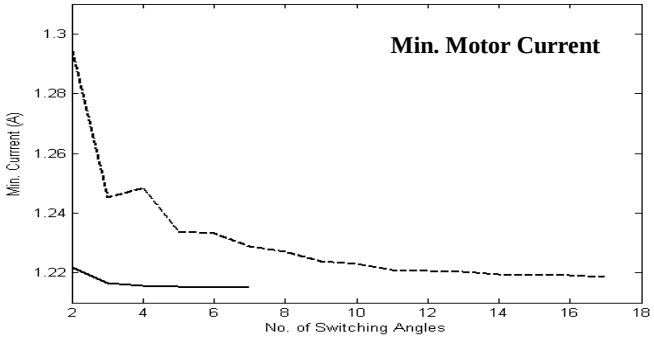
Min. Motor Current
Min. Current (A)
No. of Switching Angles

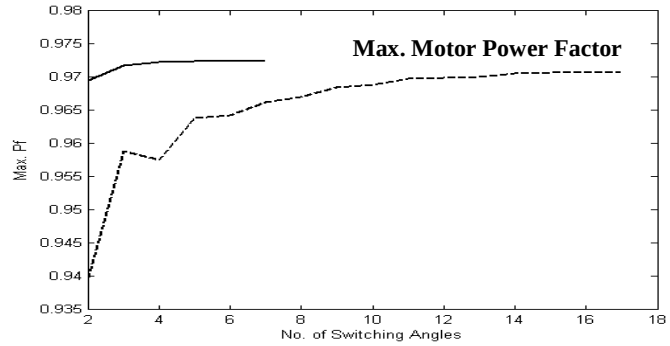
Max. Motor Power Factor
Max. Pf
No. of Switching Angles

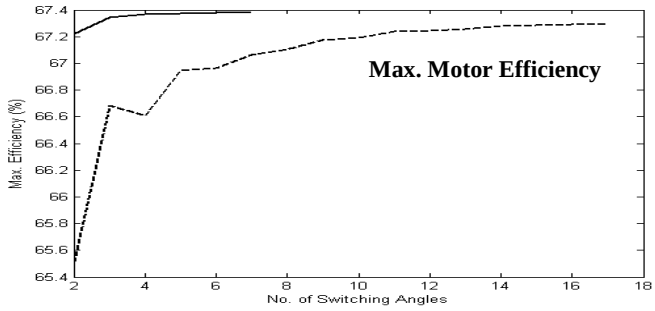
Max. Motor Efficiency
Max. Efficiency (%)
No. of Switching Angles

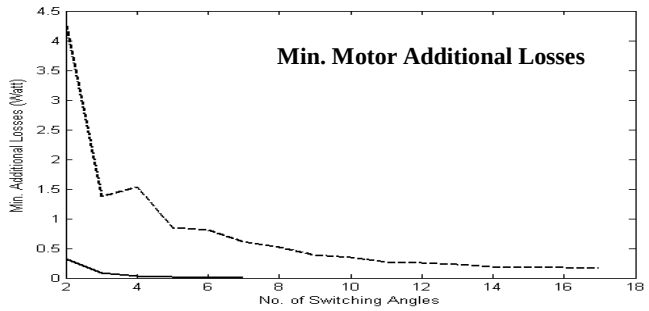
Min. Motor Additional Losses
Min. Additional Losses (Watt)
No. of Switching Angles

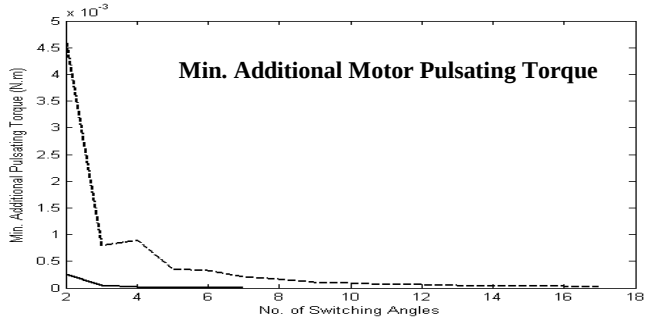
Min. Additional Motor Pulsating Torque
Min. Additional Pulsating Torque (N.m)
x 10^-3
No. of Switching Angles

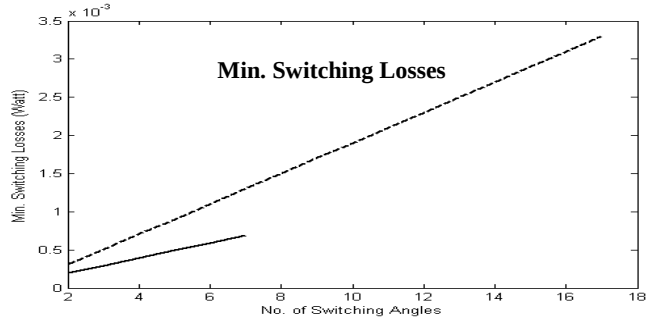
Min. Switching Losses
Min. Switching Losses (Watt)
x 10^-3
No. of Switching Angles

Fig. 7: Comparison of Performance between Motor Drive Multilevel Inverter and Traditional 3-level Inverter with Different *K*

APPENDIX

Table 1: the Optimum Performance of the Motor Drive Fed by OHESW Multilevel Inverter

No. of Levels *l*	5	7	9	11	13	15
m	1.67	2.44	3.22	4	4.15	4.925
THD_{min} (%)	16.5924	11.6262	8.9907	7.3873	7.6396	6.4554
THD_{max} (%)	32.9620	24.8098	14.6081	12.1832	9.1754	7.5029
I_{rmin} (A)	1.2218	1.2167	1.2156	1.2153	1.2152	1.2150
$\Sigma Padd_{min}$ (W)	0.328	0.08	0.0322	0.0169	0.0122	0.0071
Pin_{min} (W)	260.5941	260.1219	260.0283	259.9978	259.9887	259.9784
$Pout_{min}$ (W)	175.1772	175.1732	175.1726	175.1725	175.1725	175.1725
η_{max} (%)	67.2225	67.3427	67.3668	67.3746	67.377	67.3796
Pf_{max}	0.9695	0.9718	0.9723	0.9725	0.9725	0.9726
$Tpulsadd_{min}$(N.m)	2.5464e-4	4.8729e-5	1.6782e-5	7.7663e-6	4.3794e-6	2.3517e-6
Psw_{min}* e-4 (W)	1.9784	2.955	3.9366	4.9194	5.9028	6.8859

Table 2: The Optimum Performance of the Motor Drive Fed by SHEPWM Traditional 3-level Inverter

Switching No. (*K*)	2	3	4	5	6	7	8	9
m	0.86	0.82	0.81	0.8	0.8	0.79	0.79	0.79
THD_{min} (%)	31.5599	43.6109	44.6251	47.2747	47.3379	49.1002	48.9801	48.803
THD_{max} (%)	754.8863	671.5544	607.9097	555.3122	521.5931	446.6963	433.3106	352.5778
I_{rmin} (A)	1.2943	1.2453	1.2484	1.2339	1.2331	1.2288	1.227	1.2239
$\Sigma Padd_{min}$(W)	4.2568	1.3808	1.5275	0.8425	0.8029	0.6061	0.5254	0.3889
Pin_{min} (W)	267.6173	262.7127	262.9976	261.6739	261.596	261.2057	261.0438	260.7677
$Pout_{min}$ (W)	175.3341	175.1819	175.1836	175.1754	175.1751	175.1739	175.1735	175.1730
η_{max} (%)	65.5167	66.6819	66.6103	66.9442	66.964	67.0636	67.105	67.1759
Pf_{max}	0.9398	0.9589	0.9576	0.9639	0.9643	0.9663	0.9671	0.9685
$Tpulsadd_{min}$ (N.m)* e-4	46	7.925	9.024	3.6273	3.3608	2.1619	1.741	1.1174
Psw_{min} (W)	3.1437e-4	5.0410e4	7.0749e4	8.991e-4	0.0011	0.0013	0.0015	0.0017

Con. Table 2

Switching No. (*K*)	10	11	12	13	14	15	16	17
m	0.79	0.79	0.79	0.78	0.79	0.78	0.765	0.765
THD_{min} (%)	49.0488	48.7001	48.6333	50.0234	48.3048	49.6866	51.9878	51.6942
THD_{max} (%)	251.9755	185.042	146.6671	128.137	88.6293	59.0839	51.9878	51.6942
I_{rmin} (A)	1.2231	1.221	1.2208	1.2204	1.2194	1.2191	1.2191	1.2186
ΣP_{addmin}(W)	0.3521	0.2638	0.2532	0.2361	0.1909	0.1814	0.1784	0.1586
Pin_{min} (W)	260.6928	260.5125	260.4908	260.4559	260.3626	260.3431	260.3373	260.2961
$Pout_{min}$ (W)	175.1729	175.1727	175.1727	175.1727	175.1726	175.1726	175.1726	175.1725
η_{max} (%)	67.1952	67.2416	67.2472	67.2562	67.2802	67.2853	67.29	67.3
Pf_{max}	0.9689	0.9698	0.9699	0.9701	0.9706	0.9707	0.9707	0.9709
$Tpulsadd_{min}$* e-4 (N.m)	0.96199	0.62763	0.58992	0.51879	0.38868	0.3519	0.33021	0.27785
Psw_{min} (W)	0.0019	0.0021	0.0023	0.0025	0.0027	0.0029	0.0031	0.0033

Table 3: Parameters and Specifications of the Proposed Motor

Turn ratio	a_s	1.066	
Number of pole pair	P	2	
Main winding resistance	R_{1m}	33.5	Ω
Main winding leakage reactance	X_{1m}	27	Ω
Auxiliary winding resistance	R_{1a}	34.5	Ω
Auxiliary winding leakage reactance	X_{1a}	28	Ω
Rotor resistance	R_2	20	Ω
Rotor leakage reactance	X_2	12.5	Ω
Magnetization reactance	X_m	173	Ω
Rated supply voltage	V_1	220	V
Rated current	I	1.215	A
Total Power losses	ΣP	85	W
Output power	P_2	175	W
Efficiency	η	67.38	%
Power factor	P_f	0.9726	
Rated speed	N_r	1275	Rpm
Capacitance	C	6	μF

COMPUTER AIDED DESIGN AND IMPLEMENTATION OF CONVERTER CIRCUITS APPLIED FOR PHOTOVOLTAIC SYSTEM

Z. M. Kubba, *K. AL-shara and E. AL-Shakarchi

Physics dep. AL-Nahrain Univ, Iraq

*** Elec.& comm. Dep., Baghdad Univ.,Iraq**

ABSTRACT

This research intents to design and laboratory implementation of a power electronic converter, which is useful for home applications, industrial, communications, street light and water pumping using solar cell source. The design is based on a step up boost DC/DC converter followed by a full wave SPWM inverter. The nominal power rating is 1.25kW and can operate from any DC source such as DC battery besides fuel cells. The system which consists of the following stages (PV, converter, inverter, DC link, filter and snubber circuit), is designed primarily with a general module depending on Orcad PSPICE program to produce power output nearly 1.25kVA at 50Hz with a pure sinewave output for both voltage and current. After designing and simulating this system, the intended SPWM inverter are built experimentally to compare its results with the simulated one.

INTRODUCTION

The design of a photovoltaic (PV) system is generally addressed to the best matching between the energy supplied to the system by the sun, and the energy required by the load that is to be fed by the system. The ”best matching” can be searched in terms of minimum cost, best efficiency, reliability or a compromise between these constraints. Historically, photovoltaic systems have been used as powers supply only for special loads such as communication satellites. The continuous advances in the area of

semiconductor materials led to the development of commercial PV cells with competitive cost, as compared with conventional generating systems. As a result, PV cells are now prominent as an alternative energy source [1]. This paper presents the design and laboratory implementation of a power electronics converter. The converter is made up of a dc-dc step up boost structure and a voltage source inverter (VSI) with optimized sinusoidal pulse width modulation

(PWM) strategy. The converter uses MOSFET as power switches because it is the available device. The full bridge inverter configuration is frequently employed, wherein the power semiconductor switches can be controlled by a variety of PWM techniques (Boost and Ziogas), SPWM control strategies involving either unipolar or bipolar (Mohan) switching are quite common since the harmonics significant amplitude are pushed into the high frequency range near the carrier frequency [2].

The proposed system

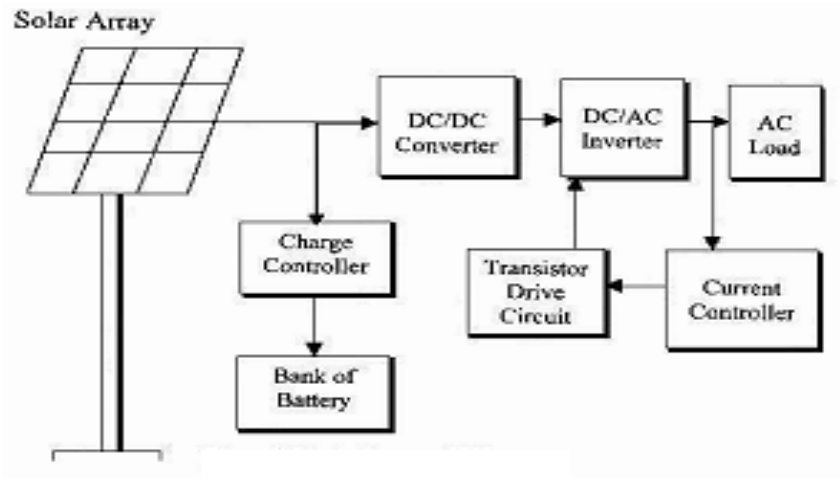

Figure 1: Block diagram of the PV system

Practical photovoltaic solar system designed with a power of 2kW is shown in fig.1. The analysis of the complete design circuit was carried out by using the PSPICE software. The PV arrays are current source so it is necessary to include a link capacitor between the array and the DC/AC inverter to obtain a voltage source in the input of the last one [3]. The step up boost converter operates in the continuous conduction mode. It has been designed for output voltage of 320V, switching frequency 2.5kHz, duty cycle .4 and 1.5kW. Figure 2 shows the boost stage as represented in PSPICE. Op1 and Op2 generate PWM as drive signal to the switching device (MOSFET – IRFP460).

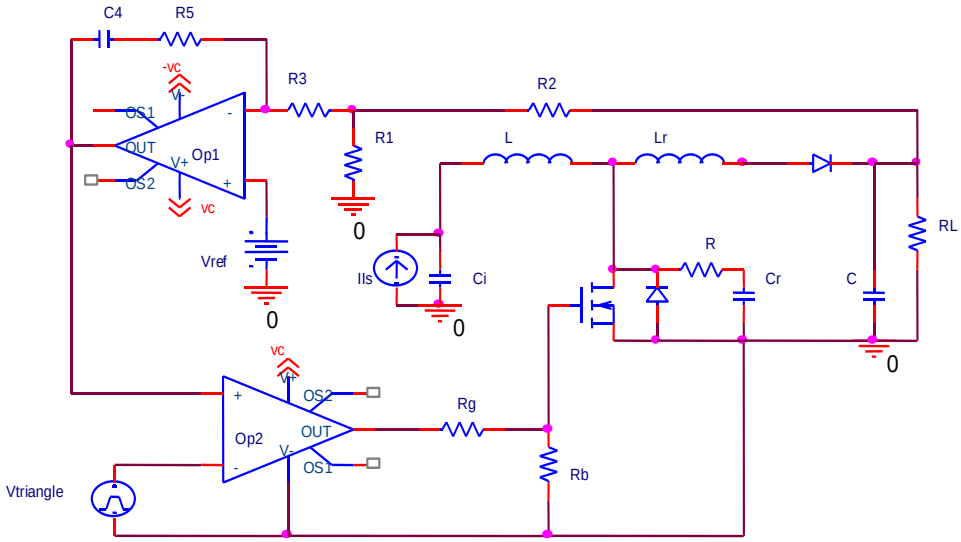

Figure 2: step-up Boost converter as represented in PSPICE

The output capacitor C for a boost stage is generally selected to limit the output ripple voltage to the required level by the specification. Its value was calculated according to the following formula [4]:

$$C \geq \frac{I_O(\max) \times D_{\max}}{f_S \times \Delta V_O} \quad (1)$$

Where:

I_o (max) is the maximum output current

D_{max} is the maximum duty cycle

The minimum value of inductor to maintain continuous conduction mode can be determined by the bellow formula [4]:

$$L_{\min} \geq \frac{Vo\ T_s}{16\ I_{o(crit)}} \quad (2)$$

$I_{o(crit)}$: the minimum output current to maintain continuous conduction mode. The complete structure of the full bridge inverter represented by PSPICE is shown in fig.3 where MOSFET (IRFP460) used as switching device and BYT30P-400 as free wheel diode, C_1, C_2, C_3 and C_4 are the resonant capacitors and act as snubbers circuit for the switches during turn off and limit the

across the switches[5]. dv/dt

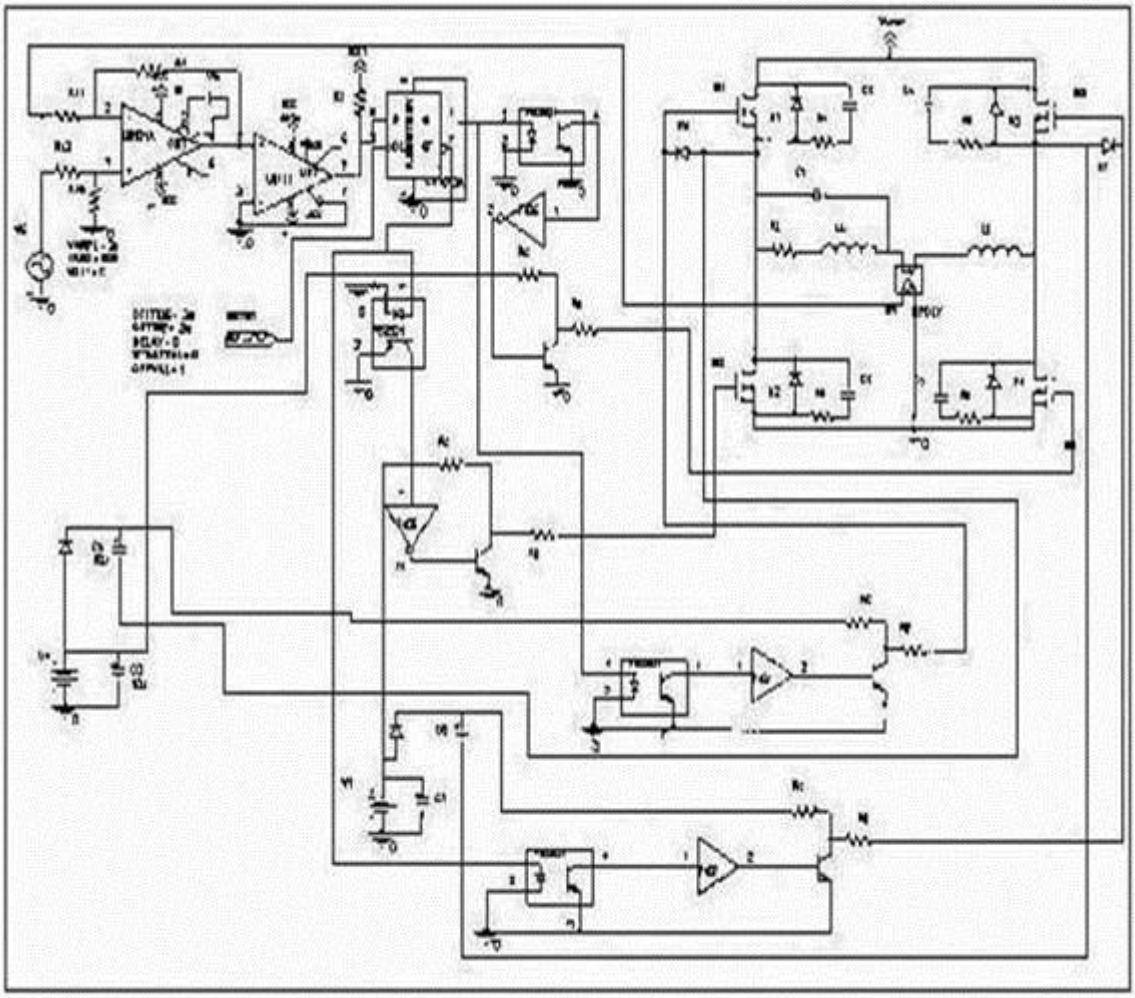

Figure 3: Full bridge SPWM inverter as represented by PSPICE

Other important parameter to consider for the power circuit design is the value of the output inductor L. The chosen value of this inductor must be a compromise between the maximum current rate at the converter output and low current ripple of the same signal. The maximum current rate happens when the sinusoidal waveform assumes a

null value. In this condition, the inductance value is determined by the input source as explained by equation (4). [6]

$$\left.\frac{di_o}{dt}\right|_{t=0} = 2\sqrt{2}\,\pi\, f_o\, I_{orms} \tag{3}$$

$$L_{\max} = E\,\frac{dt}{di_o} \tag{4}$$

This theoretical value of the inductance was chosen for an input voltage source of E=320V, f_o = 50Hz and I_{orms} = 3A. A slightly lower inductance value is adopted in the project. The results were as follows:

$$\left.\frac{di_o}{dt}\right|_{t=0} = 1332.18 A/s \text{ and } L_{adopted} = 200mH$$

If a rear sinusoidal (AC) is required, a low pass filter (consisting of L and C) is connected at the inverter output terminals in order to minimize the harmonic distortion of the load voltage.[2]

The output PWM that is obtained by comparing the output current with a reference signal the difference than it is sampled by a sampling frequency. Signal is applied to the drive circuit through an opto-coupler, which acts as isolation stage between the PWM generator and power stage. The output of the opto-coupler is applied to a buffer stage IC (7406, 7407) that feeds the bases of the transistor with appropriate signal required to drive it. The transistor supplied pulse of sufficient voltages, and drove current to the gate of the switching device (MOSFET) through a resistance R_g.

H-Bridge configuration has another unique requirement, that is the upper (power switch's) emitter is not at the ground potential, but is floating, making it necessary to employ Boot-Strapping technique to drive the power switch[7]. The complete PV system (converter and inverter circuit) with PWM and gate drive circuit is shown in fig.4.

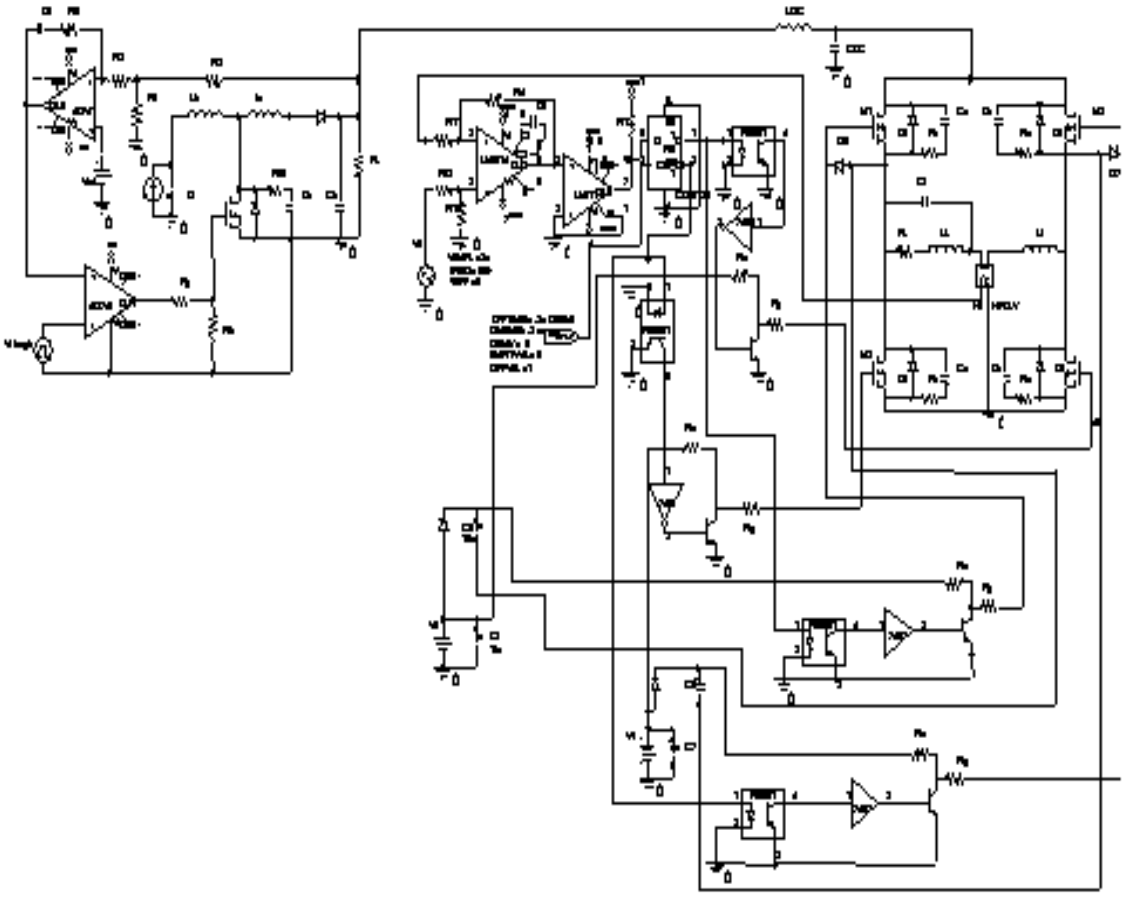

Figure 4: PV system as represented in PSPICE

RESULTS AND DISCUSSION

The PWM was implemented through experimental prototype. The parameters previously determined were used in the inverter at the sampling frequency f_c=2.5khz and output frequency f_o=50Hz. The circuit used is shown in fig.5. The pulse widths

and timing are defined using a program (supported to EPROM I.C 2716) that determines pulse requirements.

By generating a drive clock using programmable crystal oscillator (PXO600), a clock of frequency 30kHz is generated. The clock is applied to 12 bit binary counter. The outputs of the counter represent the addresses of the EPROM. The inverter performance was verified to an output active power of P_o = 1.25kVA

.

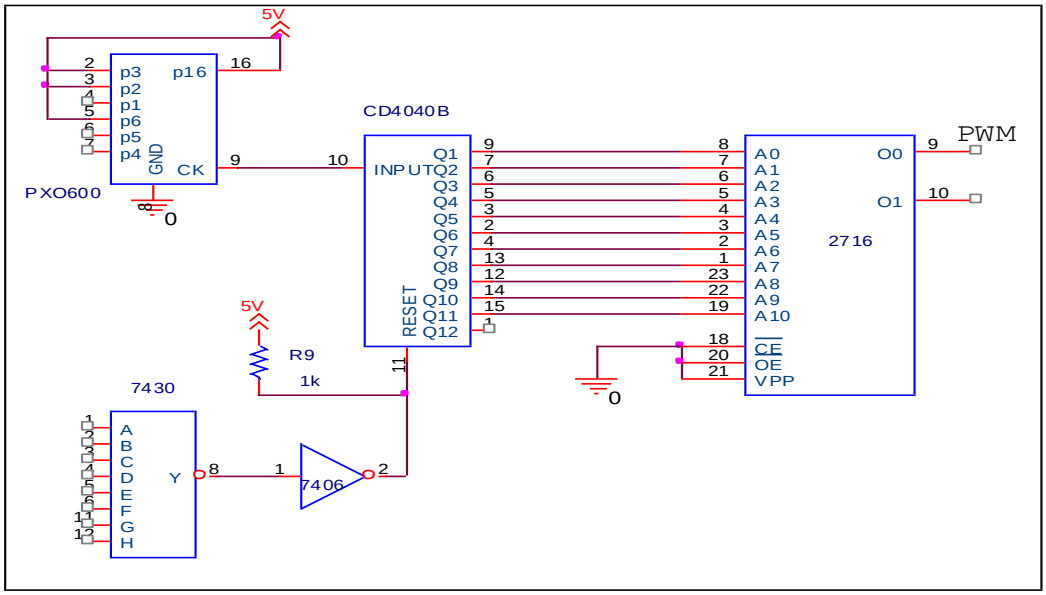

Figure 5: Pulse width modulation circuit that is used experimentally

Some experimental results are shown to demonstrate the performance of the system. Figure (6) depicts the signal at the gate of MOSFET (M_3) and MOSFET (M_4) which are shown in fig.(3). This figure explains the PWM signal, which is similar to that obtained in PSPICE simulation in number of pulses and pulse width.

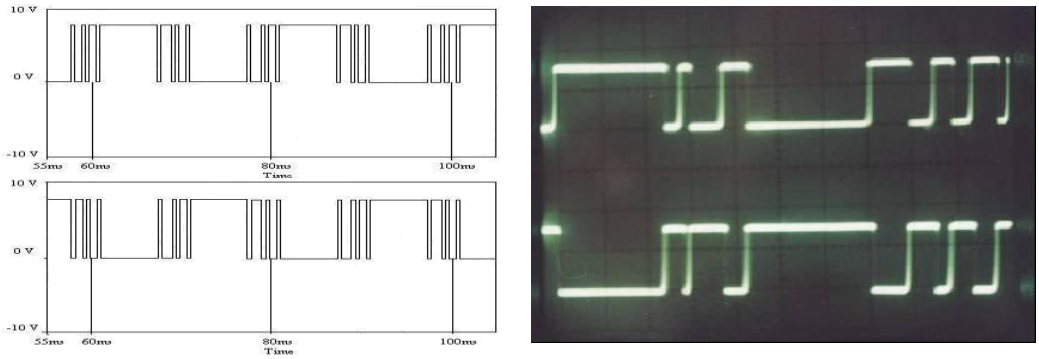

Figure 6: PWM signal from PSPICE and experimentally

Figure (7) represents the sinusoidal output current. This current have amplitude 2*2V/div divided by 1.Ω. Therefore, the rms value is equal to 3A. The scale of the time base is 5ms/div.

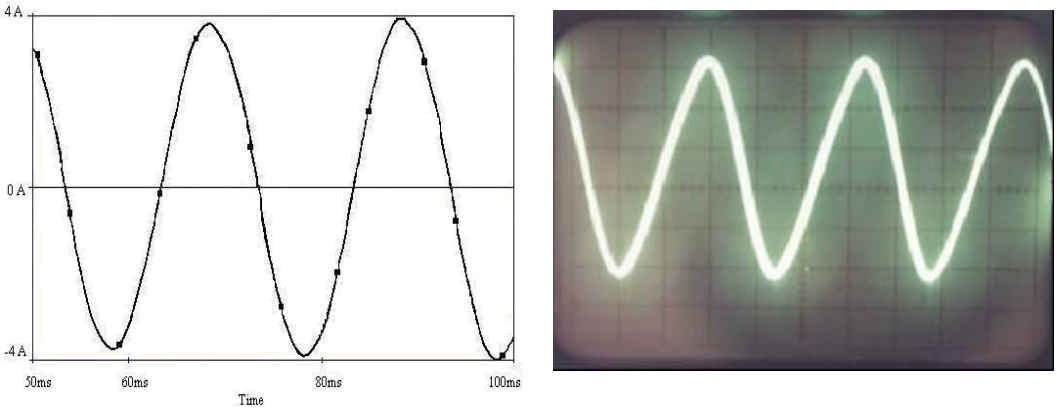

Figure 7: Output current from PSPICE and experimentally

Figure (8) shows the sinusoidal output voltage of amplitude 310V and the time base of this signal is 5ms/div. Also this signal is similar to that obtained in PSPICE.

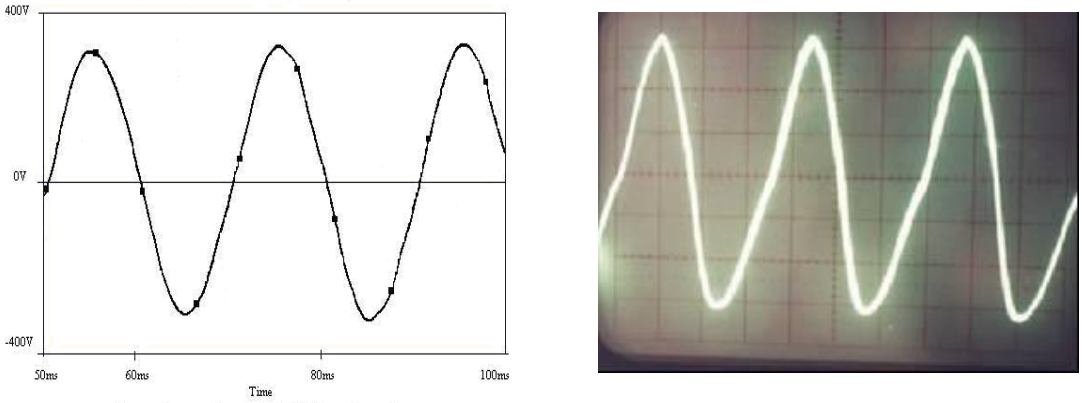

Figure 8: Output voltage from PSPICE and experimentally

In order to see the behavior of the output voltage against the frequency, fig.9 shows the maximum voltage appeared at 50 Hz. The behavior of the output current against the frequency is shown in fig.10. The peak at 50Hz has a value of about 3A; peaks at 150Hz, 250Hz and 350Hz (the 3rd 5th and 7th harmonic) have a value of about 80mA, 30mA, 25mA that is 2.6%, 1%, 0.8% of the fundamental harmonic.

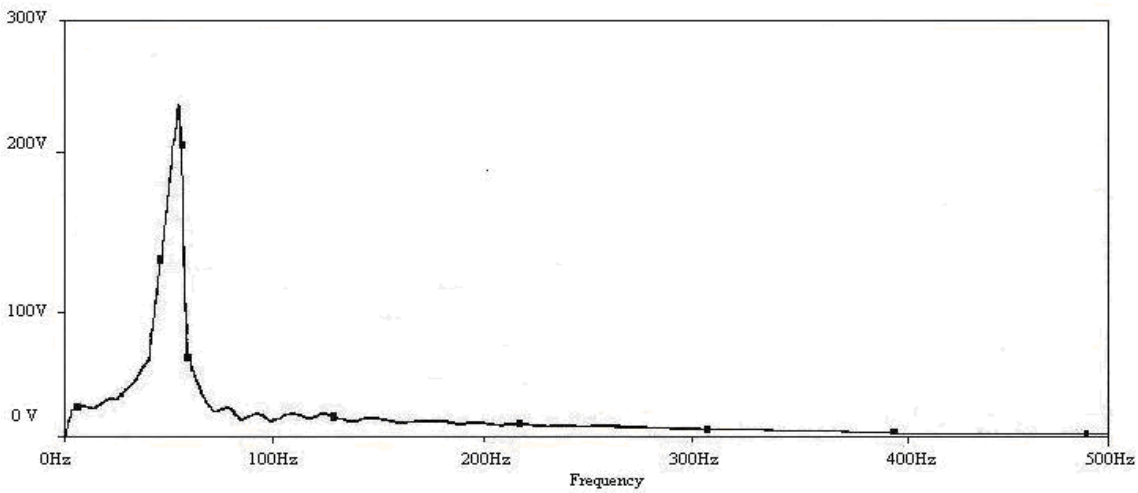

Figure 9: Harmonic distrtion spectrum for voltage

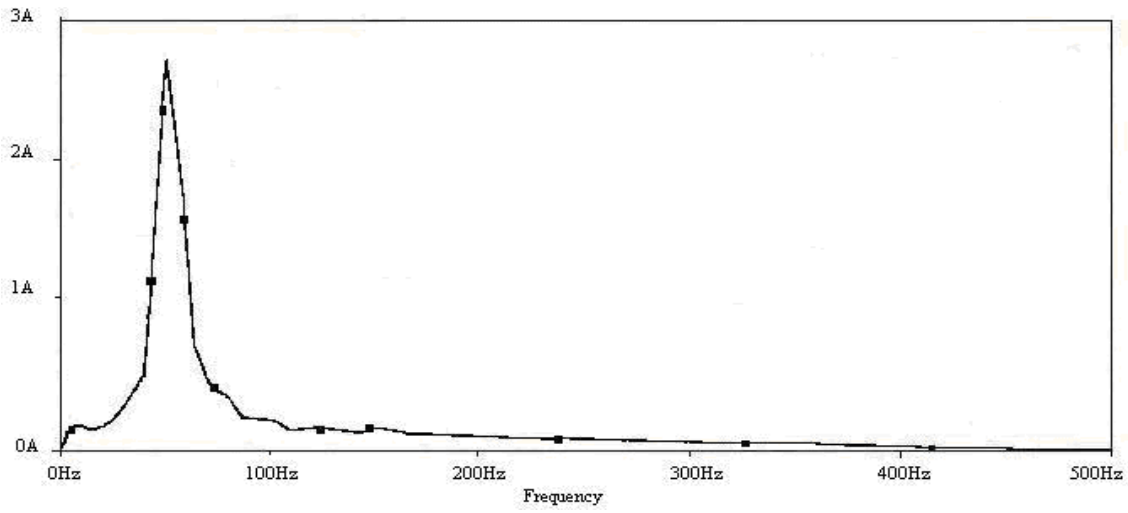

Figure 10: Harmonic distortion specturm for current

CONCLUSION

The proposed PV system circuit has been simulated with standard software (PSPICE) available and the results obtain has been compared with practical results, like the efficiency of the PV system, which is built on the laboratory, was about 93% and the result obtained from PSPICE simulation about 92% and this is agree with the efficiency obtain experimentally as well as the harmonic distortion spectrum for both the current and voltage was very low (lower than 3%).

REFERENCES

- Pedro G. Barbosa, Luis G. B. Rolim "noval control strategy for grid connected DC-AC Converters with load power factor and MPPT control" *www.sola.coppe.ufrj.br/rolim.html*

- M. I. Jahmeerbacus & M. K. Oolun “a dual stage PWM DC to AC inverter with reduced harmonic distorsion and switching losses" Science and Technology Research Journal, Vol.5, pp.80-91,2000.

- J. A. Dominguez & S. Lorenzo “Global control for two photovoltaic applications, pumping and connecting to the Grid systems” www.dte-eis.uva.es/dte/publication/congreses/EPE97B 2000

- Everett Rogers "Understanding Boost power stages in switch mode supplies" application report, Texas Instruments, 1999.

- Said EL-Barbari & W. Hofmann "Digital control of a four leg inverter for stand alone photovoltaic systems with unbalanced load

www.infotech.tu.chemnitz.de/ema/publikationen/2000Iecon2000-Japan-final

- Wail Metzker Pustorello Filho & Arnoldo Jose Perin "Delta – H modulater" 5th Brazilian power electronics conference, 1999

.

- Abhijit D.Pathak "Capacitor charge / discharge circuits"

www.ixys.com/to42502a.pdf.

INCREASING THE OUTPUT VOLTAGE OF PWM INVERTER USING HARMONIC DISTORTION

محمد حسين باقر

قاسم عبد الحسن

احمد رفعت

مدرس مساعد- معهد اعداد المدربيين

ABSTRACT

By adding a measure of third harmonic to the output of each phase of three-phase inverter, it is possible to obtain a line-to-line output voltage that is 15 percent greater than that obtainable when pure sinusoidal modulation is employed.

The line-to-line voltage is undistorted. The method permits the inverter to deliver an output voltage approximately equal to the voltage of the ac supply to the inverter. Thus an induction motor of standard rating with respect to the ac supply to the inverter can deliver very nearly full power at rated speed when supplied from the inverter. This is achieved without pulse dropping or any other form of mode changing.

الخلاصة

احدالوسائل لزيادة الاخراج للمنظومة هو بإضافة مقياس التوافقية الثالثة إلى خرج كل طور من الاطوار الثلاثية للعاكس ،من الممكن الحصول على خرج خط إلى خط، لاإخراج فولتية بنسبة 15 بالمائة، وهي أعظم من ذلك عند استخدام موجة جيبية نقية ومضمنة.فولتية الخط إلى الخط الغير مشوهة هي التي تسمح للعاكس لتجهيز فولتية الإخراج تساوي تقريباً فولتية التجهيز المتناوبة إلى العاكس .لذلك فأن المحركات الحثية ،معدل المعيار لها يتعلق بالتجهيز المتناوب إلى العاكس ،من هنا يمكن تجهيز قدرة كاملة تقريباً للمحرك الحثي بمعدل السرعة

المطلوبة عندما يكون التجهيز من خلال العاكس،وهذا يتم الحصول عليه عندما لا يكون هنالك نبض منخفض أو أي شكل آخر يؤدي الى تغير في نمط العمل للمنظومة .

INTRODUCTION

A Pulse Width Modulated (PWM) inverter, employing pure sinusoidal modulation, cannot supply sufficient voltage to enable standard motor or operate at rated power and rated speed. Sufficient voltage can be obtained from the inverter by over modulating, but this produces distortion of the output waveform. This paper demonstrates that the necessary increase in output voltage can be obtained without recourse to over modulation and without distortion of the line-to-line output waveform.

A problem is illustrated in fig.1. The dc supply for an inverter is usually obtained by rectifying a three-phase mains supply. Let the line-to-line voltage of this supply be V_{in}.

The dc link voltage will then be approximately equal to the peak voltage of the three-phase supply, therefore;

$$V_{dc} = \sqrt{2}V_{in}, \qquad (1)$$

In practice, the V_{dc} will be slightly less than this due to the forward voltage drop of the rectifier and to the ripple on the dc link.

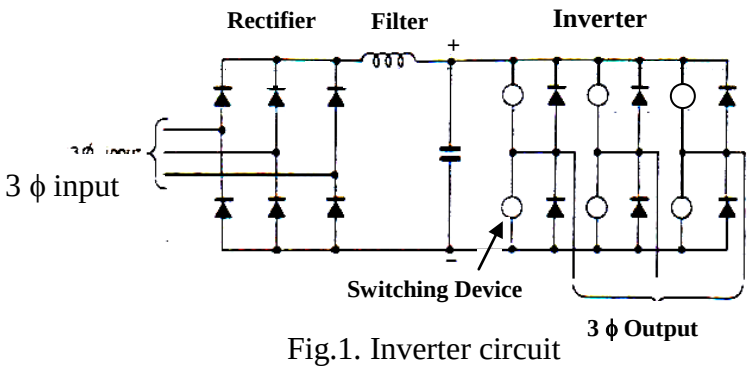

Fig.1. Inverter circuit

As fig.2 shows, the peak-to-peak output voltage obtainable from each phase of the PWM inverter is equal to the dc link voltage. Thus the rms output voltage of each phase is given by:

$$V_{out(phase)} = \frac{V_{dc}}{2}\frac{1}{\sqrt{2}} \qquad (1)$$

Substituting from (1), we obtain:

$$V_{out(phase)} = \frac{\sqrt{2}V_{in}}{2}\frac{1}{\sqrt{2}} = \frac{V_{in}}{2} \quad (2)$$

The line-to-line output voltage is therefore given by:

$$V_{out} = \sqrt{3}\frac{V_{in}}{2} = 0.866V_{in} \quad (3)$$

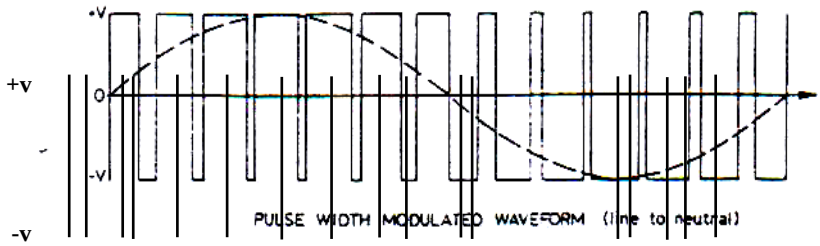

Pulsewidth modulated waveform (line-to-neutral)

Fig.2. PWM waveform with maximum output using sinusoidal modulation.

From the foregoing, it can be seen that an inverter operating from a supply of standard voltage and driving a standard voltage motor, can maintain the correct relationship between output voltage and output frequency only up to 0.866 of the supply frequency (e.g., 52Hz for 60-Hz mains, and 43Hz for 50-Hz mains).

It is of coarse, possible to increase the output voltage of an inverter beyond that which is obtainable with sinusoidal PWM. The traditional method of achieving this is by dropping pulses from the PWM waveform

This method is successfully employed in present state of the art PWM waveform, generators [1], [2]. The disadvantages of this method, however, are that the abrupt dropping of pulses may result in a step change in output voltage, which can cause motor current in stability [3], and the harmonic content of the output increases as pulses are removed from the waveform, thereby increasing motor losses. The problem of step changes in the output voltage may be negligible, or may be overcome by various techniques [4], [5], but the problem of increased output distortion remains.The aim of this paper is to show that the line-to-line output voltage of a PWM inverter can be increased by up to 15 percent without the need for pulse dropping or any other form of overmodulation, and without any material effect on the harmonic content of the line-to-line waveform.

METHOD OF DESCRIPTION

General:

The method involves the addition of triplen harmonics to the phase voltage waveforms. It is shown in the appendix that all triplen harmonics in a three-phase supply are cophasal and are therefore eliminated from the line-to-line waveforms. Although the triplen harmonics are eliminated from the line waveforms, their effect on the phase waveform is to decrease the peak voltage, has used harmonic distortion of this type to produce flat-topped phase waveforms which improve the efficiency of a class B transistor inverter [6]. This is achieved by the addition of various amounts of third, ninth, fifteenth, etc., harmonics. The method clearly has potential for the rating of all PWM inverters. However, king does not identify the optimum amount of each triplen harmonic to be used. Hodkinson and Mills have similarly employed harmonic distortion to increase the output voltage of an inverter but not analyze the process [7]. The object of the present paper is to determine the manner of distorting the phase waveform so as to obtain optimum performance from the inverter.

CALCULATION OF OPTIMUM DISTORTION:

The best modulation that can be made to the inverter phase output waveform is assumed a priori to be the addition of a measure of third harmonic. It will be subsequently shown that no further improvement can be derived from the addition of other triplen harmonics.

Assume a phase waveform of the type:

$$y = \sin\theta + \alpha \sin 3\theta \tag{4}$$

Where: θ = wt and α is the parameter to be determined. First we locate the turning points of this function by differentiating y with respect to θ and equating the result to zero. Thus:

$$\frac{dy}{d\theta} = \cos\theta + 3\alpha \cos 3\theta = 0 \tag{5}$$

The maxima and minima of the waveform therefore occur at:

$$\cos\theta = 0 \tag{6}$$

And:

$$\cos\theta = (\frac{9\alpha - 1}{12\alpha})^{1/2} \quad (7)$$

From (6) we have:

$$\sin\theta = 1 \quad (8)$$

And from (7) we have:

$$\sin\theta = (\frac{1+3\alpha}{12\alpha})^{1/2} \quad (9)$$

Using the identify that $\sin\theta = (1-\cos^2\theta)^{1/2}$.

The peak value of y can be found by substituting the values obtained for $\sin\theta$ in (8) and (9) into (4). This is facilitated by first manipulating (4) using the identity:

$$\sin 3\theta = 3\sin\theta - 4\sin^3\theta \quad (10)$$

Thus (4) becomes:

$$y = (1+3\alpha)\sin\theta - 4\alpha\sin^3\theta \quad (11)$$

Substituting for $\sin\theta$, the values obtained in (8) and (9), we have:

$$\hat{y} = 1 - \alpha \quad (12)$$

$$\hat{y} = 8\alpha(\frac{1+3\alpha}{12\alpha})^{1/2} \quad (13)$$

Where: $\hat{y}$ is the peak value of y.

The optimum value for α is that value which minimizes $\hat{y}$.

The optimum value of α can therefore be found by differentiating the expression for $\hat{y}$ and equating the result to zero. Thus from (13) [1], [2]:

$$\frac{d\hat{y}}{d\alpha} = (\frac{1+3\alpha}{12\alpha})^{1/2}(2 - \frac{1}{3\alpha}) = 0 \quad (14)$$

From which we obtain:

$$\alpha = -\frac{1}{3} \quad (15)$$

$$\alpha = \frac{1}{6} \quad (16)$$

From (12) we can see that negative values of α give values of $\hat{y}$ greater than unity and can therefore be disregarded.

The required value of α is therefore (1/6), and the required waveform is:

$$y = \sin\theta + \frac{1}{6}\sin 3\theta \qquad (17)$$

To demonstrate that no further reduction in $\hat{y}$ is possible by the addition of other triplen harmonics, the values of θ at which the peaks of y occur are found by substituting for α in (6) and (7) [3].

As may be expected, (6) gives θ: π/2, independent of α, but (7) gives:

$\cos\theta = 1/2$,

i.e.

θ = π/3, 2π/3, etc. (18)

All triplen harmonics pass through zero at these values of θ. Thus no further reduction in $\hat{y}$ can be effected by the harmonics, and the original assumption is justified.

If we now substitute these values of θ (= nπ/3) in (17), we obtain the peak values of y. Hence:

$$y = \pm\sqrt{3}/2 = \pm 0.866 \qquad (19)$$

INCREASING THE OUTPUT VOLTAGE:

As has been shown the addition of one-sixth of third harmonic to be modulated waveform has the effect of reducing the peak value of the output waveform by a factor of 0.866 without changing the amplitude of the fundamental. This process is illustrated in fig.3. It is then possible to increase the amplitude of the modulating wave by a factor (k) so that the full output voltage range of the inverter is again utilized [4], [5].

Thus the modulating waveform becomes:

$$y = k(\sin\theta + \frac{1}{6}\sin 3\theta) \qquad (20)$$

Assuming no minimum pulsewidth limitations, $\hat{y}$ can equal unity. From (19) we know that the previous peak value of (y) was 0.866.

Therefore, we have that:

$$k = \frac{1}{0.866} = 1.155 \qquad (21)$$

Thus as fig.3 shows, the addition of one-sixth of third harmonic produces a 15.5 percent increase in the amplitude of the fundamental of the phase voltage waveform and, therefore, in the line voltage waveform.

Even when minimum pulsewidth limitations are taken into consideration, a similar increase in output voltage is possible. The line-to-line waveform is undistorted since the third harmonic components in the phase waveforms are canceled. Note that it is necessary for the inverter to have a bandwidth equal to three times the wanted output frequency in order to satisfactorily handle the third harmonic [6], [7].

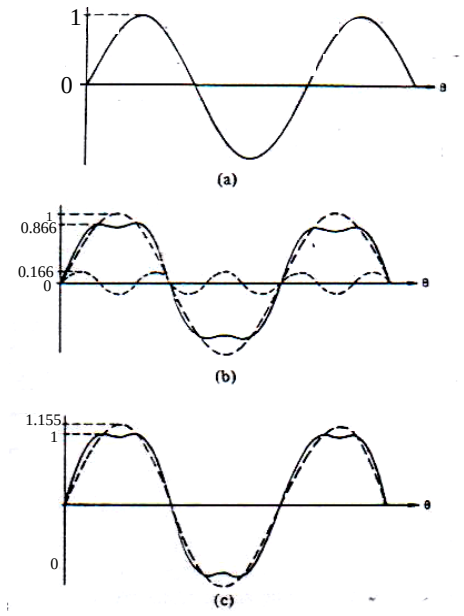

Fig.3. Increasing fundamental output voltage by addition of third harmonic.

(a) To third harmonic. Peak value = 1. Amplitude of fundamental = 1.

(b) With one-sixth of third harmonic added. Peak value = 0.866. Amplitude of fundamental = 1.

(c) With one-sixth of third harmonic added and peak value restored to one. Peak value = 1. Amplitude of fundamental = 1.55.

TEST CIRCUIT:

The principle has been proved on a 1.9 KVA three-phase inverter employing a high carrier frequency and filtering of the phase waveforms. The output waveforms are shown in fig.4. The power circuit of the inverter is shown in fig.5. The inverter uses power MOSFET's as the switching devices. The high switching speed of the MOSFET's permits the use of an ultrasonic carrier. This gives the inverter a bandwidth which encompasses both the fundamental and its third harmonic for the output frequencies far beyond normal mains frequency.

The PWM waveform was generated digitally using micro-processor-based waveform generator.

Using a carrier frequency, the carrier period is only 51 µs. To minimize the harmonic content of the PWM waveform, the positions of the edges of the waveform must be calculated every cycle for all three-phases. To make maximum use of the time available for computation, Sinewave values are stored in a lookup table in the read-only memory (ROM). The one-sixth of third harmonic is incorporated in this table.

The output of the counter external to the microprocessor is used to address the lookup table. To obtain the waveform values for each of the three-phases, an algorithm in the microprocessor program modifies these values to implement voltage control. The modified values are then supplied to counter timers to determine the instants of switching of the power devices.

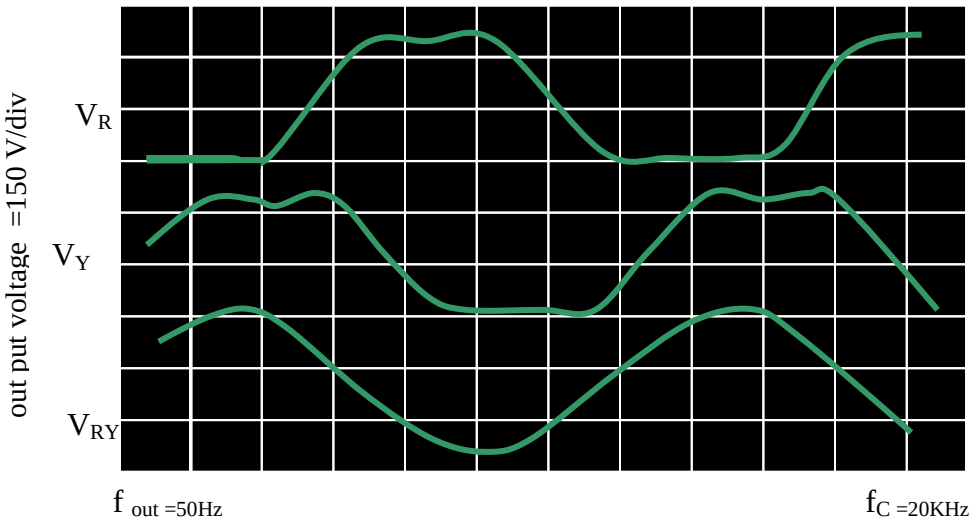

Fig.4 Output voltage waveforms.

This PWM controller by microprocessor is supplied with an input clock frequency. Hystersis between the switching points is included to avoid jitter noise. The induction motor is governed by the general expression. $V=Nd\Phi/dt$. So that maintain constant flux the voltage-time product Vt must be kept constant.

The microprocessor controller automatically satisfies the requirement by the making the output voltage directly proportional to the output frequency.

This represents of clock frequency, and connected to the input signal of the converter at the base transistor (logic signal), when maintaining (logic signal) at the recommended value and varying clock frequency controls.

The speed of the motor at constant flux rate (i.e.V/F). That i.e. varying the D.C voltage at the input of the inverter increasing or decreasing the modulation depth of the fundamental frequency.

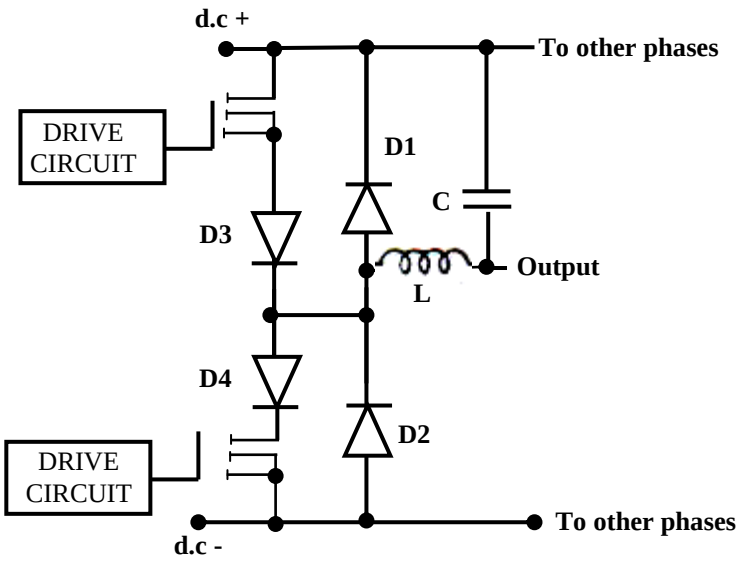

Transistors BUZ45
Diodes D1 , D2 BYV29-400
Diodes D3 , D4 BYV29-150
L = 6 mH
C = 2.2 μ F

Fig.5 Inverter Circuit.

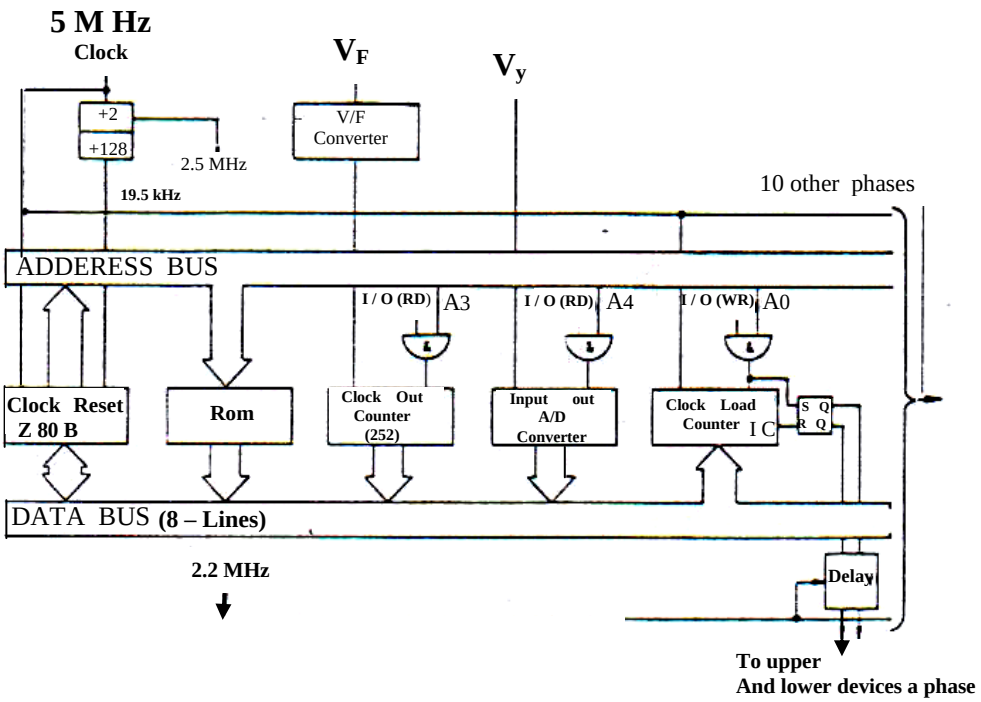

Fig.6 PWM Waveform Generator

CONCLUSION:

It is possible to increase the output voltage of a PWM inverter beyond that obtainable using pure sinusoidal modulation by adding a measure of third harmonic to the modulating waveform. The maximum increase in output voltage is obtained when the amplitude of the third harmonic is one sixth that of the fundamental. The method permits a 15 percent increase in the output voltage of PWM inverters without causing distortion of the line-to-line waveforms.

APPENDIX

Cancellation of Triplen harmonics, it can be shown that triplen harmonics contained in the phase waveforms of the output of a three-phase inverter are eliminated from the line-to-line voltage waveforms. Consider a three-phase supply, let the output waveforms be composed of the fundamentals plus an arbitrarty amount of any triplen harmonic. Therefore:

$$V_A = \sin wt + \alpha \sin 3nwt \qquad \text{(A1)}$$

$$V_B = \sin(wt - 2\pi/3) + \alpha \sin 3n(wt - 2\pi/3) = \sin(wt - 2\pi/3) + \alpha \sin(3nwt - 2n\pi) \quad \text{(A2)}$$

$$V_C = \sin(wt - 4\pi/3) + \alpha \sin 3n(wt - 4\pi/3) = \sin(wt - 4\pi/3) + \alpha \sin(3nwt - 4n\pi) \quad \text{(A3)}$$

The fundamental components of angular frequency W form a three-phase set, whereas the triplen components are Cophasal. At triplen frequency, therefore, no voltage difference exists between phases and all triplen harmonics are eliminated from the line-to-line voltage waveform.

REFERENCES:

- Mika Salo and Heikki Tuusa, " *Control of the PWM Current Source Inverter Fed Induction Motors Drive*," 2005

- P.V. Enjeti, P.D.Ziogas and J.F.Lindsay, "*Programmed PWM Techniques to Eleminate Harmonics a Cirtical Evaluation*," IEEE. Trans. Ind. Appl. Vol. 26, No. 2, MAR/APR, 1990

- N. Yadalapalli,"*Implementation of a Noval Soft Switching Inverter for Switched Reluctance Motor Drivers*," Thesis, Virginia University, 1999

- D.A. Grant, "*Technique for pulse dropping in pulsewidth modulated inverters*", Proc. Inst. Elec. Eng., pt. B, vol.128. pp. 67-72. Jan. 1981.

- D.A. Grant and R. Seidnar, "*Techniques for pulse elimination in pulsewidth modulated inverters with no waveform discontinuity*", Proc. Inst. Elec. Eng., pt. B, vol.129. pp. 205-210.July 1982.

- Jameel K. Abed AL-Jashhami," *Design of a Low Harmonics High Frequency Inverter for Control Application*," Ph.D. Thesis Submitted to the Department of Electrical and Electronic Engineering University of Technology, 2003

- Stephan J. Chapman, "*Electronic Machinery Fundamentals*," Third Edition Singapore by the McGraw-Hill Companies Inc 1999

INVESTIGATING THE EFFECT OF IRON PRESENCE IN THE MAGNETIC CIRCUIT OF A DOUBLE HELICAL WINDING INDUCTION MOTORS

Prof. Dr. J.H. Alwash and Saad Mahdi
University of Baghdad, College of Engineering, Electrical Engineering Dept.

ABSTRACT:

The paper presented a new type of double helical-winding tubular induction motor (DHWTIM). The proposed motor consists of double- layer helical windings primary arranged on the same circumference with a common secondary. By controlling the phase sequence of supply voltage for each of primary winding layers, the secondary conductor would be capable of producing pure rotary motion, pure linear motion, or helical motion. An appropriate multi-layer analysis using cylindrical geometry is presented. This has been used to study the effect of iron presence in the magnetic circuit of the machine on its performance.

KEY WORDS

Double helical windings, helical motion, induction machine, linear-rotary motion, linear induction machines.

الخلاصة

يتناول هذا البحث در اسه أداء محرك حثي اسطواني يمتلك طبقتين من الملفات ثلاثية الأطوار.المحرك المقترح يتكون من طبقتين من الملفات اللولبية (جزء الثابت)، و أن عدد الأقطاب المحيطية والمحورية متساوية في كلتا الطبقتين، مع الجزء الثانوي العام (الجزء المتحرك).

أن ألطريقه التي تم استخدامها نظريا لتحليل المحرك هي طريقه تحليليه صرفه تم استخدام أسلوب ألتغذيه الاعتيادي وتبعا لهذا تمت كتابة برنامج لهذا الغرض وتم التعرف على تأثير وجود الحديد في هيكل المحرك.

INTRODUCTION

Since the commercial motor produces only one dimensional (linear or rotary) motion, the two–dimensional motion generally requires more than two kinds of motors. The helical winding induction motor (HWIM) topology is such that the developed electromagnetic forces produce helical motion, and this would be a desirable asset to the fields of machine tools and robotic (such as valve-seat grinding).

Massoud and Cathy [1988] had presented a helical winding induction motor (HWIM) that could be used in a tandem arrangement of two units to form a direct–acting, two degree of freedom a actuator. That was capable of producing pure rotary motion, pure linear motion, or helical motion, the analysis presented, however, made use of a rotating Cartesian Coordinate, and limited the analysis to the case where only two poles exist in the circumferential direction.

Alwash [2003] had presented a tubular motor with helical winding, together with a multi-layer mathematical model chosen for the analysis. Since then few, but significant, papers relating to helical motion machines have been published.

The primary object of this paper first to develop the winding layout for such model, and second to show the effect of the presence of iron in the magnetic circuit on the performance of the machine.

WINDING LAYOUT

The basic development of the helical motion tubular induction motor can be explained with the aid of fig.(1.a). That shows a flat layout of the instantaneous pole pattern of a helical motion tubular induction motor. If this layout is rolled about an axis and applied (EE) to (FF), the result is a helical motion tubular induction motor, as shown in fig. (1.b).

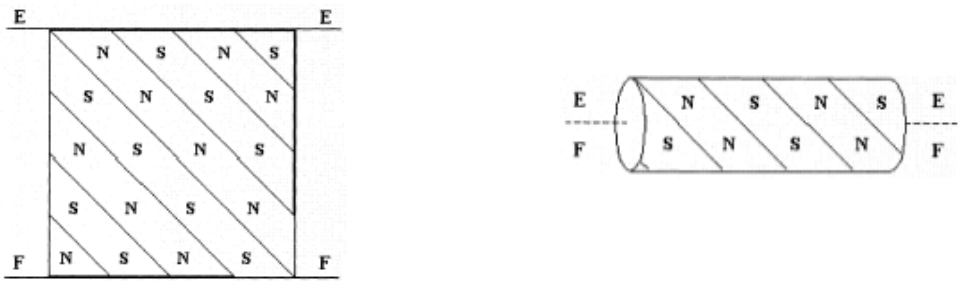

(a) **(b)**

Fig.(1). Development of a helical motion tubular induction motor.
a. Instantaneous pole pattern of a planner motor.
b. planner motor rolled to form a tubular motor.

The primary coil construction of one phase of the winding may be explained with the aid of fig. (2.a), which shows the coil structure for the planner motor. To convert this into the tubular shape, it is rolled to produce the construction shown in fig. (2.b).

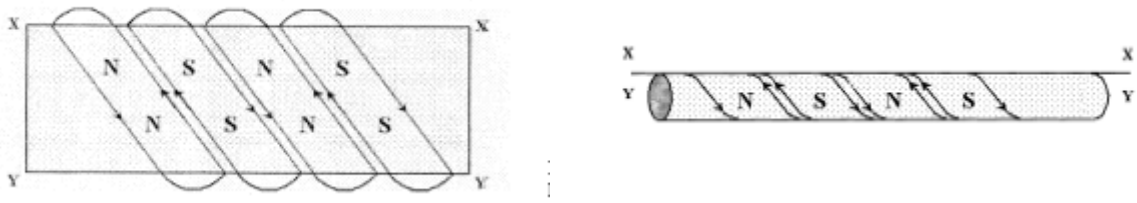

(a) **(b)**

Fig.(2). Coil structure of one phase of helical motion tubular induction motor.
a. Coil structure of a planner motor. **b. Coil structure of a tubular motor.**

Fig. (3) show the helical windings in the tubular form for two poles axially. The model shown in fig. (3.a) has two poles circumferentially while that shown in fig. (3.b) has four poles circumferentially.

(a) **(b)**

Fig. (3). A 3-phase helical motion tubular induction motor with 2-poles axially.
a. 2-Poles circumferentially **b. 4-Poles circumferentially**

Polyphase versions of the winding may of course be arranged, fig. (4) shows unrolled 3–phase configuration, with two poles circumferentially and axially.

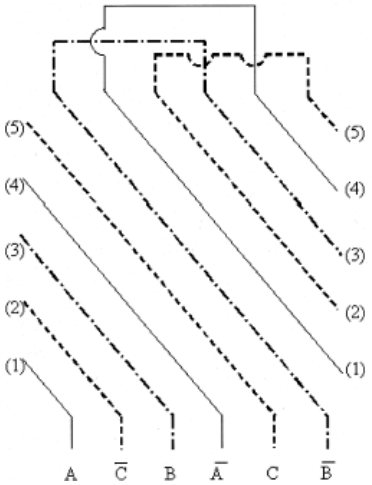

Fig. (4). An unrolled 3-phase helical motion tubular induction motor with two poles axially and circumferentially.

From this point, the developed 3-phase winding for the (DHWTIM) may be represented as shown in fig.(5).

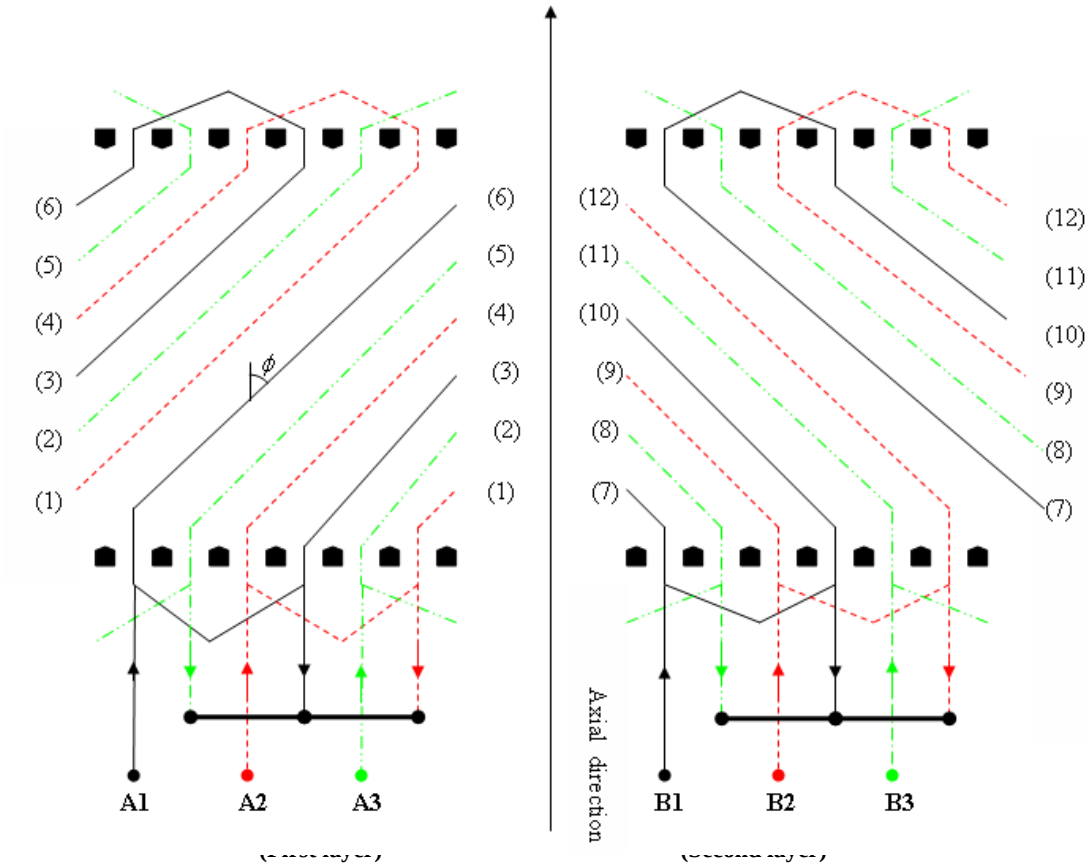

Fig. (5). An unrolled 3-phase double helical windings tubular induction motor with two poles axially and circumferentially.

THEORETICAL EVALUATION

The layer theory approach has been used to analyze this type of machines, Freeman [1968], Freeman and Smith[1970]. The mathematical analyzes of the model chosen is based on solution of Maxwell equations in a given region, with the continuity across the borders between the consecutive layers. The final governing equations are as follows:

$$E_{\theta,m} = \frac{K.r_m}{n}\left[A.I_n(\alpha_m r_m) + D.k_n(\alpha_m r_m)\right] \tag{1}$$

$$H_{Z,m} = \frac{jr_m.K}{n\omega\mu_m}\left[\left(\frac{2r_{m.}K^2}{n^2 + r_m^2K^2} - \frac{n}{r_m}\right)\left(A.I_n(\alpha_m r_m) + D.k_n(\alpha_m r_m)\right) + \alpha_m\left(A.I_{n-1}(\alpha_m r_m) - D.k_{n-1}(\alpha_m r_m)\right)\right] \tag{2}$$

The details may be seen in the M.Sc. thesis, Saad [2007], it is thought to be useful to investigate the effect of rotor and stator iron cores on both the axial and circumferential force.

Table (1) gives the machines parameters for the model chosen for the analysis.

The model under consideration posses eight degrees of freedom. These are shown in table (2), it may be seen that cases **1** to **4** each represent a type of helical motion, while cases **5** and **6** each represent a linear type of motion, and finally cases **7** and **8** each represent a rotational type of motion.

Now a helical motion model, was chosen, and the analysis been applied to investigate the variation of first the axial force with axial speed and second the variation of the circumferential torque with circumferential speed. The results are displayed respectively in fig. (6.a) and fig. (6.b).

The effect of adding iron to the rotor circuit is seen to be apparent while adding iron to stator have a greater effect on the forces, and of course adding iron to both members of the motor, have the greatest effect on forces and this is expected because the magnetic circuit becoming ideal and closed.

As a second case in the study a linear type model has been chosen for the analysis, and fig. (7) shows the variation of axial force with axial speed, and again it is clear that adding iron to both primary and secondary member of the model would produce a model with the greatest possible values of forces.

A third case was then chosen for the analysis, this is to represent the rotational type of motion, and fig. (8) shows the result of the study for such model which again shows the effect of adding iron to the model both to the stator and rotor members.

It is clear that the presence of iron in the magnetic circuit of motor increases the speed at which the maximum developed force occur. This is also expected in the conventional rotating counter part of the machine. Also it is clear that the effect of presence of iron in the stator core on the magnetic circuit is more than that in the rotor core because of the limitation of the rotor core circumference.

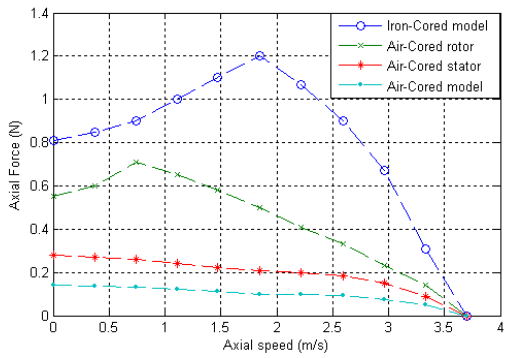

Fig.(6.a) Variation of axial force with axial speed for the mathematical model under investigation in helical motion.

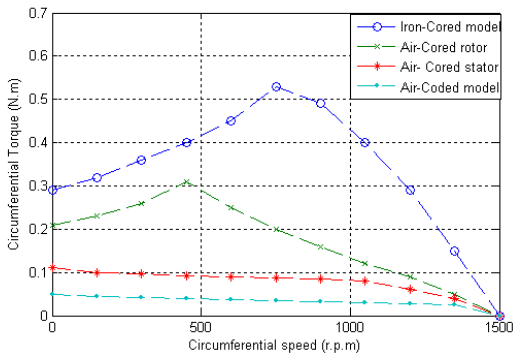

Fig.(6.b) Variation of circumferential torque with circumferential speed for the mathematical model under investigation in helical motion.

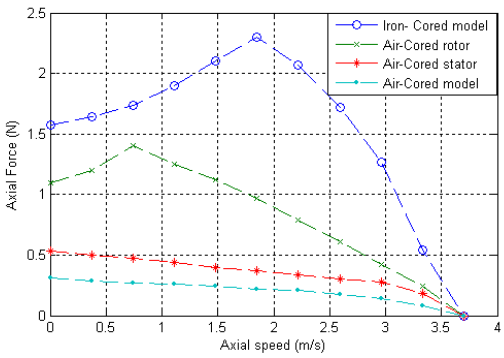

Fig.(7) Variation of axial force with axial speed for the mathematical model under investigation in linear motion.

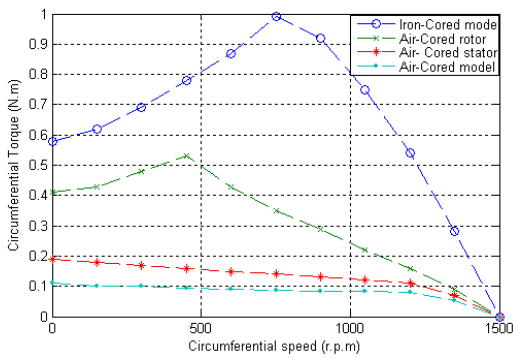

Fig.(8) Variation of circumferential torque with circumferential speed for the mathematical model under investigation in rotary motion.

Table (1)
Machine parameters

Stator length (mm)	300
Phases	3
Circumferential poles	4
Axial poles	4
Slot per pole per phase	1
Slot per pole	3
Slots, axial and circumferential	12, 12
Normal coil width (mm)	8
Normal slot pitch (mm)	12
Normal pole pitch (mm)	45.38
Helicoid angle at the average diameter of the winding (degree)	35.5
Turns per coil	140
R.M.S. stator phase current (Amp.)	1.8
Frequency (Hz)	50
Outer stator winding diameter (mm)	60.5
Air-gap length (mm)	4
Outer secondary conductor diameter (mm)	39.5
Outer stator back iron (if presence)diameter(mm)	95
Aluminum sleeve thickness (mm)	3
Iron (if presence) conductivity	5.8107

Table (2)
Eight motion of the secondary conductor by controlling the phase supply voltage for each layer

No.	Supply voltage with identical balance three-phase	Secondary conductor motion
1	Positive sequence currents were supplied to first layer only.	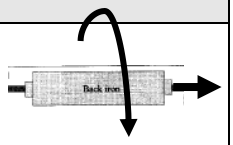
2	Negative sequence currents were supplied to first layer only.	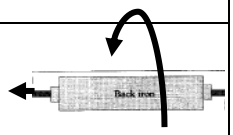
3	Positive sequence currents were supplied to second layer only.	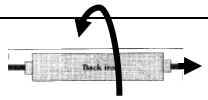
4	Negative sequence currents were supplied to second layer only.	
5	Both the first and second layer were excited by positive sequence.	
6	Both the first and second layer were excited by negative sequence.	
7	Positive sequence currents were supplied to first layer while negative sequence current were supplied to second layer.	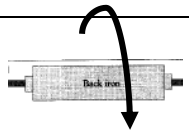
8	Negative sequence currents were supplied to first layer while positive sequence current were supplied to second layer.	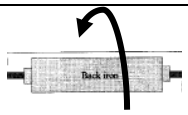

CONCLUSIONS

The paper describes a way to investigate the effect of iron presence in the rotor, in the stator, and finally in both rotor and stator of the type motor described in the M. Sc. Thesis Saad [2007], and this represent a clear addition to what is included in the reference thesis, and shows clearly that addition of iron in the stator would posses a greater effect than that obtained in adding iron to the rotor circuit.

REFERENCES

- E. M. Freeman," Traveling waves in induction machines:input impedance and equivalent circuits", proc. IEE, vol. 115, no. 12, pp. 1772-1776, Dec. 1968.
- E. M. Freeman and B. E. Smith," Surface impedance method applied to multilayer cylindrical induction devices with circumferential exciting currents", proc. IEE, vol. 117, no. 10, pp. 2012-2013, Oct. 1970
- J. H. H. Alwash, A. D. Mohssen, and A. S. Abdi, "Helical motion tubular induction motor",IEEE Trans. Energy conv. ,vol. 18, no. 3, pp. 362-369, September 2003.
- Massoud Rabiee, and Jimmie J. Cathey,"Verification of a field theory analysis applied to a helical motion induction motor",IEEE Trans. On magnetic, vol. 24, no. 4, pp. 2125-2132, July 1988.
- Saad M. Hadi, "Performance study of a double helical windings tubular induction motor", M.Sc. thesis, College Engineering Baghdad University, Baghdad 2007.

LIST OF PRINCIPAL SYMBOLES

E	Electrical-field strength, V/m
H	Magnetic-field strength, A/m
K	Wave length factor, rad/m
I_n, k_n	Modified Bessel functions of order n
m	Subscript referring to region, m
n	Circumferential pole pairs
r, θ, z	Subscripts for cylindrical coordinates
ω	Angular velocity, rad/s

EVALUATION OF THE PERFORMANCE OF THE DORA REFINERY WASTEWATER TREATMENT PLANT

Prof. Dr. Rafa H. Al-Suhaili **Muwafaq A. Abed**

Environmental Engineering Department

College of Engineering

Baghdad University

ABSTRACT

Oil refineries are major contributors to local environmental problems .The main pollutants are oil , dissolved components , spent acids , suspended solids, sludge . Technically it is possible to remove all these pollutants by Physical , chemical and biological means .Oil is initially removed in the (API) separators , by skimming, while the heavy particles by scrapping . Further removal of discrete particles is done by gravity settlement in the primary settlement tank .The remaining suspended matter is removed by chemicals , that are added in the flocculation tank , while further flocs are removed in the air flotation tank . The biological treatment follows to remove the biological pollutants , usually followed by secondary settlement to reduce the flux of suspended particles carried with the effluent water. This thesis deals with the Dora refinery wastewater treatment plant , its present performance in comparison with the designed treatment performance and its final effluents compared with the Iraqi discharged water quality limitations .In order to identify the characteristics of the refinery effluents and to evaluate the performance of the refinery wastewater treatment plant , wastewater from different treatment stages were analyzed for various physical and chemical parameters . Using these parameters as the criteria of performance , comparisons were made between the actual and the designed performance for various potential pollutants. The sampling was conducted during 6 months from May to October 2006 , with two samples in each month for each of the units, one before , and one after.The results showed that the wastewater treatment plant in Al-Dora Refinery performed significantly, where high removal efficiencies , were obtained. For T.S.S , Oil , COD , BOD , Sulfide and Phenol which were 95% , 88% , 86% , 81% , 85% and 97% respectively . And the plant was not very efficient in NH_3 , SO_4 and PO_4 removal .

الخلاصة

ان المصافي تعتبر عالميا مساهم رئيسي في مشاكل البيئة الموقعية . اهم الملوثات الناتجة من المصافي والتي تنصرف مع المياه هي النفط ومركباته ,المواد المذابة والعالقة , الحوامض , الحمأة وغيرها . فنيا بالامكان ازالتها جميعا باساليب فيزياوية , كيمياوية وبايلوجية .حيث يتم ازالة النفط اولا في محطة المعالجة في خزانات خاصة للعزل وذلك بترك المياه فيها وقشط النفط الطافي على السطح وكذلك قشط المواد المترسبة في القعر . وتكون عملية الفصل في هذه الخزانات بفعل الجاذبية الارضية .

تلي هذه المرحلة عملية فصل للمواد العالقة وذلك بخلط مواد كيمياوية مخثرة مع المياه في خزانات التخثير والدمج ومن ثم يتم تطويف المواد العالقة والمتكتلة في خزانات التطويف حيث يتم قشطها من السطح ومن قعر الخزان باستخدام القاشطات الخاصة لذلك . تتبع هذه العمليات عملية المعالجة البايلوجية , والتي يتم فيها معالجة المواد الذائبة بفعل الاحياء المجهرية (البكتريا) ومن ثم يتم فصل هذه الملوثات وترسيبها في احواض الترسيب النهائي لفصل ما تبقى من المواد العالقة والمتجمعة والاحياء الحية المجهرية لتقليل جريانها مع المواد المنصرفة الى النهر.
المعالجة البايلوجية في مصفى الدورة تستخدم التهوية الممتدة ووحدات الحمأة المنشطة . يتوفر في وحدات المشروع الاجهزة اللازمة للقشط والخلط والتهوية , وأحياء مجهرية حية تتغذى على الملوثات المجهرية .
تستخدم هذه الدراسة أسلوب البحث والتحليل الاحصائي للبيانات المستحصلة من قراءات التحاليل الكيميائية للنماذج المأخوذة من مختلف المواقع في محطة المعالجة . وطريقة اخذ النماذج المتبعة كانت نموذج قبل وبعد كل وحدة من وحدات محطة المعالجة ولمدة ستة اشهر وللفترة من ايار وحتى تشرين الاول من عام 2006 وبواقع فحصين كل شهر وللملوثات:-(pH ,Oil , T.S.S , BOD_5 ,COD ,N-NH_3 ,Sulfide ,Sulfate , Phosphorous and Phenol)
النتائج اظهرت الاداء الكفوء لمحطة المعالجة في ازالة الملوثات (T.S.S ,OIL ,BOD , COD ,Sulfide , Phenol) حيث سجلت اعلى نسبة ازالة لهذه الملوثات وهي 95% , 88% , 86% , 81% , 85% و97% على التوالي وكذلك النتائج اظهرت ان محطة المعالجة ليست كفوءة جدا في ازالة الملوثات NH_3 , SO_4 and PO_4 .

KEYWORDS
Oil Refinery effluents, wastewater treatment plant, evaluation of the performance.

INTRODUCTION

Pollution generally may be defined briefly as the total disturbance of natural surroundings. Water pollution may be defined as the existence of some , Chemical , Physical and Biological elements that exceeds the allowable standard limits. The presence in significant quantity of any extraneous material (solid , liquid , gas) in any particular location may therefore constitute pollution .

0ne of the industrial sources of pollutants is the refinery effluents, being significant water consumers and consequently large wastewater producers . In this research the performance of the wastewater treatment plant of the Dora Refinery will be studied . This study will be conducted in order to specify the problems and hence , to suggest the solution and recommendations for better performance .

GENERAL DESCRIPTION OF THE DORA REFINERY WASTEWATER TREATMENT PLANT

The Dora refinery was operated in 1955, and is located at the southern region of Baghdad city on the right bank of the Tigris river. The average Refinery Wastewater is approximately 750 cubic meter per hour ; at normal conditions ; reaching to 850 cubic meters per hour in rainy seasons . The wastewater is discharged to the Tigris River after treatment .The Dora Refinery Wastewater contains several pollutants including variable concentrations of oil, phenols, suspended solids, sulfides, oxygen demand, bearing material and other harmful contaminants. A treatment plant was constructed and operated in 1980 . In spite of this it was noticed that sometimes the quality of the refinery discharged effluents had exceeded the Iraqi discharged water quality limitations, leading to harmful environmental impact on the Tigris River.The location of Dora refinery along the Tigris river in Baghdad is just upstream of the industrial complex.The present Dora refinery wastewater treatment plant started operation in 1980 and the two old "API " separators constructed earlier in 1955 were connected with the new treatment facilities. Fig.(1) shows the treatment plant units.

Fig.(1):The Dora refinery wastewater treatment plant units .

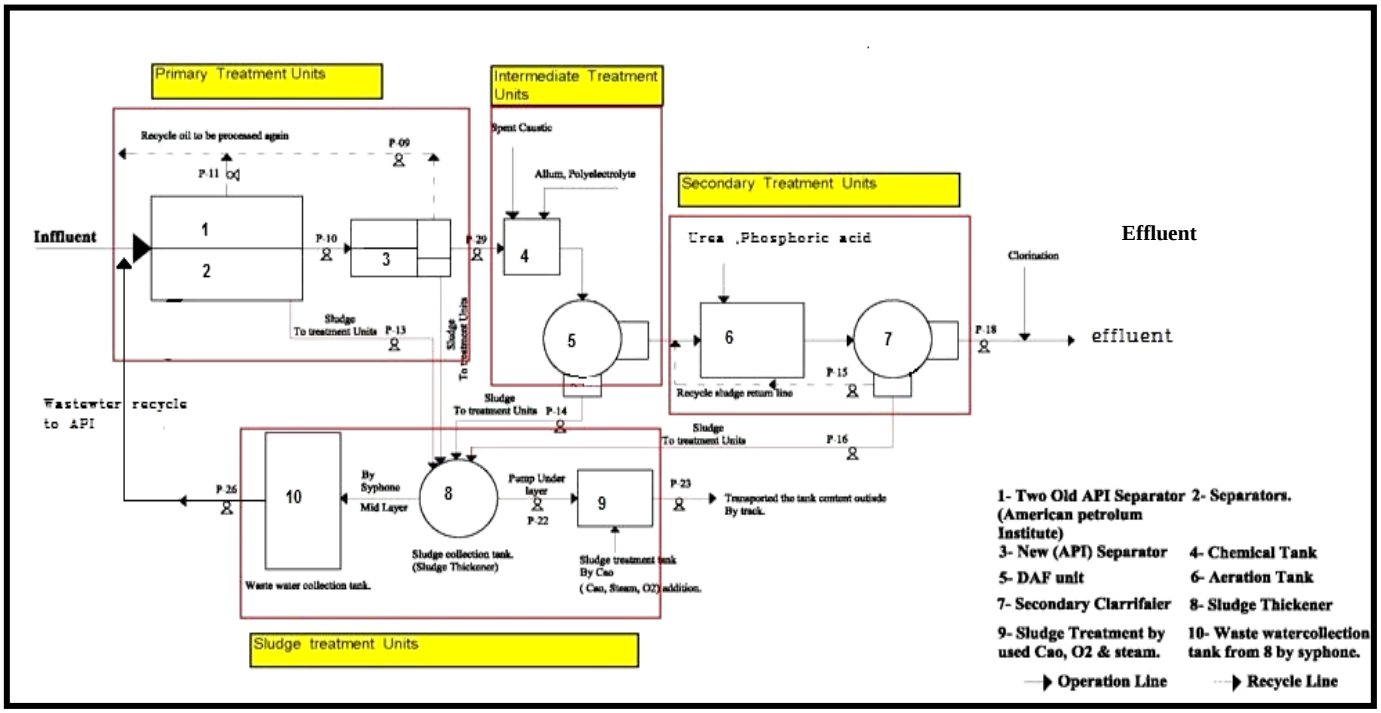

EXPERIMENTAL WORK

Parameters Needed

Before testing the quality of petroleum refinery effluents , potential parameters should be identified for successful interpretation of the experimental results obtained .The quality of refinery effluents can generally be assessed by monitoring the most popular parameters such as Oil , BOD_5 , COD , Sulfide & Sulfate , Nitrogen compounds (NH_3 ,NO_3) , Phosphorous , Suspended Solids and Phenols .[1&2] .

Sampling Technique

In this study , a series of (12 Grab Samples) were taken from 6 selected locations in the plant in order to detect the influent and effluent quality fluctuations . The total of (72 Sample) were taken during the sampling period of {14 May to 17 Oct. 2006 } . At an average of two samples per month.

Sampling Locations

In each time of the (12 Grab sampling) , samples were taken before and after each stage at the Dora refinery wastewater treatment plant . This was done in order to obtain a clear picture of the performance of each stage alone .

Experiments And Equipments Used

Experiments used for testing the Dora Refinery wastewater contaminants were chosen depending on the expected concentrations of the effluents and on the recommended tests

applied by the{Standard Methods for the examination of water & wastewater } hand

No.	Parameter	Experiment	Reference
1-	Oil & Grease	Partition – Gravimetric method	" The standard method for examination of water and wastewater " page(5-25)(18)edition
2-	Total suspended Solids	Filtration on filter paper	The same above page (2-56)
3-	pH	Direct Measurement	= = = = page (460)15th.edition
4-	BOD_5	Direct Measurement	New digital bottles
5-	COD	2 hour– Dichromate	" The standard method for examination

book,[1985 ,1988 & 1990]
These experiments were carried out in the Dora wastewater treatment plant laboratory .
The parameters tested , experiments and equipments used are stated in table (1) .

Table (1) Experiments and equipments used.

		method	of water and wastewater " page (5-7)(18)edition
6-	Ammonia (NH_3)	Nesslerization Method	= = = = page (4-78)(18)edition
7-	Nitrate (NO_3)	Not measured (unavailable reagent)	= = = = page (*)
8-	Sulfide	Spectrophotometer	New digital device
9-	Sulfate	Spectrophotometer	New digital device
10-	Phenols	Chloroform extraction method	" The standard method for examination of water and wastewater " page (5-31)(18)edition
11-	Phosphorous	Spectrophotometer	New digital device

Experimental Results

The experimental results of the Dora refinery wastewater are listed in (10) tables . These results represent the wastewater characteristics at 6 different stages & during the sampling period of [14 May to 17 October, 2006].

Note :During the sampling period the refinery was exposure to electrical shut down, that may affect the results.

ANALYSIS OF RESULTS AND DISCUSSION

Representation of Results

The experimental results that mentioned above were analyzed to obtain the following results in others 10 tables , each table is separated as the following :-

1-Table (A) involve the concentrations for each pollutants in the six treatment stages.

2-Table (B) involve the (standard deviation ,minimum ,maximum ,average & design limitation) for each pollutant in the six treatment stages.

3-Table (C) involve the pollutant removal percentage in each treatment stage ,their average and standard deviation .

The pollutants concentration in tables (B) were plotted against the designed limits of the Dora Refinery Wastewater Treatment Plant to show the difference between the design and the actual performance conditions in figures (2 to 11).The Dora Refinery discharged effluents are also studied and plotted with the Iraqi discharged water quality limitations in figures (12 to 22).Table (2) for T.S.S pollutant represent the typical table of these 10 tables that mentioned above, and the analysis of the others pollutant showed graphically.

Analysis and Discussion

The actual performance of the Dora Refinery Wastewater Treatment Plant will be analyzed and discussed according to the experimental results of the pollutants concentrations , which were considered as the criteria of performance , as follows :

Wastewater Flow Rate

Figure (12) of the wastewater flow rates show normal conditions within the design limit of (750 to 850 m^3/hr) in the (first, second, sixth, tenth, eleven and twelve) sample values are (800 m^3/hr) during this sampling period . The others six samples the values are (750 m^3/hr)..

pH Values

Figure (2) show the range of the wastewater pH at different treatment stages of the wastewater treatment plant. It can be seen that the pH values of the second stage effluent of the chemical tank and DAF unit increase slightly due to the addition of chemicals for pH adjustment in this stage .The results indicate the suitable control of pH. Fig.(13) shows the pH values of the Dora refinery final effluents discharged to the Tigris River . these discharged values are all within the range of the Iraqi water quality limitations .

Total Suspended Solids

The total suspended solids concentrations , at different treatment stages , are illustrated in table (2)(A) .These existing concentrations were plotted against the designed concentrations in fig. (3).The maximum and the minimum concentrations values seemed to be close to the design performance of the treatment plant .The total suspended solids concentration decreased with the operation of the DAF unit ,but in July and August the samples from DAF unit showed a slight increase in the T.S.S concentration. This may be related to the formulation of flocs in the chemical addition tank .because of these flocs are from the spent caustic stream(that does not enter the plant in the influent pit) did not settle properly. Also the low removal percentages in this unit is due to the low air pressure used for design Rohlich .[58] The removal reached to 3.9% for sample 1 , 15.4% for sample 9 and 8.6% for sample 11.
The T.S.S measurements from the biological treatment unit (6) were very high indicating the high micro-mass production in this tank. The removal efficiency was not recorded as this unit is not for solid settlement.The final T.S.S concentrations in the effluent were within the Iraqi discharge limitations as shown in fig.(14) and the overall removal of the plant was at an average of 95.2% .

Oil and Grease

Figure (4) also shows that the oil concentrations (max. ,min. & average) were very close to the designed performance of the treatment plant .that can be related to the API gravity separators especially the new one.The effect of the new API separator operation is clearly observed for oil removal, but it decreased to 39.1% in May and 17.8% in August .

Ingersoll ,(1951). indicated that the API performance might be disturbed by excessive concentrations of suspended solids present in the API basin , due to the presence of some suspended matter that neither floats nor settles down , thus creating a poor gravity reduction in oil and suspended solids concentrations .The DAF unit default also in oil removal in May as the removal reached 2.6% and in July 8.2% .Gehr and Henry (1978). reported that the DAF recycled liquid should always be the clearest liquid obtainable from DAF unit, in order to gain the polymer build-up in the DAF unit for better flotation process, but the refinery uses tap water . The poor performance of the DAF unit also may be related to the low saturation pressure used in pressurization tank . The oil concentrations of the final effluents

are illustrated in figure (15) . This graph shows the fluctuations in oil concentrations during the sampling period , indicating that the maximum concentration was (9.6 mg/l) of the first sample tested. Where the removal was 54.3% .The overall of the plant was between 69% - 100% . All the samples were under the Iraqi limitations of 10 mg/l .

Biochemical Oxygen Demand (BOD)

It can be seen from figure (5) that the effluent (BOD_5) values of the aeration tank were high in all samples tested . This is normally related to the suspended organic load of the biological floc which is recirculated from the final settling tank back to the aeration tank . However , these high suspended (BOD_5) values are reduced again in the final settling tank , which were less than the design limit of 20 mg/l . In figure (16) the discharged values of (BOD_5) were plotted with the Iraqi limitation of (40 mg/l).The results indicate the low (BOD_5) concentrations discharged to the Tigris River . The overall removal of the plant ranged from 68% to 90.6% .

Chemical Oxygen Demand (COD)

Figure (6) showed the COD results are within the design limitation . Excluding the API and DAF units in June where the minimum concentration were over the minimum design limits which lead to low COD removal of 9.8% and 4.4% .The COD concentrations in the final effluent ranged between 8 mg/l to 68 mg/l , that were below the Iraqi limitations of 120 mg/l .The plant had an average COD removal of 86.2%. .

Nitrogen and Phosphorous

The results of the conducted tests are plotted in figures (7 and 10) at different treatment stages , to show their fluctuations throughout the stages of treatment no design values for the internal stages were found , but only for influent and effluent from the whole treatment plant.The results indicate the degradation of NH_3 and PO_4 concentrations through the API and DAF units . But the increase in NH_3 and PO_4 concentration in the aeration tank were related to the high amounts of Urea and Phosphoric acid added in this tank as a source of nutrients . Generally , these amounts are governed by the rule of :-
100%BOD_5 : 5% Nitrogen : 1% Phosphorous . by Bush , (1980) . However , the proportions of these nutrients added in the Dora refinery wastewater aeration tank were 100% BOD_5 : 10% Nitrogen : 1% Phosphorous. The concentrations decreased in the effluent from the final settling

tank with respect to the aeration tank . The concentrations of NH_3 in most of the samples were high compared with the design limitations of 0.3 mg/l . According to Concawe limitations of 0.5 mg/l for final disposal , samples 8 and 9 showed high NH_3 concentration of 1.62 mg/l and 1.7 mg/l respectively . For PO_4 concentrations all samples of the final

effluent were low compared with the Iraqi limitations. The overall removal for NH_3 was 58.4% and 20.9% for PO_4 .

Sulfide & Sulfate

Figures (8 & 9) showed The concentration of sulfide decreased through the treatment processes , but it was difficult to evaluate the efficiency of each unit due no design

limitations. The final effluent was low in sulfide concentrations (less than 0.3 mg/l) for all of the tested samples . A high removal efficiency was observed that reached 99.2% in May . The average removal was calculated to be 85.2% . Also no design limitations were provided for sulfate removal in the treatment units . According to the Iraqi limitations for disposal , the sulfate concentration in the effluent should be (+ 1%) of the inlet . This is due to the sulfate production from the degradation of the organic matter in the treatment units . Another increase in sulfate concentration is from the oxidation of thiosulfate in the chemical addition tank .Figure (19) show the concentrations of the discharged (Sulfides) to the Tigris River , during the sampling period .The results were plotted against the English standards discharged concentrations of (Sulfide) , since no Iraqi (Sulfide) limitations exist .
Figure (20) show the (Sulfate) effluent concentrations discharged to the Tigris river . The concentrations range between 122 mg/l to 400 mg/l .

Phenols

The results indicated that the concentrations of phenol in the wastewater treatment plant for most samples tested were higher than the designed limits of Dora refinery wastewater treatment plant.The effluents from API and DAF contain phenol concentrations more than the design limitations of 0.74 mg/l and 0.72 mg/l respectively as shown in fig.(11).This may related to the in – plant treatment that was not practiced in a proper way, for separating phenol from the waste of the units which deal with phenols such as (light petroleum oil units).The decrease in phenol was observed in the aeration tank for all the samples tested and was less than 0.1 mg/l . The final effluent discharged to the river was low in phenol only for one sample tested in June which contained 0.06 mg/l compared with the Iraqi limitation 0.05 mg/l .Figure (22) show the concentrations of discharged phenols to the Tigris river .The treatment plant was efficient in phenol removal that reached to an average of 97.7% .

Table (2)-(A): ITEM NAME :-(T.S.S.)Measurements													Table(2)-(B):- Measurements Analyses					
Sample set no.	1	2	3	4	5	6	7	8	9	10	11	12						
date of experiments	14-5	28-5	05-6	25-6	02-7	23-7	13-8	28-8	05-9	27-9	9-10	17-10	ST. DEV.	Aver. Actual	Min. Actual	Max. Actual	Min. Design	Max. Design
Sample Location																		
A-Inlet	171	175	182	198	239	237	225	185	216	198	215	188	23.54	202.42	171	239		
B-API-eff-P10	14.7	20.4	22.6	32.6	34.5	34.6	20	19	21.2	16.6	28.6	23.8	6.89	24.05	14.7	34.6	500	1000
C-new API-eff-P29	12.8	18.2	15.7	21.7	22.3	27.4	11.8	11.8	15.6	8.2	15.2	N.P	5.59	16.43	8.2	27.4	50	100
D-DAF-S09	12.3	7.8	8.2	10.3	11.5	13.1	21.2	21.4	13.2	13.6	13.9	N.P	4.45	13.32	7.8	21.4	20	30
E-Bio. Treat.-S10	1482	1520	1430	3000	3700	2000	3100	3270	3340	3220	2550	2640	806.23	2604.33	1430	3700	2800	4000
F-final dis.-P18	15.8	7.8	8.3	5.5	7.8	10	9.2	7.4	9.06	9.4	14.4	9.4	2.89	9.51	5.5	15.8		10

Table (2)-(C):- (T.S.S) units percentage removal

Sample date	14-5	28-5	5-6	25-5	2-7	23-7	13-8	28-8	5-9	27-9	9-10	17-10	ST.DEV.	Average
R1%	91.4%	88.3%	87.6%	83.5%	85.6%	85.4%	91.1%	89.7%	90.2%	91.6%	86.7%	87.3%	0.03	88.2%
R2%	12.9%	10.8%	30.5%	33.4%	35.4%	20.8%	41.0%	37.9%	26.4%	50.6%	46.9%	N.P	0.23	37.2%
R3%	3.9%	57.1%	47.8%	52.5%	48.4%	52.2%	*******	*******	15.4%	*******	8.6%	N.P	*******	*******
R4%	*******	*******	*******	*******	*******	*******	*******	*******	*******	*******	*******	*******	*******	*******
R5%	98.9%	99.5%	99.4%	99.8%	99.8%	99.5%	99.7%	99.8%	99.7%	99.7%	99.4%	99.6%	0.00	99.6%
Ro%	90.8%	95.5%	95.4%	97.2%	96.7%	95.8%	95.9%	96.0%	95.8%	95.3%	93.3%	95%	0.02	95.2%

Where:-R1=eff. Of old API , R2=eff. Of new API , R3=eff. Of DAF unit , R4=eff. Of aeration tank , R5=eff. Of final clarifier, Ro=eff. Of overall treatment plant

********= Negative value**

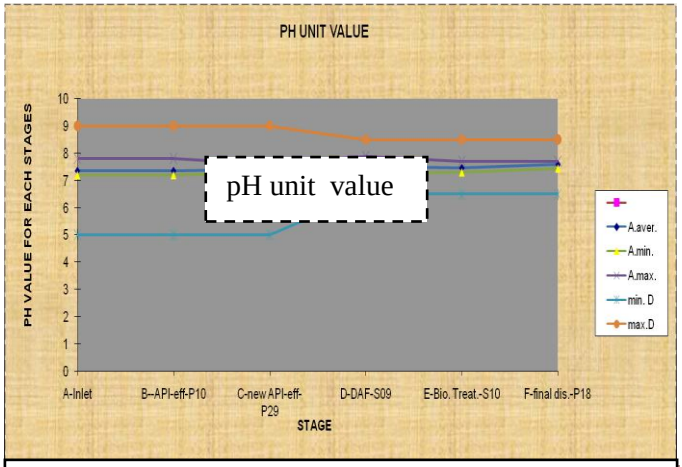

Figure (2): Existing practical and the Designed of (pH) value through stages of the Dora Refinery Wastewater Treatment Plant.

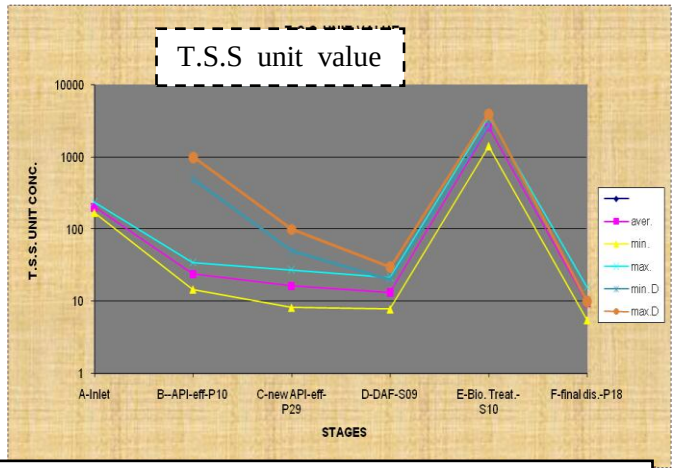

Figure (3): Existing practical and the Designed of (T.S.S.) Concentrations through stages of Dora Refinery Wastewater Treatment Plant.

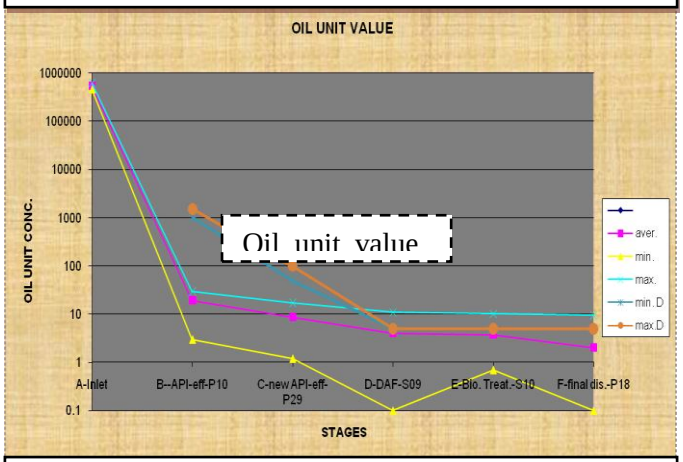

Figure (4): Existing practical and the Designed of (Oil) Concentrations through stages of Dora Refinery Wastewater Treatment Plant.

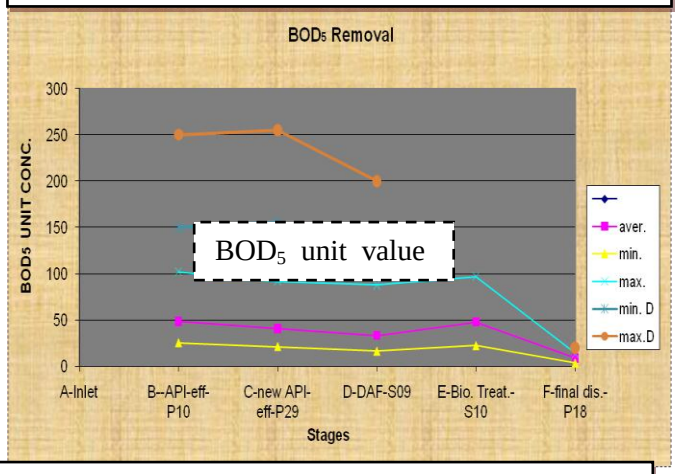

Figure (5): Existing practical and the Designed of (BOD_5) Concentrations through stages of Dora Refinery Wastewater Treatment Plant.

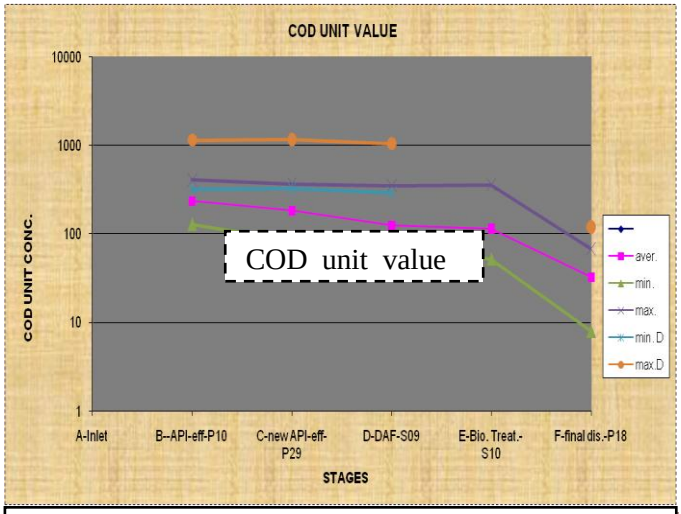

Figure (6): Existing practical and the Designed of (COD) Concentrations through stages of Dora Refinery Wastewater Treatment Plant.

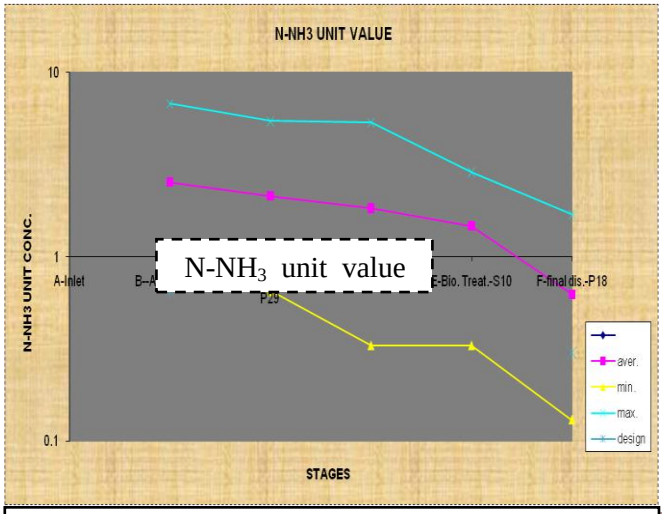

Figure (7): Existing practical and the Designed of ($N\text{-}NH_3$) Concentrations through stages of Dora Refinery Wastewater Treatment Plant.

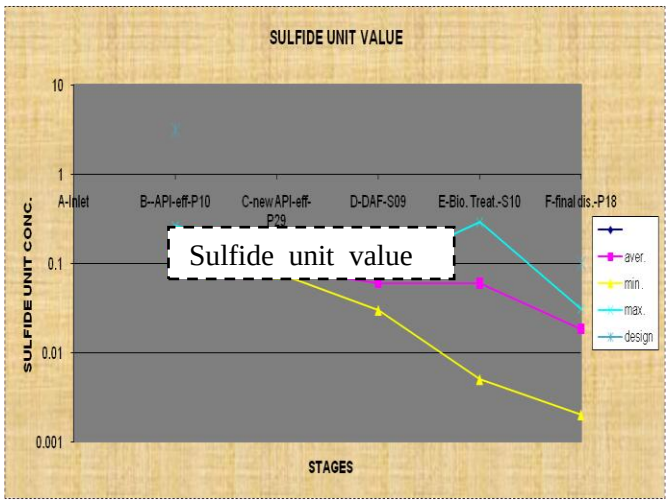

Figure (8): Existing practical and the Designed of (Sulfide) Concentrations through stages of Dora Refinery Wastewater Treatment Plant.

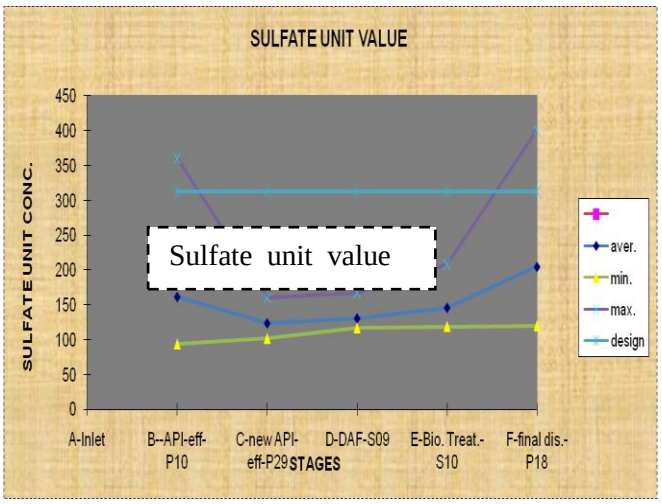

Figure (9): Existing practical and the Designed of (Sulfate) Concentrations through stages of Dora Refinery Wastewater Treatment Plant.

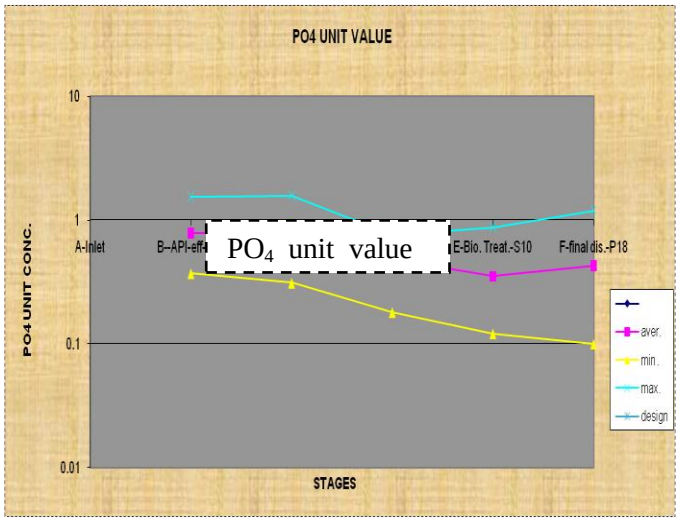

Figure (10): Existing practical and the Designed of (phosphorus) Concentrations through stages of Dora Refinery Wastewater Treatment Plant.

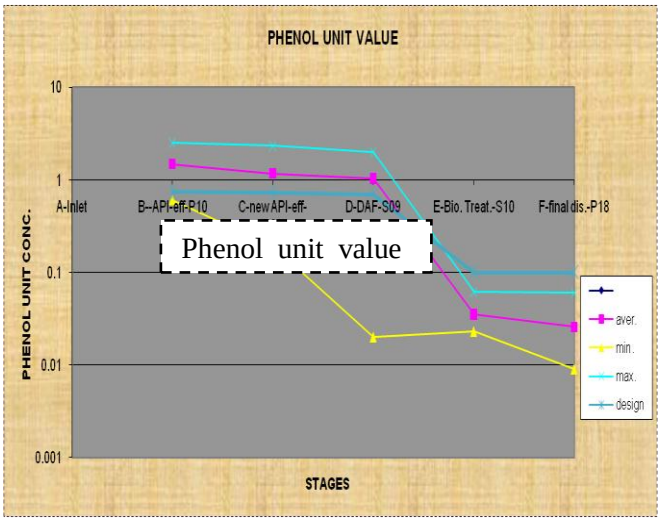

Figure (11): Existing practical and the Designed of (Phenol) Concentrations through stages of Dora Refinery Wastewater Treatment Plant.

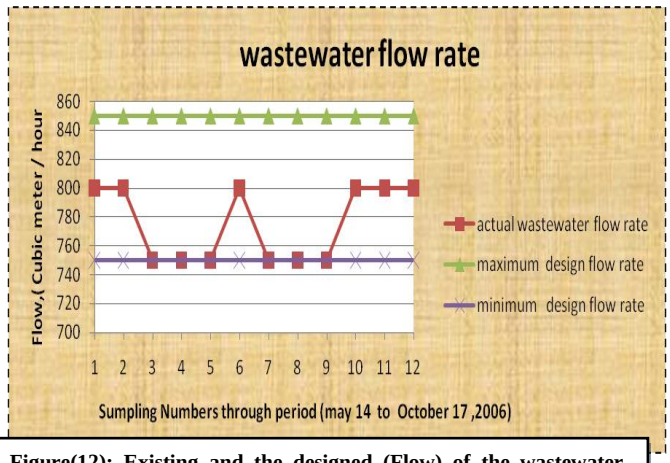

Figure(12): Existing and the designed (Flow) of the wastewater in the Dora Refinery Wastewater Treatment Plant during the sampling period .

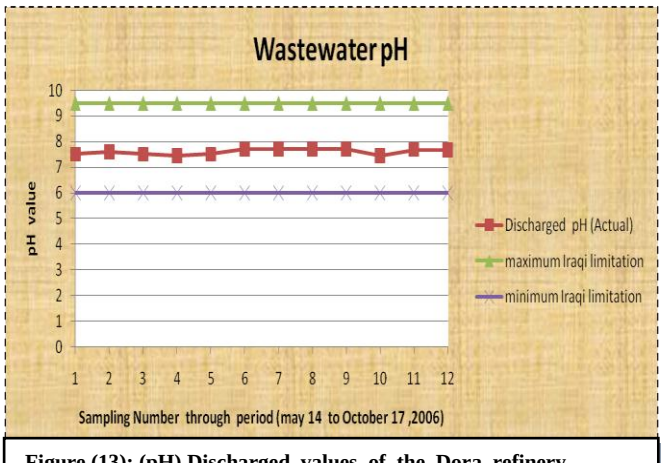

Figure (13): (pH) Discharged values of the Dora refinery wastewater treatment plant during the sampling period compared with the Iraqi Limitations .

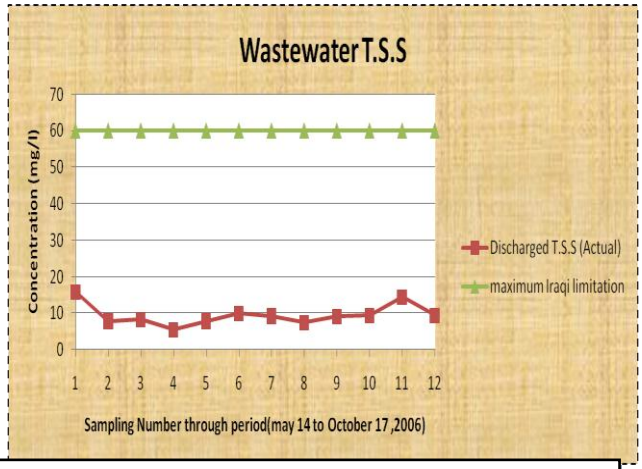

Figure (14) : (T.S.S.) Discharged Concentrations of The Dora Refinery Wastewater Treatment Plant during the sampling period compared with Iraqi discharge water Limitation .

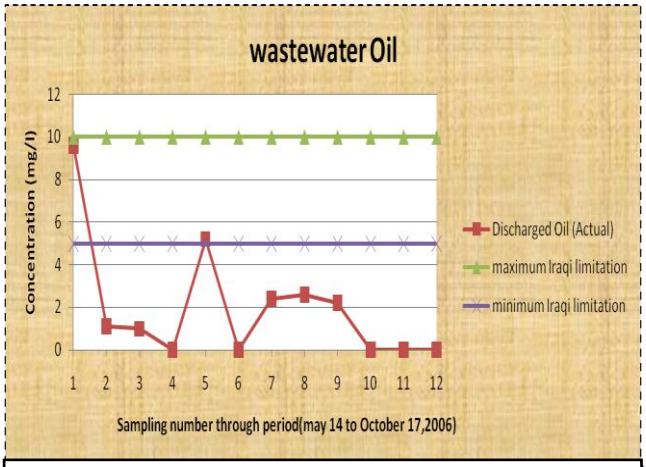

Figure (15) : (Oil) Discharged Concentrations of the Dora Refinery Wastewater Treatment Plant during the sampling period compared with Iraqi discharge water Limitations .

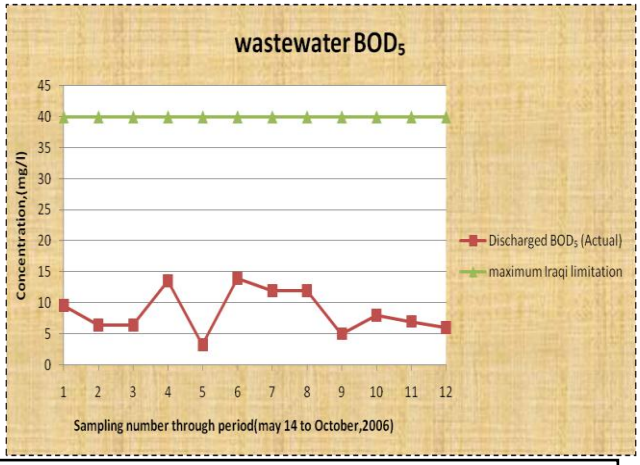

Figure (16) : (BOD_5) Discharged Concentrations of the Dora Refinery Wastewater Treatment Plant during the sampling period compared with Iraqi discharge water Limitations .

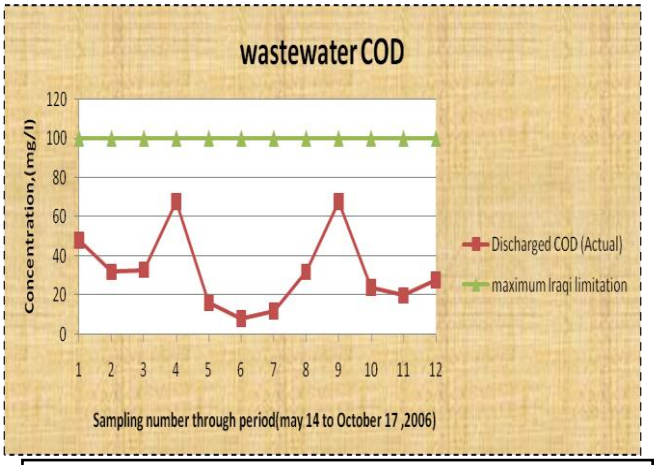

Figure(17) : (COD) Discharged Concentrations of the Dora Refinery Wastewater Treatment Plant during the sampling period compared with Iraqi discharge water Limitations .

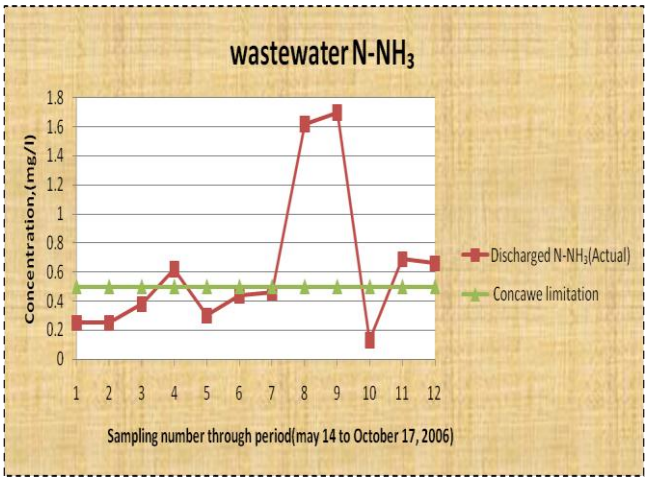

Fig.(18) : ($(N\text{-}NH_3)$ Discharged concentrations of the Dora refinery wastewater treatment plant during the sampling period compared with (Concawe) discharge water limitations .

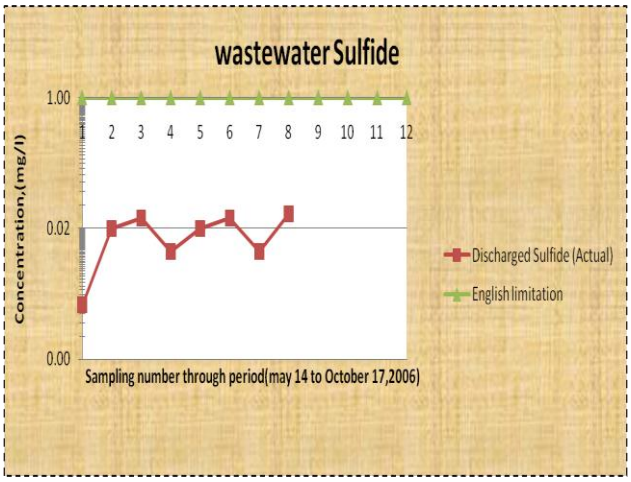

Fig.(19) : (Sulfide) Discharged concentrations of the Dora refinery wastewater treatment plant during the sampling period compared with (English) discharge water Limitations

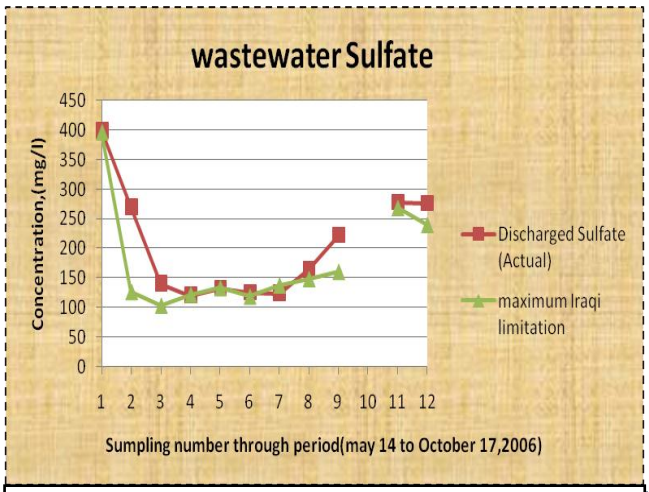

Figure(20) : (Sulfate) Discharged Concentrations of the Dora Refinery Wastewater Treatment Plant during the sampling period compared with Iraqi discharge water Limitations .

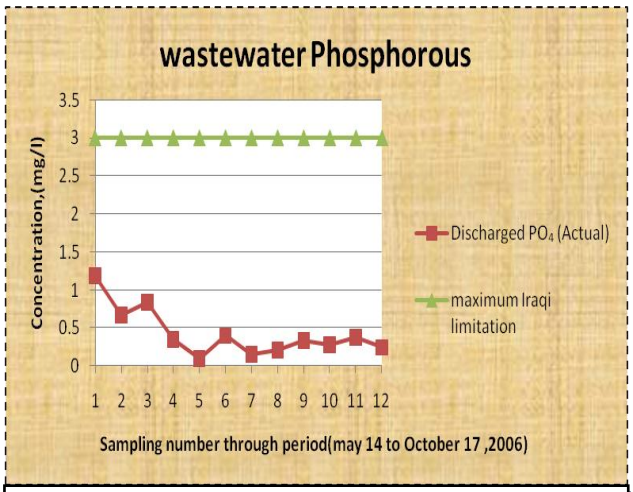

Fig.(21) : (PO_4) Discharged Concentrations of the Dora Refinery Wastewater Treatment Plant during the sampling period compared with Iraqi discharge water Limitations .

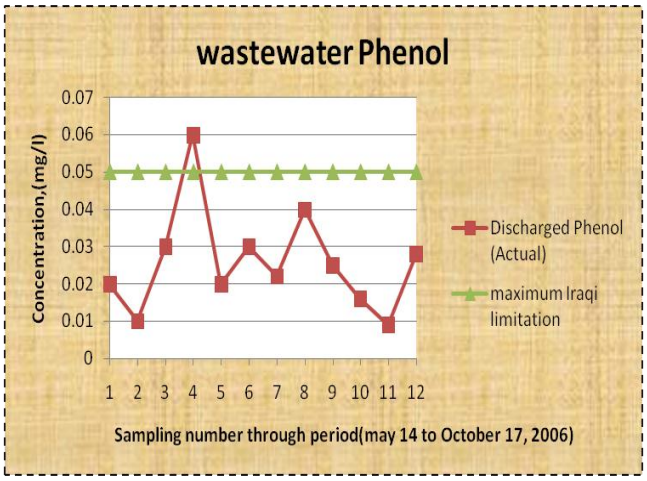

Figure (22) : (Phenol) Discharged Concentrations of the Dora Refinery Wastewater Treatment Plant during the sampling period compared with Iraqi discharge water Limitations .

CONCLUSIONS AND RECOMMENDATIONS

Conclusions

From the study of the conditions of the Dora refinery wastewater treatment plant and its final effluent discharged to the Tigris River , the following conclusions could be drawn :-

1- The influent of the treatment plant is of high diversity , in both quality and quantity , due to the fact of having a single collection system of wastewater from :different processing units of the refinery, rain water runoff , and domestic sewage wide fluctuations in the performance of the Dora refinery wastewater treatment plant were detected and can be related operational problems .

2- The performance or the API separators effects the malfunctioning in the downstream units . The API was high in oil and suspended solid removal which was reflected on the final effluent.
3- The (DAF) unit faced operational problems.Caused by, first the low air pressure to form the desired air bubble size . Second not recycling it's effluent for the formulation of the required polymer for emulsion.
4- The performance of aeration tank in regard to the removal of dissolved organics and chemical compounds was good . This is due to the good aeration process .
5- The large amounts of Urea and phosphoric acid being added to the aeration tank is believed to be the reason of the relatively high concentrations of dissolved ammonia (NH_3) and PO_4 discharged to the Tigris River.
6- The reuse or recycling some of the refinery effluents are not practiced in the Dora refinery wastewater treatment plant .
7- The treatment of sludge was practiced by adding chemical material (CaO)with steam and continuous agitation in order to change the sludge From a hazard waste to an environment friendly material.
8- In general high removal efficiencies were obtained for T.S.S , oil , COD ,BOD , Sulfide and phenol , which were 95% , 88% , 86% , 81% , 85% And 97% respectively. And the plant was not very efficient in NH_3,SO_4 and PO_4 removal.
9-The annual percentage removal of sulfide , oil ,COD ,BOD and T.S.S.,were found acceptable except for the T.S.S. value which shows relatively low removal percent 67.58% .
10-The monthly percentage removal of sulfide , oil , COD , BOD and T.S.S. shows considerable changes among different months of the years ,which may reflect considerable variation in influent water properties and treatment process.

Recommendations

1- The in- plant treatments are believed to be essential, i.e , treatment after each production unit before sending the wastewater to the sewer system .These treatments include (source reduction , reuse , recycling & recovery) .

2-Dilution of the strong influent with the less contaminated waste streams before treatment is highly recommended. This is to ensure the equalization and the utmost efficiency of the plant.
3- The separation of the different wastes reaching the inlet pit . Domestic sewage and storm water should be disposed to the main city sewer system either as in a combined or separate systems . The wastes from the processing units in the refinery should only reach the treatment plant for proper treatment.
4- The performance of the DAF unit can be improved by :-
A- using high pressure this will help for better saturation of air in water .
B- recycling of the effluent for better polymer formation .

5- Installation of interface Oil / water level indicators in the three Oil separators where Oil layer at the surface is thick, in order to improve the separation of oil and grease from the water - grease mixture and reduce the pollution of wastewater with petroleum waste.
6- Adding the proper quantities of Urea to the aeration tank will decrease the levels of the dissolved ammonia (NH_3) in the final effluents discharged to the Tigris river.
7- Installation of flow meters in the wastewater treatment plant is essential to control the addition of chemicals at different flow rates.

8- Environmental awareness and up to date operational courses are recommended to be conducted for staff members. These courses will outline the environmental impact of refinery effluents and the refineries commitment to water quality improvements.

REFERENCES

*-Askew , M.W. , Tapley , S.A., Killic , R.A. ,"Some aspects of upgrading of environmental quality standards for a refinery expansion", Proceedings of the symposium on "Protection of the environment from petroleum industry pollution",Tunis:12-15,September,PP. (365) (1982).

*-" Operations Manual for , Dora Oil refinery wastewater treatment plant".(1980).

*- Beychok , Milton R. " Aquous wastes from Petroleum and Petrochemical plants . London : John Wily &Sons 225-236. (1967).

*-Bush , K.E. , " Refinery wastewater treatment and reuse " , Chemical Engineering Magazine , PP. (13) (1980) .

*- Choong Hee Rhee , Senior Engineer Paul C. Martyn , Supervising Civil Engineer Jay G. Kremer , Head , Industrial waste section " Removal of Oil and grease in Oil processing wastewaters ".(1989).

*- Christensen , E.R. , and Plaumann , K.W. , " Waste reuse : Ultrafilteration of Industrial and municipal wastewaters ", Journal of WPCF , Vol.53 , No.7 July , PP. (1206) (1981) .

*- Cobb , C.E. ," Refinery effluents ", Oily water discharges , regulatory , technical & scientific considerations , by Johnston and Morris , Applied science publishers(1980) .

*- Egyptian Environmental Affairs Agency (EEAA) &Egyptian Pollution Abatement Project (EPAP) ," Industrial wastewater treatment plants inspection procedures manual", May ,(2002).

*- Emerson process management, "Petroleum Refining Industry- API Separators",Application Data Sheet.August , (2004).

*- Engineering Standard, "Process Design of plant solid waste treatment and Disposal systems ", Original Edition . Dec., (1997) .

*- Exploration and Production (E&P), " Waste management Guidelines " , Report No.2.58/196. Sep. , (1993).

*- General Standard for ," Disposal of Solid waste "Original Edition , Dec. (1997) updated on (2004).

*- Gehr , R. , and Henry , J.G. , " Measuring and predicting floatation performance ", Journal of WPCF , Feb. , PP. (203). (1978).

*-Huber , L.," The environmental impact of refinery effluents " CONCAWE report No. 5/79 (1979) .

*-Ingersoll , A.C., " Fundamentals and performance of gravity separators " , Petroleum refinery , Vol. 30 , No.6 , June , PP. (106) (1951).

*- King , N., " Oil and the Paris convention – the U.K. view",Oily water discharges , regulatory , technical & scientific considerations , by Johnston & Morris, Applied science publishers , page (19) (1980).

*-Kuriakose , A.P. , and Manjooran , K.B. " Bituminous paints from refinery sludge " , Surface and Coatings Technology , 145 : 132 – 138 (2001).

*- Manning , Francis S. and Eric H. Snider, "Assessment Data Base for petroleum refining wastewater and residue ",Washington: U.S. Department of Commerce, NTIS, feb.(1983),94-101 .

*- Patterson , James W." Industrial wastewater treatment technology " , Stoneham , MA: Butterworth Publishers , Inc. , Second Edition , p. (273) & (277-281) (1985) .

*-Rohlich , G.A. , " Application of air flotation to refinery wastewater " , Industrial & Engineering Chemistry , Vol. 46 , No. 2 , Feb. , PP. (304) (1954).

*- " Standard Methods for the examination of water & wastewater ".(1985 ,1988 and 1990).

*- World Bank Group, "Pollution Prevention and Abatement Hanbook : Petroleum refining", Environment Departement , Washington , D.C. Effective , July (1998).

*- WRC, (Water Research Commission), " Operation manual for Biological Nutrient Removal Wastewater treatment Works ". Report No. TT 83/97, Pretoria , South Africa (1997) .

*- Xian Lie , L. , " Wastewater treating at Lanzhou ",Hydrocarbon processing , Vol. 64 ,No. 6 , June , PP. (78) (1985) .

USING FUZZY LOGIC CONTROLLER FOR A TWO- TANK LEVEL CONTROL SYSTEM

Omar W. Abdul-Wahab

ABSTRACT
This paper presents a fuzzy logic controller for a two-tank level control system, which is a process with a dead time. The fuzzy controller is a proportional-integral (PI-like) fuzzy controller which is suitable for steady state behavior of the system. Transient behavior of the system was improved without the need for a derivative action by suitable change in the rule base of the controller. Simulation results showed the step response of the two-tank level control system when this controller was used to control this plant and the effect of the dead time on the response of the system.

الخلاصة

هذا البحث يقدم مسيطرمنطق ضبابي للسيطرة على نظام مستوى الماء في خزانين. المسيطر الضبابي هو مسيطر تناسبي- تكاملي والذي يكون مناسباً لسلوك النظام في الحالة المستقرة. أما فيما يخص سلوك الحالة الإنتقالية للنظام فقد تم تحسينه دون الحاجة إلى التأثير التفاضلي وذلك بواسطة إجراء تغيير مناسب في قاعدة بيانات المسيطر. النتائج التمثيلية بينت استجابة نظام الخزانين لإشارة الإدخال بإستخدام هذا المسيطر وكذلك بينت تأثير زمن التأخير على تلك الاستجابة.

KEYWORDS
PI-like fuzzy logic controller, two-tank level control system.

INTRODUCTION
The vast majority of conventional control techniques have been devised for linear-time invariant systems which are assumed to be completely known and well understood. In most practical instances, however, the systems to be controlled are nonlinear and the basic physical processes in it are not completely known a prior. These types of model uncertainties are extremely difficult to manage even with the conventional adaptive techniques (Abonyi, Nagy, and Szeifert 2005).

The past few years have witnessed a rapid growth in the use of fuzzy logic controllers for the control of processes that are complex and badly defined. Most fuzzy controllers developed till now have been of rule-based type (Driankov, Hellendoorn, and Reinfrank 1996), where the rules in the controller attempt to model the operator’s response to particular process situations. An alternative approach uses fuzzy or inverse fuzzy model in process control (Babuska, Sousa, and Verbruggen

1995) because it is often much easier to obtain information on how a process responds to particular inputs than to record how, and why, an operator responds to particular situations.

In recent applications, many authors started applying more sophisticated fuzzy logic controller structures in sake of a more robust fuzzy logic controller and overcoming some of the difficulties associated with fuzzy logic controller design, in general. Self organizing (Sutton and Jess 1991), self tuning (Isomursu and Rauma 1994) and adaptive (Pave and Chelaru 1992) (Fei and Isik 1992) fuzzy logic controllers have become very popular. Some of the tuning methods assume an existence of the initial fuzzy logic controller model and the availability of the plant model. However, most of the late design methods do not require any plant model at all (Ghanayem, and Reznik 1996).

THE STRUCTURE OF THE PI-LIKE FUZZY LOGIC CONTROLLER

In practice, full PID control sometimes is not desired. Instead, partial PID control in the form of PI or PD control is more effective and appropriate. This is because the derivative term tends to amplify noise and hence should be avoided if the system output is rather noisy. On the other hand, the integral term can cause slower system response and larger system overshoot (Ying 2000). PI-like fuzzy controller is known to be more practical than PD-like fuzzy controller because it is difficult for the latter to remove steady state error (Karasakal, Yesil, Guzelkaya and Eksin 2005). An equation giving a conventional PI-controller is

$$u(t) = K_P \times e(t) + K_I \times \int e(t)\,dt \tag{1}$$

where K_P and K_I are the proportional and integral gain coefficients, respectively. Differentiating Eq. (1) with respect to t yields

$$\frac{du(t)}{dt} = K_P \times \frac{de(t)}{dt} + K_I \times e(t) \tag{2}$$

The corresponding discrete-time form is

$$\Delta u(kT) = K_P \times \Delta e(kT) + K_I \times e(kT) \tag{3}$$

where T is the sampling interval.

For the PI-like fuzzy controller, the inputs are the error $e(kT)$ and the change-of-error $\Delta e(kT)$ and the output is the change-of-control $\Delta u(kT)$. To obtain the control output variable $u(kT)$, the change-of-control output $\Delta u(kT)$ is added to $u((k-1)T)$. This takes place outside the fuzzy controller and is not reflected in its rule base. A block diagram of this controller is given in **Fig. (1).**

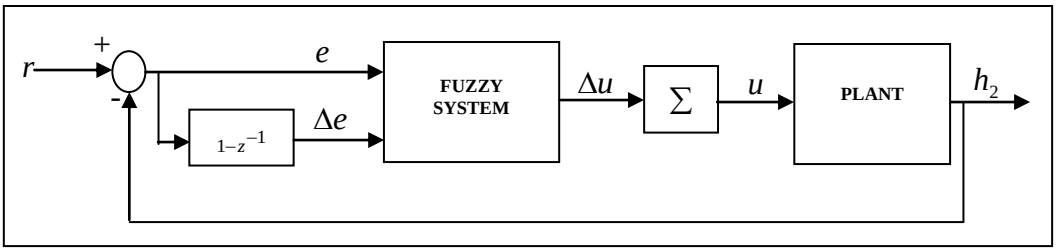

Fig (1): Block diagram of the PI-like fuzzy logic controller.

FUZZIFICATION

This controller uses singleton fuzzification method. The reason is that when singleton fuzzification is used, combining the inputs with rule premises is reduced to computing the values of the input membership functions at the current input values. Other fuzzification methods add computational

complexity to the inference process and the need for them has not been well justified. (Passino and Yurkovich 1998).

KNOWLEDGE BASE

The knowledge base of the fuzzy logic controller consists of the following parameters:

Membership Functions

For each input variable ($e(kT)$ and $\Delta e(kT)$), five fuzzy sets have been used. They are Negative Large (NL), Negative Small (NS), Zero (Z), Positive Small (PS), and Positive Large (PL). The membership function of each fuzzy set is triangular with width 2 and overlapped with the two adjacent membership functions by 0.5. The outermost two membership functions (μ_{NL} and μ_{PL}) are saturated. The equations of the three input membership functions $\mu_{NS}, \mu_Z, \mu_{PS}$ are

$$\mu_i(x) = \begin{cases} 1 - \dfrac{|x-c|}{0.5} & \text{if } c-0.5 \le x \le c+0.5 \\ 0 & \text{otherwise} \end{cases} \tag{4}$$

where $i = NS, Z, PS$, $x = e(kT), \Delta e(kT)$ and c is the center of the input membership function. The equations of the outermost membership functions μ_{NL} and μ_{PL} are

$$\mu_{NL}(x) = \begin{cases} 1 & \text{if} \quad x < -1 \\ 1 - \dfrac{x+1}{0.5} & \text{if} \quad -1 \le x \le -0.5 \\ 0 & \text{if} \quad x > -0.5 \end{cases} \qquad \mu_{PL}(x) = \begin{cases} 0 & \text{if} \quad x < 0.5 \\ 1 - \dfrac{1-x}{0.5} & \text{if} \quad 0.5 \le x \le 1 \\ 1 & \text{if} \quad x > 1 \end{cases} \tag{5}$$

For the output variable $\Delta u(kT)$, the same fuzzy sets were used with the same membership functions. The only difference is that the outermost two membership functions (μ_{NL} and μ_{PL}) are not saturated. The equations of the output membership functions are

$$\mu_i(\Delta u(kT)) = \begin{cases} 1 - \dfrac{|\Delta u(kT) - c|}{0.5} & \text{if } c-0.5 \le x \le c+0.5 \\ 0 & \text{otherwise} \end{cases} \tag{6}$$

where $i = NL, NS, Z, PS, PL$ and c is the center of the output membership function.

The input and output membership functions are shown in **Fig. (2).**

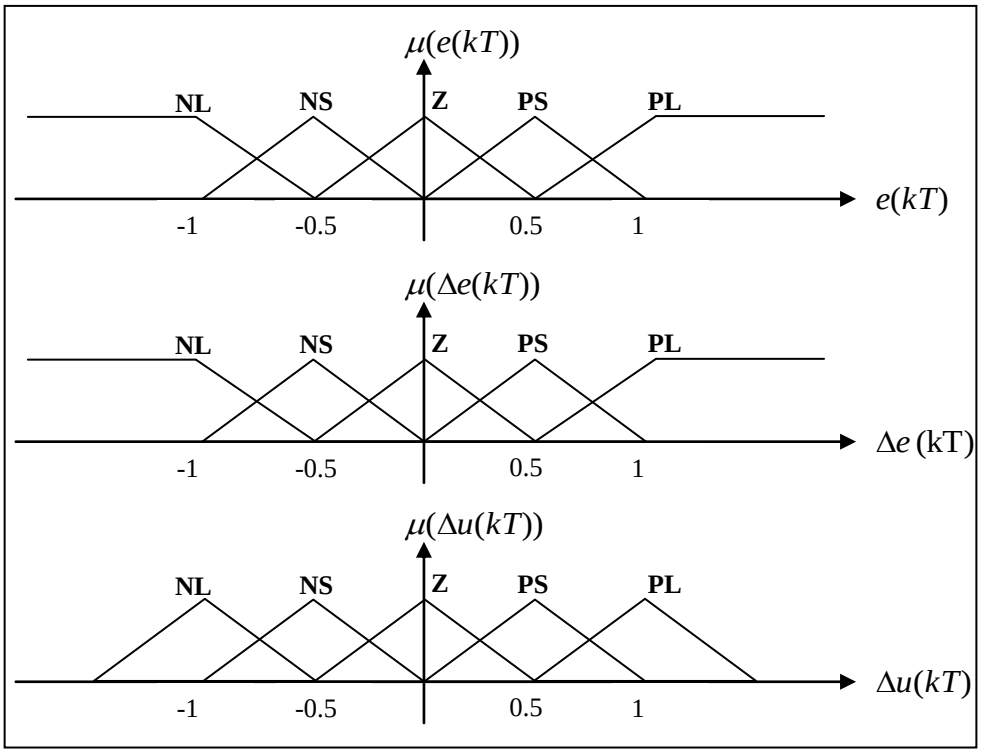

Fig (2): The input and output membership functions.

Scaling Factors

According to Eq. (3), the input scaling factors are K_P (for $\Delta e(kT)$) and K_I (for $e(kT)$). $\Delta u(kT)$ is multiplied by the output scaling factor $K_{\Delta u}$. Different values for the input scaling factors were used in the simulation to show their effect on the sensitivity of the controller with respect to the optimal choice of the operating areas of the input signals. Also different values for the output scaling factor were used to show their effect on the stability and oscillation of the system (Reznik 1997).

RULE BASE

Since the inputs of the PI-like fuzzy controller are the error $e(kT)$ and the change-of-error $\Delta e(kT)$, a standard PD-like fuzzy controller rule base was used. To form the rule base, each fuzzy set was given an index. The indices of the fuzzy sets NL, NS, Z, PS, PL are 0,1,2,3, and 4, respectively. The rule base was generated according to the following equation:

$$Rule(i,j) = \begin{cases} 0 & \text{if} \quad i+j-2 \le 0 \\ i+j-2 & \text{if} \quad 0 \le i+j-2 \le 4 \\ 4 & \text{if} \quad 4 \le i+j-2 \end{cases} \tag{7}$$

where i and j are the indices of the input membership functions and $Rule(i,j)$ is the index of the output membership function. The resultant rule base is shown in **Table (1)**.

Table (1): Rule base of a standard PD-like fuzzy controller.

$\Delta e(kT)$

$e(kT)$	NL	NS	Z	PS	PL
NL	NL	NL	NL	NS	Z
NS	NL	NL	NS	Z	PS
Z	NL	NS	Z	PS	PL
PS	NS	Z	PS	PL	PL
PL	Z	PS	PL	PL	PL

Because of the absence of the derivative action in this fuzzy controller (since the overall action of this controller after integrating the output of the fuzzy system is a PI-like fuzzy controller), an overshoot (or undershoot) may occur at some operating points. To solve this problem, the rule base can be modified so that when the output of the plant moves towards the set point and becomes near it, a reverse action is given for the change-of-control output. This is done by replacing the rule (IF $e(kT)$ is PS and $\Delta e(kT)$ is NS THEN $\Delta u(kT)$ is Z) with the rule (IF $e(kT)$ is PS and $\Delta e(kT)$ is NS THEN $\Delta u(kT)$ is NS) (to reduce overshoot) and replacing the rule (IF $e(kT)$ is NS and $\Delta e(kT)$ is PS THEN $\Delta u(kT)$ is Z) with the rule (IF $e(kT)$ is NS and $\Delta e(kT)$ is PS THEN $\Delta u(kT)$ is PS) (to reduce undershoot). The modified rule base is shown in **Table (2)**.

Table (2): The modified rule base.

$\Delta e(kT)$

$e(kT)$	NL	NS	Z	PS	PL
NL	NL	NL	NL	NS	Z
NS	NL	NL	NS	**PS**	PS
Z	NL	NS	Z	PS	PL
PS	NS	**NS**	PS	PL	PL
PL	Z	PS	PL	PL	PL

INFERENCE ENGINE

The inference step is taken by computing, for each rule, the implied fuzzy set. This is done by clipping the membership function of the consequent part of each rule according to the following equation:

$$\mu_{\text{implied}(i,j)}(\Delta u(kT)) = \mu_{\text{premice}(i,j)}(e(kT), \Delta e(kT)) * \mu_{\text{consequent}(i,j)}(\Delta u(kT)) \tag{8}$$

where $\mu_{\text{implied}(i,j)}(\Delta u(kT))$ is the membership value for the implied fuzzy set of rule (i, j), $\mu_{\text{premice}(i,j)}(e(kT), \Delta e(kT))$ is the membership value for the premise of rule (i, j) which represents the certainty that rule (i, j) holds for the given inputs, and $\mu_{\text{consequent}(i,j)}(\Delta u(kT))$ is the membership function for the consequent part of rule (i, j). By using the minimum operation as a t-norm for the intersection operation, $\mu_{\text{consequent}(i,j)}(\Delta u(kT))$ is clipped to produce $\mu_{\text{implied}(i,j)}(\Delta u(kT))$.

DEFUZZIFICATION

Since the inference step is done by computing the implied fuzzy set for each rule, center of gravity defuzzification technique was used to compute the final controller output $\Delta u(kT)$ (Passino and Yurkovich 1998).

$$\Delta u(kT) = \frac{\sum_{i=0}^{4}\sum_{j=0}^{4} center\,(Rule(i,j)) \times Area(\mu_{\text{implied}(i,j)}(\Delta u(kT)))}{\sum_{i=0}^{4}\sum_{j=0}^{4} Area(\mu_{\text{implied}(i,j)}(\Delta u(kT)))} \tag{9}$$

TWO-TANK LEVEL CONTROL SYSTEM

The two-tank level control system is shown in **Fig. (3)**. The fuzzy logic controller has to keep a constant level in the second tank. The system is nonlinear with a dead time, so it is not easy to design a conventional controller. Let the levels in tank 1 and tank 2 be h_1 and h_2, respectively, the cross-sectional areas be D_1 and D_2, and the cross-sectional areas of each pipe be A_1 and A_2. L corresponds to the dead time. Then the plant model can be described with the following equations (Reznik 1997):

$$\begin{aligned} \dot{h}_1(t) &= \frac{q_1(t-L) - q_2(t)}{D_1} \\ q_2(t) &= A_1\sqrt{2gh_1(t)} \\ \dot{h}_2(t) &= \frac{q_2(t) - q_3(t)}{D_2} \\ q_3(t) &= A_2\sqrt{2gh_2(t)} \end{aligned} \tag{10}$$

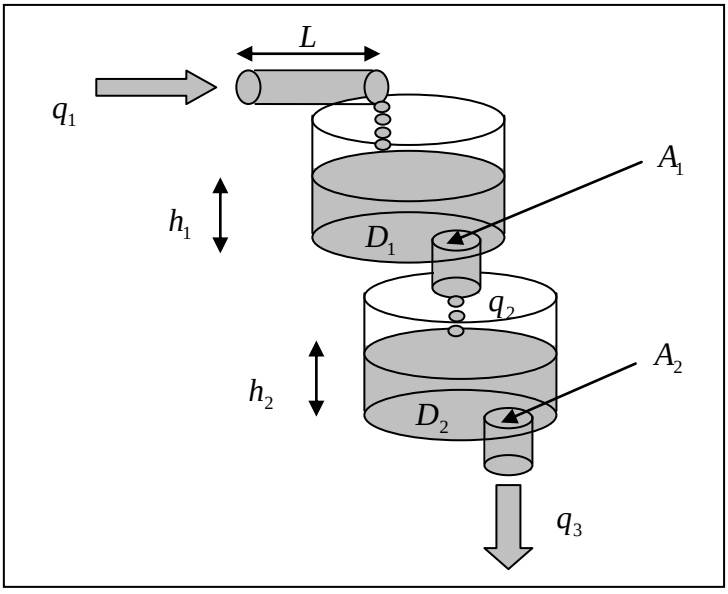

Fig (3): The two-tank level control system.

SIMULATION RESULTS

The simulation of the two-tank system needs to find the corresponding discrete-time form of Eqs (10). Euler method was used to approximate the differential equations in Eqs. (10) (i.e., the first and third equations) (Astrom and Wittenmark 1997) and (Severance 2001). The result is the following difference equations:

$$
\begin{aligned}
h_1((k+1)h) &= h_1(kh) + h \times \frac{q_1(kh-L) - q_2(kh)}{D_1} \\
q_2(kh) &= A_1\sqrt{2gh_1(kh)} \\
h_2((k+1)h) &= h_2(kh) + h \times \frac{q_2(kh) - q_3(kh)}{D_2} \\
q_3(kh) &= A_2\sqrt{2gh_2(kh)}
\end{aligned}
\tag{11}
$$

where h is the integration step size. The values of the parameters in Eqs (11) were taken as follows:

$L = 0.4\,\text{sec}$, $g = 9.8\,{}^{m}\!/_{\text{sec}^2}$, $A_1 = A_2 = 0.1\,m^2$, $D_1 = D_2 = 1\,m^2$, $h = 0.2\,\text{sec}$.

Initially, the levels in the two tanks were assumed to be 0 meters, i.e. , $h_1(0) = h_2(0) = 0\,m$.

For the controller to simulate the way that a digital control system would be implemented on a computer in the laboratory, the value of the sampling interval T must be an integer multiple of the integration step size h. In this simulation, $T = h = 0.2\,\text{sec}$.

Two Step Changes

The step response of the system has been investigated by applying two step changes to the reference input. The value of the reference input is

$$
r = \begin{cases} 2 & \text{when} \quad 0 \le kT < 100\,\text{sec} \\ 4 & \text{when} \quad 100 \le kT \le 200\,\text{sec} \end{cases}
$$

Table (1) was used for the rule base of the controller. **Fig. (4)** through **Fig. (10**) show the response of the system for different values of the scaling factors. The effect of the scaling factors on the overall response of the system is summarized in **Table (3)**.

Table (3): The effect of the scaling factors on the overall response of the system.

	Increasing K_I	Increasing K_P	Increasing $K_{\Delta u}$
Overshoot/Oscillation	Increases	Decreases	Increases
Speed of response	Increases	Decreases	Increases

Large Step Change and Overshoot

Fig (11) shows the step response of the system for a step change of 5 m. As shown, the response has an overshoot of about 5%. To reduce (or even eliminate) this overshoot, the modified rule base given by **Table (2)** was used. **Fig. (12)** shows the new step response. In both cases, the values of the scaling factors were: K_I =0.01, K_P =0.4, $K_{\Delta u}$ =1.

Effect of Dead Time Parameter *L* on the Response of the System

Processes with large dead times present a special challenge for a controller—**any** controller (http://www.expertune.com/artdt.html 2008). Dead time is the delay from when a controller output signal is issued until when the measured process variable first begins to respond. The presence of dead time is never a good thing in a control loop. For any process, as dead time becomes larger, the

control challenge becomes greater and tight performance becomes more difficult to achieve (http://www.controlguru.com/wp/p51.html 2008).

Fig. (13) shows the step response of the system for a step change of 5 m for different values of the dead time parameter L. These values are measured in seconds. This figure shows that increasing the dead time drives the system towards instability.

In each figure, the dotted line represents the reference input signal.

CONCLUSIONS

The simulation results showed that a PI-like fuzzy controller can stabilize the two-tank level control system which has a dead time with zero steady-state error. They show the effect of changing the input scaling factors on the sensitivity of the system and the effect of changing the output scaling factor on the stability and oscillation of the system. The overshoot and oscillation of the system were reduced or eliminated by a suitable change in the rule base that led to a change in the control surface so that the controller would become more reactive in the neighborhood of the set-point. Also the effect of the dead time on the response of the system was shown so that large dead time can make the system unstable.

REFERENCES

Abonyi J., Nagy L., and Szeifert F., “Adaptive Sugeno Fuzzy Control: A Case Study”, http://citeseer.ist.psu.edu/448436.html, 2005.

Astrom Karl J. and Bjorn Wittenmark, "Computer-Controlled Systems", Prentice-Hall, 1997.

Babuska R., Sousa J., and Verbruggen H. B., “Model-Based Design of Fuzzy Control Systems”. Proceedings of the EUFIT’95 837-841, 1995.

Driankov D., Hellendoorn H., and Reinfrank M., “An Introduction to Fuzzy Control”,Springer-Verlag,1996.

Fei J. and Isik C., “Adaptive Fuzzy Control Via Modification of Linguistic Variables”, IEEE International Conference on Fuzzy Systems, New York, USA, pp. 399-406, 1992.

Ghanayem O., and Reznik L., “A Universal Adaptation Procedure for Fuzzy Controller Design With The Application to Power System Stability Control”, Proceedings of the 35th Conference on Decision and Control, Kobe, Japan, 1996.

Isomursu P. and Rauma T, “A Self Tuning Fuzzy Logic Controller for Temperature Control of Superheated Steam”, Proceedings of the Third IEEE Conference on Fuzzy Systems, IEEE Word Congress on Computational Intelligence, New York, USA, vol 3, pp. 1560-1563, 1994.

Karasakal O., Yesil E., Guzelkaya M., Eksin I., " Implementation of a New Self-Tuning Fuzzy PID Controller on PLC, Turk J Elec Engin, VOL.13, NO.2, 2005.

Passino K. M. and Yurkovich S., “Fuzzy Control”, Addison Wesley, 1998.

Pave L. and Chelaru M., “Neural Fuzzy Architecture for Adaptive Control”, IEEE International Conference on Fuzzy Systems, pp. 1115-1122, New York, USA, 1992.

Reznik L., “Fuzzy Controllers”, Newnes, 1997.

Severance Frank L., "System Modelling and Simulation", John Wiley and Sons, Ltd, 2001.

Sutton R. and Jess I. M., “Real-Time Application of A Self Organizing Autopilot to Warship Taw Control”, IEEE International Conference in Control’91, pp. 827-832, Edinburgh, UK, March 1991.

Ying H., "Fuzzy Control And Modeling", Institute of Electrical and Electronics Engineers, Inc, New York, 2000.

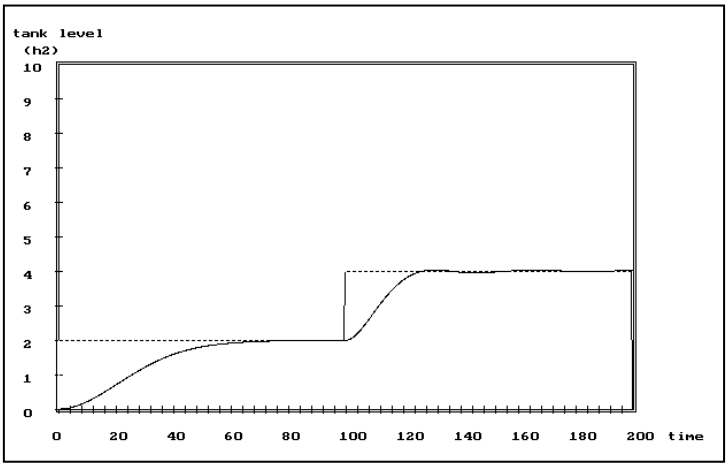

Fig (4): Two step changes response with K_I =0.01, K_P =0.55, $K_{\Delta u}$ =1.

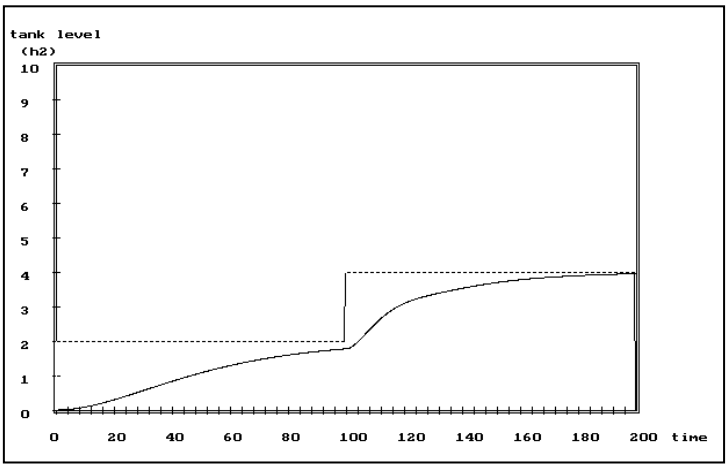

Fig (5): Two step changes response with K_I =0.005, K_P =0.55, $K_{\Delta u}$ =1.

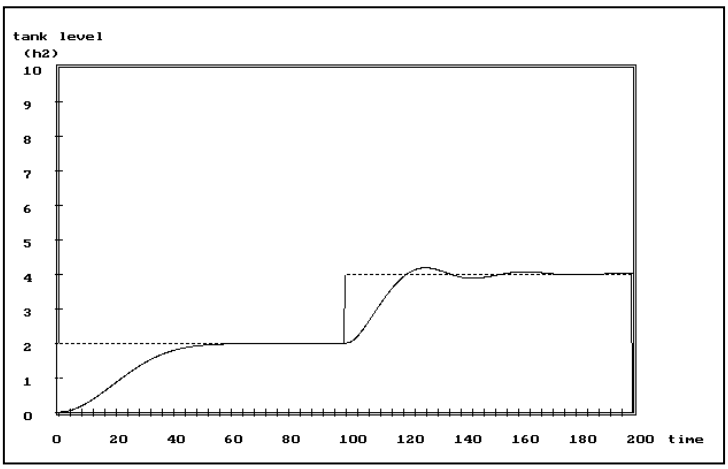

Fig (6): Two step changes response with K_I =0.012, K_P =0.55, $K_{\Delta u}$ =1.

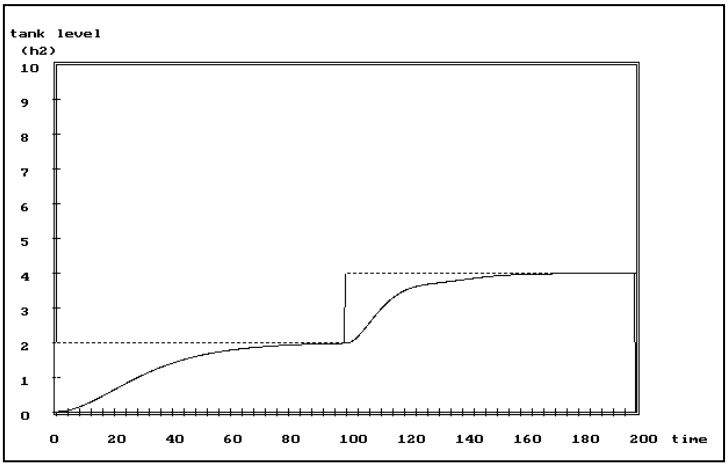

Fig (7): Two step changes response with K_I =0.01, K_P =0.8, $K_{\Delta u}$ =1.

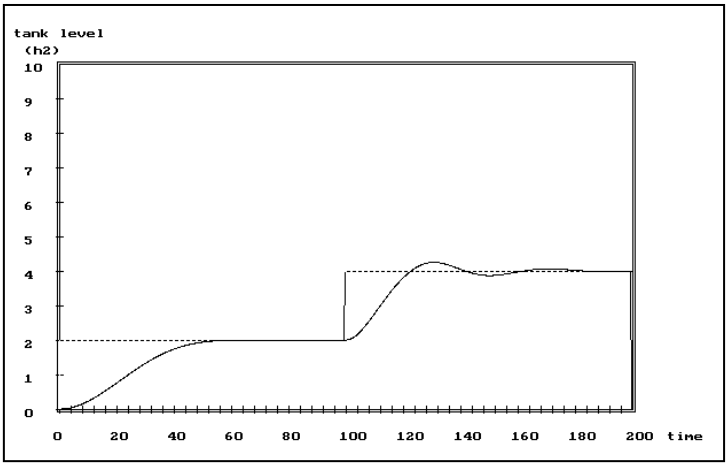

Fig (8): Two step changes response with K_I =0.01, K_P =0.4, $K_{\Delta u}$ =1.

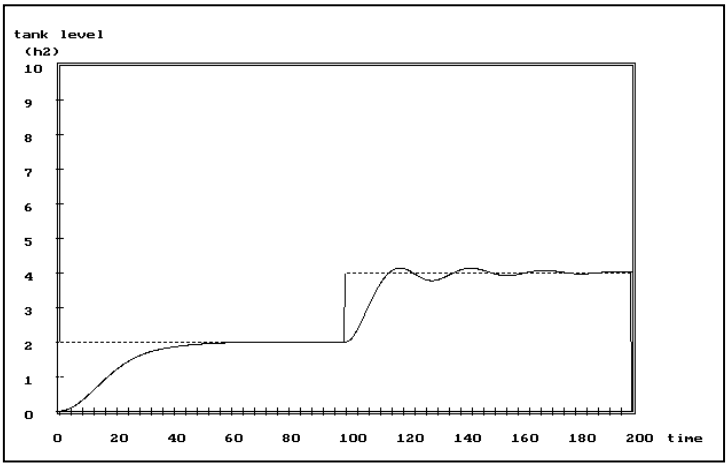

Fig (9): Two step changes response with K_I =0.01, K_P =0.55, $K_{\Delta u}$ =2.

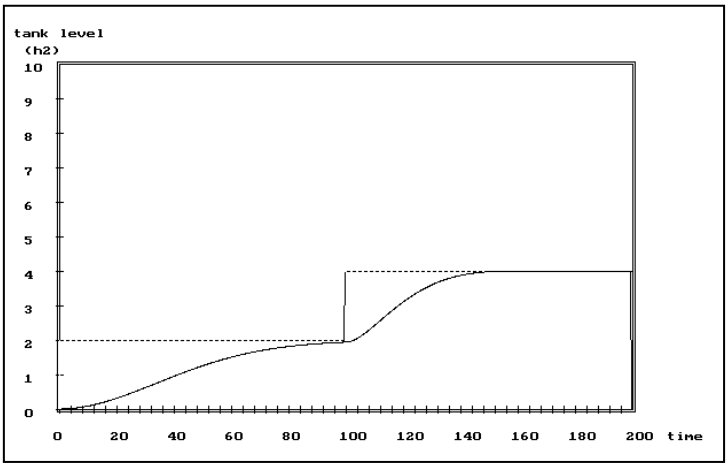

Fig (10): Two step changes response with K_I =0.01, K_P =0.55, $K_{\Delta u}$ =0.5.

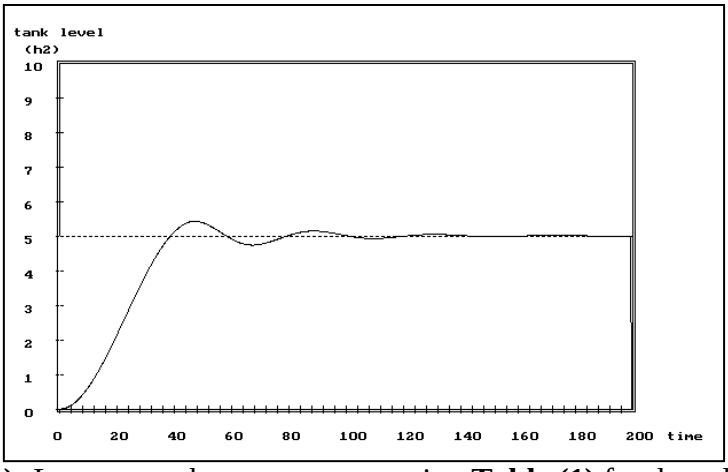

Fig (11): Large step change response using **Table (1)** for the rule base.

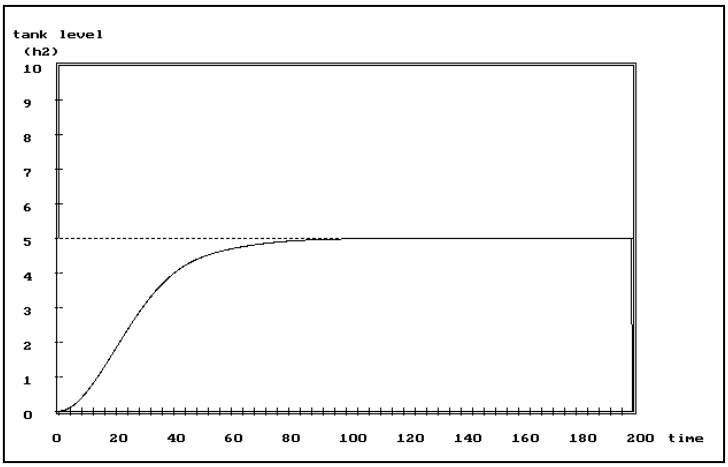

Fig (12): Large step change response using **Table (2)** for the rule base.

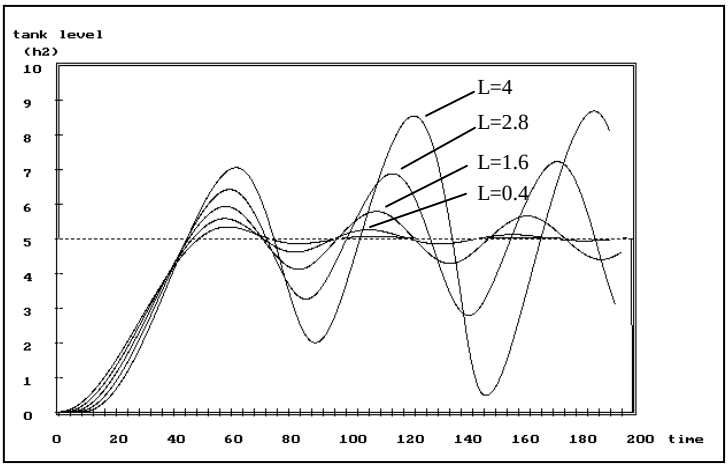

Fig (13): Effect of dead time parameter *L* on the response of the system.

SLIDING MODE VECTOR CONTROL OF A PWM INVERTER FED INDUCTION MOTOR

Aymen A. Salih
Mechatronics Engineering Dept.
University of Baghdad

Prof. Dr. Qais S. Al-Sabbagh
Computer Engineering Dept.
University of Baghdad

Asst. Prof. Azzam M. Ahmed
Information Engineering Dept.
University of Baghdad

ABSTRACT

The purpose of this paper is to analyze, study and simulate a three-phase induction motor drive using vector (field-oriented) control strategy and PWM current regulated inverter using hysteresis band current controller. The mathematical model of the induction motor and the principle of indirect field-oriented control are introduced. The Sliding Mode Controller with Boundary Layer (SMC-BL) is used as a speed controller and compared with the proportional integral (PI) controller.
A Simulink / Matlab program is written for simulating the induction motor model, SMC-BL and PI controllers and indirect field oriented control. The SMC-BL based system and PI-controller based system are compared from the point of view of speed–time response and load disturbance.
The simulation results which illustrate the performance of SMC-BL based system and PI-controller based system are plotted and discussed. These results obtained have shown improvement in the SMC-BL system performance from the point of view of variable speed tracking and load disturbance.

KEY WORD
induction motor, field oriented control, sliding mode control.

الخلاصة

الهدف من هذا البحث هو تحليل ودراسة ومحاكاة مسوق تيارمتناوب لمحرك حثي ثلاثي الطور باستخدام ستراتيجية السيطرة على اتجاه المجال(FOC) وباستخدام عاكس التيارالعامل بتضمين عرض الموجة (PWM current regulated inverter) المستخدم لمسيطر التيار المتضمن حزمة الهسترة (Hysteresis band current controller).تم تقديم النموذج الرياضي للمحرك الحثي ومباديء سيطرة المجال(FO) غير المباشر. تم أستخدام المسيطر الانزلاقي ذو المحددات (SMC-BL) كمسيطر للسرعة ومقارنتة مع المسيطر التناسبي التكاملي (PI).
استخدم برنامج (Simulink / Matlab) لمحاكاة وتمثيل نموذج المحرك الحثي و المسيطرات (SMC-BL) و (PI) و المسيطر الاتجاهي الغير مباشر(IFOC). وتمت المقارنة بين النتائج المستحصلة من تطبيق المسيطرات (SMC-BL) و (PI) من حيث الاستجابة الزمنية للسرعة وتأثيرأظطرابات الحمل (load disturbance) على السرعة.

تم رسم ومناقشة النتائج المستحصلة من المحاكاة والمتضمنة خصائص المنظومة الجديدة والمنظومة القديمة. أن النتائج النظرية اوضحت ان المنظومة الحديثة والتي تستخدم المسيطر الانزلاقي ذو المحددات هي جيدة جدا وهي افضل من المنظومة القديمة من ناحية الاستجابة الزمنية للسرع المختلفة وكذلك كبح تأثير الحمل على السرعة.

INTRODUCTION

The main types of motors that are used in speed control are dc motors and induction motors (IMs). The induction motors particularly the cage type are the most commonly used in industry due to their advantages over the dc motors. The main advantage is that induction motors do not require an electrical connection between stationary and rotating parts of the motor. Therefore, they do not need any mechanical commutator and brushes leading to the fact that they are maintenance free motors. Induction motors are cheap, robust, rugged structure, high efficiency (up to 80% higher) furthermore the induction motors can work in explosive environments because no sparks are produced.

However, the use of induction motors has several disadvantages; these include difficult controllability due to the complex mathematical model of the motors. Their nonlinear behavior during saturation, and variations of the electrical parameters due to the physical influence of temperature and a strong temperature dependency of electrical motor parameters. . For example, the rotor time constant of an induction motor can change up to 70% over a motor's temperature range. These factors make mathematical modeling of motor control systems difficult [1].

However, because of its highly non-linear and coupled dynamic structure, an induction motor requires more complex control schemes, more expensive and higher rated power converters than DC and permanent magnet motors [2].

Traditional open-loop control of the induction motors with variable frequency may provide a satisfactory solution under limited conditions. However, when high performance dynamic operation is required, these methods are unsatisfactory. Therefore, more sophisticated control methods are needed to make the performance of the induction motor comparable with DC motors such as Vector Control method.

MATHEMATICAL MODEL OF INDUCTION MOTOR

In an adjustable-speed drive the machine normally constitutes an element within a feedback loop, and therefore its transient behavior has to be taken into consideration. Besides high-performance drive control, such as vector- or field-oriented control, is based on the dynamic d-q model of the machine.

The dynamic performance of an AC machine is somewhat complex because of the three-phase rotor windings move with respect to three-phase stator windings, as shown in Figure (1 a). It can be looked on as transformer with a moving secondary coil, where the coupling coefficients between the stator and rotor phases change continuously with the change of the rotor position θ_r. The machine model can be described by differential equations with time-varying mutual inductances, but such a model tends to be very complex. A three-phase machine can be represented by an equivalent two-phase machine by using axes transformation Clark's transformation as shown in Figure (1 b), where $d^s - q^s$ correspond to stator direct and quadrature axes, $d^r - q^r$ to rotor direct and quadrature axes. This will reduce the order of the differential equations describing the machine. However, the problem of time-varying parameters still remains. This problem can be solved by replacing the machine variables (voltages, currents, and flux linkage) associated with stator windings that are fixed to stationary axes (frame) with variables associated with fictitious windings fixed to axes rotate at synchronous speed. This is called Park's transformation from stationary reference frame to synchronously rotating reference frame. This transformation will eliminates all

the time varying inductances due to the relative motion between stator and rotor electric circuit and varying magnetic reluctances [1].

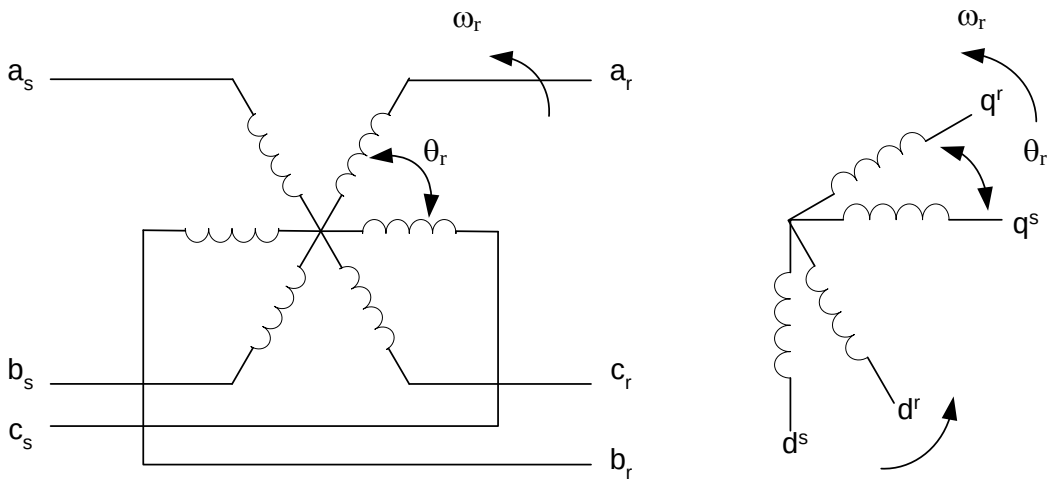

(a) (b)

Fig (1) (a) Coupling effect in three-phase stator and rotor windings of motor,
(b) Equivalent two-phase machine [1].

The mathematical model of a three phase induction motor and load is described by equations in the synchronously rotating reference frame (d^e - q^e) as [1]:

$$\begin{bmatrix} v_{qs} \\ v_{ds} \\ v_{qr} \\ v_{dr} \end{bmatrix} = \begin{bmatrix} R_s + sL_s & \omega_e L_s & sL_m & \omega_e L_m \\ -\omega_e L_s & R_s + sL_s & -\omega_e L_m & sL_m \\ sL_m & (\omega_e - \omega_r)L_m & R_r + sL_r & (\omega_e - \omega_r)L_r \\ -(\omega_e - \omega_r)L_m & sL_m & -(\omega_e - \omega_r)L_r & R_r + sL_r \end{bmatrix} \begin{bmatrix} i_{qs} \\ i_{ds} \\ i_{qr} \\ i_{dr} \end{bmatrix} \quad \textbf{(1)}$$

Where s is a d/dt operator.

For singly-fed machine (i.e. only stator be energized) such as squirrel cage motor, $v_{qr} = v_{dr} = 0$.
The speed ω_r in Equation (1) can be related to the torque as:

$$T_e = T_L + J\frac{d\omega_m}{dt} = T_L + \frac{2}{P}J\frac{d\omega_r}{dt} \quad \textbf{(2)}$$

Where

$$T_e = \frac{3}{2}\left(\frac{P}{2}\right)L_m\left(i_{qs}^e i_{dr}^e - i_{ds}^e i_{qr}^e\right) \quad \textbf{(3)}$$

And
T_e = Developed or electromagnetic torque, T_L = load torque, P = Number of poles of the motor
J = rotor inertia, ω_r = rotor speed in electrical rad/sec and ω_m = rotor mechanical speed.

Equations (1)-(3) give the complete model of the electro-mechanical dynamics for induction machine in synchronous frame.

VECTOR CONTROL

Field oriented control transforms the dynamic structure of the ac machine into that of separately excited DC machine. For a DC machine, the field flux is proportional to the field current assuming that the magnetic saturation term is negligible. If the field is assumed to be constant and independent of armature current, the armature current provides direct control of torque, so that [3]:

$$T_e \propto I_f \times I_a \qquad \textbf{(4)}$$

With the induction motor transformed to *d-q* plane, it looks like a separately exited DC machine and it can achieve four quadrant operations with fast torque response and satisfactory performance down to standstill. The space angle of the induction motor (angle between stator and rotor fields) will vary with load and; therefore, result in complex interactions between the fields. The space angle will be controlled such that the stator input current can be decoupled into flux producing (i_{ds}^s) and torque producing (i_{qs}^s) components.

There are two essentially general methods of vector control. One is called the direct or feedback method, and the other is known as the indirect or feedforward method [1]. These methods are different essentially by how the unit vector ($\cos\theta_e$ and $\sin\theta_e$) is generated for the control. It should be mentioned that the orientation of i_{ds}^e with the rotor flux λ_r, air gap flux λ_m, or stator flux λ_s is possible in vector control. However, rotor flux orientation gives natural decoupling control, whereas air gap or stator flux orientation gives a coupling effect which has to be compensated by a decoupling compensation current.

Indirect vector control method is essentially the same as direct vector control, except the unit vector signals ($\cos\theta_e$ and $\sin\theta_e$) are generated in feedforward manner. Indirect vector control is very popular in industrial applications. The fundamental principle of indirect vector control can be explained by a phasor diagram shown in Figure (2). The $d^s - q^s$ axes are fixed on the stator, but the $d^r - q^r$ axes, which are fixed on the rotor, are moving at speed ω_r as shown. Synchronously rotating axes $d^e - q^e$ are rotating ahead of the $d^r - q^r$ axes by the positive slip angle θ_{sl} corresponding to slip frequency ω_{sl}.

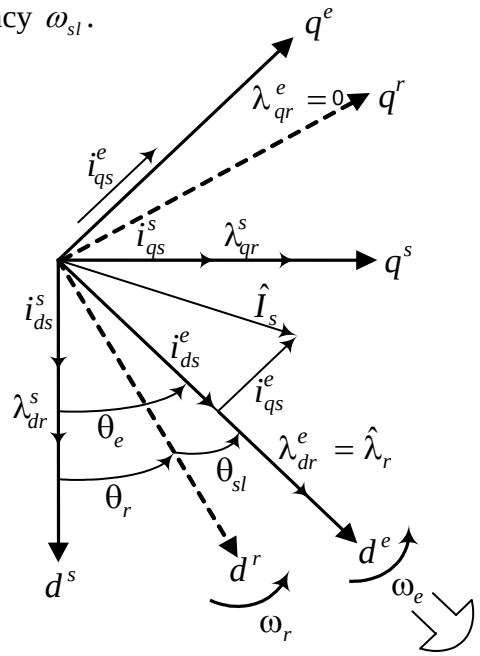

Fig (2) Phasor diagram explaining indirect vector control [1]

Since the rotor pole is directed on the d^e axis and $\omega_e = \omega_r + \omega_{sl}$, one can write

$$\theta_e = \int \omega_e dt = \int (\omega_r + \omega_{sl}) dt = \theta_r + \theta_{sl} \quad \textbf{(5)}$$

The phasor diagram suggests that for decoupling control, the stator flux component of current i_{ds}^e should be aligned on the d^e axis, and the torque component of current i_{qs}^e should be on the q^e axis.

To implement the indirect vector control strategy, equation (5) and the following equations should be applied [1]:

$$\frac{L_r}{R_r}\frac{d\hat{\lambda}_r}{dt} + \hat{\lambda}_r = L_m i_{ds}^e \quad \textbf{(6)}$$

$$\omega_{sl} = \frac{L_m R_r}{L_r \hat{\lambda}_r} i_{qs}^e \quad \textbf{(7)}$$

$$T_e = \frac{3}{2}\frac{P}{2}\frac{L_m}{L_r}\lambda_{dr}^e i_{qs}^e \quad \textbf{(8)}$$

The unit vector signals $\cos\theta_e$ and $\sin\theta_e$ are obtained from the angle θ_e by integrating ω_e signal.

VARIABL STRUCTURE WITH SLIDING MODE CONTROL

Variable structure systems (VSS) with a sliding mode (SMC) were discussed first in the Soviet literature [4,5], and have been widely developed in recent years. Comprehensive survey of variable structure control can be found in [6, 7].

VSS with SMC are characterized by control laws that are discontinuous on a certain manifold in the state space, the so-called sliding surface [5,8]. A VSS control law is designed such that the representative point's trajectories of the closed-loop system are attracted to the sliding surface and once on the sliding surface they slide towards the origin Fig (3) [9]. The dynamic performance of SMC has been confirmed to be an effective robust control approach as facing the problems of systems uncertainties and unknown disturbances, but a SMC indeed exhibits some drawbacks [10]. The major drawback in the SMC approach is the undesired phenomenon of chattering Fig (3), because of the discontinuous change of control laws across the sliding surface. In practical engineering systems, chattering may cause damage to system components, as well as excite unmodelled and high frequency plant dynamics [11].

There exist several techniques to eliminate chattering. The widely-adopted approach to chattering-free VSS is the so-called boundary layer, where the discontinuous VSS control law signum function is applied to small vicinity around the sliding surface (see [7,12]).

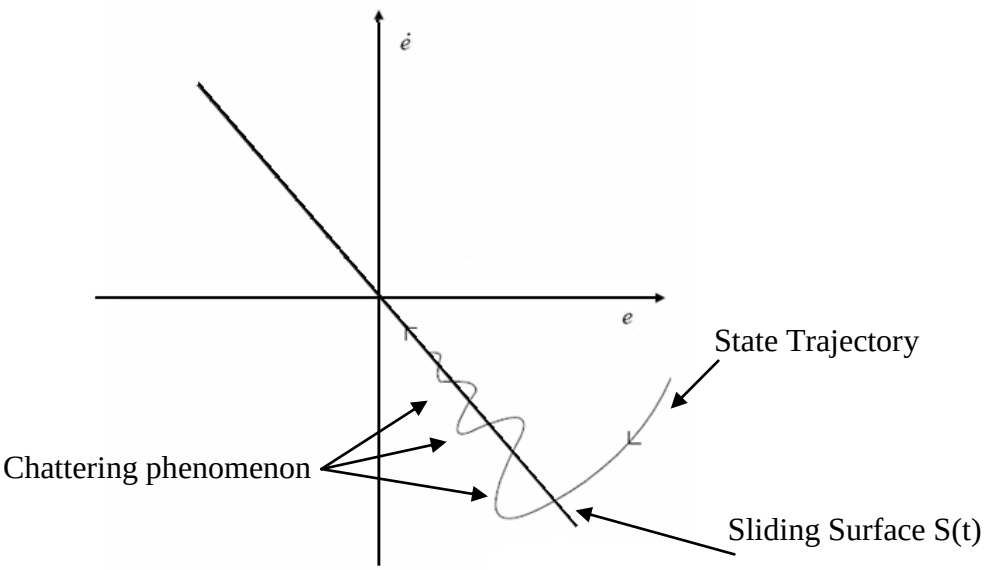

Fig (3) Sliding motion of the system

SLIDIN MODE CONTROLLER DESIGN

The sliding mode control consists of two phases [13]:

- Designing an equilibrium surface, called sliding surface S(t), such that any state trajectory of the plant restricted to the sliding surface is characterized by the desired behavior.
- Designing a discontinuous control law to force the system to move on the sliding surface in a finite time

.

Sliding mode control Law

To apply the SMC approach, we first define a time-varying sliding surface, S(t), in the state space R^n by the vector equation $S(e,e^{\bullet})=0$, where

$$S(t)=Ce+e^{\bullet} \qquad \textbf{(9)}$$

Where C is a strictly positive constant number, and e , $\dot{e}$ is the state tracking errors and their time derivatives respectively.

Sliding mode means that once the state trajectory has reached the sliding surface S=0 the system trajectory remains on it while sliding into the origin (e=0) independently of model uncertainties, unmodeled frequencies, and disturbances [13]. So, the SMC is known as being robust for model parameter variations. This property is used for compensating the effects of model uncertainties and load disturbances [14]. For the induction motor speed control, let $e=\omega_{ref}-\omega$ and $e^{\bullet}=\omega^{\bullet}{}_{ref}-\omega^{\bullet}$, where ($\omega_{ref}$) is the motor reference speed, and (ω) is the motor actual speed.

As can be seen from Eq. (9), maintaining system states on the surface $S(e,\dot{e})=0$ for all (t > 0) will "closely" satisfy the tracking requirements $\omega\rightarrow\omega_{ref}$ and $\omega^{\bullet}\rightarrow\omega^{\bullet}{}_{ref}$. Indeed, it will force e and $\dot{e}$ to approach zero, given any bounded initial conditions e(0) and $\dot{e}(0)$.

By choosing the Lyapunov function candidate $V=0.5S^{T}S$, a reaching condition (sliding condition) is obtained as [15]:

$$\dot{V} = S^T \dot{S}; S \neq 0 \quad \text{or} \qquad \textbf{(10 a)}$$

$$S^T \dot{S} \leq -\alpha \left| S^T \right| = -\alpha S^T \operatorname{sgn}(S) \qquad \textbf{(10 b)}$$

Where α is a strictly positive constant. Reaching the sliding mode means a system trajectory is outside the sliding surface but follows the reaching condition Eq.(10 b) [15].

Essentially, Eq.(10 b) states that the squared "distance" to the surface, as measured by $S^T \dot{S}$, decreases along all system trajectories. Thus, Eq. (10 b) provides a sufficient reaching condition such that the tracking error e will asymptotically converge to zero [14].
The sliding mode controller law is now chosen as follows:

$$u_{smc} = K \operatorname{sgn}(S) \qquad \textbf{(11)}$$

Where

$$S(t) = Ce + \dot{e}$$

K: +ve constant number,

$$\operatorname{sgn}(S) = \begin{cases} -1 & \text{if } S < 0 \\ +1 & \text{if } S > 0 \end{cases} \qquad \textbf{(12)}$$

The state trajectories with signum function is shown in Fig (4).

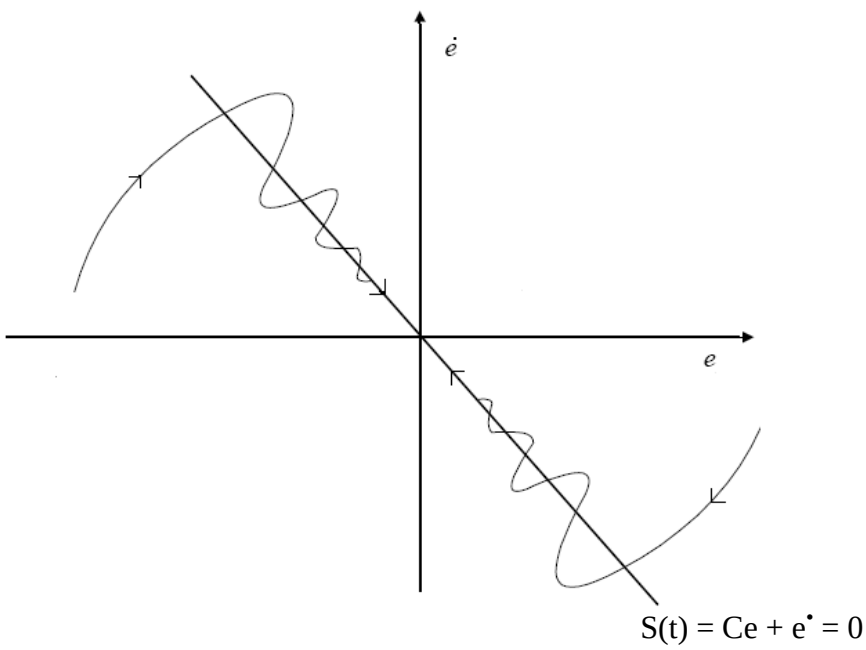

Fig (4) State trajectories with signum function [6]

Saturation Function Instead of Signum Function

To eliminate the chattering phenomenon caused by the signum function, Saturation function is used. This method is called SMC with boundary layer (BL). For each link, define thin boundary layers (BL) neighboring the sliding surfaces [12].

$$B_i(t) = \{q_i, \left| S_i(q,t) \right| \leq \Phi_i\}, \Phi_i > 0 \quad i = 1, 2, 3\ldots \qquad \textbf{(13)}$$

Where $|S_i(q,t)|$ is the distance between state e_i and sliding surface S_i, Φ_i is the boundary layer thickness and, as illustrated in Fig. (5) for i=1 in the error phase space. To remedy the control discontinuity in the boundary layer, the signum function ($\mathrm{sgn}(s)$) is replaced by a saturation function of the form [16,10].

$$sat(S_i) = \begin{cases} \mathrm{sgn}(S_i), & if\,|S_i| \geq \Phi_i \\ \dfrac{S_i}{\Phi_i}, & if\,|S_i| < \Phi_i \end{cases} \qquad i = 1, 2, 3\ldots \qquad \textbf{(14)}$$

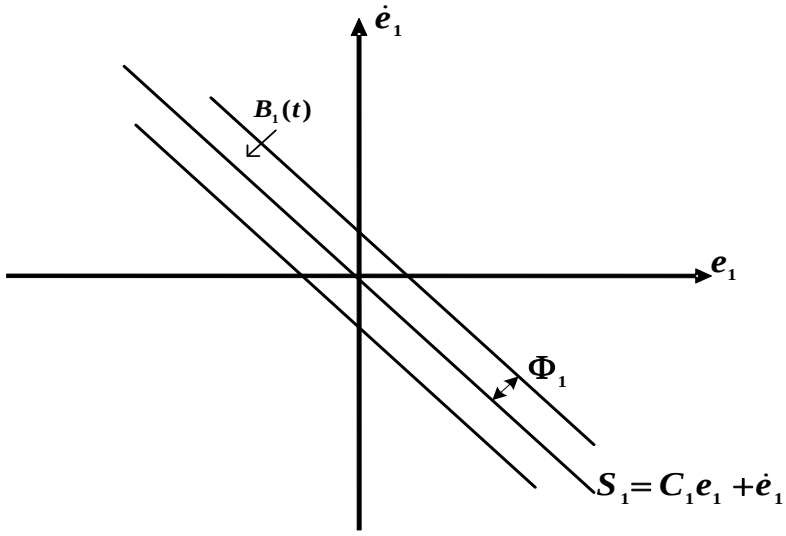

Fig (5) The sliding surface and the boundary layer [9].

However, the system state with this control law is uniform ultimate bounded with respect to a small neighborhood of the origin Fig (6) [17]. Let $\varepsilon_i = C_i^{-1}\Phi_i$, $i = 1,2,3,....$ be the boundary layer width. As shown in [18], the tracking errors exist within a guaranteed precision ε_i. Therefore, the larger the boundary layers the smaller the control chattering and the greater the tracking errors [10].

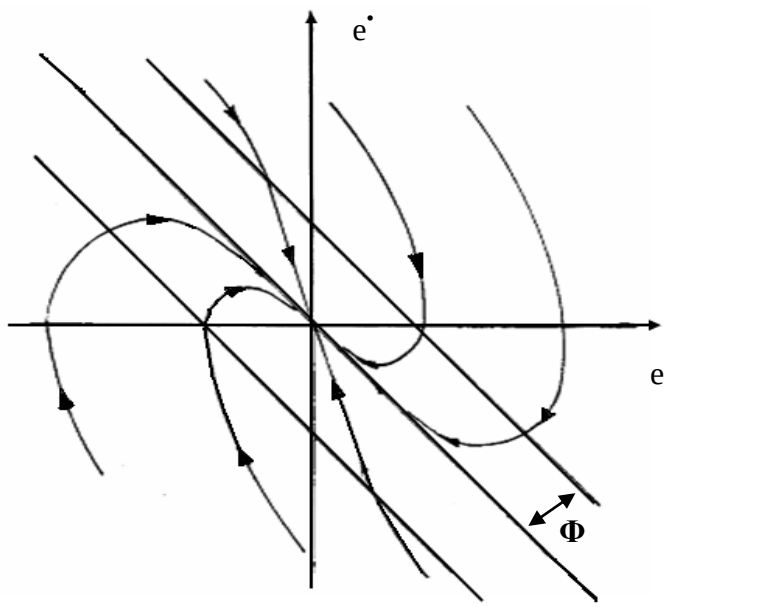

Fig (6) State trajectories with saturation function [17].

SIMULATIONS

Induction machines models are often ill – defined. Even if the machine model is well known, there may be a parameter variation problem. The *d-q* machine model discussed before was multivariable, complex, and nonlinear. Vector or Field Oriented Control of a drive can overcome this problem, but accurate vector control is nearly impossible. To overcome such problems Sliding Mode with boundary layer technique was used. The overall Simulink block diagram of the Vector Control of a three phase induction motor is shown in Fig. (7), which are taken from the MATLAB program.

The Field Oriented Control (FOC) makes the rotor shaft to follow or track the input reference speed (ω^*). The command speed signal subtracted from the measured rotor speed and generates the error signal. The error generated is then fed into a speed controller block. The speed controller block is either a Proportional Integral (PI) controller or a Sliding Mode Controller with Boundary Layer (SMC-BL) that generates a torque command (T_e^*). This torque command is used to set the electromagnetic torque induced within the induction motor by calculating an appropriate i_{qs}^* command based on the generated T_e^* signal according to Equation (8), and the flux will be computed from the resulting direct component of stator current (i_{ds}), and the flux is assumed to be constant when the motor is operated below and beyond the rated speed, and the flux-speed product is held constant. Inside the (FOC) block calculations are made and the reference direct and quadrature components of the stator current (i_{ds}^*, i_{qs}^*) are generated. These two components are fed to the (dq to abc) conversion block to generate the three phase reference currents (I_{abc}^*). These are then compared with the actual measured currents (I_{abc}) in the hysteresis band current regulator block to generate the pulses to feed the current source PWM inverter. The latter produces the driving power for a (50 Hp, 460 V, 60 Hz, 4 poles) three phase induction motor as shown in Fig. (8).

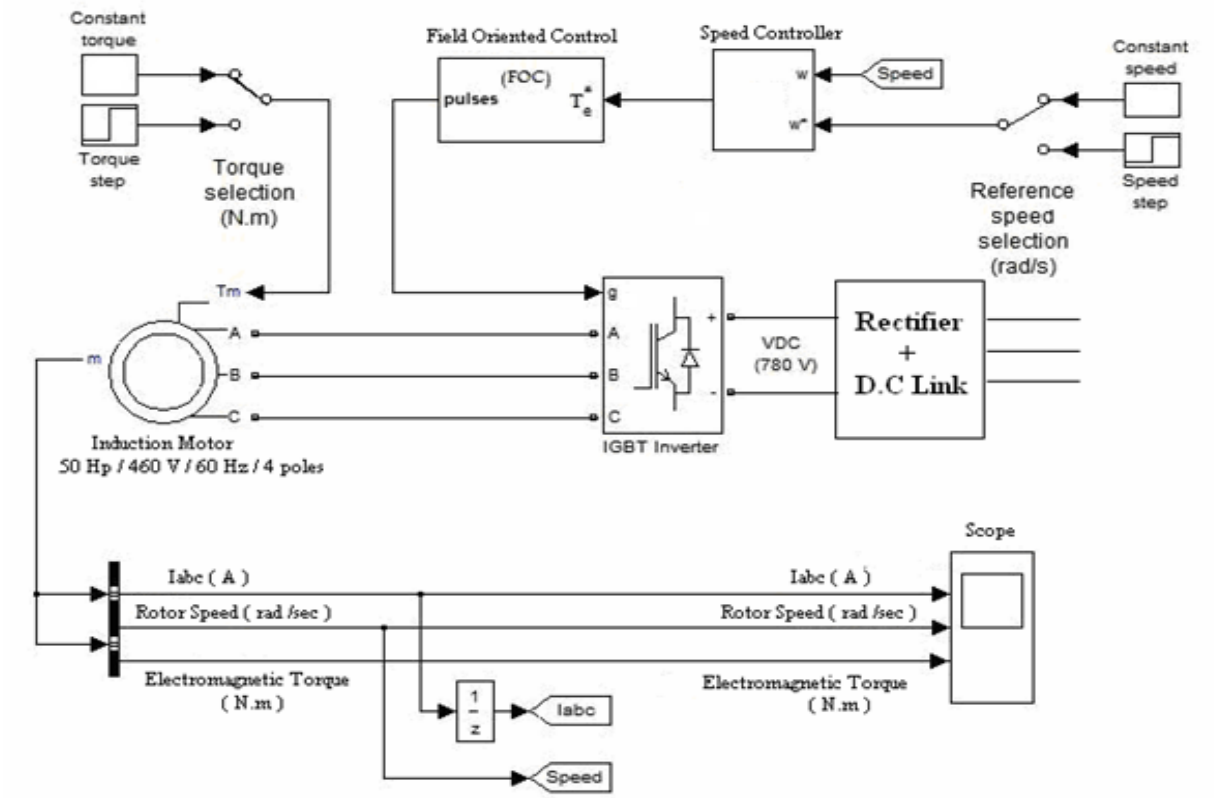

Fig (7) Overall control system [MATLAB].

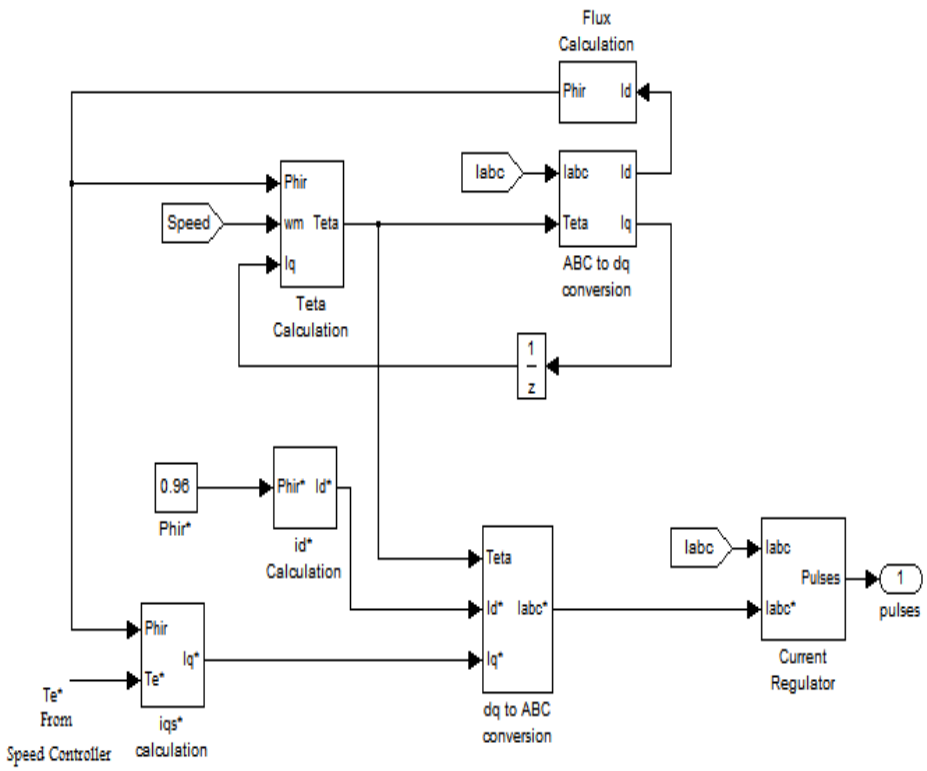

Fig (8) Inside field oriented control block [MATLAB].

SMC-BL Speed Controller Tuning

The control law of this controller is given as in equation (14):

U_{smc}= K sat (S)

Where

$$sat(S) = \begin{cases} \text{sgn}(S), & if\ |S| \geq \Phi \\ \dfrac{S}{\Phi}, & if\ |S| < \Phi \end{cases} \qquad \text{and} \qquad S(t) = Ce + \dot{e}$$

Controller parameters (K, C, and Φ) chosen should be made very carefully to satisfy the desired speed response without affecting the overall behavior of the system. Every parameter has specific effects on some region of the overall response. Where the gain (K) affects the initial starting point of the controlled variable, also it affects the transient response for the controlled system. The gain (C) affects the transient response and the steady state error, while the (Φ) parameter is used to eliminate the chattering phenomena.

For the controlled system (FOC-IM), if the value of (K) is small then the initial value of the electromagnetic torque (T_e) will be small. Then the transient response of the speed curve will be slow and it takes large time to reach steady state region, and vise versa as shown in Figures.(9, 10). If the value of (C) is small then the transient response of the speed curve will be slow and the steady state error will be large, and vise versa as shown in Figures.(11, 12). It should be noticed that there is a limit for increasing the values of (K, C) because it will no more affects the transient response but only increases the drawn currents and the electromagnetic torque at the instant of speed or torque changes during motor working.

The boundary layer (Φ) is used to eliminate the chattering, so it should be chosen small. If the boundary layer is very small then under some operating conditions chattering may re-occur. Alternatively, if the boundary layer is chosen large then chattering is completely eliminated. However, a large boundary layer results in slow system response and therefore degrades the dynamic performance of the system.

All the above tests are made on ω*=120 rad/sec, then the following values of the controller parameters are chosen to satisfy the desired speed response without affecting the overall behavior of the system:

$$K = 300,\ C = 18,\ \Phi = 2$$

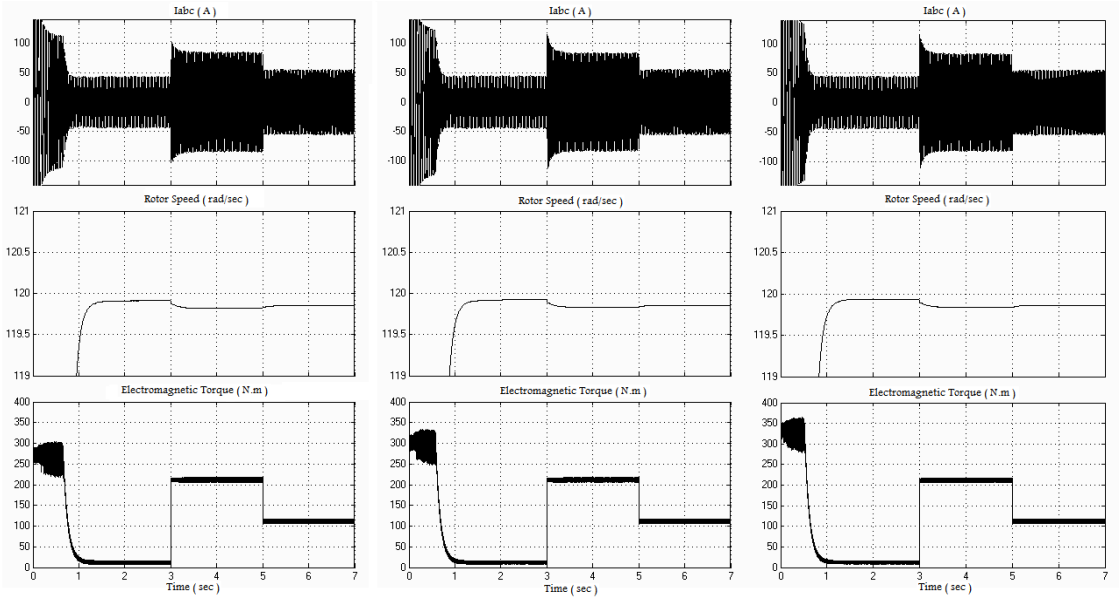

(a) K =270 (b) K= 300 (c) K= 330

Fig (9) Speed response at ω*=120 rad/sec with load step changes, at (t=3sec) from (0-200 N.m) and at (t=5sec) from (200-100 N.m).

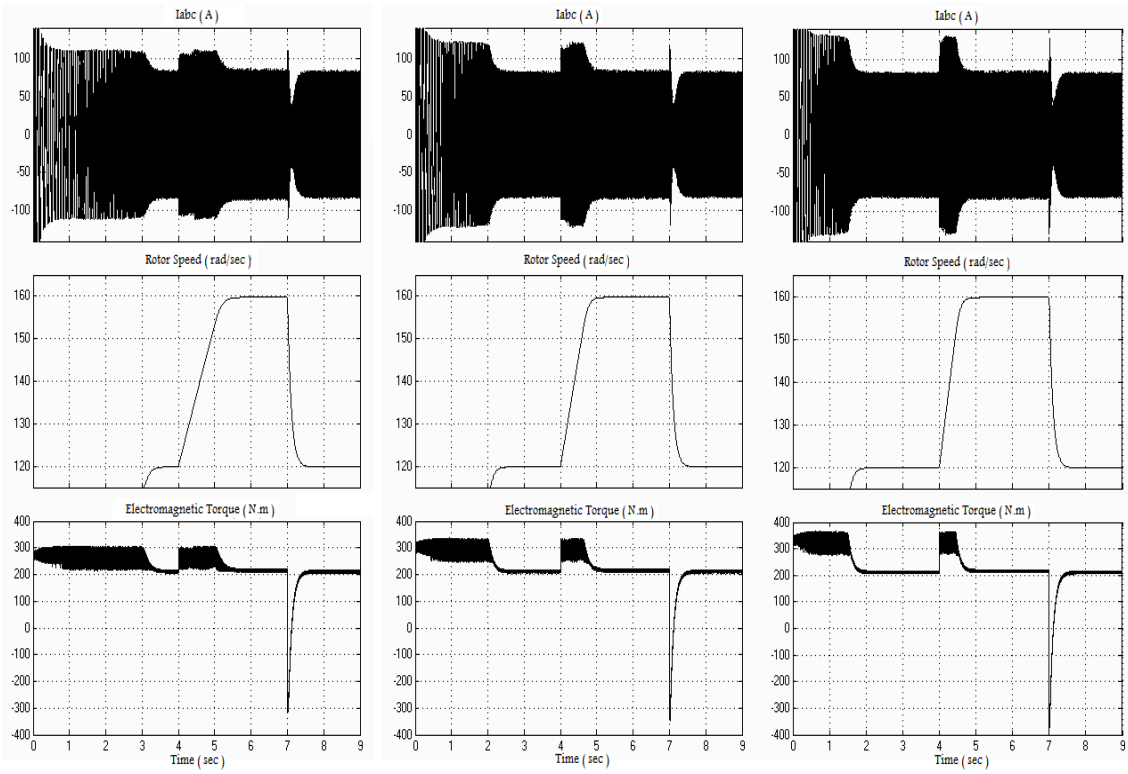

(a) K =270 (b) K= 300 (c) K= 330

Fig (10) Speed response at (200 N.m) load with speed step changes, at (t=4sec) from (120-160 rad/sec) and at (t=5sec) from (160-120 rad/sec).

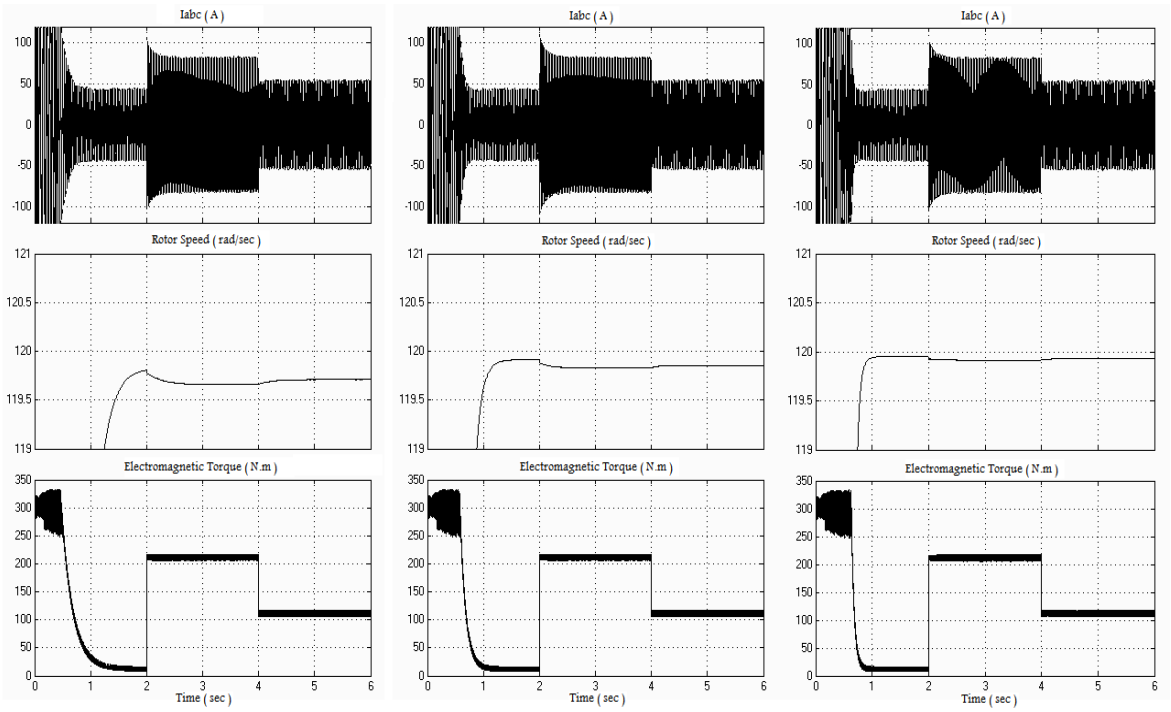

(a) C =5 (b) C= 10 (c) C= 20

Fig (11) Speed response at ω*=120 rad/sec with load step changes at (t=2sec) from (0-200 N.m) and at (t=4sec) from (200-100 N.m).

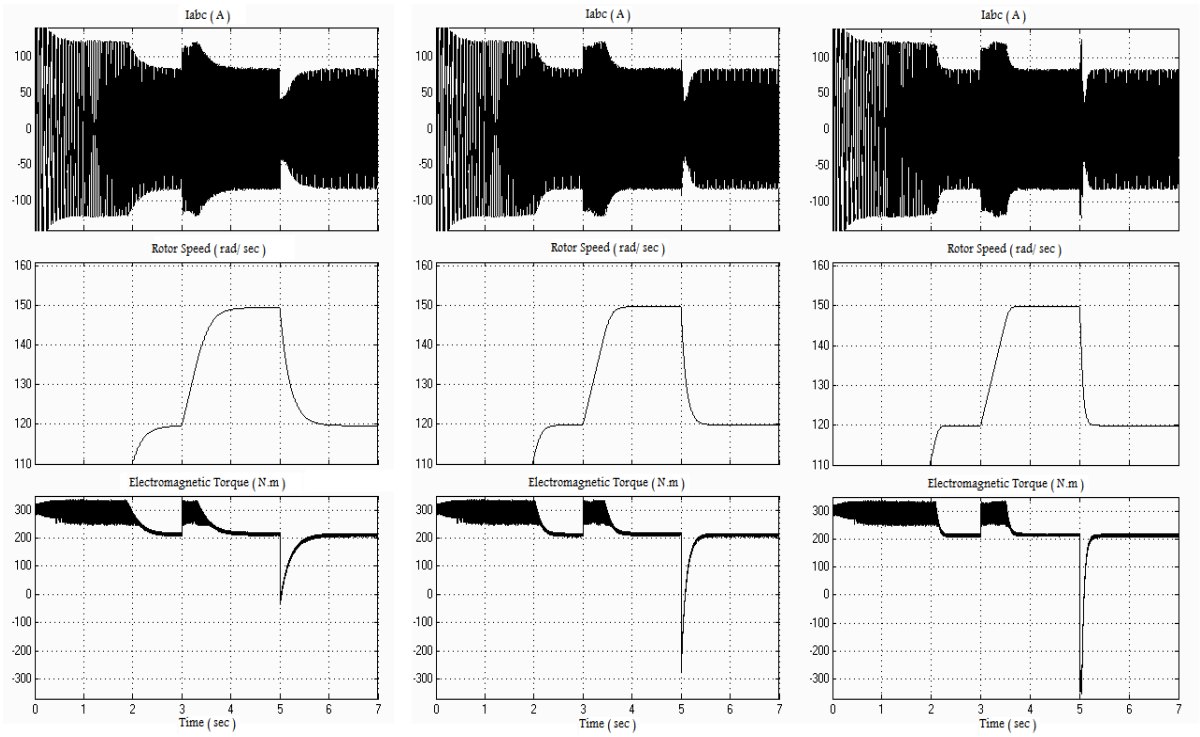

(a) C =5 (b) C= 10 (c) C= 20

Fig (12) Speed response at (200 N.m) load with speed step changes, at (t=3sec) from (120-150 rad/sec) and at (t=5sec) from (150-120 rad/sec).

RESULTS

In this section the results of simulation of sliding mode controller with boundary layer (SMC-BL) based on rotor field orientation induction motor drive are presented and discussed, also the results of simulation of conventional proportional integral (PI) controller for the same induction motor are presented and compared with the results of (SMC-BL) system from the point of view of speed tracking and load disturbance rejection on system response.

The simulation results will consist of two parts. The first part will show the System performance under no load. The second part will show the System performance under load. The parameters of the induction motor are listed in table (1):

Table (1) Parameters of induction motor.

Motor Power	50Hp
Frequency	60 Hz
Number of Poles	4
Volts	460 V
Stator resistance (R_s)	0.087 Ω
Rotor resistance (R_r)	0.228 Ω
Stator inductance (L_s)	0.8 mh
Rotor inductance (L_r)	0.8 mh
Magnetizing inductance (L_m)	34.7 mh
Friction constant (F)	0.1 N.m.s
Moment of inertia (J)	1.662 Kg.m^2

System Performance under No Load Conditions

Fig. (13) and Fig. (14) show the speed tracking performance under no load for two rated speeds (120 rad/sec), (30 rad/sec) respectively for both (SMC-BL) system and (PI) system. The motor speed (ω_r) tracks the reference model output (SMC-BL) system without overshoot, and the amount of torque ripple is much less than that of the (PI) system.

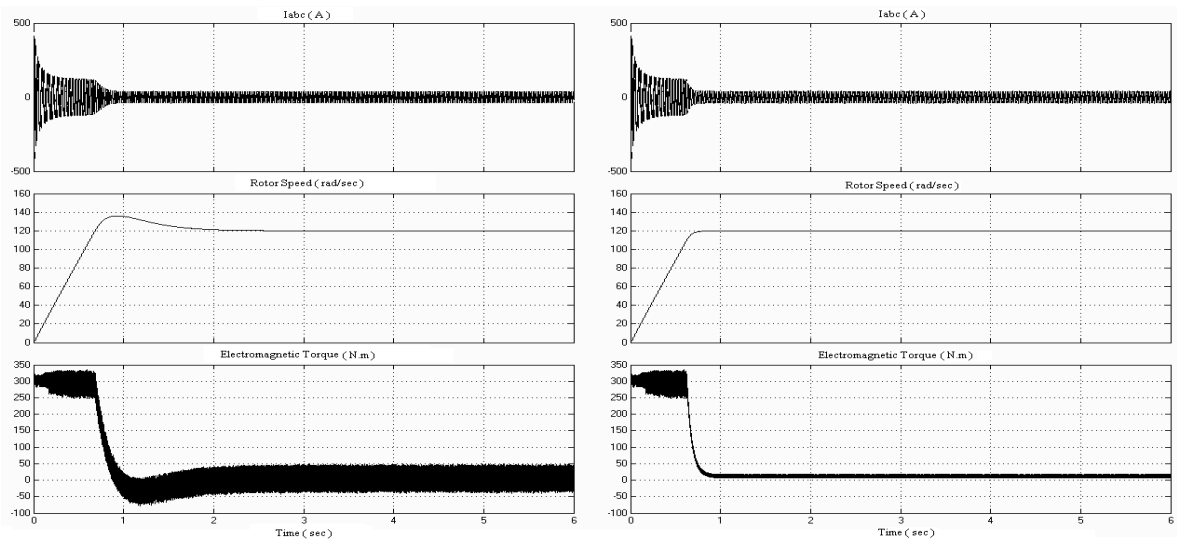

(a) PI (b) SMC-BL

Fig (13) Speed response at ω^*=120 rad/sec with no load

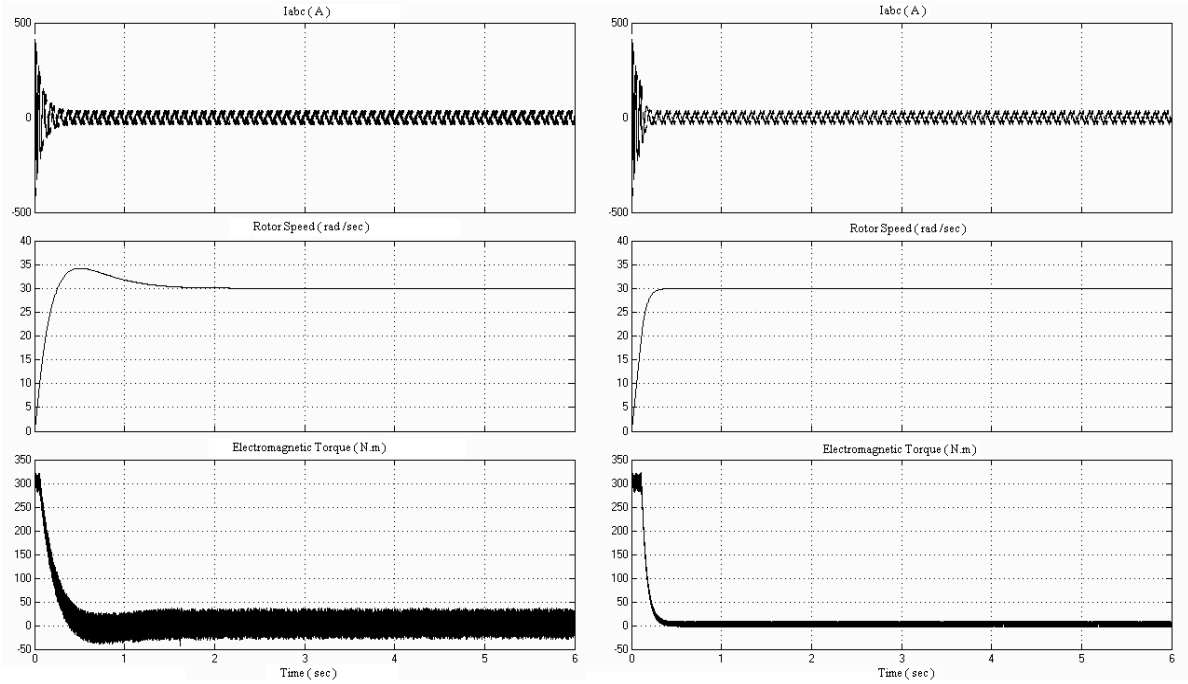

(a) PI (b) SMC-BL

Fig (14) Speed response at ω^*=30 rad/sec with no load

Fig.(15) and Fig.(16) represent the speed response for step changes of speed of the (SMC-BL) and (PI) control system for two rated speeds (120 rad/sec), (30 rad/sec) respectively. The motor speed (ω_r) tracks the reference step change model output (SMC-BL) system without overshoot and the amount of torque ripple is much less than that of the (PI) system and the speed response for the (SMC-BL) is smoother and faster than the (PI) system.

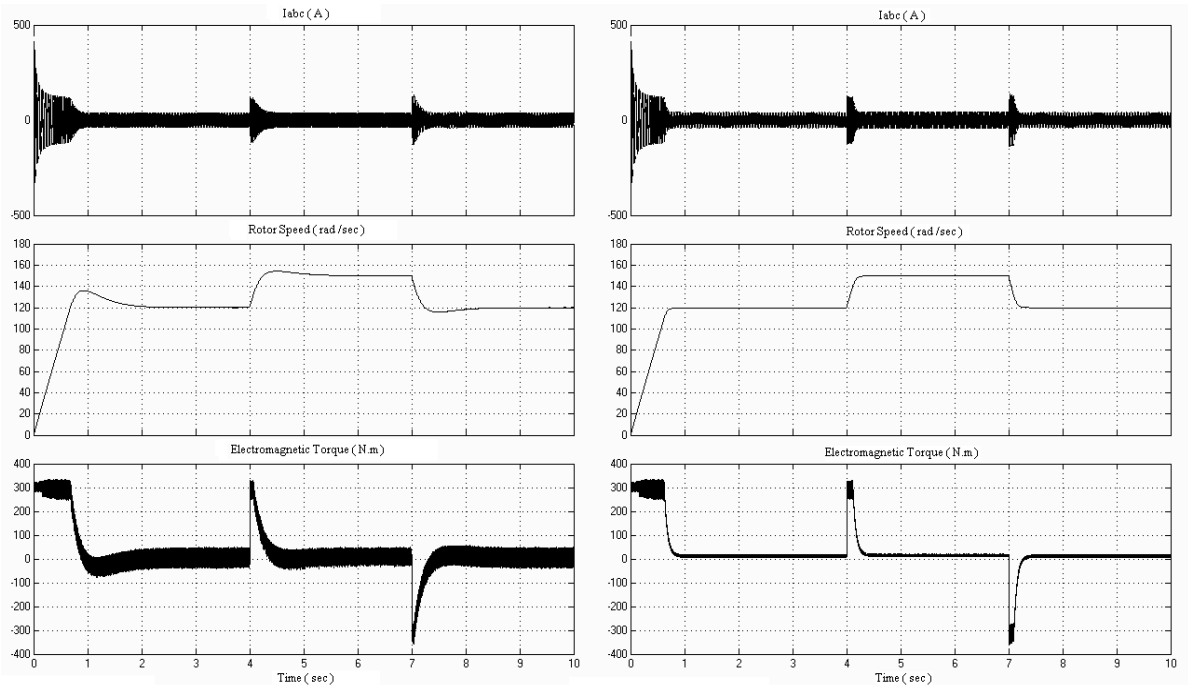

(a) PI (b) SMC-BL

Fig (15) Speed response at no load with speed step changes, at (t=4sec) from (120-150 rad/sec) and at (t=7sec) from (150-120 rad/sec).

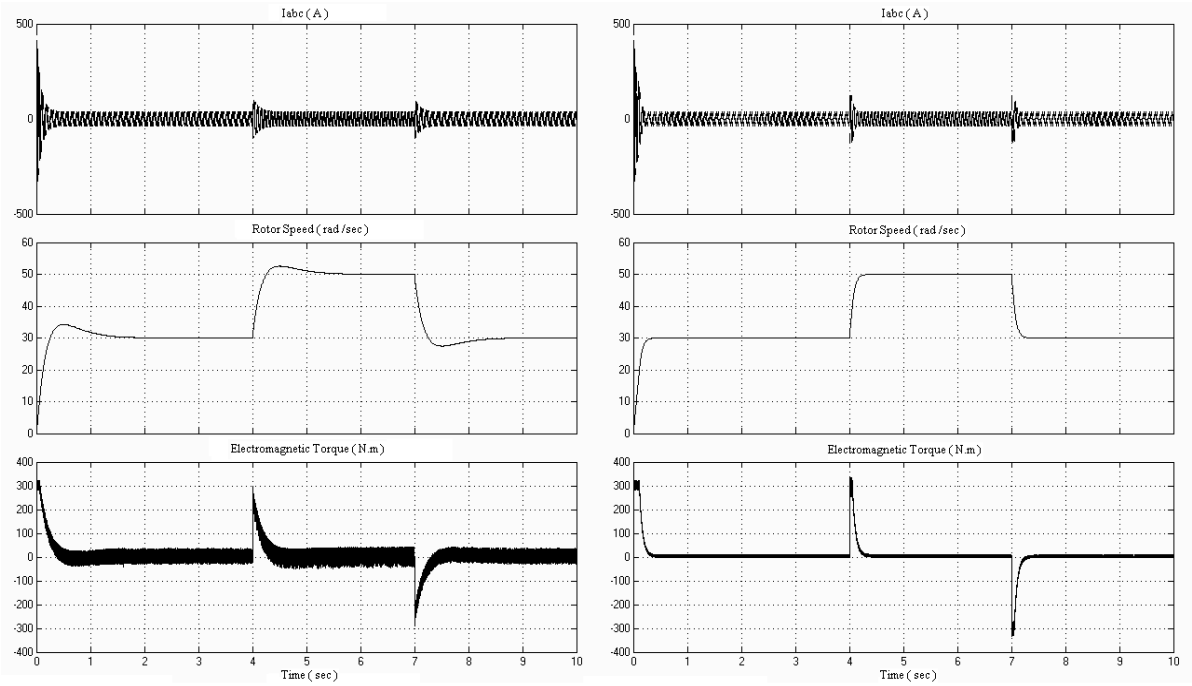

(a) PI (b) SMC-BL

Fig (16) Speed response at no load with speed step changes, at (t=4sec) from (30-50 rad/sec) and at (t=7sec) from (50-30 rad/sec).

Fig.(17) and Fig.(18) represent the speed response for forward and reverse rotating of speed of the (SMC-BL) and (PI) control system for two rated speeds (120 rad/sec), (30 rad/sec) respectively. The motor speed (ω_r) tracks the reference step change for both forward and reverse rotating case for the (SMC-BL) system without overshoot and the amount of torque ripple is much less than that of the (PI) system and the speed response for the (SMC-BL) is smoother and faster than the (PI) system.

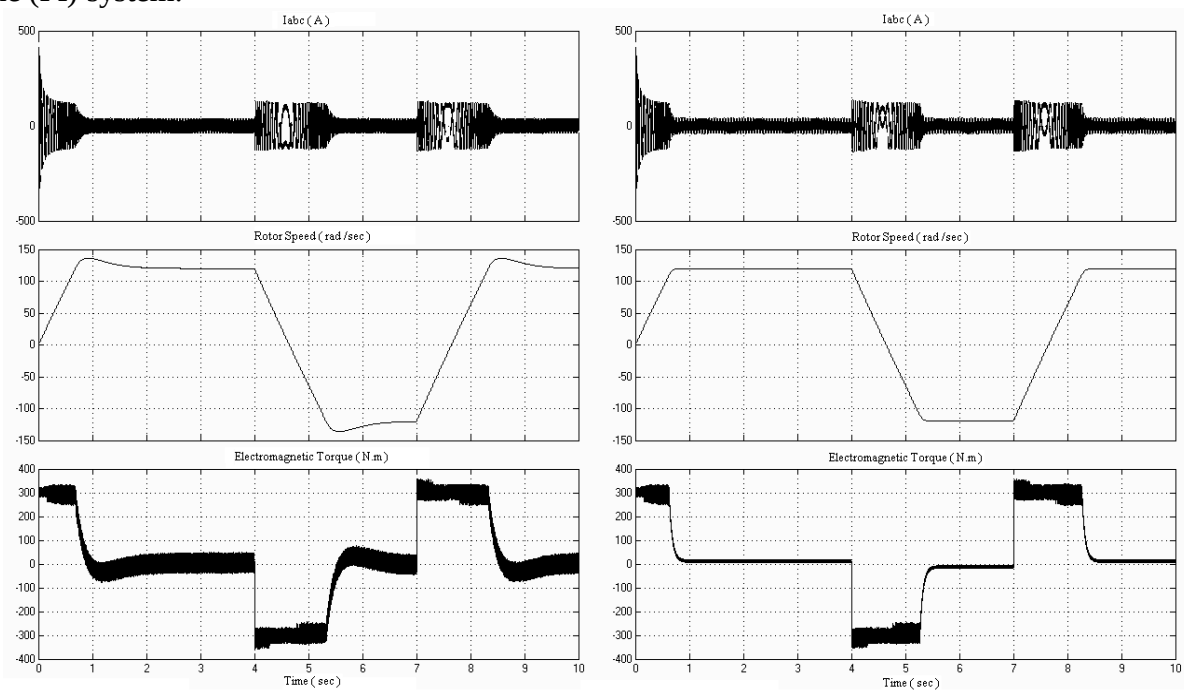

(a) PI (b) SMC-BL

Fig (17) Speed response at no load with forward and reverse speed changes, at (t=4sec) from (120 to -120 rad/sec) and at (t=7sec) from (-120 to 120 rad/sec).

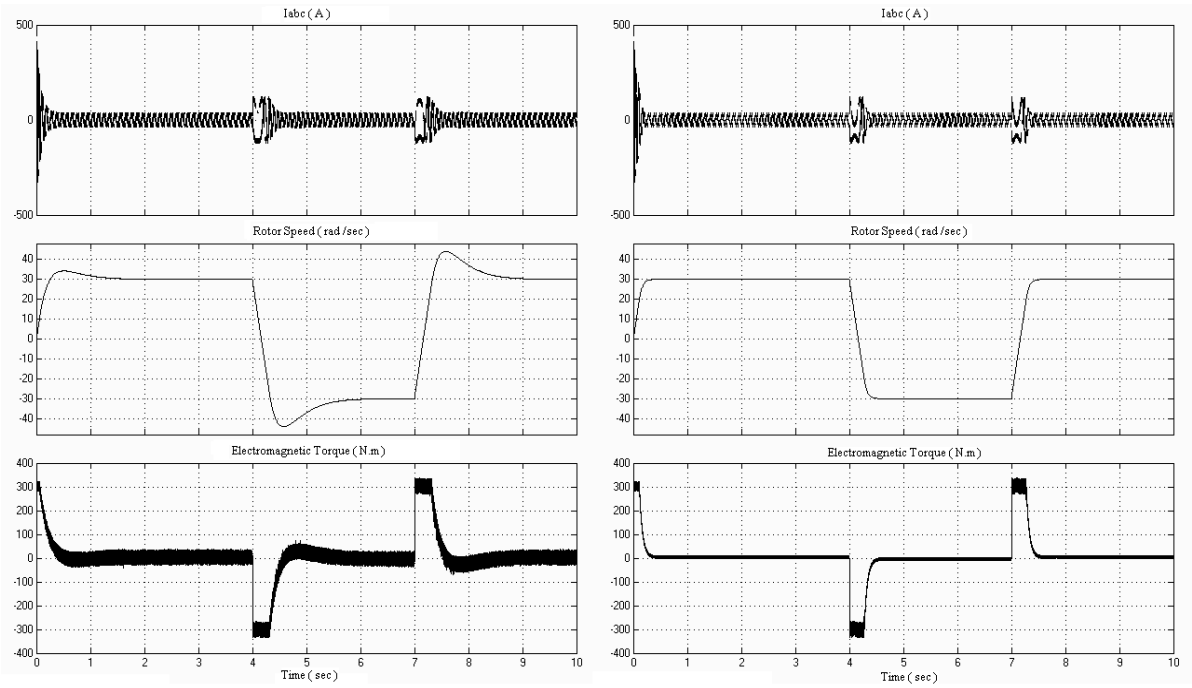

(a) PI (b) SMC-BL

Fig (18) Speed response at no load with forward and reverse speed changes, at (t=4sec) from (30 to -30 rad/sec) and at (t=7sec) from (-30 to 30 rad/sec).

System Performance under Load Conditions

Fig.(19) and Fig.(20) show the speed response for both (SMC-BL) system and (PI) system for two rated speeds (120 rad/sec), (30 rad/sec) respectively, when a set value of 200 N.m load is applied at starting. The motor speed (ω_r) tracks the reference model output (SMC-BL) system faster and without overshoot, and the amount of torque ripple at the steady state is much less than that of the (PI) system.

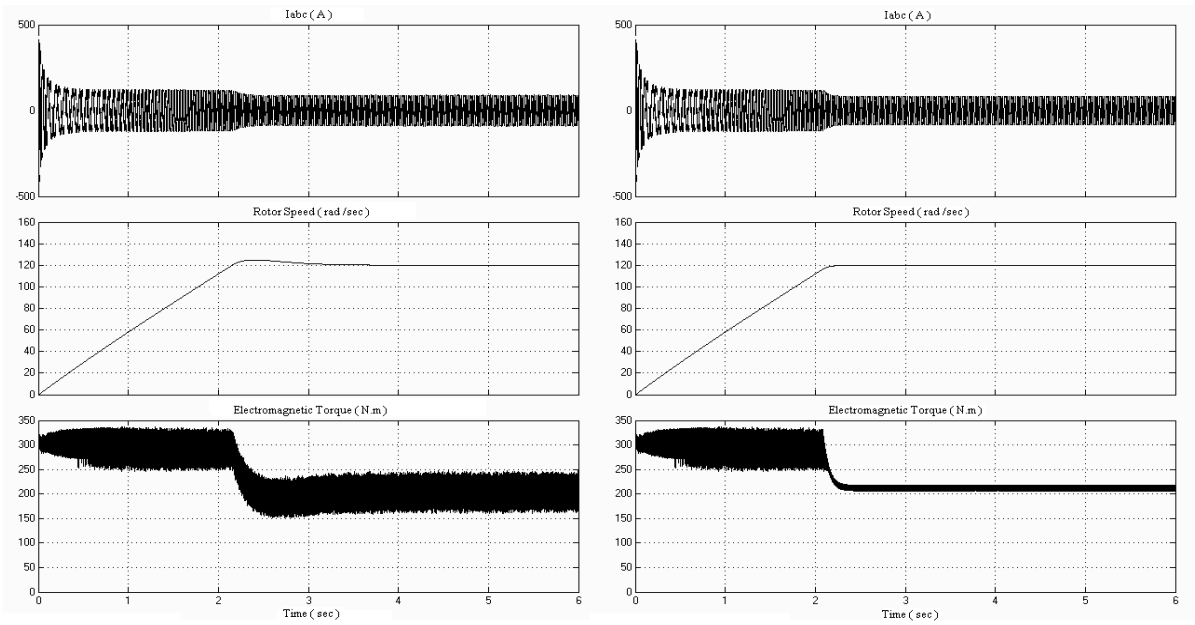

(a) PI (b) SMC-BL

Fig (19) Speed response at ω^*=120 rad/sec and constant load of 200N.m

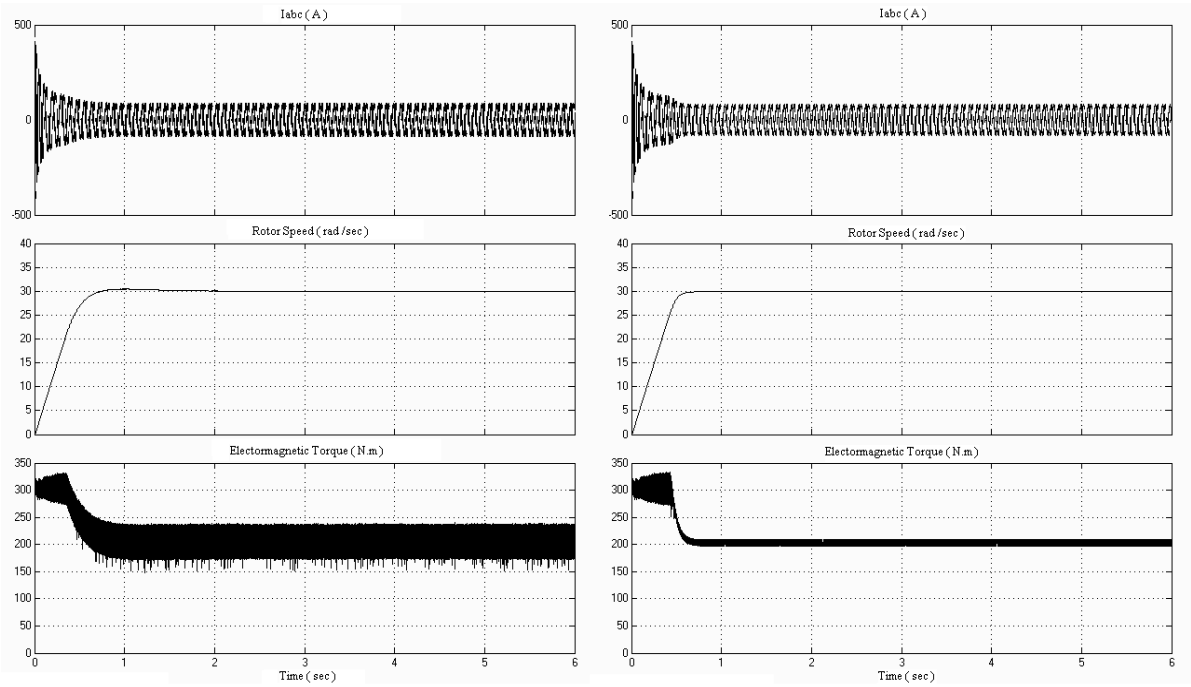

(a) PI (b) SMC-BL

Fig (20) Speed response at ω^*=30 rad/sec and constant load of 200N.m

Fig.(21) and (22) represent the speed response for step changes of load of the (SMC-BL) and (PI) control system for two speeds (120 rad/sec), (30 rad/sec) respectively. No dip or jump appears in the speed responses at the instant of applying or removing the load for the (SMC-BL) system and also the amount of torque ripple is much less than that of the (PI) system for the two rated speeds, and its obvious that the stator currents (I_{abc}) are increased when the load is applied, and the speed response for the (SMC-BL) is smoother and faster than the (PI) system.

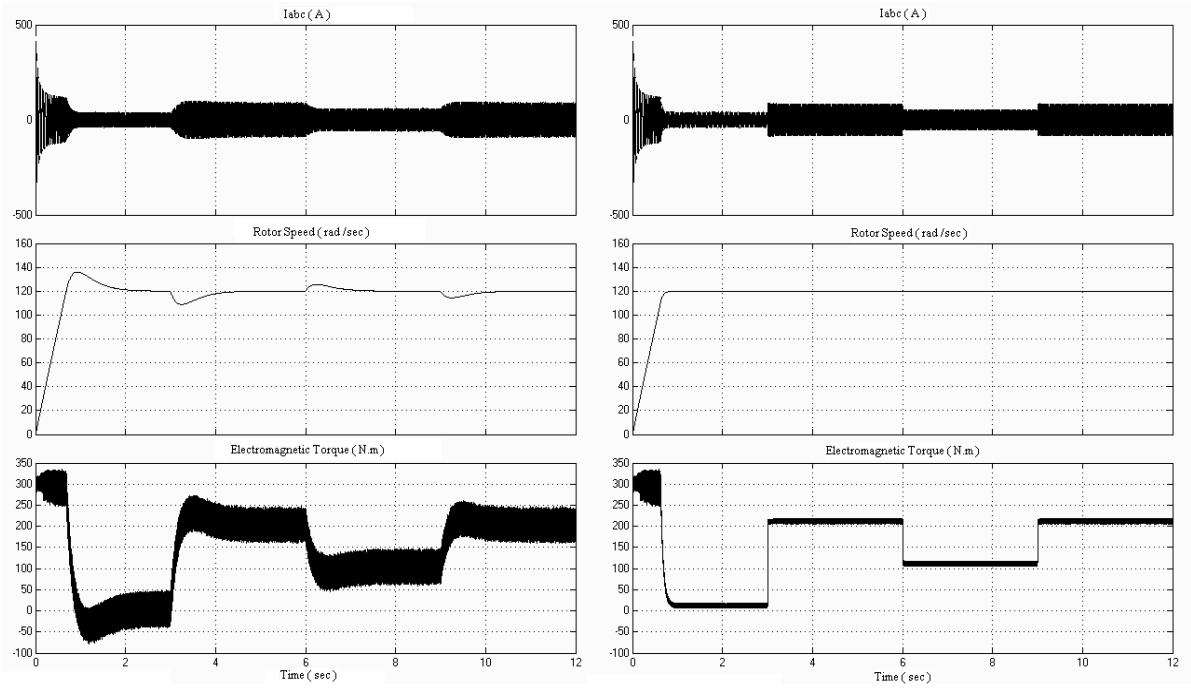

(a) PI (b) SMC-BL

Fig (21) Speed response at ω^*=120 rad/sec with load step changes, at (t=3sec) from (0-200 N.m) and at (t=6sec) from (200-100 N.m) and at (t=9sec) from (100-200 N.m).

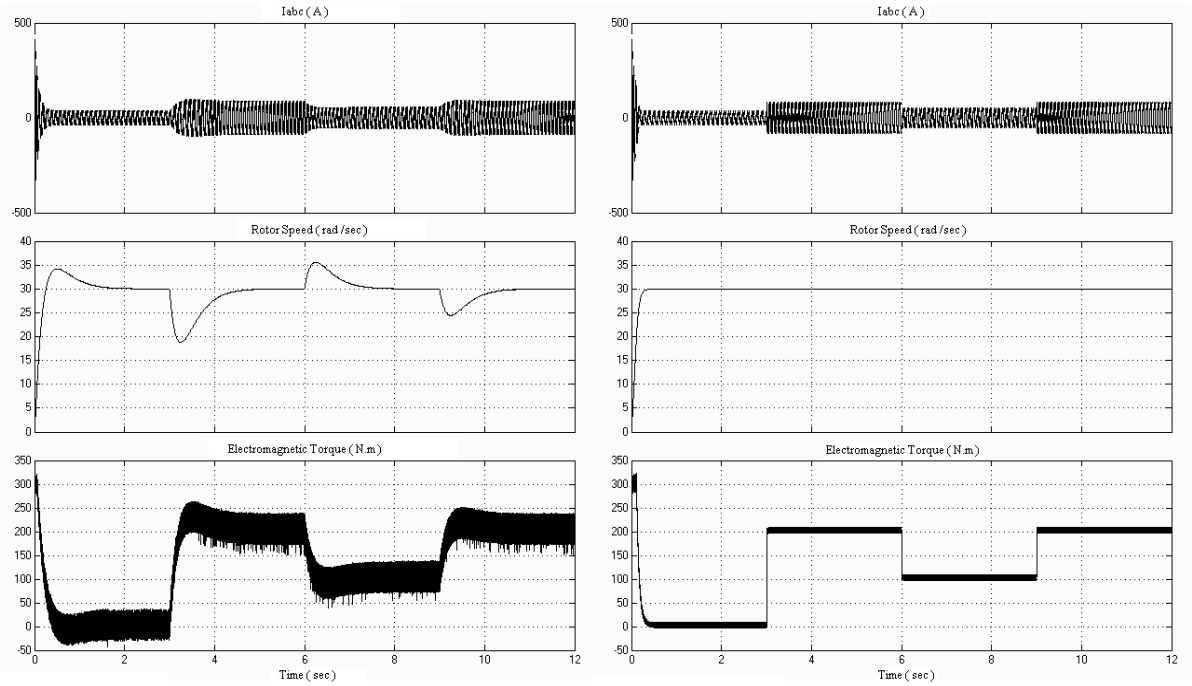

(a) PI (b) SMC-BL

Fig (22) Speed response at ω^*=30 rad/sec with load step changes, at (t=3sec) from (0-200 N.m) and at (t=6sec) from (200-100 N.m) and at (t=9sec) from (100-200 N.m).

CONCLOSIONS

Based on simulation results, the following aspects are concluded:

* The speed of the induction motor using the (SMC-BL) speed controller track the reference model output with zero steady state error and faster with no overshoot for different speeds, while the (PI) controller needs to be tuned for different speeds to insure the stability and good speed response.
* The (SMC-BL) system is more robust than the conventional system when the load disturbance occurs.
* The control techniques studied are very suitable for real time implementation due to their simplicity, robustness and ease of tuning.

REFERENCES

* B, K. Bose, ***"Modern Power Electronics and AC Drives"***, Prentice Hall Inc., USA, 2002.
* C. M. Ong, ***"Dynamic Simulation of Electric Machinery Using Matlab/Simulink"***, Prentice Hall Press, UK, 1998.
* A. M. Trzynadlowski, ***"Control of Induction Motors"***, Academic Press, UK, 2001.
* S. Emelyanov, **"*Variable Structure Control Systems*"**, Nauka Press, Moscow, Russia, 1967.
* V.I. Utkin**, "*Sliding Modes and Their Application in Variable Structure Systems*"**, Nauka Press, Moscow, Russia, 1974.
* R. A. DeCarlo, S.H Zak, and G.P. Matthews, **"*Variable Structure Control of Nonlinear Multivariable Systems: A Tutorial*",** Proceeding of IEEE, Vol.76, No.3, pp.212-232, Mar.1988.
* J. Y. Hung, W. Gao, and J. C. Hung, **"*Variable Structure Control: A Survey*",** IEEE Transactions on Industrial Electronics, Vol. 40, No.1, pp.2-22, Feb. 1993.
* Y. Itkis, **"*Control Systems of Variable Structure*"**, Wiley Press, New York, USA, 1976.

* T. V. M. Nguyen, Q. P. Ha and H. T. Nguyen, ***"A Chattering-Free Variable Structure Controller for Tracking of Robotic Manipulators"*,** Faculty of Engineering, University of Technology, Sydney, Australia, 2003.
* J. Li, **"*Design of Fuzzy Sliding-Mode Controllers and Their Applications to A Class of Mechatronic Systems* ",** Ph.D. Thesis, Department of Electrical Engineering, National Cheng Kung University Tainan, Taiwan, Repulic of China, July 2003.
* H. G. Kwatny and T. L. Siu, **"*Chattering in Variable Structure Feedback Systems*",** in Proc. IFAC 10th World Congress, Vol. 8, pp. 307-314, 1987.
* L. Zhihong, S. K. Panda, D. Q. Zhang and Y. C. Liang., ***"Modified Sliding Mode Speed Controller for Vector Controlled Induction Motor Drive"***, Proceedings of International Conference on Power Electronic Drives and Energy Systems for Industrial Growth, France, 1998.
* F. Cupertino, A. Lattanzi and L. Savatore., ***"Sliding Mode Control of an Induction Motor"***, IEE Conference on Power Electronics and Variable Speed Drives, UK, September 2000.
* A. Derdiyok, M. K. Gűven, N. Inanc, H. ur-Rehman and L. Xu., ***"A DSP – Based Indirect Field Oriented Induction Machine Control by Using Chattering–Free Sliding Mode"***, Proceedings of the IEEE National Aerospace and Electronics Conference NAECON 2000, USA, 2000.
* Y. Wang and R. Pei., ***"Speed Regulation of Induction Motor Using Sliding Mode Control Scheme"***, Conference Record of the Fourtieth Industry Applications Conference IAS Annual Meeting, USA, 2005.
* . Hazzab, I. K. Bousserhance, M. kamli and M. Rahli., ***"A New Fuzzy Sliding Mode Controller for Induction Motor Speed Control",*** IEEE Transaction on Fuzzy Systems, Vol. 7, No. 21, 2004.
* C. Gao and Y. Liu, **"*Stability of Variable Structure Control System*",** Proceeding of. American Control Conference, pp.1538-1539, Washington, USA, June 1995.
* J. E. Slotine and W. Li, **"*Applied Nonlinear Control*"**, Englewood Cliffs, Prentice Hall, Englewood cliff, new Jersey, USA, 1991.

List of symbols:

e	: Tracking error.
$\dot{e}$	: Time derivatives of the state tracking errors.
F	: Friction constant (N.m.s)
i_{qs} , i_{ds}	: q and d axis stator current (A).
i_{qr} , i_{dr}	: q and d axis rotor current (A).
I_a	: Armature current (A).
I_f	: Field current (A).
J	: Moment of inertia (Kg.m^2)
L_m	: Magnetizing inductance (H).
L_r	: Rotor inductance (H).
L_s	: Stator inductance (H).
P	: Number of machine poles
R_r	: Rotor resistance (Ω)
R_s	: Stator resistance (Ω)
$S(t)$	: Time-varying sliding surface.
$\dot{S}$	: First time-derivative of the sliding surface.
$\lvert S_i(q,t)\rvert$	: Distance between state e_i and sliding surface S_i .
T_e	: Electromagnetic Torque (N.m)

T_L	: Load torque (N.m)
v_{dr} , v_{qr}	: d and q axis rotor voltage (V).
v_{ds} , v_{qs}	: d and q axis stator voltage (V).
V	: Lyapunov function.
λ_s	: Stator flux (Wb.Turn).
λ_r	: Rotor flux (Wb.Turn).
λ_m	: Air gap flux (Wb.Turn).
λ_{qr}, λ_{dr}	: q and d axis rotor flux linkage (Wb.Turn).
λ_{qs}, λ_{ds}	: q and d axis stator flux linkage (Wb.Turn).
θ_e	: Angle between stator and rotor axes (rad).
θ_r	: Rotor position (rad)
θ_{sl}	: Slip angle (rad).
ω_r	: Angular rotor speed (electrical rad/sec).
ω_{ref}	: Desired speed (electrical rad/sec).
ω_b	: Angular Base frequency (electrical rad/sec).
ω_e	: Angular synchronous speed (electrical rad/sec).
ω_{sl}	: Slip frequency (electrical rad/sec).
Φ_i	: Boundary layer thickness.
ε_i	: Boundary layer width.

SKIN FRICTION BETWEEN UNDISTURBED OVER CONSOLIDATED SILTY CLAY SOILS AND CONCRETE

Dr. Azad Abbas Ahmed, Ph. D (C. E.)
Zuhair Kadhim JahanGer, M. Sc. (C. E.)

ABSTRACT

Up to date, in many foundation design problems (especially for piles foundation), the shear strength (skin friction) between soil and construction materials of the foundation was usually estimated or correlated without any direct methods for measurement.

The modern trend is to establish skin friction coefficients through laboratory experiments in which the factors influencing the results may be controlled quantitatively.

In this study strain controlled Direct Shear Tests were performed using shear to simulate the shear behavior area between concrete (foundation materials) and undisturbed over consolidated silty clay, to determine the shear strength of soil – foundation interface, considering the following variables : (1) Concrete, smooth surface condition, (2) Undisturbed over consolidated silty clay, (3) Variation of the normal load between the friction surface. The tests conveniently revealed both shear strength parameters as for soil test (cohesion and angle of internal friction), and interface angle of friction was in the range of 14° to 17°, while the adhesion was in the range of 13 to 16 kPa.

The ultimate shear strength was mobilized through 4 to 7 mm displacement in the direction of shear slip; this was a great advantage of Direct Shear Test performance.

KEYWORDS

undisturbed, over-consolidated, silty clay soils, soil-concrete interaction, skin friction, direct shear test.

الخلاصه

غالباً ما تستخرج معاملات مقاومة القص بين التربه ومواد الأنشاء(احتكاك التماس) في الأسس مختبرياً بدون طرق مباشِره للحساب.

يميل التوحه الحديث لأستخراج معامل التماس من تجارب مختبريه التي يمكن خلالها السيطره على الظروف والمعاملات المؤثره عليها.

في هذا البحث أجريت مجموعه من تجارب القص المباشر مسيطر الأنفعال في صندوق القص لمحاكاة تصرف القص بين الخرسانه (مواد الأساس)وتربه طينيه غرينبه مسبقه الأنضمام غير مشوشه لحساب مقاومه القص بينهما.أجريت التجارب أخذين بنظر الأعتبار المتغيرات والظروف (1)خرسانه ناعمه السطح (2) تربه طينيه غرينيه مسبقه الأنظمام غير مشوشه (3) تغيّر الحمل العمودي عل سطح التماس.عكست الأختبارات بشكل أعتيادي معاملات القص كما في تجارب التربه الطبيعيه (التلاصق وزاوية الأحتكاك الداخلي),و كانت زاوية احتكاك التماس ضمن الحدود بين 14° - 17 ° بينما ألتصاق بحدود 13 – 16 كيلوباسكال .

تأهبة مقاومة القص العظمى للتماس من 4- 7 ملم أزاحه بأتجاه شقّة القص . هذهِ هى فائدة كبيره من استخدام اختبار مقاومه القص المباشر .

* Managing Director of Andrea Engineering Laboratory for Soil Investigation and Construction Materials Testing.
** Assistant Lecturer, Baghdad University, Department of Water Resources Engineering.

INTRODUCTION

In the field of geotechnical engineering, it's well known that the designs of piles foundation depend upon end bearing and /or skin friction between the piles and soil. There are various ways to determine the pile capacity and most of them rely on full scale field tests using full size piles, but such tests are expensive and the results may apply only to the site where the test was performed. The value of skin friction factor to use in determining the load capacity of piles is a subject of much debate and testing (Budhu, M. 2000).

The soil parameters needed for static analysis of single and group piles capacity consist of the angle of internal friction φ and the cohesion c. The strength parameters have been determined from laboratory triaxial tests on undisturbed samples with experience used to extrapolate this data to obtain the design parameters. Also , they used in situ parameters of cone penetration test or pressure meter test and probably most pile design still relies heavily on standard penetration test N values in sand and field tests for shear strength in cohesive soil deposits (Bowles, J.E. 1988).

Many geotechnical problems involve estimation of stresses transferred along the interface between soils and solid surfaces. While considerable work have been done on the interfacial friction between cohesion-less soils (sands) and solid surfaces. The interfacial shear resistance between fine grained soils and solid surfaces depends on whether its mobilization takes place in the drained or in the undrained condition. Also most of these studies are on normally consolidated soils, the influence of over- consolidated soils has received little attention (Acar et. al 1982, Ampera, B. and Aydogmus, T. 2005)

The objective of this study is to use the Direct Shear Test Box to study interface friction and adhesive between undisturbed over consolidated clay soil and foundation material.

TEST PROGRAM

The test program consists of 12 Direct Shear Test on specimens of cohesive silty clay soil and concrete slice (foundation materials). The soil is placed in the bottom part of the Direct Shear Test Box and the concrete slice placed above it (in the top part of the box) as shown in **Fig.1**. Test series (S1 – S5) were performed on five undisturbed cohesive silty clay soils, a total of twelve Direct Shear Tests were carried out.

These 12 tests were conducted in such away that in the first six tests the rate of strain was higher than the second group, in addition to, the natural properties difference of the tested soils. **Table 2** shows the details information of the test series performed.

Its worth to mention, that all the soil series properties and characteristics physically and chemically, also the field work were carried out in accordance with (ASTM standards D 3080). **Table 1** presents the properties of tested soil.

SAMPLE PREPARATION

To prepare the test sample, for the direct shear test, the soil part of the specimen was undisturbed cohesive silty clay soil extracted directly from Shelby tube (Five undisturbed samples obtained from various locations in Babil governorate, 110 km south of Baghdad, were used in this work. It was extracted from different depths. The boring equipment used in carrying out the field work was rotary drills rigs, with the use of thin wall tube samplers Shelby tube for taking undisturbed samples .The disturbed samples were obtained, to determine the classification of soils, the samples that secured by the Standard Split Spoon Sampler were also used as disturbed samples, the water table was found at the time of boring be 3-4 m deep) using hollow box cutter sampler (6 × 6× 2 cm) specified for Direct Shear Test. The other part was a slice of concrete cube which was

cast using job mix (1:1.5:3) and cured for 28 days. Then the soil pushed to the bottom half of the Direct Shear Box before tighten the two halves of box. Later the concrete slice (foundation material) was put in the upper half of the Shear Box, as shown in **Fig. 1**. Finally the test was conducted in the usual manner (Das, B. M. 2002, and Lambe, T. W., 2000).

Slices of concrete cubes made to fit the Shear Box device dimension by making projection of 6 mm in the direction of applied shear and less than 1 mm in the opposite direction. The detailed characteristics of these soil samples are presented in **Table 1**. Note that the soils are denoted by series symbols (S1 – S5).

DIRECT SHEAR TEST

A conventional strain controlled Direct Shear Box machine with specimen dimensions of (6×6×2 cm) was used. Series of shear strength test on 12 samples were conducted in such away that the soil is placed in the bottom part of the Direct Shear Box and the concrete (foundation material) is placed above it, i.e. in the top part of the box. The test were carried out at two constant rate of strain 1.2 mm/min and 0.3 mm/min.

The tests were carried out in soaked condition using normal pressure ranging from 26.2 kPa to 349 kPa, as illustrated in **Table 2**.

Typical results of sample number five are shown in **Fig. 2**.

RESULTS AND DISCUSSION

Fig. 2, shows the results of Direct Shear Test between a cohesive soil and concrete (foundation material) in soaked condition at a stain rate of 1.2 mm/min. The ultimate shear strength was mobilized at about 10 % strain of sample dimension.

Fig. 3 and **Fig. 4**, illustrates the results between shear stress and normal stress for the first six specimens, the results show a friction angle and adhesion between the tested soil and concrete. The adhesion achieved from the cohesion properties of soil and angle of friction (interface friction) obtained from rough surface of concrete (foundation material).

Comparison of results of **Fig. 3** and **Fig. 4** with the results shown in **Fig. 5 and Fig. 6** indicates that testes at lower rate of strain i. e 0.3 mm/min had increased the adhesion and decreased the angle of internal friction slightly. This is due to the low applied strain that permits the soil to consolidate and to increase the contact area with the concrete face. The shear strength along the surface of contact of the soil and the foundation can be given as in eq. (1):-

$$\tau_f = c_a' + \sigma' \tan \delta' \qquad (1)$$

Where τ_f = Shear strength between the two different material.

c_a' = Adhesive.

σ' = Effective normal stress.

δ' = Effective angle of friction between the soil and the foundation material.

The shear strength parameters between a soil and a foundation material can be conveniently determined by a Direct Shear Test. The Direct Shear Test is simple to perform, but it has some inherent shortcoming .The reliability of the results may be questioned because the soil is not allowed to fail along the weakest plane but is forced to fail along the plane of split of the shear. This shortcoming is related to the original test for soil only to determine their strength parameters.

Despite of this shortcoming, this is a great advantage of the Direct Shear Test; where the shear strength between the soil and the foundation material can be obtain during ordinary site investigation for pile foundation construction.

CONCLUSIONS

This paper has presented the results of an experimental work on five different soil samples used as underneath soil for construction site. From the results of this work, the following conclusions can be warranted:

1. Interface friction angle of undisturbed cohesive soil- concrete (foundation material) can be determined using Direct Shear Test. This is a great advantage of the test.
2. The shear strength between undisturbed cohesive soils – concrete (foundation material) is mobilized at a 10 % strain of sample towards the shear direction that is about 4 – 7 mm horizontal displacement or slip.
3. The shear strength between undisturbed cohesive soils – concrete (foundation material) consisted of adhesion and interface angle of friction.
4. Normal pressure is the most effective parameter on the shear between the soil and concrete.
5. It's preferable to use this test with other tests to estimate the pile load capacity or the length of pile proposed.
6. It's recommended to do this work again, but with either foundation material and other undisturbed soils type or remolded disturbed soils.

REFERENCES

- Acar, Y. B., Durgunoglu, H. T. and Tumay, M. T. (1982) "Interface Properties of Sand." Journal of Geotechnical Engineering, ASCE, Vol. 108, No. 4, 648-654.

- Ampera, B. and Aydogmus, T. (2005) "Skin Friction between Peat and Silt Soils with Construction Materials." Ejge Paper, http://www.ejge.com/2005.

- American Society for Testing and Materials,ASTM. (1988). Annual Book of Standards, sec. 4, Vol. 04.08, West Conshohocken, Pa.

- Bowles, J, E. (1988)."Foundation Analysis and Design." 4th edition, McGraw-Hill, Inc.

- Budhu, M. (2000)."Soil Mechanics and Foundations." John Wiley and Sons, Inc, New York.

- Das, B. M. (2002)."Principles of Geotechnical Engineering." 5th edition, Brooks/Cole, pp315-322.

- Lambe, T.W. and Whitman, R.V. (2000) "Soil Mechanics." John Wiley and Sons, pp. 119-120.

Table 1 – Properties of Tested Soils

Soil Series	Depth (m.)	Sample No.	Consistency Limits		Natural Water Content (%)	Dry Density (kN/m^3)	Specific Gravity G_s	Consolidation Test				Sieve Analysis % Passing No. 200	Soil Type	Strength	SPT	Chemical Tests	
			Liquid Limit LL (%)	Plasticity Index PI (%)				Natural Void Ratio e_o	P'_c	Comp. Index c_c	Rebound Index c_r					Organic Matter (%)	Soluble Salts (%)
S1	2.0-3.0	1	40	18	17.2	15.7	2.69	0.739	120	0.18	0.031	97.4	CL	Med. To Stiff	14	8	1
		2															
S2	2.5-3.0	3	55	28	24.6	15.2	2.71	0.835	90	0.19	0.034	98.3	CH	Med. To Stiff	18	20	1
		4															
S3	3.0-4.0	5	48	25	27.2	13.9	2.69	0.851	85	0.16	0.031	96.3	CL	Med. To Stiff	16	11	1
		6															
S4	2.0-3.0	7	44	21	21.5	15.4	2.68	0.824	95	0.14	0.026	85.5	CL	Med. To Stiff	12	6	0.5
		8															
		9															
S5	5.5-6.5	10	43	23	25.9	14.4	2.68	0.788	125	0.17	0.031	97.0	CL	Med. To Stiff	23	×	×
		11															
		12															

× Not tested

Table 2 – Details of Test Series Performed

Soil Series	Sample No.	Normal Stress (kPa)			Rate of Strain (mm/min)	After Test		Interface Strength	
		1	2	3		Water Content (%)	Dry Density (kN/m^3)	Adhesion C (kPa)	Angle of interface friction Φ (°)
S1	1	41.9	71.0	129.3	1.20	26.3	15.4	36.13	14.86
	2	41.9	71.0	129.3	1.20	28.1	14.9	13.2	17.43
S2	3	41.9	71.0	129.3	1.20	25.20	15.0	16.35	10.5
	4	45	76.4	139	1.20	23.0	15.6	5.15	17.9
S3	5	45	76.4	139	1.20	29.0	14.3	4.0	18.53
	6	45	76.4	139	1.20	24.0	14.9	5.2	17.6
S4	7	45	76.4	139	0.30	24.2	15.6	12.93	16.4
	8	114	192.4	349	0.30	×	×	39.85	13.4
	9	114	192.4	349	0.30	×	×	21.49	15.10
S5	10	114	192.4	349	0.30	26.7	16.0	24.13	15.4
	11	114	192.4	349	0.30	×	×	45.8	8.3
	12	26.2	40.8	70	0.30	×	×	3.1	13.6

×Not tested

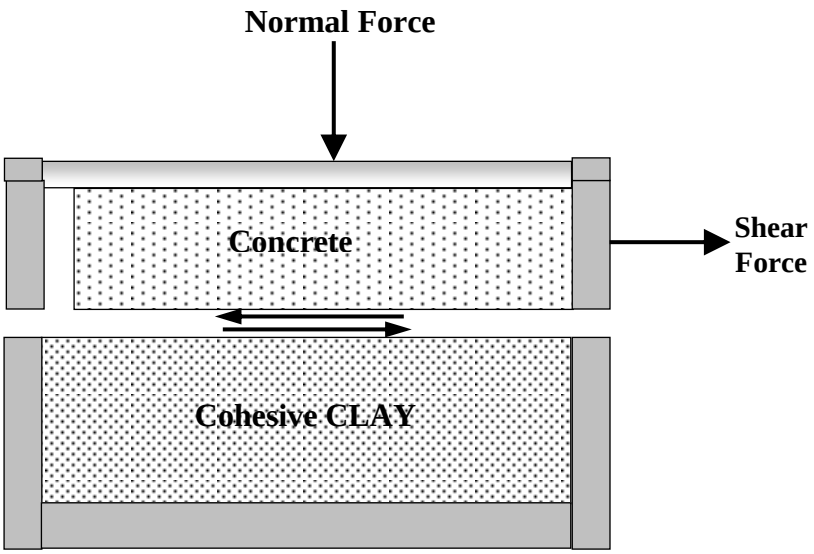

Fig. 1 Direct Shear Test to Determine Adhesion and Interface Friction Angle of Cohesive Clay – Concrete

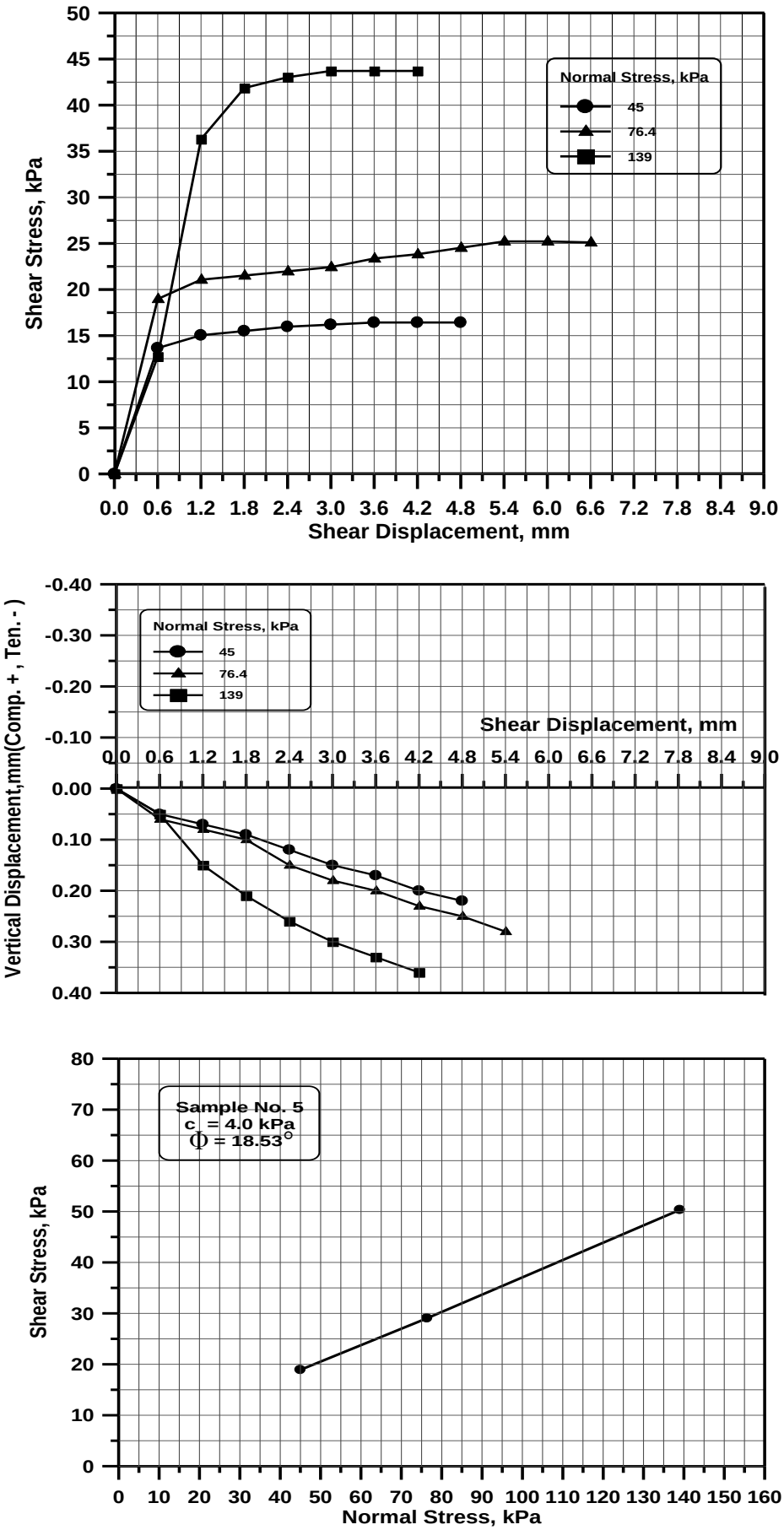

Fig. 2 Results of Direct Shear Test for Sample Number 5

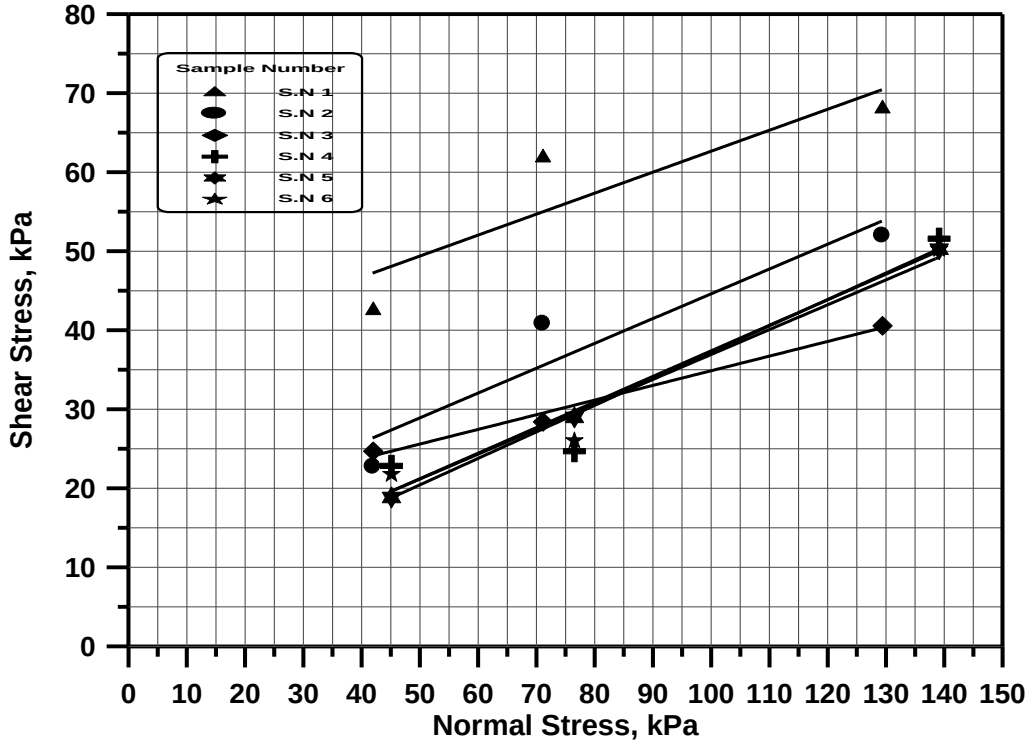

Fig. 3 Results of Direct Shear Test of over Consolidated Clay Soil-Precast Concrete in undrained Condition

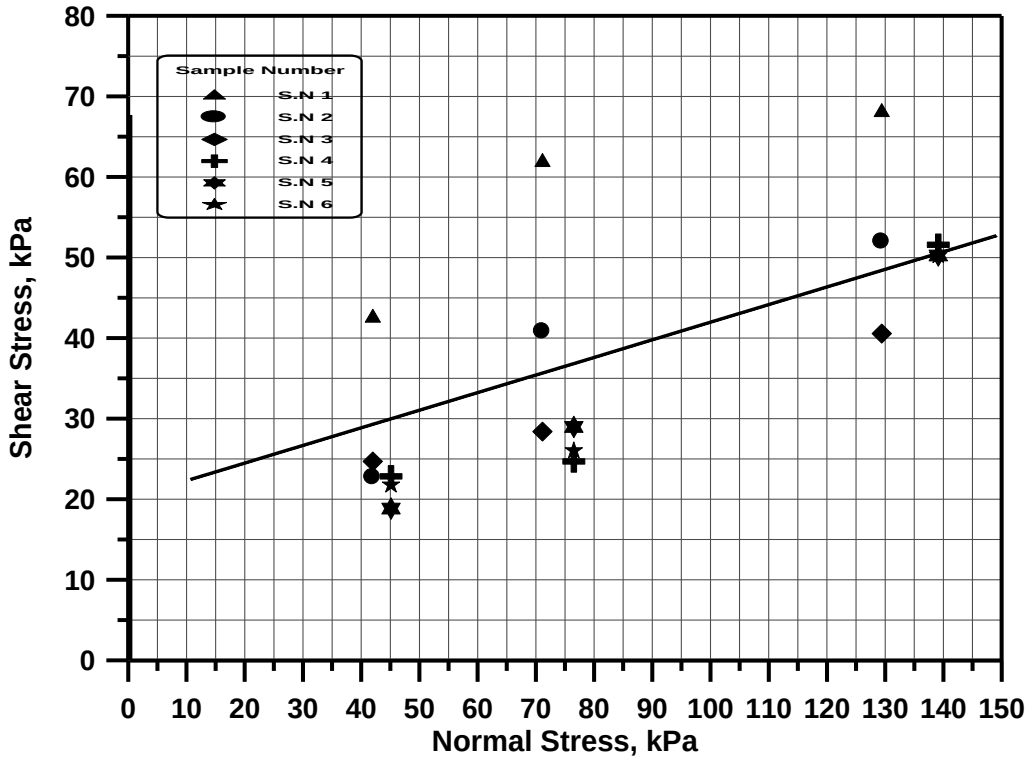

Fig. 4 Determination of Skin Friction of over Consolidated Clay – Precast Concrete in undrained Condition

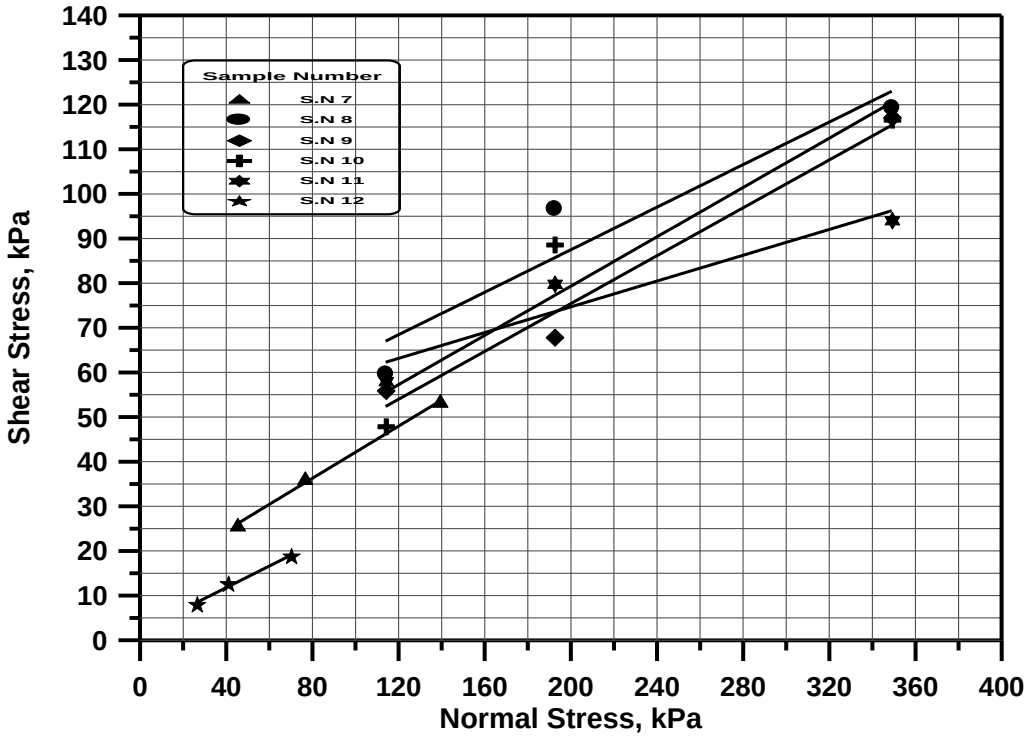

Fig. 5 Results of Direct Shear Test of over Consolidated Clay Soil-Precast Concrete in undrained Condition

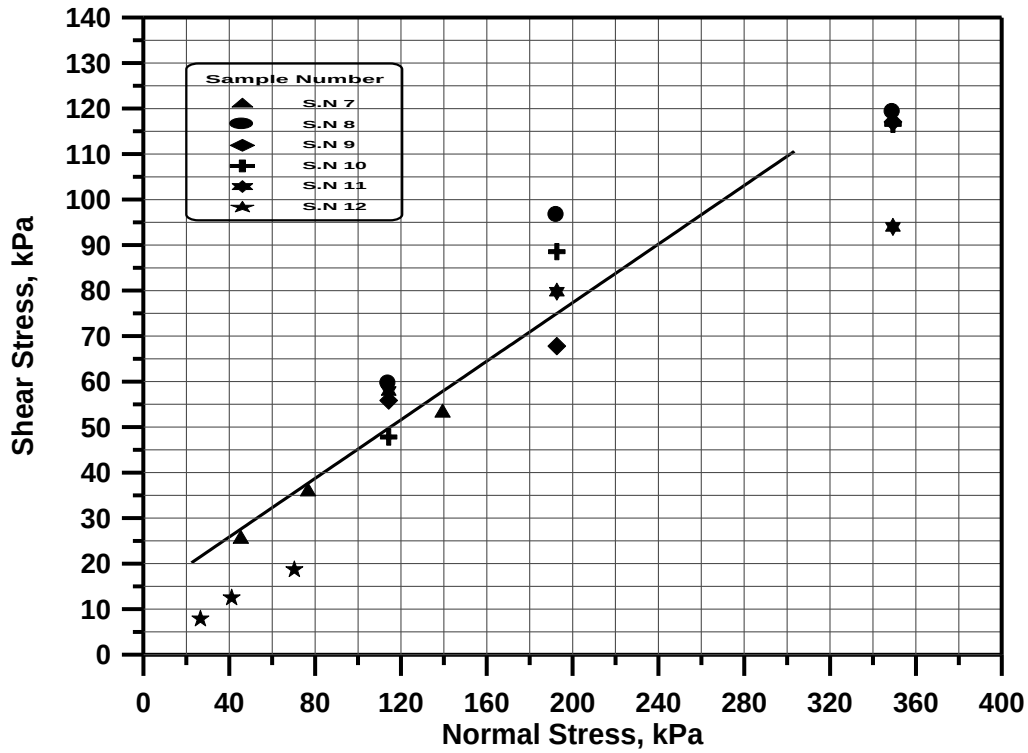

Fig. 6 Determination of Skin Friction of over Consolidated Clay – Precast Concrete in undrained Condition

LEACHING BEHAVIOR OF GYPSEOUS SOILS

Dr. Mahdi O. Karkush
Lecturer in Civil Eng. Dept.
University of Babylon

Dr. Yousif J. Al-Shakarchi
Prof. in Civil Eng. Dept.
University of Baghdad

Dr. Ala N. Al-Jorany
Asst. Prof. in Civil Eng, Dept.
University of Baghdad

ABSTRACT

A series of laboratory tests were carried out on disturbed soil samples containing different gypsum contents. The soil samples were obtained from al-Jazeera south-west of Iraq. Tests were performed to obtain the physical and mechanical properties of the soil. In addition; permeability-leaching tests were conducted by using oedometer and large-scale Rowe cell apparatus to obtain the variation of the coefficient of permeability, dissolved gypsum and leaching strain with time. All samples were tested under similar conditions, e.g. the hydraulic gradient, vertical stress and leaching period. The soil samples designated N_1, N_2, and N_3 are obtained from depths (0.5-0.75), (1.0-1.25), and (3.25-3.5) m and having gypsum content (31.43), (51.37), and (4.86) percentage respectively. Results of experimental work show that the coefficient of permeability, the percentages of dissolved gypsum and leaching strain measured from the oedometer test are higher than that measured from large-scale Rowe cell test for the same soil sample. The gypseous soil with higher gypsum content exhibited significant amount of leaching strain.

الخلاصة

اجريت سلسلة من الفحوص المختبرية على عينات مشوشة من التربة ذات محتوى جبسي مختلف. تم الحصول علي العينات من منطقة الجزيرة جنوب-غرب العراق. تم اجراء الفحوص الرئيسية للخواص الفيزياوية والميكانيكية لعينات التربة لغرض تصنيفها والاستفادة من نتائج هذه الفحوص في تفسير تصرف التربة إثناء عملية غسل الأملاح القابلة للذوبان من التربة. بالإضافة إلى ذلك تم أجراء فحص النفاذية-الغسل باستخدام جهاز الاوديوميتر وخلية رو ذات القياس الكبير لغرض حساب تغيير معامل النفاذية ونسبة الجبس المذاب وانفعال الغسل مع الزمن. تم فحص جميع العينات تحت نفس الظروف من الإجهاد العمودي والانحدار الهيدروليكي وفترة الغسل. استخدمت ثلاثة عينات من التربة في هذه الفحوص وتم ترقيمها N_1 وN_2 وN_3 والمستخرجة من الأعماق (0.5-0.75), (1.0-1.25) و (3.5- 3.25) متر وذات محتوى جبسي (31.43), (51.37) و (4.86) بالمائة على التوالي. إن معامل النفاذية ونسبة الجبس المذاب وانفعال الغسل التي تم الحصول عليها من فحص الاوديوميتر هي أعلى من تلك التي تم الحصول عليها من فحص خلية رو. هذا وان الانفعال بالغسل كبير في التربة ذات المحتوى الجبسي العالي.

KEY WORDS

Gypseous soil, Dissolution, Leaching, Gypsum, and Experimental Work.

INTRODUCTION

Gypseous soil appear to be strong, stable in their natural dry state, weak and collapsible under wetting generating large amount of settlement. The main cause of settlement is the dissolution of gypsum under wetting. The gypseous soil forms approximately (27-36) percentage of Iraqi soils (Al-Kaabi, 2007). Nashat (1990) studied the influence of soaking on the compressibility and

strength of gypseous soil. He concluded that soaking and leaching of gypsum leads to large reduction in undrained shear strength. Ismael (1993) carried out laboratory and field tests on a gypsiferous sandy silt soil. The results of tests indicate that leaching increases the permeability, void ratio, and compressibility. Al-Ani and Seleam (1993) studied the effects of initial water content and soaking pressure on the geotechnical properties of gypseous soils. They concluded that the increase in initial water content leads to decrease the collapse potential, the volumetric strain, and the compression index. Ismael and Mollah (1998) studied the effect of leaching on the properties of cemented sand deposits (natural and leached soil specimens). The results of tests indicate to an increase in the compressibility due to leaching. Al-Busoda (1999) studied the effect of leaching on the geotechnical properties of gypseous soil experimentally. The results indicate that 2.5% of dehydrate calcium chloride decreased the coefficient of permeability and the percentage of dissolved gypsum better than 5%. Al-Qaisee (2001) studied the behavior of gypseous soils under different preconsolidation pressures and different periods of soaking; also the collapse of soil during leaching using the oedometer permeability-leaching test. The test results indicate that void ratio remains constant with time for normally consolidated specimens and increases for overconsolidated specimens. Al-Rawi (2003) studied the effects of long-term soaking on the engineering properties of gypseous soil. The results obtained show that increasing the soaking period for both flowing and stable water basins decreases the percentage amount of gypsum, which remains stable in the case of gypsum saturated water basin. Mahdi (2004) conducted a non-standard field plate loading tests in six selected locations of gypseous soils. The soil was tested in its natural moisture content and after complete soaking with water. The results of tests indicated that soaking decreases the values of stiffness module, which causes an increase in settlement. Al-Obaidi (2007) investigated the leaching behavior of gypsiferous soils by using permeability-leaching oedometer test.

EXPERIMENTAL WORK

The samples were extracted by using handle excavation, with helping of a shovel, then labeled and encased in nylon cases. The laboratory tests were carried out according to the program given in Fig. 1. Note you have to omit Shear strength test and the direct shear test from Testing Program.

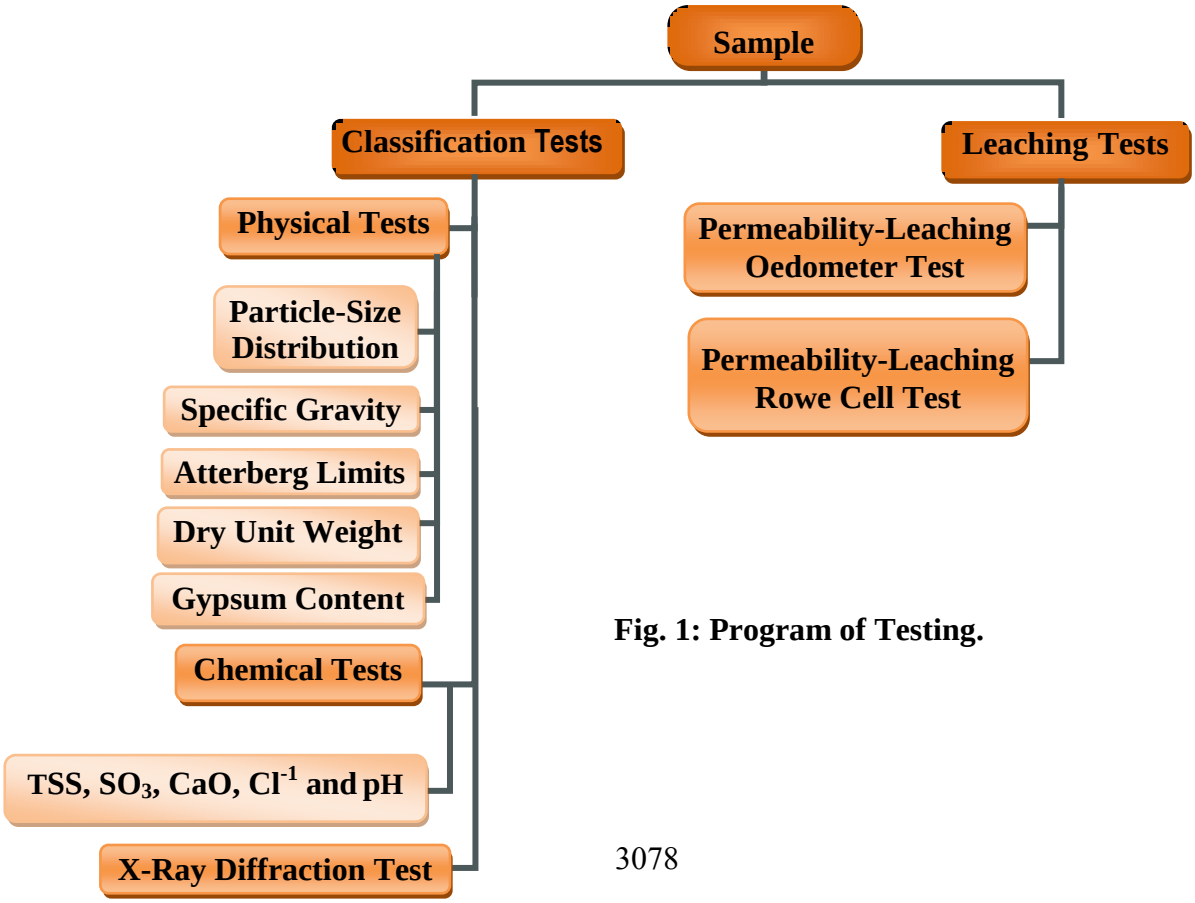

Fig. 1: Program of Testing.

CLASSIFICATION TESTS

Soil samples were classified according to the American Society for Testing and Materials (ASTM) specifications and British Standards (BS).

Particles-Size Distribution

The presence of gypsum in soil sample affects the results of particle-size distribution due to the cementation of soil particles by gypsum and its dissolution in water. Accordingly, modifications in some details of test procedure are needed to take care of the presence of gypsum in soil.

The particle-size distribution of different samples has been tested according to the standard method ASTM 422-79 (dry sieving) and by using kerosene as non-polar solvent (wet sieving). The wet sieving method involved washing the soil samples upon sieve No.200. The fraction of soil sample retained on sieve No.200 is oven dried at 45ºC and then analyzed using dry sieving. The results of particle-size distribution of the soil samples are given in Table 1 and Fig. 2.

Table 1: Classification of Soil Samples.

Sample No.	USCS
N_1	Poorly graded sand with gravel (SP)
N_2	Poorly graded sand with gravel (SP)
N_3	Poorly graded sand (SP)

Gypsum Content

The gypsum content of the soil samples was calculated by using the method proposed by Al-Mufty and Nashat (2000). In this method, the gypsum content was calculated according to the following formula:

$$\chi_{CaSo_4.\varepsilon H_2o} = \frac{W'_{s,45^oC} - W_d}{W_{s,45^oC}} * \frac{136+18\varepsilon}{36} * 100 \quad (1)$$

$$\varepsilon = \frac{2(W_{s,45^oC} - W_d)}{W'_{s,45^oC} - W_d} \quad (2)$$

Where χ is the gypsum content; ε is the number of hydration water molecules in the hydrated calcium sulfate molecules; $W_{s,45^oC}$ is the weight of soil sample oven dried after 24 hours at 45ºC; $W'_{s,45^oC}$ is the weight of soil sample after being flooded by distilled water and oven dried at 45ºC after 24 hours and W_d is the weight of soil sample oven dried at 105ºC after 24 hours.

The results of gypsum content tests are given in Table 2. The distribution of gypsum in the tested sandy soil samples is present in the form of coarse inclusions.

Table 2: Gypsum Content of the Soil Samples.

Sample No.	Gypsum Content %
N_1	31.43
N_2	51.37
N_3	4.86

Specific Gravity

The specific gravity of the tested samples was determined according to the BS 1377:1975, Test 6 (B). Kerosene was used instead of water to avoid solving of gypsum (Head,1984). The test results indicate that the specific gravity decreases with the increase of gypsum in the soil sample due to the low specific gravity of gypsum. The specific gravity of gypsum is 2.32.

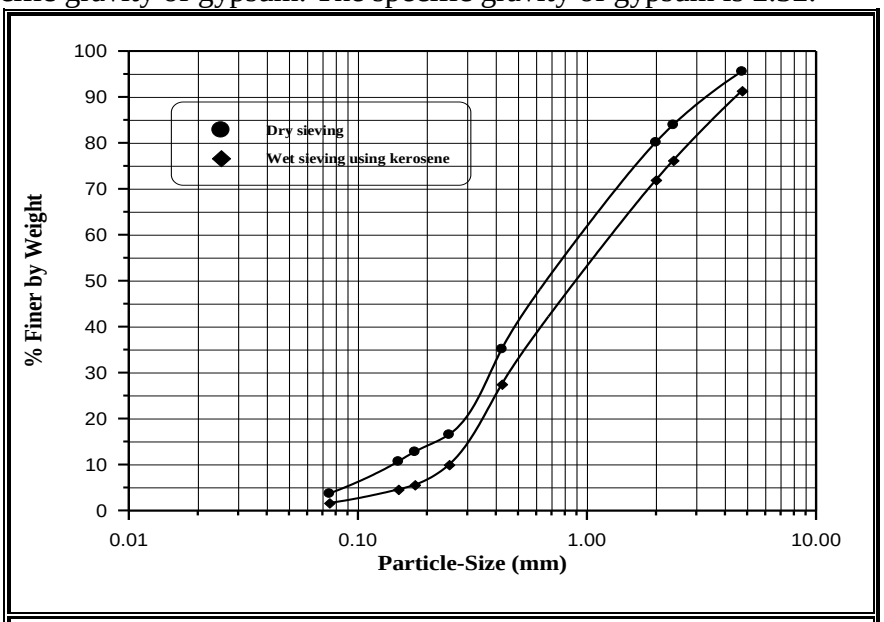

Sample N_1

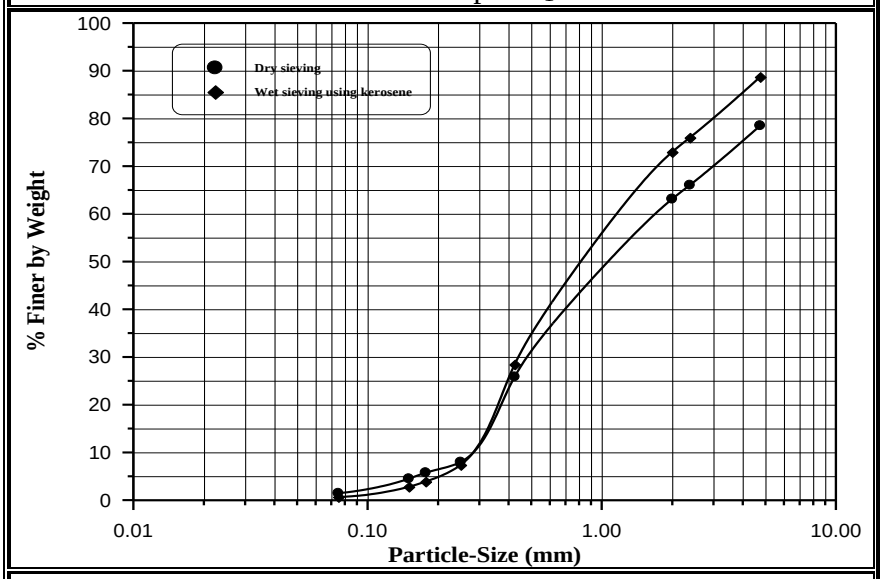

Sample N_2

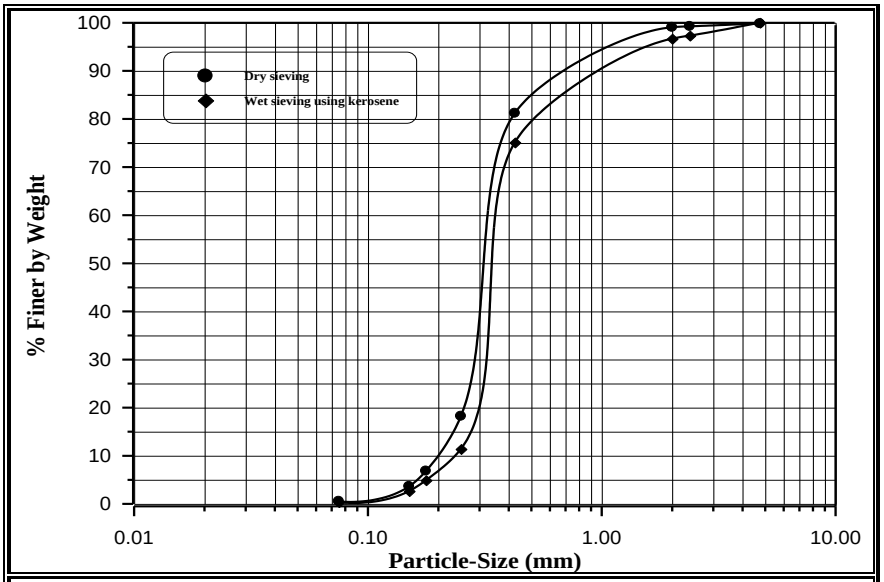

Sample N_3

Fig. 2: Particle-Size Distribution Curves of Soil Samples.

Atterberg Limits

Atterberg limits (liquid and plastic) were measured according to the BS 1377: 1975. The liquid limit was carried out according to test 2(A) using the cone penetrometer method on soil passing sieve No.40. The plastic limit was carried out according to test 3. To prevent the loss of the water of crystallization, the drying temperature must not exceed 80°C (Head,1984).

Dry Unit Weight

The minimum dry unit weight of the tested soil samples was determined according to the test described by Head (1984). It is widely accepted as a standard test for sandy soils. The maximum dry unit weight was determined according to ASTM D2049-64T (Bowles,1986). The tests results of Atterberg limits, Specific gravity, Dry unit weights, and Gypsum content are given in Table 3.

Table 3: Physical Properties of the Soil Samples.

Sample No.	Liquid Limit L.L (%)	Plastic Limit P.L (%)	Initial Void Ratio e_o	Specific Gravity Gs	Minimum dry Unit Weight (kN/m^3)	Maximum dry Unit Weight (kN/m^3)
N_1	29	NP	0.77	2.44	12.2	14.87
N_2	45	NP	0.93	2.42	10.87	13.71
N_3	25	NP	0.61	2.49	14.29	15.99

Chemical Tests

The chemical composition of the tested soil samples was calculated from several chemical tests. The results of chemical tests are given in Table 4.

Table 4: Results of Chemical Tests.

Sample No.	TSS %	SO_3 %	CaO %	Cl^{-1} %	pH
N_1	32.43	17.15	10.37	0.09	7.7
N_2	52.64	29.1	16.75	0.09	7.7
N_3	5.07	2.79	1.71	0.18	8.3

X-Ray Diffraction Test

X-ray diffraction test was carried out primarily to identify the mineral phases (classification of soil minerals into clay minerals and non-clay minerals). These tests indicate that non-clay minerals predominantly consist of quartz and gypsum while the clay minerals predominantly consist of palygorskite and mica. The results of x-ray diffraction tests are given in Table 5.

Table 5: Results of X-Ray Diffraction Tests.

Sample No.	X-Ray Diffraction	
	Non-Clay Minerals	Clay Minerals
N_1	Quartz, Gypsum, Calcite, Dolomite and Hematite	Palygorskite, Mica and Kaolinite
N_2	Quartz, Gypsum, Feldspar and Dolomite	Palygorskite, Mica, Montmorillonite and Kaolinite
N_3	Quartz and Gypsum	Palygorskite, Mica, Montmorillonite and Kaolinite

REMARKS ON SOIL PROPERTIES

The classification tests provide a reliable indication about the engineering characteristics of the soil. The particle-size distribution was found to be relevant in the engineering classification of most soils. In addition to the initial gypsum content, the chemical composition of gypsum and the distribution of the gypsum in the soil has significant role in the classification of gypseous soils.

There is a small difference between the dry and the wet methods of particle-size distribution of the soil sample as shown in Fig. 2. This difference results from washing the soil by kerosene on sieve No.200. The washing reduces the sharp edges of the soil particles and destruction some of the particles cementation resulting from the presence of minerals that dissolve in kerosene.

Atterberg limits play an important role in the classification of cohesive soils, which affect on the scale of magnitude of their many properties such as compressibility, permeability, and strength. The liquid limit increased with increasing the initial gypsum content as shown in Table 3. The presence of gypsum in the soil reduces the importance of Atterberg limits effects on the soil properties. The specific gravity is decreases with increasing the initial gypsum content as shown in Table 3 due to the lower specific gravity of gypsum, which is equal to 2.3.

LEACHING TESTS

A series of permeability-leaching tests conducted on samples of different gypsum contents by using the permeability-consolidation cell and large-scale Rowe cell. The tests were performed under similar conditions such as vertical stress, hydraulic gradient and leaching period. The hydraulic gradient was chosen in order not to affect the orientation of soil particles during leaching process (Al-Khuzaie, 1985). The measured data from these tests are the coefficient of permeability, dissolved gypsum percentage, and leaching strain.

Permeability-Leaching Oedometer Test (PLOT)

The permeability-leaching test was conducted by using a special oedometer cell called the permeability-consolidation cell of dimensions 75 mm in diameter and 19 mm in height. Fig. 3 shows the schematic diagram of the setup used in testing. The test consists of three stages: dry compression stage, saturation stage, and leaching stage. The soil samples were tested under vertical stress of 200 kPa and hydraulic gradient of 57 (Karkush,2008).

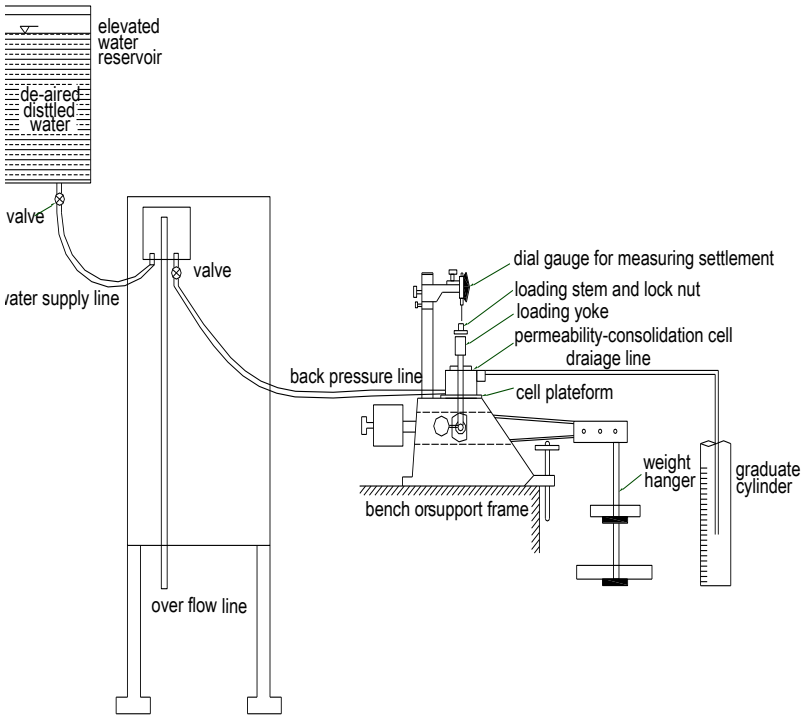

Fig. 3: The Schematic Diagram of Permeability-Leaching Test by Oedometer.

The duration of leaching stage is divided into intervals, at the end of each interval record the volume of leachate collected in a graduate cylinder to measure the change in the coefficient of permeability with time assuming laminar flow (Head, 1988).

$$k = \frac{Q_L}{60\, A_C\ i\ t} \tag{3}$$

where k is the coefficient of permeability in the flow direction (m/sec), Q_L is the volume of leachate (ml) in time t, A_C is the cross-sectional area of soil sample (mm^2), i is the hydraulic gradient ($\Delta h/H$), t is the time (min), Δh is the difference in head (mm), H is the height of soil sample (mm). Also, record the change in the height of the soil sample to calculate the leaching strain.

Permeability-Leaching Rowe Cell Test (PLRCT)

The permeability-leaching test using Rowe cell consists of three main stages: Saturation stage, Consolidation stage and Leaching stage. Large samples of Rowe cell (151.4 mm in diameter and 50 mm in height) are used to test under vertical stress of 200 kPa and hydraulic gradient of 50. The schematic diagram of the used system is shown in Fig. 4 (Karkush,2008).

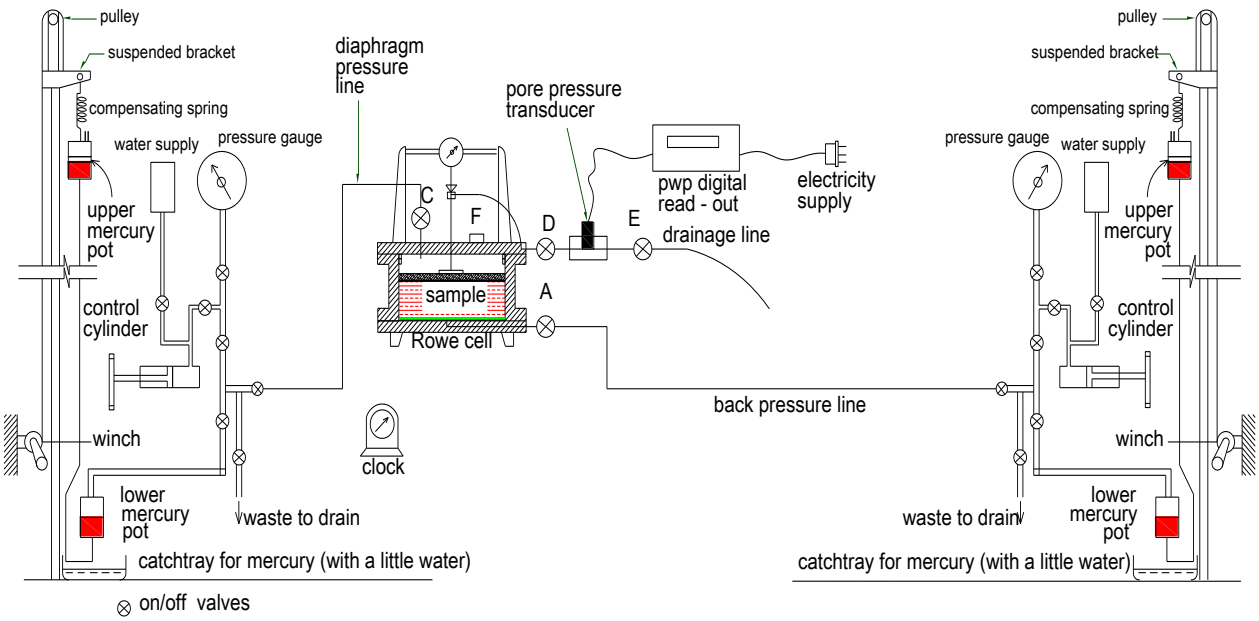

Fig. 4: The Schematic Diagram of Permeability-Leaching Test by Rowe Cell.

RESULTS AND DISCUSION

The variation of the coefficient of permeability k with time for the three tested soil samples N_1, N_2, and N_3 are shown in Fig. 5. In general, the coefficient of permeability resulting from Oedometer test decreases rapidly with the time in the first 50 hrs of time of tests.

For the three samples tested by large-scale Rowe cell, the permeability coefficient is unsteadily oscillated with time as shown in Fig. 5. The higher effective radius of soil particles means more coarse grains and consequently affects the reorientation of the soil particles during leaching process.

The final values of the coefficient of permeability were much lower than its values at the beginning of the test. The percentage of the initial gypsum content and dissolved gypsum plays a significant role in the variation of the coefficient of permeability with the time. The coefficient of permeability resulting from the oedometer test is higher than that resulting from Rowe cell test. This difference may be due to the difference in the stages of testing procedures adopted in the present study or the small difference in hydraulic gradients between the two types of tests. The variations in the percentage of dissolved gypsum and the percentage of leaching strain with the time obtained experimentally from oedometer test for the three tested soil samples are shown in Fig. 6. While, for the three tested soil samples by Rowe cell are shown in Fig. 7. The soil of initial gypsum content exceeding 50% can be treated as gypsum containing soil. The non-uniform distribution of gypsum in the soil sample leads to a difference in strain value.

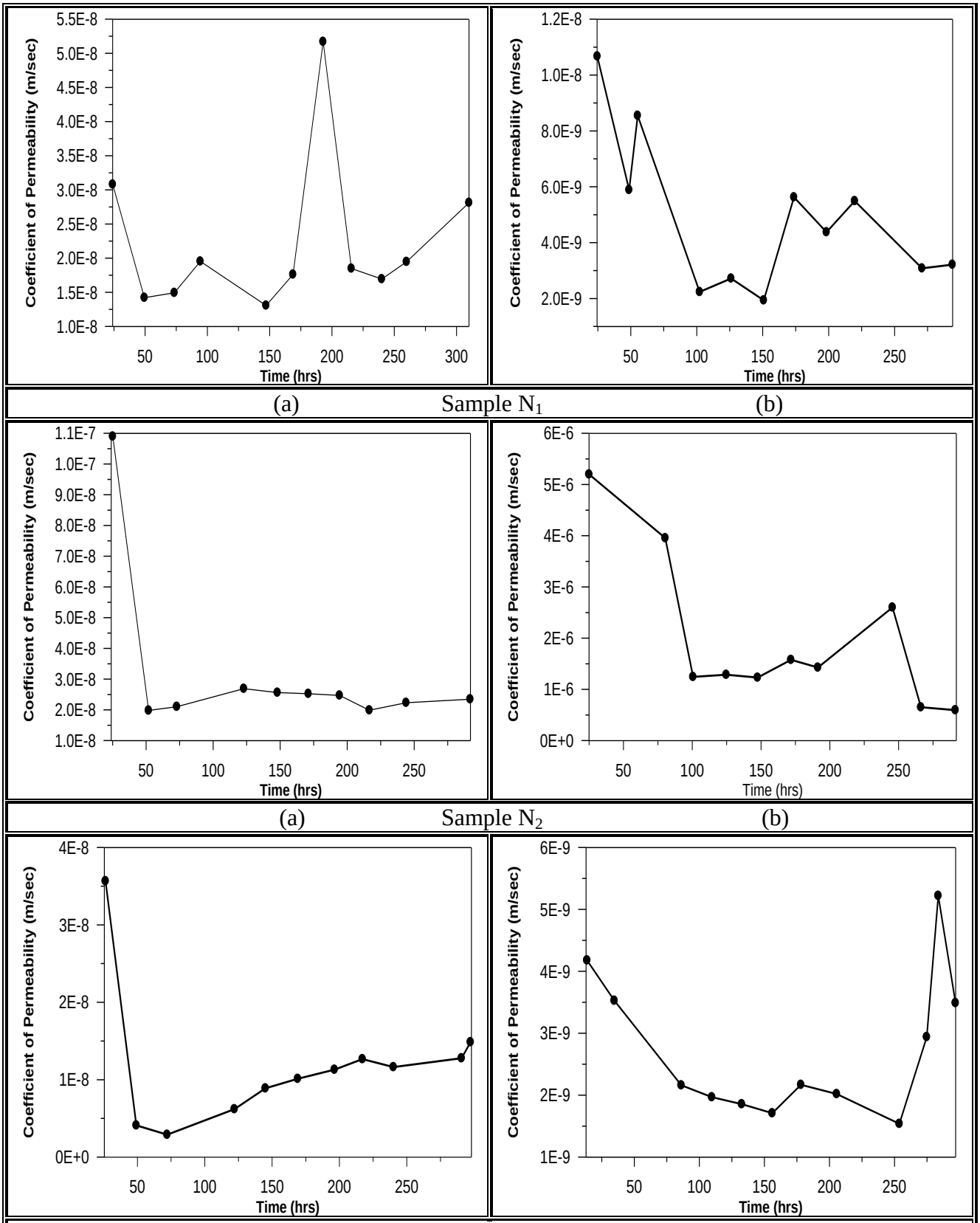

Fig. (5): Coefficient of Permeability for the Samples Tested by (a)- Oedometer and (b)- Rowe Cell.

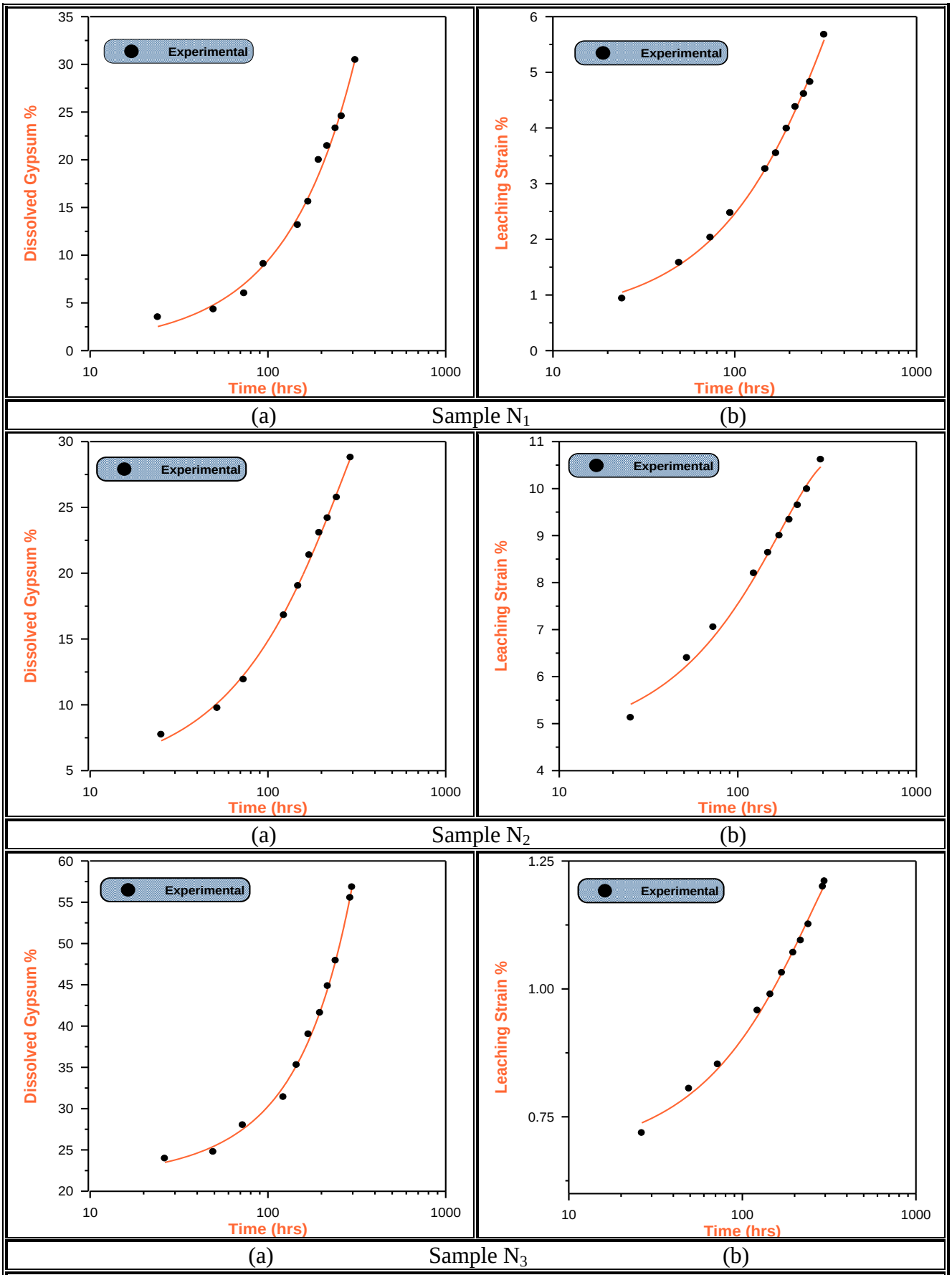

Fig. (6): Experimental Results for Samples N_1, N_2 and N_3 Tested by Oedometer: (a)-Dissolved Gypsum versus Time and (b)-Leaching Strain versus Time.

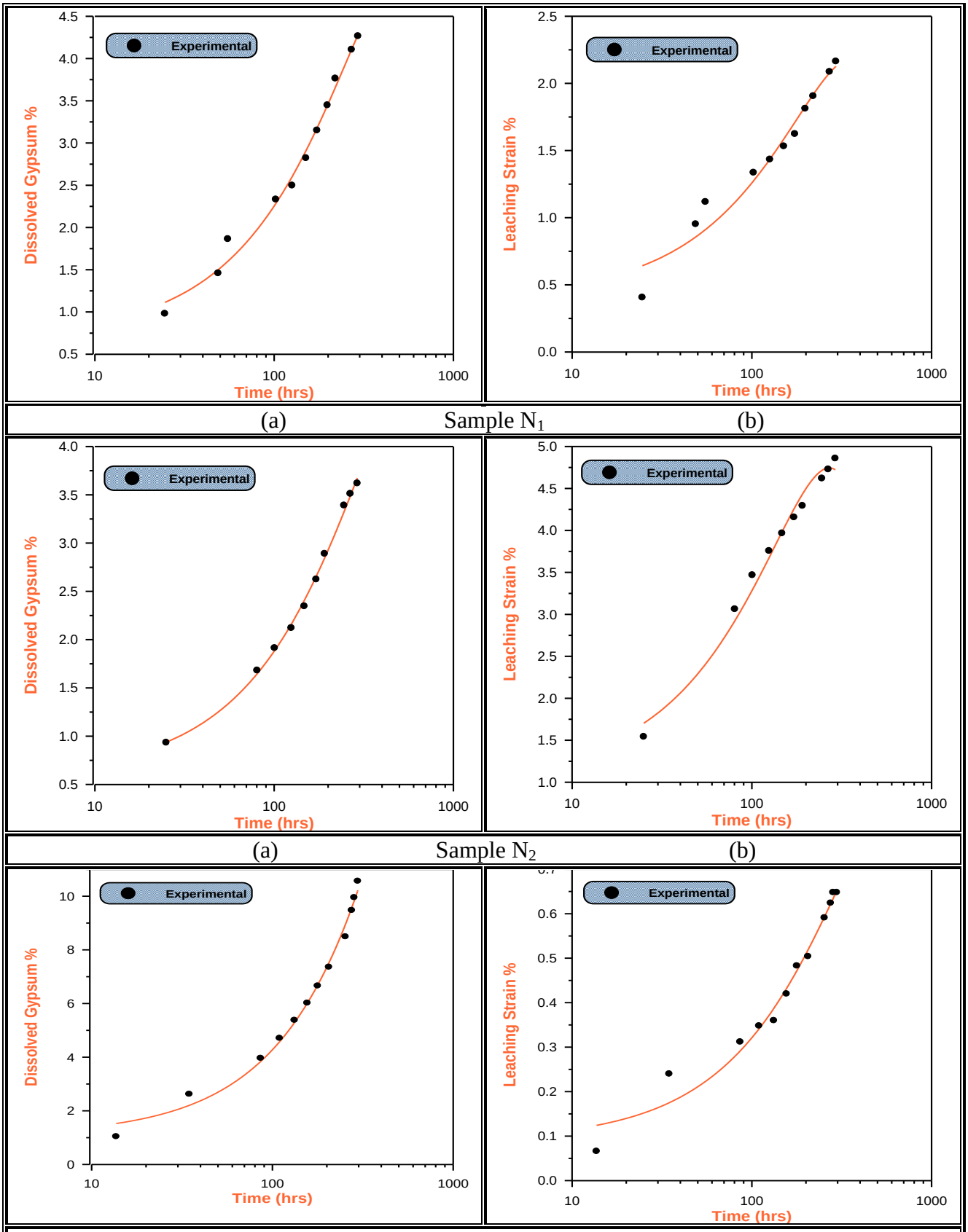

Fig. (7): Experimental Results of Sample N_1, N_2 and N_3 Tested by Rowe Cell: (a)- Dissolved Gypsum versus Time and (b)- Leaching Strain versus Time.

CONCLUSIONS

* The gypseous soil samples exhibit significant amount of leaching strain, which is larger than the initial settlement and has no definite endpoint upon the continuation of gypsum dissolution and leaching from a soil sample;
* For soil samples with high gypsum content, there is an increase in the percentage of dissolved gypsum in leaching water, consequently the leaching strain increases;
* The percentage of dissolved gypsum in leaching water decreases upon progressing of leaching process (time of leaching);
* The coefficient of permeability, the percentages of dissolved gypsum and leaching strain measured from the oedometer test are higher than that measured from large scale Rowe cell test for the same soil sample and under the same conditions, but under different sizes of soil samples;
* The permeability-leaching test by using large-scale Rowe cell gives more reliable results than those by using the ordinary permeability consolidation-cell (oedometer test).

REFERENCES

* Al-Ani, M.M., and Seleam, S.N. (1993),"Effect of Initial Water Content and Soaking Pressure on the Properties of Gypseous Soils", Al-Muhandis J., Iraqi Eng. Union, Vol.116, pp.3-12.
* Al-Busoda, B.S.Z. (1999),"Studies on the Behavior of Gypseous Soil and its Treatment during Loading", M.Sc. Thesis, Civil Eng. Dept., University of Baghdad.
* Al-Kaabi, F.S. (2007),"Distribution of the Gypsiferous Soil in Iraq", State Company of Geological Survey and Mining, Report No.3044, Iraq, Baghdad, (in Arabic).
* Al-Khuzaie, H.M.A. (1985),"The Effect of Leaching on the Engineering Properties of Al-Jazirah Soil", M.Sc. Thesis, Civil Eng. Dept., University of Mosul, Iraq.
* Al-Mufty, A.A. and Nashat, I.H. (2000),"Gypsum Content Determination in Gypseous Soils and Rocks", Third International Jordanian Conference on Mining, Amman, pp.500-506.
* Al-Obaidi, A.L.M. (2007),"Gypseferrous Soil Behaviour by Finite Element Method", Ph.D. Thesis, Civil Eng. Dept., University of Baghdad.
* Al-Qaisee, G.S.H. (2001),"Leaching Collapse of Gypseous Soils", M.Sc. Thesis, Civil Eng. Dept., University of Baghdad.
* Al-Rawi, M.K. (2003),"Effect of Long-Term Soaking on the Engineering Properties of Gypseous Soils", M.Sc. Thesis, Civil Eng. Dept., University of Mosul, Iraq.
* Annual Book of ASTM Standards (1977 & 1979),"Soil and Rock; Building; Stone; Peats", Vol.04.08, Part1.
* Annual Book of ASTM Standards (2003),"Soil and Rock; Building; Stone; Peats", Part1.
* Bowles, J.E. (1986), "Engineering Properties of Soil and their Measurement", McGraw-Hill Book Co., Fifth Edition, New York.
* BS 1377 (1976),"Methods of Testing for Civil Engineering Purpose", British Standards Institution, London.
* Head, K.H. (1984; 1988; 1986),"Manual of Soil Laboratory Testing", Vol.1; Vol.2 & Vol.3 Pentech Press, London.
* Ismeal, N.F. (1993),"Laboratory and Field Leaching Tests on Coastal Salts-Bearing Soils", Journal of Geotechnical Engineering, Vol.119, No.3, pp.453-470.
* Ismeal, N.F. and Mollah, M.A. (1998),"Leaching Effects on Properties of Cemented Sands in Kuwait", J. of Geotechnical and Geoenvironmental Eng., Vol.124, No.10, pp.997-1004.
* Karkush, M.O. (2008),"Theoretical Modeling and Experimental Investigation of the Leaching Behavior of Gypseous Soil", Ph.D. Thesis, Civil Eng. Dept., University of Baghdad.

* Lambe, T.W. and Whitman, R.V. (1995),"Soil Mechanics", John Wiley and Sons, New York.
* Mahdi, B.O. (2004),"Some Aspects of Gypseous Soil of the Middle Part of Iraq", Ph.D. Thesis, Civil Eng. Dept., University of Baghdad.

* Nashat, I.H. (1990),"Engineering Characteristics of Some Gypseous Soils in Iraq", Ph.D. Thesis, Civil Eng. Dept., University of Baghdad.

SECTIONAL CURVATURE DUCTILTY OF REINFORECD CONCRETE COLUMNS UNDER LARGE INELASTIC DEFORMATION

Dr. Raad K. Al-Azzawi
Lecturer. /Civil Eng. Dept.
College of Eng. / University of Baghdad.

ABSTRACT

A mathematical model is developed to express stress-strain relationship of normal-strength concrete confined by transverse reinforcement. The sectional ductility analysis on rectangular reinforced concrete columns is performed under axial load. Analytical modals available in the literatures for confinement concrete by different types of transverse reinforcement are used. A parametric study is performed to study the influence of these parameters on the curvature ductility of reinforced concrete columns. The main parameters introduced are the amount of longitudinal reinforcement, amount of transverse reinforcement, tie spacing and the level of the compression axial force. The experimental and analytical results available in the literatures are being compared with present study.

KEYWORDS:
Columns, Confined Concrete, Curvature Ductility, Stress-Strain Relationships.

الخلاصة:

في هذا البحث تم تطوير التمثيل الرياضي لعلاقة الإجهاد مع الانفعال للخرسانة المسلحة الاعتيادية والمحصورة بالتسليح الجانبي . تم حساب مطيلية التقوس لمقاطع أعمدة ذات خرسانة مسلحة ومستطيلة الشكل تحت تأثير القوة المحورية المسلطة. تم استخدام عدد من علاقات الإجهاد مع الانفعال للخرسانة المحصورة والمتوفرة في المصادر.

تم إجراء الدراسة بإدخال عدة متغيرات لمعرفة مدى تأثيرها على مطيلية التقوس. المتغيرات الرئيسية المستخدمة هي كمية الحديد الطولي و كمية الحديد الجانبي والمسافات بين روابط التسليح الجانبي ومقدار القوة المحورية المسلطة.تم مقارنة النتائج مع نتائج عملية متوفرة.

INTRODUCTION

Columns subjected to lateral forces such as dynamic loads must be designed according to the displacement or recently performance based approach , Bousalem, Chikh and . Hachem (2004).

A significant amount of transverse reinforcement, which has a double function in resisting shear forces as well as providing confinement to the concrete core, must be provided to achieve a ductile behavior. The presence of transverse reinforcement to increase strength and ductility in these regions of the columns is a major consideration. Therefore, tests have shown that the confinement of concrete by adequate arrangement of transverse reinforcement will cause a significant enhancement in the flexural strength capacity of the reinforced concrete column.

A mathematical model is developed to express stress-strain relationship of normal-strength concrete confined by transverse reinforcement in order to perform a moment curvature analysis with quantity of the confining steel required in reinforced concrete columns sections to achieve the ultimate curvatures required for ductility demands. The predictions of the behavior of a four representative specimens tested by Sheikh and Yeh (1990) from the considered stress-strain models for confined concrete are compared with the test results.

The unconfined moment capacity is calculated based on the equivalent rectangular concrete stress block and as stated by Bousalem, Chikh and Hachem (2004).

.

ANALYTICAL STRESS-STRAIN MODELS:

The analytical models were developed in the light of the experimental data and various stress-strain models for the prediction of the confined concrete have been illustrated and a summary of mathematical expressions of some established models is shown in **Table (1)**.

STRESS-STRAIN RELATIONSHIP MODEFIED FOR CONFINED CONCRETE:

The modefied model was developed on the basis of the observations derived from several experimental studies tested by Sheikh and Yeh (1990) and as indicated by Bousalem, Chikh and Hachem (2004).The experimental observations show that the stress strain curve of confined concrete is constantly characterized by three parts: the ascending branch, descending branch and the sustaining branch. The mathematical formulation of the stress-strain relations are shown in **Tables (1)** and **(2)**.

ULTIMATE COMPRESSION STRAIN:

As confirmed by Bousalem, Chikh and Hachem (2004), Scott et al.(1982) observed that it is reasonably conservative to define the limit of useful concrete compressive strain ε_{cu} where the first hoop fractures occurs. Recently, Priestley et al. (1996) proposed a value of ε_{cu} based on energy balanced approach and is given by the following expression;

$$\varepsilon_{cu} = 0.004 + 1.4\frac{\rho_{sh} f_{yh} \varepsilon_{sm}}{f_{cc}} \qquad (1)$$

Equation 1 has been adopted in many updating models except for Hoshikuma model(1997) where the value of ε_{cu} was used as proposed by the author and is given by equation 2.

$$\varepsilon_{cu} = \varepsilon_{cc} + \frac{f_{cc}}{2E_{des}} \qquad (2)$$

Table (1) Summary of stress- strain model for confined concrete

Author	Stress- Strain Model for Concrete		
	Ascending region	**Descending region**	**Softening rate**
Modefied (2006)	$f_c = \dfrac{f_{cc}\left(\dfrac{\varepsilon_c}{\varepsilon_{cc}}\right)r}{r-1+\left(\dfrac{\varepsilon_c}{\varepsilon_{cc}}\right)^r}$	$f_c = f_{cc} - E_{des}(\varepsilon_c - \varepsilon_{cc}) \geq 0.25 f_{cc}$	$E_{des} = \dfrac{k f_{co}^{\ 2}}{\rho_{sh} f_{yh}}$
B. Bousalem et al.(2004)	$f_c = \dfrac{f_{cc} x n}{n-1+x^n}$	$f_c = f_{cc} - E_{soft}(\varepsilon_c - \varepsilon_{cc}) \geq 0.3 f_{cc}$	$E_{soft} = \dfrac{4 f_{co}^{\ 2}}{k_e \rho_{sh} f_{yh}}$
Hoshikuma et al. (1997)	$f_c = E_c \varepsilon_c \left[1 - \dfrac{1}{n} x^{n-1}\right]$	$f_c = f_{cc} - E_{des}(\varepsilon_c - \varepsilon_{cc}) \geq 0.51$	$E_{des} = \dfrac{11.2 f_{co}^{\ 2}}{\rho_{sh} f_{yh}}$
Mander et al. (1988)		$f_c = \dfrac{f_{cc} m r}{r-1+m^r}$	

Note that:

$$r = \frac{E_c}{(E_c - E_{\sec})}$$

$$E_{\sec} = \frac{f_{cc}}{\varepsilon_{cc}}$$

$$E_c = 4730\sqrt{f_{cc}}$$

And the analytical expression of k is proposed to be equal to:

$$k = 6.25 + \frac{f_{co}}{\rho_{sh} f_{yh}}$$

Table (2) Analytical expressions of K_s et K_d values for rectangular section columns

Authors	**Proposed equation for** $K_s = \dfrac{f_{cc}}{f_{co}}$	**proposed equation for** $K_d = \dfrac{\varepsilon_{cc}}{\varepsilon_{co}}$
Mander et al.	$-1.254 + 2.254\sqrt{1 + 7.94\dfrac{f_1'}{f_{co}}} - 2\dfrac{f_1'}{f_{co}}$	$1 + 5\left[\dfrac{f_{cc}'}{f_{co}} - 1\right]$

Hoshikuma et al.	$1+0.73\dfrac{\rho_{sh} f_{yh}}{f_{co}}$	$1+4.98\dfrac{\rho_{sh} f_{yh}}{f_{co}}$
B.Bousalem et al.	$1+0.4\dfrac{k_e \rho_{sh} f_{yh}}{\sqrt{f_{co}}}$	$1+2.7\dfrac{k_e \rho_{sh} f_{yh}}{\sqrt{f_{co}}}$

MOMENT-CUTVATURE RELATIONSHIPS:

Fig.(1) shows a typical stress-strain curves for two representative specimens, A3 and A11, as predicted from using different confinement models. It is clear that Mander model predict respectively higher strength and lower ductility of confined concrete compared with other models and also as indicated by Bousalem, Chikh and Hachem (2004).
The stress strain curves for concrete and the stress strain model for longitudinal reinforcement proposed by Mander et al.(1984), a series of analytical moment curvature curves can be generated taking into account the different influencing parameters.

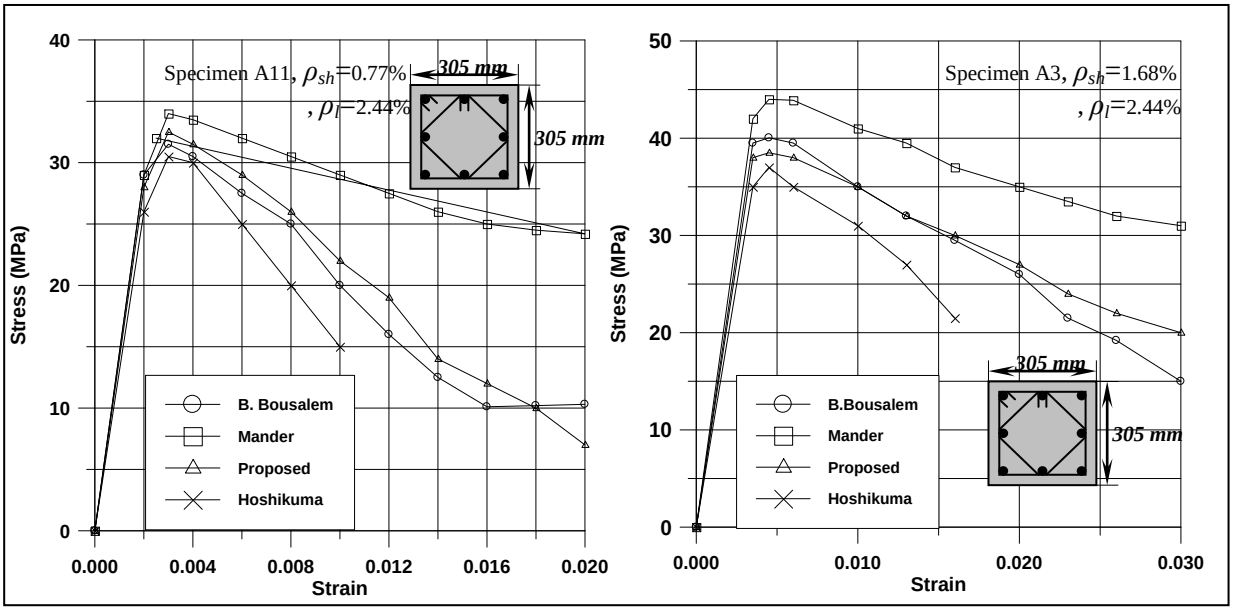

Fig. (1) Analytical stress-strain curves for confined concrete

As confirmed by Bousalem, Chikh and Hachem (2004) and other literatures listed through this study, the assumptions used in theoretical moment curvature analysis are as follows.

- Plane section before bending remain plane after bending,
- Tensile strength of concrete is ignored,
- Stresses in concrete are derived from the appropriate stress strain curves respectively for confined and unconfined concrete
- Stresses in longitudinal reinforcement are derived from the stress strain curve using Mander model and experimental data including strain hardening
- Perfect bond between steel and concrete
- In the application of the analytical models, the lateral steel stress is suggested to be equal to yield stress
- The ultimate state is reached when one of the three limit is attained:

1. The concrete strain at the extreme compression fiber reaches the specified value ε_{cu},

2. The steel strain in the tension zone reaches the specified value ε_{su} ,
3. The flexural moment drops to a value of 0.8 M_{max} .

PARAMETRIC STUDY USING IN THE MODEL:

As stated in previous studies and illustrated in this study, the effect of different variables is considers by comparing moment curvature relations of the column sections in which only one major variable differed significantly. These variables included the level of axial load, the amount of both transverse and longitudinal steel, and the tie spacing.

Level of Axial Load:

The effect of axial load on moment curvature relationship is shown in **Fig.(2)**. The level of axial load simulates the column axial load from medium to high stories. This level is defined as F equal to $P/f_c' A_g$ where p is the compressive axial load on the columns. The moment curvature curves were derived using the experimental data of column A3 tested by Sheikh et al.(1990) where the confining and longitudinal steel ratios were 1.68 and 2.44% respectively. It is observed that the ductility reduces as a result of higher axial load levels, and the moment beyond the maximum point degrades more rapidly as the level of axial load increases and as confirmed by Bousalem, Chikh and Hachem (2004).

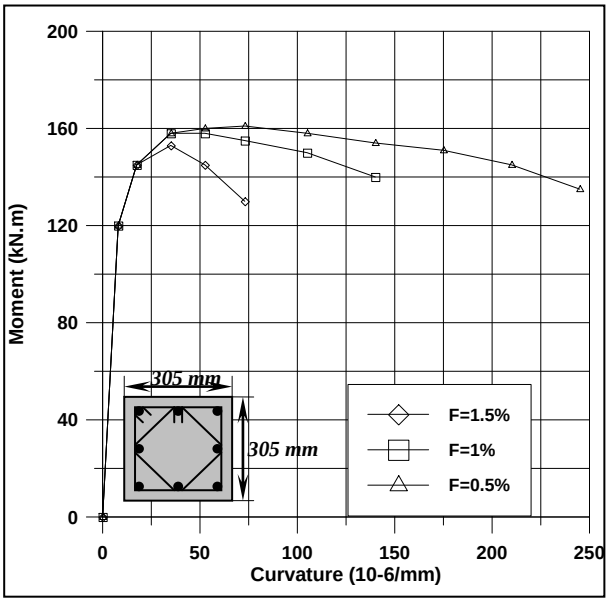

Fig. (2) Effect of axial load level

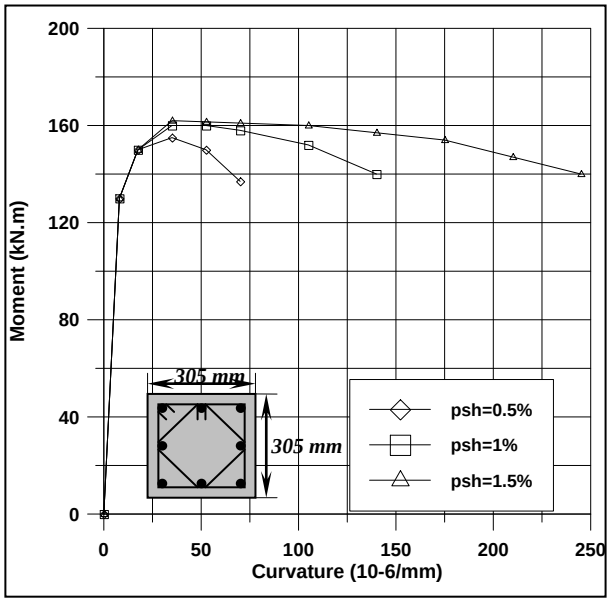

Fig. (3) Effect of amount of transverse steel

Amount of Lateral Reinforcement:

The effect of this variable is clearly evaluated by comparing the behaviour of the three curves shown in **Fig. (3)**.The identical ascending parts of the curves indicate that the quantity of transverse steel don't influence the section behaviour prior to the first cracking of unconfined concrete. It can be noticed that the ductility increase with the increase of transverse steel content. It is apparent that with lower lateral volumetric ratios, the confining pressure is not sufficient enough to maintain the moment capacity of the section and as confirmed by Bousalem, Chikh and Hachem (2004).

.

Amount of the Longitudinal Reinforcement:

Fig. (4) illustrates the effect of longitudinal steel content on the moment curvature curve for a specimen having the same details as specimen A11. It is demonstrate that the increase of the moment capacity of the section with the increase of the amount of longitudinal steel is small. The post peak behaviour is characterized by gradual drop in the moment capacity of the section where it reaches approximately a same value at ultimate curvatures. However a large longitudinal steel content means that less reliance is placed on the concrete capacity, and therefore the moment capacity can be better maintained at high curvatures and as confirmed by Bousalem, Chikh and Hachem (2004). .

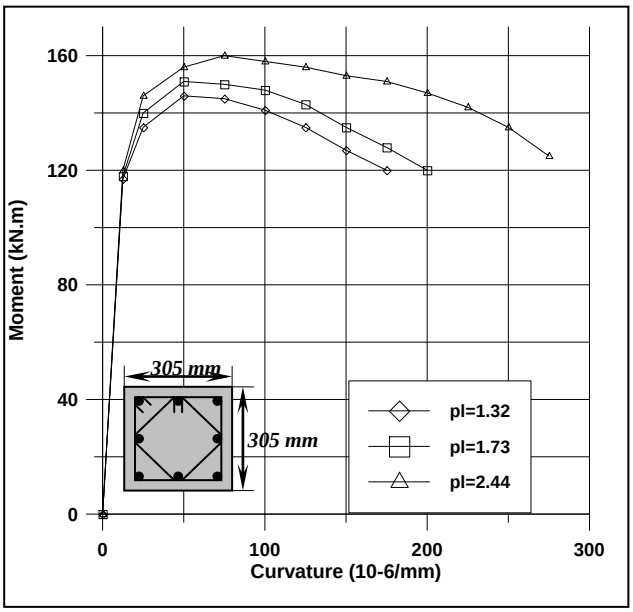

Fig. (4) Effect of the amount of longitudinal steel

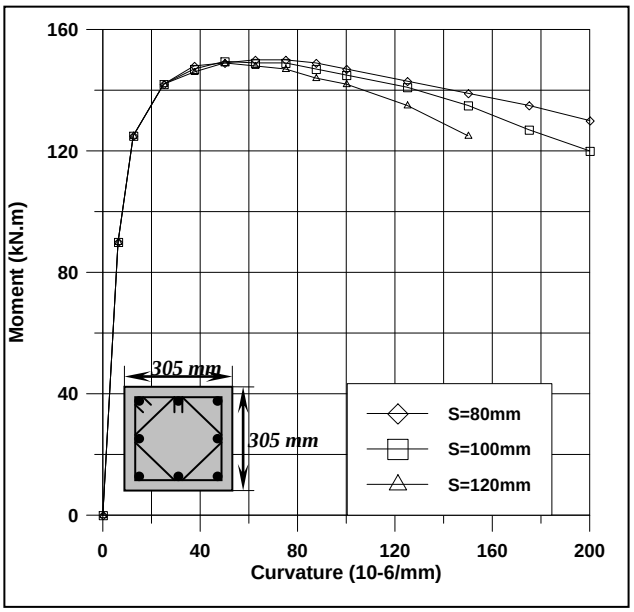

Fig. (5) Effect of tie spacing

Tie Spacing:

The effect of tie spacing on the moment curvature behaviour of the section is shown in **Fig.(4)** for specimen A11 and subjected to a load level of 0.5%. In general smaller tie spacing resulted in higher curvature ductility. The moment capacity in this case also increased by reducing of tie spacing and as confirmed by Bousalem, Chikh and Hachem (2004). .

MOMENT-CURVATURE CURVES:

Figs.(6) and **(7)** show the comparisons between the moment curvature relations for four representative specimens (Sheikh and Yeh 1990) and those derived from numerical analysis from the four models discussed previously. Except for specimen D5, ρ =2.58%, ρ_{sh} =1.68%, the model by Hoshikuma et al.(1994) constantly overestimated the moment capacity of the sections. The other models tend to underestimate the moment capacity of the sections and this underestimation is even larger for specimen D5 with higher volumetric ratio of longitudinal steel and lower level of axial load. Sheikh et al.(1990) reported in their experimental investigation that in the case of specimen D5, it has been observed that yielding of steel took place before a significant drop in the moment capacity, indicating that crushing of core had started after lateral steel became effective, this may explain the discordance of the theoretical results compared with the experimental ones in spite they are on the conservative side.

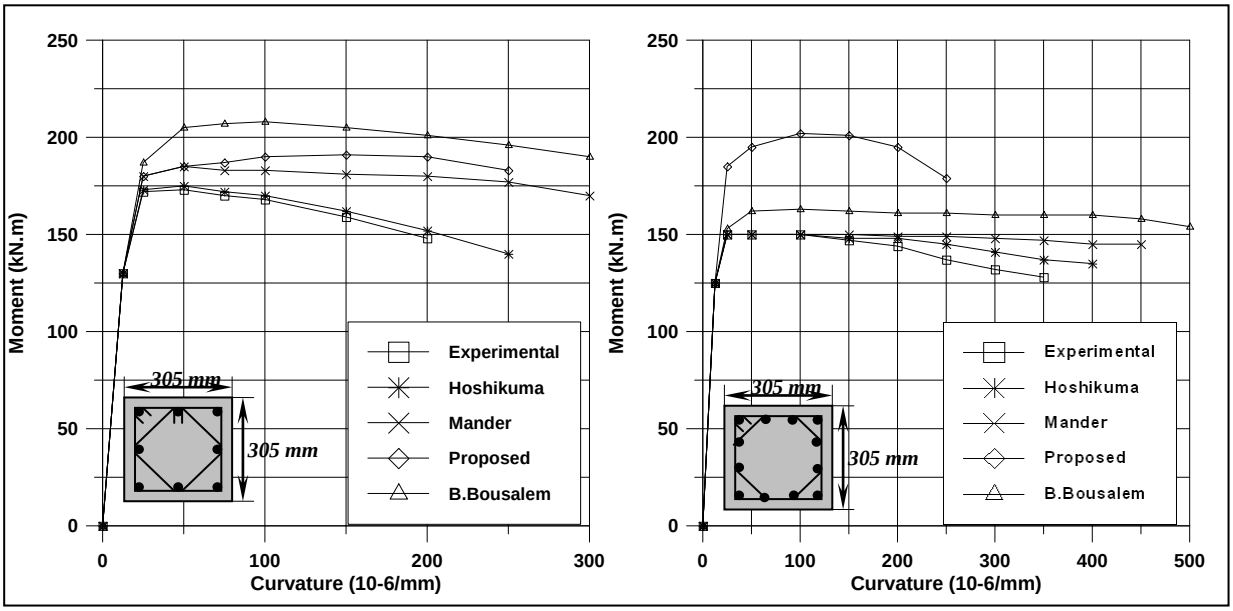

Fig. (6) Comparison of experimental and analytical curves for specimens A3 and D5

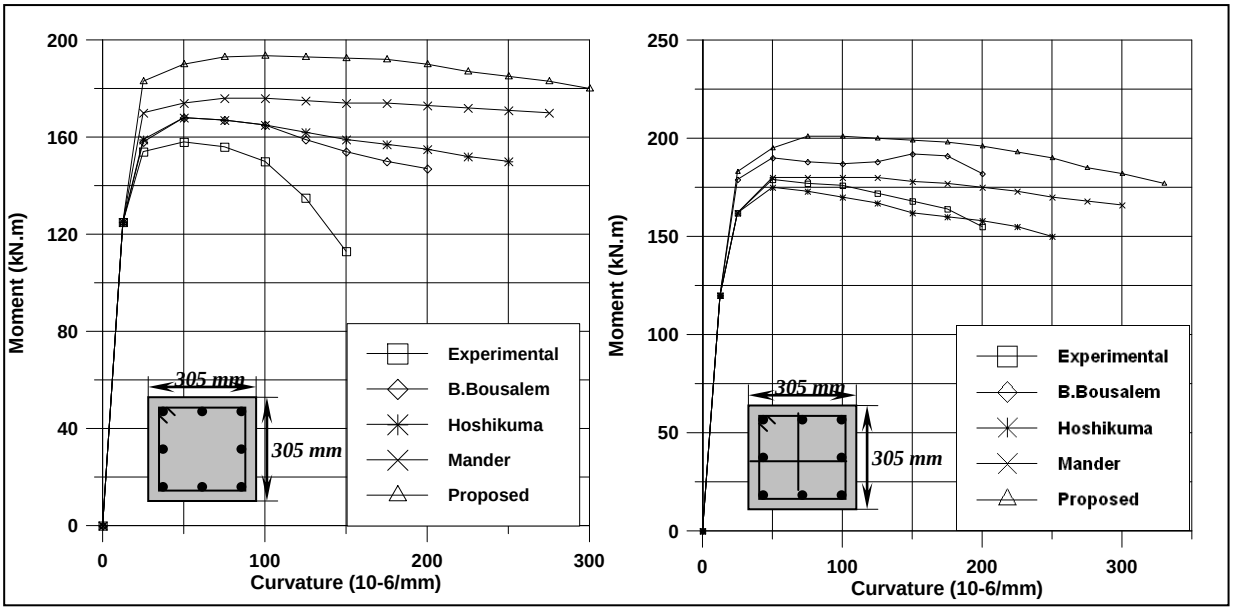

Fig. (7) Comparison of experimental and analytical curves for specimens E2 and F4

CONCLUSIONS

The conclusions reached from this analysis for the range of variables considered in this study and as confirmed by Bousalem, Chikh and Hachem (2004) are as follows:

1. The large transverse steel content and reduced tie spacing increase the ductility and enable the moment capacity to be better maintained at higher curvatures.
2. The level of axial load reduces the ductility and the moment beyond the maximum point degrades more rapidly as the level of axial load increases.

3. The increase of the amount of longitudinal steel on the moment capacity of the section is small. However a large longitudinal steel content means that less reliance is placed on the concrete capacity, and therefore the moment capacity can be better maintained at high curvatures.
4. The proposed model reflects well the influence of the variables considered in this study, namely the axial load level, the transverse and longitudinal steel content and the tie spacing. The accuracy of the model in the representation of experimental results is acceptable.

NOTATIONS:

f_{cc}',f_{co}'= confined & unconfined concrete compressive strength in members.
f_y =steel yield strength.
f_{yt} =yield strength of transverse reinforcement.
ε_c =concrete strain.
ε_{cc} =strain corresponding to peak stress of confined concrete.
ε_{01} =strain corresponding to peak stress of unconfined concrete.
ε_{85} =strain corresponding to 85% of peak stress of confined concrete.
ε_h =static strain hardening initiation strains of steel.
ε_u =static ultimate strains of steel.
E_c =modulus of elasticity for concrete.
E_{sec} =secant modulus of elasticity for concrete.
E_s =modulus of elasticity for steel.
ρ_{sh} =total transverse steel area in two orthogonal directions divided by corresponding concrete area.
S =spacing of transverse reinforcement.
S_L =spacing of longitudinal reinforcement laterally supported by corner of hoop or hook of cross tie.

REFEENCES

- B. Bousalem, N. Chikh and R. Hachem, Curvature Ductility of rectangular Reinforced Concrete Columns, ICCT 2004-I-(17).
- S.A.Sheikh and C. Yeh., Tied concrete columns under axial load and flexural. Journal of Structural Engineering, 116(10), October 1990, 2780-2800.
- J. B. Mander, M. J. N. Priestley and R. Park, Theoretical Stress-Strain Model for Confined Concrete, Journal of Structural Engineering, 114(8), August, 1988, 1804-1826.
- S. Murat and S. R. Razvi, Strength and ductility of confined concrete, Journal of Structural Engineering, 1992, 118(6), 1590-1607.

- J. Hoshikuma, K. Kawashima, K. Nayaga and A. W. Taylor, Stress –strain model for confined RC in bridge piers, journal of Structural Engineering, 1994, 123(5), 624-633.

- B. D. Scott, M. j. N. Priestley and R. Park, Stress- strain behavior of concrete confined by overlapping hoops at low and high strain rates, ACI Journal, Jan. Feb., 1982, 13-27.

- M. J. N. Priestley, F. Seible and G. m. Calvi, Seismic design and retrofit of bridges, John Wiley, 1996, 686 pp.

- J. B. Mander, M. J. N. Priestley and R. Park, Seismic design of bridge piers, Research report 84-2, Department of civil engineering, University of Canterbury, 1984, p. 483.

STATIC AND DYNAMIC ANALYSIS OF STIFFENED PLATE USED IN MACHINE TOOL COLUMN

Wedad I. Alazzawy

Baghdad University – Eng.College

Mechanical Department

ABSTRACT

Static behavior (under torsion and bending loading) of machine tool column was studied in this paper. The effects of changing the cross sectional area of the column itself on the deformations (design parameters) was investigated. The adding of stiffeners and changing the stiffeners cross sectional area are also verified. The results show that using of stiffeners can produse a great reduction in deformation of the column structure under the stastic loading mentioned above. Also using stiffeners with different cross-sectional areas suggest the best stiffener cross-sectional shape can be used to give the minimum deformations of column structure. Dynamic analysis of column involves calculating natural frequencies and mode of different column structure mentioned above, these frequencies are fairly insensitive of adding stiffeners to colmn structures.

KEYWORDS

Static analysis, Dynamic analysis, Stiffened Pplates, Machine Tool Column, Natural Frequencies

الخلاصة:

تم في هدا البحث دراسة التصرف الستاتيكي (تحت حمل الالتواء والانحناء) لهيكل عمود ماكنة تشغيل ميكانيكي. حيث تم دراسة تاثير تغيير شكل المساحة المقطعية للعمود للتشوهات (عنصر التصميم). كما تم دراسة تاثير اضافة دعامات لهيكل العمود وكدلك التحقق من تاثير تغيير المساحة المقطعية لهده الدعامات.تبين النتائج ان اضافة الدعامات يمكن ان ينتج تقليل كبير في تشوهات العمود تحت تأثير الاحمال الستاتيكية المدكورة كدلك استخدم دعامات بمساحات مقطعية مختلفة يقترح اعطاء افضل شكل الدي يعطي اقل تشوه لهيكل العمود.التحليل الديناميكي للعمود تضمن قياس التردد الطبيعي لهياكل العمود المختلفة المدكورة اعلاه ، وقد تبين ان هده الترددات تتأثر قليلاً بأضافة الدعامات لهيكل العمود .

NTRODUCTION:

Stiffened plates are structural component consisting of plate reinforced by a system of ribs to enhance their load-carring capacity. These structural components have been widely applied to aircraft, ships, bridges, buildings, rockets and machine tool structures as well as in many other branches of structural engineering. Thus, there are many circumstances in which stiffened plate structure is exposed to static and dynamic load. Different approaches have been suggested for static and vibration analysis of stiffened plates, **(Rossow and Ibrahinkhail 1978)** applied the constraint method to the finite element static analysis of concentrically and eccentrically stiffened plates, the displacement fields in the stiffener are expressed in term of the displacements of the middle surface of the plate.

Supposing the strain energy of plate and stiffener, the stiffness matrix of compound structure is obtained, for arbitrary order of approximating polynomials. **(Mokhopadhyay 1981)** suggested a new approach to account for the stiffeners within the plate element under plane stress. It caters accurately the spacing and orientation of the stiffeners, the results of stiffened deep beams, a rectangular ship plating and typical web frame of tanker obtained by using this new approache. **(Deb and Booton 1988)** used linear finite element models based on Mindlins shear distortion theory for bending of eccentrically stiffened plates subjected to transverse loading. Two models using discrete plate-beam formulation are given superiority of one over the other discussed, also additional formulation applicable to technically orthotropic plate under distributed lodaing is included. **(Palani et al 1992)** proposed isoperimetric finite element models, the eight – noded and nine-noded models have been arrived at by appropiatly combining Lagrangian plate shell elements with three node isoperimetric beam element. **(Omurtag and Akoz 1992)** presented a new functional for thin cylindrical shells and space bars with geometric and dynamics boundary conditions, using Gateaux diffrentials. **(Rao et al 1993)** applied a finite element analysis of the large deflection behavior of stiffened plates using isoperimetric quadratic stiffened bending element. The evaluation of fundemental equations of stiffened plates is based on Von Kerman s theory. **(Singh and Miller 1992)** deal with the design analysis of a twin head horizontal press using finite element model, developed for the press, quantitative results useful to press designers. Some suggestions are made to improve the stiffness and torsion rigidity of the press. In modeling the twin head horizontal hydrualic press, different elements types are used, rectangular, quadrilateral, traingular, beam and 8-node solid element. The entire model possesses 4542 degree of freedom. In present work finite element approach is applied to analyze the static and dynamic behavior of stiffened plates for analysis of machine tool column.

MODELING OF THE COLUMN:

Software Nastran(70.7) and Patran(90) are used in analyzing the machine tool column, through the following steps:

1. Geomatry modeling.
2. Solution.
3. Getting the results.

The (3D) column structure is modeled using shell (elastic shell) element with both bending and membrane capabilities **Fig.1-a**. The element has both bending and membrane capabilities, both in-plane and transverse loads are permitted and six degree of freedom, translation in the nodal X,Y,Z directions and rotation about nodal X,Y,Z axes.

While stiffeners of this column are modeled using beam (1-D elastic beam) element. This beam is uniaxial element with tension, compression, bending and torsion capabilities. The element has two degree of freedom at each node, translation in X axis and rotation about Y axis, **Fig.1-b**. The element position is defined by offsetting from the column structure shell.

Solution steps consist of applying the boundary conditions (the column modeled as cantilever), setting the load (6kNm for bending or torsion) and solve the eq.(1) to get the displacement which is the most impotrant design variable for the column, while obtaining the natural frequencies of this column is done by solving eq.(2):

$$[K] \times \{U\} = \{F\} \qquad (1)$$

$$([K] - \omega^2[M])\{U\} = 0 \qquad (2)$$

RESULTS AND DISCUSSIONS:

Comparison of Results:

For verification, simply supported steel square stiffened plate (Dep and Booton 1988) is modeled under a uniform distributed load with (4+4) orthogonally placed stiffeners of rectangular section, the obtained result for max. deflection is (2.921E-3) and gives good agreement with the published result (3.365E-3) in meter.

Stiffened Column:

The column structure of machine tool has been verified for different cases to study the effects of some design variables on the static behavior of that structure.

Machining forces, which are transmitted to column structure by the slides causing torsion and bending of the column, can be calculated as shown below (Sen and Bhattacharyya 1975):

$$F_x = (C_p) \times (K_p) \times (K_B) \times (d^{xp}) \times (S^{yp}) \qquad (3)$$

$$M_T = (C_m) \times (K_p) \times (K_B) \times (d^{xm}) \times (S^{ym}) \qquad (4)$$

$$F_y = M_T \times \left({}^{2}/_{d}\right) \quad (5)$$

$$T = F_y \times X \quad (6)$$

$$M_B = F_x \times Z \quad (7)$$

$$F_T = \left({}^{T}/_{Y}\right) \quad (8)$$

$$F_B/_2 = M_B/Z \quad (9)$$

The first design variable is changing the cross-sectional area of the column as in **Fig.2-a**, the cross-sectional area and material properties of each structures are given in **Table 1**, these three column structure are analyzed under bending and torsion loading as shown in **Fig.2-b**, the deformations results of these structures are compared in **Table 2** and plotted against the length of the column in **Fig.3** in which column with square section has minimum deformations.

The second variable is adding of orthogonal stiffeners (12 vertical stiffeners and 10 rings spaced equally) to the three column mentioned above, also the effect of this parameter on the deformation of these structures under the two static loading types are compared in **Table 2** and shown in **Fig.4,5** and **6**.

The third parameter is changing the cross-sectional area of the orthogonal stiffeners which are added to the three column structure as mentioned above, the cross-sectional area and material specifications of each beam type are given in **Table 1**. Studying the effects of this variable is shown in **Table 2** and **Figs. 4, 5** and **6** in which column stiffened with I- section beams has the minimum deformations.

Knowledge of natural frequencies and modes is important from a design viewpoint to avoid resonance conditions and it is also the foundation for forced response calculations. The natural frequencies of this column with different cross-sectional area and with stiffeners are obtained in **Table 3**, while the first mode of different cross-section area without stiffeners are shown in **Fig.7**.

CONCLUTIONS:

It is apparent from the obtained results that the best cross-sectional area of the column structure without stiffeners is the square shape which gives a reduction of 62.685% in deformation of the column under bending loading, also under torsion loading it gives 66.885% reduction of the deformation (compared with maximum deformation for both cases).

Adding the stiffeners to the column structure improve the static behavior of the column, the best reduction in deformation of the structure is done with a beam of I cross-sectional area which gives 72.224% reduction of deformation (with column of square section) under bending load and 91% reduction of deformation (with column of circular section) under torsion loading (compared with maximum deformation in both cases), while adding of these stiffeners have a little effect on the natural frequencies of different column structures because these structures are stiff and heavy.

Table 1: Geometry and material properties of column and its stiffeners.

Column				Stiffeners		
Cross-Section	**Square**	**Circular**	**Hexagonal**	**I section**	**Rectangular**	**Circular**
Area(mm^2)	**47760**	**47752.208**	**47814.3595**	**1386**	**1386**	**1386**
E(GN/m^2),v	**210 .3**	**210 .3**	**210 .3**	**210**	**210**	**210**

Table 2: Column max. displacement component(mm).

Stiffeners type	**Bending Load**			**Torsion Load**		
	Square column	**Circular column**	**Hexagonal column**	**Square column**	**Circular column**	**Hexagonal column**
Without stiff.	**.072315**	**.143215**	**.1938**	**.161357**	**.283126**	**.487274**
I-section	**.053829**	**.055092**	**.088833**	**.071935**	**.043848**	**.13738**
Rect.	**.056879**	**.062494**	**.102152**	**.08853**	**.07373**	**.181651**
Circ.	**.059229**	**.069587**	**.113294**	**.098704**	**.10092**	**.223053**

Table 3: Natural frequencies (Hz) for column.

Mode no.	**Square column**				**Circular column**				**Hexagonal column**			
	Without stiff.	**I-section**	**Circ.**	**Rect.**	**Without stiff.**	**I-section**	**Circ.**	**Rect.**	**Without stiff.**	**I-section**	**Circ.**	**Rect.**
1	**125.6**	**91.7**	**100.5**	**94.2**	**118.8**	**82**	**89.1**	**85.5**	**134.2**	**91.2**	**93.9**	**92.6**
2	**125.6**	**91.7**	**100.5**	**94.2**	**118.8**	**82**	**89.1**	**85.5**	**134.2**	**91.2**	**93.9**	**92.6**
3	**133.3**	**100**	**109.3**	**102.6**	**162.5**	**118.7**	**130.1**	**125.2**	**140.4**	**105.3**	**109.5**	**108.1**
4	**133.3**	**100**	**109.3**	**102.6**	**162.5**	**118.7**	**130.1**	**125.2**	**140.4**	**105.3**	**109.5**	**108.1**
5	**157.4**	**125.9**	**133.7**	**130.6**	**260.9**	**208.7**	**216.5**	**206.1**	**300.9**	**240.7**	**252.7**	**246.7**

a)-Quad 4 (b)-Bar2

(Fig. 1: Element type that used in modeling the column structure.

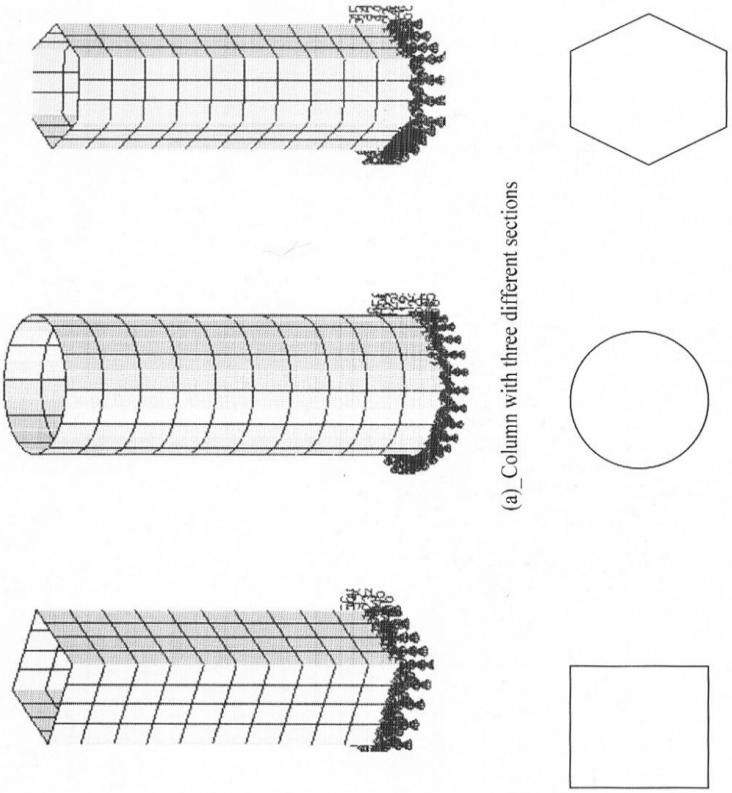

(a)_ Column with three different sections

(b)_ Top view of column structure

Fig. 2: F.E. model of column structure

5

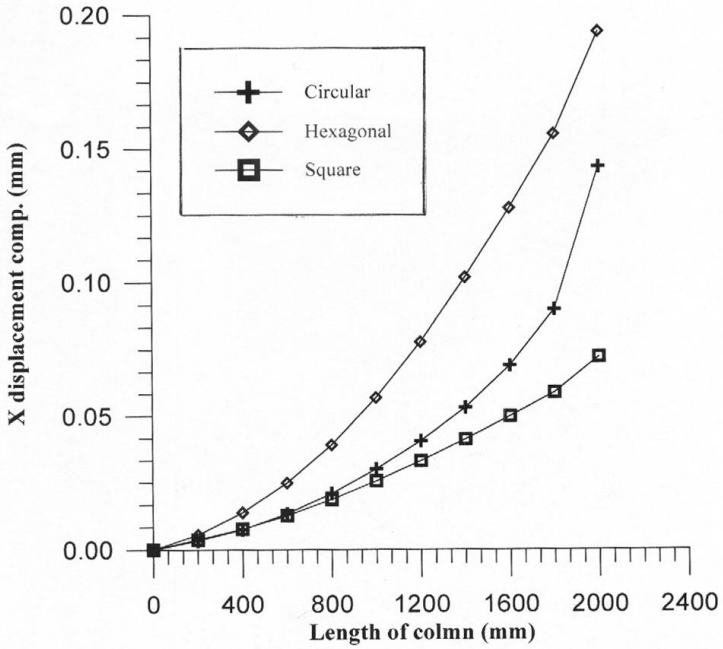

(a)_Bending load

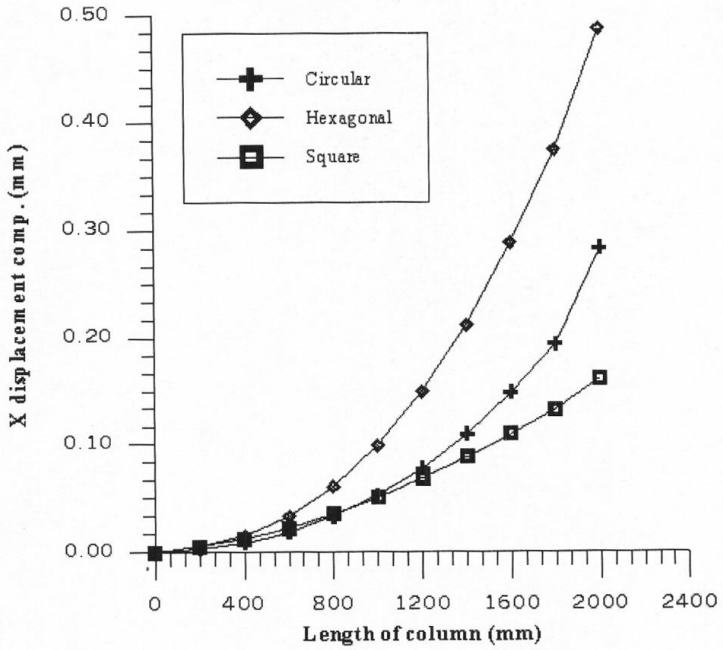

(b)_Torsion load

Fig.3 : Max. displacement of column with different cross-section

6

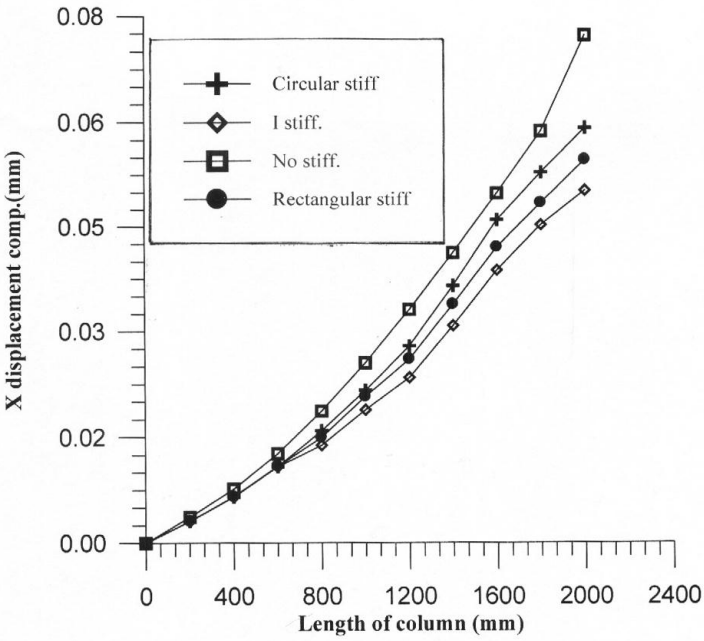

(a)_Bending load

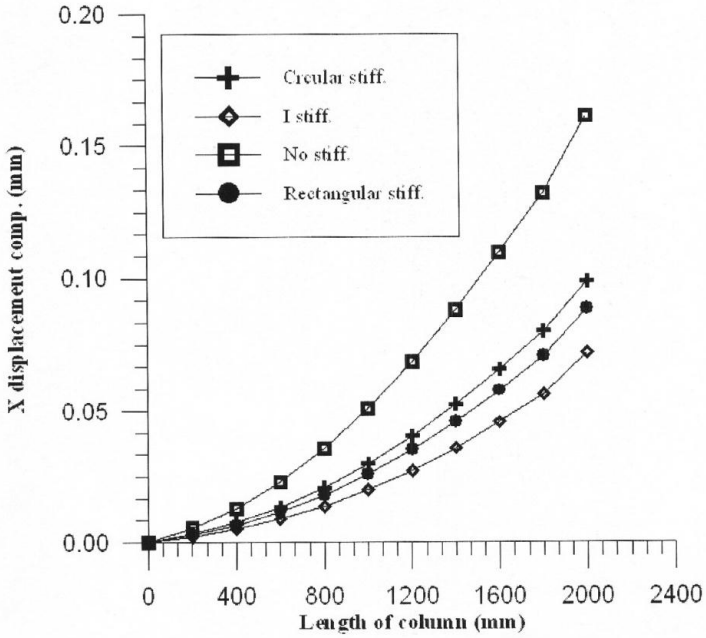

(b)_Torsion load

Fig.4 : Max. displacement of column with square cross-section

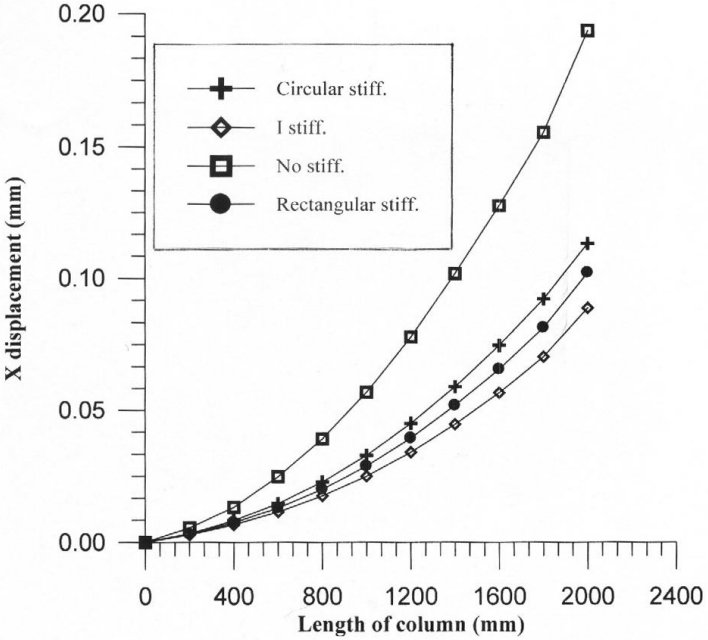

(a)_Bending load

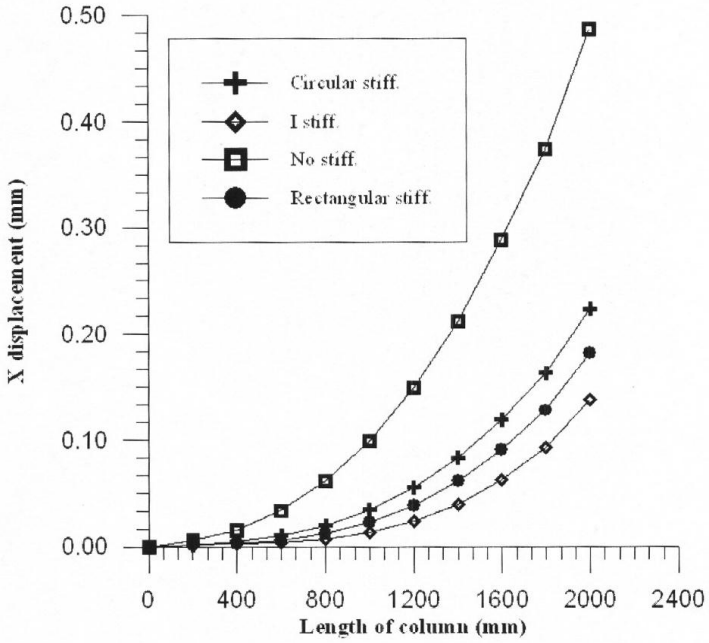

(b)_Torsion load

Fig. 5 : Max. displacement of column with hexagonal cross-section

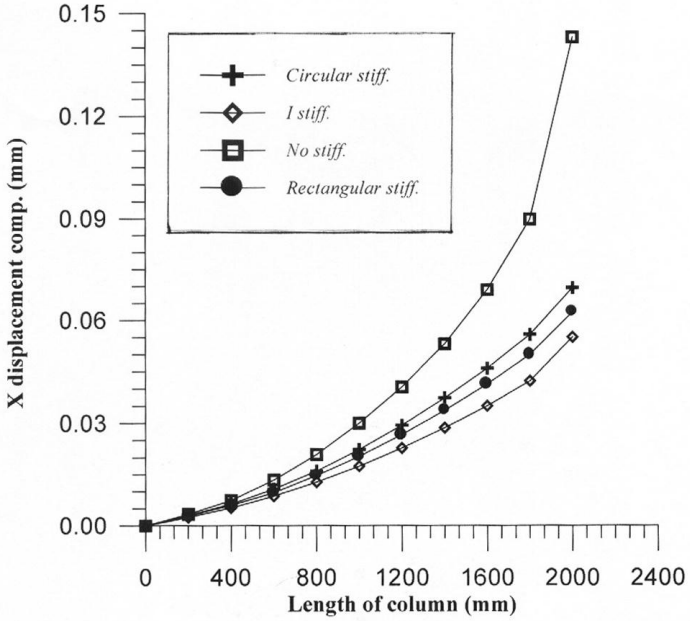

(a)_Bending load

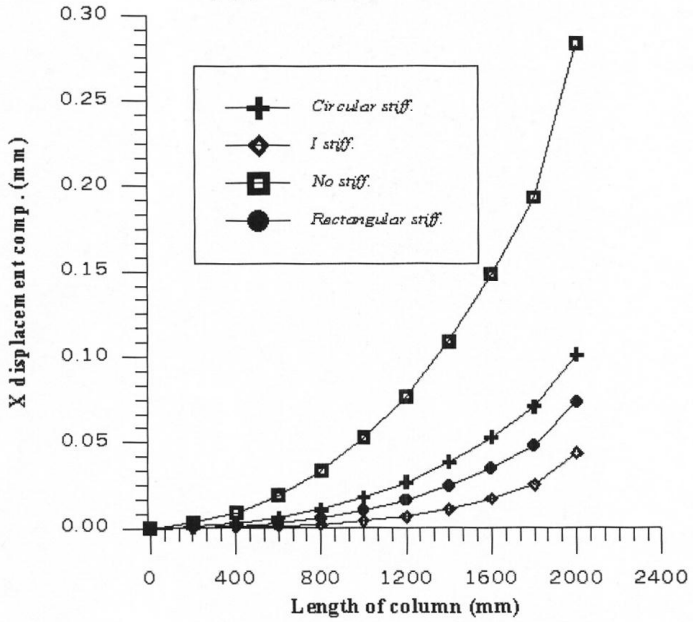

(b)_Torsion load

Fig. 6 : Max. displacement component of acolumn with circular cross-section

9

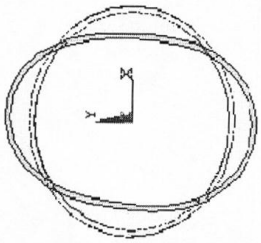

a- First mode of circular cross section column with no stiffeners (ω = 118.88Hz)

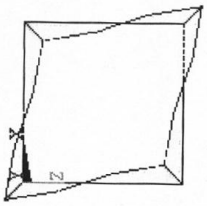

b- First mode shape of square cross section column with no stiffeners (ω= 125.67Hz)

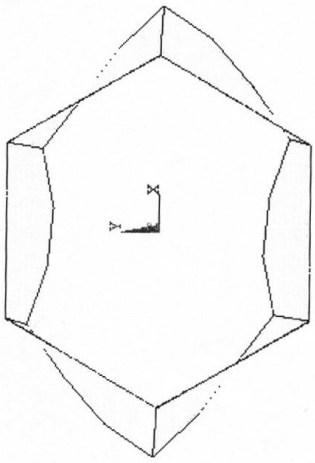

c- First mode shape of hexagonal cross section column with no stiffeners (ω= 134.24Hz)

Fig. 7: First mode shape of a column with different cross section area

10

REFERENCES

*A.Deband M.Booton "Finite element models for stiffened plates under transverse loading", Comp.&Stru., V.28, No.3, 1988.

* Backlund Jesper "Free vibration analysis of rocket nozzles using energy methods", Masters Thesis, Luleal Tekniska University, 1998.

*D.Venugopal Rao, A.H.Sheikh and M.Mukhopadhayay "A finite element large displacement analysis of stiffened plates", Comp.&Stru., V.47, No.6, 1993.

* G.S.Palani, N.R.Iyer and T.V.S.R.Appa Rao "An efficient finite element model for static and vibration analysis of eccentrically stiffened plates shells", Comp.&Stru., V.43, No.4, 1992.

* G.C.Sen and Bhattacharyya,"Principles of machine tools", New Central Book Agency,Calcutta 700009, India, 1975.

* I.E.Harik and M.Guo "Finite element analysis of eccentrically stiffened plates in free vibration", Comp.&Stru., V.49, No.6, 1993.

* M.P.Rossow and A.K.Ibrahimkhail "Constraint method analysis of stiffened plates", Comp.&Stru., V.8, 1978.

* M.Mukjopadhyay "stiffened plates element for analysis of ships structures", Comp.&Stru., V.13, 1981.

* M.H.Omurtag and A.Y.Akoz "Mixed finite element formulation of eccentrically stiffened cylindrical shell", Comp.&Stru., V.42, No.5, 1992.

* U.P.Sigh and P.P.Miller "Design analysis of twin head horizontal hydraulic press", J.of Eng. For industry, V.114,1992.

NOMENCLATURE:

C_p, C_m=material constant

d=tool diameter(mm)

F_x, F_y=Force components(N)

F_T, F_B=Torsion and bending forces(N)

[K]=Column stiffness matrix (N/mm)

K_p=Coefficient taking into account the effect of point angle.

K_B= Coefficient taking into account the effect of Brinell hardness-number.

[M]=Column mass matrix(g).

M_T,M_B= Torsion and bending moments(Nmm).

S=Feed rate(mm/rev.).

T=Column torque(N .mm).

xm,ym=Exponent of tool diameter while calculating tool torque.

xp, yp= Exponent of tool diameter while calculating tool thrust.

Y=Length of tool(mm).

Z=Length of column(mm).

Ω^2=Column natural frequency(Hz).

CAPABIIITY OF FORGING TECHNIQUE TO PRODUCE ROUND SHAPE FLANGE USING (POM) MATERIAL UNDER COLD AND HOT CONDITIONS

Talib.H.Rashid
Assis.leucturer
Mech.Eng. Department.
Baghdad University

ABSTRACT

The paper studied capability of forging process to produce round shape flange using acetal (celcon^R) polymer which is an engineering crystalline material having a good ductility if it is preheated The process done under cold & hot conditions This kind of technique guarantees a product with high strength and stiffness better than what injection molding could achieve. The products showed crack and curling traces on the flange under cold forging, but a good product was achieved by heating the billet and the tools to (100C^o)with improvement in the mechanical properties. The paper discussed also through (stress – strain) curves manner of deformation through forging action. The results explained that POM (celcon^R) is forgeable polymer if it is preheated at (100 C^o) using slow speed press by closed die forging process under applied pressure of 170Mpa to produce round shape flange, while this technique failed to forge same polymer at room temperature.

الخلاصة

درست الورقة امكانية طريقة الكبس بالقوالب المغلقة فى انتاج (شفة دائرية) من مادة (اسيتيل سيلكون) وهي مادة بلاستيكية هندسية بلورية لها القابلية على مطاوعة الكبس كلما كانت ساخنة. وقد اجريت التجربة وذلك بالكبس على البارد مرة وبالكبس بعد تسخين القطعة المشغولة مرة اخرى . هذه الطريقة تضمن صلادة و مقاومة للمنتج افضل مما تفعله طريقة البثق . كانت النماذج المنتجة تحت ظروف درجة حرارة الغرفة تحوى عيوب التكسر والالتواء, بينما كانت النماذج في الحالة الثانية حيث تم تسخين القطعة المشغولة والقالب لدرجة100مئوى كاملة الشكل والأبعاد مع تحسن في الخصائص الميكانيكية. الورقة درست كذلك سلوك المادة اثناء عملية الكبس من خلال منحنيات الجهد والاجهاد. النتائج اوضحت ان الاسيتل له المطاوعه الكافيه اذا تم تسخينه لدرجة(100مئوى) لكى ينتج شفة دائرية بواسطة طريقة الكبس بالقوالب المغلقة تحت صغط (170 ميكاباسكال), بينما فشلت النماذج التى انتجت دون تسخين مسبق باستخدام نفس طريقة الصنع .

KEY WORDS

(Forging _ POM_ recovery _ dwell time _billet _ SPF)

CLAIMS:

1. Forgeability of acetal (celcon^R) through closed die forging technique to produce flange under cold (room temp.) & hot (100 C^o) conditions
2.Behaviour of the polymer through forging action taking into consideration that typical forging process using acetal is usually done at (155C^0) **(Kulkarni1995)** . Melting temperature for it about (165C^0)

INTRODUCTION

Closed die forging is a process in which a billet or blank is subjected to bulk deformation by application of compressive pressure with constraining dies which are generally made from steel **(Coffman1990).** The billet (POM) is made of formaldehyde and it always has been referred to as (acetal). This polymer as an engineering material had been fabricated by forging process which was previously applied only to metals; it has been successfully employed with many types of polymeric materials **(Kulkarni, yong-Seon Lee 2002)** which have to be ductile, with most deformation non-recoverable to minimize spring back and time dependent strain. (POM) can be difficult cold forged **(Kulkarni 1995)**. It typically fabricated after heating at (155C^0). Cold forming implies that the process is performed at room temperature with out heating the material or the tools. In general a polymer can be either cold or warm formed. Solid phase forming (spa) indicates any of them. The process is selected depending on the application. This technique insures better mechanical properties and can produce a complex shape with high thickness or deals with polymers of (ultra high molecular weight) which are mostly beyond the capability of injection molding process **(kulkarni 995).**

DIMENSIONS AND MEASUREMENTS:

- **Billet dimensions**: the billet was solid plastic rod

Cross-section area = 25mm
Height = 65mm

- **Die dimensions**: the die was made of hardened carbon steel

Outside diameter = 51mm
Inside diameter = 39mm
Height = 10mm
Cone diameter (bottom part) = 28mm
Cone height = 5mm

- **Billet test measurements :**

mechanical properties

Tensile strength at 1%strain	Modulus tensile	Modulus flexural	Hardness(ROCKWELL) (wt=100gm)
62Mpa	2.87Gpa	2 Gpa at 23C^0 0.9 Gpa at 100 C^o	M84

Table 1

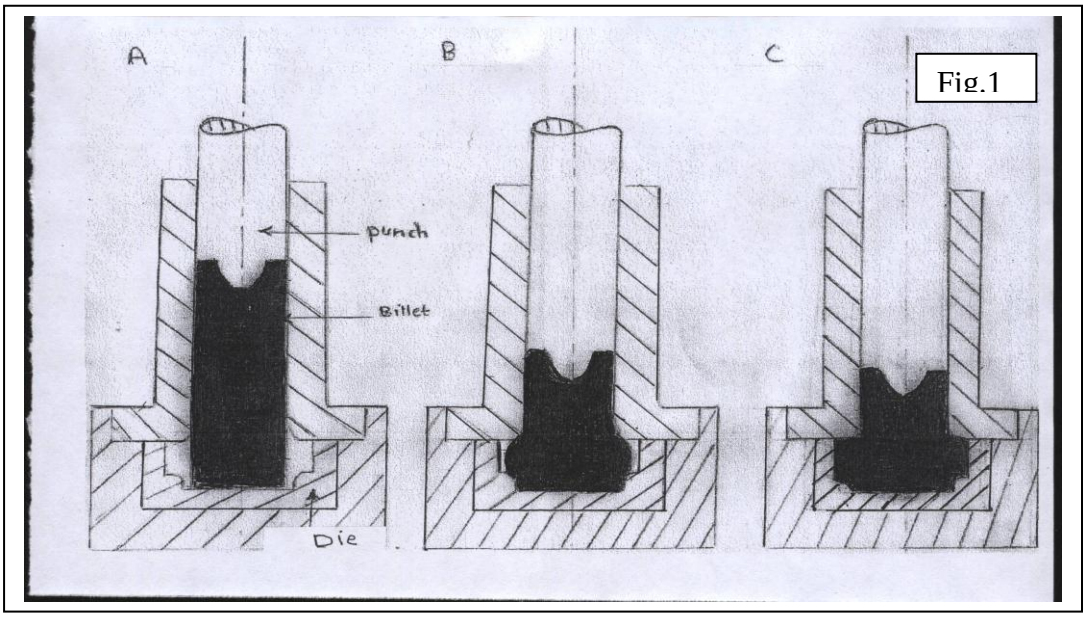

(Fig. 1): shows steps of forging actions

- (A) punch is ready to start forging
- (B) Punch is moving down pushing the polymer according to load increasing, and then gradually the die filled with polymer except corners.
- (C) Increasing of pressure gradually to fill corners.

This process influenced by load increase which was done gradually while trial and error were the only way to examine what was going on inside die cavity step by step, so many samples were spent for this purpose

EXPERIMENTAL PROCEDURES:

1. The process was done using slow speed press.
2. A load cell consisted of strain gauge was used to transmit the compressive load to the strain recorder then to an amplifier. The amplifier then connected to Bryan X-Y plotter to get graphs of load against displacement, then to be converted later to (stress-(strain) curves describing the style of flow done by yielding action.

A. Cold forging

The billet was simply put into the die at room temperature, and then forging carried out. .

Load would then be increased and when the pen on the plotter started to move vertically (Fig.2), load then held constant at that particular value for (2 minutes) to prevent recovery.

B. Hot forging

The billet was put into the die and whole assembly was placed in an oven over night. The temperature was adjusted at 100C^{o}. The strain gauge was insulated from the hot punch by the use of an asbestos slab to prevent unwanted effect of strain gauge due to

heating. After putting the die assembly below the machine punch, switching on, then the head of machine was brought down and the forging carried out. When the pen of the plotter started to move vertically, load was again held constant at that particular value (100second).

RESULTS AND DISCUSION:

* RESULTS:

Product test.
Dimensions stability = within 1 % in all directions
Modulus improvement increased by 50% in one direction
Tensile strength increased by 150% in one direction

* DISCUSSION:

Typical forging pressure for preheated billet (5 C^o) below softening point is around 40Mpa. Cold forging pressure recorded in such work to be (3-5)times that of typical heating, while in the case of heating billet and tools to(100C^o) would be (2- 3) times that of typical heating(Coffman1990) , sometimes the use of (MoS_2) based lubricant gives an advantage by lowering forging force value. .
In this paper, a cold forging at room temperature and a hot forging at (100 C^o) had been done using MoS_2 based lubricant to reduce forging pressure, the results indicated that curling, and cracks traces appeared on the flange under cold forging. On the other hand smooth product -with improvements in the mechanical properties -was achieved by heating the billet and the tools at (100 C^o).

A. Load –displacement curves behavior: (see Fig.2)
Curves at both conditions showed viscoelastic behavior of (POM)
1. OA-section which represented a behavior of elastic material.
2. AB-section which represented viscous non-linear deformations because of this polymer behavior, AB line was not fully horizontal straight line.
The load required to form the general shape of flange was at ranges:

- (40-65 KN) to achieve (11.5) mm as reduction in height at cold forging for (section AB).
- (20-35 KN) to achieve (10) mm as reduction in height at hot conditions for (section AB).
  3. BC-section which indicated load applied to fill the corners which were last part of flange to achieve:
- Total reduction in height was (22.5mm) including elastic part using range of loads (65-90 KN) at cold forging.
- Total reduction in height was (20mm) including elastic part using range of loads approached (85 KN) at hot conditions. (Fig.1) shows the details of the forging process stages.

The total percentage reduction in height in each case was (34%)

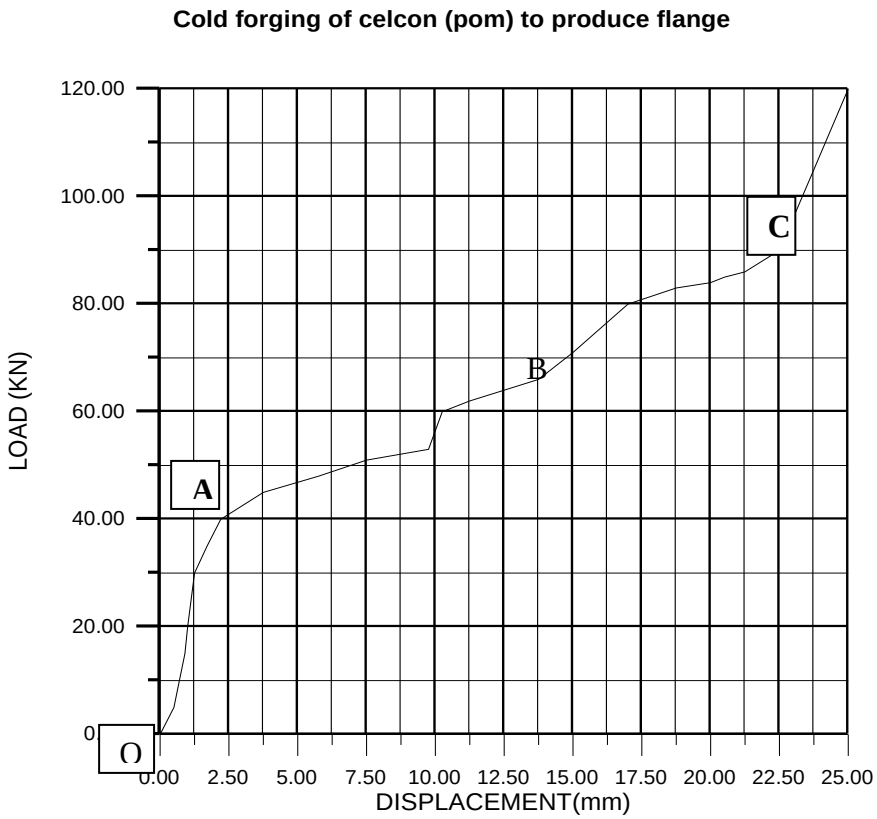

Fig.2-a Load-displacement graph

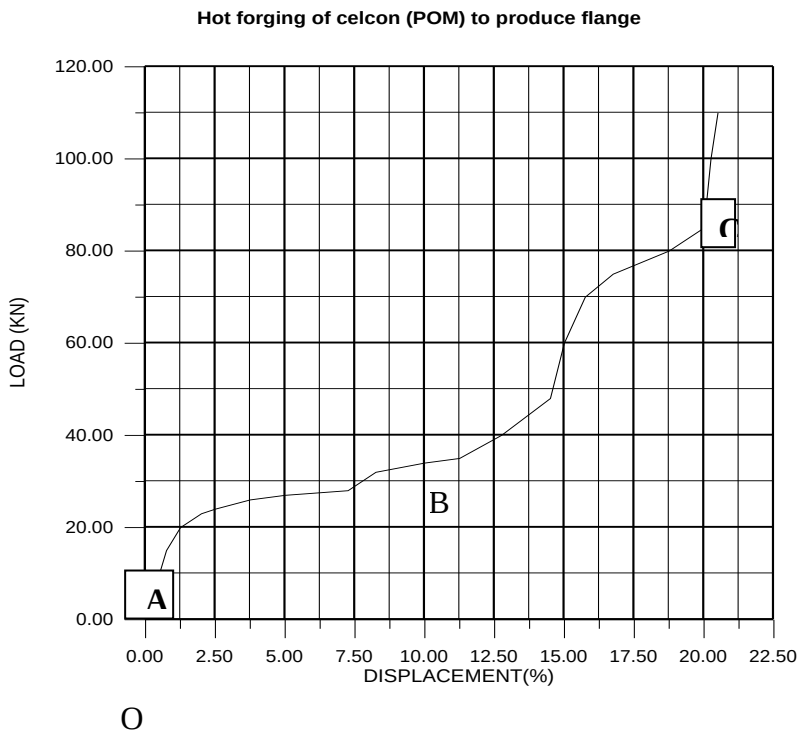

Fig.2-b Load - displacement graph

B. Strain rates:

According to the types of deformation shown on Fig.3

There are two parts of strain:

- Elastic part which obeys Hooks law, hence
  Stain = stress/ modulus
- Viscous non-linear part: This polymer is viscoelastic material, so no straight linear deformation. The polymer behaved as viscous material & as non- linear, in this meaning,

The total strain –according to Maxwell model- is equal to both. (Crawfor 1985)

So, total strain = (stress1/modulus) + (stress2/vicous element).

Any way, from fig.3:

The strains at

cold condition = 37%, achieved under applied pressure of 180 Mpa

hot condition = 30%, achieved under applied pressure of 170 Mpa

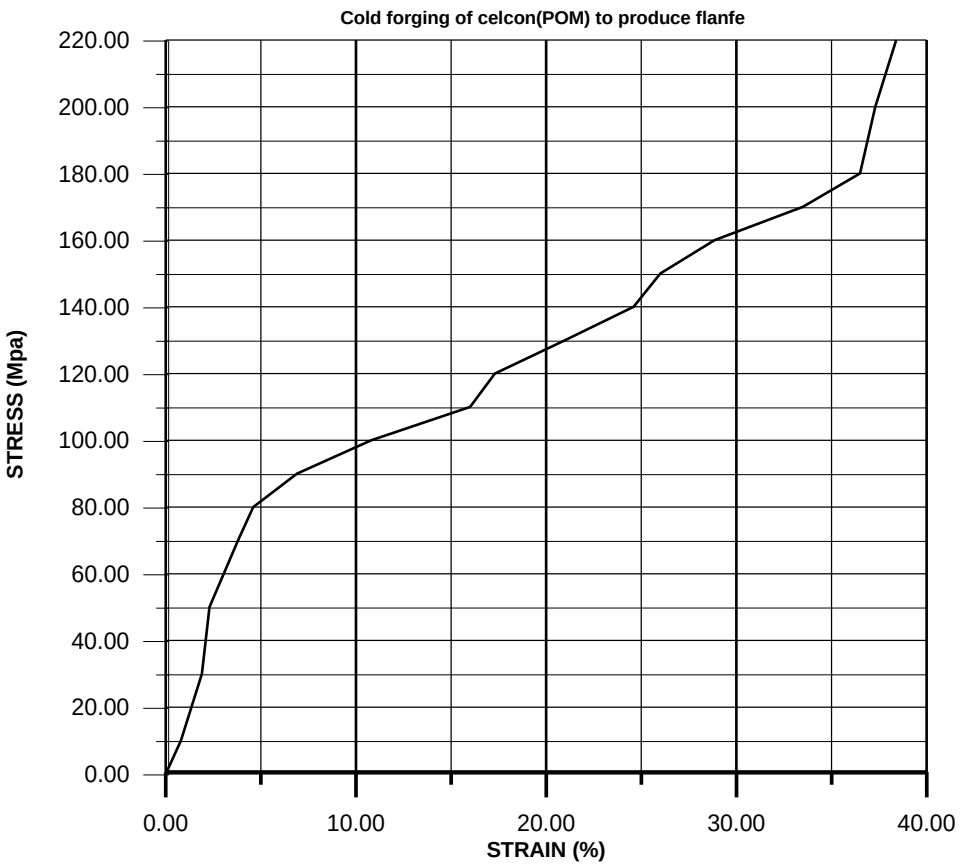

Fig.3-a stress-strain graph explains the type of deformation of POM during cold forging process under increased pressure.

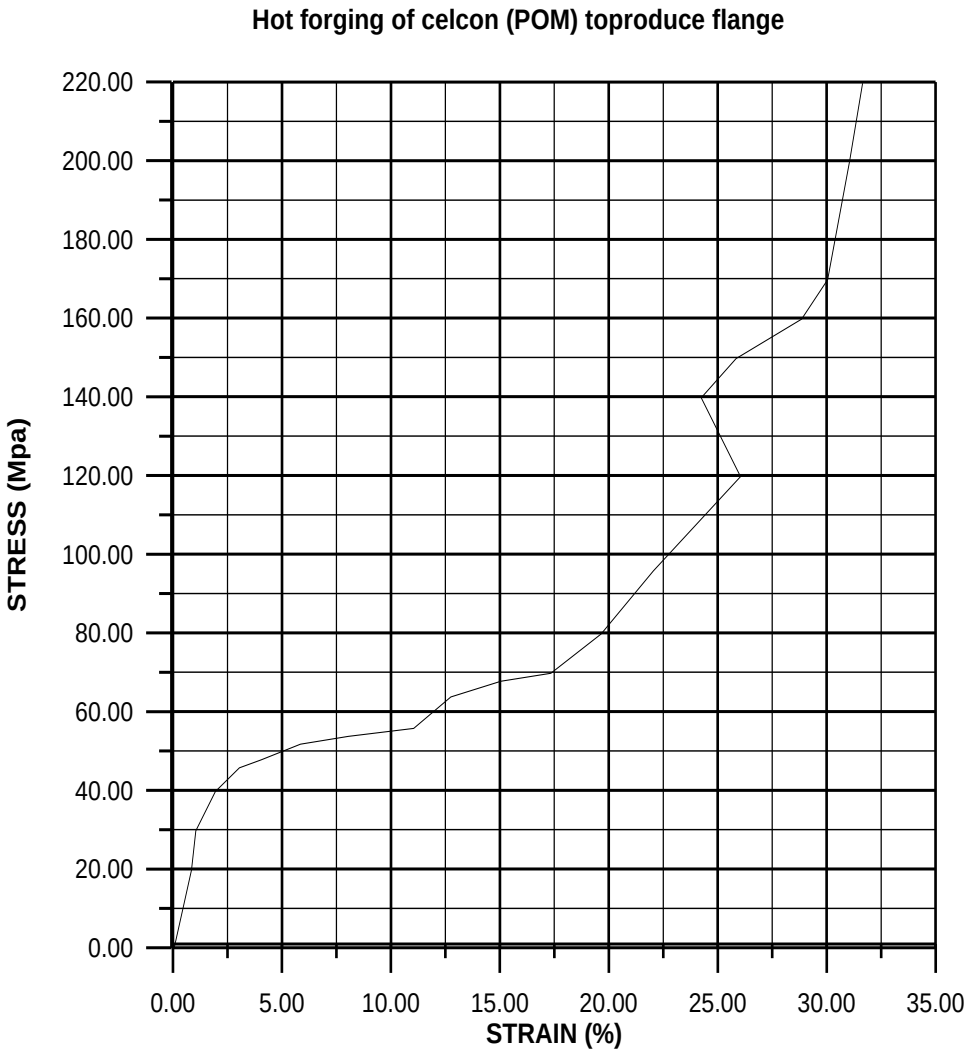

Fig.3-b stress-strain graph explains the type of deformation of preheated POM polymer during forging process under increased pressure.

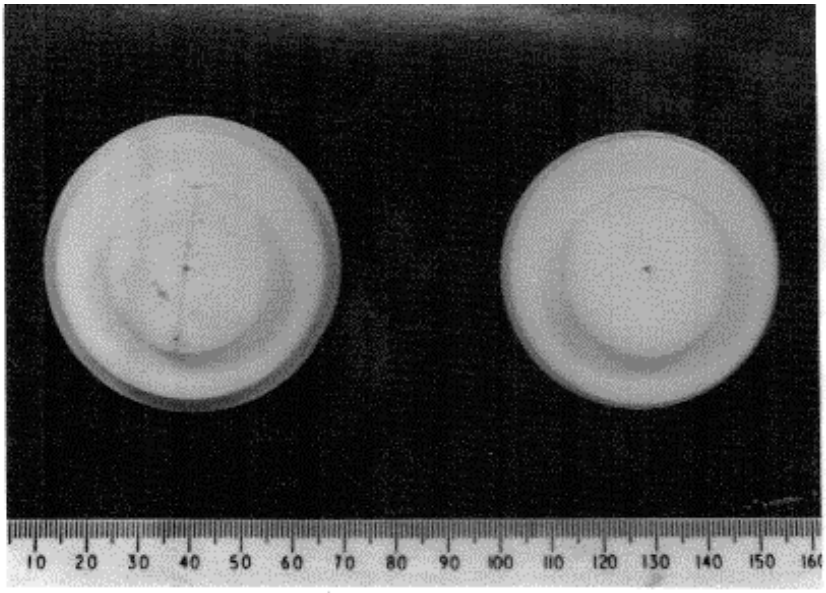

(1) (2)

FIG. 4.1-A BOTTOM VIEW

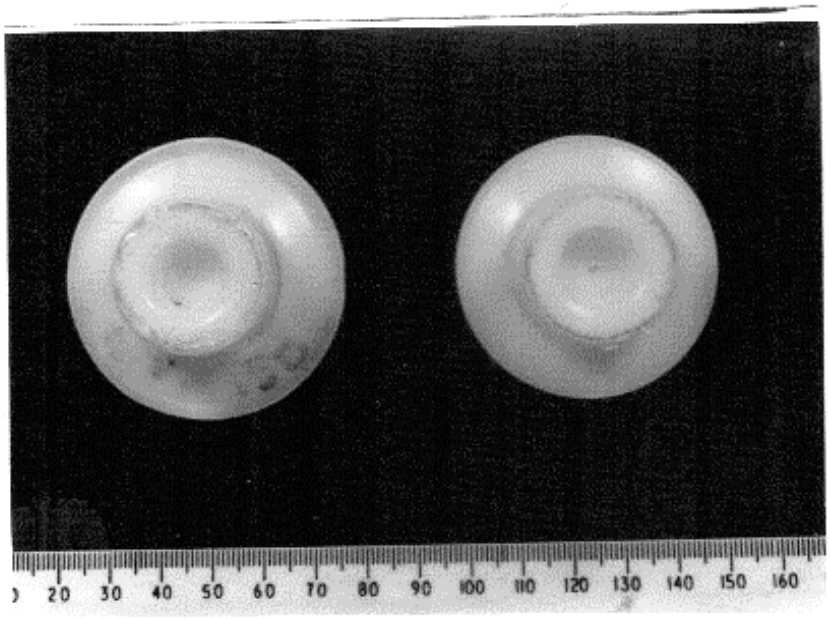

(1) (2)

FIG. 4.1-B TOP VIEW

Fig.4: (Pictures show a complete shinny flanges produced at (100C^{o}) by closed die forging process under pressure about 170Mpa

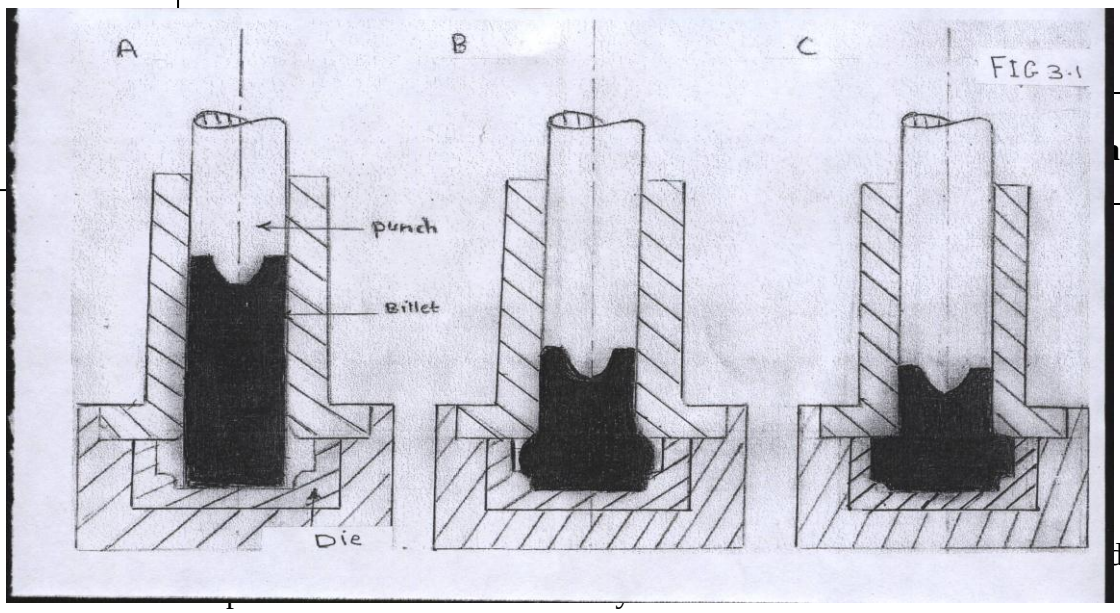

de them for those

2. Products that produced at cold condition showed curling and crack traces.
3. a smooth & shinny flange as shown in (Fig.4.1) was produced with improvement in the mechanical properties as mentioned before.
4. This work insured forgeability of acetal (celcon^{R}) at (100C^{o}) by closed die forging process at applied pressure around 170 Mpa.
5. The paper discussed the behavior of the polymer at cold & hot conditions
6. The disadvantages:
   - Too long dwell time (100sec.)
   - High pressure was required comparing to typical forging process.
7. This kind of flanges is similar to those used in following applications:
Timing pulley flange, vacuum flange, pipe fitting.

REFERENCES

* Api-Kolon(1995)- Engineering plastics

* K.M.KULKARNI(1995)- Review of forging

* P.M.COFFMAN (1990)- Forging of plastics by metal working technique

* PARSONS, I.M. WARD, P.S. HOPE and S.HENDERSON (1985)
journal of mechanical working technology

* R.J.CRAWFOR(1985)- Plastic engineering

* Yong-Seon Lee & Junes-Hwan(2002) "Experimental & analysis evaluation for elastic deformation behaviors of forging" Journal of materials processing technology, Vol.127
.
.

Simulation of Scheduling Production System by Using Integrating Simulation Models with Artificial Neural Network Model

Dr. Z. I. AL-Daoud
Assistant Professor
College of Engineering
University of Baghdad

Ouf A. Shams
M.Sc. Student
College of Engineering
University of Baghdad

ABSTRACT
Traditional methods of dealing with finding the relationship between the inputs data of simulation models and the outputs data fail or takes a long time to find this relationship. Artificial neural networks (ANNs) have the ability to learn complex relationships between inputs and outputs. Their use can greatly enhance simulation models and allow for more accurate representations of real life scenarios. This paper is concerned with the application of the mechanism of integrating simulation models with artificial neural network (ANN) model. This mechanism was tested by integrating simulation models of re-tubing heat exchangers line (RTHEL) with ANN model to schedule entering exchangers to inside re-tubing workshop. The result of applying this mechanism of integration in system (RTHEL) was in reducing completion time of re-tubing batches of heat exchangers by about (12.5%).

الخلاصة
النظريات التقليدية المستخدمة لأيجاد العلاقة بين البيانات الداخلة لنماذج المحاكاة والناتجة منها قد تفشل أو تأخذ وقت طويل لأيجاد هذه العلاقة. شبكات الخلايا العصبية الأصطناعية لها القابلية على التعلم لأيجاد أصعب العلاقات بين المدخلات والمخرجات (النواتج). أن أستخدام هذه الشبكات يحسن نماذج المحاكاة كثيراً وتسمح بتمثيل أدق لسيناريوهات العمل الحقيقية للأنظمة. يهتم هذا البحث بدراسة تطبيق آلية تكامل لنماذج المحاكاة بنموذج لشبكة خلايا عصبية أصطناعية. هذه الآلية أختبرت عن طريق تكامل نماذج المحاكاة لخط أعادة تأهيل المبادلات الحرارية مع نموذج لشبكة خلايا عصبية أصطناعية لجدولة دخول المبادلات الى داخل ورشة أعادة التأهيل. أن تطبيق آلية التكامل هذه على خط أعادة تأهيل المبادلات سوف يقلل من الوقت الكلي لأعادة تأهيل دفعات من المبادلات الحرارية بمقدار (١٢.٥%).

KEYWORDS
Integration; Simulation Models; Artificial Neural Network; Scheduling

INTRODUCTION
The risk of failing to complete activities and entire industrial projects on time is critical element of project management. Therefore, the decision making of scheduling is important to complete manufacturing the products on desired time. The importance of decision making in scheduling

production lines for complete all activities on time needs for an estimation tool for both engineers and managers.

Simulation offers a powerful tool to study, planning and improving simple and complex systems. In some cases of decision making by using simulation models, there is a difficulty to find the relationship between inputs data and outputs data. Therefore, intensive interest to use (ANNs) with simulation because; ANNs are effective tools capable of learning complex relationships between inputs data and outputs data **(G. Roberts 2004)**.

One method of integrating neural networks with simulation models is to simply use a separate program such as NeuralWorks **(NeuralWare 2006)** to develop a neural network, provide it with the desired inputs values, obtain the outputs and use outputs as parameters to the simulation program.

A generic approach for integrating simulation models with external systems such as neural networks is required. This approach should be able to encapsulate these external processes and provide standard access methods for exchanging information with the simulation models.

The objective of this paper is to develop a mechanism of integration discrete-event simulation (DES) models of RTHEL with ANN model to scheduling enters of heat exchangers to inside re-tubing workshop (find best array) with smallest completion time of re-tubing it.

SIMULATION MODELS

Building a simulation model can be a difficult and time-consuming task, it will be useful if decision maker could reuse a simulation model if possible and change it to solve a different problem or evaluate another option. Thus, it is desirable to have adoptable simulation models that are easy to change with little or no programming effort.

The RTHEL is one of primitive production lines; where it depends largely on performance, skills and experience mankind; and also for separation this line from automation. Therefore, there are two main reasons which cause a big varying in times of activities. The first reason is human factors and the second reason is the ancientness of machines and tools which they are using in this line. This leads to separate from recording times of all activities.

According to that, there is no history data for all activities times of this re-tubing line. For this situation (no history data exist), the suitable form to estimate the times of activities is (minimum, most likely and maximum values) **(Richard B. 2004)**. Therefore, in this work a use of PERT/CPM technique to estimate the times of activities from **eq. (1)**, concurs the critical path (C.P) and calculate the probability to meet the desired date from **eq. (2)** and **Table 1**.

$$ET = \frac{(T_a + 4T_m + T_b)}{6} \tag{1}$$

$$Z = \frac{(D - T_E)}{s_{cp}} \tag{2}$$

$$s_{cp} = \sum_{i=1}^{n} s \tag{3}$$

$$s = \frac{(T_b - T_a)}{6} \tag{4}$$

Where: ET = Expected Activity Time.
T_a = Optimistic Duration.
T_m = Most Likely Duration.
T_b = Pessimistic Duration.
σ = Standard Deviation of Activity Duration.
σ_{cp} = Standard Deviation of the Critical Path.
n = Activities Number of the Critical Path.
Z = Number of Standard Deviations (of a Standard Normal Distribution) that the Project, Due Date is from the Expected Completion Time.
D = Desired Completion Data for the Project.
T_E = Expected Completion Date for the Project.

Table 1: Standard Normal Cumulative Distribution (Mario F. Triola 2005)

Z	0.00	0.01	0.02	0.03	0.04	0.05	0.06	0.07	0.08	0.09
0.0	0.5000	0.5040	0.5080	0.5120	0.5160	0.5199	0.5239	0.5279	0.5319	0.5359
0.1	0.5398	0.5438	0.5478	0.5517	0.5557	0.5596	0.5636	0.5675	0.5714	0.5753
0.2	0.5793	0.5832	0.5871	0.5910	0.5948	0.5987	0.6026	0.6064	0.6103	0.6141
0.3	0.6179	0.6217	0.6255	0.6293	0.6331	0.6368	0.6406	0.6443	0.6480	0.6517
0.4	0.6554	0.6591	0.6628	0.6664	0.6700	0.6736	0.6772	0.6808	0.6844	0.6879
0.5	0.6915	0.6950	0.6985	0.7019	0.7054	0.7088	0.7123	0.7157	0.7190	0.7224
0.6	0.7257	0.7291	0.7324	0.7357	0.7389	0.7422	0.7454	0.7486	0.7517	0.7549
0.7	0.7580	0.7611	0.7642	0.7673	0.7704	0.7734	0.7764	0.7794	0.7823	0.7852
0.8	0.7881	0.7910	0.7939	0.7967	0.7995	0.8023	0.8051	0.8078	0.8106	0.8133
0.9	0.8159	0.8186	0.8212	0.8238	0.8264	0.8289	0.8315	0.8340	0.8365	0.8389
1.0	0.8413	0.8438	0.8461	0.8485	0.8508	0.8531	0.8554	0.8577	0.8599	0.8621
1.1	0.8643	0.8665	0.8686	0.8708	0.8729	0.8749	0.8770	0.8790	0.8810	0.8830
1.2	0.8849	0.8869	0.8888	0.8907	0.8925	0.8944	0.8962	0.8980	0.8997	0.9015
1.3	0.9032	0.9049	0.9066	0.9082	0.9099	0.9115	0.9131	0.9147	0.9162	0.9177
1.4	0.9192	0.9207	0.9222	0.9236	0.9251	0.9265	0.9279	0.9292	0.9306	0.9319
1.5	0.9332	0.9345	0.9357	0.9370	0.9382	.09394	0.9406	0.9418	0.9429	0.9441
1.6	0.9452	0.9463	0.9474	0.9484	0.9495	0.9505	0.9515	0.9525	0.9535	0.9545
1.7	0.9554	0.9564	0.9573	0.9582	0.9591	0.9599	0.9608	0.9616	0.9625	0.9633
1.8	0.9641	0.9649	0.9656	0.9664	0.9671	0.9678	0.9686	0.9693	0.9699	0.9706
1.9	0.9713	0.9719	0.9726	0.9732	0.9738	0.9744	0.9750	0.9756	0.9761	0.9767
2.0	0.9772	0.9778	0.9783	0.9788	0.9793	0.9798	0.9803	0.9808	0.9812	0.9817
2.1	0.9821	0.9826	0.9830	0.9834	0.9838	0.9842	0.9846	0.9850	0.9854	0.9857
2.2	0.9861	0.9864	0.9868	0.9871	0.9875	0.9878	0.9881	0.9884	0.9887	0.9890
2.3	0.9893	0.9896	0.9898	0.9901	0.9904	0.9906	0.9909	0.9911	0.9913	0.9916
2.4	0.9918	0.9920	0.9922	0.9925	0.9927	0.9929	0.9913	0.9932	0.9934	0.9936
2.5	0.9938	0.9940	0.9941	0.9943	0.9945	0.9946	0.9948	0.9949	0.9951	0.9952
2.6	0.9953	0.9955	0.9956	0.9957	0.9959	0.9960	0.9961	0.9962	0.9963	0.9964
2.7	0.9965	0.9966	0.9967	0.9968	0.9969	0.9970	0.9971	0.9972	0.9973	0.9974
2.8	0.9974	0.9975	0.9976	0.9977	0.9977	0.9978	0.9979	0.9979	0.9980	0.9981
2.9	0.9981	0.9982	0.9982	0.9983	0.9984	0.9984	0.9985	0.9985	0.9986	0.9986
3.0	0.9987	0.9987	0.9987	0.9988	0.9988	0.9989	0.9989	0.9989	0.9990	0.9990
3.1	0.9990	0.9991	0.9991	0.9991	0.9992	0.9992	0.9992	0.9992	0.9993	0.9993
3.2	0.9993	0.9993	0.9994	0.9994	0.9994	0.9994	0.9994	0.9995	0.9995	0.9995
3.3	0.9995	0.9995	0.9995	0.9996	0.9996	0.9996	0.9996	0.9996	0.9996	0.9997
3.4	0.9997	0.9997	0.9997	0.9997	0.9997	0.9997	0.9997	0.9997	0.9997	0.9998

3.50 and up	**0.9999**									

Therefore, the use of the most familiar technique for building the DES models of RTHEL which is Network Technique; because this technique shows the interdependencies and relationships between events and activities. There are other reasons of using network technique for building model. First, the decision to use PERT/CPM technique is to estimate time of each activity and which activities are critical, where PERT is one of network‘s techniques. Second, network is easy to change with little or no programming effort and change it to solve a different problem. Third, network is a suitable model to DES, because network model can be make changes in it; when changing occur at discrete periods of time in system which network represents it.

Simulation models of RTHEL to re-tubing several types of heat exchangers are building and run by using *simulation software* which develops by using Visual Basic 6.0 language. **Fig. 1** show the main window of software, using this window the data is entered to *Master Database* of software or doing any change on this data. **Fig. 2** show the window of simulation models, using this window a simulation model of re-tubing one heat exchanger is built and run it to estimate completion time, concurs (C.P) and calculate the probability to meet the desired time. **Fig. 3** show the window which contain the draw of network (simulation model).

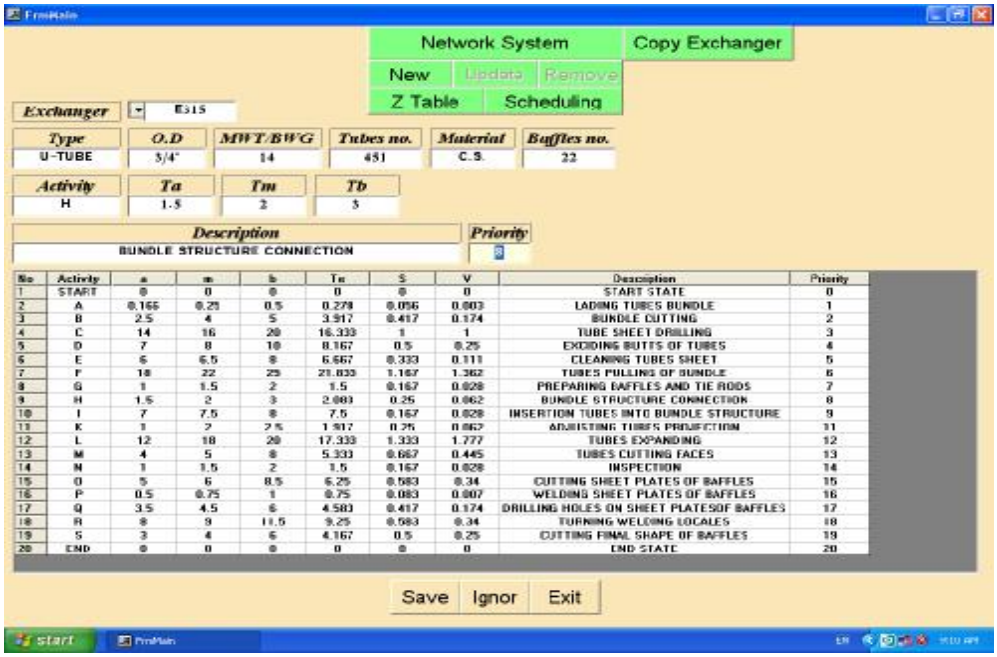

Fig. 1: The main window of simulation software

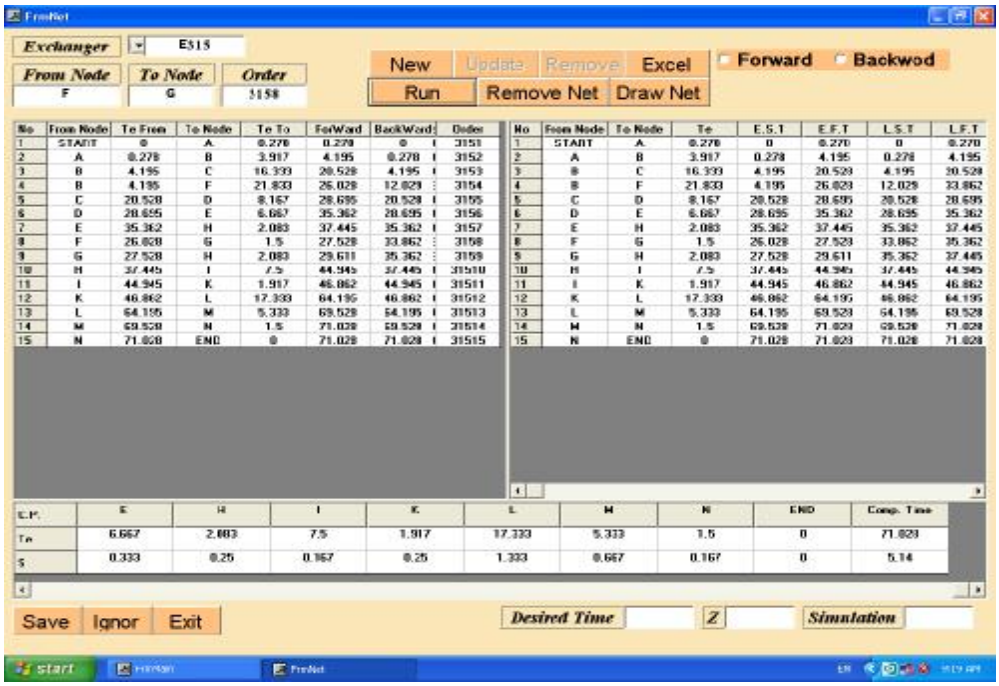

Fig. 2: The window of simulation models

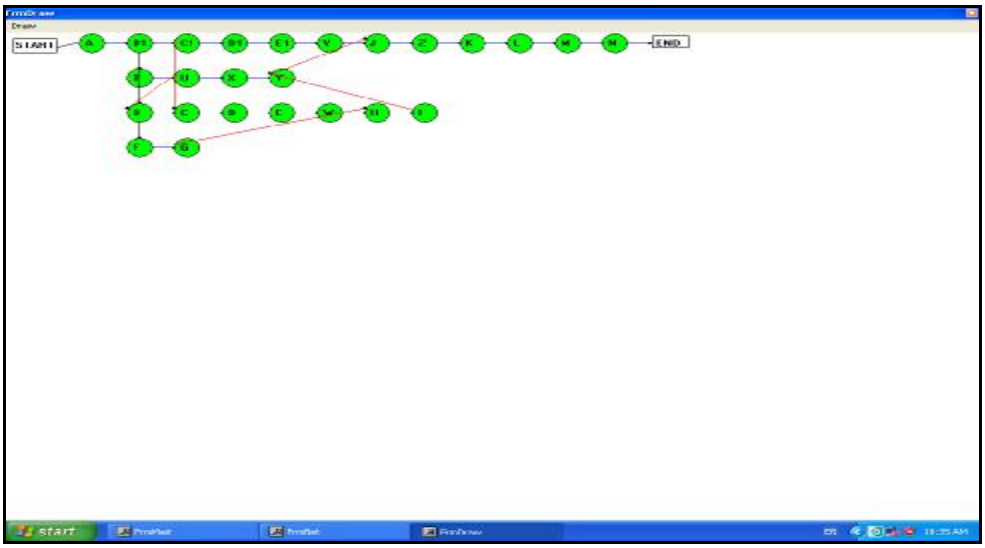

Fig. 3: The window drawing of simulation models

ARTIFICIAL NEURAL NETWORKS (ANNs)

The inspiration for artificial neural networks originated from the study of processes in the human brain. Neural networks are comprised of multiple simple element called artificial neurons **Fig. 4**, the network acquires knowledge through a learning process. The inter-neuron connection strengths known as synaptic weight are used to store the knowledge **(Haykin S. 1994)**. This learning ability of neural networks gives an advantage in solving complex problems whose analytic or numerical solutions are hard to obtain **(Rafiq MY. 2001)**. The scheduling production line is one of those problems.

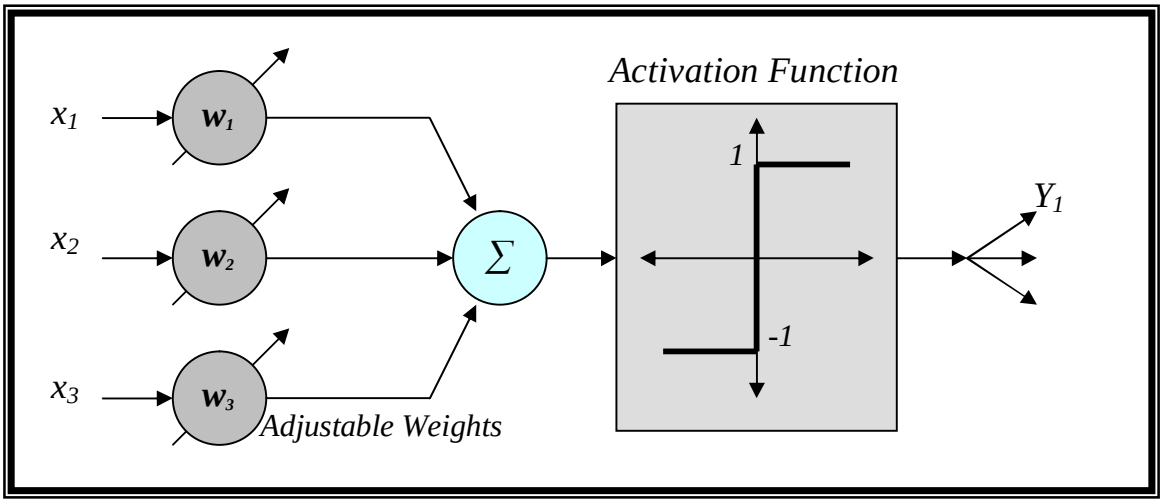

Fig. 4: Artificial neuron

The Design of Artificial Neural Network Model

The problem presented in this paper is based on optimum design and prediction utilizing a multi-layer feed-forward neural network (MLFFNN) architecture and new supervised learning algorithm.

The model has been developed in three phases; the modeling phase, the training phase and the testing phase. The modeling phase involves the analysis of data, the identification of time estimation parameters and the selection of the network architecture and of the internal rules. The training phase requires the preparation of the data and the adoption of the learning law for the training. The testing phase evaluates the prediction accuracy of the model.

The Modeling Phase

The modeling phase includes the design of the neural network architecture. It is a complex and dynamic process that requires the determination of the internal structure and rules (i.e., the number of hidden layers and the type of activation function). The model is designed according to the type of the data and the response required by the application.

The current model has been designed to include an input layer of (p) processing elements (neurons) corresponding to the (p) input parameters and an output layer of one processing element (neuron) as the target. One hidden layer of (h) processing elements was selected according the nature of problem **(D. T. Pham 2003)** as shown in **Fig. 5**.

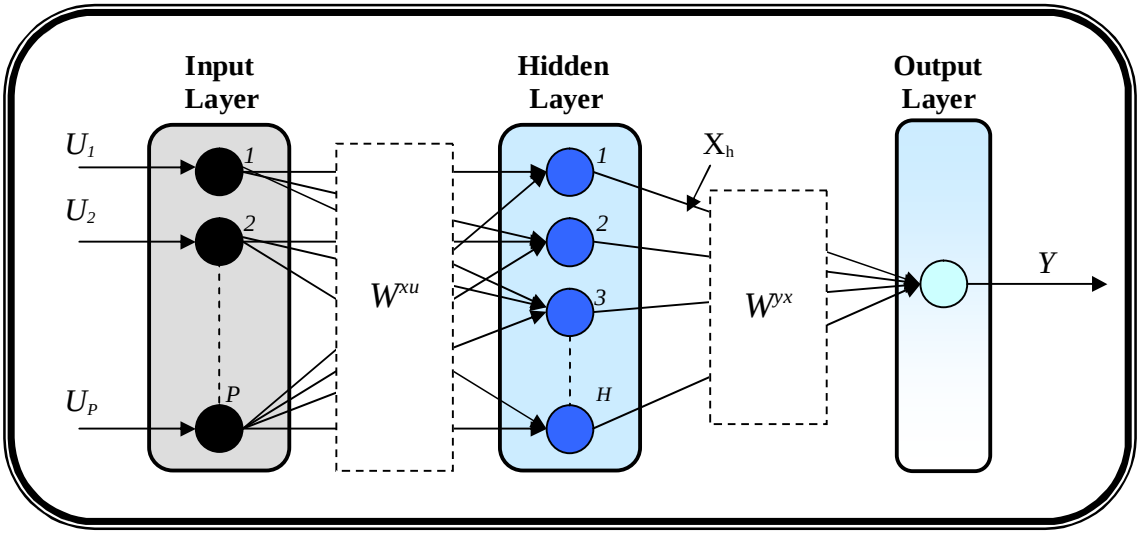

Fig. 5: The architecture of MLFFNN of problem in this work

Therefore, an effective number of processing elements is usually determined by trials for the hidden layers, since there is no rule to determine it **(Albino V. 1998)**, **(Setyawati BR 2002)**. In this work, the author finds equation can be determine the number of processing elements for the hidden layer of neural network of this work as shown in **eq. 5**.

$$h = p! \tag{5}$$

Where: h = Number of nodes in hidden layer.
p = Number of nodes in input layer.

A neuron basically computes the sum of their weighted inputs, subtracts its threshold from the sum, and transfers these results by a function. This can be explained mathematically as (Eq. (6)):

$$Y = f(net) \tag{6}$$

$$Net = \sum_{h=1}^{H} w_h x_p \tag{7}$$

Where: Y = Output of a neuron.
w_h =Weight associated with the input p.
h = Number of nodes in hidden layer = {1, 2 . . . . H}.
x_p = Input units.
f =Transformation function.

The neurons are interdependent on each other via weighted connections. These weights form the power of the influence between the neurons. All neurons are connected to the other neurons in the next layer.

The function of the hidden layer is to extract and remember the useful features and the sub features from the input patterns to predict the outcome of the network (values of the output layer) **(Rafiq MY. 2001)**. The characteristics of the activation function are important since it defines the behavior of the network model. An activation function is used because several impacts, if applied

additively, might cause these quantities (i.e., target values) to fall below the lower or rise above the upper bound.
The function adopted for the current completion time estimation problem was a linear function, given by **eq. 8**.

Linear function = $c \times net$ (8)

Where: c = neuron gain.

To learn this neural network, author decides to use supervised learning to learn MLFFNN of this work because; the inputs and the output of ANN are known. In general, there is a useful correspondence between the type of training that is appropriate and the type of problem. Additionally, there is a relationship between the number of learning epochs and the desired characteristics of the output **(D. T. Pham 2003).**

According the nature of problem of this work and the desired characteristics of the output, the ANN use to scheduling the entering of heat exchangers to inside workshop and find the best array from multi arrays, it is the same process to find minimum value from multi values. For this purpose, ANN need to one learning epoch to find the best array. Also, weights between input-hidden layers (W^{xu}) are fixed; and learning rate (η) and error goal (eg) are equal to zero because; there is no need to iterative training.

Therefore, author applies a new supervised learning algorithm to train the neural network. New supervised learning algorithms represent one of attempts to improving the learning speed of these learning algorithms for example; BP algorithm, which are still too slow to be applied in real-world applications even for a very simple problem.

The Training Phase

An important issue to be resolved when applying ANNs to a problem is to determine which training procedure to adopt. In this work a new supervised learning algorithm is applied to learn neural network. The steps which use to training the neural network in this work to find the best array with minimum value of completion time are explained as follows:

Step 1: Input units (x_p) (p = 1, 2 ….. P); receive input signal U_p.

$$x_p(k) = U_p(k) \quad (9)$$

Step 2: The interconnection weight (W_p^{xu}) of input-hidden layer have to be assumed (1) for each connection.

Step 3: Compute the outputs of hidden layer (X_h) by use the following equation:

$$X_h = \sum_{p=1}^{P} W_p^{xu} x_p \quad (10)$$

Where: X_h = outputs of nodes of hidden layer.
x_p = nodes of input layer.
p = Number of nodes in input layer = {1, 2 . . . . P}

W_p^{xu} = interconnection weight of input- hidden layer.

Step 4: The interconnection weight (W_h^{yx}) of hidden-output layer will be assumed as below:

- For the smallest value (W_h^{yx}) equal (1)
- For the other values (W_h^{yx}) equal (0)

Step 5: Compute the output of output layer (Y) by use the following equation:

$$Y = \sum_{h=1}^{H} W_h^{yx} X_h \tag{11}$$

Where: Y = output of output layer (output of network).
X_h = outputs of hidden layer.
h = Number of nodes in hidden layer = {1, 2 . . . . H}.
W_h^{yx} = interconnection weight of hidden-output layer.

THE INTEGRATION MECHANISM

The situation of analysis and decision making in fast paced, rapidly changing venues; such as job shop scheduling. In this situation, there is simply no time to perform multiple replications for the selected values of the decision variables. Also, some times it is difficult to solve some problems with traditional technique.

The problem of this work; which is scheduling the entrees of heat exchangers to inside re-tubing workshop, so as to finding the best array of entrance of the batch of heat exchangers to re-tubes it with smallest completion time of re-tubing. It is difficult to solve it through simulation models just and also it takes long time to get right decision. Therefore, it is necessary to integrate simulation models with other tool to solve this problem. Simulation models are integrated with ANN model because; ANN provides an effective tool for evaluating relationships between input data and result output.

Integrating simulation with other systems involves a careful analysis of the nature of the information that needs to be exchanged. Ideally, the integration mechanism should be generic enough to be used to link simulation models to ANN models as well as many other elements such as databases as shown in **Fig. 6**.

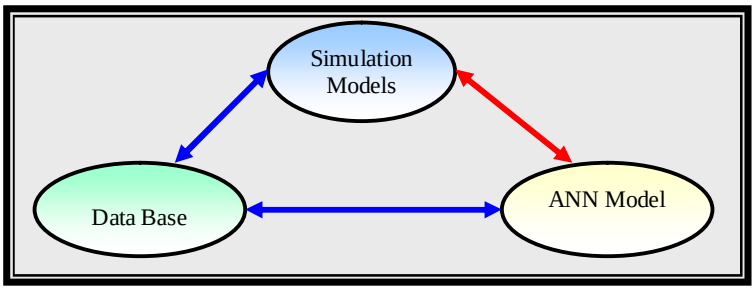

Fig. 6: Integrating Simulation with ANN and Databases

The mechanism of integrating simulation models with ANN model which is used in this work; is explain as follows:

1. The start begins with insertion of the order of manager RTHEL; which represent the batch of heat exchangers that wants to re-tubes it. This order takes as the inputs to ANN model.

2. The interconnections between nodes of input-hidden layers and hidden-output layers are fully connected.
3. There are two connections (one way) between hidden layer - master database of software and master database - simulation models.
4. There is a connection (two ways) between hidden layer and simulation models to transfer models for each node in hidden layer.
5. The nodes in hidden layer represent the probabilities of array. In each node, the simulation models are merging and then, compute the forward time (completion time).
6. There is a connection (one way) between output NN and simulation models to transfer the best array. Then, compute the backward time of this array to detect the critical path.

Fig. 7 shows the integration mechanism between simulation models and ANN model in simulation software and how the data of exchangers transfer between models.

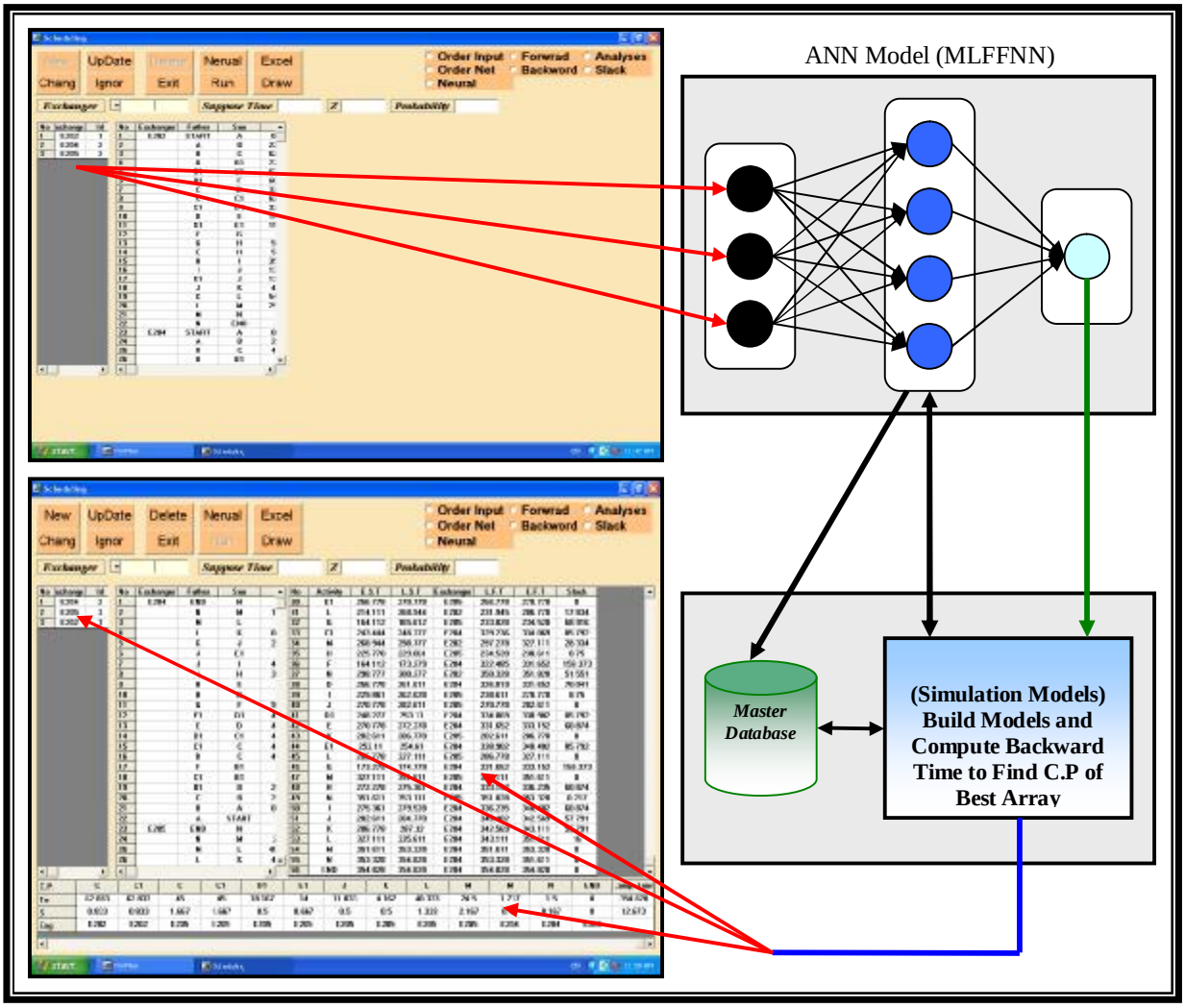

Fig. 7: The integration mechanism between simulation models and ANN model

The simulation software is designed to scheduling the entrees of heat exchangers, so as to find the best array to enter exchangers inside re-tubing workshop by using integrating simulation models

with ANN model. Then, compute the completion time of this array and detects the critical path of this production process. Also, evaluate the probability to meet the desired completion time. **Fig. 8** show the window of scheduling, from this window it can find the best array of entering batch of heat exchangers by merging simulation models of these exchangers and run it to estimate completion time, concurs (C.P) and calculate the probability to meet the desired time. **Fig. 9** show the window which contains the table of ANN results. **Fig. 10** show the window which contain the draw of merging networks (merging simulation models).

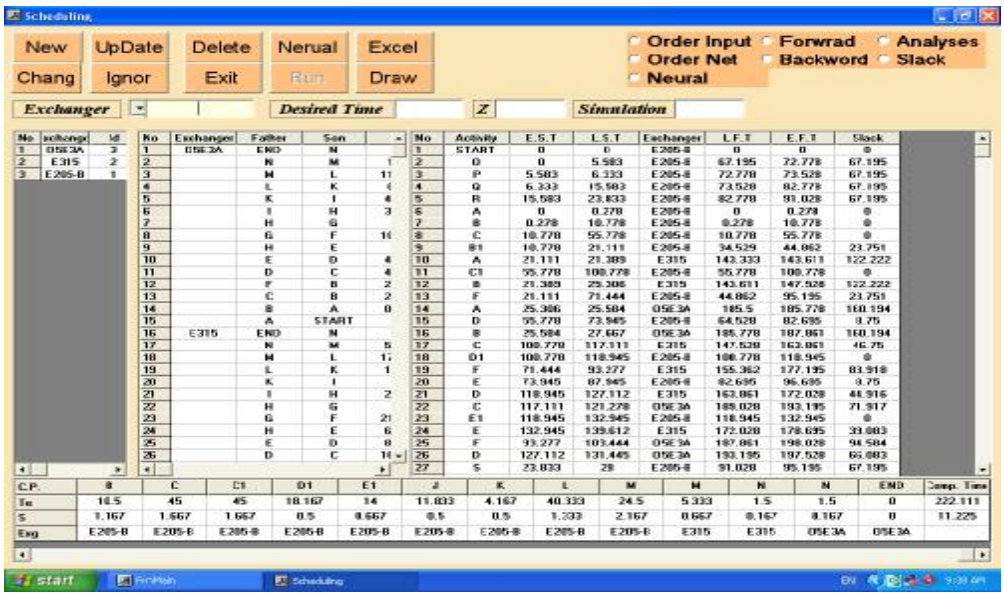

Fig. 8: The window of scheduling

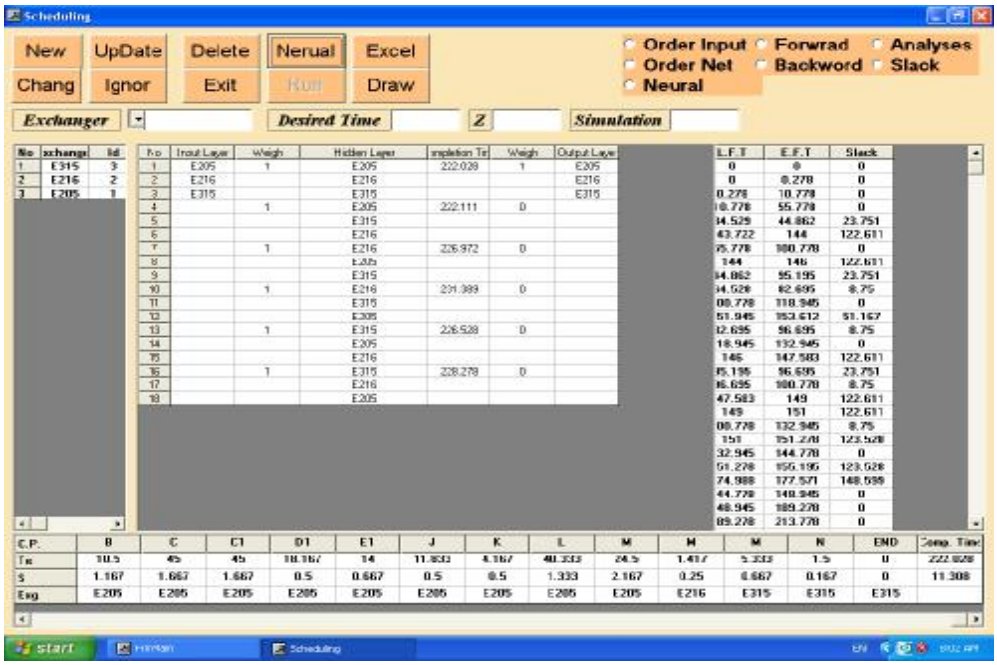

Fig. 9: The window of scheduling which contains the table of ANN results

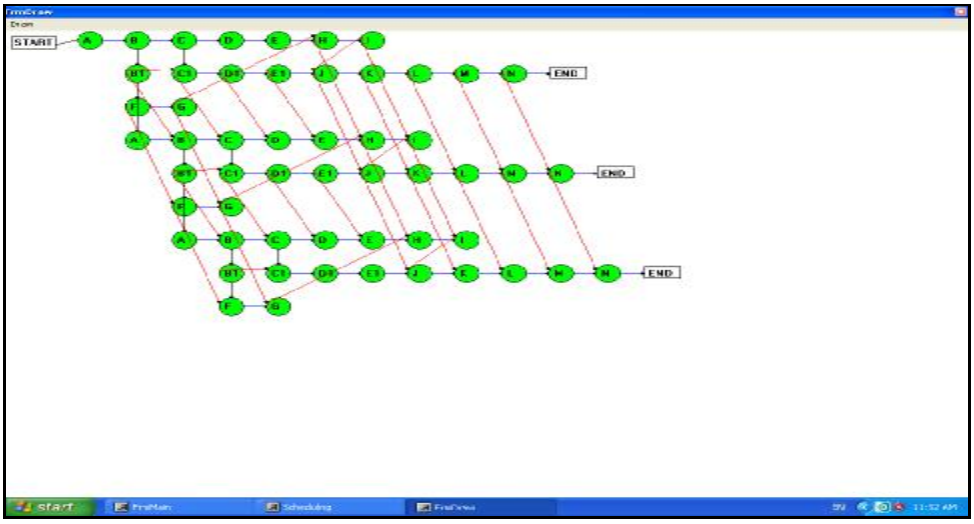

Fig. 10: The window drawing of merging simulation models

THE TESTING PHASE

After applying the integration mechanism, the output of this mechanism is tested by using validation technique called "*Validation Using Testing against Historical Data*". In this technique, author compared the results of simulation software with the actual data (historical data) of completion time for re-tubing some batches of heat exchangers as shown in **Table 2**.

Table 2: Results of simulation software and actual data of completion time for re-tubing some batches of heat exchangers

No. of Batch	Re-tubing Completion Time						
	Probability of Array						
	1	2	3	4	5	6	Actual
1st	**315.277**	**303.777**	**318.638**	**325.833**	**337.972**	**329.833**	**345.5**
2nd	**216.111**	**225.277**	**228.528**	**242.195**	**230.972**	**227.389**	**247**
3rd	**319.994**	**305.994**	**326.638**	**340.5**	**311.856**	**322.5**	**348**
4th	**219.028**	**228.278**	**233.972**	**247.389**	**226.528**	**238.278**	**252.5**

Then, it can be recognized from **Table 2** that the results of integration mechanism are close from the historical data of real system. This result leads that mechanism of integrating simulation models with ANN model is acceptable and it can represent the real system for finding best array.

RESULTS

The run of integration mechanism takes the shortest time to find the best array to entering the batches of heat exchangers to inside re-tubing workshop with its completion time and also concurs the (C.P) without any error in runs. The results of simulation software (simulation data) of completion time for re-tubing some batches of heat exchangers are summarized in **Table 3**, and then convert to **Fig. 11**.

Table 3: Simulation Data and Actual Data of Completion Time for Re-tubing some Batches of Heat Exchangers

	Completion Time of Re-Tubing Batch of Heat Exchangers			
Batch	First	Second	Third	Fourth
Actual Data	**345.5**	**247**	**348**	**252.5**
Simulation Data	**303.777**	**216.111**	**305.994**	**219.028**

From **Fig. 11**, it can be seen that completion time of re-tubing batch of heat exchangers has decreased about (12.5%) after applying the mechanism of integration simulation models of re-tubing heat exchangers with ANN model

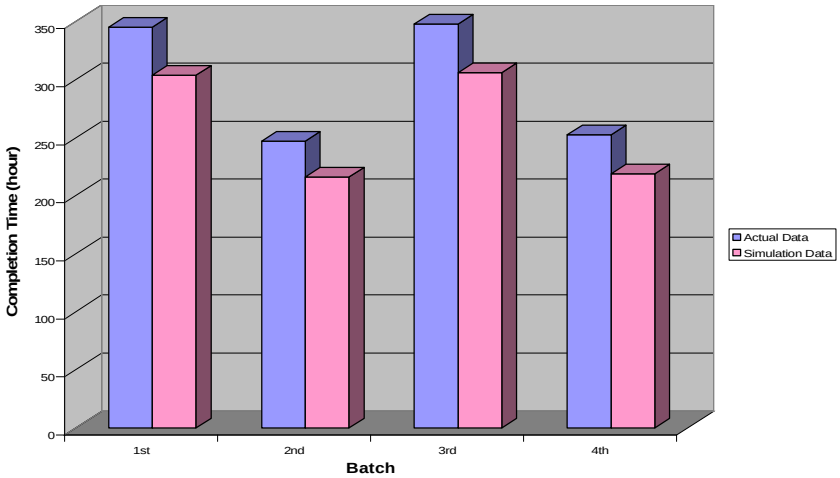

Fig. 11: Histogram of Completion Time for Re-tubing some Batches of Heat Exchangers

CONCLUSIONS

An approach has been presented to achieve the integration of simulation models with ANN model. The approach was designed to allow for future integration with other types of models as well.

Integration of the ANN model with re-tubing simulation models allows for more accurate representation of the real life operations as complex relationships between the heat exchangers needs to re-tubes it and the best array of entering these exchangers to inside re-tubing workshop.

REFERENCES

*Albino V, Garavelli AC. A neural network application to subcontractor rating in construction firms. J Project Manage 1998; 16 (1): 9-14.

*D. T. Pham and X. Liu. Neural Networks for Identification, Prediction and Control. Springer-Verlag: New York. 2003.

*G. Roberts. Intelligent Mechatronics. Computing and Control Engineering Journal, IEE Control Division, Vol.4, No.6, December 2004, PP. 257-264.

*Haykin S. Neural Network: A Comprehensive Foundation. New York: Macmillan; 1994.

*Mario F. Triola. Essentials of Statistics. New York: Pearson. 2005. 2nd edition.
NeuralWare, 2006. Neural works Professional. Detailed information available on http://www.neuralware.com/ . Version: 2006.

*Rafiq MY, Bugmann G, Easterbrook DJ. Neural network design for engineering applications. Comput Struct 2001; 79: 1541-1552.

*Richard B. Chase, F. Robert Jacobs and Nicholas J. Aquilano. Operations Management for Competitive Advantage. New York: McGraw-Hill, 2004, 10th edition.

*Setyawati BR, Sahirman S, Creese RC. Neural networks for cost estimation. AACE International Transactions; 2002, ABI/IN-FORM Global: EST.13.1-EST.13.9.

NOMENCLATURE

Symbol	Description
ANN	Artificial Neural Network
ANNs	Artificial Neural Networks
C.P	Critical Path
CPM	Critical Path Method
C	Neuron Gain
D	Desired Completion Data for the Project
DES	Discrete-Event Simulation
ET	Expected Activity Time
e.g	Error Goal
f	Transformation Function
h	Number of Nodes in Hidden Layer
n	Activities Number of the Critical Path
MLFFNN	Multi-Layer Feed-Forward Neural Network
PERT	Program Evaluation and Review Technique
p	Number of Nodes in Input Layer
RTHEL	Re-Tubing Heat Exchanger Line
Ta	Optimistic Duration
Tb	Pessimistic Duration
Tm	Most Likely Duration
T_E	Expected Completion Date for the Project
U	The External Inputs to the Neural Network
w	The weight of interconnection neuron
W^{xu}	Weighted Interconnection for Input-Hidden Layers
W^{yx}	Weighted Interconnection for Hidden-Output
x	Input units
X	The Output of Hidden Units

Y	The Output of Neural Network
Z	The Number of Standard Deviations (of a Standard Normal Distribution) that the Project Due Date is from the Expected Completion Time.
σ	Standard Deviation of Activity Duration
s_{cp}	Standard Deviation of the Critical Path
η	Learning Rate

COMPUTATIONAL METHOD FOR UNSTEADY MOTION OF TWO-DIMENSIONAL AIRFOIL

Anmar H. Ali

Asst. Lect.Mechanical Engineering Dept.

College of Engineering

University of Baghdad

ABSTRACT

A numerical method is developed for calculation of the wake geometry and aerodynamic forces on two-dimensional airfoil under going an arbitrary unsteady motion in an inviscid incompressible flow (panel method). The method is applied to sudden change in airfoil incidence angle and airfoil oscillations at high reduced frequency. The effect of non-linear wake on the unsteady aerodynamic properties and oscillatory amplitude on wake rollup and aerodynamic forces has been studied. The results of the present method shows good accuracy as compared with flat plate and for unsteady motion with heaving and pitching oscillation the present method also shows good trend with the experimental results taken from published data. The method shows good results for a wide range of unsteady motion of a two-dimensional airfoil.

الخلاصة:

تم تطوير طريقة عددية لحساب القوى الهوائية وشكل الاعقاب خلف مطيار ثنائي الابعاد واقع تحت تاثير حركة غير متوازنة لجريان غير لزج وغير قابل للانضغاط (طريقة البوابات). طبقت الطريقة على المطيار الذي يبدا بحركة فجائية وبزاوية هجوم معينة كذلك المطيار الذي يتحرك بتذبذب ذو قيمة اهتزازية عالية. ان تاثير التصرف اللاخطي للاعقاب على الخواص الهوائية وقيم العليا للحركة الاهتزازية وتاثيراتها على الالتفاف الحاصل بالاعقاب خلف المطيار والقوى الهوائية المتولدة حيث تمت دراستها. اوضحت الطريقة المستخدمة حاليا نتائج جيدة اذا ما قورنت مع الاسطح المستوية كذلك فان الحركة الاهتزازية الرفعية والانحنائية اظهرت تطابق جيد من حيث التصرف مع النتائج العملية المتحصلة من بحوث سابقة. ان الطريقة الحالية تظهر نتائج جيدة ولمديات واسعة في الحركة الغير مستقرة لمطيار ثنائي البعد.

KEYWORDS

Airfoil Oscillations, Panel Method, Unsteady Aerodynamics, Aerodynamic Coefficients, Hydrofoils, Lift, Pressure Distribution

INTRODUCTION:

One of the basic assumptions of airfoil theory deal with the presence of stagnation point at the sharp trailing edge, what is commonly called Kutta Condition. While the existence of this condition is well established for steady non-separated flow situation, its validity for time-dependent cases is still controversial **(Hess & Smith 1966)**.

It can be shown that Kutta Condition can be applied for force and moment prediction in unsteady small amplitude non-separated high Reynolds Number flows. As a first approximation it is reasonable assume that the flow can be regarded as inviscid so long as the flow in the region of the trailing edge is not separated.

For general unsteady motion it is possible to obtain numerical solutions by imposing either the condition of finite velocities about the trailing edge or the condition of zero loading about the trailing edge **(Basu and Hancock 1978).**

The most comprehensive numerical solution is due to **(Gesing 1968)** and is based on (**Hess & Smith 1966)** procedure to solve two-dimensional airfoil in steady incompressible flow by using source and vortex distribution on the surface and by using Kutta condition invoked velocities equal in both magnitude and direction at midpoint of the two trailing edge elements. The method discrete vortex shedding from the trailing with strength equal to the negative vortex strength of the airfoil, it found that the approach gives good behavior of the wake and loads when the airfoil move in unsteady motion. **(Basu and Hancock 1978)** developed a numerical method to calculate two-dimensional airfoil under going an arbitrary unsteady motion in an inviscid incompressible flow. The method of **Gesing** is modified by adding additional panel at the trailing edge with length and angle depends on the solution of airfoil vorticity and by application of zero loads at the trailing edge, so that, a system of non-linear equation is produced due to this element and with iteration technique is used to solve these equations. Good results obtained with this modification as compared with **Gesing**. **(Chen and Sheu 1980)** used the interior singularities to solve the unsteady incompressible inviscid airfoil. Same approach of **Basu and Hancock** for oscillations motion analysis although results have been presented for a sudden change in incidence at high frequency oscillation and entry into a sharp-edge gust, the method is completely general. **(Kats and Weihs 1981)** used a thin airfoil theory to solve the unsteady motion, as compared with other published experimental data. It is found that when the trailing edge displacement is small the range of linearized theory calculations using Kutta condition can be extended far beyond reduced frequency larger than 1. **(Poling and Telionis 1986)** presented two cases of unsteady flow field over a NACA 0012 airfoil at an angle of attack, the results indicates that the unsteady Kutta condition proposed by **Gesing** is examined and some evidence is provided for its support.

In the present work will adapt the method stated by **(Katz and Plotkine 1991)** which created to solve the unsteady flow about thin (Flat Plate) airfoil, and then coupled with **Hess & Smith** method to solve thickness problem (e.g. NACA 0012). Some modification presented to solve airfoil load coefficients which illustrated in numerical procedure.

MATHEMATICAL MODEL:

The flow field is assumed to be potential (inviscied and irrotational) and incompressible. In that case velocity potential satisfies the laplace equation:

$$\Delta\phi = 0 \qquad (1)$$

The equation is the same, both for steady and unsteady flows. Owing to that, methods for steady cases can be applied for the solution of unsteady flow problems, as well. Unsteadiness is introduced by the unsteady boundary condition:

$$\vec{Q}.\vec{n} = 0 \qquad (2)$$

Of the Kelvin theorem:

$$\frac{D\Gamma}{Dt} = 0 \qquad (3)$$

And the unsteady form of the Bernoulli equation:

$$\frac{p - p_\infty}{0.5\rho_\infty} = V_\infty^2 - Q^2 - 2\frac{\partial\phi}{\partial t} \qquad (4)$$

In order to define the aerodynamic characteristics of the airfoil, two models should be established: airfoil model and wake model.

The airfoil model is modeled by **(Hess & Smith 1966)** method, which enables to model airfoil with different shape by using constant source and vortex panel on the airfoil surface.

Numerical modeling of the wake must be done carefully due to its high influence on the lift force generation. To satisfy the unsteady Kutta Condition at the trailing edge, the pressure coefficient for the unsteady flow is defined as:

$$C_p = 1 - \frac{Q^2}{V_\infty} - \frac{2}{V_\infty}\frac{\partial\phi}{\partial t} \qquad (5)$$

According to that, the difference between the upper and lower surface pressure coefficients at the trailing edge is:

$$\Delta C_p = -\frac{Q_u^2 - Q_l^2}{V_\infty^2} - \frac{2}{V_\infty^2}\frac{\partial}{\partial t}\left(\phi_u - \phi_l\right) = 0 \qquad (6)$$

Where u and l are the upper and lower surface value;

The potential difference is:

$$\Gamma = \phi_u - \phi_l \qquad (7)$$

The Kutta condition can be expressed as the uniqueness of the pressure coefficients at the trailing edge, which mathematically expressed, takes the form:

$$\frac{\partial\Gamma}{\partial t} = -V_\infty \gamma_{TE} \qquad (8)$$

From this equation it can be clearly seen that the variation of airfoil circulation in time can be compensated by releasing vortices of magnitude γ_{TE}.

NUMERICAL METHOD:

The solution for the flow about an airfoil under going an arbitrary time-dependent motion which started at t = 0 is calculated at successive intervals of time.

$$t_k \ (t_0 = 0, k=1,2,3\ldots..) \qquad (9)$$

By a method based on **(Hess and Smith 1966)** approach to solve steady linear incompressible flow about airfoil at time t_k, the model of non-linear unsteady incompressible flow is shown in **Fig (1).**

The airfoil contour at time t_k is replaced by N straight-line elements. A uniform source distribution $(\sigma_i)_k$ and a uniform vorticity distribution $(\gamma)_k$ are placed on i^{th} element (i =1,2,…..,N) where $(\sigma_i)_k$ varies from element to element but $(\gamma)_k$ is the same for all elements on airfoil and the subscript k refer to the time t_k. The over all circulation (Γ_k) can be calculated from $(\gamma)_k$ * (airfoil perimeter).

The unsteady motion of the airfoil is characterized by the presence of the trailing vortex wake emanating from the trailing edge of the airfoil. The vorticity shed during any time t_k is equal in magnitude and opposite in sign to the change in circulation about the airfoil during t_k.

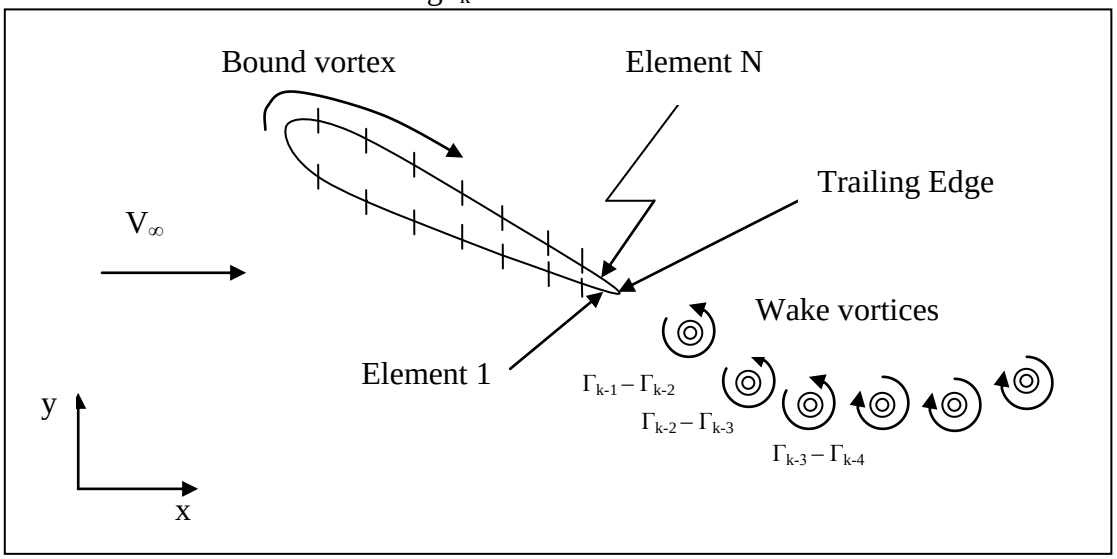

Fig (1): The unsteady motion of a two-dimensional airfoil**.**

Once the vorticity is shed it moves as a fluid particle subjected firstly to the onset flow and secondly to the perturbation velocity due to the airfoil and then to the induced velocity due to the remainder of the shed vorticity, this procedure is implemented as indicated in **Fig (2).** From any initial stage the prescribed movement of the airfoil during next t_k is carried out and the vorticity shed during t_k is computed from the simultaneous application of the usual Kutta condition at the trailing edge of the airfoil and the vorticity conservation low mentioned above. This vorticity is placed in the fluid as a line vortex at a location representative of the average fluid velocity over the trailing edge locus during t_k. Finally, all previously shed line vortices are moved to new locations using a predictor-corrector method. As shown in the **Fig (2).**

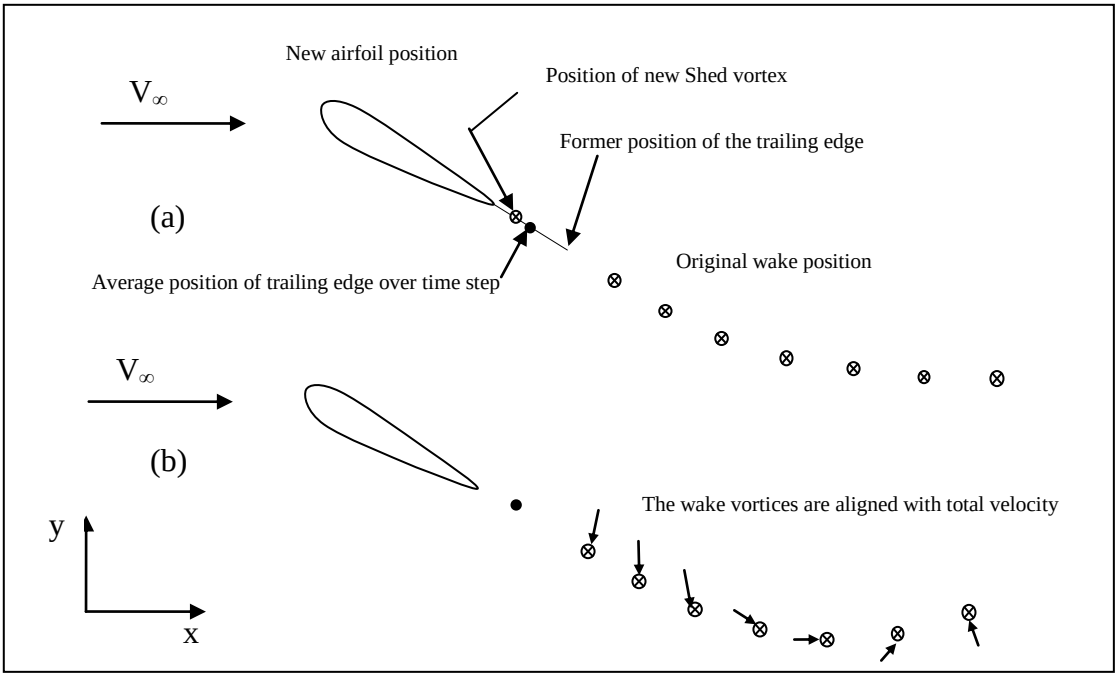

Fig (2): (a) Airfoil Moves. (b) Wake Moves **(from Hess J. L. 1975)**

The solution can be summarized at time t_k, there are N+2 unknowns $(\sigma_i)_k$ (i =1,2,3,……,N) , $(\gamma)_k$ and the Γ_W. The basic set of equations can be formulated as follows;

1- the condition of zero normal velocity (Q_n) at the external midpoint of each airfoil element **j** at time t_k such that,

$$\left(Q_{n\,j}\right)_{k=0} = 0 \qquad \textbf{(10)}$$

2- the condition of equal velocities at the midpoint of the two elements on the airfoil on either side of the trailing edge is,

$$(Q_{t1})_k = (Q_{tN})_k \qquad \textbf{(11)}$$

Where Q_{t1}, Q_{tN}: is the total tangential velocity at the midpoint of element 1 and N at time t_k.

3- the vorticity conservation low (the Kelvin's Conditions),

$$\Gamma_W = \Gamma_k - \Gamma_{k-1} \qquad \textbf{(12)}$$

Where Γ_W = is the Wake Circulation.
Γ_k = is the circulation about airfoil at time t_k.

Since the problem is concerned with incompressible flow the formula for the induced velocities by source and vorticity distributions are the same as for the steady case. Thus the experience gained with the steady **(Hess and Smith 1966)** method carries over to the unsteady problem.

4- The boundary condition of the equations represents the normal velocity component due to the motion of the airfoil which is known from kinematics equation. Since the strength of the other wake vortices is known from the previous time steps. So that, their effect on the normal velocities will be included in the boundary condition also.

5- Solving the set of equations and once the source and vorticity strengths and wake vortex have been determined the velocity distribution on the airfoil or at any point in the flow field is known. The unsteady Bernoulli's equations namely**(Basu and Hancock 1978)**.

$$C_P = 1 - \frac{Q^2}{V_\infty} - \frac{2}{V_\infty^2}\frac{\partial \phi}{\partial t} \qquad \textbf{(13)}$$

Where Q**:** is the total velocity on the outer airfoil surface and ϕ is the velocity potential.

6- The forces and moments are obtained by direct integration of the pressure distributions. In calculation of unsteady pressure coefficient, ($\frac{\partial \phi}{\partial t}$) has to be determined. In the present numerical method the value of ($\frac{\partial \phi}{\partial t}$) at the midpoint of the jth element at time t_k is approximated by;

$$\left(\frac{\partial \phi}{\partial t_j}\right)_k = \left\{(\phi_j)_k - (\phi_j)_{k-1}\right\}/(t_k - t_{k-1}) \qquad \textbf{(14)}$$

7- The velocity potential (ϕ) is obtained by integrating the velocity field along the x-axis from upstream of the airfoil and then around the airfoil surface

8- Once the solution at time t_k has been determined, the model stepped for time t_{k+1}, with the wake pattern calculated from the solution at time t_k. The distributed vorticity on the wake element at time t_k is now assumed to be concentrated into a vortex strength (Γ_W) at time t_{k+1} situated at ,

$$\begin{aligned} x_{k+1} &= (x_{TE})_k + (U_W)_k \Delta t \\ y_{k+1} &= (y_{TE})_k + (V_W)_k \Delta t \end{aligned} \qquad \textbf{(15)}$$

The resultant velocity at the center of each of the other concentrated vortices in the wake is calculated from the solution at time t_k. Then the position of that vortex at time t_{k+1} follows directly.

A computer program has been developed in **FORTRAN** power Station, and is applied to,

i. Sudden Change in Angle of Attack:

The analytic solution of impulsive incidence (for flat plate thin airfoil) was studied by Wagner in 1925 and illustrated in **(Yuong 2006),** who provided what is now referred to as the Wagner Function. The Wagner Function has else where been used as a validation of unsteady panel method (e.g. **Katz and Plotkin 1991**). The lift

coefficient ratio $\frac{c_l}{c_l(t=\infty)} = 1 + \phi(t)$ with $\phi(t)$ is an approximation to the Wagner function,

$$\phi(t) = -0.165e^{-0.091t} - 0.335e^{-0.6t} \quad (16)$$

This equation is valid for angle of attack of 5 deg.

ii. Heaving Oscillation:

The general equations of motion and parametric nomenclature for the configuration used to simulate numerical solution are illustrated in **Fig (3).** The equations of motion are shown. From the equations illustrated in the figure the airfoil will oscillate up and down the x–axis with amplitude equal to h. this oscillation create a velocity on the boundaries of the airfoil showed in terms of u/V_∞ and v/V_∞. It must be note that these velocities must be in concluded in the boundary condition of the zero normal velocity. The equations show a harmonic behavior so that, it expected the results has these effects.

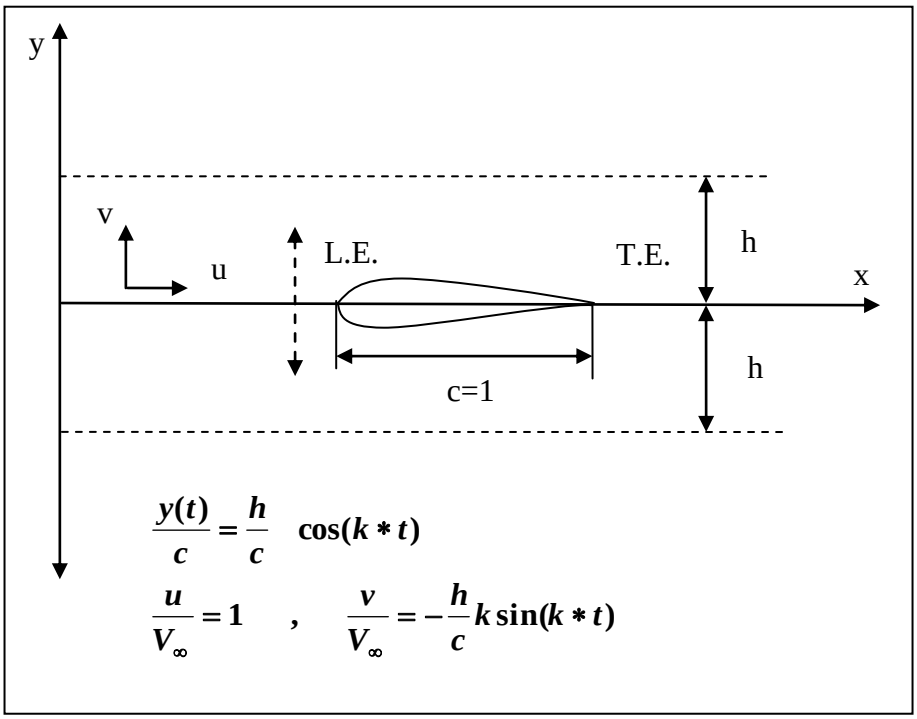

Fig (3): Equation of motion of heaving oscillation and nomenclature.

iii. Pitching Oscillation:

The pitching motion and its equations are illustrated in fig (4). The figure shows that the airfoil will translate with pitching motion about a pivot point called x_{cp}. The position of this point is changed to study its effect on the airfoil wake and forces coefficients.

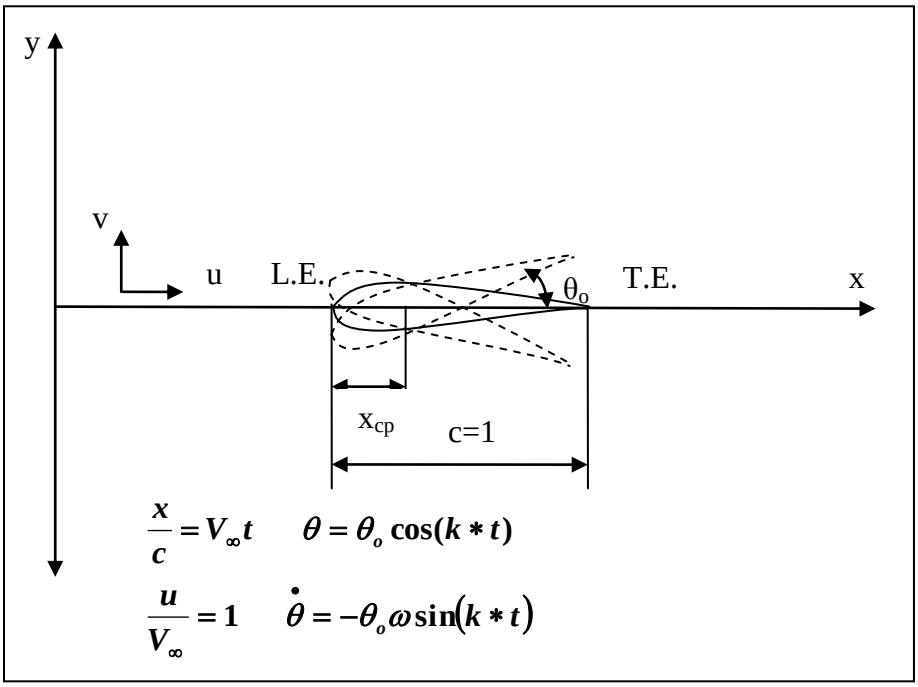

Fig (4): Equation of motion of Pitching oscillation and nomenclature**.**

NACA 0008 thick symmetrical airfoil is used in pitching oscillation for a mean incidence angle of 0 deg. At high reduced frequency k=20 with amplitude of θ_o=0.01 rad., So that, the results can be compared with those obtained from (**Basu and Hancock 1978)**.

RESULTS AND DISCUSSION:

For sudden change in angle of attack calculation presented in **Fig (5)** is at angle of attack equal to 5° and $\frac{\Delta t V_\infty}{c} = 0.25$. The results for computation of lumped vortex method (**LVM**) which is used to find the unsteady flow over thin airfoils is also shown in the figure for comparison. The **LVM** depends on using lumped vortex on the quarter chord and Kutta condition was valid at third quarter chord of the airfoil. The wake rollup calculation and forces such that at each time interval (dt) a vortex shed from the Trailing edge where the strength of each vortex is equal in magnitude and opposite in sign to the change in circulation of the airfoil bound circulation. This procedure is continued for the next time steps. The results obtained is in good accuracy as compared with the other approaches, and it could be conclude that at time t=0 there are an impulse lift which arises from instantaneous change in ϕ with time as shown in pressure coefficient **Eq (5).** This change in ϕ with time due to acceleration of the flow becomes smaller with reduced influence of the starting vortex.

Fig (6) show that there is a drag force, this force could be divided into two components, first is the wake induced downwash and the second is due to fluid acceleration these two components calculated and presented in figure.

While examining the wake vorticity as presented in **Fig (7),** it can be observed that the first vortices are the strongest and that all vortices have a counterclockwise

values. Also if the wake is allowed to rollup, due to the velocity field induced by the wake and the airfoil, the shape is as shown in **Fig (8).** It could be concluding that the present method gives at least good behavior and trends for sudden change in angle of attack motion of the airfoil.

For heaving oscillation **(Katz and Plotkine 1991)**, presented a wake shape visualizations for a flat plate under going heaving oscillation (Plunging motion), corresponding solution were performed with the present Method for comparison. Assume that thickness of the airfoil is NACA 0001 (i.e. 1% thickness) instead of flat plate.

Three results were performed with k = 8.5, k = 2.1 and k =0.6 with amplitude h = 0.019. Fig (10,11 and 12), show a very close agreement with **(Kats and Plotkine 1991)** results in terms of the shape of the wake and the degree of self induced roll-up.

Overall the present method demonstrated excellent qualitative and quantitative agreement with published Panel Method data.

Other comparisons are performed between experimental wake visualization of airfoil NACA 0012 oscillating in different reduced frequencies and amplitudes with computational procedure discussed in the previous section and illustrated in **Fig (13).**

Also figures shows wake behavior of the airfoil with lines represents positive vortices(clock wise) and lines which represents negative vortices (counter clock wise). So that, with simple procedure solution depending on linear equations the non-linear behavior of the problem was solved with good accuracy.

For the airfoil thickness NACA 0008 the calculation of heaving oscillation for the mean angle of incidence 0 deg with an amplitude h=0.018 c and reduced frequency k = 8.5.

The lift and drag coefficients for the upper conditions are presented in **Fig (14).** Due to the strong non-linear effects of the discrete vortices in the wake, the variations of lift and drag distribution are not simply harmonic.

The comparison shows good trends between experimental and computations. So that, it could be find complex and nonlinear problems by a linear solution with good accuracy.

For pitching oscillation, generally speaking, the non-linearity in the problem arises from the wake, it is non-linear process to find the position and the shape of the wake, the wake pattern in the **Fig (15),** shows the rollup of the wake vorticity into discrete vortices of opposite sign.

Fig (16) show the wake rollup for NACA 0008 thick symmetrical airfoil in pitching oscillating with various oscillatory amplitudes θ_o and various oscillatory positions x_{cp} on mean chamber line at reduced frequency 20 respectively. It could be shown that the effect of oscillatory amplitude $\theta_o$on the wake rollup is significant if the airfoil is oscillating about the position between the leading edge x_{cp} =0 and the mid-point on the mean camber line x_{cp} =c/2.

The lift and drag forces coefficients are predicted and simulated in **Fig (17).** The variation in lift and drag are not simply harmonic behavior due to the skew ness and the phase shift in the neighborhood of the peak values.

The vorticity distributions will influence the vortex shedding from the trailing edge and overall lift and drag distributions on the airfoil surface.

CONCLUSIONS:

The numerical method out lined in this paper leads to the calculation of the inviscid flow field about an airfoil undergoing an arbitrary time-dependent motion. If it is assumed that the flow remains attached and that it separates at the trailing edge of the airfoil. Although results have been presented for a sudden change in incidence and a high frequency oscillation the method is completely general.

The wake rollup calculations show good agreement with the available flow visualization data. The effects of the wake rollup on the calculation of unsteady lift and drag coefficients are significant.

REFERENCES:

***Basu B. C., Hancock G. J. (1978)**, "The Unsteady Motion of A Two-Dimensional Aerofoil in Incompressible Inviscid Flow", J. Fluid Mech. 87(I), 159-178.

***Chen D. R., Sheu M. J. (1980)**, "Numerical Solutions for Oscillatory Aerofoil", Comput. Methods in Appl. Mech. Vol(1), 1024-1028

***Gesing J. P. (1968)**, "Nonlinear Two-Dimensional Unsteady Potential Flow with Lift", J. Aircraft 5, 135-143.

***Hess J. L. (1975),** "Review of Integral-Equation Techniques for Solving Potential-Flow Problems with Emphasis on Surface-Source Method", Comput. Methods in Appl. Mechanics and Eng., 5, 145-196.

*** Hess J. L., Smith A. M. O. (1966)**, "Calculation of Potential Flow about Arbitrary Bodies", Progress in Aeronautical Science, Vol. 8, Pp. 1-138, Pergamon Press Oxford.

***Katz J., Plotkin A. (1991),** "Low-Speed Aerodynamics from Wing Theory to Panel Methods", International Edition, McGraw-Hill.

***Katz J., Weihs D. (1981)**, "Wake Rollup and the Kutta Condition for Airfoils Oscillating at High Frequency", AIAA J. 19(12), 1604-1606.

***Poling D. R., Telionis S. P. (1986)**, "The Response of Airfoils to Periodic Disturbance-the Unsteady Kutta Condition", AIAA J. 24(2), 193-199.

***Young J. (2006),** "Numerical Simulation of The Unsteady Aerodynamics of Flapping Airfoils", Ph.D. Thesis, School of Aerospace, Civil and Mechanical Eng., University of New South Wells.

Nomenclature:

c	Chord length (m)
C_d	Drag coefficient per unit span $D/(q_\infty c)$
C_l	Lift coefficient per unit span $L/(q_\infty c)$
C_p	Pressure coefficient
h	Amplitude level in heaving oscillation (m)
k	Reduced frequency, $\omega c/ 2V_\infty$
Q	Total velocity on the airfoil surface (m/s)
Q_n	Total normal velocity on the airfoil surface (m/s)
Q_t	Tangential velocity on the airfoil surface (m/s)
t	Time (s)
u	horizontal kinematic velocity (m)
U_w	Wake influence velocity in x-direction (m/s)
v	Vertical kinematic velocity (m/s)
V_∞	Free stream velocity (m/s)
V_w	Wake influence velocity in y-direction (m/s)
x	Horizontal displacement of airfoil in terms of c
x_{cp}	Pivot point at which the airfoil pitching in terms of c
x_{TE}	Airfoil trailing edge displacement in horizontal displacement
y	Vertical displacement of airfoil in terms of c
y_{TE}	Airfoil tailing edge displacement in vertical oscillation
Γ_w	Wake vorticity
Γ_k	Vorticity due to airfoil motion at k^{th} step
ϕ_∞	Uniform flow velocity potential
γ	Vorticity strength distribution
α	Angle of attack
ω	Circular frequency
θ_o	Amplitude angle in pitching oscillation
θ	Pitching angle of oscillating airfoil
$\dot{\theta}$	Angular velocity of pitching oscillation airfoil
ϕ	Velocity potential and Wagner function

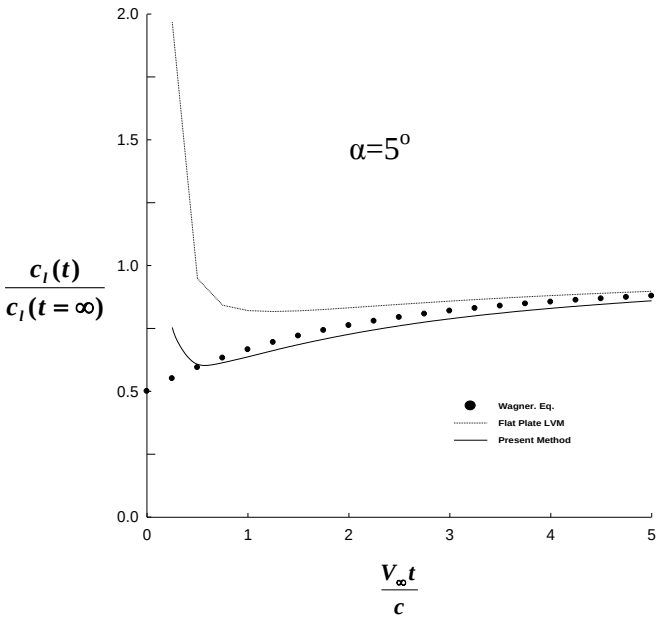

Fig (5): Variation of lift after initiation of sudden forward motion of two-dimensional airfoil.

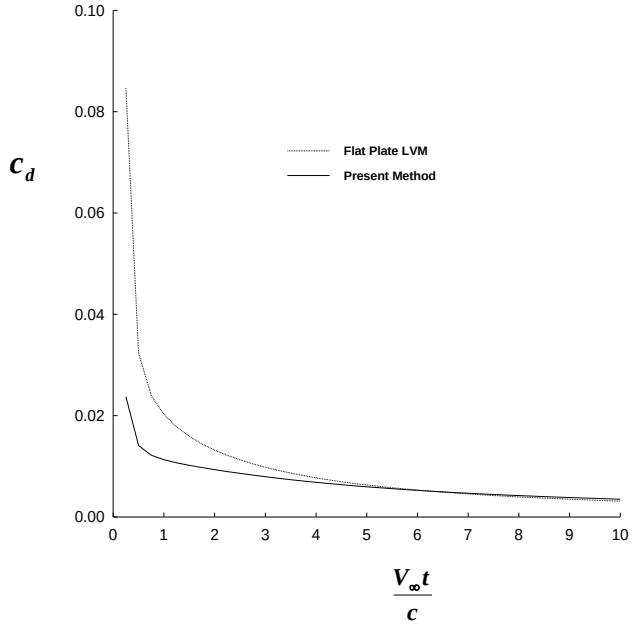

Fig (6): Variation of drag after initiation of sudden forward motion of two-dimensional airfoil.

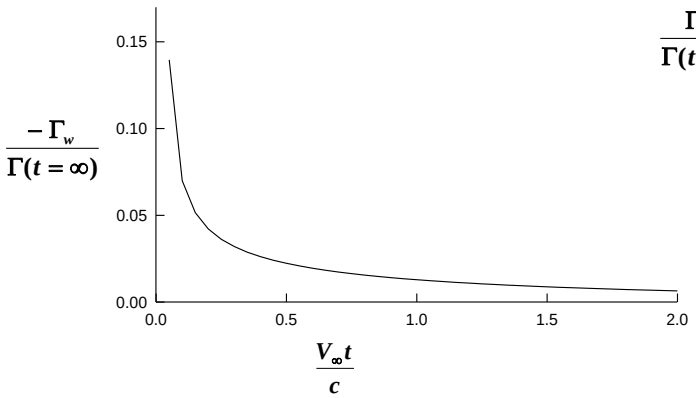

Fig (7): Wake circulation behined the airfoil which was suddenly set into motion.

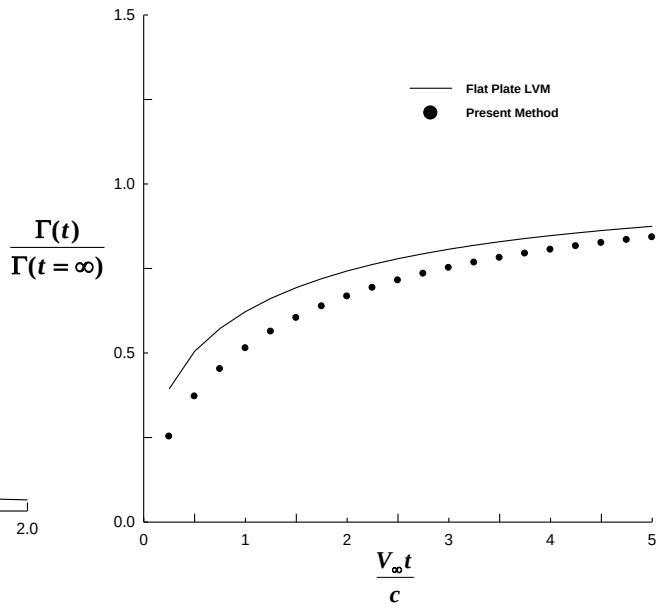

Fig (8): Variation of airfoil circulation after initiation of sudden forward motion of two-dimensional airfoil.

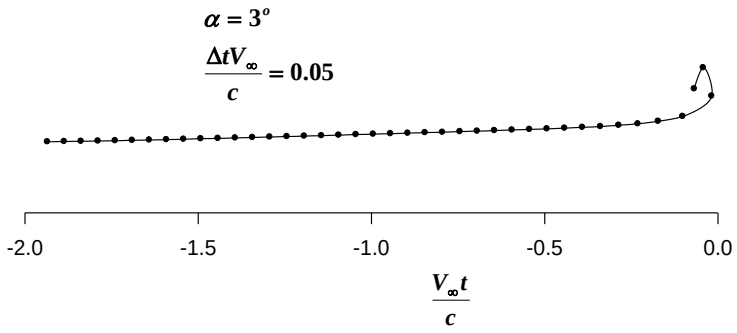

Fig (9): Wake rollup behind a two-dimensional airfoil which was suddenly set into motion.

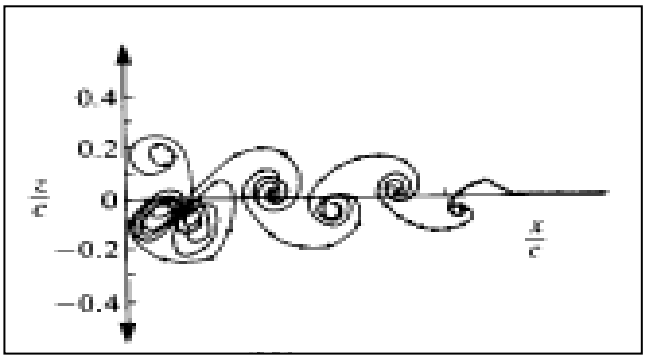

(a) Katz and Plotkin (1991)

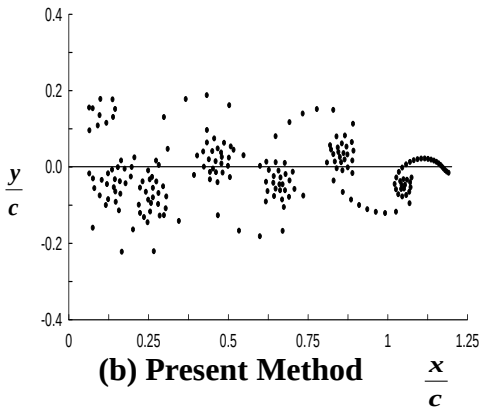

(b) Present Method

Fig (10): Wake pattern calculated from **Katz and Plotkin (1991)** and corresponding present calculations for heaving oscillation of $k = \frac{\omega c}{2V_\infty}$ =8.5 and h=0.019.

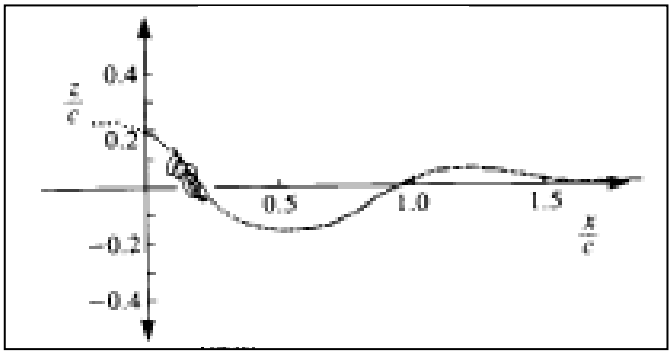

(a) Katz and Plotkin (1991)

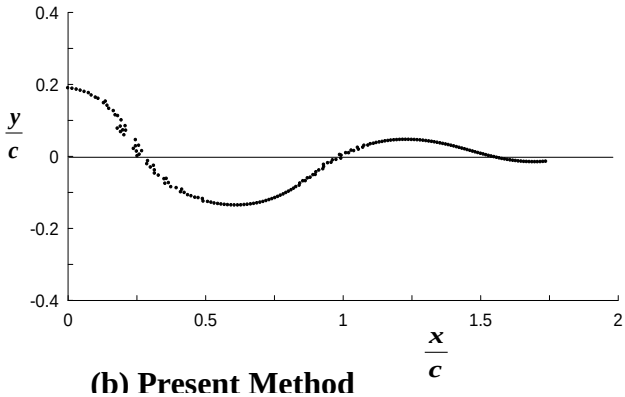

(b) Present Method

Fig (11): Wake pattern calculated for heaving oscillation of $k = \frac{\omega c}{2V_\infty}$ =2.1 and h=0.019.

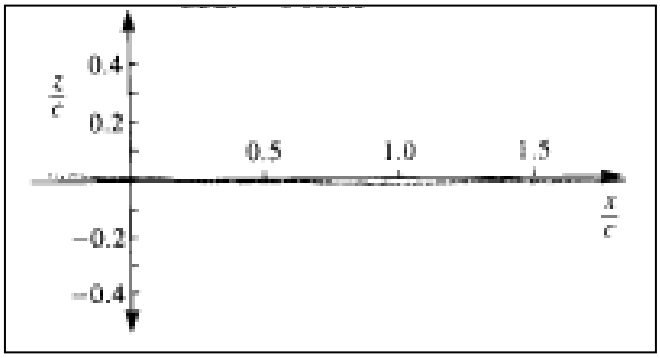

(a) Katz and Plotkin (1991)

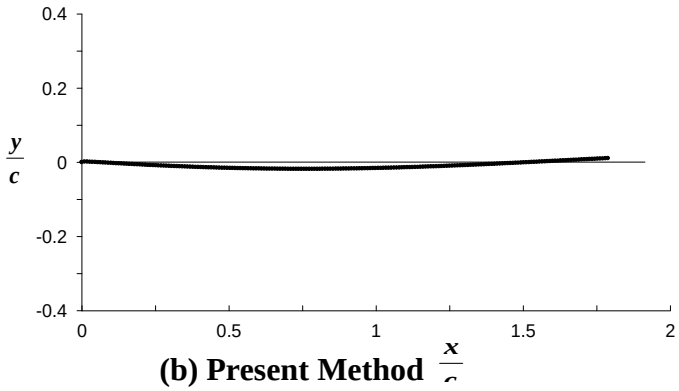

(b) Present Method

Fig (12): Wake pattern calculated for heaving oscillation of $k = \frac{\omega c}{2V_\infty}$ =0.6 and h=0.019.

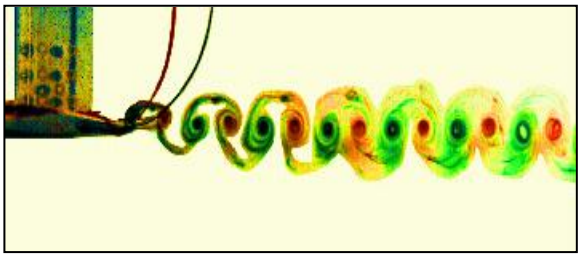

k=7.85
h=0.0125

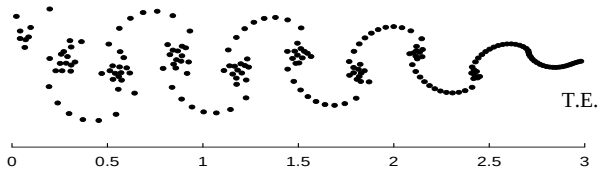

k=7.85
h=0.025

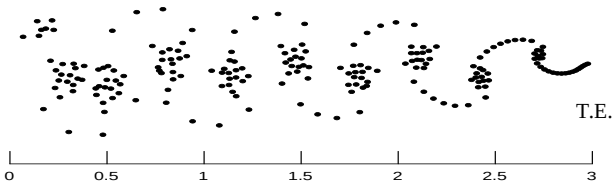

k=7.85
h=0.05

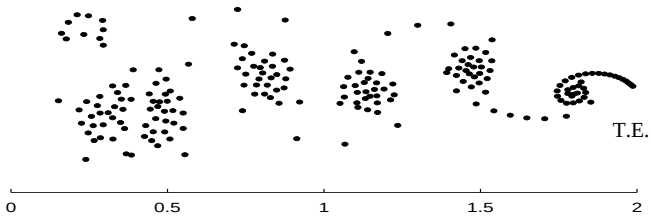

(a) Young J. (2006) **(b) Present Method**

Fig (13): NACA 0012 Wake pattern visualization from **Young J. (2006)** as compared with computed wake for heaving oscillations at various amplitudes .

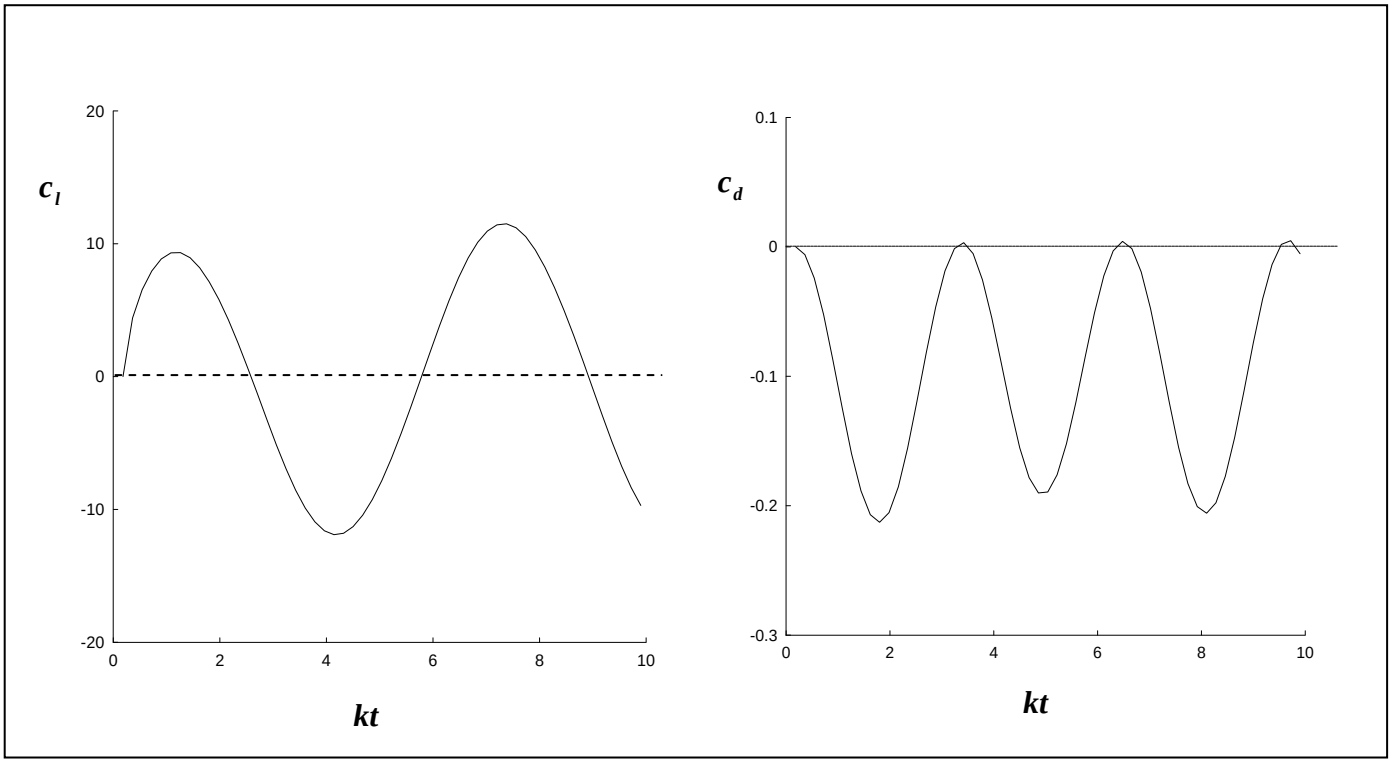

Fig (14): Lift and Drag coefficients of NACA 0008 airfoil oscillating with Heaving motion k=8.5, h=0.018.

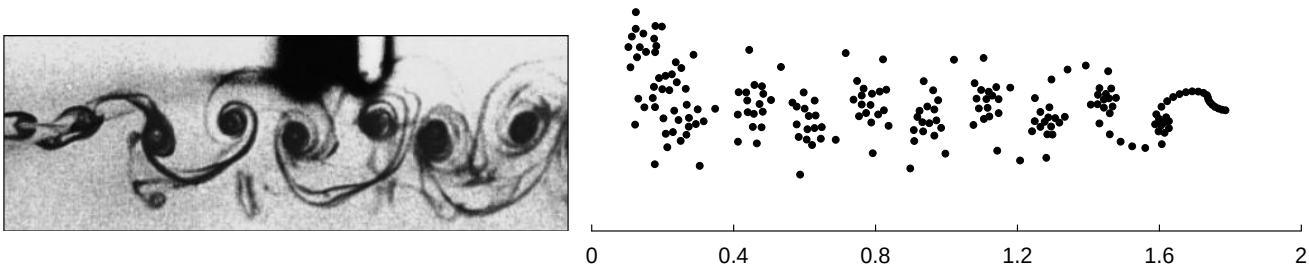

(a) Basu and Hancock (1978) **(b) Present method**

Fig (15): Wake Pattern for pitching oscillation as compared with **Basu and Hancock (1978)**, airfoil with k=20, θ_o=0.01 rad.

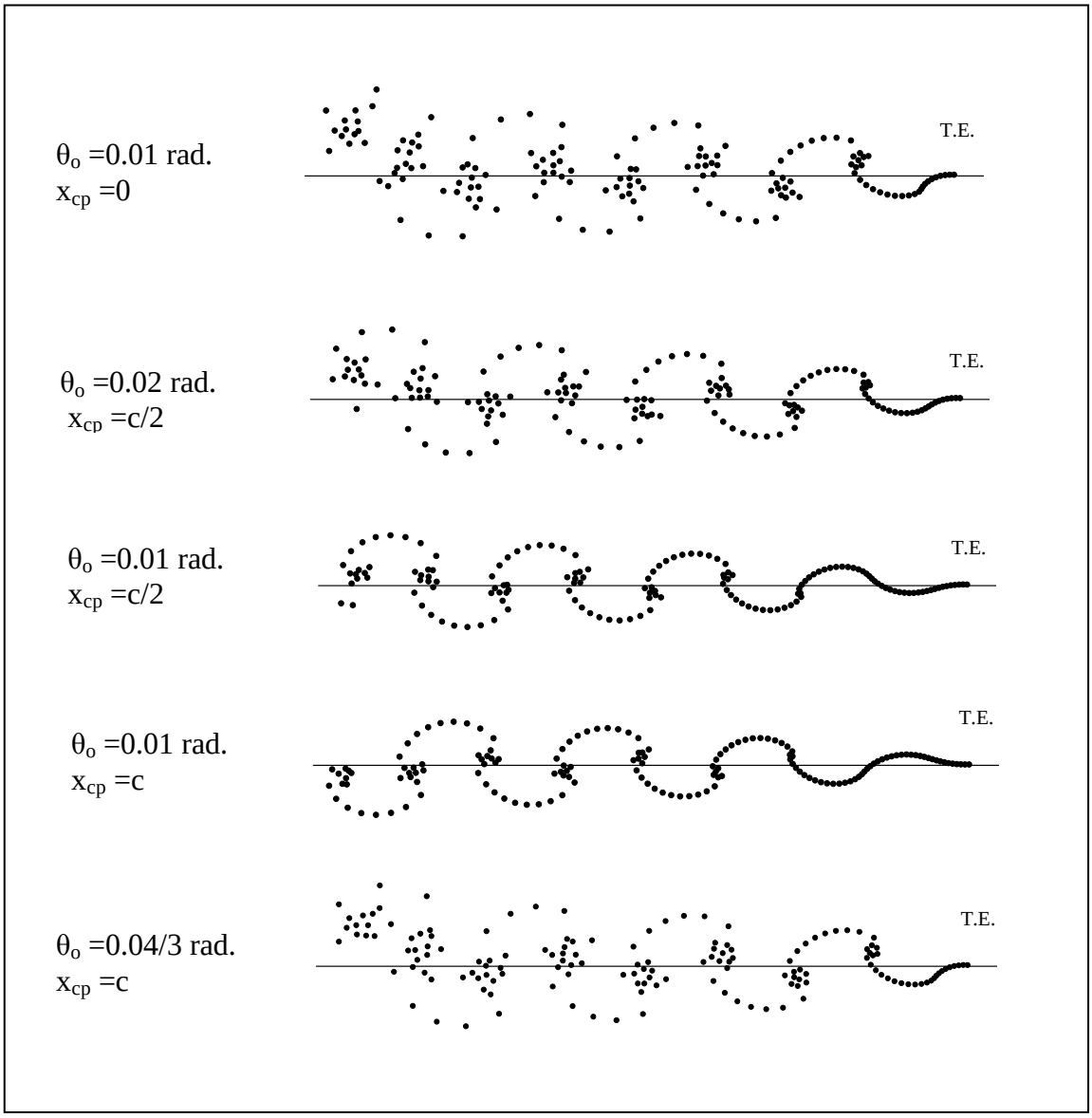

Fig (16): Wake patterns for NACA 0008 thick symmetrical aerofoil in pitching oscillation at reduced frequency k=20.

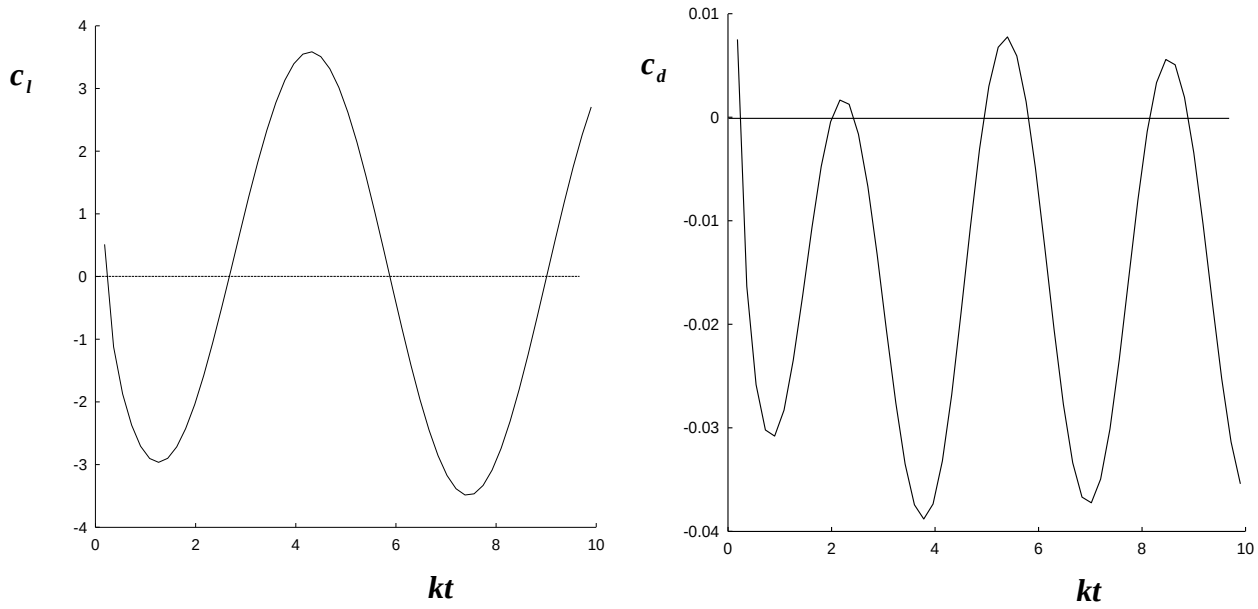

Fig (17): Lift and Drag coefficients of NACA 0008 airfoil oscillating with pitching motion k=20, θ_o =0.01 rad.

INFLUENCE OF RUBBER CONSTITUENTS ON PERFORMANCE OF ASPHALT PAVING MIXTURES

Dr. Ayad A. F. Al-Dulaimi
College of Engineering
University of Baghdad

ABSTRACT

Environmental problems created by discarded waste rubbers, such as potential fire and disease hazards, have become significant in recent years. In connection with rubber recycling, a comparative study of laboratory performance of application of two polymer types: styrene butadiene rubber (SBR) and polyethylene–vinyl acetate (PVA) in asphalt paving mixtures is presented. These mixtures are usually employed in construction the surface courses in Iraq. These modified asphalt mixtures were prepared with asphalt cement previously modified by using three percents of polymer (1, 3 and 5) percent by weight of modified asphalt. Two control mixes are adopted for comparison purpose. The first control mix was produced with 40/50 penetration asphalt cement while the second was produced with 60/70 penetration asphalt cement.

To evaluate the mixture characteristics of the modified and conventional mixes: laboratory tests of Marshall, indirect tensile strength, indirect tensile resilient modulus, indirect tensile fatigue and incremental indirect tensile creep were conducted on a compacted Marshall specimens. The VESYS 5W software program was used to investigate the effect of polymer type on rut depth occurring in whole selected pavement structure.

The results of the present study indicated that the modified mixtures exhibited higher tensile strength characteristics than the control mixtures. The modified asphalt mixtures showed overall better performance indices (rut depth and fatigue cracks) than the corresponding control mixtures. Also, the addition of (SBR) polymer type to the mixture improves asphalt mixture performance, especially, when it is added by 1 % by weight of asphalt.

KEYWORDS

Rubber recycling, styrene butadiene rubber (SBR), polyethylene–vinyl acetate (PVA), indirect tensile strength, indirect tensile resilient modulus, indirect tensile fatigue and rut depth.

الخـلاصـــة:-

أن المشاكل البيئية المتولدة عن طرح مخلفات المطاط والمتمثلة بالحرائق والأمراض تعد من القضايا التي اكتسبت اهتمام كبير في السنوات الأخيرة. ولأجل تدوير مخلفات المطاط، تم تقديم دراسة مختبريه للمقارنة بين أداء تطبيق نوعين من البوليمرات هما styrene butadiene rubber (SBR) و polyethylene-vinyl acetate (PVA) في خلطات التبليط الإسفلتي. أن هذه الخلطات تستخدم عادة في إنشاء الطبقة السطحية في العراق والتي يتم تحضيرها باستخدام الإسفلت الأسمنتي والذي يعدل باستعمال ثلاث نسب من البوليمر (١,٣,٥) بالمائة من الإسفلت المعدل. تم اختبار خلطتين سيطرة لغرض المقارنة حيث أن خليط السيطرة الأول أنتج باستخدام أسفلت أسمنتي ذو اختراق 40/50 بينما الثاني أُنتج باستخدام أسفلت أسمنتي ذو اختراق 60/70.

لتقييم خصائص الخلطات المُعَدَّلة والسيطرة أجريت الاختبارات التالية على نماذج مارشال المحدولة وهي مارشال، مقاومة الشد غير مباشر، معامل الرجوع الشدّ غير المباشر، الكلل شدّ غير مباشر والزحف التراكمي شدّ غير مباشر. تم استخدام برنامج VESYS 5W لبحث تأثير نوع البوليمر على عمق التخدد الحاصل في منشأ التبليط الكلي المختار.

تشير نتائج هذه الدراسة إلى أن الخلطات المُعَدَّلة أظهرت خصائص مقاومة الشدّ أعلى من خلطات السيطرة. كذلك أظهرت الخلطات الإسفلتية المعدلة عموماً مؤشرات أداء (عمق تخدد وشقوق كلل) أفضل من خلطات السيطرة. كذلك أظهرت الخلطات الإسفلتية المعدلة عموماً مؤشرات أداء (عمق تخدد وشقوق كلل) أفضل من خلطات السيطرة المقابلة. أخيراً فيما يتعلق بنتائج البحث فان إضافة نوع بوليمر (SBR) إلى الخليط يحسن أداء الخليط الإسفلتي، خصوصاً عندما يضاف بمقدار ١% من وزن الإسفلت.

INTRODUCTION AND BACKGROUND

Presently and into the future, waste rubber (for example tires, tubes…….etc) could potentially become a serious environmental problem. Many methods have been used to dispose waste rubber. One method is to recycle waste by cutting and scraping them into small sizes down to powder particles and reuse as reclaimed rubber material. The use of reclaimed rubber as an additive in various types of bituminous construction not only solves a waste disposal problem and offers the benefit of resource recovery; it is also of interest to the paving industry because of the additional elasticity imparted to the binder and pavement system (Nukulchai et al., 2007).

Many asphalt additives are polymers and the interaction with asphalt may result in a complex blends. The polymer may have no interaction with the asphalt (phase separate), partial interaction (swollen polymer domains), or strong interaction (thermodynamic dissolution of polymer). Polymer additives differ in molecular weight, shape (linear, branched, star, etc…), repeat unit …etc. Polymer amount, strain and thermal history may alter the morphological and physical properties of the modified asphalt (Wegan and Brule, 1999). In particular, the relationship of fatigue properties to asphalt chemistry is not well understood and the incorporation of additives only complicates an analysis (Little et al., 1999).

The ability of polymer-modified asphalts to improve asphalt pavement resistance to permanent deformation is well documented (Institute for Transportation Studies, 1994 and Bahia et al., 2001). In cases where high-quality aggregates are used, polymer modification for the purpose of permanent deformation resistance may not be necessary, at least for some airfield asphalt mixtures. However, modified asphalt mixtures may either degrade or enhance asphalt mixture fatigue life as measured by flexural beam tests (Institute for Transportation Studies, 1994 and Newman, 2000).

Studies by Harvey and Monismith have shown that the addition of a modifier to certain asphalts may reduce the number of strain cycles to failure or increase the rutting. The same modifier mixed with other asphalt produced opposite results in that the fatigue life increased and rutting decreased (Harvey et al., 1994, Harvey et al., 1995, Harvey et al., 1997). These studies indicated that the modifiers had different effects on mix stiffness, fatigue life and the cumulative dissipated energy. Stiffness of unmodified asphalt mixtures and cycles to failure in flexural beam tests has been shown to correlate well with fatigue life. Fatigue life estimates using ‘surrogate’ stiffness of asphalt mixtures were developed for cases in which beam testing was not available. However, with polymer-modified asphalt mixtures, fatigue life models were unreliable. Khattak and Baladi have shown

significant effects of modifier type, concentration on fatigue and indirect tensile properties (Khattak and Baladi, 2001).

Many factors contribute to the degradation of asphalt pavements. When high quality materials are used, distresses are typically due to traffic loading, resulting in rutting or fatigue cracking. Environmental conditions such as temperature and water can have a significant effect on the performance of asphalt concrete pavements as well. The presence of water (or moisture) often results in premature failure of asphalt pavements in the form of isolated distress caused by debonding of the asphalt film from the aggregate surface or early rutting/fatigue cracking due to reduced mix strength. Moisture sensitivity has long been recognized as an important mix design consideration. The moisture affects asphalt mixes in three ways: loss of cohesion, loss of adhesion and aggregate degradation. The loss of cohesion and adhesion are important to the process of stripping. A reduction in cohesion results in a reduction in strength and stiffness. The loss of adhesion is the physical separation of the asphalt cement and aggregate, primarily caused by the action of moisture. The air void system in the asphalt concrete provides the means by which moisture can enter the mix. Once moisture is present through voids or from incomplete drying during the mixing process, it interacts with the asphalt-aggregate interface. Numerous test methods have been developed and used to evaluate the moisture susceptibility of HMA mixes (Taylor and Khosla, 1983 and Khosla, 2000).

* EXPERIMENTAL WORK

Material

Asphalt cement 40/50 and 60/70 brought from Daurah refinery with the physical properties given in Table (1), were used in the present study. Coarse and fine aggregate, Bulk specific gravity of 2.77 and 2.68 respectively, were used in the preparation of the asphalt concrete mixtures. Limestone was used as mineral filler which was obtained from Karbala'a factory with specific gravity of 2.773. Table (2) presents the selected mix gradation for surface course.

Table 1: Properties of used asphalt cement.

Property	Test Results		Requirements Penetration –Graded Asphalt Cement	
			(40/50)	(60/70)
1.Penetration at 25 ^{o}C , (0.10mm)	48	66	40-50	60-70
2. Ductility at 25 ^{o}C , (cm)	110	120	>100	>100
3.Specific gravity at 25 ^{o}C	1.03	1.01	------	-----
4.Flash point ,(^{o}C)	275	249	>232	>232
5.Solubility in trichloroethylene	99.37	99.26	>99	>99
6.Residue from thin –film oven test - Retained penetration , % of original -Ductility at 25 ^{o}C, (cm)	 68 57	 61 73	 >55 >25	 >52 >50

Table 2: Selected mix gradation for surface course.

Sieve	19 mm	12.5 mm	9.5 mm	No.4	No.8	No.50	No.200
% Passing	100	95	83	59	43	13	7

In general, polymer types are classified into four main types: polymer latex (or polymer dispersion), redispersible polymer powder, water-soluble polymer and liquid polymer. In particular, the commercial polymer latexes widely used in the world are styrene-butadiene rubber (SBR) and

polyethylene–vinyl acetate (PVA). The chemical structures of the (SBR) and (PVA) are $(-CH-CH=CH-CH_2-CH_2-CH-C_6H_5)_n$ and $(-CH_2-CH_2-CH_2-CH-OCOCH_3)_n$ respectively.

Asphalt mixtures code

The fourteen asphalt mixture types adopted in the present study are listed in Table (3).

Table 3: The code for the six asphalt mixture types.

Asphalt mixture code	Description
Mix 1	Control mix 48 penetration grade asphalt
Mix2	Control mix 66 penetration grade asphalt
Mix3	Modified mix 48 penetration grade asphalt and 1 % SBR polymer
Mix 4	Modified mix 48 penetration grade asphalt and 3 % SBR polymer
Mix 5	Modified mix 48 penetration grade asphalt and 5 % SBR polymer
Mix 6	Modified mix 48 penetration grade asphalt and 1 % PVA polymer
Mix 7	Modified mix 48 penetration grade asphalt and 3 % PVA polymer
Mix 8	Modified mix 48 penetration grade asphalt and 5 % PVA polymer
Mix 9	Modified mix 66 penetration grade asphalt and 1 % SBR polymer
Mix 10	Modified mix 66 penetration grade asphalt and 3 % SBR polymer
Mix 11	Modified mix 66penetration grade asphalt and 5 % SBR polymer
Mix12	Modified mix 48 penetration grade asphalt and 1 % PVA polymer
Mix 13	Modified mix 48 penetration grade asphalt and 3 % PVA polymer
Mix 14	Modified mix 48 penetration grade asphalt and 5 % PVA polymer

Sample prepartions

Asphalt cement content of 5% by weight of total mixture was used based on Marshall Stability mix design method. Polymer of (1, 3 and 5) % by weight of asphalt was used for the tested specimens. The used polymer was blended with the asphalt binder at a temperature of 160°C using conventional mixer. All examined asphalt concrete mixtures were prepared in accordance to (ASTM Designation: D1559-89) (ASTM, 2003) with the standard 75-blow Marshall design method for designing hot asphalt concrete mixtures, designated as using automatic compaction.

Asphalt mixture properties

The Marshall test was performed during the mix design according to the (ASTM Designation: D 1559-89) (ASTM, 2003). This test is performed at a deformation rate of 51 mm/min (2 inch/min) and a temperature of 60ºC. The properties obtained from this test are the Marshall stability and flow. The Marshall stability of an asphalt mixture is the maximum load that the material can be carried when tested in the Marshall apparatus. The Marshall flow is the deformation of the specimen when the load starts to decrease. Stability is reported in (KN) and flow is reported in (mm) of deformation. Three specimens were tested and an average is reported and used in the analysis. Marshall properties at 5% asphalt content by weight of total mix and SCRB (SCRB, 2003) specifications for asphalt mixes used as a surface course are presented in Table(4).

Table 4: Marshall properties of different asphalt mixture types.

Mix type	Asphalt paving properties				
	Marshall stability (KN)	Marshall flow(mm)	Voids in total mix (%)	Voids in mineral aggregate (%)	Voids filled with asphalt (%)
Mix 1	13.6	2.9	4.2	16.2	70.1
Mix2	10.3	3.1	4	15.9	74.8
Mix3	12.7	3.0	4.1	16.0	74.4
Mix 4	12.0	3.1	3.9	14.9	73.8
Mix 5	12.4	3.1	3.9	14.9	73.8
Mix 6	10.7	3.2	3.8	14.9	74.5
Mix 7	10.4	3.2	4.1	16.3	74.8
Mix 8	10.0	3.3	4.2	16.0	73.8
Mix 9	9.5	3.1	4	15.9	74.8
Mix 10	9.0	3.3	3.9	15.8	75.3
Mix 11	8.6	3.3	4.2	16.0	73.8
Mix12	8.5	3.4	4.3	16.3	73.6
Mix 13	7.5	3.3	4.3	16.2	73.5
Mix 14	7.2	3.3	4.4	16.5	73.3
SCRB specification	Min. 8 KN	2-4 mm	3-5 %	Min.14	65-85%

* MECHANICAL BEHAVIOR TESTS

The mechanical behavior of the polymer-modified and unmodified mixtures was evaluated based on the indirect tensile strength**,** indirect tensile resilient modulus, indirect tensile fatigue and the unconfined compressive strength.

Indirect tensile strength test

The indirect tensile strength tests were conducted using the standard method ASTM D4123 (ASTM, 2003). The experimental procedure used to determine the tensile, or splitting, strength of a cylindrical specimen is based on loading it diametrically in compression to create a tension zone along the specimen's loaded diameter. The expression for the maximum tensile strength generated can be stated as:

$$s_t = \frac{2P_{max}}{p\,HD} \tag{1}$$

Where σ_t is the indirect tensile strength, Pa, P_{max} is the maximum applied load, N, and H&D is the height and the diameter of the specimen in m, respectively.

Indirect tensile resilient modulus test

The indirect tensile resilient modulus test is conducted at temperatures of 5, 25 and 40ºC according to the modified ASTM D4123 (Mohammad and Paul, 1993). It is a repeated load indirect tension test for determining the resilient modulus of the asphalt mixtures. The recoverable horizontal deformation, δH, was used to calculate the indirect tensile resilient modulus, M_R in eq.2.

$$M_R = \frac{P(0.27 + m)}{t.dH} \tag{2}$$

Where M_R Resilient Modulus, Pa, P Applied vertical load, N, t Sample thickness, m, μ Poisson's ratio (assumed equal to 0.35 for asphalt concrete mixtures) and δH Horizontal deformation, m.

Indirect tensile fatigue test

To determine the fatigue resistance of the asphalt concrete samples, this test was conducted at 25°C temperature and applied on the Marshall specimen (101.6mm diameter X 63.5 mm height). The (10%) of the test failure load obtained from indirect tensile test was used as the peak value of the cyclic load with loading duration of 0.10 second followed by a rest period of 0.90 second was applied to the test specimen (Loulizi et al., 2002).The number of cycles were monitored through the duration of test and the test was terminated when the specimen reached to failure. The fatigue testing procedure is described in NLT-350 standard (Spanish Ministry of Public Works, 1990). The failure criteria are related to a decrease in the needed load below 50% of the initial value for each imposed strain. A total of three Marshall Specimens are tested to measure average fatigue life for each mix being studied.

3-4) Incremental indirect tensile creep test

At testing temperature of 40°C, a compressive stress of 0.138 MPa (20 psi) was applied on the Marshall specimen. The loading times include (3, 5, 10, 100 and 1000 seconds) and rest periods are (2, 2, 2, 4 and 8 minutes). The total permanent strains, ε_P (in/in), at the end of each rest period were measured. In last loading time (1000 seconds), the creep deformations were measured after (3, 6, 10, 30, 60,100, 300, 600, and 1000 seconds) durations. The creep compliance, C (t), at each of these loading durations is calculated as follows:-

$$C(t) = \epsilon(t) / \sigma_o \qquad (3)$$

Where C(t) creep compliance at (1/MPa), Є(t) vertical strain at loading duration t (mm/mm) and σ_o applied stress (MPa).

*** RESULTS AND DISCUSSION**

Laboratory characteristics of mixtures

Only the surface course mixtures were evaluated in the paper. An average of three specimen results was reported. The air voids for the laboratory test specimens were 4±1%. Fig.1 presents the results of Marshall Tests. It shows that the conventional mixtures had higher or equal values of Marshall Stability than the polymer modified asphalt mixtures.

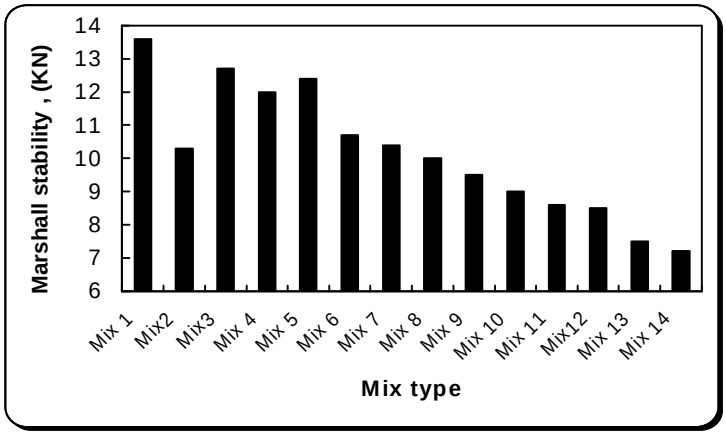

Fig.1: Effect of mix type on Marshall Stability values.

Fig.2 presents the average results of the indirect tensile strength (ITS) test for the surface course mixtures. The present modified mixtures exhibited higher indirect tensile strength values than the two control surface course mixes. Especially, the 1% SBR or PVA polymer modified asphalt mixtures have higher strengths than the other mixture types wearing course mixes. Higher strength indicates the mixes to be more resistance under tension. This characteristic is desired for mixtures to resist fatigue cracks.

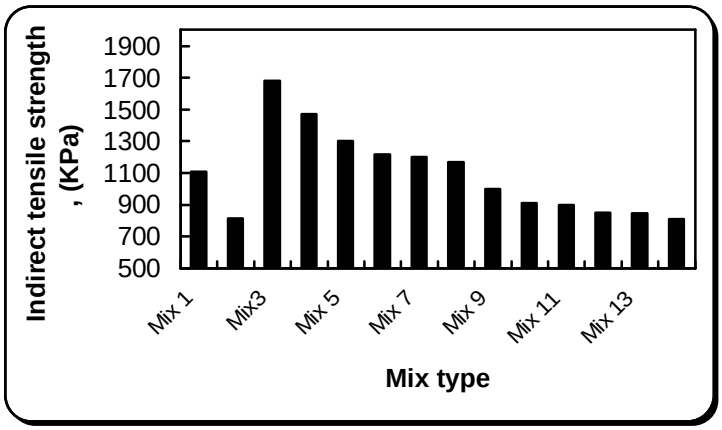

Fig.2: Effect of mix type on indirect tensile strength values.

Fig.3 presents the results of the indirect tensile resilient modulus (MR) of the surface course mixtures at 40°C test temperature. The test results indicated that the modified mixtures exhibited higher values of M_R than the control asphalt mixtures.

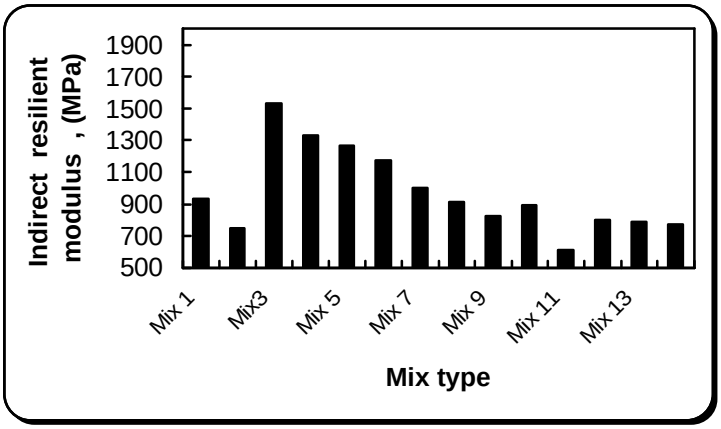

Fig.3: Effect of mix type on indirect resilient modulus values.

The results of the indirect tensile fatigue test for various mix types are presented in Fig.4. While evaluating the fatigue resistance of asphalt concrete mixes, the number of cycles to failure is used as performance indicators. A high number of cycles to failure are the desired properties to resist fatigue cracking.

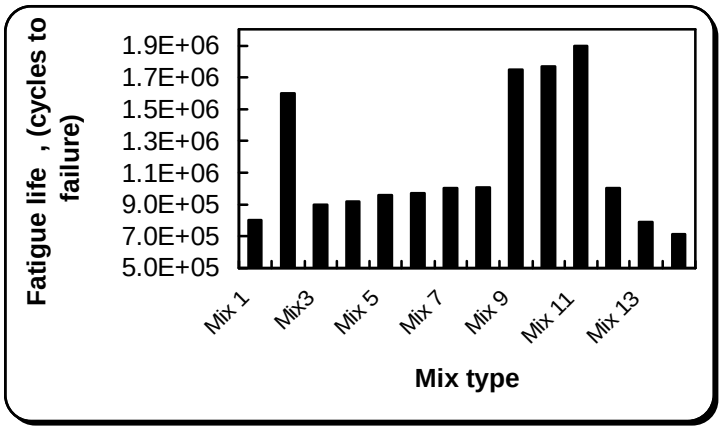

Fig.4: Effect of mix type on indirect fatigue life values.

Fig.4 indicates the modified asphalt mixtures with two selected polymer types (SBR or PVE) exhibited higher resistance to fatigue than the control mixes and the asphalt grade has effect on fatigue life values of modified asphalt mixtures.

Rut depth calculations

VESYS 5W software program is short from Visco-Elastic Pavement System Analysis Program Prediction (FHWA, 2003). The rut depth computed by the VESYS 5W software program is the summation of the permanent deformation of all layers. Therefore, the input data required to the

VESYS 5W software program are material properties of the layers, the thicknesses of each layer, traffic data and environmental conditions. These input data will be described in as follows:

To obtain input parameters required for the VESYS 5W software, an average curve of creep compliance C(t) versus time is constructed on a log-log graph and extrapolated backward to obtain values of C(t) at 0.1 and 0.30 seconds. The total permanent strain versus incremental time of loading is, also, plotted on a log-log graph and the best-fit line is obtained. The intersection of the line with the vertical axis is denoted by (i) and the slope by (s). The permanent deformation properties μ and α are determined as follows: $\mu = (i \times s)/\varepsilon$ and $\alpha = 1-s$ where ε is the recovered strain which was obtained from resilient modulus test. Creep properties of various asphalt mixtures at average test temperatures of 40 ^{0}C are obtained by conducting incremental creep test on various mix types.

Resilient modulus values α and μ parameters for surface course were determined from laboratory tests. Cross section of flexible pavement used for a multilane highway is considered in the present study. The selected pavement structure consists of five courses as shown in Fig.5.

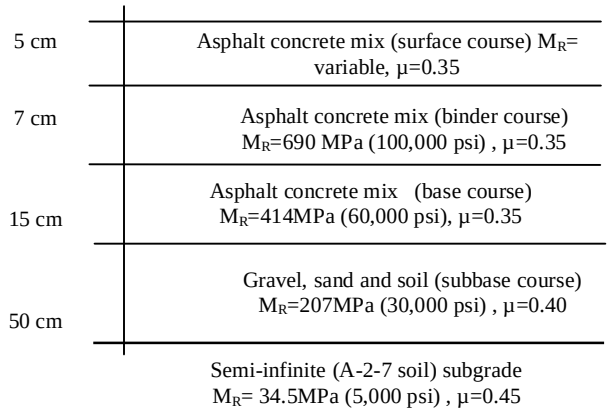

Fig.5: Cross section of the selected pavement structure.

Initially an equivalent 124 MPa (18000 psi) single axle load (ESAL) with dual tires was adopted. Traffic loading is assumed to be one million ESAL with tire pressure of 552 KPa (80 psi) and radius of contact area is 6 inches. Annual growth rate is assumed to be 8 percent. Average temperature of 40°C was used in estimation of rut depth value within selected pavement structure. Fig.6 illustrates the effect of various mix types on rut depth values.

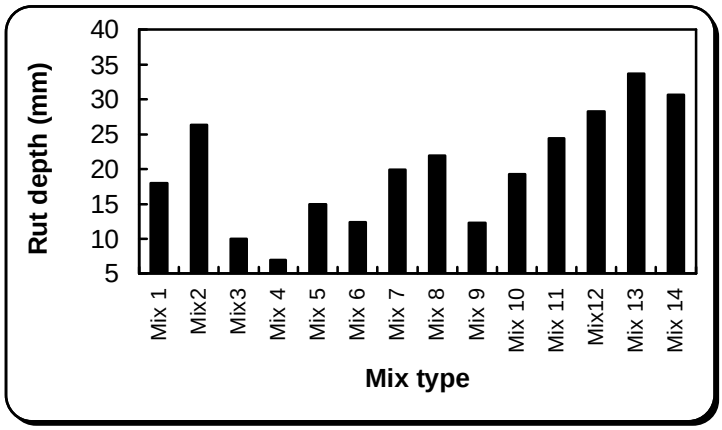

Fig.6: Effect of mix type on rut depth values.

As shown in Fig.6, the addition of polymer to asphalt paving mixture reduces the rut depth values in case using the modified asphalt mixes in construction of surface course for the selected pavement structure especially for modified mixes containing polymer percent of 1% by weight of modified asphalt. Also, the modified mixture with SBR polymer gives rut depth values lower than that modified mixture with (PVA) polymer regardless the polymer percent.

* CONCLUSIONS

- Modified asphalt mixtures with 1% SBR or PVA polymer have higher strengths than the other mixture types. Higher strength indicates that the mixes to be more resistance under tension. This characteristic is desired for mixtures to resist fatigue cracks.
- For the particular asphalt used in the present study SBR and PVA modified polymer mix types affect the number of cycles to failure and would be expected to provide an increased level of protection against cracking due to repetitive loads. Also, the modified asphalt mixtures with two selected polymer types exhibited higher resistance to fatigue than the control mixes and the asphalt grade has effect on fatigue life values of modified asphalt mixtures.
- The rutting distress analysis results shown that the addition of polymer to asphalt paving mixture will reduce the rut depth values in whole pavement courses structure especially for modified mixes which containing polymer percent of 1% by weight of modified asphalt.
- The modified asphalt mixtures with (SBR) polymer show excellent performance (high fatigue life, high tensile strength, low rut depth), especially, at 1% when compared with other modified with (PVA) polymer and control asphalt cement mixes.

REFERENCES

- ASTM Standards, (2003), *"Roads and Paving Materials"*, Annual Book of the American Society for Testing and Materials Standards, Section 4, Vol. 04-03.

- Bahia, H.U., Hanson, D.I., Zeng, M., Zhia, H., and Khatri, M.A., and Anderson, R.M., (2001), *"Characterization of Modified Asphalt Binders in Superpave Mix Design"*, NCHRP Report 459.

- FHWA, (2003),*"VESYS 5W's User Manual "*, Federal Highway Administration Office (FHWA) of Infrastructure Research and Development, Truck Pavement Interaction Program, June 26, Washington, D.C.

- Harvey, J., Lee, T., Sousa, J., Pak, J., and Monismith, C.L., (1994), *"Evaluation of Fatigue and Permanent Deformation Properties of Several Asphalt-Aggregate Field Mixes Using Strategic Highway Research Program A-003A Equipment"*, Transportation Research Record 1454, 123, 1994.

- Harvey, J., J.A. Deacon, B. Tsai, and C.L. Monismith, (1995), *"A Fatigue Performance of Asphalt Concrete Mixes and its Relationship to Asphalt Concrete Pavement Performance in California"*, California Department of Transportation, Report No. RTA-65W485-2, October.

- Harvey, J.T., J.A. Deacon, A.A. Tayebali, R.B. Leahy, and C.L. Monismith, (1997) *"A Reliability-Based Mix Design and Analysis System for Mitigating Fatigue Distress"*, Eighth International Conference on Asphalt Pavements, Seattle, Washington, 1997.

- Institute for Transportation Studies, University of California at Berkeley, (1994), *"Fatigue Response of Asphalt-Aggregate Mixes "*, SHRP-A-404.

- Institute for Transportation Studies, University of California at Berkeley, *"Permanent Deformation Response of Asphalt-Aggregate Mixes"*, SHRP-A-415, 1994.

- Khattak, M.J. and Baladi, G.Y., (2001), *"Fatigue and Permanent Deformation Models for Polymer-Modified Asphalt Mixtures"*, Transportation Research Record 1767, 135.

- Khosla, N. P., Brian Birdsall, and S. Kawaguchi, (2000), *"Evaluation of Moisture Susceptibility of Asphalt Mixtures – Conventional and New Methods"* Transportation Research Record No. 1728.

- Little, D.N., Lytton, R.L., Williams, D., and Kim, Y.R.,(1999), *"An Analysis of the Mechanism of Microdamage Healing Based on Application of Micromechanics First Principles of Fracture and Healing"*, Journal of the Association of Asphalt Paving Technologists 68, 501.

- Loulizi, A., Al-Qadi, I.L., Lahour, S., and Freeman, T.E., (2002), *"Measurement of Vertical Compressive Stress Pulse in Flexible Pavements and Its Representation for Dynamic Loading"*, Transportation Research Board, Paper No.02-2376.

- Newman, J.K., (2000) , *"Polymer Modification of Asphalt Mixtures Designed for Military Airfield Pavements; Fatigue Properties According to AASHTO TP-8"*, Transportation Systems 2000 Workshop, San Antonio, Texas, February 28-March 3.
- Nukulchai, W.K., Kongsuwan, S., Sawatparnich, A., and Singhatiraj, P., (2007), *"Rubber-Modified Asphalt for Better Road Pavement"*, www.doh.go.th./dohweb/project/rubber.pdf.

- Mohammad, L.N. and Paul, H., (1993), *"Evaluation of the Indirect Tensile Test for Determining the Structural Properties of Asphalt Mix"*, Transportation Research Record, No. 1417, TRB, National Academy of Science, Washington, D.C.

- Robber, F.L., Kandhal, P.S., Brown, E.R., and Dunning, R.L., (1989), *"Investigation and Evaluation of Ground Tire Rubber in Hot Mix Asphalt "*, National Center for Asphalt Technology.

- State Commission of Roads and Bridges (SCRB), (2003), *"General Specification for Roads and Bridges "*, Republic of Iraq, Ministry of Housing and Construction, Department of Planning and Studies, Baghdad, Revised Edition, Addendum No.3.

- Spanish Ministry of Public Works, (1990), *"NLT-350 Flexural Test to Measure the Fatigue Strength of Bituminous Mixtures"*, Madrid.

- Taylor, M. A. and N. P. Khosla., (1983), "*Stripping of Asphalt Pavements: State of the Art*", Transportation Research Record 911. TRB, National Research Council, Washington, DC, 1983.

- Wegan, V. and Brule, B., (1999), *"The Structure of Polymer Modified Asphalt Binders and Corresponding Asphalt Mixtures"*, Journal of the Association of Asphalt Paving Technologists, 68, 64.

SYMBOLS

C(t)	Creep compliance	[1/MPa]
D	Diameter of the specimen	[m]
H	Height of the specimen	[m]
P_{max}	Maximum applied load	[N]
P	Applied vertical load	[N]
M_R	Resilient modulus	[Pa]
t	Sample thickness	[m]

Greek symbols

δH	Horizontal deformation	[mm]
Є(t)	vertical strain	[mm/mm]
m	Poisson's ratio	[unitless]
σ_o	Applied stress	[Pa]
σ_t	Indirect tensile strength	[Pa]

DERIVATION OF STIFFNESS MATRIX FOR A GENERAL TWO DIMENSIONAL CURVED ELEMENT IN GENERAL GLOBAL COORDINATES SYSTEM

Mus'ab Aied Q. Al-Janabi
Assistant Lecturer
Department of Civil Engineering
University of Babylon

Balqees Abdul Wahid Ahmed
Assistant Lecturer
Department of Civil Engineering
University of Baghdad

ABSTRACT

In the present paper , the derivation of stiffness matrix for a general two dimensional curved element in global coordinates system is presented. The derivation depends on the assumption that any curved in-plane element can be approximated by a specified curve in polar coordinates. The polar curve assumed in this polar depends on some variables that enable it to represent any two dimensional curved element. The derivation process accompanied by complex integrals which are evaluated by using **(Gaussian Quadrature)** method of numerical integration. One numerical example is presented to verify the accuracy and efficiency of the derived stiffness matrix. The verification contains a comparison with the results of the exact solution. Very good agreement is obtained between the results of the derived stiffness matrix and the results of the exact model.

الخلاصة

في هذا البحث تم اشتقاق مصفوفة الجساءة لأي عنصر مقوس ثنائي الأبعاد وبنظام الإحداثيات العام. الاشتقاق يعتمد على فرضية أن أي عنصر مقوس ثنائي الأبعاد يمكن أن يقرب بمنحني معين بالإحداثيات القطبية. المنحني القطبي المفروض في هذا البحث يعتمد على بعض المتغيرات التي تمكنه من تمثيل أي عنصر منحني ثنائي الأبعاد. عملية الاشتقاق صوحبت بتكاملات معقدة والتي تم حسابها باستخدام طريقة **(Gaussian Quadrature)** للتكاملات العددية. تم حل مثال واحد لغرض إثبات دقة وفاعلية المصفوفة الجديدة. تم مقارنة النتائج التي تم الحصول عليها مع الحل المضبوط ومن خلال المقارنة تم الحصول على نتائج قريبة جدا من الحل المضبوط وبفرق لايزيد عن (1,7%).

KEYWORDS

Stiffness matrix; two dimensional element; general curved element; global coordinates

INTRODUCTION

In the past, the curve beam or arch represents one of the few structural systems which make it possible to cover large spans. The earliest inhabitants developed the arch as an important element of their architecture as expressed by remaining bridges, aqueducts and large public buildings. To day, the same importance is presented especially in bridge construction. Typical forms of curved beams are: circular arches, cantilever-curved beams, elliptical arches, cubic, square arches and catenary curved beams. Most of early modern curved beams have semicircular shapes. Now, curved beams or arched structures are constructed in different shapes and from variable materials as brick, steel, reinforced concrete, ferrocement and timber. The main aim of the curved beam is to enhance the load carrying capacity, which may come from stiffening beavior due to membrane action. A literature survey indicates that a substantial amount of works that deal with the analysis of arches by using circular curved finite element. **Just(1982)** presented the exact $(6*6)$ stiffness matrix for a circularly curved beam subjected to loading in its own plane. This matrix was derived from the governing differential equations and from the finite element procedure. The strain energy contributed axial and flexural actions were considered. **Akhtar(1987)** expressed the stiffness matrix of a single circular member of uniform cross-section. He also obtained the fixed end actions due to concentrated load acting at any point on the member making any angle with radial direction at this point. The effect of shear deformations was neglected. **Litewka and Rakowski(1998)** derived the exact stiffness matrix for a curved beam element with constant curvature(circular curved element). The plane two node six-degree-of-freedom element was considered. **Hadi(2002)** developed a circular curved beam element stiffness matrix. He included the effect of shear deformations. The derived matrix is used in the nonlinear analysis of reinforced concrete circular arches. It is clear from the preceding review that there is no formulation of a more general stiffness matrix for a curved element including circular and non-circular curved elements. The objective of the present paper is to derive a more general stiffness matrix that deals with circular and non-circular curved elements by using the principle of the strain energy. In addition, the derived stiffness matrix is in global coordinates system and can be applied on any curved element without any transformation.

- Derivation of Stiffness Matrix For a General Curved Beam Element:

Before the derivation of stiffness matrix, a general equation for any curved in-plane element must be found. In this paper, a general equation in polar coordinates is suggested to represent any plane curved element. The suggested equation is:

$$r = a \cos n\theta \qquad (1)$$

Which represents a family of (flower-shaped) curves or roses depending on the value of (n) equally spaced petals of radius $(a \ at \ \theta = 0)$. So, if one takes the first quadrant of eq.(1) , any plane curved element can be fitted by choosing a specified values for (n) and (a) depends on span length and a number of known $(x-y)$ coordinates for the curve. For $(n=1)$, the curve represents a circle as shown in **Fig.1** and for $(n=2)$ represents a rose of $(2n)$ equally spaced petals if (n) is even $(n=2,4,6,....)$ and of (n) equally spaced petals if (n) is odd $(n=3,5,7,.....)$. As (n) reaches high values, the above eq.(1) represent a straight beam. So, the chosen polar curve represents an infinite number of curves varies from a circle $(n=1)$ and the degree of curvature will decrease with the increment of (n) until it will reach to a straight element $(n \approx \infty)$ or large values. The above explanation can be seen in **Fig.1**.

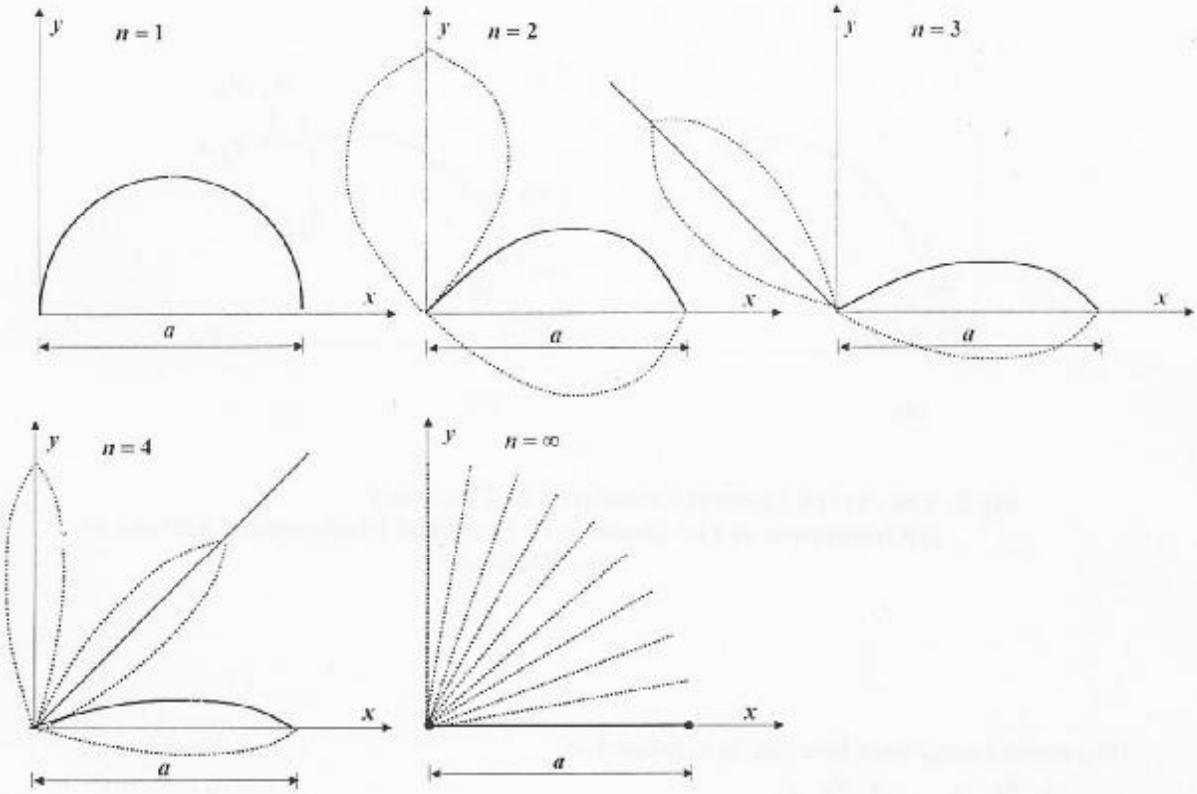

Fig.1: The Graph of $r = a\cos n\theta$

The derivation of the stiffness matrix depends on the principle of the strain energy. The model forces and displacements of a curved element are shown in Fig.2. The internal forces can be expressed in terms of the nodal forces at node (i) by using the static equilibrium equations. The global coordinates system is considered for the directions of the nodal forces and displacements. Hence, by using the suggested polar equation, the following internal forces can be obtained

$$P = P_i \cos\beta + Q_i \sin\beta \tag{2}$$

Where (β) is the inclination angle of the tangent to the polar curve at a point having coordinates (r,θ) which can be expressed as

$$\tan\beta = \frac{dy}{dx} = \frac{dy/d\theta}{dx/d\theta} = \frac{n\sin n\theta \sin\theta - \cos n\theta \cos\theta}{r\sin n\theta \cos\theta + \cos n\theta \sin\theta} \tag{3}$$

In which $x = r\cos\theta, y = r\sin\theta, r = a\cos n\theta$

$$M = Q_i(r\cos\theta - r_2\cos\theta_2) - (P_i(r\sin\theta - r_2\sin\theta_2) + M_i) \tag{4}$$

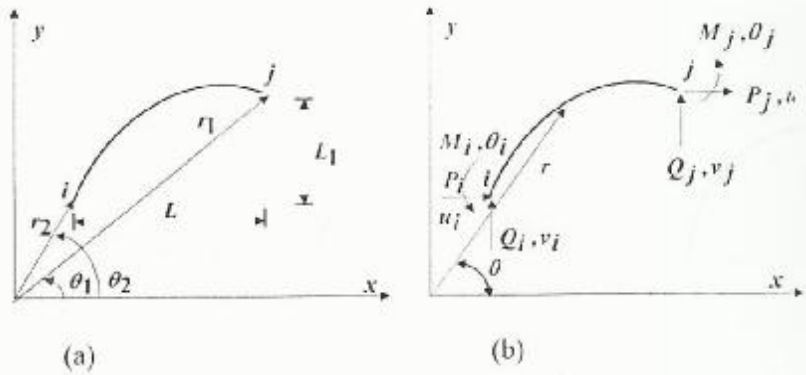

Fig.2: The curved Element Considered In This Study
(a)Orientation of The Element (b) Force and Displacement Systems on The Element

The strain energy used here can be expressed as

$$U = \frac{1}{2EI}\int_{\theta_1}^{\theta_2} M^2 ds + \frac{1}{2AE}\int_{\theta_1}^{\theta_2} P^2 ds \tag{5}$$

Where $\left(ds = a\sqrt{(\cos n\theta)^2 + n^2(\sin n\theta)^2}\ d\theta\right)$ is the length of the curve segment in polar coordinates used to find the strain energy along the curve , **Anton et al (2002).**
By substituting expressions (2) and (4) into the equation of the strain energy (5) one can get

$$U = \frac{1}{2EI}\begin{bmatrix} Q_i^2(a_1) - 2Q_iP_i(a_2) - 2Q_iM_i(a_3) + P_i^2(a_4) + 2P_iM_i(a_5) + M_i^2(a_6) + \\ \frac{I}{A}(P_i^2(a_7) + P_iQ_i(a_8) + Q_i^2(a_9)) \end{bmatrix} \tag{6}$$

Where

$$a_1 = \int_{\theta_1}^{\theta_2}\left[\left[a^3(\cos n\theta)^2(\sin n\theta)^2 - 2a^2r_2\cos\theta_2(\cos n\theta\cos\theta) + ar_2^2(\cos\theta_2)^2\right]\left(\sqrt{(\cos n\theta)^2 + n^2(\sin n\theta)^2}\right)\right]d\theta \tag{7}$$

$$a_2 = \int_{\theta_1}^{\theta_2}\left[\left[\frac{1}{2}a^3(\cos n\theta)^2(\sin 2\theta) - a^2r_2\cos\theta_2(\cos n\theta\sin\theta) - a^2r_2\sin\theta_2(\cos n\theta\cos\theta) + \frac{1}{2}ar_2^2(\sin 2\theta_2)\right]\left(\sqrt{(\cos n\theta)^2 + n^2(\sin n\theta)^2}\right)\right]d\theta$$

(8)

$$a_3 = \int_{\theta_1}^{\theta_2}\left[\left[a^2(\cos n\theta\cos\theta) - ar_2\cos\theta_2\right]\left(\sqrt{(\cos n\theta)^2 + n^2(\sin n\theta)^2}\right)\right]d\theta \tag{9}$$

$$a_4 = \int_{\theta_1}^{\theta_2}\left[\left[a^3(\cos n\theta)^2(\sin\theta)^2 - 2a^2r_2\sin\theta_2(\cos n\theta\sin\theta) + ar_2^2(\sin\theta_2)^2\right]\left(\sqrt{(\cos n\theta)^2 + n^2(\sin n\theta)^2}\right)\right]d\theta \tag{10}$$

$$a_5 = \int_{\theta_1}^{\theta_2} \left[\left[a^2 (\cos n\theta \sin\theta) - a r_2 \sin\theta_2 \right] \left[\sqrt{(\cos n\theta)^2 + n^2 (\sin n\theta)^2} \right] \right] d\theta \tag{11}$$

$$a_6 = \int_{\theta_1}^{\theta_2} \left[a \sqrt{(\cos n\theta)^2 + n^2 (\sin n\theta)^2} \right] d\theta \tag{12}$$

$$a_7 = \int_{\theta_1}^{\theta_2} \left[a (\cos\beta)^2 \sqrt{(\cos n\theta)^2 + n^2 (\sin n\theta)^2} \right] d\theta \tag{13}$$

$$a_8 = \int_{\theta_1}^{\theta_2} \left[a (\sin 2\beta) \sqrt{(\cos n\theta)^2 + n^2 (\sin n\theta)^2} \right] d\theta \tag{14}$$

$$a_9 = \int_{\theta_1}^{\theta_2} \left[a (\sin\beta)^2 \sqrt{(\cos n\theta)^2 + n^2 (\sin n\theta)^2} \right] d\theta \tag{15}$$

Integrations of eqs.(7 to 15) is complicated, so, it can be found by using **Gaussian-Quadrature** method of numerical integration (see Appendix –A). It is found that three Gaussian points give close results to the exact solution for the example presented in this paper. The stiffness coefficients corresponding to the degrees of freedom shown in **Fig.2(b)** can be obtained by using **Castigliano's** second theorem **Boresi and Schmidt (2003)**, which states that the deflection caused by an external force is equal to the partial derivative of the strain energy (U) with respect to that force.
The partial derivatives of the strain energy (U) with respect to (P_i), (Q_i) and (M_i) respectively are:

$$\frac{\partial U}{\partial P_i} = \frac{1}{2EI} \left[P_i (c_1) + Q_i (c_2) + M_i (c_3) \right] \tag{16}$$

$$\frac{\partial U}{\partial Q_i} = \frac{1}{2EI} \left[P_i (c_2) + Q_i (c_4) + M_i (c_5) \right] \tag{17}$$

$$\frac{\partial U}{\partial M_i} = \frac{1}{2EI} \left[P_i (c_3) + Q_i (c_5) + M_i (c_6) \right] \tag{18}$$

Where

$$\left.\begin{aligned} c_1 &= 2(a_4) + \frac{2aI}{A}(a_7) \\ c_2 &= \frac{aI}{A}(a_8) - 2(a_2) \\ c_3 &= 2(a_5) \\ c_4 &= 2(a_1) + \frac{2aI}{A}(a_9) \\ c_5 &= -2(a_3) \\ c_6 &= 2(a_6) \end{aligned}\right\} \tag{19}$$

The stiffness coefficient (K_{ij}) can be defined as the force of type (i) which required to cause a unit displacement of type (j) with all other types of displacements equal to zero. Therefore, equations (16), (17) and (18) will be used to fined the stiffness matrix of the element.

2.1 Axial Stiffness

Consider the element shown in **Fig.3** which is subjected to a unit axial displacement. The stiffness coefficients corresponding to that displacement can be obtained by setting expressions (16),(17) and (18) equal to 1,0 and 0 respectively, hence

$$P_i (c_1) + Q_i (c_2) + M_i (c_3) = 2EI \tag{20}$$

$$P_i(c_2)+Q_i(c_4)+M_i(c_5)=0 \tag{21}$$

$$P_i(c_3)+Q_i(c_5)+M_i(c_6)=0 \tag{22}$$

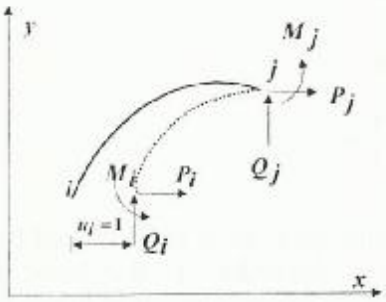

Fig.3: Curved Element Subjected to a Unit Axial Displacement

Solving eqs. (20), (21) and (22) simultaneously yields

$$P_i=\frac{2EI}{A_1} \tag{23}$$

$$Q_i=\frac{2EI}{A_1}Z_1 \tag{24}$$

$$M_i=\frac{-2EI}{A_1}\left[\frac{c_3+c_5Z_1}{c_6}\right] \tag{25}$$

Where

$$A_1=\left[c_1+c_2Z_1-\frac{c_3}{c_6}(c_3+c_5Z_1)\right],\ Z_1=\frac{(\frac{c_5c_3}{c_6}-c_2)}{(c_4-\frac{c_5^2}{c_6})}$$

From equilibrium requirements

$$P_j=-P_i=\frac{-2EI}{A_1} \tag{26}$$

$$Q_j=-Q_i=\frac{-2EI}{A_1}Z_1 \tag{27}$$

$$M_j=Q_iL-(P_iL_1+M_i)$$
$$=\frac{2EI}{A_1}\left[Z_1L-(L_1-(\frac{c_3+c_5Z_1}{c_6}))\right] \tag{28}$$

*** Lateral Stiffness**

Proceeding as in the previous section, stiffness coefficients due to a unit lateral displacement at a node (i) (Fig.4) can be found by making expressions (16),(17)and (18) equal to 0,1 and 0 respectively, hence

$$P_i(c_1)+Q_i(c_2)+M_i(c_3)=0 \tag{29}$$

$$P_i(c_2)+Q_i(c_4)+M_i(c_5)=2EI \tag{30}$$

$$P_i(c_3)+Q_i(c_5)+M_i(c_6)=0 \tag{31}$$

Again, by solving the above three equations simultaneously, the following expressions can be obtained

$$P_i=\frac{-2EI}{A_2}\left[\frac{c_2+c_3Z_2}{c_1}\right] \tag{32}$$

$$Q_i=\frac{2EI}{A_2} \tag{33}$$

$$M_i=\frac{2EI}{A_2}Z_2 \tag{34}$$

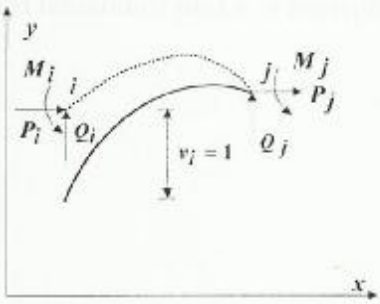

Fig.4: Curved Element Subjected to a Unit Lateral Displacement

Where

$$A_2=\left[c_4+c_5Z_2-\frac{c_2}{c_1}(c_2+c_3Z_2)\right],\ Z_2=\frac{(\frac{c_3c_2}{c_1}-c_5)}{(c_6-\frac{c_3^2}{c_1})}$$

Also, due to equilibrium requirements

$$P_j=\frac{2EI}{A_2}\left[\frac{c_2+c_3Z_2}{c_1}\right] \tag{35}$$

$$Q_j=\frac{-2EI}{A_2} \tag{36}$$

$$M_j=Q_iL-(P_iL_1+M_i)$$
$$=\frac{2EI}{A_2}\left[L-(Z_2-(\frac{c_2+c_3Z_2}{c_1})L_1)\right] \tag{37}$$

- Rotational Stiffness

Stiffness coefficients corresponding to a unit rotational displacement at a node (i) **(Fig.5)** can be found by setting expressions (16),(17)and (18) equal to 0,0 and 1 respectively, hence

$$P_i(c_1)+Q_i(c_2)+M_i(c_3)=0 \tag{38}$$

$$P_i(c_2)+Q_i(c_4)+M_i(c_5)=0 \tag{39}$$

$$P_i(c_3)+Q_i(c_5)+M_i(c_6)=2EI \tag{40}$$

Solving eqs.(38),(39), and (40) simultaneously, one can get

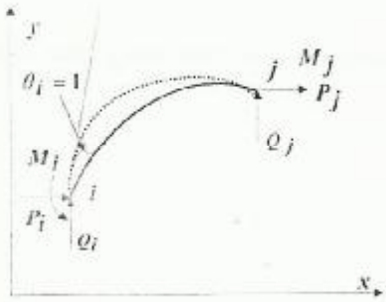

Fig.5: Curved Element Subjected to a Unit Rotational Displacement

$$P_i = \frac{-2EI}{A_3}\left[\frac{c_2 Z_3 + c_3}{c_1}\right] \tag{41}$$

$$Q_i = \frac{2EI}{A_3} Z_3 \tag{42}$$

$$M_i = \frac{2EI}{A_3} \tag{43}$$

In which

$$A_3 = \left[c_6 + c_5 Z_3 - \frac{c_3}{c_1}(c_3 + c_2 Z_3)\right], Z_3 = \frac{\left(\frac{c_3 c_2}{c_1} - c_5\right)}{\left(c_4 - \frac{c_2^2}{c_1}\right)}$$

From equilibrium requirements, the following expressions can be obtained

$$P_j = \frac{2EI}{A_3}\left[\frac{c_2 Z_3 + c_3}{c_1}\right] \tag{44}$$

$$Q_j = \frac{-2EI}{A_3} Z_3 \tag{45}$$

$$M_j = Q_i L - (P_i L_1 + M_i)$$
$$= \frac{2EI}{A_3}\left[Z_3 L - \left(1 - \left(\frac{c_2 Z_3 + c_3}{c_1}\right) L_1\right)\right] \tag{46}$$

All other stiffness coefficients can be found from symmetry and equilibrium requirements. The coefficients of the (6*6) stiffness matrix in the global coordinates system according to the degrees of freedom shown in Fig.2 **(b)** is as follows:

$$K_{11} = \frac{2EI}{A_1} \tag{47}$$

$$K_{21} = \frac{2EI}{A_1} Z_1 \tag{48}$$

$$K_{31} = \frac{-2EI}{A_1}\left[\frac{c_3 + c_5 Z_1}{c_6}\right] \tag{49}$$

$$K_{41} = \frac{-2EI}{A_1} \tag{50}$$

$$K_{51} = \frac{-2EI}{A_1} Z_1 \tag{51}$$

$$K_{61} = \frac{2EI}{A_1}\left[Z_1 L - (L_1 - (\frac{c_3 + c_5 Z_1}{c_6})) \right] \tag{52}$$

$$K_{22} = \frac{2EI}{A_2} \tag{53}$$

$$K_{32} = \frac{2EI}{A_2} Z_2 \tag{54}$$

$$K_{42} = \frac{2EI}{A_2}\left[\frac{c_2 + c_3 Z_2}{c_1} \right] \tag{55}$$

$$K_{52} = \frac{-2EI}{A_2} \tag{56}$$

$$K_{62} = \frac{2EI}{A_2}\left[L - (Z_2 - (\frac{c_2 + c_3 Z_2}{c_1}) L_1) \right] \tag{57}$$

$$K_{33} = \frac{2EI}{A_3} \tag{58}$$

$$K_{43} = \frac{2EI}{A_3}\left[\frac{c_2 Z_3 + c_3}{c_1} \right] \tag{59}$$

$$K_{53} = \frac{-2EI}{A_3} Z_3 \tag{60}$$

$$K_{63} = \frac{2EI}{A_3}\left[Z_3 L - (1 - (\frac{c_2 Z_3 + c_3}{c_1}) L_1) \right] \tag{61}$$

$$K_{44} = \frac{2EI}{A_1} \tag{62}$$

$$K_{54} = \frac{2EI}{A_1} Z_1 \tag{63}$$

$$K_{64} = \frac{-2EI}{A_1}\left[Z_1 L - (L_1 - (\frac{c_3 + c_5 Z_1}{c_6})) \right] \tag{64}$$

$$K_{55} = \frac{2EI}{A_2} \tag{65}$$

$$K_{65} = \frac{-2EI}{A_2}\left[L - (Z_2 - (\frac{c_2 + c_3 Z_2}{c_1}) L_1) \right] \tag{66}$$

$$K_{66} = \left[(K_{62}) L - ((K_{61}) L_1 + K_{63}) \right] \tag{67}$$

The above coefficients can be written in a matrix form as follows

$$[K] = \begin{bmatrix} K_{11} & & & & & \\ K_{21} & K_{22} & & & sym. & \\ K_{31} & K_{32} & K_{33} & & & \\ K_{41} & K_{42} & K_{43} & K_{44} & & \\ K_{51} & K_{52} & K_{53} & K_{54} & K_{55} & \\ K_{61} & K_{62} & K_{63} & K_{64} & K_{65} & K_{66} \end{bmatrix}$$

- Numerical Example

To verify the validity and efficiency of the derived matrix, a cantilever-curved beam shown in **Fig.6** is analyzed by using the derived stiffness matrix. The curved beam is analyzed previously by **Just(1982)** by using an exact circularly curved beam element derived by him. In this element, the strain energy contributed by axial and flexural actions was considered. Three subtended angles (γ) of the curved cantilever were investigated. The beam was analyzed by using a single curved element and also by approximating it into a various numbers of equal straight segments. In the present study, the end displacements of point (B), (u_B, v_B) are found by using the derived stiffness matrix for the three values of (γ). The results are listed in **Table (1)** . Through the comparison of the two solutions, it is found that the results obtained by using the derived stiffness matrix is close to the exact solution obtained by **Just(1982).**

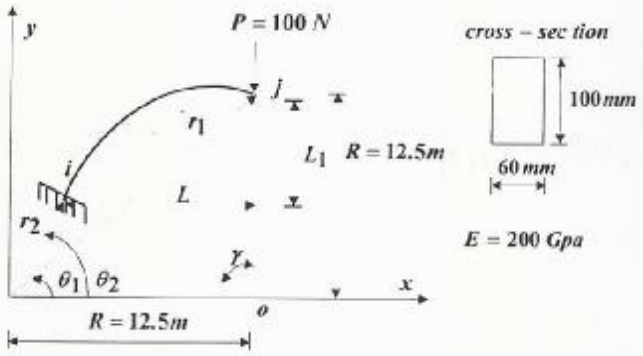

Fig.6: Curved Cantilever of The Numerical Example

In the above figure, the unknowns ($r_1, r_2, \theta_1, \theta_2$) can easily found from the geometry of the curved beam.

Table (1): Comparison of Results of The Numerical Example

End Deflections (mm)	γ	Number of Straight Elements Just (1982)			Exact Just (1982)	Present Analysis
		1	2	3		
$v_B \downarrow$	90°	94.28	138.13	152.11	157.08	156.908
$u_B \rightarrow$		94.28	97.67	99.37	100.00	100.448
$v_B \downarrow$	60°	50.00	58.08	60.55	61.42	60.975
$u_B \rightarrow$		28.87	25.88	25.22	25.00	24.58
$v_B \downarrow$	30°	8.63	8.93	9.03	9.06	9.174
$u_B \rightarrow$		2.31	1.92	1.83	1.79	1.805

- CONCLUSIONS

The derived stiffness matrix is found to be efficient for the analysis of curved beams as shown by the comparison of results obtained from the present analysis and the exact solution. It is found that the difference between the present and the exact analyses is not more than (1.7%). The derived stiffness matrix can be used for a wide range of curved elements starting from circular curved elements to straight elements. In addition, the global coordinates system is considered in the derivation of stiffness matrix, so, it can be used without any transformation. This will offer an economical time and fewer calculations solution than the derivations presented by different researchers.

- REFERENCES

Akhtar, M.N.," Element Stiffness of Circular Member ", Journal of Structural Engineering, Vol.113,No.4, April, (1987), pp.867-872.

Anton, H., Bivens, Irt., and Davis,S.," Calculus" Seventh Edition, John Wiley&Sons,Inc.,(2002).

Boresi, A.P. and Schmidt, R.J." Advanced Mechanics of Materials ", Sixth Edition, John Wiley&Sons, Inc. (2003).

Hadi, W.K." Elastic-Plastic Analysis of Reinforced Concrete Shallow Arched Frames Using Curved Beam Element" M.Sc. Thesis, Departement of civil Engineering, University of Babylon,(2002).

Just,D.J.," Circularly Curved Beams Under Plane Loads" , Journal of the Structural Division,ASCE, Vol.108, No.ST8, August, (1982), pp.1858-1873.

Litewka, P. and Rakowski,J., " The Exact Thick Arch Finite Element" ,Computers and Structures, Vol.68 ,1998,pp.369-379

- NOTATIONS

The following symbols are used in this paper

A : cross-sectional area of the element

E : modulus of elasticity

I : the moment of inertia about the major axis

K_{ij} : coefficients of stiffness matrix $[K]$

L : the horizontal projection length of the curved element on $x-axis$ (span length)

L_1 : the vertical projection length of the curved element on $y-axis$

M : internal moment at a point with (r,θ) coordinates on the curved element

P : internal axial force at a point with (r,θ) coordinates on the curved element

Q : internal shear force at a point with (r,θ) coordinates on the curved element

u_i, u_j :horizontal displacements at the node (i) and (j) respectively

v_i, v_j : vertical displacements at the node (i) and (j) respectively

Appendix-A (Numerical Integration)

One of the most formulas which is used for numerical integration is(**Gaussian Quadrature**) formula . To estimate the value of the integration ($\int_{\theta_1}^{\theta_2} f(\theta)d\theta$) according to (**Gaussian Quadrature**) formula, the interval of the integration will be changed from $[\theta_1,\theta_2]$ to $[-1,1]$ by a suitable transformation of variable. Let the new variable (α), where $-1 \le \alpha \le 1$, be defined by

$$\alpha = \frac{2\theta-(a+b)}{b-a} \qquad \text{(A-1)}$$

Also define a new function $F(\alpha)$ so that

$$F(\alpha) = f(\theta) = f(\frac{(b-a)\alpha+(b+a)}{2}) \qquad \text{(A-2)}$$

Then, integration of $F(\alpha)$ between the integration limit $[-1,1]$ can be found as follows

$$\int_{-1}^{1} F(\alpha)d\alpha = \sum_{i=1}^{n} w_i F(\alpha_i) \qquad \text{(A-3)}$$

Where n is the number of Gaussian points. So, according to eq.(A-3) and by the subistitutions

$$\theta = \frac{(a+b)+(b-a)\alpha}{2}, and, \quad d\theta = \frac{(b-a)}{2}\, d\alpha$$

$$\int_{a}^{b} f(\theta)\, d\theta = \frac{(b-a)}{2}\left[\sum_{i=1}^{n} w_i f(\frac{(a+b)+(b-a)\alpha_i}{2})\right] \qquad \text{(A-4)}$$

Where (w_i) is the weight factor and (α_i) is the corresponding base point.

Example:

Find $A = \int_{\pi/4}^{\pi/2} (\cos\theta)^4\, d\theta$

a) Exact solution

$$A = \left[\frac{1}{4}(\cos\theta)^3 \sin\theta + \frac{3}{4}(\frac{1}{2}\theta + \frac{1}{4}\sin 2\theta)\right]_{\pi/4}^{\pi/2}$$

$$= 0.04447$$

b) Approximate solution

Using three Gussian points, the corresponding base point and weight factors are:

$\alpha_1 = 0.0 \qquad w_1 = 0.8888888 \qquad \theta_1 = 1.178$

$\alpha_2 = +0.77459 \qquad w_2 = 0.5555555 \qquad \theta_2 = 1.482$

$\alpha_3 = -0.77459 \qquad w_3 = 0.5555555 \qquad \theta_3 = 0.874$

Hence,

$$A = \int_{\pi/4}^{\pi/2} (\cos\theta)^4 \, d\theta = \frac{(b-a)}{2}\left[\sum_{i=1}^{3} w_i (\cos\theta_i)^4\right] = 0.3927[0.88888(0.021466) + 0.55555(0.16969)]$$

$A = 0.0445$

It can be seen that the two solutions are very close to each other.

Table (A-1): The values of the appropriate base points and the corresponding weight factors for $n = 1,2,3,.....,6$ points formula

Roots(α_i)	$\int_{-1}^{1} F(\alpha)d\alpha = \sum_{i=1}^{n} w_i F(\alpha_i)$	Weight factors (w_i)
+0.57735 02691 89626	Two- point Formula	1.00000000000000000000
-0.57735 02691 89626		1.00000000000000000000
0.00000000000000000	Three- point Formula	0.88888888888888888888
+0.77459 66692 41483		0.55555555555555555555
-0.77459 66692 41483		0.55555555555555555555
+0.33998 10435 84856	Four- point Formula	0.65214 51548 62546
-0. 33998 10435 84856		0.65214 51548 62546
+0.86113 63115 94053		0.34785 48451 37454
-0.86113 63115 94053		0.34785 48451 37454
0.00000000000000000	Five- point Formula	0.56888 88888 88889
+0.53846 93101 05683		0.47862 86704 99366
-0.53846 93101 05683		0.47862 86704 99366
+0.90617 98459 38664		0.23692 68850 56189
-0.90617 98459 38664		0.23692 68850 56189
+0.23861 91860 83197	Six- point Formula	0.46791 39345 72691
-0.23861 91860 83197		0.46791 39345 72691
+0.66120 93864 66256		0.36076 15730 48139
-0.66120 93864 66256		0.36076 15730 48139
+0.93246 95142 03152		0.17132 44923 79170
-0.93246 95142 03152		0.17132 44923 79170

PREDICTION OF INDUCED STRESSES WITHIN SOIL MASS USING ARTIFICIAL NEURAL NETWORK

Zainal, Abdul Kareem Esmat

ABSTRACT

In this paper, an Artificial Neural Network (ANN) is applied to predict the soil stress within a soil mass for a variety of depths and displacements under applied loading. The neural network model is created and applied for two cases, point load, and Uniform rectangular load.

Theses two cases were selected among many other cases of loading as a representation of the capabilities of ANN in finding proper solutions. The first case needs one input to get one output, where in the second case we need two inputs, to get one output only.

Results revealed that function approximation using neural network can be applied easily and can give accurate results by choosing the appropriate learning algorithm, number of layers, and number of neurons to solve the problem. ANN model can provide reasonable accuracy for civil engineering problems, and a more effective tool for engineering applications.

الخلاصة

في هذا البحث، تم تطبيق استخدام الشبكات العصبية في محاولة لتخمين قيمة الاجهادات في التربة لأعماق وإزاحات مختلفة تحت موقع تسليط الحمل على سطح التربة. تم إيجاد موديل باستخدام الشبكات العصبية وتطبيقه على حالتين من حالات تسليط الإجهادات وهما الحمل النقطي، والإجهاد المنتظم على شكل مستطيل.

تم اختيار هاتين الحالتين من بين عدة حالات تحميل للتربة كنموذج لبيان إمكانية الشبكات العصبية في إيجاد حلول مناسبة. الحالة الأولى تحتاج إلى مُدخل واحد للحصول على نتيجة واحدة، والحالة الثانية تحتاج إلى مُدخلين اثنين للحصول على نتيجة واحدة فقط.

أسفرت النتائج عن إمكانية استخدام الشبكات العصبية كأداة للحصول على قيم تقريبية للدوال بشكل دقيق مع سهولة الاستخدام وذلك باختيار خوارزمية التعليم المناسبة، عدد الطبقات المناسب، وعدد الخلايا العصبية المناسب لمعالجة المشكلة. إن استخدام الشبكات العصبية في أعمال الهندسة المدنية بشكل عام يعتبر أداة فعالة ومؤثرة لمعالجة بعض المشاكل والتطبيقات التي لا يمكن حلها بالطرق التقليدية إلا بصعوبة.

Keywords

Artificial neural network, artificial intelligence, civil engineering, stresses within soil mass, function approximation.

INTRODUCTION

The origins of artificial neural networks (ANN) are in the field biology. The biological brain consists of billions of highly interconnected neurons forming a neural network. Human information processing depends on this connectionist system of nervous cells. Based on this advantage of information processing, neural networks can easily exploit the massively parallel local processing and distributed storage properties in the brain (Jeng, et al., 2003).

A classical comparison of information processing by a human and a computer is focused on the ability of pattern recognition and learning. The computer can calculate large numbers at high speeds

but it cannot recognize something such as a classification problem, written text, data compression and a learning algorithm. On the contrary, humans easily recognizes and deals with the challenges mentioned above by processing information with highly distributed transformations through thousands of interconnected neurons in the brain.

Generally speaking, an ANN is an informational system simulating the ability of a biological neural network by interconnecting many simple neurons (Fig. 1). The neuron accepts inputs from a single or multiple sources and produces outputs by simple calculations, processing with a predetermined non-linear function. Therefore, the primary characteristics of an ANN can be presented as following: (1) the ability of learning; (2) distributed memory; (3) fault tolerance and (4) operating in parallel.

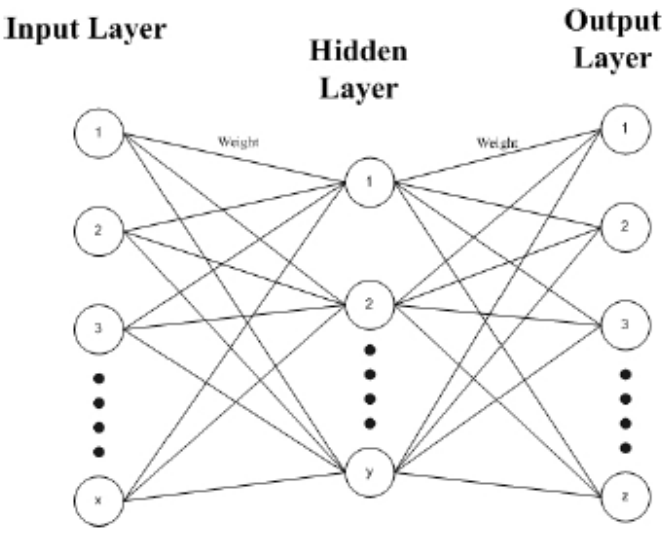

Fig. 1. Structure of Artificial Neural Network model.

Recently, artificial neural network (ANN) models have been widely applied to various relevant civil engineering areas such as geotechnical engineering, water resources and coastal engineering.

CASES STUDIED

Two cases of loading are studied here to determine the stress within soil mass, the cases are:

1. Point load (one input, one output),
2. Uniform Rectangular load (two inputs, one output).

To determine the increase of stresses within a soil mass for a specific depth and displacement that results from applying a certain loading condition, we usually use the classical graphs, complex equations, or approximate methods.

Graphical approach gives approximate results, and usually has an error tolerance according to the human judgment of determining the required value, while using the complex equations which are already built on several assumptions may lead to unnecessary excessive effort of calculations.

Using ANN is just like using a memory. Artificial Networks can remember the values that we teach them to memorize (using the appropriate learning algorithm, number of layers, and number of neurons), then we can recall these values back when needed, this process needs to be done only once. With some extensive learning and suitable algorithms, this network can predict values that never been taught before, these predicted values usually have some error tolerance that we try to minimize.

Case 1 Stresses Inside a Soil Mass Due to Surface Point Load P.
Theoretical approach

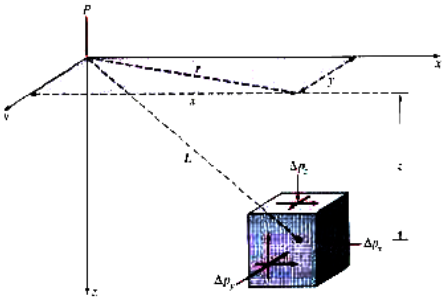

$$\Delta p_x = \frac{P}{2\pi}\left\{\frac{3x^2 z}{L^5} - (1-2\mu)\left[\frac{x^2-y^2}{Lr^2(L+z)} + \frac{y^2 z}{L^3 r^2}\right]\right\}$$

$$\Delta p_y = \frac{P}{2\pi}\left\{\frac{3y^2 z}{L^5} - (1-2\mu)\left[\frac{y^2-x^2}{Lr^2(L+z)} + \frac{x^2 z}{L^3 r^2}\right]\right\}$$

$$\Delta p_z = \frac{3P}{2\pi}\frac{z^3}{L^5} = \frac{3P}{2\pi}\frac{z^3}{(r^2+z^2)^{\frac{5}{2}}} = \frac{P}{z^2}\left\{\frac{3}{2\pi}\frac{1}{\left[\left(\frac{r}{z}\right)^2+1\right]^{\frac{5}{2}}}\right\} = \frac{P}{z^2}I_1$$

Fig 2 Mathematical solution for Point Load

Boussinesq published in 1883 a mathematical solution to the problem of finding the stress at any point in a homogeneous, elastic and isotropic medium due to a vertical point load P applied upon the surface of a semi-infinitely large space, as shown below (Das, 1998).
For a different ratio of r/z (as defined in eq.1), the value of I_1 can be calculated and obtained as shown in the second field of table (1).
The last equation in fig. 2 which is:

$$\Delta P_z = \frac{P}{z^2}\left\{\frac{3}{2\pi}\frac{1}{\left[\left(\frac{r}{z}\right)^2+1\right]^{\frac{5}{2}}}\right\} = \frac{P}{z^2}I_1 \qquad (1)$$

where
P = Point load
z = depth
r = distance from the load
Is used in this case, r/z (which is the only variable here) will represent the input value and I_1 will be obtained as the output value. Obtaining I_1 makes it possible to calculate ΔP_z as shown in eq. (1).

Implementation of ANN

MatLab version R2008a was used in designing and implementation of the ANN. To find the most appropriate design and learning algorithm, the method of trial and error was used by choosing different learning algorithms, layers, and neurons, as follows:

1. Ten different learning algorithms were used as shown in table A–1.
2. Three different numbers of layers were used, 1 layer, 2 layers, and 3 layers.
3. Four different numbers of neurons were used, 10, 20, 30, and 40 neurons in each layer.

First, the data was calculated using eq. (1) as shown in table (1), the first column (r/z) was used as the input data and the second column (I_1) was used as the target data which represents the values that we aim to reach after teaching the neural network. The ratio (r/z) was taken from 0.0 to 4.0 where the calculated values of I_1 beyond this range of r/z are very small and can be considered negligible in geotechnical problems.
Verifying data were also prepared, which are random data taken for the ratio r/z and the corresponding values of I_1 are calculated as shown in table (2), 75% of these data were for

interpolation where the values of (r/z) are between 0.0 and 4.0, the other 25% are used for extrapolation to examine the reliability of the solution for the values of (r/z) outside the given range. Different number of neurons, networks, and training algorithms (tables A–1, A–2) were tried to get the best solution, which is considered to have:

1. maximum correlation ratio between the target data and the output data obtained,
2. maximum correlation ratio between verifying data and the output obtained, and
3. minimum time to reach solution.

Logsig (log–sigmoid) transfer function was used fig. (3) (Demuth, et al., 2008, Zurada, 1992) for the hidden layers and the output layer. This function gives an output value of $0 \leq a \leq 1$ (eq. 2), which is exactly what we need to obtain the value of the output I_1.

The value of (a) can be described as:

$$a = f(n) = \frac{1}{1+e^{-\beta n}} \qquad (2)$$

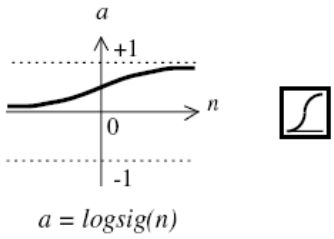

Fig. 3 Log–Sigmoid Transfer Function

Table 1 value of r/z vs. I_1 as calculated by eq. (1)

r/z	Calculated I_1	r/z	Calculated I_1
0	0.47746	2.1	0.00701
0.1	0.46573	2.2	0.00579
0.2	0.43287	2.3	0.00481
0.3	0.38492	2.4	0.00402
0.4	0.32946	2.5	0.00337
0.5	0.27332	2.6	0.00285
0.6	0.22136	2.7	0.00241
0.7	0.17619	2.8	0.00205
0.8	0.13862	2.9	0.00176
0.9	0.10833	3.0	0.00151
1.0	0.08440	3.1	0.00130
1.1	0.06576	3.2	0.00113
1.2	0.05134	3.3	0.00098
1.3	0.04023	3.4	0.00085
1.4	0.03167	3.5	0.00075
1.5	0.02507	3.6	0.00066
1.6	0.01997	3.7	0.00058
1.7	0.01600	3.8	0.00051
1.8	0.01290	3.9	0.00045
1.9	0.01046	4.0	0.00040
2.0	0.00854		

Table 2 Verifying Data for Case 1

r/z	Calculated I_1
0.05	0.47449
0.25	0.41032
0.65	0.19559
1.03	0.07831
1.56	0.02186
1.85	0.01161
2.27	0.00508
2.78	0.00212
3.75	0.00054
4.20	0.00032
4.70	0.00019
5.00	0.00014

The values of (r/z) were gathered in one vector (the input vector) and the values of I_1 are gathered in another vector (the target vector) then the learning process was applied to the network until one of these criteria is met:

- *mse* (Mean Squared Error) of 1×10^{-10} is reached, or
- Maximum number of iterations (*Epochs* as called in MATLAB) of 10000 is reached, or
- Minimum gradient of 1×10^{-6} is reached, or
- Minimum step size of 1×10^{-6} is reached.

Each training algorithm depends on one or more of these criteria to reach the end of the training process and gives the solution, the solution is a trained network that gives the expected output to a specific input value (this process is called *simulation*) .

The results of these tries are shown in table (A–2). Figure (4) summarizes the Maximum correlation ratios and the minimum time to obtain solution in seconds. It is not necessary that the values for the correlation ratio and the minimum time are for the same learning algorithm, but it gives an idea of the optimum performance of each try.

These tries revealed that the most suitable solution for this case is by using (Levenberg-Marquardt with 2 layers 40, 40 neurons) as it gives the most accurate results with minimum time.

The Artificial Network model used was as follows:

1. 1 node as an input layer,
2. 40 nodes as hidden layer 1,
3. 40 nodes as hidden layer 2, and
4. 1 node as an output layer.

The output is shown in table (3) for the simulated data and in table (4) for the verifying data. Time to reach solution was 6 seconds with 9 iterations.

Correlation ratio was calculated to observe the fitness of the simulated data to the calculated data; also the correlation ratio was calculated for the verifying data and the predicted output data. A correlation ratio of 1 and 0.999987812 was obtained for both outputs respectively.

Figure (5) show the data regression between input and target data, figure (6) shows the performance where the value of *mse* was reached in 9 Epochs (iterations), where figure (7) shows the output data, and the verifying data and how they fit to the target data.

Table 3 r/z, I_1 Calculated Values, and I_1 Simulated Values for case 1

r/z	Calculated I_1	Output Value I_1	r/z	Calculated I_1	Output Value I_1
0	0.47746	0.477463584	2.1	0.00701	0.007013647
0.1	0.46573	0.465731470	2.2	0.00579	0.005794614
0.2	0.43287	0.432860895	2.3	0.00481	0.004813168
0.3	0.38492	0.384911411	2.4	0.00402	0.004020859
0.4	0.32946	0.329444563	2.5	0.00337	0.003375093
0.5	0.27332	0.273308334	2.6	0.00285	0.002846994
0.6	0.22136	0.221351186	2.7	0.00241	0.002413953
0.7	0.17619	0.176182178	2.8	0.00205	0.002056527
0.8	0.13862	0.138617682	2.9	0.00176	0.001758853
0.9	0.10833	0.108323893	3.0	0.00151	0.001510348
1.0	0.08440	0.084403204	3.1	0.00130	0.001302479
1.1	0.06576	0.065759708	3.2	0.00113	0.001128002
1.2	0.05134	0.051341152	3.3	0.00098	0.000980044
1.3	0.04023	0.040236740	3.4	0.00085	0.000854248
1.4	0.03167	0.031677664	3.5	0.00075	0.000747481
1.5	0.02507	0.025078250	3.6	0.00066	0.000656436
1.6	0.01997	0.019972652	3.7	0.00058	0.000578020
1.7	0.01600	0.016001569	3.8	0.00051	0.000510310
1.8	0.01290	0.012901423	3.9	0.00045	0.000452432
1.9	0.01046	0.010465445	4.0	0.00040	0.000401220
2.0	0.00854	0.008541327			

Table 4 Simulated Values for Verifying Data

r/z	Calculated I_1	Output Value I_1
0.05	0.47449	0.467757196
0.25	0.41032	0.406451657
0.65	0.19559	0.192011980
1.03	0.07831	0.075212898
1.56	0.02186	0.021337445
1.85	0.01161	0.011383963
2.27	0.00508	0.005019298
2.78	0.00212	0.002098753
3.75	0.00054	0.000532549
4.20	0.00032	0.000366514
4.70	0.00019	0.000366513
5.00	0.00014	0.000366513

Fig. 4 Max. Correlation Ratios for Case 1(see Table A–2)

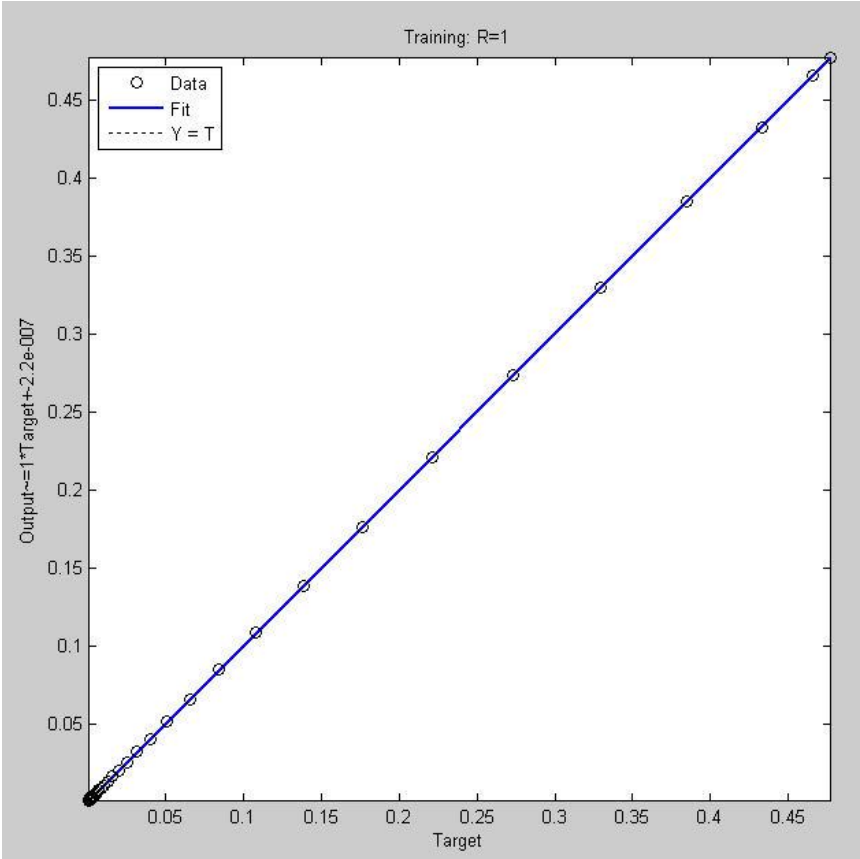

Fig. 5 Regression for ANN Simulated Data

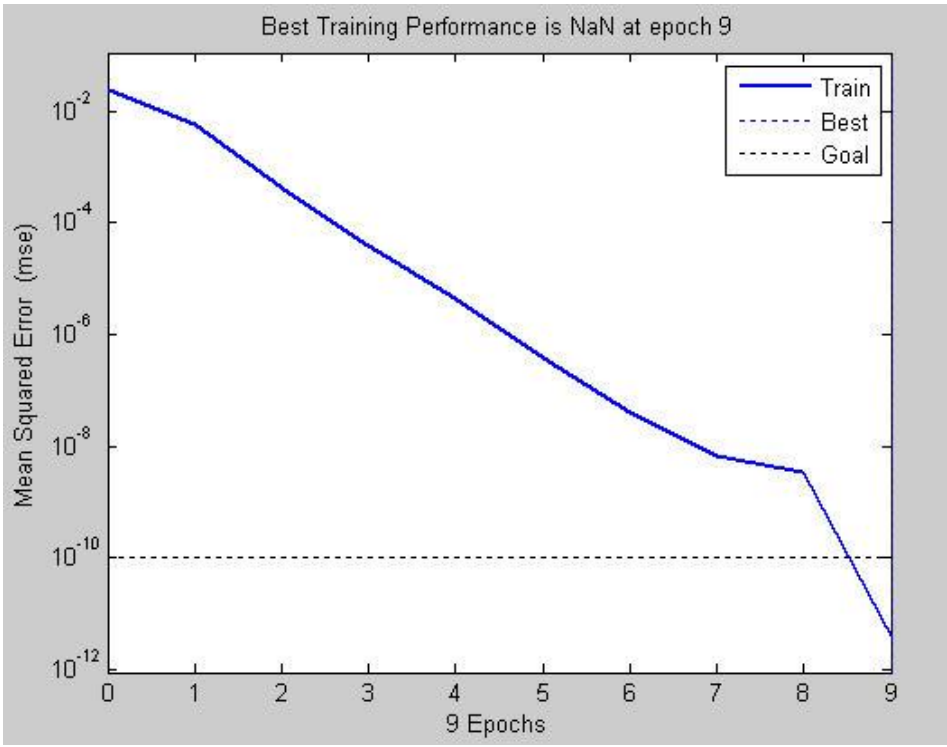

Fig. 6 Performance for Simulated Data with LM Algorithm

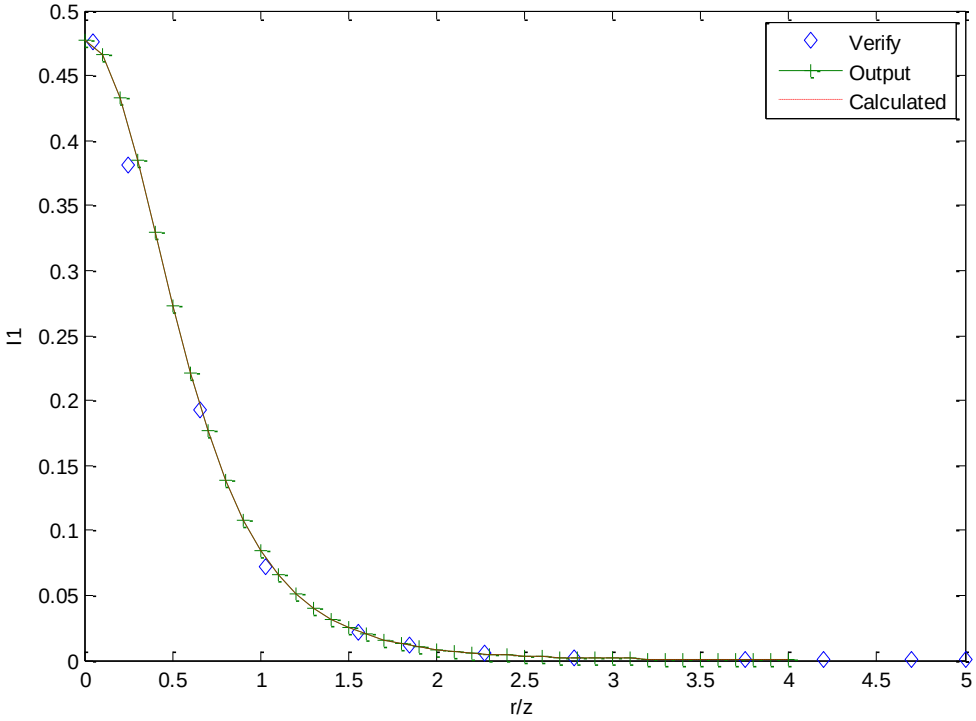

Fig. 7 (r/z) vs. I_1 for Output, Calculated, and Verify Data

Case 2 Uniform Rectangular Load
Theoretical Approach

The increase in the vertical stress at point A is due to the contribution of each *dq* of area (*dxdy*), added up over the length **L** and the width **B**.
Therefore, *dq* = q *dx dy* and the increase in vertical stress is, (Das, 1998)

$$dp = \frac{3q\ dx\ dy\ z^3}{2\pi(x^2+y^2+z^2)^{5/2}}$$

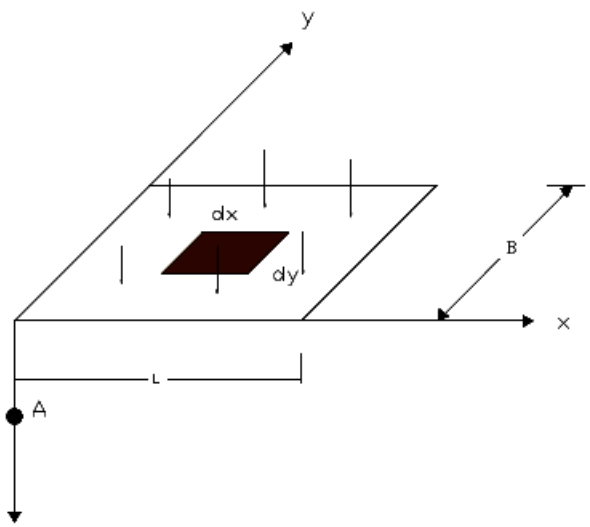

Fig. 8 Mathematical Solution for Uniform Rectangular Load

$$\Delta p = \int dp = \int_{y=0}^{B} \int_{x=0}^{L} \frac{3q\, dx\, dy\, z^3}{2\pi (x^2 + y^2 + z^2)^{5/2}} = qI_3$$

where,

$$I_3 = \frac{1}{4\pi}\left[\frac{2mn\sqrt{m^2+n^2+1}}{m^2+n^2+m^2n^2+1}\left(\frac{m^2+n^2+2}{m^2+n^2+1}\right) + \tan^{-1}\left(\frac{2mn\sqrt{m^2+n^2+1}}{m^2+n^2-m^2n^2+1}\right)\right] \quad \textbf{(3)}$$

$$m = \frac{B}{z} \quad and \quad n = \frac{L}{z}$$

The increase of the vertical stress Δp_z at point A due to the load *dq* can be determined by integration that gives $\Delta p_z = qI_3$, where I_3 is defined by eq. (3) for different values of *m* and *n*.
Therefore, finding the value of I_3 (through this complex equation (3)) is the key for finding Δp_z that represents the increase in the vertical stress under the corner of a rectangular loaded area.

Implementation of ANN

MatLab version R2008a was also used in implementing the ANN for the uniformly loaded rectangular area. The input data used are shown in table (5). Values of *m* and *n* were transformed into 2 × 400 input matrix holding different combinations of *m* and *n* in each column, and 1 × 400 target vector holding the value of I_3 that correspond to the values of *m* and *n* (in this case we need 2 inputs, *m* and *n* (as they are the two variables here), and to get 1 output which is I_3). The values of *m* and *n* were taken from 0.0 to 6.0 as shown in the table (5). Verifying data were also prepared as random combinations of *m* and *n* with the corresponding values of I_3 as shown in table (7), 75% of these data were taken for interpolation where the values of *m* and *n* are between 0.0 and 6.0, the other 25% are used for extrapolation to examine the reliability of the solution for the values of *m* and *n* outside the given range.
Different number of neurons, networks, and training algorithms (table A–1) were tried to get the best solution, which is also considered to have:

1. maximum correlation ratio between the target data and the output data obtained,
2. maximum correlation ratio between verifying data and the output obtained, and
3. minimum time to reach solution.

Logsig (log–sigmoid) transfer function was also used here as the transfer function for the same reason. The results of these tries are shown in table A–3 and summarized in fig. (9) where a close examination of the values obtained could help in choosing a suitable learning algorithm, number of layers, and number of neurons.
The most suitable algorithm was found to be (**CGB** Conjugate Gradient with Powell/Beale Restarts, with 2 layers, each layer having 10 neurons) as it gave high correlation ratio for both, simulated data and verifying data with little execution time as shown in table (A–3). So, the CGB learning algorithm is considered to be the most promising model with:

1. 2 node as an input layer,
2. 10 nodes as hidden layer 1,
3. 10 nodes as hidden layer 2, and
4. 1 node as an output layer.

With correlation ratio of 0.999928637 for simulated data and 0.999904893 for verifying data, with 22 seconds needed to complete the solution.
This compromization of choosing the most suitable solution is absolutely a human judgment and may differ according to the accuracy needed and the type of problem solved.

- **RESULTS AND DISCUSSION**

Results are shown in tables (3, 4, 6, and 7) and figures (5, 6, 7, and 10). In general, the correlation ratio for all tries show a great relationship between the results obtained and the target values (the calculated values). A little decrease in correlation ratio was observed for the verifying data results.

Verifying data was further investigated, and a few samples were taken randomly for analysis for both cases where the 75% interpolation data were separated from the 25% extrapolation data and the correlation ratio was examined for each case separately.

For case 1, it was observed that the interpolation results agree very much with the calculated data (higher correlation ratio) where the extrapolation data have relatively lower correlation ratio, which indicates that the decrease in total correlation ratio is mainly due to the extrapolation data results.

For case 2, after examining the interpolation data separately from the extrapolation data, there was no indication that the decrease in total correlation ratio is due to extrapolation only, but it is the result of the contribution of both interpolation and extrapolation data.

Generally, the results reveal that the use of ANN gives very good agreement between calculated data and simulated data which makes the ANN a very good tool for function approximation method to obtain results, it is also very good for obtaining interpolation results, but less dependant on obtaining extrapolation results on some situations.

Table 5 Input Data for case 2

Table with the variation of I_3 with m and n for a rectangular loaded area.

											m									
n	0.1	0.2	0.3	0.4	0.5	0.6	0.7	0.8	0.9	1.0	1.2	1.4	1.6	1.8	2.0	2.5	3.0	4.0	5.0	6.0
0.1	0.0047	0.0092	0.0132	0.0168	0.0198	0.0222	0.0242	0.0258	0.0270	0.0279	0.0293	0.0301	0.0306	0.0309	0.0311	0.0314	0.0315	0.0316	0.0316	0.0316
0.2	0.0092	0.0179	0.0259	0.0387	0.0387	0.0435	0.0474	0.0504	0.0528	0.0547	0.0573	0.0589	0.0599	0.0606	0.0610	0.0616	0.0618	0.0619	0.0620	0.0620
0.3	0.0132	0.0259	0.0374	0.0474	0.0559	0.0629	0.0686	0.0731	0.0766	0.0794	0.0832	0.0856	0.0871	0.0880	0.8870	0.0895	0.0898	0.0901	0.0901	0.0902
0.4	0.0168	0.0328	0.0474	0.0602	0.0711	0.0801	0.0873	0.0931	0.0977	0.1013	0.1063	0.1094	0.1140	0.1126	0.1134	0.1145	0.1150	0.1153	0.1154	0.1154
0.5	0.0198	0.0387	0.0559	0.0711	0.0840	0.0947	0.1034	0.1104	0.1158	0.1202	0.1263	0.1300	0.1324	0.1340	0.1350	0.1363	0.1368	0.1372	0.1374	0.1374
0.6	0.0222	0.0435	0.0629	0.0801	0.0947	0.1069	0.1168	0.1247	0.1311	0.1361	0.1431	0.1475	0.1503	0.1521	0.1533	0.1548	0.1555	0.1560	0.1561	0.1562
0.7	0.0242	0.0474	0.0686	0.0873	0.1034	0.1169	0.1277	0.1365	0.1436	0.1491	0.1570	0.1620	0.1652	0.1672	0.1686	0.1704	0.1711	0.1717	0.1719	0.1719
0.8	0.0258	0.0504	0.0731	0.0931	0.1104	0.1247	0.1365	0.1461	0.1537	0.1598	0.1684	0.1739	0.1774	0.1797	0.1812	0.1832	0.1841	0.1847	0.1849	0.1850
0.9	0.0270	0.0528	0.0766	0.0977	0.1158	0.1311	0.1436	0.1537	0.1619	0.1684	0.1777	0.1836	0.1874	0.1899	0.1915	0.1938	0.1947	0.1954	0.2956	0.1957
1.0	0.0279	0.0547	0.0794	0.1013	0.1202	0.1361	0.1491	0.1598	0.1684	0.1752	0.1851	0.1914	0.1955	0.1981	0.1999	0.2024	0.2034	0.2042	0.2044	0.2045
1.2	0.0293	0.0573	0.0832	0.1063	0.1263	0.1431	0.1570	0.1684	0.1777	0.1851	0.1958	0.2028	0.2073	0.2103	0.2124	0.2151	0.2163	0.2172	0.2175	0.2176
1.4	0.0301	0.0589	0.0856	0.1094	0.1300	0.1475	0.1620	0.1739	0.1836	0.1914	0.2028	0.2102	0.2151	0.2184	0.2206	0.2236	0.2250	0.2260	0.2263	0.2264
1.6	0.0306	0.0599	0.0871	0.1114	0.1324	0.1503	0.1652	0.1774	0.1874	0.1955	0.2073	0.2151	0.2203	0.2237	0.2261	0.2294	0.2309	0.2320	0.2323	0.2325
1.8	0.0309	0.0606	0.0880	0.1126	0.1340	0.1521	0.1672	0.1797	0.1899	0.1981	0.2103	0.2183	0.2237	0.2274	0.2299	0.2333	0.2350	0.2362	0.2366	0.2367
2.0	0.0311	0.0610	0.0887	0.1134	0.1350	0.1533	0.1686	0.1812	0.1915	0.1999	0.2124	0.2206	0.2261	0.2299	0.2325	0.2361	0.2378	0.2391	0.2395	0.2397
2.5	0.0314	0.0616	0.0895	0.1145	0.1363	0.1548	0.1704	0.1832	0.1938	0.2024	0.2151	0.2236	0.2294	0.2333	0.2361	0.2401	0.2420	0.2434	0.2439	0.2441
3.0	0.0315	0.0618	0.0898	0.1150	0.1368	0.1555	0.1711	0.1841	0.1947	0.2034	0.2163	0.2250	0.2309	0.2350	0.2378	0.2420	0.2439	0.2455	0.2461	0.2463
4.0	0.0316	0.0619	0.0901	0.1153	0.1372	0.1560	0.1717	0.1847	0.1954	0.2042	0.2172	0.2260	0.2320	0.2362	0.2391	0.2434	0.2455	0.2472	0.2479	0.2481
5.0	0.0316	0.0620	0.0901	0.1154	0.1374	0.1561	0.1719	0.1849	0.1956	0.2044	0.2175	0.2263	0.2324	0.2366	0.2395	0.2439	0.2460	0.2479	0.2486	0.2489
6.0	0.0316	0.0620	0.0902	0.1154	0.1374	0.1562	0.1719	0.1850	0.1957	0.2045	0.2176	0.2264	0.2325	0.2367	0.2397	0.2441	0.2463	0.2482	0.2489	0.2492

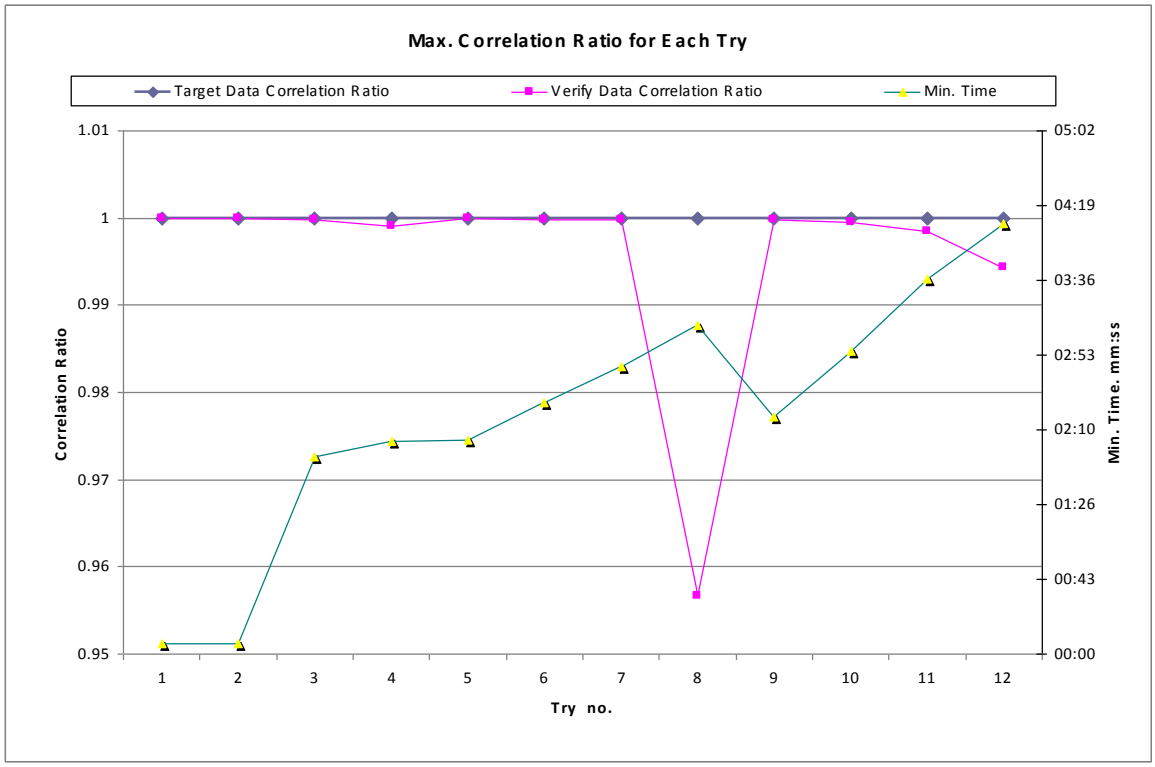

Fig. 9 Correlation Ratios for Case 2 (Table A–3)

Table 6 Output Data (Simulated Data) for case 2

n \ *m*	0.1	0.2	0.3	0.4	0.5	0.6	0.7	0.8	0.9	1.0	1.2	1.4	1.6	1.8	2.0	2.5	3.0	4.0	5.0	6.0
0.1	0.0061	0.0102	0.0142	0.0177	0.0205	0.0230	0.0250	0.0266	0.0279	0.0288	0.0302	0.0310	0.0316	0.0321	0.0325	0.0332	0.0334	0.0315	0.0330	0.0328
0.2	0.0105	0.0184	0.0261	0.0326	0.0380	0.0426	0.0463	0.0493	0.0516	0.0534	0.0558	0.0573	0.0582	0.0589	0.0595	0.0606	0.0607	0.0590	0.0610	0.0605
0.3	0.0148	0.0265	0.0381	0.0479	0.0561	0.0630	0.0686	0.0732	0.0767	0.0795	0.0831	0.0853	0.0867	0.0877	0.0885	0.0897	0.0899	0.0891	0.0906	0.0898
0.4	0.0183	0.0333	0.0482	0.0610	0.0716	0.0806	0.0879	0.0938	0.0985	0.1022	0.1071	0.1100	0.1119	0.1131	0.1140	0.1154	0.1159	0.1160	0.1167	0.1157
0.5	0.0210	0.0387	0.0563	0.0715	0.0843	0.0949	0.1036	0.1107	0.1164	0.1208	0.1268	0.1305	0.1327	0.1342	0.1352	0.1368	0.1376	0.1384	0.1383	0.1372
0.6	0.0232	0.0430	0.0630	0.0802	0.0946	0.1066	0.1165	0.1246	0.1310	0.1361	0.1431	0.1474	0.1500	0.1517	0.1528	0.1545	0.1559	0.1567	0.1563	0.1552
0.7	0.0249	0.0466	0.0684	0.0873	0.1031	0.1163	0.1272	0.1361	0.1432	0.1488	0.1567	0.1615	0.1645	0.1664	0.1677	0.1695	0.1713	0.1719	0.1714	0.1705
0.8	0.0263	0.0495	0.0730	0.0933	0.1102	0.1243	0.1360	0.1456	0.1533	0.1595	0.1682	0.1735	0.1768	0.1789	0.1802	0.1822	0.1845	0.1846	0.1842	0.1834
0.9	0.0274	0.0518	0.0767	0.0982	0.1161	0.1310	0.1433	0.1535	0.1617	0.1683	0.1777	0.1835	0.1871	0.1893	0.1908	0.1929	0.1955	0.1951	0.1950	0.1944
1.0	0.0283	0.0537	0.0796	0.1021	0.1208	0.1363	0.1492	0.1598	0.1685	0.1755	0.1855	0.1917	0.1956	0.1980	0.1995	0.2017	0.2046	0.2038	0.2041	0.2038
1.2	0.0294	0.0561	0.0836	0.1074	0.1272	0.1436	0.1573	0.1686	0.1780	0.1856	0.1966	0.2036	0.2080	0.2107	0.2124	0.2147	0.2177	0.2170	0.2180	0.2180
1.4	0.0300	0.0574	0.0857	0.1103	0.1308	0.1478	0.1620	0.1739	0.1837	0.1917	0.2036	0.2112	0.2159	0.2188	0.2206	0.2230	0.2258	0.2260	0.2275	0.2276
1.6	0.0304	0.0581	0.0868	0.1120	0.1329	0.1503	0.1649	0.1770	0.1872	0.1955	0.2080	0.2160	0.2211	0.2241	0.2260	0.2284	0.2308	0.2322	0.2338	0.2339
1.8	0.0308	0.0587	0.0876	0.1130	0.1342	0.1519	0.1667	0.1791	0.1894	0.1980	0.2108	0.2192	0.2244	0.2277	0.2296	0.2321	0.2343	0.2364	0.2378	0.2380
2.0	0.0313	0.0593	0.0883	0.1138	0.1352	0.1530	0.1680	0.1805	0.1910	0.1997	0.2127	0.2213	0.2267	0.2300	0.2321	0.2346	0.2371	0.2393	0.2405	0.2407
2.5	0.0325	0.0608	0.0900	0.1156	0.1370	0.1549	0.1699	0.1825	0.1930	0.2017	0.2150	0.2238	0.2295	0.2332	0.2357	0.2391	0.2414	0.2430	0.2437	0.2439
3.0	0.0336	0.0620	0.0910	0.1165	0.1379	0.1557	0.1706	0.1830	0.1935	0.2022	0.2156	0.2248	0.2311	0.2353	0.2381	0.2422	0.2429	0.2444	0.2449	0.2453
4.0	0.0329	0.0605	0.0894	0.1154	0.1376	0.1562	0.1716	0.1845	0.1952	0.2042	0.2177	0.2269	0.2333	0.2376	0.2401	0.2423	0.2441	0.2460	0.2474	0.2496
5.0	0.0330	0.0601	0.0890	0.1156	0.1383	0.1570	0.1722	0.1844	0.1945	0.2031	0.2166	0.2261	0.2326	0.2371	0.2403	0.2441	0.2448	0.2469	0.2493	0.2490
6.0	0.0330	0.0612	0.0900	0.1156	0.1375	0.1561	0.1719	0.1851	0.1960	0.2048	0.2178	0.2265	0.2325	0.2366	0.2394	0.2436	0.2463	0.2489	0.2486	0.2491

Table 7 Verifying Data (Calculated and Simulated)

m	*n*	Calculated Data	Simulated Data
0.05	0.05	0.001188709	0.003061156
1.10	2.20	0.208105692	0.208031476
2.40	0.75	0.176836343	0.175824553
1.03	0.85	0.165927416	0.165769742
1.56	0.30	0.086847463	0.086495926
1.90	4.30	0.237935443	0.238111898
2.25	4.70	0.242047436	0.241577197
3.78	2.50	0.243242079	0.242648952
4.45	3.10	0.246134235	0.244890620
6.40	2.50	0.244163366	0.244000887
7.30	3.60	0.247790018	0.250191178
8.00	0.11	0.034731558	0.032693384

- **CONCLUSIONS AND RECOMMENDATIONS**

ANN implementation in geotechnical problems as a function approximation for predicting stresses in soil mass is found to be very good. The results obtained for the two cases of loading gave a correlation ratio of not less than 0.95 for the simulated data in the worst case.

As mentioned earlier, ANN is just like memory that can be taught some information to memorize then we can recall these information back. Therefore, with the appropriate learning rules and a suitable number of neurons and layers, a very good solution can be obtained in solving geotechnical problems, as one good trained network can remember a lot of information and can be used for prediction in a way that is similar to the human brain.

This method can be combined with more complex artificial intelligence and expert systems to solve more complex problems in geotechnical engineering, and generally civil engineering problems.

The following recommendations could be of great benefits for future work:

1- Finding a solution for more complex functions solving geotechnical problems.
2- Combining more cases of stress loading with one network where this network can give a solution for more than one case of loading.
3- Using more fields of Artificial Intelligence and expert systems to find solutions for geotechnical problems.

REFERENCES

- Das, B.M., 1998, “Principles of Geotechnical Engineering”, PWS Publishing Company, Boston.
- Demuth, H., Mark B., and Martin H., 2008, ” Neural Network Toolbox™ 6 User’s Guide”, The MathWorks, Inc.
- Jeng, D.S., Cha D. H. and Blumenstein M., 2003, “Application of Neural Network in Civil Engineering Problems“, Proceedings of the International Conference on Advances in the Internet, Processing, Systems and Interdisciplinary Research (IPSI-2003).
- Zurada, J. M., 1992, “Introduction to Artificial Neural Systems“, PWS Publishing Company.

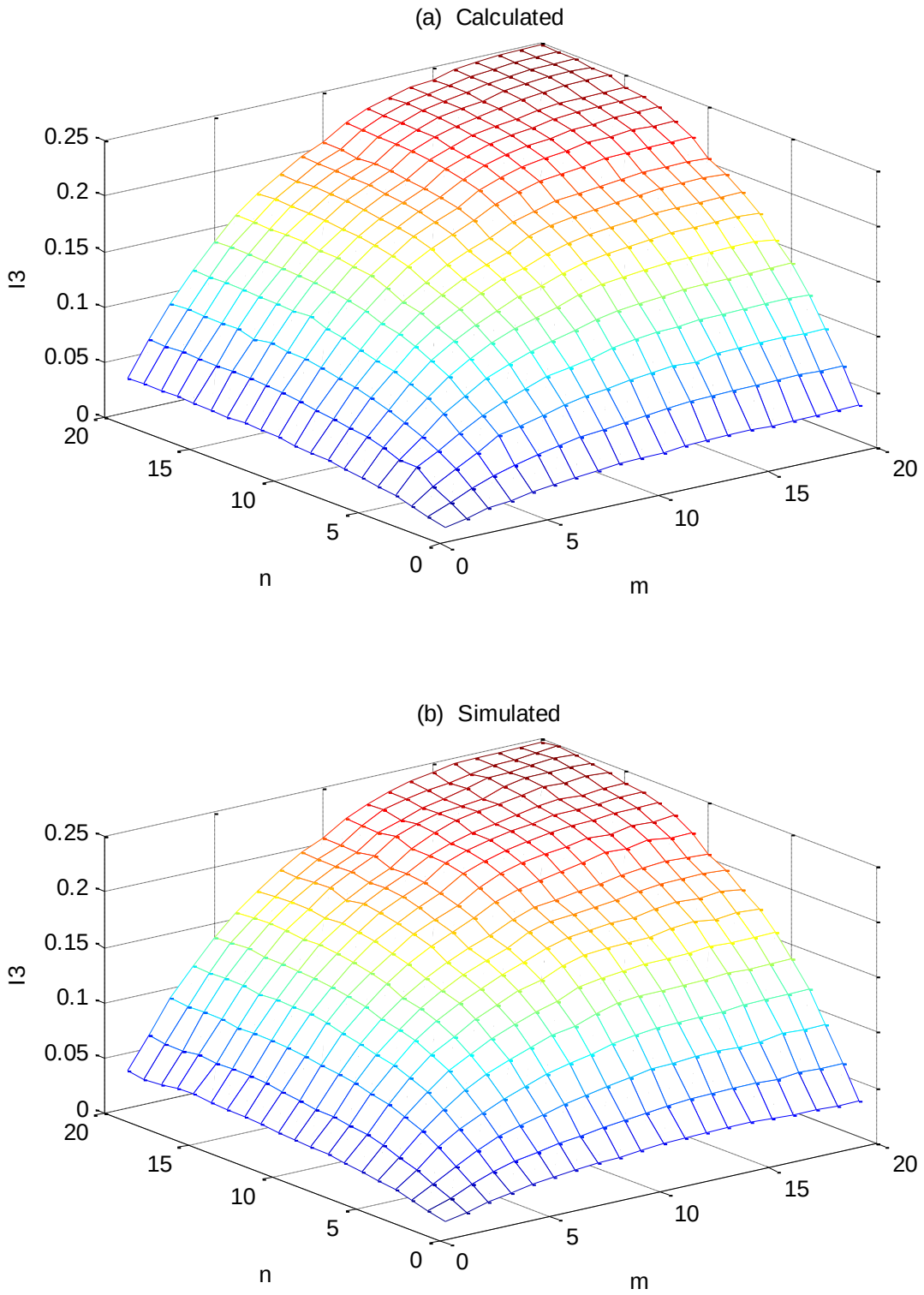

Fig. 10 a) Calculated Data, b) Simulated Data Using CGB 10,10 Neurons

Appendix A

This appendix contains three tables, table A–1 is a list of ten learning algorithms and their abbreviations as used by MATLAB (Demuth, et. al., 2008). These abbreviations were used in table A–2 and A–3 to show the performance of each learning algorithm when tested for a specified number of layers and neurons.

Table A–1 Training Algorithms Names and Symbols

Symbol	Algorithm Name
GDA	Backpropagation training with an adaptive learning rate
GDX	adaptive learning rate with momentum training
RP	Resilient Backpropagation
CGF	Fletcher-Powell Conjugate Gradient
CGP	Polak-Ribiére Conjugate Gradient
LM	Levenberg-Marquardt
BFG	BFGS Quasi-Newton
SCG	Scaled Conjugate Gradient
CGB	Conjugate Gradient with Powell/Beale Restarts
OSS	One Step Secant

Table A–2 Correlation Ratio and Time to Obtain Solution for Each Learning Algorithm, Case 1

Size		GDX	LM	BFG	RP	CGP	CGF
1 1 Layer 10 Neurons	simulated data	0.999654268	0.999999998	0.999974471	0.999994856	0.999689497	0.998935533
	verify data	0.999564824	0.999998664	0.999985423	0.999992449	0.999697215	0.99748201
	Time to reach Solution mm:ss	01:13	00:05	00:02	01:30	00:02	00:01
2 1 Layer 20 Neurons	simulated data	0.999887993	0.999999998	0.999969126	0.999998361	0.994836809	0.999975446
	verify data	0.99991002	0.999994758	0.999883621	0.999565628	0.998366133	0.999942052
	Time to reach Solution mm:ss	01:13	00:05	00:02	01:30	00:01	00:04
3 1 Layer 30 Neurons	simulated data	0.999903148	0.999999998	0.999982061	0.999998876	0.999985799	0.999979182
	verify data	0.999657258	0.999725836	0.999817677	0.999124495	0.999853799	0.999849619
	Time to reach Solution mm:ss	01:13	00:01	00:02	01:31	03:15	00:05
4 1 Layer 40 Neurons	simulated data	0.999925388	0.999999998	0.999982977	0.999999976	0.999977561	0.999827721
	verify data	0.999868643	0.992037779	0.999846374	0.998608843	0.997504938	0.999472775
	Time to reach Solution mm:ss	01:15	00:01	00:03	00:17	01:30	00:03
5 2 Layers 10 x 10 Neurons	simulated data	0.999886681	0.999999997	0.999977361	0.999999359	0.970815555	0.999993597
	verify data	0.999936907	0.999998713	0.999991644	0.999996637	0.979495316	0.999994631
	Time to reach Solution mm:ss	01:19	00:07	00:07	01:37	00:01	00:08
6 2 Layers 20 x 20 Neurons	simulated data	0.999952208	1	0.999982813	0.999999997	0.999988324	0.999996521
	verify data	0.999880492	0.999951412	0.999955936	0.999903009	0.999950285	0.999961913
	Time to reach Solution mm:ss	01:22	00:01	00:57	00:23	00:08	00:17
7 2 Layers 30 x 30 Neurons	simulated data	0.999978976	1	0.999997074	0.999999998	0.999995185	0.996383211
	verify data	0.999430234	0.999661826	0.999859665	0.99790594	0.999716004	0.996033786
	Time to reach Solution mm:ss	01:34	00:03	07:17	00:01	00:06	00:01
8 2 Layers 40 x 40 Neurons	simulated data	0.999985139	1	0.506677097	0.999999997	0.999987578	0.999998062
	verify data	0.999780676	0.999987812	0.697834879	0.996756997	0.99990708	0.999912867
	Time to reach Solution mm:ss	01:26	00:06	00:28	00:14	00:05	00:26
9 3 Layers 10 x 10 x 10 Neurons	simulated data	0.99998686	0.999999997	0.999988897	0.999999993	0.999981582	0.999997282
	verify data	0.999988507	0.99999969	0.999310864	0.999995224	0.999965553	0.999997825
	Time to reach Solution mm:ss	01:31	00:08	00:33	01:45	00:09	00:19
10 3 Layers 20 x 20 x 20 Neurons	simulated data	0.999967055	0.999999998	0.99998969	0.999999997	0.999996346	0.999997943
	verify data	0.999896482	0.999939485	0.999980226	0.999875488	0.999955602	0.999966711
	Time to reach Solution mm:ss	01:30	00:16	07:04	00:03	00:11	00:19
11 3 Layers 30 x 30 x 30 Neurons	simulated data	0.999993711	1	0.999998249	0.999999998	0.999997149	0.999999645
	verify data	0.999506264	0.999275545	0.999604536	0.999122072	0.999470174	0.999626002
	Time to reach Solution mm:ss	02:09	00:24	36:29	00:01	00:09	00:33
12 3 Layers 40 x 40 x 40 Neurons	simulated data	0.999971275	1	0.999264321	0.999999998	0.99999236	0.999999724
	verify data	0.999928194	0.999944212	0.998731643	0.999069412	0.999913901	0.999712451
	Time to reach Solution mm:ss	01:45	00:38	39:27	00:02	00:06	00:26

Table A–2 Continued

Size		GDA	CGB	SCG	OSS	Max. Value Min Time
1 1 Layer 10 Neurons	simulated data	0.999666514	0.998761755	0.999925306	0.999935355	0.999999998
	verify data	0.999955245	0.998627971	0.999924218	0.999978577	0.999998664
	Time to reach Solution mm:ss	01:15	00:01	00:04	03:12	00:01
2 1 Layer 20 Neurons	simulated data	0.999591775	0.999847813	0.999979631	0.999997225	0.999999998
	verify data	0.999663038	0.999891158	0.999962418	0.999926147	0.999994758
	Time to reach Solution mm:ss	01:15	00:01	00:06	02:53	00:01
3 1 Layer 30 Neurons	simulated data	0.999936424	0.99997307	0.999995115	0.999998675	0.999999998
	verify data	0.999852982	0.999782103	0.999847051	0.999821996	0.999853799
	Time to reach Solution mm:ss	01:20	00:03	00:04	02:55	00:03
4 1 Layer 40 Neurons	simulated data	0.99969054	0.999992138	0.999994962	0.999998074	0.999999998
	verify data	0.999814941	0.999138924	0.997849328	0.999845586	0.999868643
	Time to reach Solution mm:ss	01:02	00:11	00:09	02:41	00:01
5 2 Layers 10 x 10 Neurons	simulated data	0.999734388	0.999866841	0.999989427	0.999996428	0.999999997
	verify data	0.992158466	0.999841064	0.999975637	0.999994309	0.999998713
	Time to reach Solution mm:ss	01:06	00:02	00:07	03:00	00:01
6 2 Layers 20 x 20 Neurons	simulated data	0.999902432	0.999984293	0.999996627	0.999996659	1
	verify data	0.999902629	0.99994639	0.999906829	0.999981756	0.999981756
	Time to reach Solution mm:ss	01:09	00:05	00:12	03:00	00:01
7 2 Layers 30 x 30 Neurons	simulated data	0.999940514	0.999997308	0.999999045	0.99999981	1
	verify data	0.999676993	0.999799644	0.999798234	0.999974154	0.999974154
	Time to reach Solution mm:ss	01:12	00:04	00:11	03:06	00:01
8 2 Layers 40 x 40 Neurons	simulated data	0.99992327	0.999992737	0.999999439	0.999999841	1
	verify data	0.999288164	0.999707704	0.999961055	0.999956722	0.999987812
	Time to reach Solution mm:ss	01:14	00:04	00:13	03:12	00:04
9 3 Layers 10 x 10 x 10 Neurons	simulated data	0.999882979	0.999966795	0.999992395	0.999997898	0.999999997
	verify data	0.999910773	0.999975854	0.99998874	0.999954502	0.99999969
	Time to reach Solution mm:ss	01:13	00:03	00:18	03:11	00:03
10 3 Layers 20 x 20 x 20 Neurons	simulated data	0.999871778	0.999965098	0.999997622	0.999997538	0.999999998
	verify data	0.999919554	0.999861734	0.999978875	0.999933998	0.999980226
	Time to reach Solution mm:ss	01:17	00:03	00:13	03:19	00:03
11 3 Layers 30 x 30 x 30 Neurons	simulated data	0.999937628	0.999996323	0.999999768	0.999999808	1
	verify data	0.999245187	0.999541516	0.999665832	0.999474113	0.999665832
	Time to reach Solution mm:ss	01:35	00:04	00:21	03:50	00:01
12 3 Layers 40 x 40 x 40 Neurons	simulated data	0.999973088	0.999996136	0.999999415	0.999999903	1
	verify data	0.99982772	0.999764675	0.999670247	0.999983231	0.999983231
	Time to reach Solution mm:ss	01:38	00:04	00:14	03:57	00:02

Table A–3 Correlation Ratio and time to obtain solution for each learning Algorithm case 2

Size		GDX	LM	BFG	RP	CGP	CGF
1 1 Layer 10 Neurons	simulated data	0.997421716	0.999969763	0.999014114	0.999213905	0.99771077	0.998553091
	verify data	0.995884694	0.999893625	0.999367354	0.999172877	0.998582663	0.998684718
	Time to reach Solution mm:ss	00:38	01:17	00:04	00:46	00:04	00:09
2 1 Layer 20 Neurons	simulated data	0.995336219	0.999982973	0.999852751	0.999502653	0.999848426	0.998388063
	verify data	0.924061144	0.999998649	0.991147479	0.969938723	0.999954383	0.993569279
	Time to reach Solution mm:ss	00:43	01:33	00:25	00:51	00:50	00:07
3 1 Layer 30 Neurons	simulated data	0.996806751	0.999985597	0.999903201	0.998806597	0.998807389	0.999438118
	verify data	0.992795757	0.975812633	0.99986166	0.964759798	0.966495175	0.997367799
	Time to reach Solution mm:ss	00:51	01:59	00:21	00:57	00:18	00:14
4 1 Layer 40 Neurons	simulated data	0.997892925	0.9999861	0.999905937	0.998788153	0.99945839	0.999224168
	verify data	0.986097452	0.143796811	0.867275277	0.737279256	0.980675097	0.998992426
	Time to reach Solution mm:ss	00:50	02:21	00:46	00:59	00:27	00:26
5 2 Layers 10 x 10 Neurons	simulated data	0.996890395	0.999997582	0.999852129	0.999569505	0.9986369	0.999854326
	verify data	0.912433348	0.999404815	0.512562258	0.910469786	0.999706186	0.99876493
	Time to reach Solution mm:ss	00:58	02:32	01:12	01:02	00:10	00:24
6 2 Layers 20 x 20 Neurons	simulated data	0.996142221	0.99999999	0.999884894	0.999850083	0.99973115	0.999603252
	verify data	0.909444391	0.936508981	0.994932753	0.942481183	0.999825778	0.946697531
	Time to reach Solution mm:ss	00:59	10:20	04:16	01:12	00:15	00:30
7 2 Layers 30 x 30 Neurons	simulated data	0.996598329	0.99999999	0.999942195	0.999960039	0.999768294	0.999905451
	verify data	0.636405873	0.67423607	0.973376501	0.967667176	0.998951902	0.999808203
	Time to reach Solution mm:ss	01:08	12:50	28:50	01:17	00:29	01:08
8 2 Layers 40 x 40 Neurons	simulated data	0.997748529	0.99999901	0.998822264	0.999960711	0.999767041	0.999879413
	verify data	0.630516212	0.667252486	0.851514957	0.956629571	0.833867299	0.822350015
	Time to reach Solution mm:ss	01:18	26:05	56:25	01:27	00:53	01:05
9 3 Layers 10 x 10 x 10 Neurons	simulated data	0.997350202	0.999999773	0.999888087	0.999929652	0.999682006	0.999907425
	verify data	0.992936228	0.999353912	0.998986038	0.989582256	0.998938213	0.999864811
	Time to reach Solution mm:ss	00:55	04:17	01:57	01:10	00:27	00:36
10 3 Layers 20 x 20 x 20 Neurons	simulated data	0.996257627	0.99999999	0.999940914	0.999945295	0.999762082	0.999829242
	verify data	0.978996204	0.685547129	0.814073295	0.732601706	0.862005909	0.994203739
	Time to reach Solution mm:ss	01:29	23:27	19:18	01:23	00:26	00:56
11 3 Layers 30 x 30 x 30 Neurons	simulated data	0.997686728	0.99999999	0.999585112	0.999972564	0.999949771	0.999943743
	verify data	0.947105816	0.970780874	0.977114937	0.893065588	0.986427798	0.998443019
	Time to reach Solution mm:ss	01:37	32:07	01:32:04	01:53	01:07	01:20
12 3 Layers 40 x 40 x 40 Neurons	simulated data	0.995687483	0.999999966	0.997994709	0.99998398	0.999916312	0.999956099
	verify data	0.445215417	0.939654085	0.984840882	0.988761096	0.994385995	0.881900269
	Time to reach Solution mm:ss	02:00	01:47:39	03:55:40	01:49	00:59	02:53

Table A–3 Continued

Size		GDA	CGB	SCG	OSS	Max. Value Min. Time
1 1 Layer 10 Neurons	simulated data	0.993069265	0.998929287	0.998957846	0.998689024	0.999969763
	verify data	0.995344777	0.999273071	0.994336215	0.999396451	0.999893625
	Time to reach Solution mm:ss	00:39	00:10	00:22	01:32	00:04
2 1 Layer 20 Neurons	simulated data	0.992847871	0.998185191	0.999893027	0.999363396	0.999982973
	verify data	0.796550721	0.998664137	0.999726489	0.999642399	0.999998649
	Time to reach Solution mm:ss	00:44	00:06	00:27	01:42	00:06
3 1 Layer 30 Neurons	simulated data	0.957142332	0.999768934	0.999880579	0.999429077	0.999985597
	verify data	0.617977696	0.996636178	0.98631191	0.99255058	0.99986166
	Time to reach Solution mm:ss	00:51	00:29	00:36	01:54	00:14
4 1 Layer 40 Neurons	simulated data	0.975834402	0.999865384	0.999918645	0.99936063	0.9999861
	verify data	0.920799101	0.968838149	0.993225527	0.963971922	0.998992426
	Time to reach Solution mm:ss	00:51	00:37	00:52	02:03	00:26
5 1 Layer 10 x 10 Neurons	simulated data	0.968764374	0.999928637	0.999749657	0.999307618	0.999997582
	verify data	0.776141122	0.999904893	0.99879928	0.821808487	0.999904893
	Time to reach Solution mm:ss	00:51	00:22	00:29	02:04	00:10
6 2 Layers 20 x 20 Neurons	simulated data	0.992261753	0.99980772	0.999936415	0.999589259	0.99999999
	verify data	0.974546767	0.994357189	0.993112716	0.893312454	0.999825778
	Time to reach Solution mm:ss	01:02	00:16	00:47	02:25	00:15
7 2 Layers 30 x 30 Neurons	simulated data	0.992262839	0.999921395	0.999954975	0.999464822	0.99999999
	verify data	0.976899059	0.912104144	0.953475843	0.961125015	0.999808203
	Time to reach Solution mm:ss	01:07	00:27	00:35	02:46	00:27
8 2 Layers 40 x 40 Neurons	simulated data	0.986202936	0.999896374	0.999973346	0.999797966	0.99999901
	verify data	0.935001304	0.875996341	0.756037951	0.332080011	0.956629571
	Time to reach Solution mm:ss	01:17	00:31	01:53	03:10	00:31
9 3 Layers 10 x 10 x 10 Neurons	simulated data	0.994952231	0.997526044	0.99994114	0.999439923	0.999999773
	verify data	0.986227565	0.996553965	0.994876201	0.998729027	0.999864811
	Time to reach Solution mm:ss	00:58	00:03	00:28	02:17	00:03
10 3 Layers 20 x 20 x 20 Neurons	simulated data	0.988980895	0.999873191	0.999965168	0.999747848	0.99999999
	verify data	0.792296992	0.999569785	0.979908348	0.837947791	0.999569785
	Time to reach Solution mm:ss	01:13	00:28	01:21	02:55	00:26
11 3 Layers 30 x 30 x 30 Neurons	simulated data	0.992739047	0.999899804	0.99997531	0.999843149	0.99999999
	verify data	0.974915566	0.861619169	0.833139766	0.952912463	0.998443019
	Time to reach Solution mm:ss	01:27	00:58	01:41	03:37	00:58
12 3 Layers 40 x 40 x 40 Neurons	simulated data	0.984708694	0.99980022	0.999977051	0.999820369	0.999999966
	verify data	0.880740521	0.896155879	0.659881142	0.908629323	0.994385995
	Time to reach Solution mm:ss	01:40	00:33	02:07	04:09	00:33

IMPROVEMENT OF SOIL USING GEOGRIDS TO RESIST ECCENTRIC LOADS.

Prof. Dr. Mosa J. Al-Mosawe
Civil Engineering Department, College of Engineering, University of Baghdad.

Dr.A′amal A. Al-Saidi

Civil Engineering Department, College of Engineering, University of Baghdad

Faris W. Jawad
Civil Engineering Department, College of Engineering, University of Baghdad.

ABSTRACT

This paper presents the results of experimental investigations to predict the bearing capacity of square footing on geogrid-reinforced loose sand by performing model tests. The effects of several parameters were studied in order to study the general behavior of improving the soil by using the geogrid. These parameters include the eccentricity value, depth of first layer of reinforcement, and vertical spacing of reinforcement layers. The results of the experimental work indicated that there was an optimum reinforcement embedment depth at which the bearing capacity was the highest when single-layer reinforcement was used. The increase of (z/B) (vertical spacing of reinforcement layer/width of footing) above 1.5 has no effect on the relative improvement for the soil and the relative improvement (%) of the reinforced soil can be predicated by using a simple equation .

االخاصة

يستعرض هذا البحث النتائج لدراسة مختبرية لتقدير قابلية التحمل لتربة رملية مفككة بعد تسليحها بال (geogrid) . و قد تمت دراسة تأثير بعض العوامل لغرض الحصول غلى التصرف العام للتربة المحسنة بال (geogrid) وتشمل هذه العوامل الانحراف المركزي ، عمق الطبقة الاولى من التسليح ، والمسافة العمودية بين طبقات التسليح . وقد بينت النتائج الى ان هنالك عمق امثل لطبقة التسليح الذي يعطي اعلى قابلية تحمل ، زيادة نسبة (Z/B) (المسافة العمودية لطبقة التسليح / عرض الاساس) اكثر من 1.5 ليس لها تأثير على نسبة التحسين للتربة ،كما تم الوصول الى معادلة بسيطة لايجاد نسبة التحسين للتربة المسلحة .

INTRODUCTION

The reinforced earth has been most widely applied with something in excess of one million square meters of wall facing benign erected to the end of end of 1978, Mickittrick and Darbin (1979).The soil particles in direct contact with the reinforcements tend to slide over them under the effect of the load. The sliding is reduced by the frictional resistance between the particles and the surface of the reinforcement. Consequently this resistance will produce a tensile force along the reinforcing element which will acts as a tie between the particles surrounding it. The soil particles which are in direct contact with the reinforcement are bounded to other particles by the interlocking action. The frictional resistance will be transferred through the reinforced mass (Vidal, 1969).

The present study was undertaken to investigate the bearing capacity of square footings on geogrid-reinforced sand. The parameters investigated include

1)- Eccentricity value (e)

2)- Depth Ratio of first layer (u/B), where u and B are depth of first reinforced layer and footing width, respectively.

The symbols of the geometric parameters used in this present paper are shown in Fig (1).

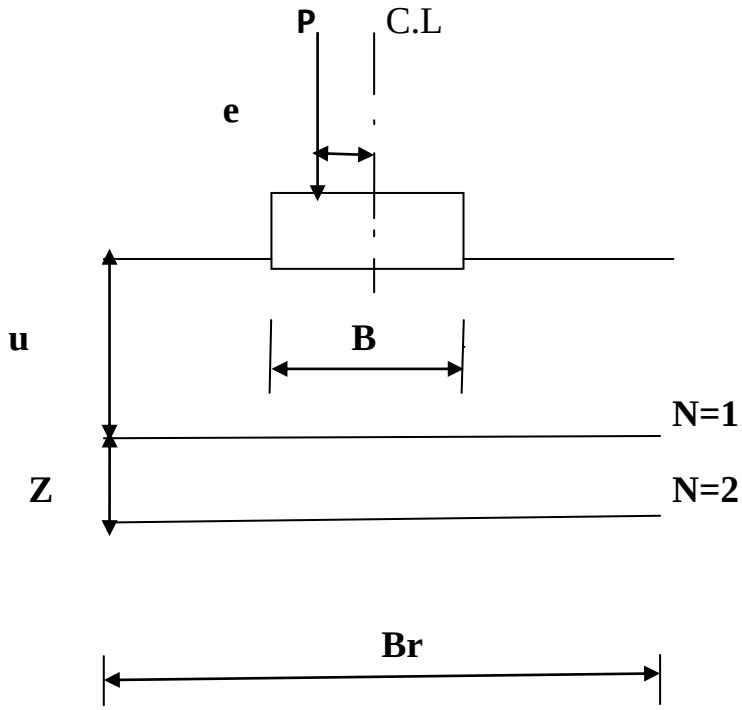

Figure (1) Geometric parameters of Reinforced Foundation.

EXPERMENTAL TESTS AND TESTS PROCEDURE

A series of model loading tests were conducted inside steel box of 600 X 600mm in plane and 700mm in depth. The box was made of steel plate of 3mm thickness, stiffened with angle sections, as shown in Plate (1) . The internal faces of the box were covered with polyethylene sheets in order to reduce the slight friction which might be developed between the box surface and soil. Static vertical loads were applied using electrical hydraulic pump. Loads transferred from the pump to a hydraulic jack were carefully recorded by proving ring installed between the jack and the tested footing.

The footing was loaded at a constant loading rate to failure. The ultimate bearing capacity state was defined as the state at which either the load reached a maximum value where settlement continued without further increase in load or where there was an abrupt change in the load –settlement relationship. Settlement of the footing was measured using two dial gauges fixed in the middle and edge of footing.

The test footing was a square steel plate 60mm in plane and 5mm thick.

Plate (1) General View of Testing Equipment

SOIL PROPERTIES

Clean, oven-dried, uniform quartz sand (Kerbela sand) was used in the tests. The sand was placed in the test box at unit weight of approximately 15.2 kN/m^3 (relative density is 31%). Some properties of the sand are given in Table (1).

Table (1) Sand Properties.

Property	Values
Specific Gravity	Gs= 2.63
Void Ratio and Dry Unit Weight	e_{max}=0.8, γ_{dmax}=17.39kN/m^3 e_{min}=0.5, γ_{dmin} =14.4 kN/m^3 e_{used}=0.74, γ_{dused}=15.2kN/m^3
Relative Density	Dr=31%
Angle of Internal Friction	Ø=29˚

The value of (Ø) was obtained from the result of triaxial test (UU.test) in accordance with ASTM(D2850-95).

REINFORCEMENT PROPERTIES.

The reinforcement used is polymer geomesh the general view for three types used in tests described, Plate (2) .The dimensions of the geogrid samples used in this study are listed in Table (2).The physical and chemical properties for sample used were listed in Table (3). The technical properties for sample used were listed in Table (4).

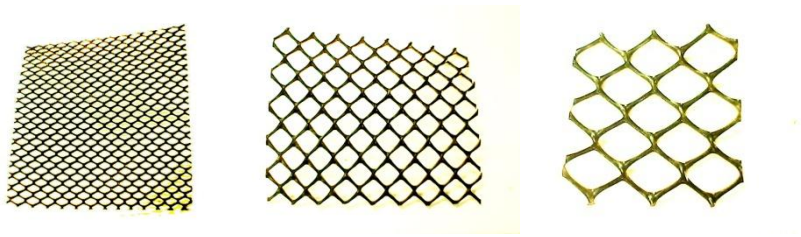

Geogrid No.1 Geogrid No.2 Geogrid No.3

Plate (2) The Reinforcement Used.

Table (2) Dimensional properties for geogrids used. .(Latifia Geogrid)

Property	Unit	Data for geogrid No.1	Data for geogrid No.2	Data for geogrid No.3
Aperture Size	mm	6x10	55x55(±4)	39x39(±2)
Mass Per Unit Area	g/m^2	700	520(±%)	770(±40)
Roll Width	m	2.0	1.0	2.5
Roll Length	m	20	20	30
Roll Diameter	m	0.40	0.43	0.50
Cross Roll Weight	kg	28.0	10.4	57.75

Table (3) The physical, chemical and biological properties for geogrids used. .(Latifia Geogrid)

Property	Data for Geogrid No.1	Data for Geogrid No.2	Data for Geogrid No.3
Structure	Extruded Geogrid	Extruded Geogrid	Extruded Geogrid
Mesh Type	Diamond	Square	Diamond
Standard Color	Black	Black	Black
Polymer Type	HDPE	HDPE	HDPE
U.V Stabilized	Carbon Black	Carbon Black	Carbon Black
Chemical Resistance	Excellent	Excellent	Excellent
Biological Resistance	Excellent	Excellent	Excellent
Packaging	Rolls	Rolls	Rolls

Table (4) The technical properties for geogrid used.(Latifia Geogrid)

Property	Unit	Data for Geogrid No.1	Data for Geogrid No.2	Data for Geogrid No.3
Tensile Strength at 2% Strain	kN/m	5.1	2.3	4.3
Tensile Strength at 5% Strain	kN/m	9.1	4.0	7.7
Peak Tensile Strength	kN/m	16.0	7.1	13.5
Yield Point Elongation	%	20.0	20.0	20.0

VARIABLES STUDIED

Effect of Depth Ratio

The relative improvement for soil versus depth ratio for each value of eccentricity is shown in Fig (2). The optimum depth ratio (u/B= 0.75, 0.5, 0.25) show the maximum rate of strength improvement is define [{(Pr/P) -1}*100] where Pr and P is the max load for reinforced and un reinforced sand for eccentricity values (e= 0.05B, 0.135B, 0.22B) respectively. It is noted that for depth ratios (u/B=1.0), improvement values decreased and approach a constant for eccentricity values (e= 0.05B, 0.135B and 0.22B). The relative improvement increases with decreased the values of eccentricity.

It should be pointed out that there is no general consensus regarding the effect of depth ratio on the relative improvement of the soil . Singh (1988), based on the study of square footing on sands reinforced with mild steel grids (also called "welded mesh"), indicated that the effect of depth ratio on the bearing capacity was independent of the number of

reinforcement layers and the optimum depth ratio was about 0.25. Selvadurai and Gnanendran, (1989) to improve the bearing capacity of footing located on slope fill using geogrids, showed that when (u<B), the failure path is penetrated below the reinforcement while when (u>B) the failure occurs at the soil geogrid interface (i.e. the failure path is limited in narrow zone) and the deep location of the geogrid layer at (u>2B) does not lead to any improvement in either the carrying load or the stiffness of the footing

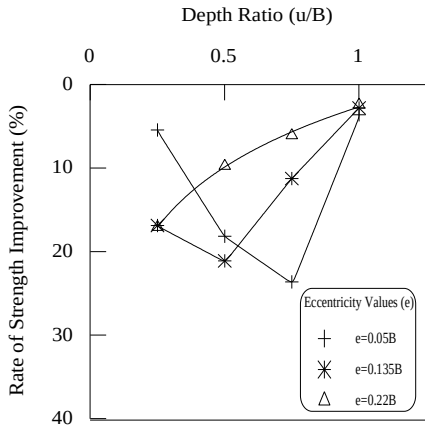

Figure. (2) Improvement versus Depth Ratio for Different Eccentricity Values, and Br /B=3.

The maximum improvement versus eccentricity values when depth ratio is optimum value (u/B=0.75, 0.5 and 0.25) for eccentricity value (e=0.05B, 0.135B and 0.22B) respectively is illustrated in Fig. (3). This figure shows the deterioration in strength with increasing eccentricity values.

The general equation for the relative improvement (%) for the soil can be expressed as follows:

$$q=25.863 - 6.563e \qquad \text{.....} \qquad (1)$$

Where q= maximum rate of strength improvement (%)

e= eccentricity value (mm).

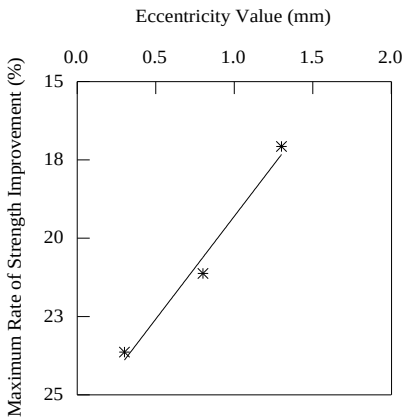

Figure (3) Maximum Improvement Versus Eccentricity Values for Optimum Depth Ratio and Br/B=3.

Effect of Vertical Spacing of Reinforcement Layers :

Figure (4) shows the relative improvement (%) versus vertical spacing ratio(z/B=0.5, 0.75, 1.0 and 1.5) for different eccentricity values (e= 0.05B, 0.135B and 0.22B).This figure illustrated the maximum improvement for eccentricity values (e= 0.05B, 0.135B and 0.22B) at z/b=0.5. It can be seen that the rate of strength improvement equals (0) for vertical spacing ratio (z/B= 1.5) for different eccentricity values thus the increase of (z/B) above 1.5 has no effect on the relative improvement for the soil. Similar to these findings were found by Fukuda et. al., (1987) who tested concentric load applied on footing with polymer grid reinforcement showed that the optimum vertical spacing between reinforcement is 2/3B. Guido et al (1987) indicated that the bearing capacity decreased with increasing vertical spacing ratio for Tensar SS1, SS and SS3 geogrid.

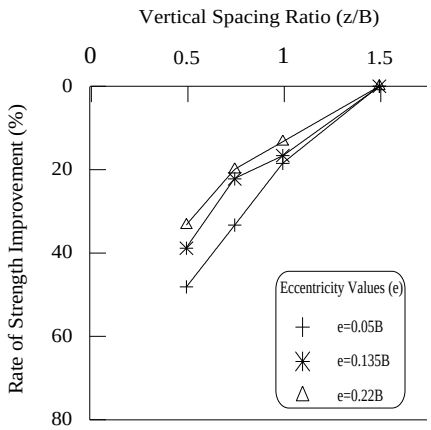

Figure (4) The Relative Improvement Versus Vertical Spacing Ratio for (u/B=Optimum Value and Br/B=3)

The maximum relative improvement versus eccentricity values is shown in Fig. (5). This figure illustrats that the maximum rate of strength improvement decreased with increasing eccentricity values. For any value of eccentricity value and (z/B)=0.5, the relative improvement can be obtained according to the equation (2).

q= exp (-0.368e) * 53.239 …… (2)

where

q= maximum rate of strength improvement (%) .

e=eccentricity values (mm).

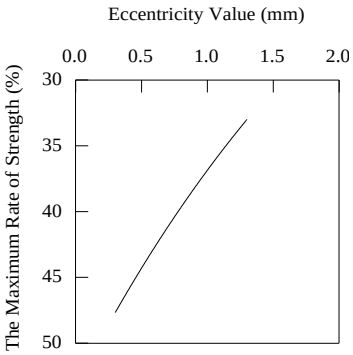

Figure (5) Maximum Rate of Strength Improvement Versus Eccentricity Values for (z/B=0.5, u/B=Optimum Value, N=2, Br/B=3).

CONCLUSIONS

* For single-layer reinforced sand, there is an optimum depth ratio of the first layer at which the bearing capacity is the highest. The tests indicated that the optimum depth ratio of reinforcement of the first layer is equal to (u/B=0.75, 0.5 and 0.25) for eccentricity values (e=0.05, 0.135 and 0.22B), respectively.

* The increase of (z/B) (vertical spacing of reinforcement layer/width of footing) above 1.5 has no effect on the relative improvement for the soil.

* The relative improvement (%) of the reinforced sandy soil can be predicated by using a simple equation (q=25.863 - 6.563e).

* For any value of eccentricity value and (z/B) =0.5, the relative improvement can be obtained t according to the equation { q= exp (-0.368e) * 53.239}.

REFERENCES

- Fukuda, N., Taki, M., and Sutoh, Y., 1987. Foundation Improvement by Polymer Grid reinforcement. Proceedings of the 8th Asian Regional Conference on Soil Mechanics and Foundation Engineering, pp. 365-368.
- Guido, V.A., Knueppel, J.D., and Sweeny, A.1987. Plate loading test on geogrid reinforced earthslabs. Proceedings Geosynthetics' 87 Conference,New Orleans. pp216-225
- Mckittrick, D. P. and Darbin, M., (1979); "World- Wide Development and Use of Reinforced Earth Structures", Ground Engineering, Vol. 12, No.2, p.p. 15-21.
- Selvadurai, A.P.S. and Gnanendran, C.T., 1989. An Experimental Study of a Footing Located on a Sloped Fill: Influence of a Soil Reinforcement Layer. *Canadian Geotechnical Journal*, Vol. 26, No. 3, pp. 467-473.
- Singh, H.R. 1988. Bearing capacity of reinforced soil beds. Ph.D. Thesis . Indian Institute of Science, Bangalore, India
- Vidal, H., (1969); "The Principle of Reinforced Earth", Highway Research Record, HRR-282, p.p. 1-16.

HYDROLOGICAL MODELING OF ASSANNA'F MARSH

Riyadh Z. Al Zubaidy, Ph. D.
Department of Water Resources Engineering, University of Baghdad
Hayder A. Al Thamiry, Ph. D.
Department of Water Resources Engineering, University of Baghdad
Mahmoud S. Al Khafaji, M. Sc.
Department of Building and Construction, University of Technology

ABSTRACT

AsSanna'f Marsh is one of the southern Iraqi Marshes. It is considered as a seasonal marsh. During rainy season, the marsh feeders start to fill the nearly empty region of the marsh and the water levels start to increase gradually. After the water level reaches a specific value, it starts to flow toward Al Huwayza Marsh.

Studies on the hydrological properties of AsSanna'f Marsh are rare and there is a lack of hydrological data of AsSanna'f Marsh feeders. Generally, this paper was prepared to predict missing hydrological data, a procedure was developed and applied for this purpose, and to be used with the available hydrological and topographical data for modeling and analysis the hydrological properties of AsSanna'f Marsh.

The topographical survey and the hydrological field measurements for a period of six months, which were carried out by the Center for Restoration of Iraqi Marshlands, CRIM, of the Ministry of Water Resources, MOR, were used in the hydrological analysis carried out by this paper.

The area and storage elevation curves were computed in two different methods satisfying the existing behavior of the flow condition through the marsh. Relations between the inflow, out flow with the water level elevation, and storage and losses within the marsh were obtained.

The hydrological routing showed the dykes surrounding AsSanna'f Marsh must be at least 11m.a.s.l to increase the Marsh outflow into Al Huwayza Marsh. especially at the south east boundary of the marsh near Al Msharah River. Maximum and minimum storages and the extended wetted area of the marsh were specified. The required inflow and outflow of AsSanna'f Marsh was studied, taking in consideration the wet, normal, and dry years. The maximum allowable AsSanna'f Marsh inflow into Al Huwayza Marsh is specified for flooded year satisfying different the design criteria of the control structures of the outlets of Al Huwayza Marsh and Kmait Flood Escape. A control structure was suggested at the outlet of AsSanna'f Marsh to ensure the full restoration of Al Huwayza Marsh.

الخلاصة

هور السناف احد اهوار العراق الجنوبية الموسمية. يبدأ الماء بالتجمع في هذا الهور من مغذياته خلال موسم الامطار الى ان تصل مناسيب المياه فيه الى حد محدد عندها يبدا الماء بالانسياب باتجاه هور الحويزة.

الدراسات الهيدرولجية التي تمت لهور السناف محدودة كما ان البيانات المطلوبة لانجاز الدراسات الهيدرولوجية قليلة وما متوفر منها يقتصر على فترة محدودة. عموما، اعدت هذه الدراسة لاستنباط البيانات الهيدرولوجية الناقصة وفق سياق اعد في هذه الدراسة لهذا الغرض ومن ثم وبالاعتماد على هذه البيانات وما متوفر من بيانات هيدرولوجية وطوبوغرافية تم نمذجة وتحليل الخواص الهيدرولوجية لهور السناف.

اعتمد في هذا البحث المسح الطوبوغرافي والقياسات الحقلية الهيدرولوجية المنجزة من قبل مركز انعاش الاهوار العراقية التابع لوزارة الموارد المائية لمدة ستة أشهر.

تم في هذا البحث حساب العلاقة بين منسوب الماء مع الخزين والمساحة السطحيةفي هور السناف والتي اعتمدت على اسلوبين مختلفين لتحقيق واقع حال الماء الجاري ضمن الهوركما وتم الاستفادة من القياسات الحقلية في منطقة هور السناف في ايجاد العلاقة بين الماء الداخل والخارج مع مناسيب المياه والخزن والضائعات ضمن هذا هور . ان الاستنتاجات المستحصلة من خلال استتباع الجريان خلال موسم الفيضان بان منسوب التكتيف المحيط بالهور يجب ان لا يقل عن 11م فوق مستوى سطح البحر وخصوصا الجزء الجنوبي الشرقي من هورالسناف قرب نهر المشرح لزيادة تصريف الهور باتجاه هور الحويزة وكذلك تم تحديد اقصى تصريف ممكن اطلاقه من هور السناف باتجاه هور الحويزة محققا مختلف المعايير التصميمية لمنشأت السيطرة على مخارج هور الحويزة ومهرب كميت الفيضاني اضافة لاستعراض اسلوب التشغيل الامثل للمنشأ المقترح على مخرج هور السناف لضمان الانعاش الكلي لهور الحويزة..

KEY WORDS
Flow routing, Hydrological modeling, Hydrological routing, Iraqi Marsh Lands.

INTRODUCTION

Fig. 1 shows a schematic diagram of AsSanna'f Marsh and its feeders, the marsh area reaches 360km^2 during rainy seasons. The marsh area lies along left hand side of Am'arah-Msharah main road. Flood protections dykes lie along the south boundary of the marsh started from Ghzayla Bridge until the dykes of Sa'ad Drain River. Al Fakka–Ghzayla road is the north-east boundary of the marsh. The north boundary of the marsh is a varying boundary that depends on the levels of the stored water within the marsh. The average ground level is around 5m.a.s.l at its southern part and increases gradually in north and north-west directions. The maximum recorded water level in the marsh was 6.5m.a.s.l at Ghzayla Bridge in March of 1988.

The main feeders of AsSanna'f Marsh are: AtTeeb, Dwayreach, Kmait Rivers, the Drain water of Sa'ad River irrigation project, and the surface runoff of AshShmasher catchment area. The catchments area of AtTeeb and Dwayreach Rivers are 2670km^2 and 3270km^2, respectively. These catchment areas lie within the Iranian borders and discharging into AsSanna'f Marsh. AtTeeb River has a length of 500km; its peak discharge is about 1100m^3/sec. While Dwayreach River has a length of 202km, its peak discharge is about 930m^3/sec. These two rivers are seasonal rivers they have flow during January to March. There is no hydraulic structure that can be used to control the inflow from these feeders, Al-Furat Center for studies and designs of irrigation projects, 2003.

Kmait River was designed as a flood escape, its intake has a design discharge of 400m^3/sec and a crest level of 8m.a.s.l, which is located at north of Al Am'arah Barrage. The river is extended from Tigris River towards AshShmasher dykes with a length of 3.4km, then its

direction is changed to the right along these dykes, and this part of river is known as AshShmasher channel, Al-Furat Center for studies and designs of irrigation projects, 1993.

Sa'ad River irrigation project area is about 90000Donams which is located between Al Msharah and Kmait Rivers. This project is served by a drain system in which the drain water is collected by a main collector draining called Sa'ad River irrigation project drain which is finally pumped at a rate of 11m^3/sec to the Kmait River and at a rate of 4 m^3/sec directly to AsSanna'f Marsh by another pump station.

The catchment area of AshShmasher surface runoff is 1300km^2, its surface runoff of about 600m^3/sec is discharge along AsSanna'f Marsh west dyke, between Ghzayla Bridge and AshShmasher dykes. The water passes this dyke through groups of pipes, Al-Furat Center for studies and designs of irrigation projects, 2003, General Directorate of Water Resources Management, Center of hydrology, 2004.

During rain season, water from AsSanna'f Marsh feeders starts to fill empty region of the marsh and the levels are increased gradually. Then water of this marsh is directed to Al Huwayza Marsh after it reaches a specified level.

Fig. 1. Layout of AsSanna'f Marsh and its feeders, *after CRIM 2006*.

AVAILABLE DATA

Some of the hydrological and topographical data required to carry out the flow routing through AsSanna'f Marsh were available at the CRIM, these data are presented in the following sections.

Topographical Data

A topographical survey of AsSanna'f Marsh area was carried out by CRIM, 2006. **Fig. 2** shows the topographical map of AsSanna'f Marsh.

Hydrological Data

The monthly Evapo-transpiration, evaporation and water used by plants, are essential factor in estimating the water losses. **Table 1** presents the calculated monthly Evapo-transpiration for Al Huwayza Marsh and was adopted in AsSanna'f Marsh hydrologic routing, Ministry of Water Resources, et. al. 2006.

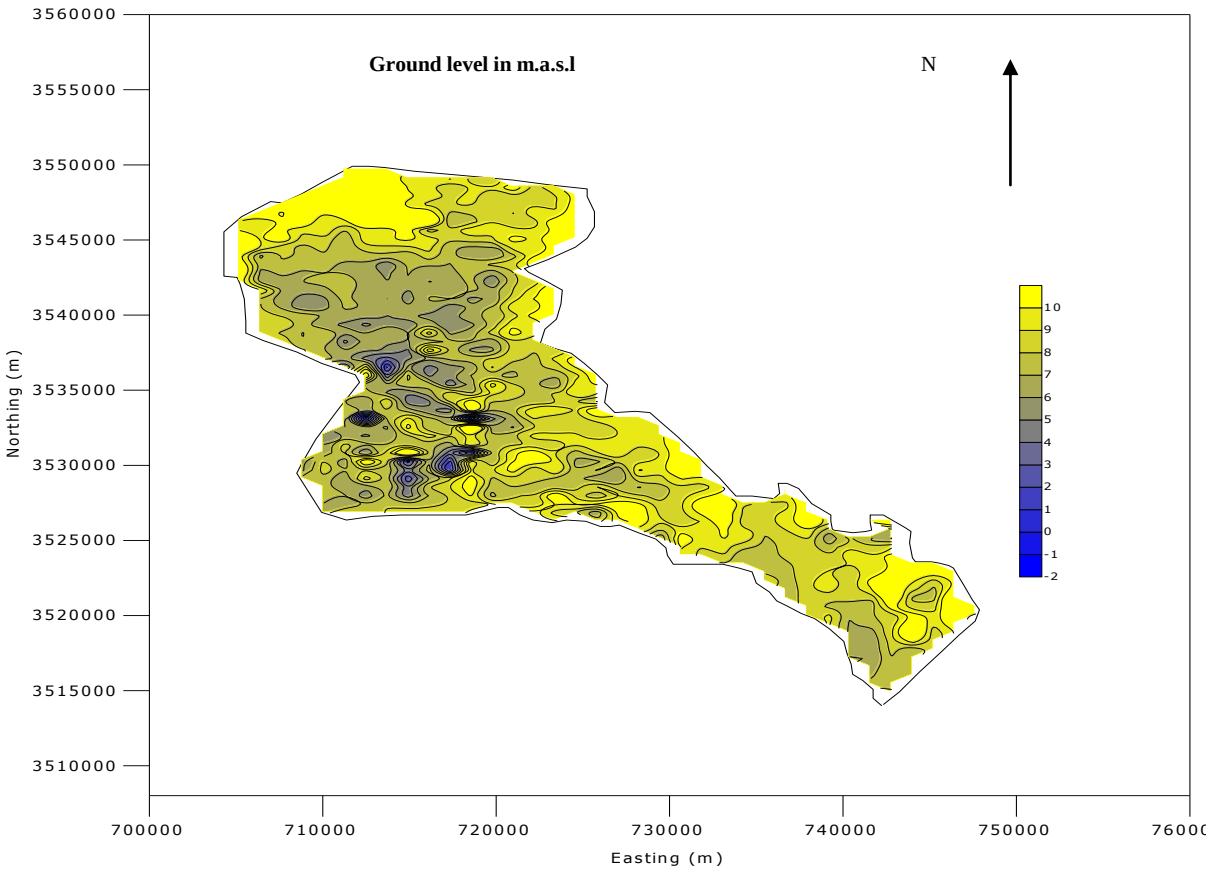

Fig. 2. Topographical map of AsSanna'f Marsh, *after CRIM 2006*.

Table 1. Monthly evapo-transpiration in Al Huwayza Marsh, ***after Ministry of Water resources et. Al. 2006.***

	Month												
	Jan.	Feb.	Mar.	Apr.	May	Jun.	Jul.	Aug.	Sep.	Oct.	Nov.	Dec.	Total
Evapo-transpiration mm/month	53.5	76.8	126.1	199.9	278.4	375.2	423.2	390.9	279.1	174.4	99.1	59	2536.3

Hydrological Field Measurements

Twelve discharge and stage measurements at four measurement stations, two measurements every month, were carried out during the period from January 2006 to July 2006 by the CRIM. These stations are shown in **Fig. 3.**

The discharge and stage measurements records in all stations are presented in **Table 2.** The recorded discharge at Kmait station is zero during the study period, since there is no inflow water from Kmait flood escape. The stage within this station is approximately constant and equal to 6m.a.s.l.

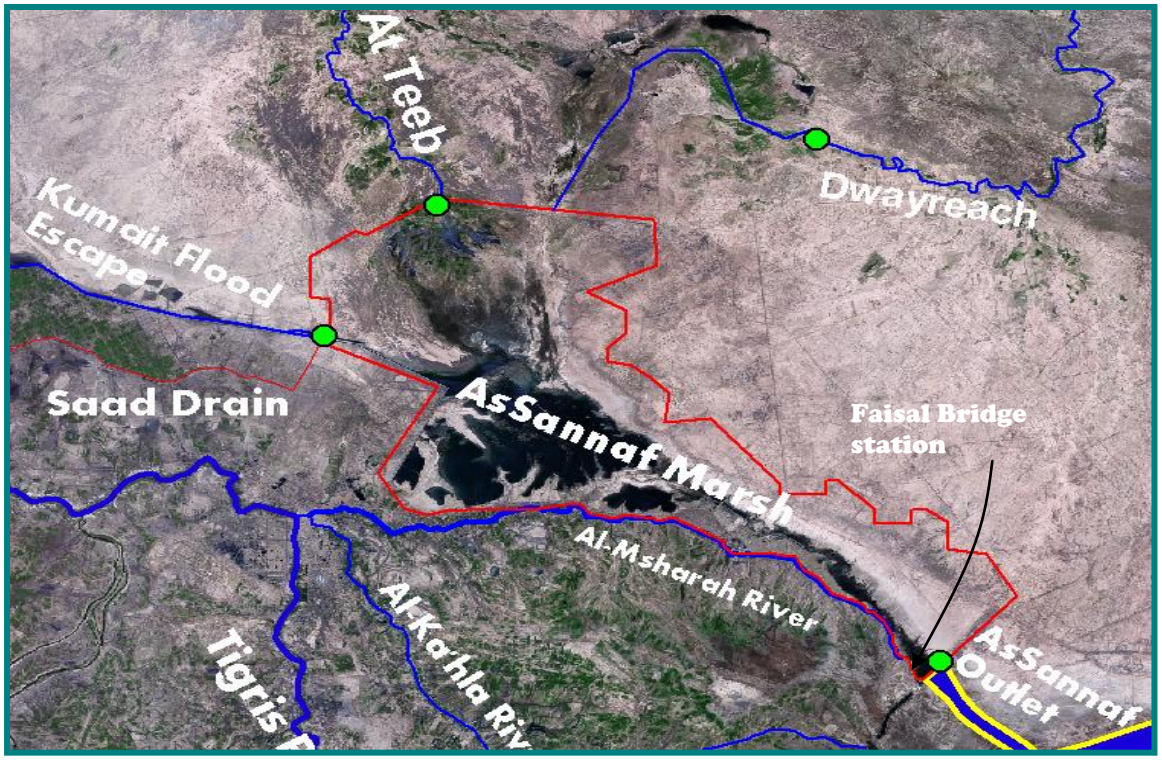

Fig. 3. Hydrological field measurements Stations.

Table 2. Measured discharge and stage at the measuring stations. ***After CRIM, 2006*****.**

Measurement date	Discharge Q ,m^3/sec- Stage m m.a.s.l.					
	Dwayreach Station		AtTeeb Station		Faisal Bridge station	
23/1/2005	202.00	21.90	154.00	17.40	210.00	7.64
08/2/2005	94.50	20.86	55.20	15.99	152.00	6.89
16/3/2005	0.18	18.75	1.55	13.44	94.80	6.14
30/3/2005	0.16	18.50	1.55	13.44	17.20	6.06
13/4/2005	0.15	18.75	1.40	14.19	3.55	6.16
27/4/2005	0.06	18.78	1.38	13.87	3.78	6.13
01/5/2005	0.06	18.82	1.31	13.78	9.48	6.17
25/05/2005	0.00	18.50	0.74	13.71	7.23	6.09
08/06/2005	0.00	18.50	0.51	13.69	6.07	6.09
22/06/2005	0.00	18.50	0.72	13.71	3.23	6.04
06/07/2005	0.00	18.50	0.74	13.71	0.00	5.64
20/07/2005	0.00	18.50	0.71	13.72	0.00	5.64

PREDICTED HYDROLOGICAL DATA

There is a lack of hydrological data of AsSanna'f Marsh feeders. The discharge hydrographs of these feeders have been estimated by utilizing the hydrological field

measurements during the period of the study. An accurate estimation of the surface runoff of AshShmasher catchment area is very difficult because of the absence of the accurate historical data and the interface between this runoff and the water of AtTeeb and Dwayreach Rivers before the entrance of this runoff into AsSanna'f Marsh. Prediction of AshShmasher catchment area surface runoff was carried out depending on the topographical and climatologically similarity. The catchment area of AtTeeb and Dwayreach Rivers lies within the same region of AshShmasher area and have approximately same conditions. By assuming a linear relation between catchment area and runoff, the surface runoff of AshShmasher area surface runoff hydrograph is approximated to be the runoff of AtTeeb and Dwayreach runoff multiplied by area ratio. The catchment area of AshShmasher area, AtTeeb, and Dwayreach Rivers are 1300, 2670, and 3270 km^2, respectively, General Directorate of Water Resources Management, Center of Hydrology, 2004, UNEP, January 2004

The average ratio of AshShmasher catchment area to AtTeeb River catchments area is (0.49), and Dwayreach River catchments area, (0.4), is 0.44. This ratio, 0.44, has been adopted as the ratio of AshShmasher area surface runoff from the average of AtTeeb and Dwayreach Rivers discharges. Predicted data of AshShmasher catchment area surface runoff is presented below in **Table 3**.

The discharges of AsSanna'f Marsh feeders, AtTeeb River, Dwayreach River and AshShmasher surface runoff, during the dry and wet years were estimated by making use of the measured discharges during the study period. These measured discharges have been considered as AsSanna'f Marsh feeders' discharges during a normal year.

Table 3. Predicted surface runoff (m^3/sec) of AshShmasher Catchments Area.

Months	Surface Runoff (m^3/sec)		
	AtTeeb River	Dwayreach River	AshShmasher Area
Oct.	0.73	0.00	0.16
Nov.	0.73	0.00	0.16
Dec.	0.73	0.00	0.16
Jan.	154.0	202.0	78.3
Feb.	55.2	94.5	32.9
Mar.	1.55	0.17	0.38
Apr.	1.39	0.11	0.33
May	1.03	0.03	0.23
Jun.	0.62	0.00	0.14
Jul.	0.73	0.00	0.16
Aug.	0.73	0.00	0.16
Sept.	0.73	0.00	0.16

The ratio of discharge of each feeder to AsSanna'f Marsh outflow, at Faisal bridge station, was calculated for normal year. The calculated ratios have been considered as the amount of share of each feeder from the marsh outflow for the dry and wet years. The predicted discharges of AsSanna'f Marsh feeders, AtTeeb River, Dwayreach River and AshShmasher catchment area surface runoff, during the dry, normal, and wet years are shown in **Figs. 4, 5 and 6.**

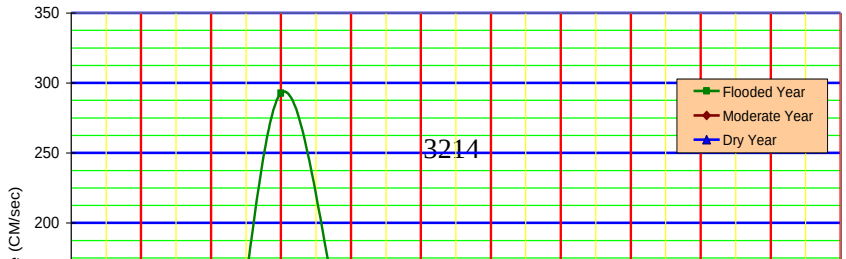

Fig.4. Averaged monthly flow of AtTeeb River averaged.

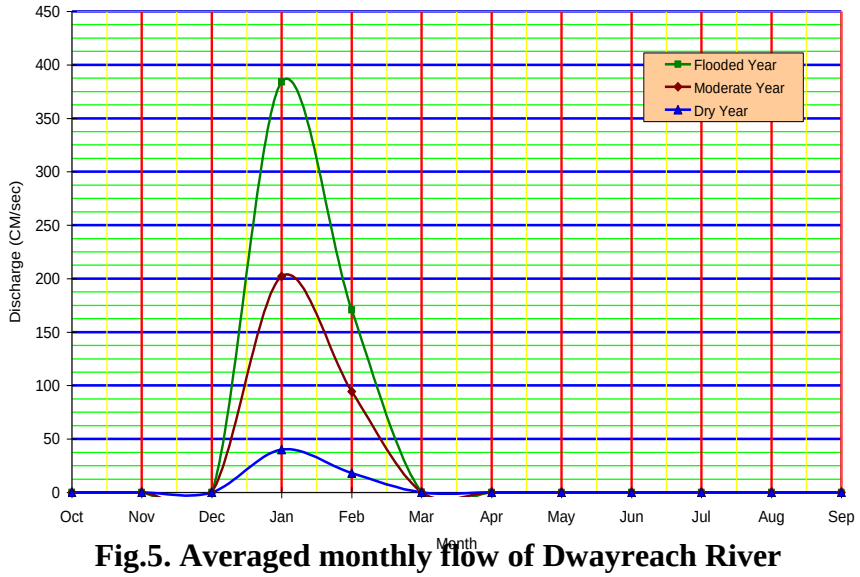

Fig.5. Averaged monthly flow of Dwayreach River

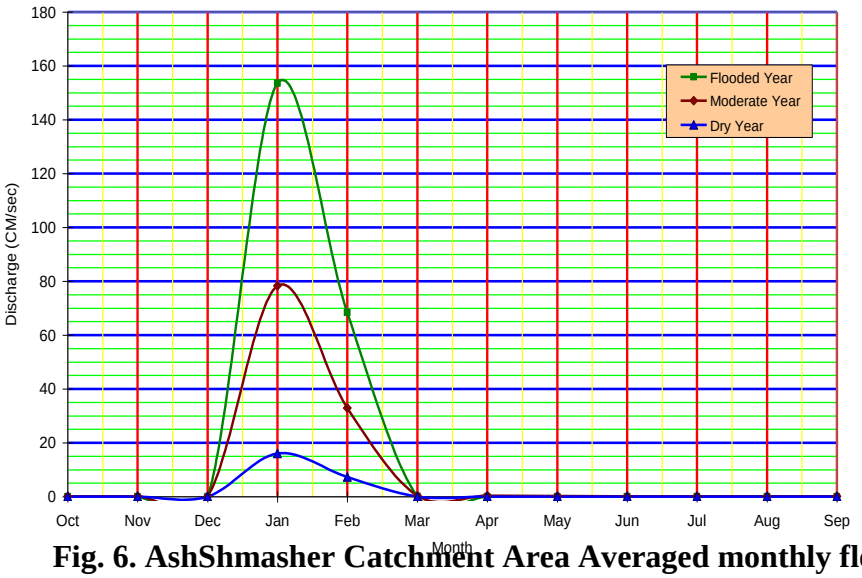

Fig. 6. AshShmasher Catchment Area Averaged monthly flow.

STORAGE CAPACITY RELATION

AsSanna'f Marsh extension is decided depending on the actual height of the marsh dykes. The minimum dykes level is about 9 m.a.s.l at the south boundary of the marsh near Al Msharah River. Therefore, the marsh boundary is the within the contour of 9 m.a.s.l. if 1m is considered as a free board, then the maximum allowable water level within the marsh is 8m.a.s.l.

The area and storage elevation curves were computed for two different cases satisfying the existing behavior of the water flowing through the marsh. The first case, when there is inflow and no outflow from the marsh toward Al Huwayza Marsh, or there is no inflow and there is outflow from the marsh or there is no inflow and no outflow. This case occurs when the marsh is starting store water or when the feeders are depleted at the end of the rainy season. In this case the water level within AsSanna'f Marsh is approximately horizontal and the Arc-View GIS software is used to evaluate the area elevation and storage elevation relations.

The second case, when the water level near AsSanna'f Marsh outlet is higher than the 5.65 m.a.s.l, i.e. water is discharged from this marsh towards Al Huwayza Marsh with the existing of upstream feeding. In this case the marsh is treated as a river basin and the water level along the marsh will not be a horizontal. Since the marsh width is not constant a long its length, the water surface elevation will have significant variation along the marsh length. This variation in water levels increases the surface area and storage in the upstream part of this marsh.

A one dimensional steady hydraulic model was developed using the HEC-RAS software in order to estimate the surface area and the storage within the marsh. Development of this model required implementation of the geometrical and hydraulic data. ARC-View GIS Software with DEM of AsSanna'f Marsh is used in the construction of the geometrical data. Layout of the implemented cross sections is shown in **Fig. 7.**

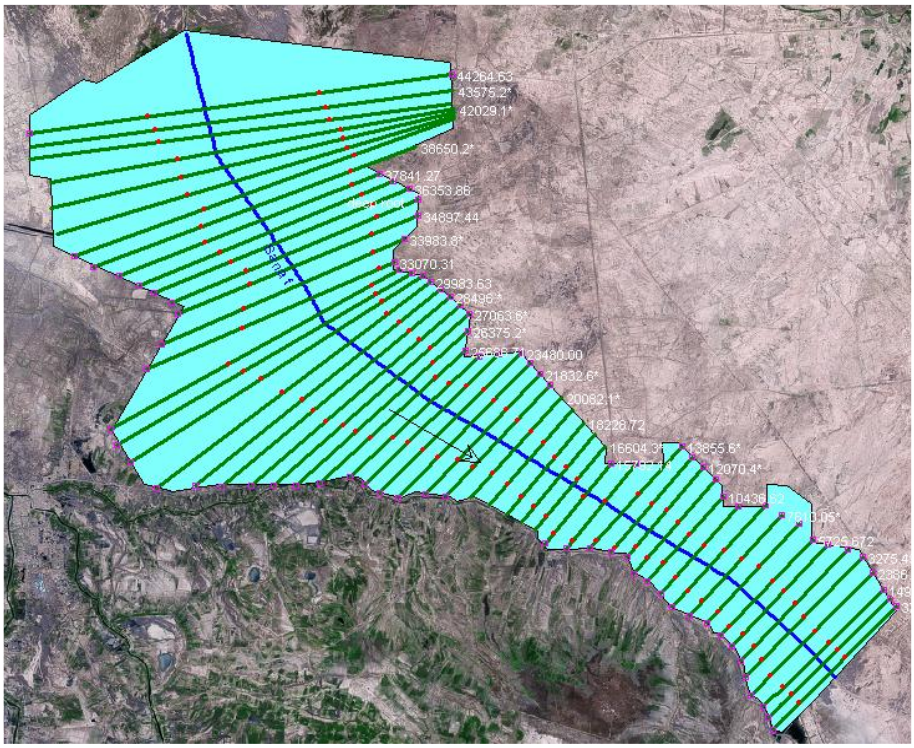

Fig.7. Implemented cross sections along AsSanna'f Marsh.

The upstream boundary condition is a known range of flow rates while the downstream boundary condition is rating curve, according to the filed measurements at Faisal Station during the study period. According to each computed water level, the surface area and storage are evaluated from the developed model. The constructed area-elevation and storage–elevation curves

for the two cases are shown in **Fig. 8** and **9**. The constructed area-elevation curves and storage elevation curves for the flow conditions are based on the water elevation at location of Faisal station. The maximum surface area of AsSanna'f Marsh with 8m.a.s.l is 360 km^2 with storage capacity of 750 million m3. It is to be noticed that, the dykes surrounding the marsh are equal or higher than 9m.a.s.l.

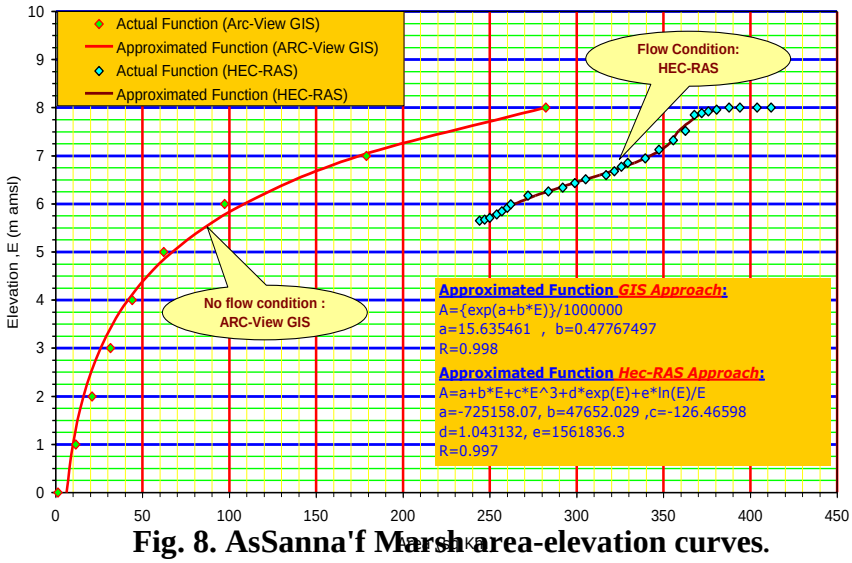

Fig. 8. AsSanna'f Marsh area-elevation curves.

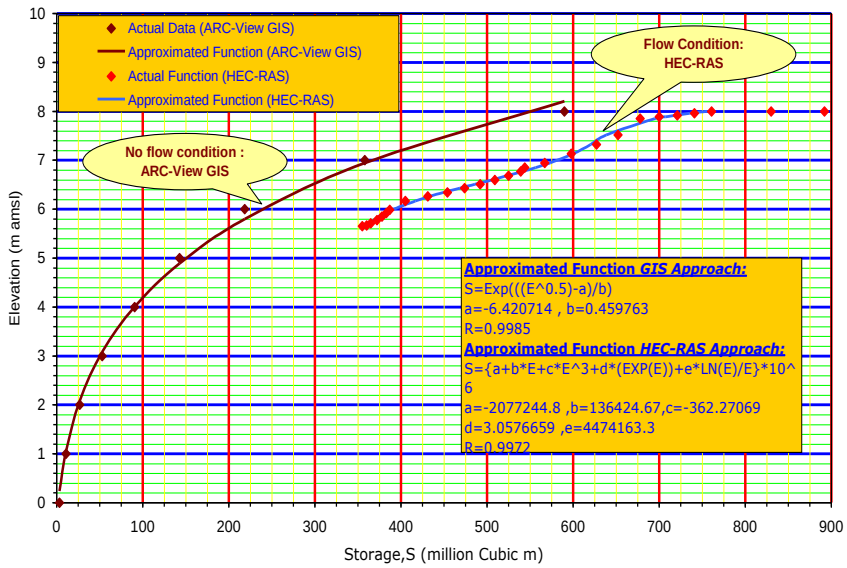

Fig. 9. AsSanna'f Marsh storage-elevation curves.

HYDROLOGICAL ROUTING

There is some uncertainty in the flow routing of AsSanna'f Marsh arising from its behavior and the lack of infiltration losses data within the marsh. To take these two points into account, the following methodology was adopted in the hydrological study. A hydrological routing for normal year is presented by the period of this study using the twelve measured discharges that were carried out at all feeders and outlet of the marsh and comparing of the resulting storage within the marsh with the existing storage according to the recorded stages at Faisal station. The effect of the infiltration losses is considered as a part of the required storage in the first period of storing water, when there is inflow and no outflow from the marsh. These infiltration losses are considered with the calibration of the model.

The implementation of the hydrologic routing model for calibration purposes depends on the inflow into AsSanna'f Marsh, measured at: AtTeeb, Dwayreach, and Kmait hydrological measuring stations, the outflow, measured Faisal bridge hydrological measuring station, the area – elevation curves, storage –elevation curves, and evapo-transpiration of the study area. It was noted, during the period of the study that there is no inflow towards AsSanna'f Marsh from the Kmait Flood Escape at Kmait station. The recorded water levels at Kmait station is approximately constant and is about 6m.a.s.l. The outflow form AsSanna'f Marsh was measured at Faisal Bridge station. These data were used as an input for the hydraulic mathematical model to verify the flow and obtain the relation between the inflow and out flow with the water level elevation, storage and losses within the marsh. The resulting marsh storage for normal year is shown in **Fig. 10.**

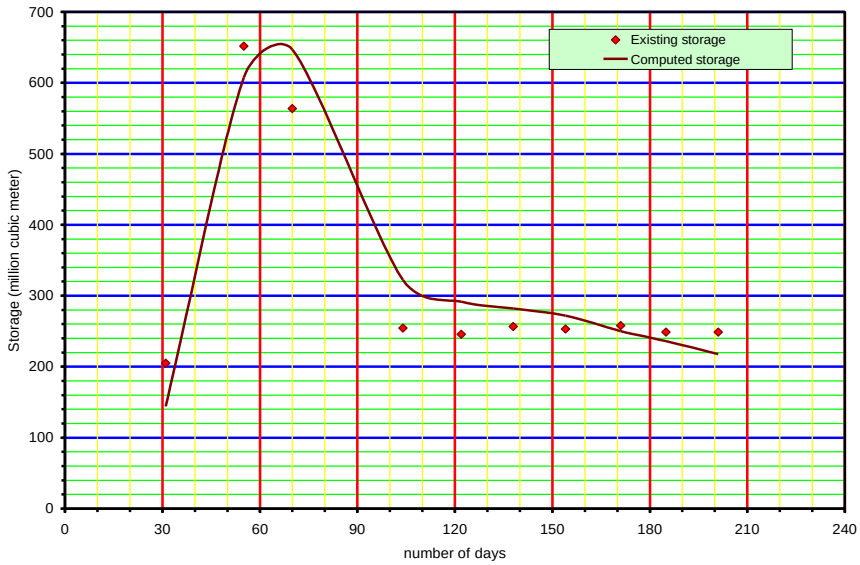

Fig.10. Computed and existing storage within AsSanna'f Marsh during January to October, 2006.

Additional important results from the hydrological routing are the total volume of inflow, outflow and the losses within the marsh are 11012.10, 8810.67 and 2201.43 million m^3 respectively. The evaporation and infiltration losses within the marsh are about 21% from the total inflow. All above results are considered for normal years only

Due to the lack of data records concerning the wet and dry years, the constructed stage-outflow curve for normal year, **Fig. 11**, (it is constructed according to the existing field measurements) will be adopted in the implementation of the hydrological routing for the two situations.

Hydrological Routing During Wet and Dry Years

Two individual hydrological routing were made for wet and dry years, to predict the storage, outflow, and the water levels within the marsh. AsSanna'f Marsh starts its depletion at the end of the rain season and starts its restoration in sequent new rain season. So, this marsh starts its hydrological cycle as a dry marsh. The main limitations that are considered in the construction of the hydrological routing are:

- The maximum storage within the marsh is considered with water level of 8 m, dykes are considered to be at 9 m.a.s.l. The surrounding dykes must be raised to the safe height and new area-elevation and storage elevation curves must be achieved when levels are higher than 8 m.a.s.l.
- The minimum water level is 5.65m.a.s.l, which is the ground level at AsSanna'f Marsh outlet.

- The wet year data of all feeders and the required outflow are considered as detailed in **Table 4**.

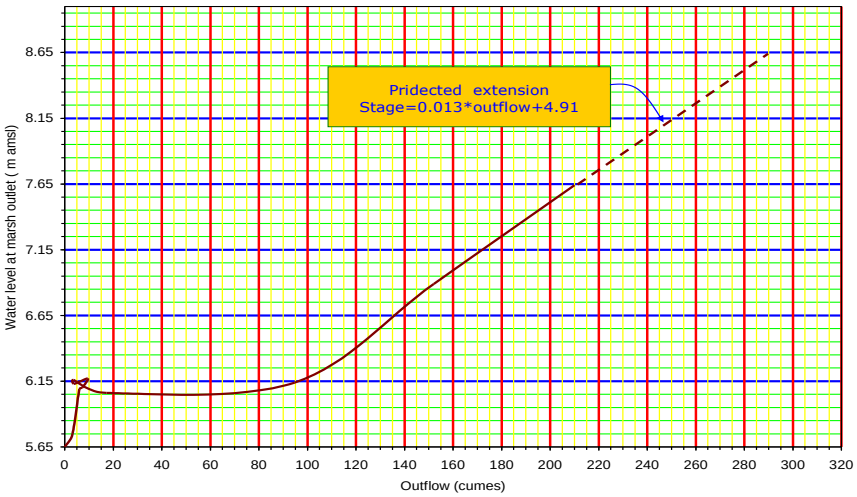

Fig. 11. AsSanna'f Marsh outflow-stage curve.

Table 4. Monthly discharge, m^3/sec, into AsSanna'f Marsh from all feeders during wet years.

Month	Feeder				Total Outflow[b]	The required Outflow[c]
	AshShmasher Run off [a]	Dwayreach River[a]	AtTeeb River[a]	Total Inflow		
Oct.	0	0	1	1	0	0
Nov.	0	0	1	1	0	0
Dec.	0	0	1	1	0	0
Jan.	154	384	293	831	388	264
Feb.	68	171	100	339	367	170
Mar.	0	0	2	2	240	33
Apr.	0	0	2	2	103	33
May	0	0	1	1	67	8
Jun.	0	0	1	1	0	6
Jul.	0	0	1	1	0	0
Aug.	0	0	1	1	0	0
Sept.	0	0	1	1	0	0

a:predicted **b:**hydrologic routing **c:** CRIM, 2006.

According to the hydrological routing and the predicted outflow from the marsh the maximum water level within the marsh reaches 10.15m.a.s.l during January at Faisal bridge station.. The stored water, the surface area and water level variations during the flood season are shown in **Figs. 12, 13** and **14** are respectively.

The dykes of AsSanna'f Marsh must be at least 11m.a.s.l surrounding the marsh especially at the south east boundary of the marsh near Al Msharah River. The maximum expected outflow into Al Huwayza Marsh is 388m^3/sec. Additional routing is needed for Al Huwayza Marsh during flooded year, since the required inflow from this feeder into Al Huwayza Marsh is 264m3/sec at January. The capacity of Al Huwayza Marsh and its outlet designed structures must be able to carry the surplus inflow of 124m^3/sec**,** CRIM, 2006. When the dykes surrounding AsSanna'f Marsh become equal to (or higher than) 11 m.a.s.l, the maximum storage and surface area of the marsh will be 1480 million m^3 and 426km^2, respectively.

The maximum allowable inflow into Al Huwayza Marsh from AsSanna'f Marsh for flooded year is listed in **Table 5**. The Kmait flood escape structure must be a gated control structure with maximum capacity of 250m^3/sec.This control structure must be operated according to the maximum allowable inflow from Kmait Escape**.**

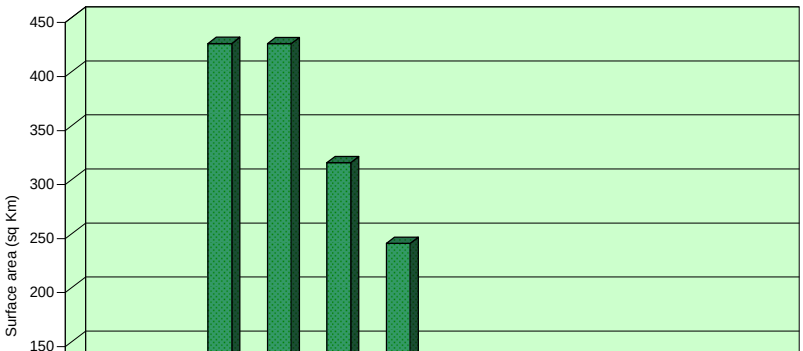

Table 5. Maximum allowable inflow into Al Huwayza Marsh from its feeders during wet year with Al Huwayza Marsh outlets is

Fig.12. The Surface area variation within AsSanna'f Marsh.

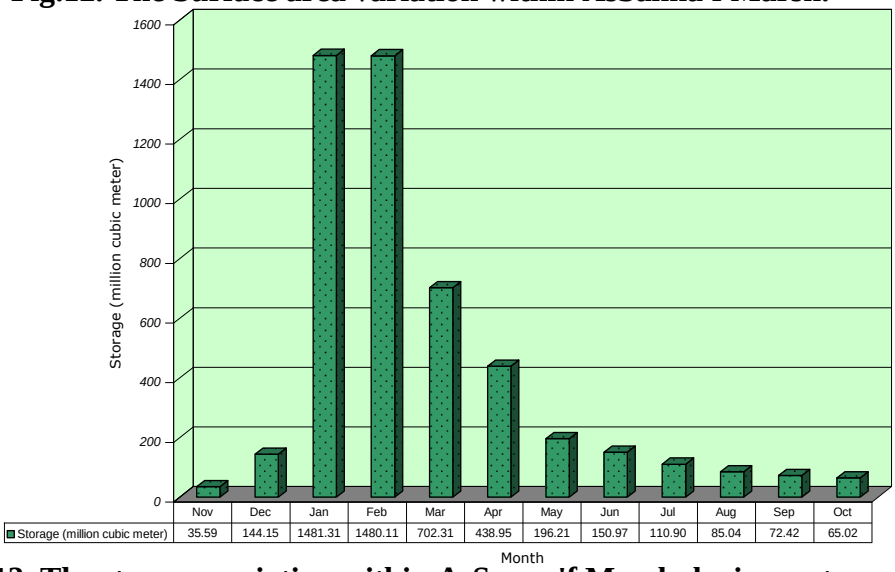

Fig. 13. The storage variation within AsSanna'f Marsh during wet year.

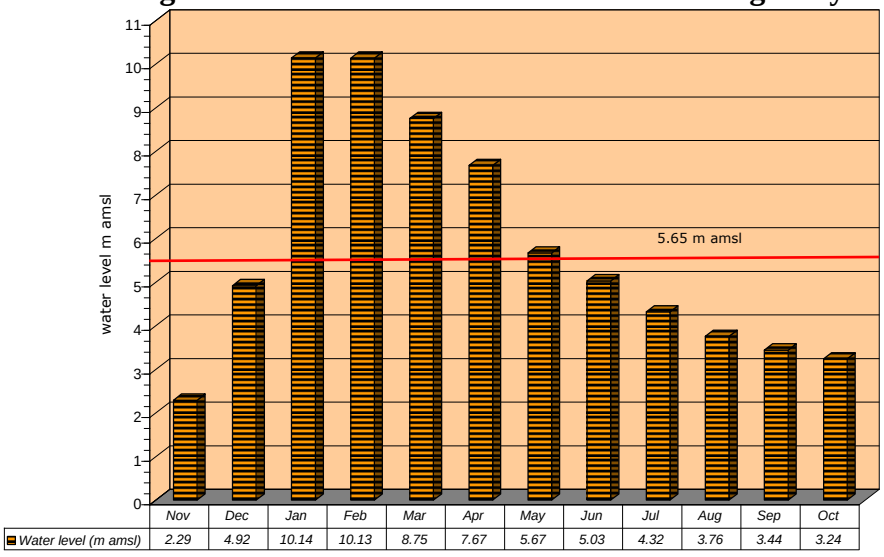

Fig.14. Water level variation within AsSanna'f Marsh during wet year.

e maximum allowable inflows from Kmait flood escape were 181 m^3/sec, 111 m^3/sec, 95m^3/sec, 230 m^3/sec and 177 at Jan., Feb., Mar., Apr. and May, respectively. While the design capacity of this escape is 400m^3/sec. According to the hydrological routing of AsSanna'f

Month	Max. allowable inflow into Al Huwayza Marsh	The total required inflow Into Al Huwayza Marsh	Max. surplus inflow into Al Huwayza Marsh	Available inflow from AsSanna'f Marsh	Required inflow from AsSanna'f Marsh	Surplus inflow from AsSanna'f Marsh	Max. allowable inflow From Kmait Escape	Max allowable inflow from AsSanna'f Marsh
Oct.	459	144	315	0	0	0	315 = 250	315
Nov.	528	218	310	0	0	0	310= 250	310
Dec.	519	209	310	0	0	0	310= 250	310
Jan.	799	494	305	388	264	124	181	388*
Feb.	755	447	308	367	170	197	111	388 *
Mar.	751	449	302	240	33	207	95	335
Apr.	850	550	300	103	33	70	230	333
May	608	372	236	67	8	59	177	244
Jun.	311	206	105	0	6	-6	111	335
Jul.	249	144	105	0	0	0	105	333
Aug.	357	132	225	0	0	0	225	244
Sept.	445	130	315	0	0	0	315= 250	335

There is no flood risk, so the maximum allowable discharge must be limited by the proposed Kmait escape control structure maximum capacity , 250 m^3/sec.

*** Maximum capacity of AsSanna'f Marsh outfall.**

Marsh, refer to **Table 4,** the outflow of AsSanna'f Marsh into Al Huwayza Marsh will 388m^3/sec, 367m^3/sec, 240m^3/sec, 103m^3/sec, and 67m^3/sec during Jan., Feb., Mar., Apr. and May respectively. An additional safe inflow from Kmait Escape can be discharged into Al Huwayza Marsh through AsSanna'f Marsh considering the maximum capacity of AsSanna'f Marsh outlet. The maximum safe additional inflow from Kmait escape is 223m^3/sec which occurred at May.

According to the hydrological routing of Al Huwayza Marsh, CRIM, 2006, the designed discharges of Al Huwayza Marsh outlets control structures must be increased to 550m^3/sec in order to safely discharges this surplus inflow into Tigris river and Shat Al Arab River, the client recommendation for the maximum capacity of Al Huwayza Marsh outlets is 325m^3/sec, The New Eden group, 2005. The design capacity of the Al Huwayza Marsh outlets must be 200m^3/sec of Al Kassara River and 350m^3/sec of AsSuwayb River hydraulic structures. The maximum allowable inflow into Al Huwayza Marsh from AsSanna'f Marsh for flooded year is listed in **Table 6.** The Kmait flood escape structure must be a gated control structure of 400m^3/sec maximum capacity. This control structure must be operated according to the maximum allowable inflow from Kmait escape, **Table 6.**

The dry year data of all feeders are considered as detailed in **Table 7**.The required outflow into Al Huwayza marsh routing is considered to be zero as a worst case, refer to CRIM, 2006**,** for more details.

The results of the hydrological routing were based on the achieved routing in the normal year and the related relations. The maximum water level at Faisal station will be 6.44 m.a.s.l with storage and surface area of 289.8 million m^3 and 133.7 km^2, respectively. The outflow is predicted by trail and error process where, the main constrain is the water level at Faisal bridge station and the losses within the marsh. The monthly variation in storage, surface area and water levels are shown in **Figs. 15, 16** and **17** respectively. According to the hydrological routing and the predicted outflow from the marsh that is listed in **Table 7**.

Table 6. The maximum allowable inflow into Al Huwayza Marsh from its feeders for wetyear with Al Huwayza Marsh outlets is

Month	Max. allowable inflow into Al Huwayza Marsh	The total required inflow Into Al Huwayza Marsh	Max. surplus inflow into Al Huwayza Marsh	Available inflow from AsSanna'f Marsh	Required inflow from AsSanna'f Marsh	Surplus inflow from AsSanna'f Marsh	Max. allowable inflow from Kmait escape	Max allowable inflow from AsSanna'f Marsh
Oct.	684	144	540	0	0	0	400	388*
Nov.	741	218	535	0	0	0	400	388*
Dec.	743	209	535	0	0	0	400	388*
Jan.	1024	494	530	388	264	124	264	388*
Feb.	980	447	530	367	170	197	191	388*
Mar.	973	449	530	240	33	207	181	388*
Apr.	1078	550	525	103	33	70	318	388*
May	834	372	461	67	8	59	329	388*
Jun.	536	206	330	0	6	-6	336	336
Jul.	473	144	330	0	0	0	330	330
Aug.	582	132	450	0	0	0	400	402*
Sept.	670	130	540	0	0	0	400	402*

Table 7. Monthly feeders discharges, m^3/sec, into AsSanna'f Marsh during dry years.

Month	AshShmasher Run off [1]	Dwayreach River[1]	AtTeeb River[1]	Total Inflow	Total Outflow[2]	Required Outflow[3]
Oct.	0	0	1	1	0	0
Nov.	0	0	1	1	0	0
Dec.	0	0	1	1	0	0
Jan.	16	40	31	87	0	0
Feb.	7	18	11	36	13	13
Mar.	0	0	1	1	28	28
Apr.	0	0	1	1	0	0
May	0	0	1	1	0	0
Jun.	0	0	0	0	0	0
Jul.	0	0	1	1	0	0
Aug.	0	0	1	1	0	0
Sept.	0	0	1	1	0	0

1: Predicted, 2:Resulting from the hydrological routing, 3: CRIM, 2006.

*** Maximum capacity of AsSanna'f Marsh outfall.**

The stored water, the surface area and water level variations in the marsh during the rainy months are shown in **Figs. 18,19** and **20**, respectively.

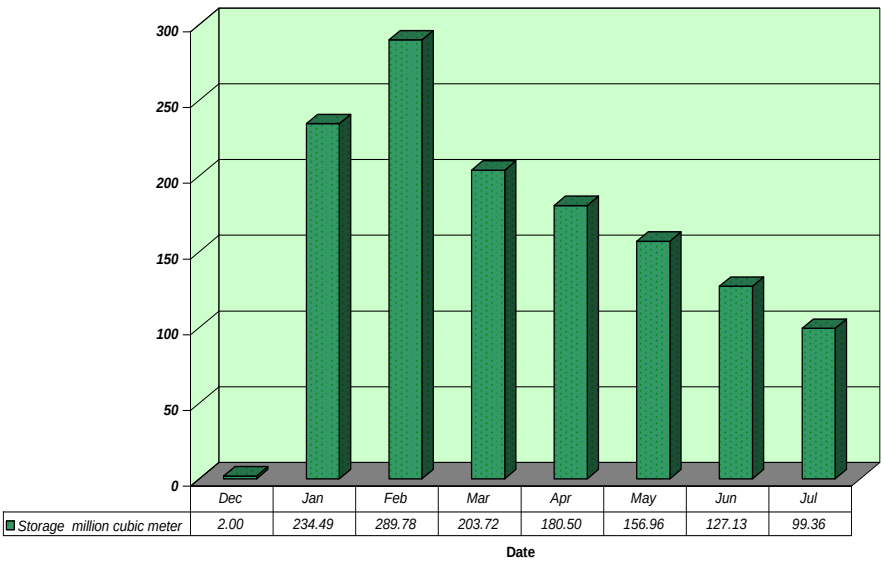

Fig. 15. Storage variation within AsSanna'f Marsh.

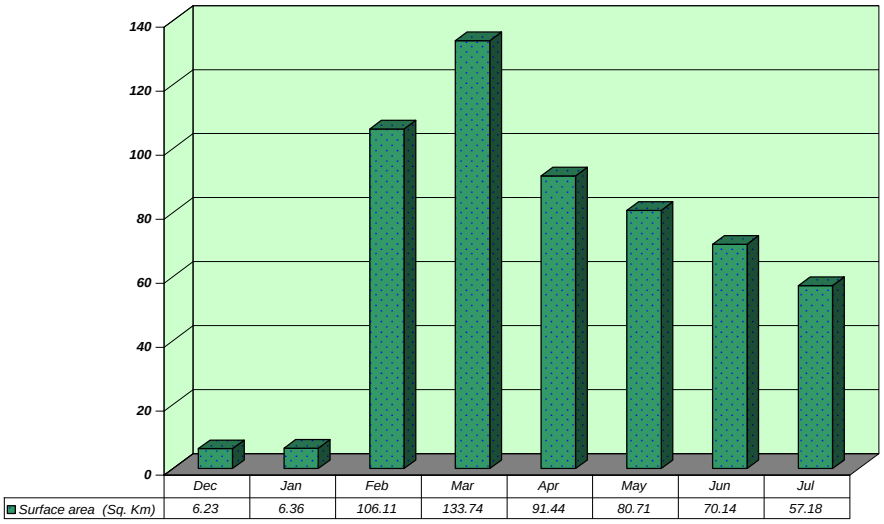

Fig. 16. AsSanna'f Marsh surface area variation during dry year.

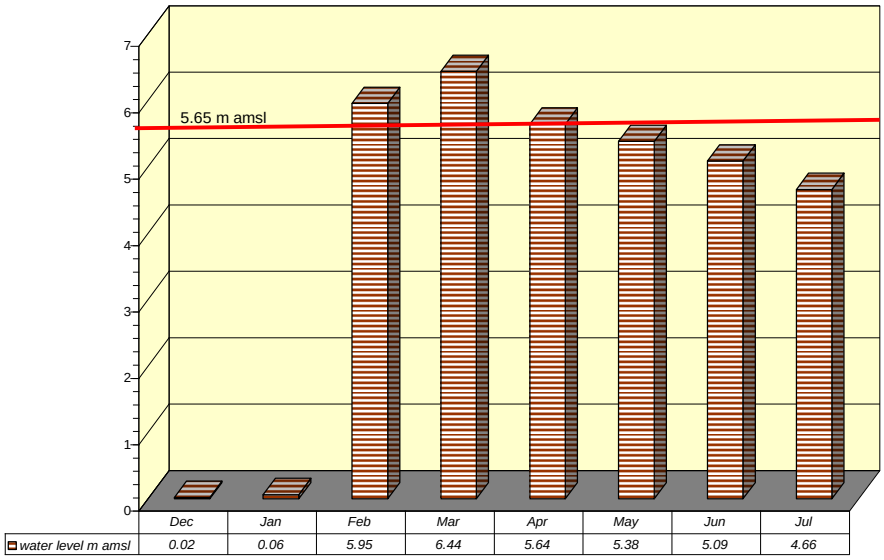

Fig. 17. AsSanna'f Marsh water level variation during dry year.

Water levels within AsSanna'f Marsh

The water levels within AsSanna'f Marsh are affected by the fluctuations of the water levels within Al Huwayza Marsh. if Al Huwayza Marsh water levels or AsSanna'f Marsh water level were higher than 5.65m, AsSanna'f Marsh outlet bed level, there will be an interface between these marshes. When the amount of flow from AsSanna'f toward Al Huwayza Marsh will be varied according to the head difference and type of flow, free or submerged. Comparison of Al

Huwayza Marsh water levels which computed in the hydrological routing of this marsh, CRIM, 2006, with AsSanna'f Marsh water levels which computed in the hydrological routing of this marsh show that Al Huwayza Marsh water levels are higher than that of AsSanna'f Marsh and AsSanna'f Marsh outlet bed level during the period from March to September for flooded and moderate years, as shown in **Figs. 18** and **19**. The flow rates due to the head difference are estimated according to the suitable open channel hydraulic formula. These flow rates are shown in **Table 8**. The yearly stored water in AsSanna'f Mash according to the estimated inflow is 1118 million m^3 and 680 million m^3 for flooded and moderate years respectively.

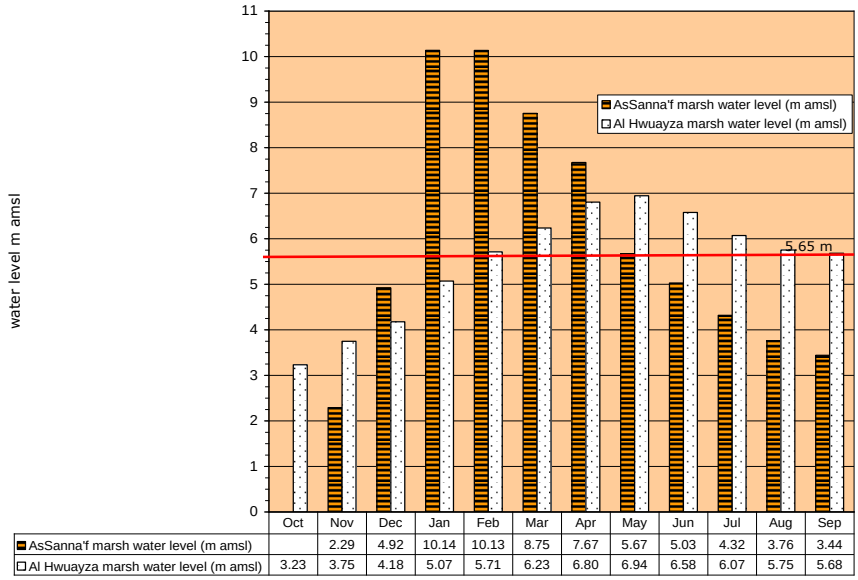

Fig. 18. Al Huwayza Marsh and AsSanna'f Marsh water levels during wet year.

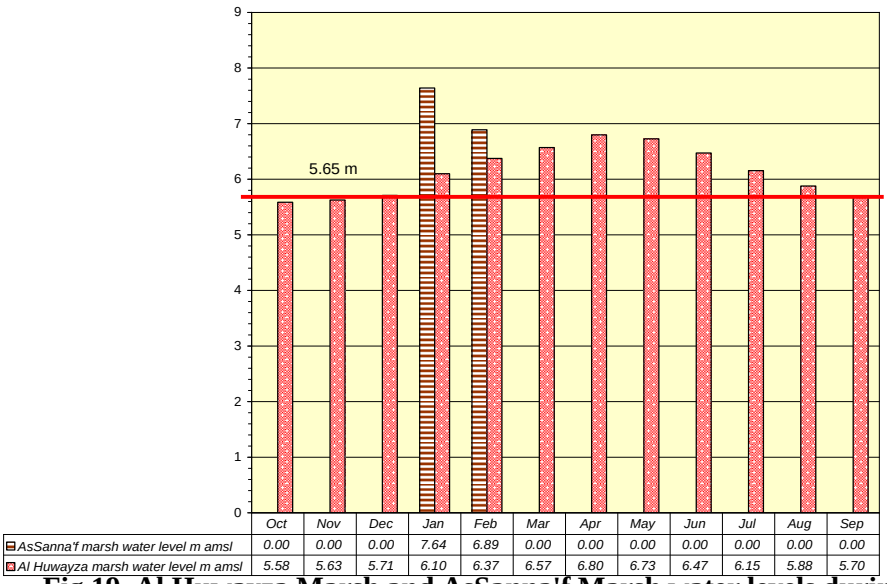

Fig.19. Al Huwayza Marsh and AsSanna'f Marsh water levels during normalyear.

Table 8. Al Huwayza Marsh flow, m^3/sec, into AsSanna'f Marsh during wet and normal years.

Month	Oct	Nov	Dec	Jan	Feb	Mar	Apr	May	Jun	Jul	Aug	Sep
Wet year	0	0	0	0	0	44.2	122.7	145.4	88.3	27.0	3.3	0.5
Normal year	0	0	0	0	0	53.6	87.0	76.7	44.1	0.6	0.2	0

These storages represent about 149 % from the maximum allowable storage of AsSanna'f Marsh when the minimum dykes level is 8 m.a.s.l, so AsSanna'f Marsh will be flooded due to this rate, and 91 % from the maximum allowable storage of AsSanna'f Marsh when the minimum dykes level is 8 m.a.s.l, so AsSanna'f Marsh will be flooded in the next year due to inflow of AtTeeb and Dwayreach rivers to AsSanna'f Marsh. While, these storages represent about 76 % and 46 % from the maximum allowable storage of AsSanna'f Marsh when the minimum dyke's level is raised to 11m.a.s.l, so AsSanna'f Marsh will be flooded in the next year due to inflow of AtTeeb and Dwayreach rivers to AsSanna'f Marsh. According to the above conclusions, a control structure at Faisal bridge station must be constructed at AsSanna'f Marsh outlet to satisfy the positive operation of AsSanna'f Marsh. The design discharge of the suggested control structure is 425m^3/sec with the spillway crest level of 7m.a.s.l. This control structure must be operated according to **Table 9**.

Table 9. Operation of the proposed control structure at AsSanna'f Marsh outlet.

Month	Oct	Nov	Dec	Jan	Feb	Mar	Apr	May	Jun	Jul	Aug	Sep
Flood year												
Moderate year												

Fully opened , **Fully closed**

CONCLUSIONS

1- The dykes surrounding the marsh must be at 11 m.a.s.l.
2- Ghzayla Bridge width must be increased 30m in order to develop its discharge capacity.
3- A control structure at Faisal bridge station must be constructed at AsSanna'f Marsh outlet to satisfy the positive operation of AsSanna'f Marsh. The design discharge of the suggested control structure is 425m^3/sec with the spillway crest level of 7m.a.s.l. This control structure must be operated according to **Table 9.**
4- In order to use Kmait flood escape during the flooded years to discharge 400m^3/sec into Al Huwayza Marsh through AsSanna'f Marsh, the design capacity of Al Huwayza Marsh outlets hydraulic structures must be: 200m^3/sec of Al Kassara River and 350m^3/sec of AsSuwayb River and Kmait flood escape structure must be a gated control structure with maximum capacity of 400m^3/sec and the operation of this escape must be based on **Table 6**.
5- The suggested maximum design discharges of Al Huwayza Marsh outlets, 550 m^3/sec may not be adopted if a new gated hydraulic structure is a accomplished at Kmait Flood Escape inlet with maximum discharge of 250 m^3/sec instead of that of 400 m^3/sec. The operation of this escape must be satisfying the maximum allowable inflow into Al Huwayza Marsh, **Table 5**.

RECOMMENDATIONS

- The hydrological system of AsSanna'f Marsh requires continuous observations on all its feeders using the existing hydrological stations. Extensive reading is required during rain season.
- The expected outflow from the marsh into Al Huwayza Marsh during flooded and dry years must be calibrated with observation data of more than 6 years.
- Studying the morphological changes within AsSanna'f Marsh area resulting from the sediment transportation from its feeders.
- Studying the ability of controlling AtTeeb and Dwayreach flow discharges into AsSanna'f Marsh.

REFERENCES

- Ministry of Water Resources, Al-Furat Center for studies and designs of irrigation projects, 2003, *Restoration of southern Iraqi Marshlands*, (in Arabic).

- Ministry of Water Resources, General Directorate of Water Resources Management, Center of hydrology, 2004, *Border Rivers between Iraq and Iran*, Translated from Arabic.

- Ministry of Water Resources, Al-Furat Center for studies and designs of irrigation projects, 1993, *Kmait Flood Escape project*, Translated from Arabic

- Ministry of Water Resources, Center of Restoration of the Iraq Marshlands, CRIM, 2006, *Study The Rehabilitation of Al Huwayza Marsh Ecological Syste.*.

- Ministry of Water Resources, Ministry of Environment , Ministry of Municipalities, and Public Works which Prepared in cooperation with the Italian Ministry for the environment and Territory and the Free Iraq Foundation, 2006, NEW *EDEN Master Plan for Integrated Water Resources Management in the Marshlands area.*

- UNEP, January 2004, *Azadegan Environmental Baseline Study*, Iran.

- The New Eden group, 2005, *Design Criteria for Optimum Regulation of Haweizhe Marshes*.

OPTIMAM SHAPE OF TAPERED COLUMNS UNDER AXIAL COMPRESSIVE FORCE

Wisam Victor Yousif, PhD.
Structural lecturer, Water recourses Department-University of Baghdad, Iraq
Ehab Nabil Issa, Bch.
Civil Engineer, Baghdad University Graduated
Rasha Atwan Faraj, Bch.
Civil Engineer, Baghdad University Graduated

ABSTRACT:

The continuous and rapid development of shapes for architectural members and structural researches development in stability field encourage the designers and researchers to study the effect of member shape on the load capacity. The optimum strength of compression members with economical dimensions can be obtained to satisfy the architectural and technical requirements. A different nonlinear tapered member shapes have been studied under compression axial force with simply supported end conditions. Then graphical comparisons for different member shapes are presented to find the maximum axial force and minimum member volume at buckling state. This study is based on modified stability functions that have been based on Bessel functions. The results of this study provide structural and architectural designers the most proper member's shape, with more economical dimensions to carry the design load.

ألخلاصه:

إن التطور المتزايد و المستمر في الشكل المعماري للعتبات الإنشائية و كذلك تطور البحوث في ميدان الاستقرارية حث الباحثين والمصممين على دراسة الشكل المعماري وتأثيره على قابلية تحمل العتبات للاحمال المحورية لايجاد التحمل الاقصى لهذه العتبات والذي يحقق الجانب الاقتصادي في نفس الوقت مع توفر كافة المتطلبات المعمارية والفنية. وتم في هذه الدراسة تقديم انواع من العتبات متساوية الطول والحجم ومختلفة من حيث تخصر الشكل متضمنة التخصر المقعر والمحدب والخطي وهي نماذج العتبات التي تم دراستها تحت تأثير الأحمال المحورية ومسندة إسنادا بسيطا. ثم تم عرض منحنيات للمقارنة بين العتبات المختلفة توضح أقصى قوة محورية يمكن إن تحمّل واقل حجم مطلوب لهذه العتبات قبل حصول فشل الانبعاج.ان هذه الدراسة تمت بالاعتماد على دوال الاستقرارية المحدثة والتي تم اشتقاقها في البحوث السابقة وهذه الدوال تستند على الدوال الرياضية التي تدعى دوال بسل ذات النوع الأول من الدرجة n. أن نتائج هذه الدراسة تمكّن أي مصمم إنشائي أو معماري على اختيار العتبات ذات الشكل المناسب والإبعاد الأكثر اقتصادية وتحقق في نفس الوقت قدرة هذه العتبات على تحمل الحمل التخميني المطلوب.

KEY WORDS:

Stability function, Non-linearity shape, Tapered member, Bessel function, Concave, Convex and Axial load.

INTRODUCTION:

The model of this study is a tapered member in both dimensions. The section depth and width along the member length producing the linearly or non-linearly tapered member is shown in **Fig. (1)**. This model is subjected to compression axial force. Increasing the section dimensions will

enhance the strength of the individual structural members and enhance the whole structure load capacity.

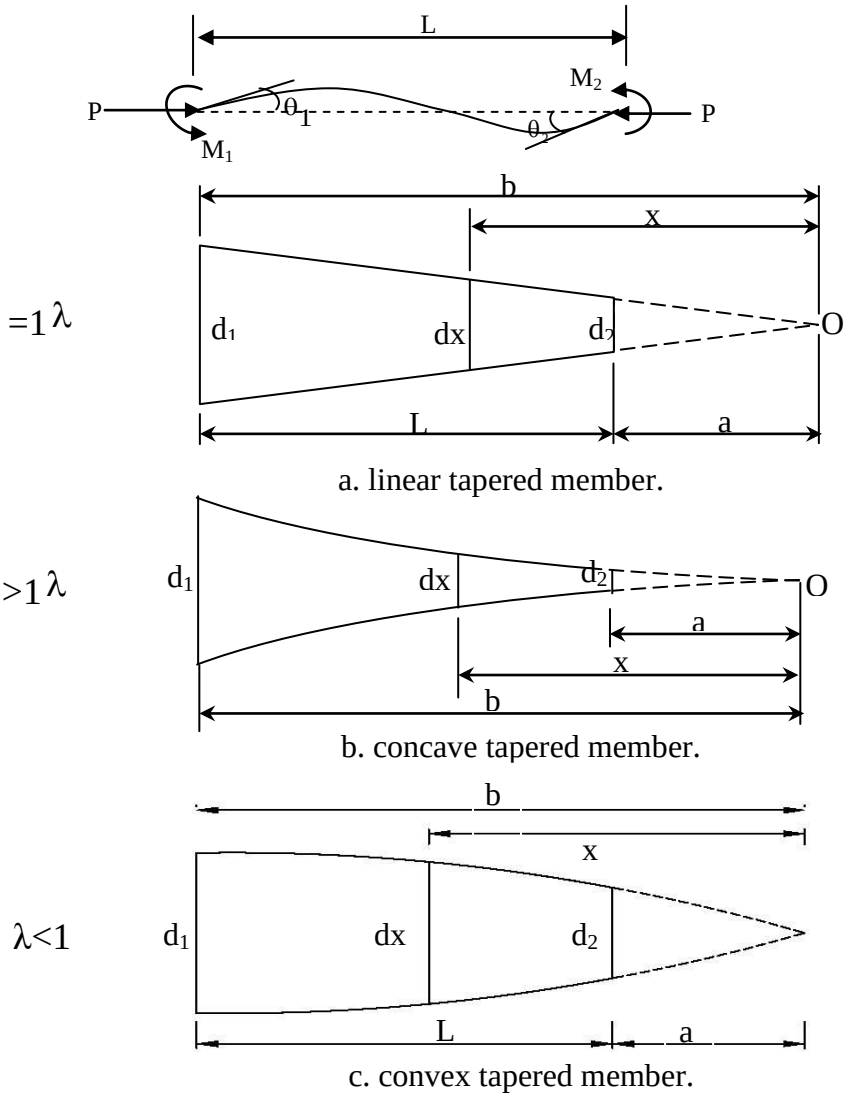

Fig. 1: Tapered beam-column member.

MODIFIED STABILITY FUNCTIONS:

The modified stability functions of non sway and non-prismatic members in different non-linear configuration shape as derived in previous researches by (AL-Damluji and Yossif 2005), (Al-Sarraf and Yossif 2005) and (Yossif 2006) can be written in the form of modified slope deflection equations as given in eq. (1) and eq. (2) below:

$$M_1 = \frac{EI_2}{L}\left(S_1\theta_1 + SC\,\theta_2\right) \qquad (1)$$

$$M_2 = \frac{EI_2}{L}\left(SC\,\theta_1 + S_2\,\theta_2\right) \tag{2}$$

These two equations can be written in matrix form as given in eq. (3).

$$\begin{Bmatrix} M_1 \\ M_2 \end{Bmatrix} = \frac{EI_2}{L}\begin{bmatrix} S_1 & SC \\ SC & S_2 \end{bmatrix}\cdot\begin{bmatrix} \theta_1 \\ \theta_2 \end{bmatrix} \tag{3}$$

Therefore the stiffness matrix $[K]$ for simply supported beam-column member can be written as given in eq. (4).

$$[K] = \frac{EI_2}{L}\begin{bmatrix} S_1 & SC \\ SC & S_2 \end{bmatrix} \tag{4}$$

Where I_2 is the moment of inertia at smaller depth of member, S_1, SC and S_2 are the modified stability functions and L is the member length.

The derivation of the modified stability functions based on the exact solution given in eq. 5 of second order differential equation of the deflected shape of beam column member subjected to compression axial force and bending moments.

$$EI(x)\frac{d^2y}{dx^2} + Qy = \frac{M_1}{L}(x-a) + \frac{M_2}{L}(x-b) \tag{5}$$

where I(x) is the moment of inertia at distance x from origin O that can be written with respect to member dimensions as given in eq. (6) and with respect to member depth as given in eq. (7): –

$$I(x) = I_2\left(x/a\right)^{\overline{m}} \tag{6}$$

$$I(x) = d(x)^4/12 \tag{7}$$

Where $\overline{m}$ is the modified shape factor as obtaine from eq. (8). Otherwise the equation of shape factor can be obtained using eq. (9) (Al-Sarraf , 1979) and (Al-Damarchi, 1999) which depends on logarithm ratio of moment of inertia between two ends and tapering ratio: –

$$\overline{m} = \lambda m \tag{8}$$

$$m = \log\left(I_2/I_1\right)/\log u \tag{9}$$

In fact, the non-linear shape of non-prismatic members can be classified in three types according to the non-linearity factor λ:

1. $\lambda > 1$, for concave tapered member along its axis.
2. $\lambda = 1$, for linear tapered member along its axis.
3. $\lambda < 1$, for convex tapered member along its axis.

Where u and $\overline{u}$ are the tapering ratio and modified tapering ratio respectively that can be obtained from eq. (10), eq. (11) and eq. (12): –

$$\overline{u} = a/b \tag{10}$$

$$\bar{u} = u^{\frac{1}{\lambda}} \tag{11}$$

$$u^{\frac{1}{\lambda}} = a/b \tag{12}$$

Where b and a are the distance from origin O to end 1 and end 2 respectively as shown in Fig. (1). The depth d (x) may be expressed by eq. (13):

$$d(x) = d_2 (x/a)^{\lambda} \tag{13}$$

From eq. (13), the depth d_1 at end 1 when x = b can be obtained from eq. (14):

$$d_1 = d_2 (b/a)^{\lambda} \tag{14}$$

The moment of inertia of the strut may be expressed in the form shown in eq. (15):

$$I(x) = I_2 (x/a)^{\lambda m} \tag{15}$$

The basic differential equation of beam- column as given in eq. (5) can be written as in eq. (16) after substituting eq. (8) and eq. (15) into eq. (5).

$$EI_2 \left(\frac{x}{a}\right)^{\bar{m}} \frac{d^2 y}{dx^2} + Qy = \frac{M_1}{L}(x-a) + \frac{M_2}{L}(x-b) \tag{16}$$

The right hand side of eq. (16) can be reduced to zero by replacing “y” by “Z” when

$$Z = y - \frac{M_1}{QL}(x-a) - \frac{M_2}{QL}(x-b). \tag{17}$$

Thus, the differential equation becomes:

$$\frac{d^2 Z}{dx^2} + \omega^2 x^{-\bar{m}} Z = 0 \tag{18}$$

Where

$$\omega^2 = Qa^{\bar{m}} / EI_2 \ . \tag{19}$$

Eq. (18) can be transformed into Bessel Equation of the form shown in eq. (20) (McLachla, 1961):

$$\frac{d^2 Z}{dx^2} - \frac{(2\alpha - 1)}{x} \cdot \frac{dZ}{dx} + \left(\beta^2 \gamma^2 x^{2\gamma - 2} + \frac{\alpha^2 - n^2 \gamma^2}{x^2}\right) Z = 0 . \tag{20}$$

This equation has a general solution (McLachlan, 1961):

$$Z = x^{\alpha} \left[A J_n (\beta x^{\gamma}) + B J_{-n} (\beta x^{\gamma}) \right] \tag{21}$$

Depending on (n) is not an integer; here J_n is the Bessel functions of the first kind of order n; A and B are the constants of integration. Therefore, the solution can be written down in terms of Bessel functions by giving particular values to the constants α, β, γ and n, by comparing the two equations eq. (18) and eq. (20), the constants α, β, γ and n can be obtained: –

$$\alpha = 0.5 \ , \ \beta = \pm\frac{2\omega}{2-\overline{m}} \ , \ \gamma = \frac{2-\overline{m}}{2} \ , \ n = \pm\frac{1}{2-\overline{m}}$$

Hence, the general solution of the fundamental eq. (16) is:

$$y = \sqrt{x}\left[AJ_n\left(\beta x^{\gamma}\right) + BJ_{-n}\left(\beta x^{\gamma}\right)\right] + \frac{M_1}{QL}(x-a) + \frac{M_2}{QL}(x-b) \qquad (22)$$

There are four unknowns A, B, M_1, and M_2, which have to be determined from the following boundary conditions:

at $x = a$, deflection $y = 0$ and rotation $dy/dx = \theta_2$,
and $x = b$, deflection $y = 0$ and rotation $dy/dx = \theta_1$.

The solution of the basic differential equation as given in eq. (22) can be represented by the modified stability functions for each type of nonlinear shape as given in **Table (1)** (Abdul Mahdi, 2002), (Al-Azawi 2005) and (Yossif, 2006).

Table (1): Modified stability functions for different non-linearity shape (Yossif, 2006).

	m	λ	$\overline{m}$	S_1	SC	S_2
Concave	4	0.2	0.8	$\frac{(\omega Lf_4 - Za^{0.4})}{[\omega PEI_2/LZQb^{0.4}]}$	$\frac{(\omega Lf_5 - Za^{-0.1}b^{0.5})}{[-\omega PEI_2/LZQa^{0.5}b^{-0.1}]}$	$\frac{(\omega Lf_3 - Zb^{0.4})}{[-\omega PEI_2/\ LZQa^{0.4}]}$
	4	0.4	1.6	$\frac{(\omega Lf_4 - Za^{0.8})}{[\omega PEI_2/\ LZQb^{0.8}]}$	$\frac{(\omega Lf_5 - Za^{0.3}b^{0.5})}{[-\omega PEI_2/\ LZQa^{0.5}b^{0.3}]}$	$\frac{(\omega Lf_3 - Zb^{0.8})}{[\omega PEI_2/\ LZQa^{0.8}]}$
	4	0.6	2.4	$\frac{(\omega Lf_4 + Za^{1.2})}{[-\omega PEI_2/\ LZQb^{1.2}]}$	$\frac{(\omega Lf_5 + Za^{0.5}b^{0.7})}{[\omega PEI_2/LZQa^{0.7}b^{0.5}]}$	$\frac{(\omega Lf_3 + Zb^{1.2})}{[-\omega PEI/\ LZQa^{1.2}]}$
	4	0.8	3.2	$\frac{(\omega Lf_4 + Za^{1.6})}{[-\omega PEI_2/LZQb^{1.6}]}$	$\frac{(\omega Lf_5 + Za^{0.5}b^{1.1})}{[\omega PEI_2/LZQa^{1.1}b^{0.5}]}$	$\frac{(\omega Lf_3 + Zb^{1.6})}{[-\omega PEI_2/LZQa^{1.6}]}$
Linear	4	1	4	$\frac{(\omega Lf_4 + Za^{2})}{[-\omega PEI_2/LZQb^{2}]}$	$\frac{(\omega Lf_5 + Za^{0.5}b^{1.5})}{[\omega PEI_2/LZQa^{1.5}b^{0.5}]}$	$\frac{(\omega Lf_3 + Zb^{2})}{[-\omega PEI_2/LZQa^{2}]}$
Conv ex	4	1.4	5.6	$\frac{(\omega Lf_4 + Za^{2.8})}{[\omega PEI_2/LZQb^{2.8}]}$	$\frac{(\omega Lf_5 - Za^{0.5}b^{2.3})}{[\omega PEI_2/LZQa^{2.3}b^{0.5}]}$	$\frac{(\omega Lf_3 + Zb^{2.8})}{[\omega PEI_2/\ LZQa^{2.8}]}$

	4	1.8	7.2	$\frac{(\omega Lf_4 + Za^{3.6})}{[\omega PEI_2/LZQb^{3.6}]}$	$\frac{(\omega Lf_5 - Za^{0.5}b^{3.1})}{[\omega PEI_2/LZQa^{3.1}b^{0.5}]}$	$\frac{(\omega Lf_3 + Zb^{3.6})}{[\omega PEI_2/LZQa^{3.6}]}$
	4	2.2	8.8	$\frac{(\omega Lf_4 + Za^{4.4})}{[-\omega PEI_2/LZQb^{4.4}]}$	$\frac{(\omega Lf_5 + Za^{0.5}b^{3.9})}{[\omega PEI_2/LZQa^{3.9}b^{0.5}]}$	$\frac{(\omega Lf_3 + Zb^{4.4})}{[-\omega PEI_2/LZQa^{4.4}]}$
	4	2.6	10.2	$\frac{(\omega Lf_4 + Za^{5.2})}{[-\omega PEI_2/LZQb^{5.2}]}$	$\frac{(\omega Lf_5 + Za^{0.5}b^{4.7})}{[\omega PEI_2/LZQa^{4.7}b^{0.5}]}$	$\frac{(\omega Lf_3 + Zb^{5.2})}{[-\omega PEI_2/LZQa^{5.2}]}$

Where any symbol in the above equations is defined in appendix A1, A2 andA3

ELASTIC CRITICAL LOAD:

A compression force Q if loaded axially on any beam-column member by a small value that is applied through the centroid of the cross section, the column remains straight and undergoes only axial compression. This straight form of equilibrium is stable, which means that the column returns to the straight position if it is disturbed. For instance, if a small lateral load is applied which causes the column to bend, the deflection will disappear and the column will return to the original position when the lateral load is removed. As the axial load is gradually increased, it reaches a condition of neutral equilibrium in which the column may have a bent shape. The ideal column may undergo small lateral deflections with no change in the axial force, and a small lateral load will produce a bent shape that does not disappear when the lateral load is removed. The stiffness matrix of beam-column member is gradually vanished at this load therefore such a load is called the elastic critical load.

The elastic critical load Q_c of any tapered member shape can be obtained using eq. (23) as given below:

$$Q_c = \rho . Q_E . \qquad (23)$$

Where: ρ_c is non-dimensional axial force parameter at the elastic critical load.

Q_E is the equivalent Euler load for tapered member which equal to $EI_2\pi^2/L^2$

E is modules of elasticity for steel

I_2 is the moment of inertia at smaller end depth

L is member length

The elastic critical load is obtained for linear tapered members and five types of tapering ratio which equal to 1.5, 2, 3, 4 and 5, then tabulated with respect to the properties ratio I_2/L^2 as given in **Table (2)** and presented graphically as shown in **Fig. (2)**.

The value of non-dimensional axial force parameter at the elastic critical load can be obtained using stability equations that given in **Table (1).**

Table (2): Elastic critical load for different depth at smaller depth's end

I_2/L	Elastic Critical Load Q (kN)				
	b/a=1.5	**b/a=2.0**	**b/a=3.0**	**b/a=4.0**	**b/a=5.0**
0.000833333	3.70	6.58	14.80	26.32	41.12
0.013333333	59.22	105.28	236.87	421.10	657.97
0.067500000	299.79	532.96	1199.16	2131.83	3330.99
0.213333333	947.48	1684.41	3789.93	6737.65	10527.58
0.520833333	2313.19	4112.34	9252.75	16449.34	25702.09
1.080000000	4796.63	8527.34	19186.51	34109.35	53295.86

2.000833333	8886.35	15797.95	35545.38	63191.79	98737.17
3.413333333	15159.71	26950.60	60638.85	107802.40	168441.25
5.467500000	24282.93	43169.65	97131.71	172678.60	269810.31
8.333333333	37011.02	65797.36	148044.07	263189.45	411233.52
12.20083333	54187.83	96333.92	216751.32	385335.67	602086.99
17.28000000	76746.04	136437.41	306984.18	545749.64	852733.82
23.80083333	105707.16	187923.85	422828.66	751695.39	1174524.05
32.01333333	142181.52	252767.15	568726.08	1011068.59	1579794.68
42.18750000	187368.27	333099.15	749473.08	1332396.59	2081869.68
54.61333333	242555.40	431209.60	970221.59	1724838.38	2695059.98
69.60083333	309119.71	549546.15	1236478.84	2198184.61	3434663.45
87.48000000	388526.85	690714.39	1554107.39	2762857.58	4316964.97
108.6008333	482331.27	857477.81	1929325.07	3429911.24	5359236.31
133.3333333	592176.26	1052757.80	2368705.06	4211031.21	6579736.27

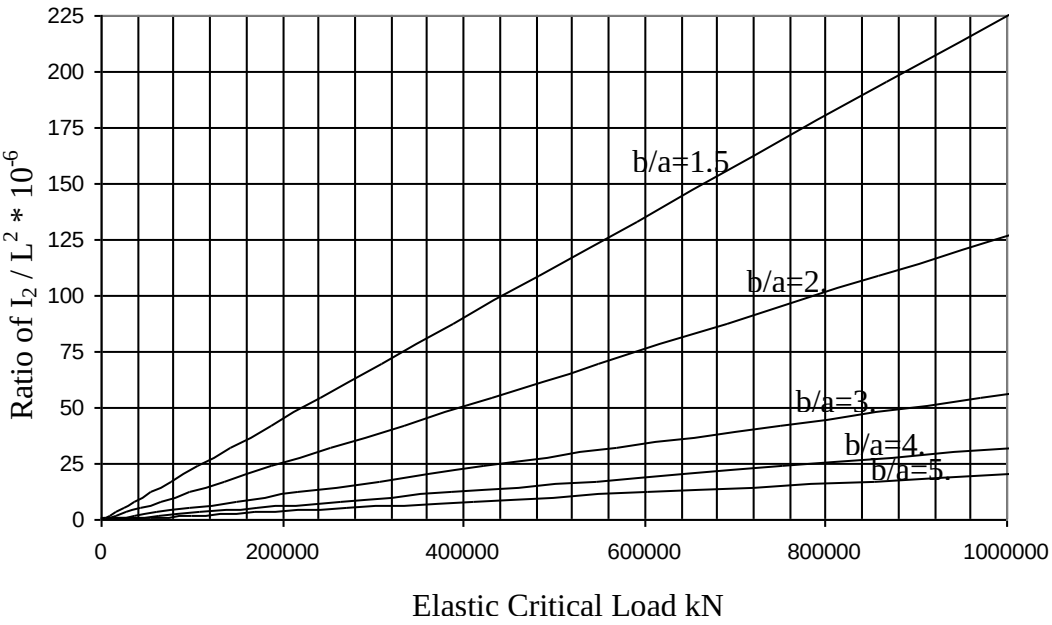

Figure (2): Elastic critical load for different tapering ratio of linear tapered shape

Then the modified stability function values substituted into the matrix given in eq. (4) with different compressive axial force value until the equation of stiffness matrix becomes equal to zero. At this case the axial load is the elastic critical load. The non-dimensional axial force parameter at elastic critical load are tabulated for nine different non-linearity shape and five tapering ratio as given in **Table (3)**.

Table (3): Non-dimensional Axial Force Parameter

λ	b/a=1.5	b/a=2.0	b/a=3.0	b/a=4.0	b/a=5.0
0.2	1.190	1.364	1.685	1.982	2.263
0.4	1.408	1.821	2.727	3.69	4.716
0.6	1.657	2.358	4.232	5.995	8.978
0.8	1.935	3.134	6.297	10.461	15.611
1.0	2.250	4.000	9.000	16.000	25.000

1.4	2.991	6.219	16.518	32.005	52.706
1.8	3.892	9.139	27.001	54.812	92.567
2.2	4.963	12.793	40.532	84.453	144.561
2.6	6.212	17.198	56.088	12.902	203.633

ECONOMICAL AND OPTIMUM SHAPE:

The economical member shape in this study represents the member that has a minimum material weight i.e. minimum member volume while the optimum member shape can be defined as the member which has minimum shape volume with maximum load capacity. The optimum shape is not necessarily being the economical member shape.

The optimum member shape depends on the optimum degree ratio represented by the ratio between member capacity and member volume. That mean the member shape convergence to the case of optimum shape when the optimum degree increased.

Nine different shapes of tapered beam-column members are presented in this study assigned according to the degree of non-linearity factor. General volume equations for different cross section area of tapered member derived as a function of non-linearity degree as given in **Table (4)** that can be used to compare between volumes of different member shapes having the same capacity of axial load.

Table (4): General volume equation

Section Type	Volume Function
Square section	$\dfrac{d_2^{\,2}\left(b^{2\lambda+1}-a^{2\lambda+1}\right)}{a^{2\lambda}(2\lambda+1)}$
Rectangular section	$\dfrac{\psi_2.d_2^{\,2}\left(b^{2\lambda+1}-a^{2\lambda+1}\right)}{a^{2\lambda}(2\lambda+1)}$
Circular section	$\dfrac{d_2^{\,2}.\pi.\left(b^{2\lambda+1}-a^{2\lambda+1}\right)}{4.a^{2\lambda}(2\lambda+1)}$

The ratio of the elastic critical loads of different non-linearity shape from the elastic critical loads of linear tapered member at tapering ratio u=2 are presented in **Table (5)** as the first numerical comparison between different tapered member shapes having the same other properties.

Table (5): Ratio of elastic critical load from linear tapered shape

λ	b/a=1.5	b/a=2	b/a=3	b/a=4	b/a=5
0.2	1.35930	1.35456	1.34557	1.33771	1.33122
0.4	1.34392	1.30339	1.24151	1.18318	1.13540
0.6	1.31595	1.20208	1.06945	0.87873	0.84358
0.8	1.27325	1.12498	0.86182	0.67749	0.54964
1	1.22161	1.00000	0.65237	0.44444	0.31868
1.4	1.09224	0.73125	0.31682	0.15197	0.08113
1.8	0.94111	0.48686	0.12854	0.04121	0.01585

2.2	0.78294	0.29878	0.04549	0.00950	0.00259
2.6	0.63044	0.17111	0.01426	0.00195	0.00037

The comparison presented in **Table (5)** explains that the convex shape has a more axial load capacity than other shapes in which it will reach about to 136% from the linear shape capacity; on the other hand the concave shape is less axial load capacity than other shapes in which it will be reach less than 0.04% from the linear shape capacity.

The elastic critical load of different non-linearity shape as a ratio from linear tapered shape is presented as the first comparison in graphical curve for different tapering ratio as shown in **Fig. (3)** for members having the same member length, volume and support conditions.

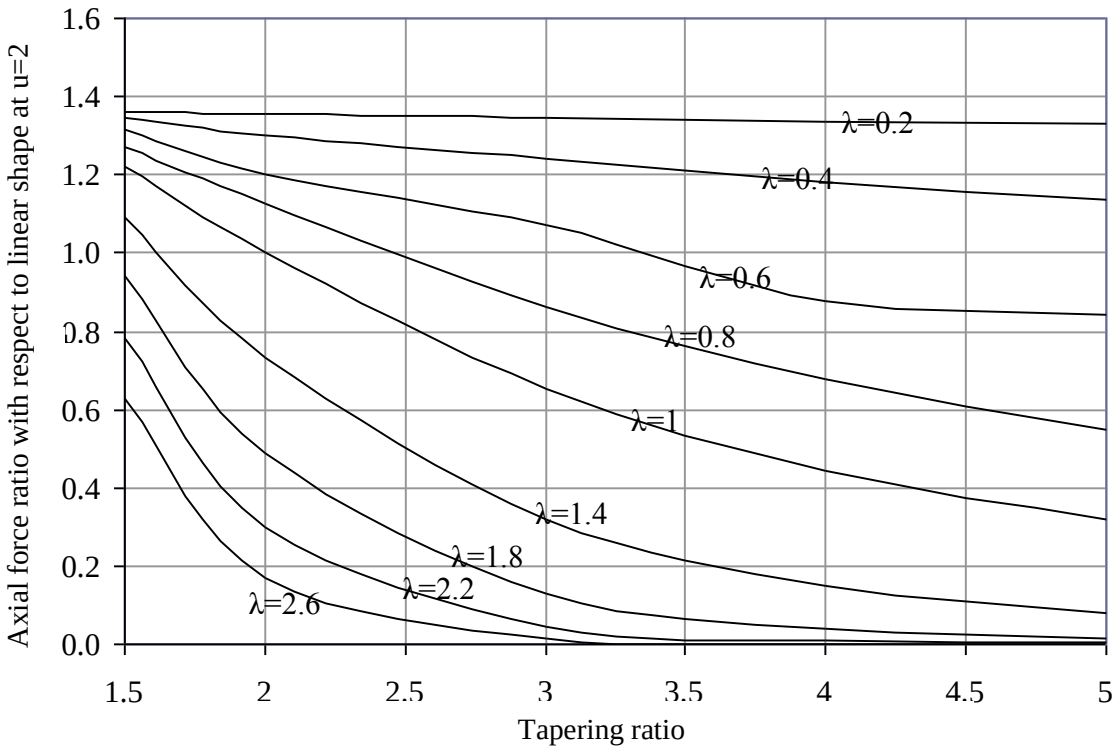

Figure (3): Comparison of models according to elastic critical loads

The ratio of members volume from the volume of linear tapered member at tapering ratio u=2 is presented in **Table (6)** as the second numerical comparison for different non-linearity shape and different tapering ratio.

Table (6): Volume ratio with respect to linear shape at u=2

Tapering ratio, u	**λ=0.2**	**λ=0.4**	**λ=0.6**	**λ=0.8**	**λ=1**	**λ=1.4**	**λ=1.8**	**λ=2.2**	**λ=2.6**
1.5	0.86	0.86	0.87	0.89	0.90	0.96	1.03	1.13	1.26
2	0.86	0.88	0.91	0.94	1.00	1.17	1.43	1.83	2.42
3	0.86	0.90	0.97	1.08	1.24	1.77	2.79	4.68	8.37
4	0.86	0.92	1.07	1.21	1.50	2.56	4.92	10.25	22.63
5	0.87	0.94	1.09	1.35	1.77	3.51	7.94	19.61	52.16

The comparison of **Table (6)** explains that the convex shape needs more volume than other shapes to carry the same axial load capacity which can be reached to 5216% as that of the linear shape. On the other hand the concave shape needs less volume than other shapes to carry the same axial load capacity which can be reached to 86% as that of the linear shape.

The volume for members having the same length and the same elastic critical load capacity with different tapering ratios is presented as the second comparison in another graphical curve as shown in **Fig. (4)**.

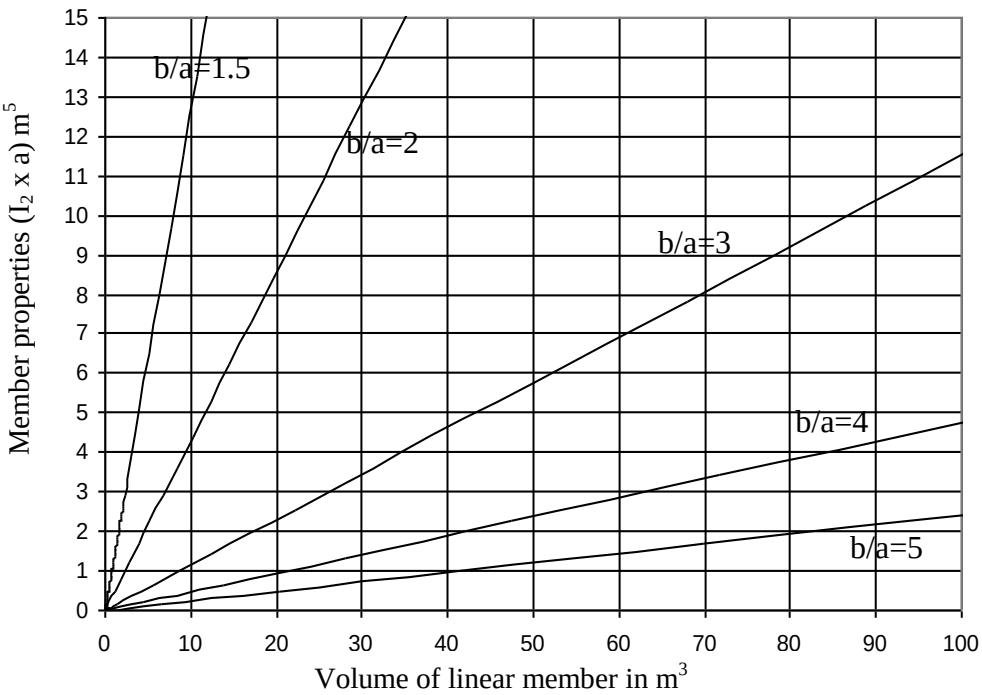

Figure (4): Comparison of models according to member volume

APPLICATIONS:-

The three simply supported steel beam-column members subjected to a compressive axial force with equal lengths of 4.0 m and solid rectangular cross sections tapered in different configuration shapes:

1-linear tapered member

2-concave tapered member with non-linearity equal to 2.6

3-convex tapered member with non-linearity equal to 0.2

The members have the same dimensions at the smaller depth's end which is equal to 5 cm for members depth and width, and the same tapering ratio of 3.

The comparison of the elastic critical force and volume for the three members are tabulated to verify the optimum member's shape:

First member:

The elastic critical load of this member can be obtained using eq. (23) and **Table (3)** as given below:

$$Q = \rho.\frac{EI_2\pi^2}{L^2} = 9.\frac{200000000 \text{ x } 0.05^4/12 \text{ x } \pi^2}{4^2} = 578.3\text{kN}$$

The volume of this beam-column can be obtained using **Table (5)** as given below:

$$V = \frac{d_2{}^2.\left(b^{2\lambda+1} - a^{2\lambda+1}\right)}{a^{2\lambda}\left(2\lambda+1\right)} = \frac{0.05^2.\left(6^{2\times1+1} - 2^{2\times1+1}\right)}{2^{2\times1}\left(2\times1+1\right)} = 0.043\ \ m^3$$

Second member:

The elastic critical load of this member can be obtained using eq. (23) and **Table (3)** as given below:

$$Q = \rho.\frac{EI_2\pi^2}{L^2} = 56.088.\frac{200000000\,x\,0.05^4/12x\,\pi^2}{4^2} = 3604\,kN$$

The volume of this beam-column can be obtained using **Table (5)** as given below:

$$V = \frac{d_2{}^2.\left(b^{2\lambda+1} - a^{2\lambda+1}\right)}{a^{2\lambda}\left(2\lambda+1\right)} = \frac{0.05^2.\left(6^{2\times2.6+1} - 2^{2\times2.6+1}\right)}{2^{2\times2.6}\left(2\times2.6+1\right)} = 0.732\ m^3$$

Third member:

The elastic critical load of this member can be obtained using eq. (23) and **Table (3)** as given below:

$$Q = \rho.\frac{EI_2\pi^2}{L^2} = 1.685.\frac{200000000\,x\,0.05^4/12\,x\,\pi^2}{4^2} = 108.3\,kN$$

The volume of this beam-column can be obtained using **Table (5)** as given below:

$$V = \frac{d_2{}^2.\left(b^{2\lambda+1} - a^{2\lambda+1}\right)}{a^{2\lambda}\left(2\lambda+1\right)} = \frac{0.05^2.\left(6^{2\times0.2+1} - 2^{2\times0.2+1}\right)}{2^{2\times0.2}\left(2\times0.2+1\right)} = 0.013\,m^3$$

The above results are tabulated according to the non-linearity degree as given in **Table (8)**:

Table (8): Application Results

	Concave λ=2.6	Linear λ=1.0	Convex λ=0.2
Elastic critical load Q, kN	3604	578.3	108.3
Elastic critical load Q, %	623%	100%	18.7%
Volume V, m^3	0.732	0.043	0.013
Volume V, %	1702%	100%	30%
$\frac{Q\%}{V\%}$	36.6%	100%	62.3%

CONCLUSIONS:

This study is based on mathematical solution of nine different models of tapered members having square or circular solid cross-sectional area to find mathematical functions which named modified stability functions which are used to obtain the elastic critical load for each member shape.

The results of this study are presented by two comparison tables and graphical curves. The maximum shape strength is obtained at the non-linearity factor of 2.6 “concave shape” with tapering ratio of 1.5 which is equal to 136% of the linear shape strength. The minimum shape strength is also found at the non-linearity 0.2 “convex shape” with tapering ratio of 5 which is less than 0.04% of the linear shape strength. Then the more economical shape is found at the non-linearity degree of 0.2 and tapering ratio of 1.5 in which it requires about 86% of the linear shape volume to carry the same axial load, on the other hand the least economical shape is found at the

non-linearity degree of 2.6 and tapering ratio of 5 which is required about 5216% of the linear shape volume to carry the same load.
Another comparison can be resulted from the application using load capacity-volume ratio in which the first optimum degree is obtained in the non-linearity degree equal to 1"linear shape", and the less optimum degree when the non-linearity value convergence to 1.

REFERENCES:

Abdul Mahdi, H., "Large Displacement Elastic Plastic Analysis of Plane Frames with Non-Prismatic Member of Non-Linearly Varying Sections", Ph.D Thesis, University of Technology, Iraq, 2002.

Al-Azawi, T.K., "Stability Analysis for Columns of Concave Configuration Using the Finite Element Method", Journal of Engineering, College of Engineering University of Baghdad, Vol.11 No.4, December 2005.

Al-Damarchi, H. T., "Large Displacement Elastic-Plastic Analysis of Non-Prismatic Members", Ph.D Thesis, University of Technology. Iraq, 1999.

AL-Damluji, O., and Yossif, W.V., "Elastic Stability of Frames Having Concave Tapered Struts", Journal of Engineering, College of Engineering University of Baghdad, Vol.11, No.1, March 2005, pp149-164.

Al-Sarraf, S. Z., "Elastic Instability of Frames with Uniformly Tapered Members", The Structural Engineer, March 1979, pp. 18-24.

Al-Sarraf S.Z., and Yossif, W.V., "Elastic Instability of Frames with Non-linear Tapered members" Journal of Babylon University, Vol.13, No.5, 2005.
Mckachlan N. W., "Bessel Functions for Engineering", Clarendon Press Oxford, 1961.

Yossif, W.V., Modified Stability Functions with Shear Effect for Non-Prismatic Members In Steel Plane Frames And Member Inside Soils", Ph. D. Thesis, University of Baghdad, Baghdad April 2006.

SYMBOLS:

d_1 and d_2	: Depth at end 1 and end 2 respectively
$f_1, f_2, ...f_6$	: Parameters function
K	: Stiffness of the strut
$m, \overline{m}$	: Shape factor and modified Shape factor respectively
n	: The order of Bessel function
y	: Deflection
u	: Tapering ratio
$\bar{u}$	: Modified tapering ratio
E	: Young's modulus
I_1 , I_2	: Moment of inertia at end 1and end 2 respectively
L	: Member length
M_1, M_2	: Bending moments at end 1 and 2 of the member
Q	: Axial load

Q_c : Elastic critical load
Q_E : Eular load = EI_2L^2/π^2
S_1, S_2 : Modified stability function at end 1and end 2 respectively
SC : Carrying factor of the modified stability function
λ : Non-linearity factor
θ_1, θ_2 : Rotation at end 1 and 2 of member due to bending moment and axial force
ρ : Non-dimensional axial force parameter
ρ_c : Elastic critical load parameter
ψ_2 : Ratio of member cross sectional dimensions (width to depth) at smaller depth

APPENDIX A

Table A-1: Symbols of Stability Equations for members having λ=0.2, 0.4 and 0.6

Symbol	$\overline{m}=0.8 \quad \lambda=0.2$	$\overline{m}=1.6 \quad \lambda=0.4$	$\overline{m}=2.4 \quad \lambda=0.6$
Z	$J_{-0.166}(\alpha)J_{0.166}(\beta)-J_{0.166}(\alpha)J_{-0.166}(\beta)$	$J_{-2.5}(\alpha)J_{0.2.5}(\beta)-J_{2.5}(\alpha)J_{-2.5}(\beta)$	$J_{2.5}(\alpha)J_{-2.5}(\beta)-J_{-2.5}(\alpha)J_{2.5}(\beta)$
ω	$\left(a^{0.8}\,Q/EI_2\right)^{0.5}$	$\left(a^{1.6}\,Q/EI_2\right)^{0.5}$	$\left(a^{2.4}\,Q/EI_2\right)^{0.5}$
α	$1.667\omega a^{0.6}$	$5\omega a^{0.2}$	$5\omega a^{-0.2}$
β	$1.667\omega b^{0.6}$	$5\omega b^{0.2}$	$5\omega b^{-0.2}$
A	$-\dfrac{M_1J_{-0.167}(\alpha)\sqrt{a}+M_2J_{-0.167}(\beta)\sqrt{b}}{\sqrt{a}\,\sqrt{b}\,ZQ}$	$-\dfrac{M_1J_{-2.5}(\alpha)\sqrt{a}+M_2J_{-2.5}(\beta)\sqrt{b}}{\sqrt{a}\,\sqrt{b}\,ZQ}$	$\dfrac{M_1J_{-2.5}(\alpha)\sqrt{a}+M_2J_{-2.5}(\beta)\sqrt{b}}{\sqrt{a}\,\sqrt{b}\,ZQ}$
B	$\dfrac{M_1J_{0.167}(\alpha)\sqrt{a}+M_2J_{0.167}(\beta)\sqrt{b}}{\sqrt{a}\,\sqrt{b}\,ZQ}$	$\dfrac{M_1J_{2.5}(\alpha)\sqrt{a}+M_2J_{2.5}(\beta)\sqrt{b}}{\sqrt{a}\,\sqrt{b}\,ZQ}$	$-\dfrac{M_1J_{2.5}(\alpha)\sqrt{a}+M_2J_{2.5}(\beta)\sqrt{b}}{\sqrt{a}\,\sqrt{b}\,ZQ}$
f_1	$J_{-1.166}(\alpha)J_{1.166}(\beta)-J_{1.166}(\alpha)J_{-1.166}(\beta)$	$J_{-3.5}(\alpha)J_{3.5}(\beta)-J_{3.5}(\alpha)J_{-3.5}(\beta)$	$J_{-3.5}(\alpha)J_{3.5}(\beta)-J_{3.5}(\alpha)J_{-3.5}(\beta)$
f_2	$J_{-0.166}(\alpha)J_{0.166}(\beta)-J_{0.166}(\alpha)J_{-0.166}(\beta)$	$J_{-2.5}(\alpha)J_{2.5}(\beta)-J_{2.5}(\alpha)J_{-2.5}(\beta)$	$J_{-2.5}(\alpha)J_{2.5}(\beta)-J_{2.5}(\alpha)J_{-2.5}(\beta)$
f_3	$J_{-0.166}(\alpha)J_{1.166}(\beta)+J_{0.166}(\alpha)J_{-1.166}(\beta)$	$J_{-2.5}(\alpha)J_{3.5}(\beta)+J_{2.5}(\alpha)J_{-3.5}(\beta)$	$J_{-2.5}(\alpha)J_{3.5}(\beta)+J_{2.5}(\alpha)J_{-3.5}(\beta)$
f_4	$J_{-0.166}(\beta)J_{1.166}(\alpha)+J_{0.166}(\beta)J_{-1.166}(\alpha)$	$J_{-2.5}(\beta)J_{3.5}(\alpha)+J_{2.5}(\beta)J_{-3.5}(\alpha)$	$J_{-2.5}(\beta)J_{3.5}(\alpha)+J_{2.5}(\beta)J_{-3.5}(\alpha)$
f_5	$J_{0.166}(\beta)J_{-1.166}(\beta)+J_{-0.166}(\beta)J_{1.166}(\beta)$	$J_{2.5}(\beta)J_{-3.5}(\beta)+J_{-2.5}(\beta)J_{3.5}(\beta)$	$J_{2.5}(\beta)J_{-3.5}(\beta)+J_{-2.5}(\beta)J_{3.5}(\beta)$
f_6	$J_{-0.166}(\alpha)J_{1.166}(\alpha)+J_{0.166}(\alpha)J_{-1.166}(\alpha)$	$J_{-2.5}(\alpha)J_{3.5}(\alpha)+J_{2.5}(\alpha)J_{-3.5}(\alpha)$	$J_{-2.5}(\alpha)J_{3.5}(\alpha)+J_{2.5}(\alpha)J_{-3.5}(\alpha)$
P1	$(f_5b^{0.5}-f_3a^{0.5})$	$(f_5b^{0.5}-f_3a^{0.5})$	$(f_5b^{0.5}-f_3a^{0.5})$
P2	$\left(f_4b^{0.5}-f_6a^{0.5}\right)$	$\left(f_4b^{0.5}-f_6a^{0.5}\right)$	$\left(f_4b^{0.5}-f_6a^{0.5}\right)$
P	$Z\left[-a^{-0.1}P_1-b^{-0.1}P_2\right]-\omega Lf_1f_2$	$Z\left[b^{0.3}P_2-a^{0.3}P_1\right]-\omega Lf_1f_2$	$Z\left[a^{0.7}P_1-b^{0.7}P_2\right]-\omega Lf_1f_2$

Table A-2: Symbols of Stability Equations for members having λ=0.8, 1.0 and 1.4

Symbol	$\overline{m}=3.2 \quad \lambda=0.8$	$\overline{m}=4 \quad \lambda=1$	$\overline{m}=5.6 \quad \lambda=1.4$
Z	$J_{0.833}(\alpha)J_{-0.833}(\beta)-J_{-0.833}(\alpha)J_{0.833}(\beta)$	$J_{0.5}(\alpha)\,J_{-0.5}(\beta)-J_{-0.5}(\alpha)\,J_{0.5}(\beta)$	$J_{0.78}(\alpha)J_{-0.278}(\beta)-J_{-0.278}(\alpha)J_{0.278}(\beta)$
ω	$\left(a^{3.2}\,Q/E\,I_2\right)^{0.5}$	$\left(a^{4}\,Q/EI_2\right)^{0.5}$	$\left(a^{5.6}\,Q/EI_2\right)^{0.5}$
α	$0.56\omega a^{-1.8}$	ω/a	$0.556\omega a^{-1.8}$
β	$1.667\omega b^{-0.6}$	ω/b	$0.56\omega b^{-1.8}$
A	$\dfrac{M_1J_{-0.833}(\alpha)\sqrt{a}+M_2J_{-0.833}(\beta)\sqrt{b}}{\sqrt{a}\,\sqrt{b}\,ZQ}$	$\dfrac{M_1J_{-0.5}(\alpha)\sqrt{a}+M_2J_{-0.5}(\beta)\sqrt{b}}{\sqrt{a}\,\sqrt{b}\,ZQ}$	$\dfrac{M_1J_{-0.278}(\alpha)\sqrt{a}+M_2J_{-0.278}(\beta)\sqrt{b}}{\sqrt{a}\,\sqrt{b}\,ZQ}$
B	$-\dfrac{M_1J_{0.833}(\alpha)\sqrt{a}+M_2J_{0.833}(\beta)\sqrt{b}}{\sqrt{a}\,\sqrt{b}\,ZQ}$	$-\dfrac{M_1J_{0.5}(\alpha)\sqrt{a}+M_2J_{0.5}(\beta)\sqrt{b}}{\sqrt{a}\,\sqrt{b}\,ZQ}$	$-\dfrac{M_1J_{0.279}(\alpha)\sqrt{a}+M_2J_{0.278}(\beta)\sqrt{b}}{\sqrt{a}\,\sqrt{b}\,ZQ}$
f_1	$J_{-1.833}(\alpha)J_{1.833}(\beta)-J_{1.833}(\alpha)J_{-1.833}(\beta)$	$J_{-1.5}(\alpha)\,J_{1.5}(\beta)-J_{1.5}(\alpha)\,J_{-1.5}(\beta)$	$J_{-1.278}(\alpha)J_{1.278}(\beta)-J_{1.278}(\alpha)J_{-1.278}(\beta)$
f_2	$J_{-0.833}(\alpha)J_{0.833}(\beta)-J_{0.833}(\alpha)J_{-0.833}(\beta)$	$J_{-0.5}(\alpha)\,J_{0.5}(\beta)-J_{0.5}(\alpha)\,J_{-0.5}(\beta)$	$J_{-0.278}(\alpha)J_{0.278}(\beta)-J_{0.278}(\alpha)J_{-0.278}(\beta)$
f_3	$J_{-0.833}(\alpha)J_{1.833}(\beta)+J_{0.833}(\alpha)J_{-1.833}(\beta)$	$J_{-0.5}(\alpha)\,J_{1.5}(\beta)+J_{0.5}(\alpha)\,J_{-1.5}(\beta)$	$J_{-0.278}(\alpha)J_{1.278}(\beta)+J_{0.278}(\alpha)J_{-1.278}(\beta)$
f_4	$J_{-0.833}(\beta)J_{1.833}(\alpha)+J_{1.833}(\beta)J_{-1.833}(\alpha)$	$J_{-0.5}(\beta)\,J_{1.5}(\alpha)+J_{0.5}(\beta)\,J_{-1.5}(\alpha)$	$J_{-0.278}(\beta)J_{1.278}(\alpha)+J_{0.278}(\beta)J_{-1.278}(\alpha)$
f_5	$J_{-0.833}(\beta)J_{1.833}(\beta)+J_{0.833}(\beta)J_{-1.833}(\beta)$	$J_{0.5}(\beta)\,J_{-1.5}(\beta)+J_{-0.5}(\beta)\,J_{1.5}(\beta)$	$J_{0.278}(\beta)J_{-1.278}(\beta)+J_{-0.278}(\beta)J_{1.278}(\beta)$
f_6	$J_{-0.833}(\alpha)J_{1.833}(\alpha)+J_{1.833}(\alpha)J_{-1.833}(\alpha)$	$J_{-0.5}(\alpha)\,J_{1.5}(\alpha)+J_{0.5}(\alpha)\,J_{-1.5}(\alpha)$	$J_{-0.278}(\alpha)J_{1.278}(\alpha)+J_{0.278}(\alpha)J_{-1.278}(\alpha)$
P1	$(f_5b^{0.5}-f_3a^{0.5})$	$(f_5b^{0.5}-f_3a^{0.5})$	$(f_5b^{0.5}-f_3a^{0.5})$
P2	$\left(f_4b^{0.5}-f_6a^{0.5}\right)$	$\left(f_4b^{0.5}-f_6a^{0.5}\right)$	$\left(f_4b^{0.5}-f_6a^{0.5}\right)$
P	$Z\left[a^{0.5}P_1-b^{0.5}P_2\right]-\omega Lf_1f_2$	$Z\left[a^{1.5}P_1-b^{1.5}P_2\right]-\omega Lf_1f_2$	$Z\left[a^{2.3}P_1-b^{2.3}P_2\right]-\omega Lf_1f_2$

Table A-3: Symbols of Stability Equations for members having λ=1.8, 2.2 and 2.6

Symbol	$\overline{m}=7.2 \quad \lambda=1.8$	$\overline{m}=8.8 \quad \lambda=2.2$	$\overline{m}=10.4 \quad \lambda=2.6$
Z	$J_{-0.192}(\alpha)J_{0.192}(\beta)-J_{0.192}(\alpha)J_{-0.192}(\beta)$	$J_{0.147}(\alpha)J_{-0.147}(\beta)-J_{-0.147}(\alpha)J_{0.147}(\beta)$	$J_{0.119}(\alpha)\,J_{-0.119}(\beta)-J_{-0.119}(\alpha)\,J_{0.119}(\beta)$
ω	$\left(a^{7.2}\,Q/EI_2\right)^{0.5}$	$\left(a^{8.8}\,Q/EI_2\right)^{0.5}$	$\left(a^{10.4}\,Q/EI_2\right)^{0.5}$
α	$0.385\,\omega a^{-2.6}$	$0.294\omega a^{-3.4}$	$0.238\,\omega\,a^{-4.2}$
β	$0.385\,\omega b^{-2.6}$	$0.294\omega b^{-3.4}$	$0.238\omega\,b^{-4.2}$
A	$\dfrac{M_1J_{-0.192}(\alpha)\sqrt{a}+M_2J_{-0.192}(\beta)\sqrt{b}}{\sqrt{a}\,\sqrt{b}\,ZQ}$	$\dfrac{M_1J_{-0.147}(\alpha)\sqrt{a}+M_2J_{-0.147}(\beta)\sqrt{b}}{\sqrt{a}\,\sqrt{b}\,ZQ}$	$\dfrac{M_1J_{-0.119}(\alpha)\sqrt{a}+M_2J_{-0.119}(\beta)\sqrt{b}}{\sqrt{a}\,\sqrt{b}\,ZQ}$

B	$-\frac{M_1 J_{0.192}(\alpha)\sqrt{a}+M_2 J_{0.192}(\beta)\sqrt{b}}{\sqrt{a}\sqrt{b}\,ZQ}$	$-\frac{M_1 J_{0.147}(\alpha)\sqrt{a}+M_2 J_{0.147}(\beta)\sqrt{b}}{\sqrt{a}\sqrt{b}\,ZQ}$	$-\frac{M_1 J_{0.119}(\alpha)\sqrt{a}+M_2 J_{0.119}(\beta)\sqrt{b}}{\sqrt{a}\sqrt{b}\,ZQ}$
f_1	$J_{-1.192}(\alpha)J_{1.192}(\beta)-J_{1.192}(\alpha)J_{-1.192}(\beta)$	$J_{-1.147}(\alpha)J_{1.147}(\beta)-J_{1.147}(\alpha)J_{-1.147}(\beta)$	$J_{-1.119}(\alpha)J_{1.119}(\beta)-J_{1.119}(\alpha)J_{-1.119}(\beta)$
f_2	$J_{-0.192}(\alpha)J_{0.192}(\beta)-J_{0.192}(\alpha)J_{-0.192}(\beta)$	$J_{-0.147}(\alpha)J_{0.147}(\beta)-J_{0.147}(\alpha)J_{-0.147}(\beta)$	$J_{-0.119}(\alpha)J_{0.119}(\beta)-J_{0.119}(\alpha)J_{-0.119}(\beta)$
f_3	$J_{-0.192}(\alpha)J_{1.192}(\beta)+J_{0.192}(\alpha)J_{-1.192}(\beta)$	$J_{-0.147}(\alpha)J_{1.147}(\beta)+J_{0.147}(\alpha)J_{-1.147}(\beta)$	$J_{-0.119}(\alpha)J_{1.119}(\beta)+J_{0.119}(\alpha)J_{-1.119}(\beta)$
f_4	$J_{-0.192}(\beta)J_{1.192}(\alpha)+J_{0.192}(\beta)J_{-1.192}(\alpha)$	$J_{-0.147}(\beta)J_{1.147}(\alpha)+J_{0.147}(\beta)J_{-1.147}(\alpha)$	$J_{-0.119}(\beta)J_{1.119}(\alpha)+J_{0.119}(\beta)J_{-1.119}(\alpha)$
f_5	$J_{0.192}(\beta)J_{-1.192}(\beta)+J_{-0.192}(\beta)J_{1.192}(\beta)$	$J_{0.147}(\beta)J_{-1.147}(\beta)+J_{-0.147}(\beta)J_{1.147}(\beta)$	$J_{0.119}(\beta)J_{-1.119}(\beta)+J_{-0.119}(\beta)J_{1.119}(\beta)$
f_6	$J_{-0.192}(\alpha)J_{1.192}(\alpha)+J_{0.192}(\alpha)J_{-1.192}(\alpha)$	$J_{-0.47}(\alpha)J_{1.147}(\alpha)+J_{0.147}(\alpha)J_{-1.147}(\alpha)$	$J_{-0.119}(\alpha)J_{1.119}(\alpha)+J_{0.119}(\alpha)J_{-1.119}(\alpha)$
P1	$(f_5 b^{0.5}-f_3 a^{0.5})$	$(f_5 b^{0.5}-f_3 a^{0.5})$	$(f_5 b^{0.5}-f_3 a^{0.5})$
P2	$(f_4 b^{0.5}-f_6 a^{0.5})$	$(f_4 b^{0.5}-f_6 a^{0.5})$	$(f_4 b^{0.5}-f_6 a^{0.5})$
P	$Z[a^{3.1}P_1-b^{3.1}P_2]-\omega L f_1 f_2$	$Z[a^{3.9}P_1-b^{3.9}P_2]-\omega L f_1 f_2$	$Z[a^{4.7}P_1-b^{4.7}P_2]-\omega L f_1 f_2$

EFFECTS OF SKEW ANGLE ON BENDING MOMENT'S DISTRIBUTION IN THE SKEW BRIDGE DECK

Ghaidak A. Fadhil
Assistant Lecturer, University of Baghdad, Iraq

ABSTRACT

In this paper the effect of skew angle on reinforced concrete skew bridges deck is presented by using the grillage analogy. The actual decking system of the bridge is represented by an equivalent grillage of beams. A span 24 m of simply supported right bridge deck with I-section prestressed concrete girders is taken as the case study to obtain the values of the bending moment's distribution for the two types of skewness (types 1 and 2) and the results of skew types are compared against the moments of the right deck span of the bridge. In the skew type 1 the deck span is increased as skew angle increased while in type 2 there is no increase in the desk span. The analysis results for the span are obtained dead and live loads (Iraqi standard load and walkway loading) using STAADPRO computer program. The analysis provided useful information about the variation of moments with respect to change in skewness. It is concluded that in skew bridge deck, the bending moment is increased with increasing the skew angle in skew type 1 while it is decreased with increasing the skew angle in skew type 2 and the negative bending moment in transverse direction and the torsion are increased.

KEY WORDS

Skew bridge deck, grillage analogy, bending moment, standard Iraqi load

الخلاصة

في هذا البحث تم دراسة تاثير زاوية الانحراف (Skew angle) على الجسور الخرسانية باستخدام طريقة المشبكات (grillage analogy) حيث تم نمثيل نظام الارضية الحقيقية للجسر بشبكة مكافئة من الروافد.ارضية الجسر بالاسناد البسيط وذات الفضاء المستقيم الذي يبلغ طوله ٢٤ متر مع الروافد الخرسانية مسبقة الجهد ذات مقطع عرضي بشكل حرف I استخدمت في هذا البحث لتحديد قيم العزوم الداخلية للجسر بعد تدويره بطرقتين مختلفتين من طرق تدوير الجسور الممستخدمة واقعيا ومقارنة النتائج مع العزوم المستحصلة من الحالة المستقيمة للجسر. النوع الاول من التدوير يسبب زيادة في طول فضاء الجسر وهو قليل الاستخدام واقعيا اما النوع الثاني يبقى محافظا على طول فضاء الجسر وهوالاكثر شيوعا في الجسور. نتائج التحليل فد حددت تحت تاثير الحمل الميت والحمل الحي (الحمل العراقي القياسي يالاضافة الى الحمل الحي على المماشي الجانبية للجسر) باستخدام برنامج الحاسبة STAAD PRO . التحليل اعطى معلومات مفيدة حول تغيير العزوم قياسا بتغيير زاوية الانحراف للجسر. حيث وجد ان عزم الانحناء يزداد بزيادة زاوية الانحراف وذلك للنوع الاول من انواع التدوير للجسور. كما وجد ان عزم الانحناء يقل بزيادة زاوية الانحراف وذلك للنوع الثاني من انواع تدوير الجسور يرافق هذا النقصان في عزم الانحناء زيادة في عزم اللي (torsion) وكذلك زيادة في عزم الانحناء السالب الذي يظهر بالاتجاه العرضي للجسر.

INTRODUCTION

Nowadays many of bridge decks are built with some form of skew. The bridge skewness is used in order to increase high speeds and more safety requirements of the traffic, modern as connection of highways with bridges are to be continuous as far as possible. The skew angle is the inclination of the centerline of traffic to the normal to the centerline of the river in case of a river bridge or other corresponding obstruction. The increasing demand for high skew bridges has been accompanied by the development of computer aided methods of analyze, and it is now generally possible to analysis and design a structure at any angle of skewness (Hambly, 1976; Gupta and Misra, 2007).

Many methods are used in analysis of skew bridges such as grillage and finite element methods. Generally, grillage analysis is the most common method in bridge analysis. In this method the deck is represented by an equivalent grillage of beams (Kakish, 2007), the finer grillage meshes, provides more accurate results. The method is applicable to bridge decks with simple as well as complex configurations with almost the same ease and confidence.

The main aim of the present study is to investigate the maximum moments of highway bridges by the use of grillage method to idealize the bridge deck systems under effect of standard Iraqi load UDL (Iraqi Standard, 1978). The present paper is carried out for beam and slab deck system, 14 m in width of deck forming a 9m carriageway and two sidewalks 2.5m each is analyzed for 24 m right span for skew angle of 0, 10, 20, 30, 40, 50 and 60 degrees by using two types of skewness as shown in **Fig. 1**. In the skew type 1 (Cussens, 1975; Gupta and Misra, 2007) the deck span is increased with increasing of skew angle, the span of a skew bridge measured along an unsupported edge of the bridge in plan is the skew span and the perpendicular distance between the two lines of supports is considered the right span. In the skew type 2 (Hambly, 1976; Bakht, 1988) there is no increase in the deck span and the rotation is done in the supported edge, this type of skewness is more efficient than skew type 1 because there is no need to increase in girders and deck slab length.

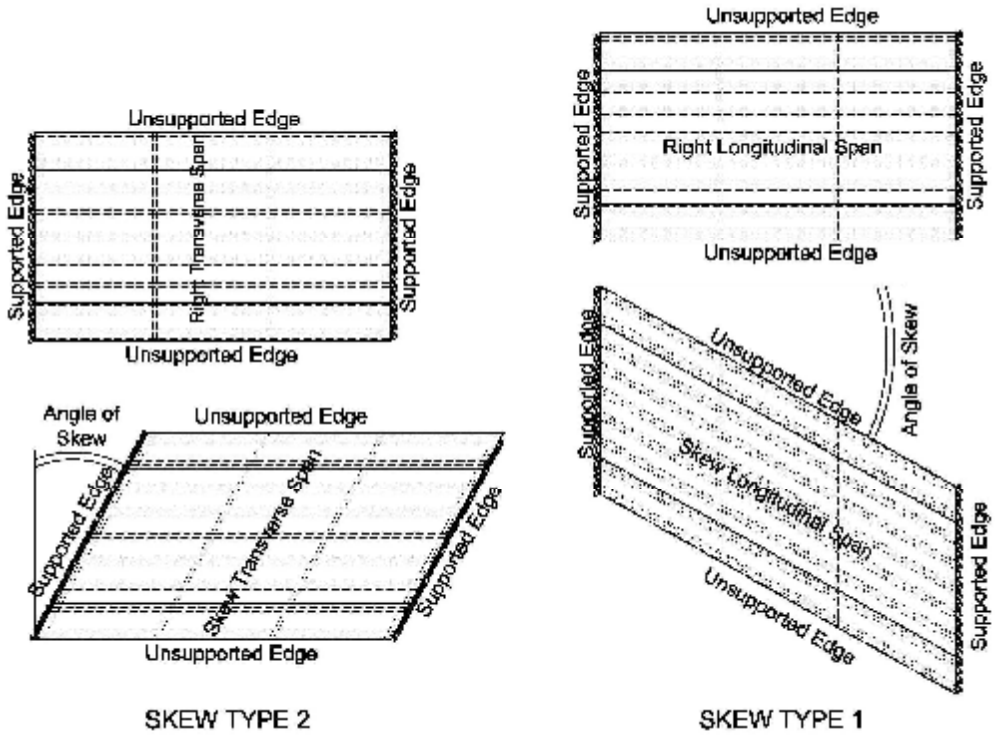

Fig. 1, Types of skew decks

ANALYSIS LAYOUT

The analysis layout in this paper is relatively inexpensive and has been proved to be reliably accurate for a wide variety of bridges as in below articles.

Information About Selected Bridge

The bridge deck type is a beam and slab deck of simply supported span length (24m) center to center of piers, the total width of deck is (14m), the span of the bridge deck is constructed of the nine precast concrete girders I-cross section with depth (1.2m) which are connected by cast in situ deck slab of thickness (20cm) and four diaphragms as shown in **Fig. 2**. The deck slab is covered by asphalt surfacing layer of (7cm), the slab thickness is increased by additional concrete layer to be (40cm) for (2.5m) width at the two sides of the (9m) carriageway (Al-Sabbagh, 1999).

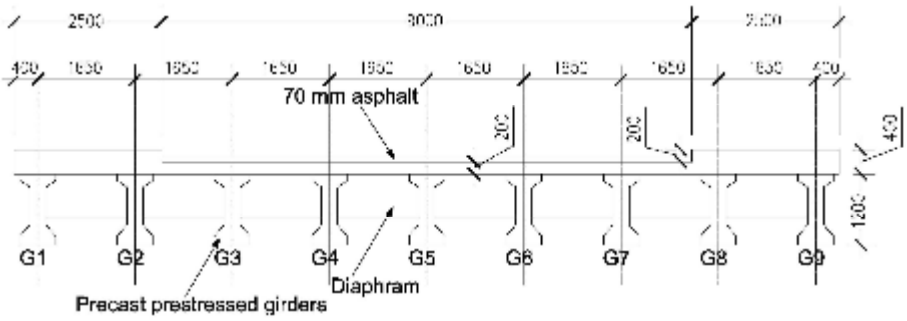

a-cross section

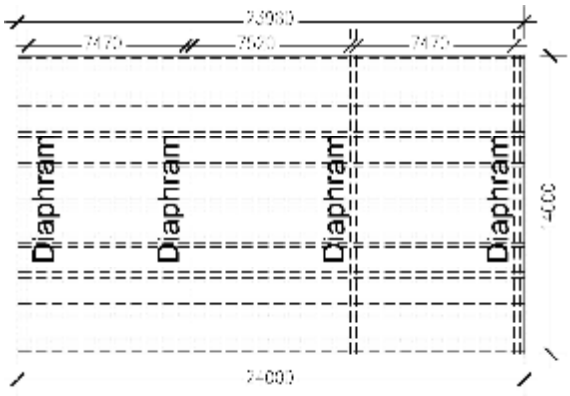

b-top view bridge deck

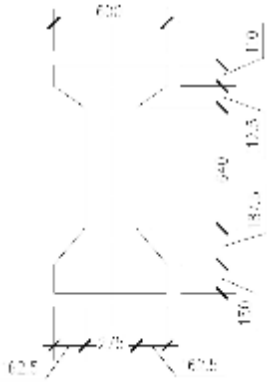

c-girder dimensions details

Fig. 2, Selected bridge layouts (Al-Sabbagh, 1999)

Idealization of the Bridge by Grillage

The grillage analogy is used in the analysis of the bridge deck (Hambly, 1976). This method is based on representing the actual decking system of the bridge by an equivalent grillage of beams. For the purpose of analysis the distributed bending and torsional stiffness of the decking system are assumed to be concentrated in these beams.

The concrete bridge span is idealized by substituting it by (162) longitudinal grillage members located along the webs centerlines and (152) transverse grillage members as shown in **Fig. 3**. The grillage members were rigidly connected at the intersection joints and the span is supported at its ends on the line of supports as in

Fig. 3. A linear elastic analysis was used. The recommendations suggested by (West, 1973) were used to compute the properties of the grillage members. The required section properties are the flexural inertia (I), the torsional inertia (J), the cross section area (A) of each grillage members, the cross section area is used to include the shearing deformation in deflection calculations. The grillage members were classified into nine (T1-T9) types for this span according to the section type. **Table 1** shows the grillage members properties, where I and J are calculated by using the computer program PROKON.

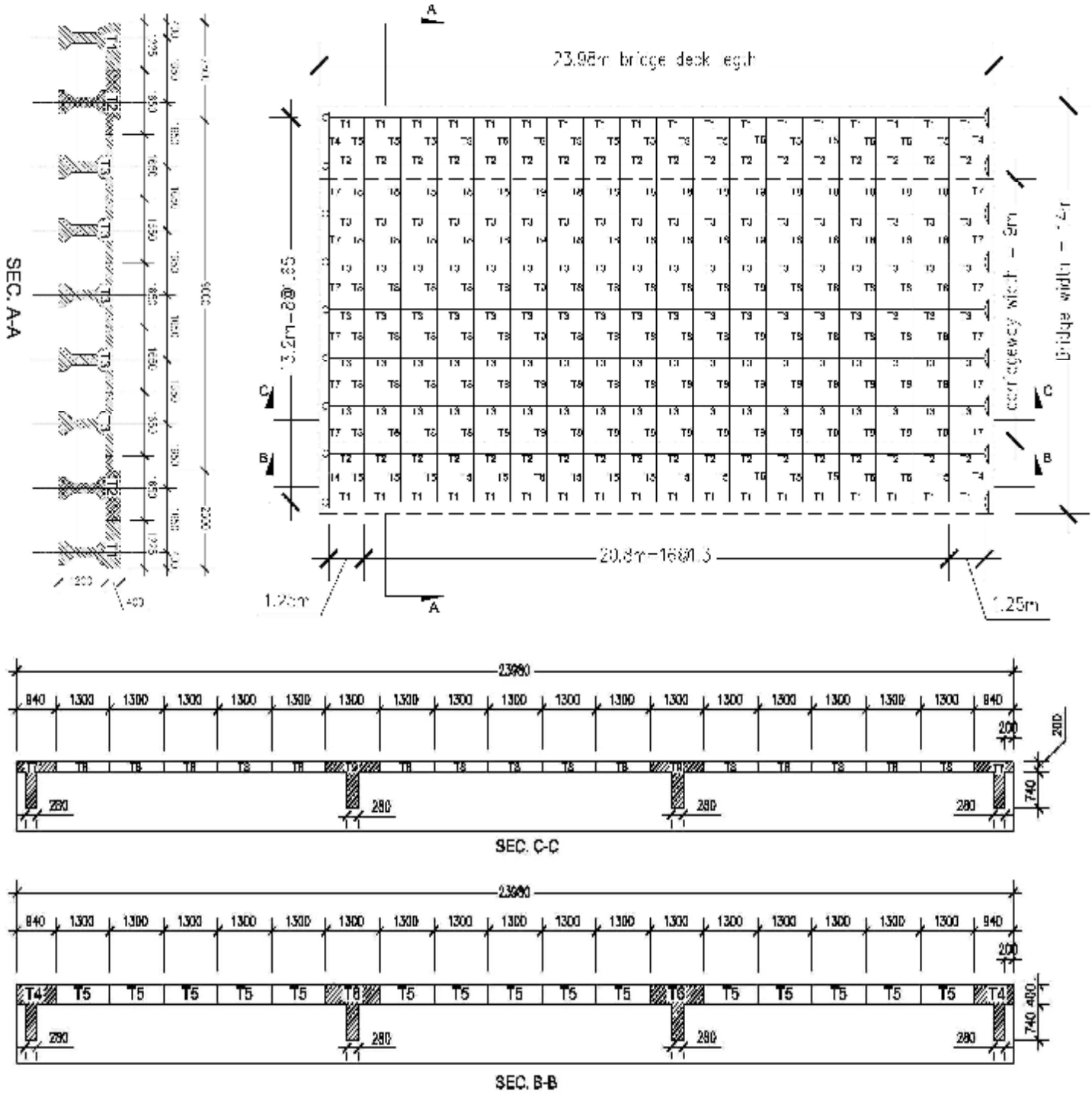

Fig. 3, Grillage mesh and types of its members

Table 1, Grillage member properties

Member type	I (mm^4)	J (mm^4)	A (mm^2)
1	226.58×10^9	43.1×10^9	890050
2	234.68×10^9	46.3×10^9	985050
3	165.79×10^9	17.5×10^9	730050
4	57.871×10^9	22.4×10^9	583200
5	6.9333×10^9	22.4×10^9	520000
6	64.527×10^9	8.86×10^9	727200
7	31.855×10^9	7.97×10^9	395200
8	866.67×10^6	3.16×10^9	260000
9	35.793×10^9	8.86×10^9	467200

The (T1-T9) types can be divided in longitudinal and transverse members, where the first group represent the main girders composite with deck slab, and the other group represent the deck slab itself in the transverse direction. The spacing of transverse grillage members has been selected, so that, it does not exceed (1.5) times the spacing of longitudinal members.

The analysis is accomplished by the software program "STAAD PRO" for grillage structure. This program is the most popular structural engineering software and the program enables the user to input the difference level of the neutral axes of the grillage members at each start and end joints of a member. **Table 2** gives the offsets of the grillage members (all offsets are in the vertical direction on grillage plane). Grillage member type (3) is assumed to be at level 0.0 in x-z plane. So, the offset values for other member types have been measured according to this level.

Table 2, Grillage members offset (in mm)

Grillage member types	1	2	3	4	5	6	7	8	9
Member offset (mm)	127	155	0.0	297.5	500	337.6	153.6	400	191.6

Application of Loading

In the analysis all cases are considered for both dead and live loadings which are applied on the deck that was modeled by grillage meshes and the bridge deck responses are determined.

The dead load of the bridge deck can be calculated according to the deck cross section, where the precast girder, deck slab, diaphragms and asphalt are considerable in the dead load calculations with concrete density = 25 kN/m^3 and asphalt density = 22 kN/m^3, these dead loads were applied for the concrete span and the responses are obtained.

In the live load applications, two types of loadings which are taken into consideration, the first is the Iraqi specifications of highway bridge loading issued by the Development Board in June 1962 and revised in 1972 and 1978 and adopted for global analysis (Iraqi Standard, 1978). The standard loading (S.L) as uniformly distributed lane loading (UDL) per linear meter of notional lane. This load is to be decreased as the loaded length and lane width are increased. In addition to (UDL) a concentrated knife-edge load (KEL) which is uniformly distributed across the width of the notional lane is also considered. The carriageway of the bridge is divided into

three notional lanes each of (3.0m). Full S.L is to be applied to two notional lanes and one-third of S.L to other lane. Two cases of standard loading distribution were considered as shown in **Fig. 4**, the values of nominal lane loading for the effective length (23.3m) of the span as follows:-

$$S.L = 10.3\frac{kN}{m^2} \qquad KEL = 39.42\frac{kN}{m}$$

The other type of the live load is the walkway loading that was taken 4 kN/m^2, the effect of the critical walkway were added to the effect of the critical standard load by superposition.

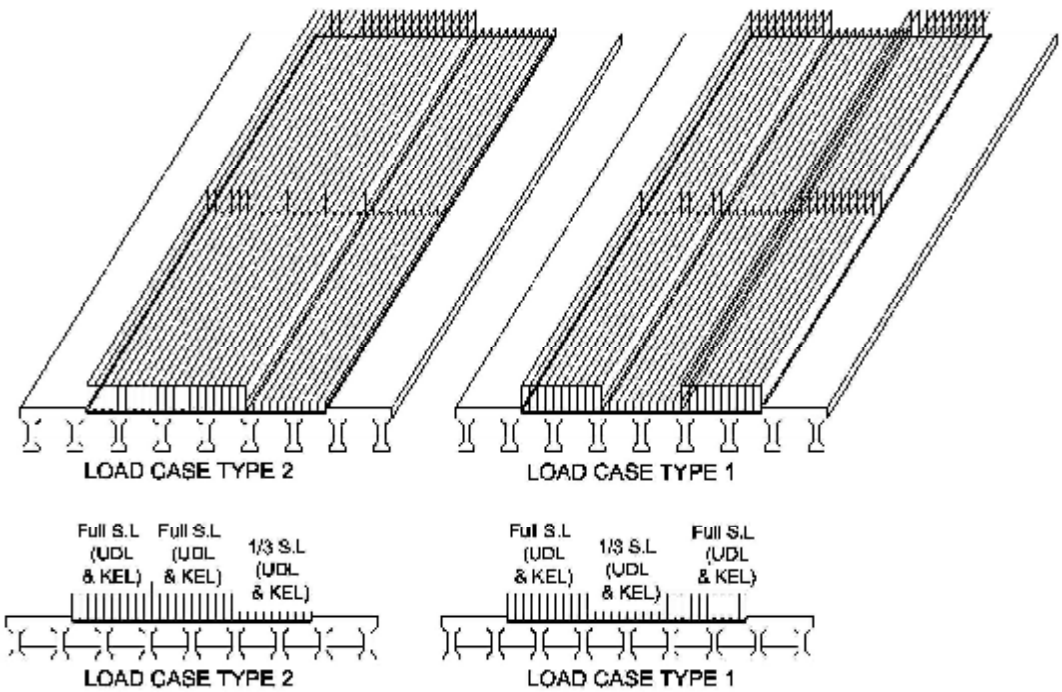

Fig. 4, Live load cases for Iraqi standard loadings

RESULTS AND DISCUSSIONS

To assess quantitatively the effect of analyzing real life skew bridges, several skew angles (0°, 10°, 20°, 30°, 40°, 50° and 60°) for two types of skewness are analyzed and compared with right bridge to examine the effects on the major principal moments

Skew Type (1)

In this type of skewness the span is rotated at the required angle and set the abutment at the same arrangement. The analysis is done with the abutment set at the same length (which means the perpendicular distance between girders decreases) for angles (0° to 60°) with fixing the applied loads and idealization system to find the effect of the skew angle on the maximum moment, then the results from the output of analysis of bridge decks are obtained. The maximum moments have been calculated for this type of skewness under the effect the dead load, the live load and the total load separately. **Fig. 5** shows that the relationship between the maximum moments and the skew angles and also it presents a comparison between the maximum moments

obtained from the different types of loadings. The maximum moment under the effect of total loads at 0° skew angle is 2963 kN which increases to 5143 kN at 60° skew angle. The relationships between the ratios of increased maximum moments to the original moment versus the skew angles for different types of loadings are given in **Fig. 6**.

To keep the same traffic width (perpendicular distance to the span) a new mesh is used to idealize the bridge for each skew angle because the horizontal distances between joints are increased which means that the abutment stays in the same arrangement but its length is increased. The relationship between the maximum moments and the skew angles under the total load effect is shown in **Fig. 7**. The maximum moment under effect of the total loads at 0° skew angle is 2963 kN which increases to 10381 kN at 60° skew angle.

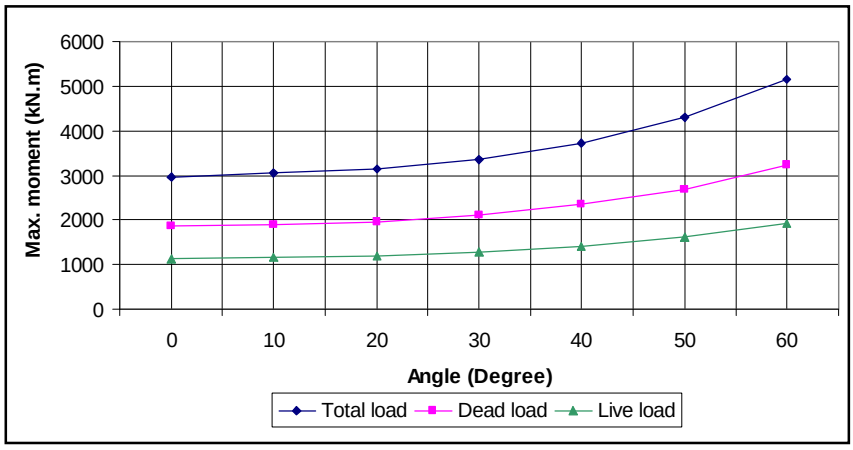

Fig. 5, Maximum moments for 24 m right span (skew type 1)

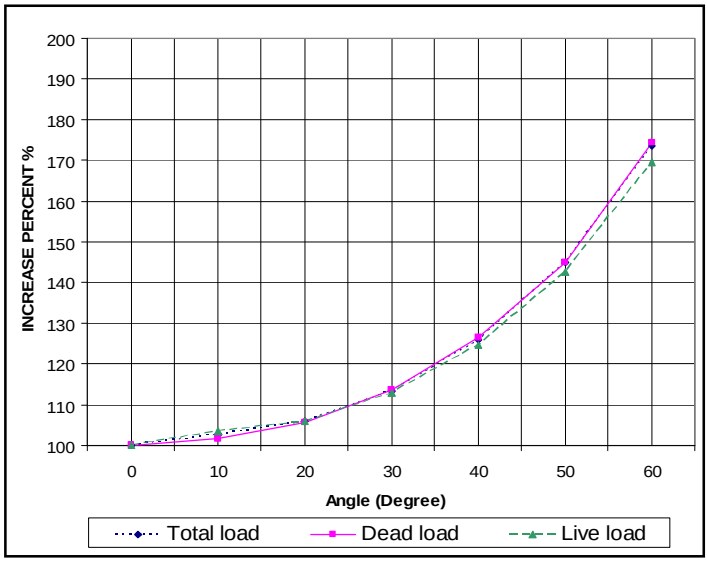

Fig. 6, Increase percent in the moments for 24 m right span (skew type 1)

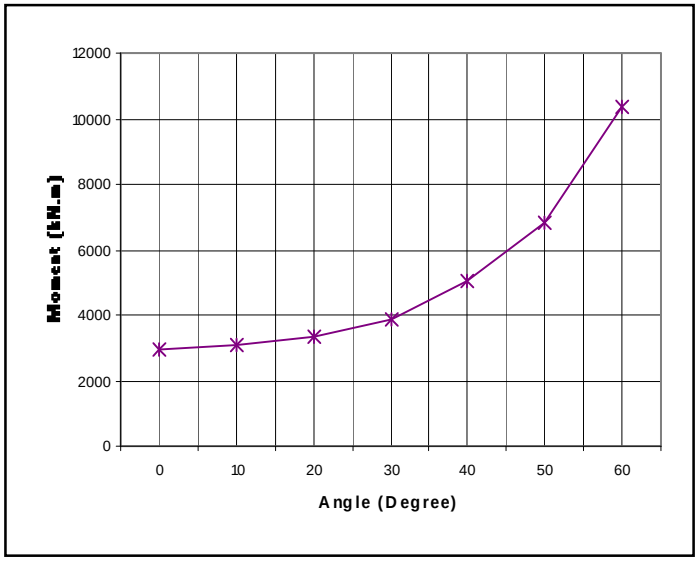

Fig. 7, Maximum moments for 24 m right span (skew type 1 with mesh modification)

Skew Type (2)

This type of skew has the most publicity and widespread use in the construction of highway bridges. In this type of skewness the abutment is rotated at the required angle with keeping the span between the abutments at the same length.

In the present paper, the analysis is done for angles (0° to 60°) to find the effect of the skew angle on the maximum moment then the results from the output of analysis of bridge decks are obtained.

The maximum moments have been calculated for this type of skewness under the effect of dead load, live load and total load separately. **Fig. 8** shows that the relationship between the maximum moments and the skew angles and also it presents a comparison between the maximum moments obtained under the different types of loadings. The maximum moment under the effect of total loads at 0° skew angle is 2963 kN which decreases to 2551 kN at 60° skew angle, and the maximum moment under the effect of live loads at 0° skew angle is 1128 kN which decreases to 981 kN at 60° skew angle. Also the maximum moment under the effect of dead loads at 0° skew angle is 1855 kN which decreases to 1613 kN at 60° skew angle.

The relationship between the maximum torsions and the skew angles under the total load effect is shown in **Fig. 9**. The maximum torque under the effect of total loads at 0° skew angle is 31 kN which increases to 345 kN at 60° skew angle.

The relationship between the maximum negative moment in transverse direction and the skew angles under the total load effect is shown in **Fig. 10**. The maximum moment in diaphragms under the effect of total loads at 0° skew angle is -74 kN which increases to -317 kN at 60° skew angle.

Table 3 shows the values of maximum moments and torque in longitudinal direction and maximum moment in transverse direction under the effect of live, dead and total loads.

Table 3, Maximum values of moments and torque

angle	Max. moment in longitudinal dir.			Torque	Max. neg. moment in transv. dir.
	Total load	Live load	Dead load		
0	2963.235	1127.985	1854.526	30.734	-73.951
10	2960.808	1126.481	1852.617	63.486	-80.83
20	2946.713	1119.303	1844.03	98.364	-94.186
30	2917.07	1105.358	1826.701	146.942	-117.542
40	2860.194	1079.445	1794.436	203.624	-152.918
50	2753.352	1032.787	1733.861	270.509	-207.453
60	2551.314	980.845	1612.683	344.843	-316.46

Fig. 11 shows the bending moment diagrams for the girder G1 that is located approximately in the edge span, under the effect of total loads. The relationship between the distance and the average moment in the joints is appearing clearly in this figure for the different skew angles from 0° to 60°. The value of moment diagrams are decreased with the increasing of the skew angles in all joints except the joints at supports at which the moment approaches to zero (simply supported span). **Fig. 12** shows the bending moment diagrams for the girder G5 which is located in the mid-span under the effect of total loads. The relationship between the distance and the average moment in the joints is appearing clearly in this figure for different skew angles from 0° to 60°. The values of moment diagrams are decreased with increasing the skew angles.

The bending moment diagrams for the diaphragm that is located at first span under the effect of total loads is shown in **Fig. 13**. The relationship between distance (the length of diaphragm) and the moments (two moments at each internal joint) is appearing in this figure for different skew angles from 0° to 60°. The bending moment diagrams for the diaphragm that is located at one-third span under the effect of total loads is shown in **Fig. 14**. The relationship between distance (the length of diaphragm) and the moments (two moments at each internal joint) is appearing in this figure for different skew angles from 0° to 60°.

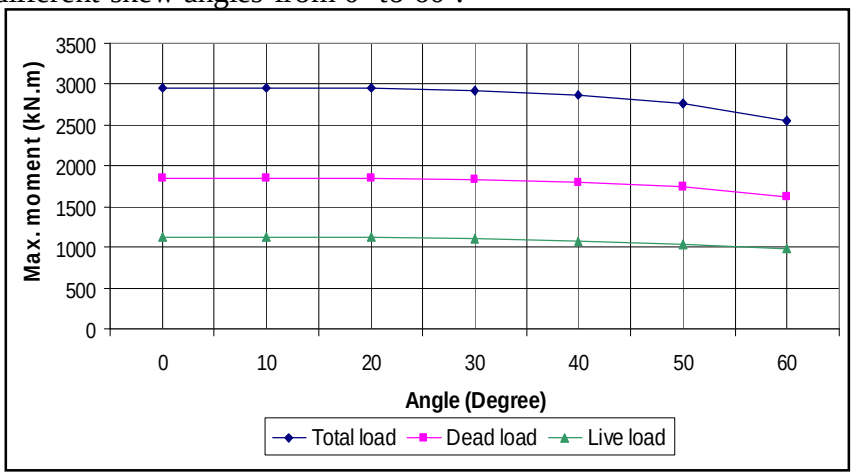

Fig. 8, Maximum moment for 24 m right span (skew type 2)

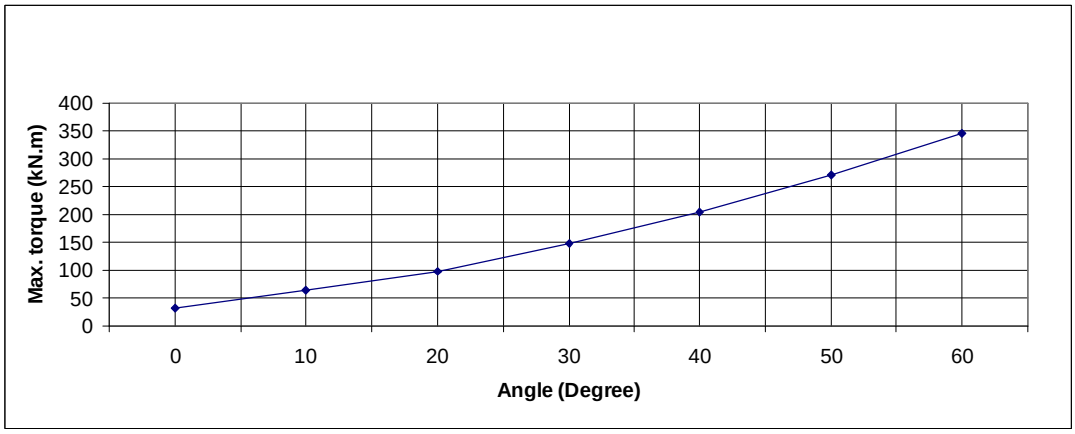

Fig. 9, Maximum torque for 24 m right span (skew type 2)

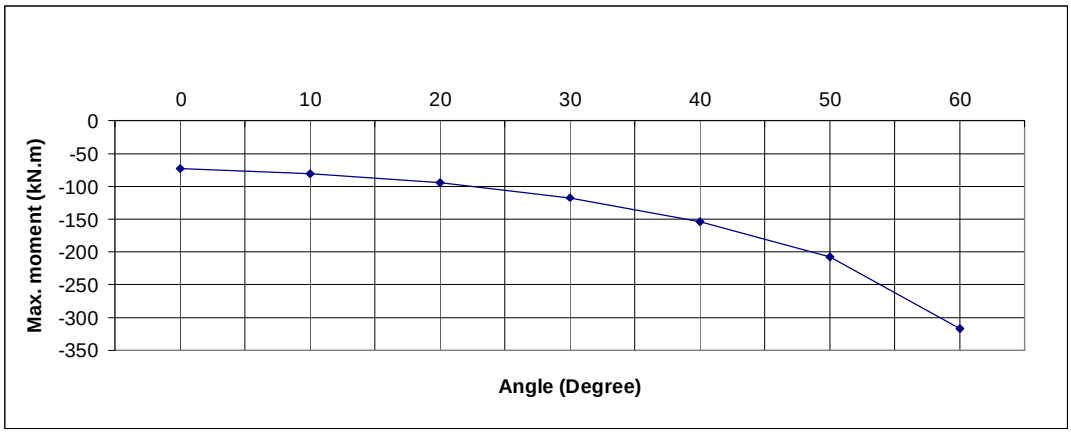

Fig. 10, Maximum negative moment in transverse members for 24 m right span (skew type 2)

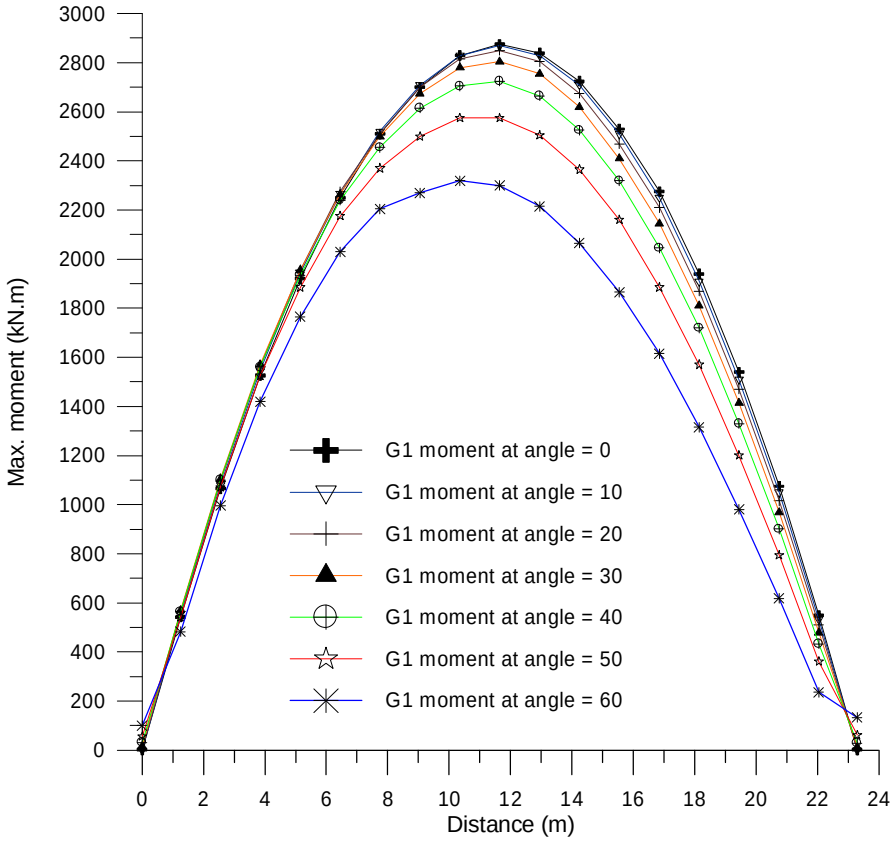

Fig. 11, Bending moment diagrams in the G1 location at edge span (skew type 2)

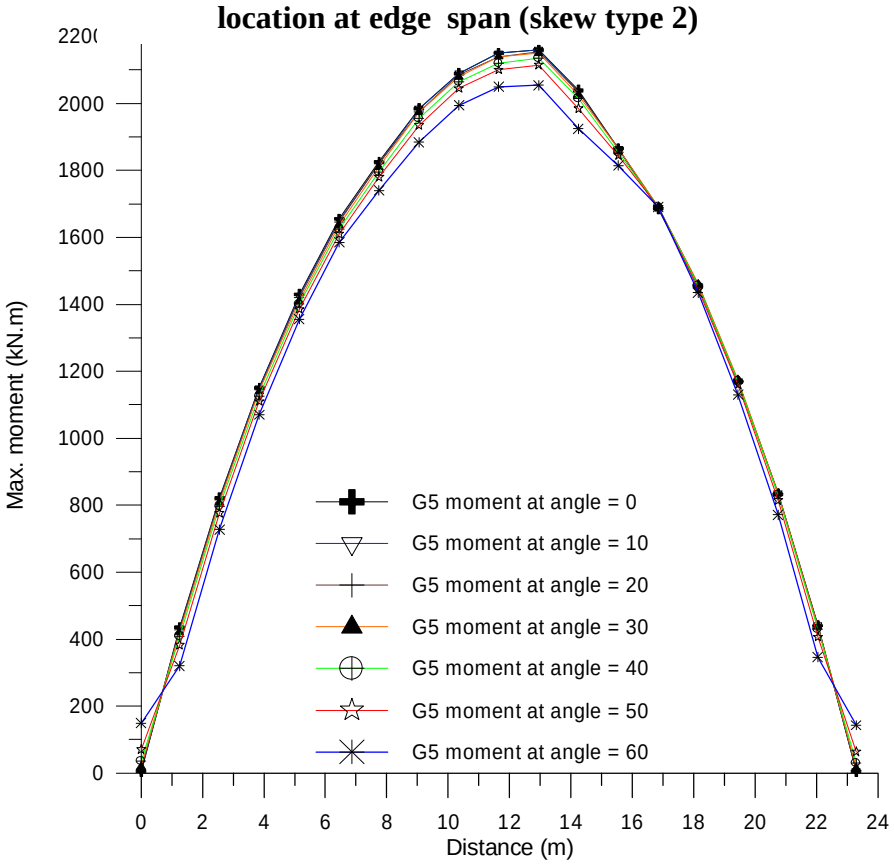

Fig. 12, Bending moment diagrams in the G5 location at mid span (skew type 2)

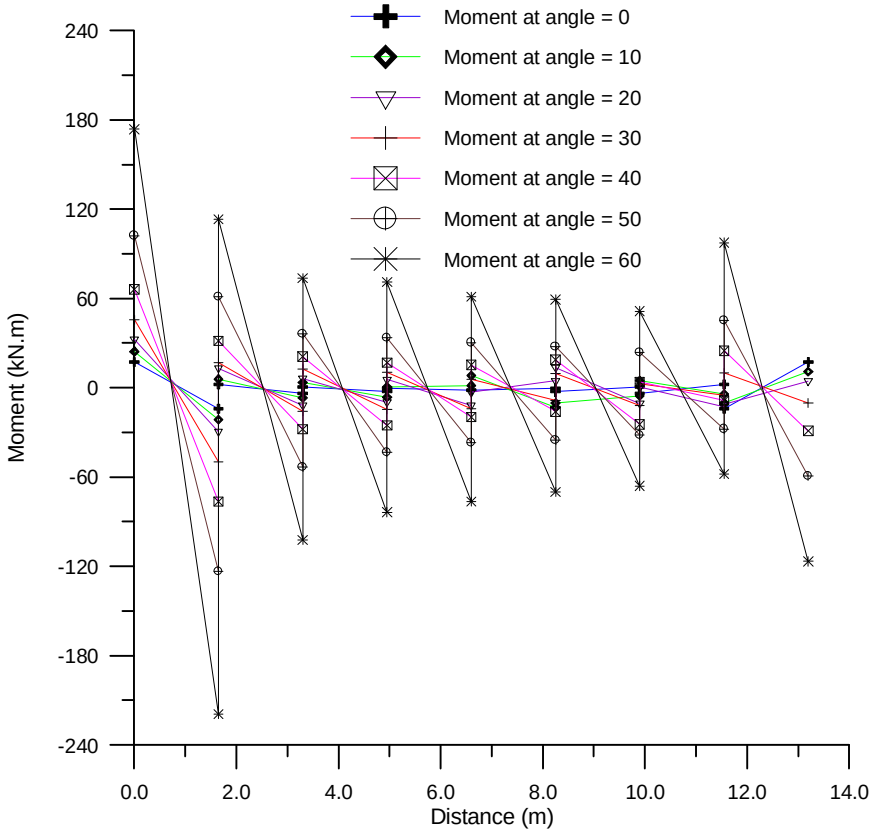

Fig. 13, Bending moment diagrams in the diaphragm location at first span (skew type 2)

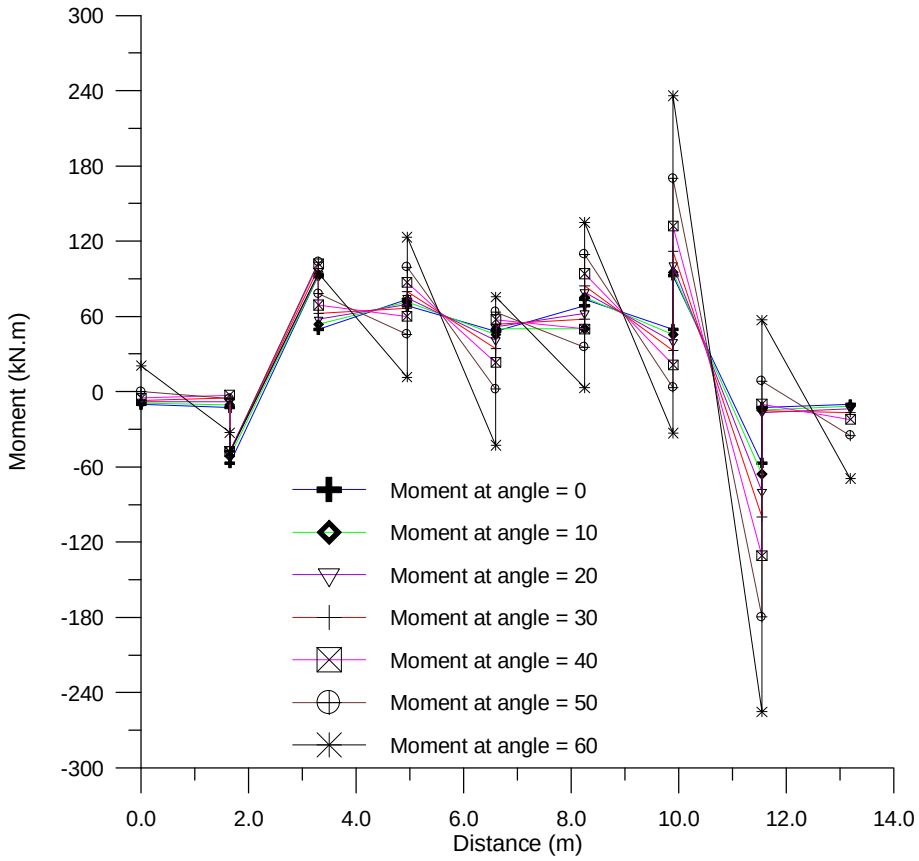

Fig. 14, Bending moment diagrams in the diaphragm location at one-third span (skew type 2)

CONCLUSIONS

The grillage analogy of analysis for bridge decks is versatile, easy for engineers to visualize and prepare the data. It has been found that in skew bridges, the moments develop with the change of skew angle. Based on the results of the analysis, the following conclusions are drawn:

- In the skew type 1 which is used in the special case of highway bridges the maximum moment increases with increases of skew angle. The maximum moment is reached at angle 60° to 175% than the maximum moment at right span, so, it depends on the skew angle only and this percent is increased up to 350% when the effect of increasing the dead load and the live load (due to increase of the span) are taken into consideration.
- In the skew type 2 which is more widespread in the skew highway bridges the maximum moment in the longitudinal direction decreases with increases in the skew angle. The maximum moment is reached to 86% at skew angle 60°, on the other hand the maximum torque increases with increases of skew angle for more than ten times that the torque in the right span at angle 60°. Also the maximum negative moment in the transverse direction increases as the skew angle increases this increase reaches to four times it values at right span when the skew angle reaches to 60°.
- According to the results obtained here, it is preferable to use the skew type 2 in the highway bridge decks more than skew type 1.

REFERENCES

- Al-Sabbagh, L. A. M., 1999,"Structural Evaluation of the Superstructure of Al-Kut Reconstructed Highway Bridge", M.Sc. Thesis presented to the University of Baghdad.

- Bakht, B., October 1988,"Analysis of Some Skew Bridges as Right Bridges", Journal of Structural Engineering, ASCE, Vol. 114, No. 10, 2307-2322.

- Cussens, A. R., and Pama, R. P., 1975,"Bridge Deck Analysis", John Wiley and Sons, London.

- Gupta, T., and Misra, A., February 2007," Effect on Support Reactions of T-Beam Skew Bridge Decks", ARPN Journal of Engineering and Applied Sciences, Vol. 2, No. 1.

- Hambly, E. C.,1976, "Bridge Deck Behaviour", Chapman and Hall, London.

- Iraqi standards, 1978, "Iraqi Standard Specifications for Roads and Bridges (Loadings)", Ministry of Housing and Construction, State Organization of Roads and Bridges, Baghdad.

- Kakish, M., 2007,"Bending Moments Distribution at the Main Structural Elements of Skew Deck-Slab and Their Implementation on Cost Effectiveness", American Journal of Applied Sciences, Vol. 4, Issue 12, 1036-1039.

- West, R., 1973," Recommendations on the Use of Grillage Analysis for Slabs and Pseudo-Slab Bridge Decks", Cement and Concrete Association.

FEASIBILITY STUDY OF POWER SAVING BASED ON USING EMMEDUE M2 BUILDING SYSTEM

Dr. Akram. W. Izzat
Mechanical Engineering Department
University of Baghdad

ABSTRACT

The present work concentrates on the feasibility of the heat load reduction by utilizing some structural material with very poor heat conductivity as isolators for heat transmission. Average annular heating and cooling load is estimated for a typical building of certain area and design using ordinary structural material and EMMEDUE M2 building system. The basic element of the new structural material is made of a foam polystyrene core that is self extinguishing and chemically inert with varying density and thickness depending on panel type. The calculations are based on the average maximum and minimum monthly temperature in Baghdad. Building heating load could mainly depend on the average temperature difference per each daily hour per year, while building cooling load components are; direct solar radiation, transmission load, ventilation/infiltration load and internal load. Except the transmission load which depends on the same average temperature difference the other factors could be calculated separately.A reduction of 55% in the annual load is estimated per each house using the new building technology. For a district sums up 1000 houses of the new structural design the total saving of power will be 10.45 MW. The saving in heating and cooling cost is estimated based on capital cost of the diesel generation system and the fuel consumption cost. It has been concluded that the passive structural heat isolation is a very effective manner in countries like Iraq which has severe temperature differences between the summer and winter seasons.

الخلاصة:

يتركز البحث على مدى عملية تقليل الحمل الحراري بأستخدام مواد بناء ذات توصيل حراري ضعيف كمواد عازلة للأنتقال الحراري. تم تخمين معدل الحمل الحراري والتريد السنوي لبناية نموذجية ذات مساحة وتصميم معين بأستخدم مواد بناء عادية مقارنة بمادة بناء EMMEDUE M2. العنصر الأساسي في مادة البناء الجديدة مكونة من مادة البوليسترين الرغوية ذات قابلية الأطفاء التلقائي وغير الفعالة كيمياويا وبكثافات مختلفة وسمك يعتمد على نوع القطعة.تم بناء الحسابات على معدل القيم العليا والسفلى لدرجات الحرارة الشهرية في مدينة بغداد. يعتمد الحمل

الحراري على معدلات فرق درجات الحرارة اليومية على مدار السنة بينما يعتمد حمل التبريد على: أشعة الشمس المباشرة, الحمل الأنتقالي، حمل التهوية، والحمل الداخلي. بأستثناء الحمل الأنتقالي الذي على نفس معدلات فروقات درجات الحرارة فأن بقية العوامل تحسب بشكل مذ صل.
تم تخمين مفدار النقصان في قيمة الحمل السنوي بقيمة مقدارها ٥٥% لكل بناية يتم فيها أستخدام مواد البناء العازلة والمشار اليها في البحث. لحي سكني مكون من ١٠٠٠ بناية مبنية من مادة البناء العازلة يكون مقدار الأدخار في طاثة التدفئة والتبريد ١٠.٤٥ ميكاواط. تم حساب معدل الأدخار في كلفة التدفئة والتبريد بناءا على القيمة الفعالة لمنظومة التوليد وكلفة الوقود المتسخدم لمدة سنة. حيث تم الأستنتاج من البحث أن أستخدام مواد البناء العازلة في دول ذات مناخ قاري يكون ذا جدوى اقتصادية عالية جدا.

KEYWORDS
EMMEDUE M2, Heating & Cooling Load, Feasibility, Annual Load

INTRODUCTION

From the beginning of recorded human history people have sought shelter from wind, rain, and snow either in caves or in buildings which they have built for that purpose. In addition to shelter from the elements the buildings provide an opportunity to control the temperature and humidity of the air inside them. People are most comfortable when the temperature is around 70°F and the humidity is moderate. When the outside air is very cold, a furnace or some kind of a heat source inside the building can heat the inside air. When it is very hot outside, we try to control the flow of heat energy into the building and we may even cool the air with air-conditioning equipment. In either case the choice of building materials plays a critical role in our ability to maintain a comfortable temperature inside. The ground tends to remain cool, so caves, basements....buildings built partially underground tend to be cool in those parts that are underground. Certain types of brick or clay change in temperature slowly and tend to “hold in” the heat. Walls of these materials might heat up during the day - soaking in heat from the sun and from the inside air, and cool down at night - radiating to the cold night sky and also radiating energy to the inside air. Thick walls of brick, clay, or stone often provide a cool daytime shelter and a warm night shelter in hot climates. Thinner walls made of wood planks will not have the same properties. Unless we add other materials to those walls it will usually be difficult to maintain a different temperature inside relative to the outside temperature.
Heat energy flows from hot spaces to cold spaces and the rate at which this energy flow increases as the temperature difference increases. The material which separates the temperature extremes has a certain resistance to energy flow. When the resistance is high, the rate at which energy flows through the material is low; when the resistance is low, high energy flow rates are expected. We insulate walls to lower the rate at which energy flows through the walls. Insulation increases the thermal resistance or “R value” of the wall.

The second important factor which is taken under consideration is the heat capacity of the building materials. Heat capacity is a measure of a material’s ability to store heat energy. Metals tend to have low heat capacities. When heat energy flows through a metal, it changes temperature quickly. On the other hand, stone or cement has a much higher heat capacity. When heat energy flow into stone it changes temperature very slowly and tends to “store” the heat energy. Passive solar homes usually include a large mass of stone, rock, or other material with a high heat capacity. This thermal mass will heat up during the day when the sun shines. At night when it is cooler, energy can be drawn from the thermal mass.

ANSARI investigated the effect of building parameters like orientation, windows type wall insulation and roof & floor type on heating and cooling load calculations. ASHREE Handbook is based for all the heating and cooling load calculations.
One of the structural materials which have common use now in the world is the

EMMEDUE M2 Building System.

The IRISH agreement board proved that the EMMEDUE system meets the requirements of the building regulations 1997-2002, as indicated in section 1.2 of their certificate.

DESCRIPTION OF EMMEDUE BUILDING SYSTEM

Fundamentals of the System

The basis of the EMMEDUE construction system is based on a serious of a polystyrene panels and steel wire mesh, whose shape has been especially designed to apply structural plaster during panel installation. The aim is that of providing a system of industrialized modular panels that bodies requiring shorter erection time compared to the conventional systems, permits to copy with structural and load bearing functions, offering in the same time a fast assembling and laying, high thermal and sound coefficient and a wide range of shapes and finishes that may be achieved during the building process.

Composition of the EMMEDUE Panel

The basic element is made of:

1. A foam polystyrene core that is self extinguishing and chemically inert with varying density and thickness depending on panel type, see **Fig. (1)**.
2. Electro welded steel wire mesh made of galvanized drawn steel wires placed on both sides of polystyrene sheet and connected by means of joints of the same material. The wire gauge of the net varies according to panel type and mesh direction.

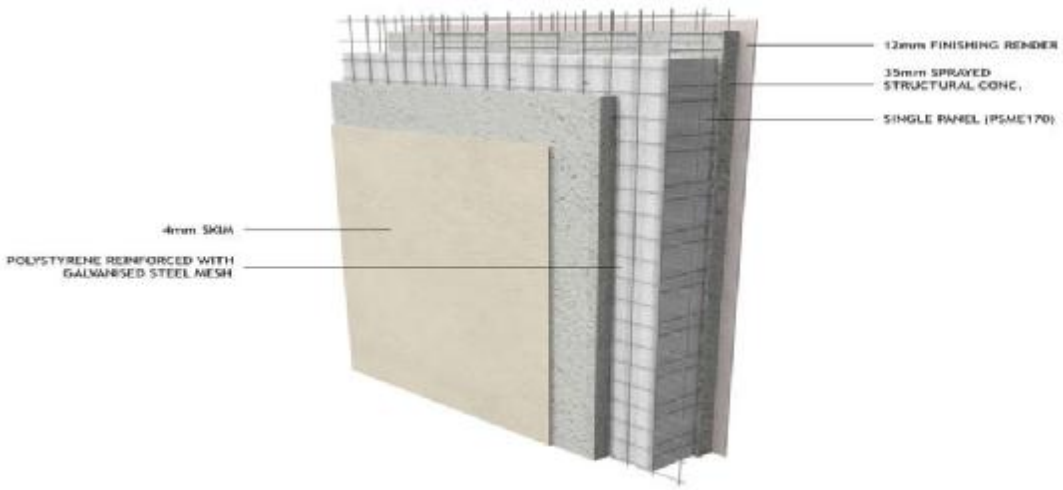

Fig. (1): EMMEDUE single panel Figure

Plastering

After Panel assembly, structural plaster should be sprayed and / or poured on the panel depending on the panel type.

Classification of the EMMEDUE Products

The various types of EMMEDUE panels, their fields of application, standard sizes and complementary EMMEDUE products are described EMMEDUE Me2 Building system catalogue certified by the IRISH AGREEMENT BOARD.
The thickness of the polystyrene sheets as well as the length of the panels may be customized according to different project requirements of customers.
Generally speaking the thickness the panels is usually determined according to its different conditions of heat insulation and required structural behavior. In the later case in fact, a greater moment of inertia may be achieved by increasing the interval between the concreted or plastered surfaces.
As far as the degree of heat insulation of polystyrene is concerned, a finished panel of 10 cm thickness with 4 cm thick polystyrene core corresponds to an ordinary brick wall 64 cm thickness.

HEAT LOAD CALCULATIONS

Assumptions and Postulates

The present research investigates the effect of the structural material selection on power saving based on heat load calculations for typical building in Baghdad.
Outside ambient temperature is estimated based on the annual temperature records in Baghdad for certain year.
This approach takes under consideration that the design temperature inside the building according to the national standards is 22 ^{o}C.
As the heat load is directly proportional to the temperature difference between the inside building design temperature and the surrounding temperature these differences are averaged per 12 months to facilitate the estimation of the annual power consumption saving due to implementation of the M2 material.
The dimension of the building is assumed according to a typical house building layout in Baghdad. Two types of structural material are selected for comparison purposes (conventional concrete and brick versus M2 EMMEDUE building system including the other structural material used with each of the two types).
The power saving calculation bases on the comparison between the energy required for the typical house building when two structural materials are used in construction. This calculation takes under consideration both the capital cost and the fuel cost required to ensure electric power for a district consists of 1000 house buildings per one year. The cost of the unit price of each of the constructional material is assumed to be equal.

Annual Temperature Records

The average values of the maximum and minimum temperatures per each month investigated from the annual temperature records in Baghdad is estimated based on the references of the Iraqi Meteorological Directorate, IMD, see **Table (1)**.
The calculation bases on averaging the temperature differences between the building inside design temperature and the surrounding higher temperature / or lower temperature per each day / or night intervals per each month assuming equal, (12) hours, for each of day and night, see **Table (2)**.

Table (1): Annual temperature records in Baghdad based on IMT references

Month	Minimum Temperature ^{o}C	Maximum Temperature ^{o}C
January	4	16
February	6	18
March	9	22
April	15	30
May	20	37
June	23	41
July	25	43
August	25	43
September	21	40

October	16	33
November	11	23
December	6	18

Table (2): Temperature differences between the building inside design temperature, 22 ^{o}C and the surrounding higher temperature / or lower temperature per each day / or night intervals per each month.

Month	Temperature difference at night, ^{o}C	Temperature difference at day, ^{o}C	Total temperature difference per day per month, ^{o}C
January	(22-4)	(22-16)	24
February	(22-6)	(22-18)	20
March	(22-9)	(22-22)	13
April	(22-15)	(30-22) *	15
May	(22-20)	(37-22) *	17
June	(23-22)	(41-22) *	20
July	(25-22)	(43-22)*	24
August	(25-22)	(43-22)*	24
September	(22-21)	(40-22)*	19
October	(22-16)	(33-22)*	17
November	(22-11)	(23-22)	12
December	(22-6)	(22-18)	20
Average temperature difference per each daily hour per year			18.75 ^{o}C

THERMAL PROPERTIES OF THE BUILDING MATERIAL

The rate at which heat gets transferred depends upon the thickness of the material, the thermal conductivity, k (this depends on the composition of the material), surface area of the material, A, and the temperature difference between the reservoirs.

In particular the rate of the heat transfer = A. k. (Th – Tc) / L. This equation shows that the thicker the material that separating the two reservoirs, the smaller the surface area that is contact, or the smaller the temperature difference, the slower the rate of heat transfer through the substance. When it comes to heating and cooling our homes, this is exactly what we need to strive for in order to reduce our energy bills.

In our homes the exterior surfaces are usually comprised of more than one type of material. For instance, a wall can be composed of 3 ½ inches of fiberglass insulation which is covered by ½ inches of sheetrock on the inside and plywood and brick on the exterior. When two or more different materials are between the hot and cold reservoir, the equation on the previous page can become quite messy since there will be various thermal conductivities and thicknesses with which to deal.

The equation is greatly simplified if we consider the R-value of objects instead of their thermal conductivity. This is a measure of how well the material resists the flow of heat

through it, and it combines the thermal conductivity and thickness into one term (R-value = thickness / thermal conductivity = L / k). While the common units for the R-value is ft^2. hr.^{o}F / Btu, these are often not quoted. It is likely to just see the R-value of a substance to just be quoted as a number as in "Fiberglass R-value = 13".

The R-factor of a surface determines how quickly heat is conducted across it. The values shown in **Table (3)** illustrate some of common R-factors for surfaces found on typical homes.

Table (3): R-factors for typical construction material

Exterior walls with siding

Concrete block (8")	Factor
(a.) Concrete block (8")	2.0
With foam insulated cores	20
With 4" on non-insulated stud wall	4.3
With 4' insulated stud wall	14
Brick (4")	
With 4" non-insulated stud wall	4
With 4" insulated stud wall	4
Wooden Frame	
Non-insulated with 2"x4" construction	4.6
With 1 ½" fiberglass	9
With 3 ½" fiberglass stud; studs 16' O.C	12
With 3 ½" fiberglass and 1" foam	20

Roof /Ceiling

Material	Factor
No insulation	3.3
3 ½" fiberglass	13
6" fiberglass	20
6" cellulose	23
12' fiberglass	43
12" cellulose	46
14" cellulose	54

Windows and Sliding glass walls

Glass	Factor	Low Emissivity	Drapes	Quits
Single panel	0.9	1.1	1.4	3.2
Single w / storm window	2.0		2.5	4.2
Double pane, ¼"air space	1.7		2.2	4.0
½" air space	2.0	2.99	2.5	4.3
Triple pane, ¼" air space	2.6		3.0	4.8
Triple pane, ½"air space	3.2	3.7	3.7	5.5

PRESENT CALCULATION APPROACH

The purpose from our calculation is to estimate the annual power saving based on both cooling and heating loads rather than investigation of the design parameters and requirements for the air conditioning system which mainly depends on the maximum outside temperature conditions.

In our case building cooling load and heating load are calculated together. Building heating load could mainly depend on the average temperature difference per each daily hour per year, see **Table (2)**, while building cooling load components are; direct solar radiation, transmission load, ventilation/infiltration load and internal load.

Except the transmission load which depends on the same average temperature difference the other factors could be calculated separately.

Calculating all these loads individually and adding them up gives the estimate of total load. The load, thus calculated, constitutes total sensible load. Normal practice is that, depending on the building type, certain percent of it is added to take care of latent load. Applying the laws of heat transfer and solar radiation makes load estimations.

Step by step calculation procedure has been adequately reported in the literature issued by ANSARI.

In our case we base the effect of the solar radiation on the cooling load only for the period at which the temperature differences represent the days of the seasons when there is direct sun radiation and which are marked by (*) in **Table (2)**.

Overall heat transfer coefficients for all the components of the building are computed with the help of thermal properties of the building materials. For the design conditions and the building materials used, cooling and heating load temperature difference, solar heat gain factors and cooling load components are calculated. Principles of solar energy calculation are applied to determine the direct and indirect solar heating component of the building.

First principle is applied to yields the rates of heat transfer through different building components. All these components, when added up, give the total cooling and heating load of a building.

The following assumptions are made to estimate the heating and cooling loads:

1. One story building, shown in **Fig. (2)**, is based for the load calculations.
2. The heating and cooling load based on transmission factor uses an effect factor of (1).
3. The lightening, equipment and personnel loads use an effect factor of (1), the building dimensions and internal details is shown in **Fig. (2)**.
4. The outside air flow uses an effect factor of (1).
5. The solar radiation factor for cooling load uses an effect factor of (0.5x0.85) where 0.5 represent the percentage of the sunny hours to total day hours, while (0.58) assumes the percentage of the days within one year when the outside temperature becomes higher than the building inside temperature.
6. Referring to **Table (3)** the heat conductance of the main structural material using the foam insulated core in 8” concrete block to that without insulation for both wall and ceiling material is assumed to be (0.15) for heat transmission factor.

7. The heating and cooling load calculations for isolated roof and walls are based on the double glass of glass block.
8. The air flow, lightening, equipment and personnel factors are shown in **Table (4)**.
9. **Table (4)** shows the main equation used for calculating the heating and cooling load components.
ASHREA handbook is used as basis for these calculations together with the assumptions implemented by RUDOY.

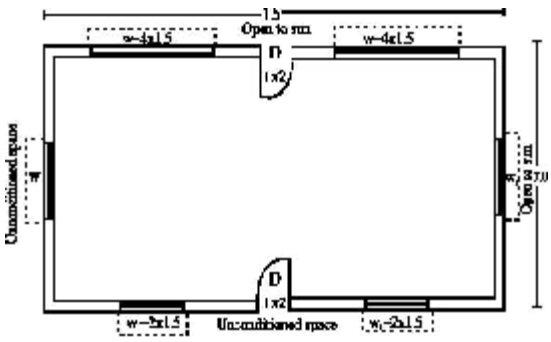

Fig.(2): Typical one story Building based for heating and cooling load calculations.

Table (4): Cooling and heating load estimations and equations

1. Direct solar radiation: (Figure all windows for each exposure, but use only the exposure with the largest load)		**For glass black reduce factor by 50%: for storm windows or double glass reduce factor by 15%.**		
Direction	**Windows Area, m2**	**No Shading Awn**	**Inside shade**	**Outside**
North-east	**4.5**	**190**	**79**	**63**
East	**12.0**	**158**	**126**	**79**
South-east		**237**	**95**	**63**
South	**4.5**	**237**	**111**	**63**
South-west		**347**	**142**	**95**
West	**6.0**	**473**	**205**	**111**
North-west		**379**	**158**	**95**
2. Window Transmission :				
Double glass of glass block (Area = 27m2)		**0.46241 + 3.026* ΔT**		
3. Walls:				
No insulation (brick, frame etc.), (Area=132m2)		**8.3932 + 1.21465* ΔT**		
4. Roofs:				

No insulation (Area= 105m2)	**48.82+1.55* ΔT**
5.Outside Air per cubic meter of flow area / 20 frequent door usage (Floor area=105m2)	**(2.01 + 0.71 * ΔT) / m2 floor area**
6. Lightening (Area=105m2)	**16.65 w/m2**
7. Equipment	**750 w**
8. Personnel	**440 w**

RESULTS AND CALCULATION

The results of the heating and cooling load calculations for a house of typical design, shown in **Fig. (2),** give a total load of 18,900 KW when ordinary concrete structure is used, while this load is reduced to 8,450 KW when the concrete structure is replaced by EMMEDUE isolated structure based on the assumptions clarified in previous section.

A reduction of 55% in the annual load is estimated per each house using the new building technology. For a district sums up 1000 houses of the new structural design the total saving of power will be 10.45 MW. The reduction in the power consumption will affect both the capital cost and the fuel consumption cost.

Based on the diesel power generation technique which is the main power generation source in Iraq and an estimated fuel consumption rate of 0.25 liter/hour/ KW the fuel consumption saving will be around 22.88xE03 cubic meter. The total fuel cost saving will be around 12 M USD in yearly base. Adding this value to the capital cost of 10.45 MW diesel generation plant price (roughly 0.35 M USD / MW), (total 3.66 M USD). The total power saving cost will be (14.11 M USD) per 1000 single story houses of around 105 square meters per each house.

These results show the effect of building isolation techniques on the power saving in Iraq rather than other countries due to the large temperature differences between the winter and summer seasons.

CONCLUSION AND RECOMMENDATION

It is concluded from the research that the cost benefit form the utilization of isolated structural material in the buildings has an effective impact on the total heating and cooling cost required in the these buildings specially in countries that have a big differences in the summer and winter temperature differences.

Using the identified structural material EMMEDUE M2 did not have any additional cost impact when it is compared to the ordinary structural material. Another benefits from using such type of material summarized in low weight reasonable strength and high acoustic insulation which add some structural privileges in addition to its excellent thermal properties.

Such type of material is became recommended in special usage building that require an optimum design specification between strength, architectural, thermal and acoustic properties.

REFERENCES

- **ANSARI, F. A.** A simple Approach for Building Cooling Load Estimation, American Journal of Environmental Sciences, 1 (3):209-212, 2005.

- **ASHRAE Handbook, Fundamentals Volume,** 1981. American Society of Heating, Refrigerating and Air Conditioning.

- **IRISH AGREEMENT BOARD,** EMMEDUE M2 Building system, National standards authority of IRELAND (NSA), Certificate No. 06/0241.

- **Standard for Ventilation Required for Minimum Acceptable Indoor Air Quantity,** ASHRAE Standard 62-81, 1981. American Society of Heating, Refrigerating and Air Conditioning Engineers, Atlanta, Ga.

- **Thermal Environmental Conditions for Human Occupancy**, ASHRAE Standard 55-81, 1981, American Society of Heating, Refrigerating and Air Conditioning Engineers, Atlanta, Ga.

- **RUDOY, W., 1979, Cooling and Heating Load Calculation Manual,** American Society of Heating, Refrigerating and Air-Conditioning Engineers, Atlanta, GA.

مدن الصحراء
بين المكونات الايكولوجية والحلول التخطيطية

د. لؤي طه الملا حويش
استاذ مساعد
المعهد العالي للتخطيط الحضري ولاقليمي
جامعه بغداد

د. انتصار قدوري جمعة
مدرس
القسم المدني/ معهد التكنلوجيا /بغداد

احلام المؤمن
مهندسة

الخلاصـــة

يبدو واضحاً الأثر الكبير للمكونات الايكولوجية على تشكيل النسيج الحضري لمدن الصحراء والمستقرات الحضرية في المناطق القارية عموماً, إلا إن تلك العوامل لا تمثل علة كافية في الاستقرار وعملية تشكل الهيئة الحضرية حينما يذهب الفعل الإنساني في ذلك ابعد من الاستجابة لتلك العوامل في محاولة تضمينه خصائصه الحضارية المميزة في ذلك النتاج.

فهذا البحث يحاول أن يلقي ضوءاً على هذه المقابلة الدقيقة بين عوامل البيئة والنزوع الحضاري في نواتج صنع الإنسان لبلورة أفكاراً في طريق بناء استراتيجيات للتوجه الواعد للمستقرات الحضرية في الصحراء .

ABSTRACT

It seems very clear to us that the great influence of the ecologic component of forming urban texture on the desert cities and the civiled constanity of tropical places in general , but these factors dont represent an aadequit reason of settlement and the process of forming urban society specially when the action of huminity goes farther than reaction to the mentioned factors in away to include its specified properties in that product .

This research focuses the accurate interaction between invironment factors and civilization nature as aresult in the development of socity and develop or built strategies of new fonomenas of desert urbanization . .

المقدمـــــــــة

على الرغم من الأثر الكبير للعوامل الايكولوجية في تشكيل النسيج الحضري للمستقرات الصحراوية. غير إن جوهر فعل الإنسان التنظيمي تجاه محيطه كجزء من عملية التمثيل والملائمة المكانية يذهب ابعد من مواجهة العوامل الايكولوجية ليحاول تضمين خصائصه الحضارية المميزة في نتاجه الحضري, وعندئذ يدخل المجتمع في طبيعة ذلك النتاج. وتحدث مقابلة دقيقة بين عوامل البيئة الخارجية والنزوع الحضاري للإنسان والمجتمع بكل أبعاده الذاتية والكونية. هذه المقابلة تميزت في النتاج الحضري التقليدي بتماهي طرفيها في هذا النتاج.

هذا من جانب ومن جانب آخر هناك مفارقة واضحة بالتوجه الحالي والواعد للمستقرات الحضرية نحو البيئة الصحراوية. وتقف خلف هذا التوجه عوامل مستجدة تمثلت في محاولة وقف الزحف الحضري نحو الأراضي الزراعية والأكثر خصوبة من جهة وظهور أسس لبؤر اقتصادية في الصحراء تمثلت في التعدين وبعض الصناعات الاستخراجية فضلا عن العوامل القديمة – الجديدة والمتمثلة بالمناطق الجاذبة والواقعة على طرق التجارة البرية وكذلك عوامل الاستقرار ذات الطبيعة العسكرية في مناطق الحدود الصحراوية.

هذا التوجه الأخير خلق تحديات جديدة للمخططين في التعامل مع البيئة الصحراوية غير إن من حسن الحظ إن التراث الحضري التقليدي (خاصة مدننا العربية) يقدم لنا حلولاً امتزج فيها ما هو حضاري بما هو بيئي بشكل مثير.

وهكذا يمكن تصور إشكالية الاستقرار الحضري الجديد في الصحراء بين أهداف ومفاهيم المخططين المعاصرين, والصحراء بكافة جوانبها الطبيعية, الاجتماعية, الاقتصادية والحضارية.

وهنا يتبلور هدف البحث في تقصي أسس التشكيل العمراني المتوافق مع البيئة الصحراوية وفقاً لملامح ومقومات المكان الطبيعية والاجتماعية والثقافية.

وتتبلور مشكلة البحث:

مشكلة البحث

عدم وضوح التصورات المنهجية والعملية (التخطيطية – التصميمية) للتنمية الاقليمية والاستقرار الحضري الصحراوي مع تزايد الحاجة والاسباب الدافعة لهذا من النوع من المستقرات, وتعقد العلاقة بين

المتطلبات الايكولوجية والحلول (التخطيطية- التصميمية) الشاملة لجميع النواحي الطبيعية من جهة والحضارية (الاجتماعية – الاقتصادية – التقنية) من جهة اخرى.

ويتضح من هذه المشكلة طبيعتها المركبة التي تتوزع الى المستويات المنهجية والمفاهيمية والمعالجات والحلول التخطيطية – التصميمية.

وفي ضوء ذلك يتحدد هدف البحث:

هدف البحث

وضع التصورات المنهجية والمفاهيمية للكشف عن اهم الخصائص التخطيطية – التصميمية للمقترب البيئي الملائم للتنمية والاستقرار الحضري الصحراوي وبكافة جوانبه الطبيعية, الاجتماعية, الاقتصادية والتقنية.

منهجية البحث

اما المنهج الذي اتبعه البحث في التشخيص والكشف عن تلك التصورات هو الاستدلال والانتقال من العام الى الخاص ومن الرؤى والمقتربات المنهجية العامة في التنمية الاقليمية والحضرية في الصحراء الى المفاهيم التخطيطية والتصميمية, ومن ثم وضع التصورات لاهم الخصائص وملامح المعالجات التخطيطية التصميمية من خلال تحليل اثر المكون الايكولوجي وتكامله مع العوامل الاخرى في صياغة تلك المناهج والمفاهيم والحلول.

- **المقتربات المنهجية التخطيطية في التعامل مع الاستقرار الحضري الصحراوي**

يمكن تقصي أهم المقتربات المنهجية والتخطيطية التي تناولت مفهوم مدن الصحراء في سياق تنمية الأقاليم الصحراوية من خلال طروحات عدد من المخططين والكتاب لكي يمكن وضع تصور منهجي للتعامل مع إشكاليات هذا النمط من الاستقرار الحضري وأيضا في التعامل مع مدننا القائمة:-

* حيث يرى Gollany ضرورة تبني مدخل التخطيط الشامل للتعامل مع إشكاليات المجتمعات الصحراوية, حيث يتوافق التخطيط العضوي والرؤى الشاملة للمدينة ككل مع مفهوم تنمية المدينة. كما يقترح تجميع المجتمعات العمرانية الصحراوية في نمط مجموعات صغيرة بدلا من المجتمعات الفردية المنعزلة لتحقيق الاكتفاء الذاتي حيث تؤثر العوامل الإقليمية للمناطق الصحراوية الشديدة الجفاف في أبعاد أطوال امتدادات الخدمات والبنية الأساسية والمواصلات, وكما يؤثر العامل النفسي للإحساس بالانعزال حيث يوفر التجمع الإقليمي "Regional Clustering" للمجتمعات المنفردة أو المجتمعة التماسك الاجتماعي وتقارب الاحتياجات اليومية الأساسية وتكون إدارة المجتمعات أكثر فعالية.

* في حين يؤكد " Ledreaa "أهمية تبني مقترب تخطيط الصحراء الايكولوجي "Ecological Desert Planning " ويرى تكوين المدينة من مجتمعات صغيرة مكتفية – "Small Self Contained Communities" موزعة في تدرج هرمي للوحدات والوحدات الفرعية.

* في حين يحدد Barton مفهوم الاكتفاء الذاتي المحلي Local Self- Sufficiencyمن خلال رؤية التنمية ككائن حي قادر على الإنتاج وتجديد نفسه كنظام بيئي مصغر"MiniEcosystem" ابتداءاً من وحدة المسكن وحتى المدينة حيث البيئة المحلية للإنسان ويشكل الظروف المناخية المحلية وأساليب الراحة الفردية. ويقترح زيادة مستوى استقلالية النظام البيئي بتقليل الاعتماد على موارد البيئة الهائلة وتقليل تلوث البيئة وتحديد مفهوم المحلية "Locality " من خلال نمط السلوك الإنساني والابتعاد عن الرؤى الأحادية وإحلال التنوع المحلي "Local Diversity " فبدلاً من نطاق الاستعمال الواحد استخدام نظام اختلاط وتكامل الاستعمالات المختلفة والمتنوعة.

غير انه من الجدير بالإشارة هنا هو تأكيد "Gollany " على أهمية دراسة عمران المجتمعات الصحراوية التقليدية وعناصر تصميم الموقع من خلال الدراسات التحليلية لمورفولوجية المدينة وشبكة الحركة وتوجيه المدينة وتخطيط مواقع استعمالات الأرض وعلاقتها مع بعضها البعض.

وهكذا يمكن التوصل إلى إن مدخل التخطيط البيئي هو (احد) مداخل التعامل مع المجتمعات الصحراوية وأساسا لصياغة إستراتيجية التنمية الشاملة للصحراء, وذلك من خلال مفاهيم تحقيق الاكتفاء الذاتي والاستقلالية المحلية والرضا الاجتماعي, ويمكن من خلاله تصنيف وتحديد خصائص أنواع البيئة الصحراوية وتصنيف الصحراء إلى وحدات تخطيطية متجانسة طبقاً للخصائص الجغرافية والطبيعية والاجتماعية بالإضافة إلى تكامل الموارد.

- **دوافع توجه الاستقرار الحضري نحو الصحراء**

مع النمو والتوسع الحضري الكبير الذي ظهر بوتائر عالية منذ بدايات القرن الماضي كأحد آثار التغير الصناعي ثم ما تلاه من هجرة كبيرة من الريف إلى المدن خاصة في البلدان العربية منذ منتصف القرن الماضي, كل هذا أدى إلى تقليص وتآكل الأراضي الزراعية التي توسعت نحوها المدن القائمة, الأمر الذي شجع نحو التوجه إلى مواقع جديدة للاستقرار الحضري ومنها الصحاري والمناطق المحاذية لها بسبب قلة المساحات المعدة للسكن ضمن التصاميم الاساسية للمدن .

وفضلا عن هذا السبب المستجد فان هناك عوامل أخرى تشجع توجه الاستقرار الحضري في الصحراء وتطوير الأقاليم الصحراوية ومنها:-

أ. **التعدين:** وهو من أهم الأسباب في إنشاء المستقرات الحضرية في الصحراء التي غالبا ما تقع فيها الخامات المعدنية وكذلك النفط الأمر الذي يتطلب إنشاء مجمعات حضرية لاحتياجات العاملين, كما هو الحال في غرب العراق (منطقة عكاشات).

ب.الصناعة: حيث إن هناك بعض الصناعات التي تنشأ في مناطق صحراوية أما لقربها من المواد الأولية أو لكونها تلوث البيئة. كما هو الحال في بعض التجمعات الحضرية التي أنشأت في جنوب العراق.

ج.العوامل العسكرية: حيث إن بعض المتطلبات العسكرية والملاحة الجوية في المناطق الصحراوية الحدودية قد تكون حافزا لإنشاء مستقرات صحراوية وذلك لتواجد المخافر والمعسكرات التدريبية.

د.السياحة: حيث إن هناك بعض المناطق الصحراوية التي تتمتع بإمكانيات سياحية من الممكن استغلالها لتكون عامل جذب سياحي لسكان المدن وبالتالي تكون حافزا للاستقرار الحضري فيها, ومثال ذلك الحبانية, بحيرة ساوة أو قد تكون مناطق أثرية كمدينة الحضر.

ه.العوامل التجارية: حيث إن هناك مناطق تقع على مفارق الطرق التجارية البرية يمكن أن تستغل لإنشاء مدن أو تجمعات حضرية فيها.

ولكن المهم في كل هذا هو التأكيد على إن عناصر البيئة الطبيعية لها دور تعديلي وليس جوهري في عملية النتاج الحضري التي يمارس فيها الإنسان تضمين خصائصه الحضارية العميقة ورؤاه الكونية بحيث يدخل المجتمع في طبيعة ذلك النتاج, لذلك لا يمكن تفسير شكل ذلك النتاج وطبيعته بلغة الوظائف والتأثيرات البيئية فقط.

وسنتناول الآن العوامل الايكولوجية المؤثرة قبل التعرض لعناصر التشكيل الحضري المتوافقة معها.

- **المنظومة الايكولوجية**

تتشكل المنظومة الايكولوجية الشاملة للإقليم من ثلاثة مستويات:-

أولاً. ويضم المكونات الايكولوجية الأساسية غير الحية وتتمثل بالعوامل الجيولوجية, الهيدرولوجية, الطبوغرافية, التربة وعوامل المناخ.

ثانياً. ويضم الموارد النباتية والحيوانية والتي تتفاعل مع المكونات الأساسية من خلال مجتمعاتها.

ثالثاً. ويضم الإنسان من خلال مستقراته وهو المستوى الأكثر تعقيداً للمنظومة حيث يتفاعل مع المكونات الايكولوجية الباقية على انفراد من خلال تأثير مستوطنه.

المكونات الايكولوجية

سنحاول أن نستعرض بإيجاز المكونات الايكولوجية الأساسية وأثرها العام في الاستقرار في البيئة الصحراوية قبل أن نتناول التأثير الأكبر لبعض العوامل الايكولوجية في المستقرات الصحراوية:-

أ. جيولوجية الإقليم :- حيث يعطينا التركيب الجيولوجي للإقليم ,البعد التاريخي لتطور تربة الموقع ويساعدنا في تحديد توقعات تغيراتها المستقبلية نتيجة لأعمال التشييد أو الزراعة والري وغيرها...

وتلعب المعلومات الجيولوجية دورا مهماً في تحديد طبيعة الأسس للأبنية وكيفية تصريف المصادر المائية المختلفة وتعيين قنوات مجاري المياه الجوفية.

ب.هيدرولوجية الإقليم وموارده المائية:- ويعتبر العامل الأساس والمتحكم بإمكانيات تطوير الأقاليم الصحراوية خاصة وإمكانية إنشاء وتوسع المدن فيها. فتصبح نقطة البداية في مشروع الاستقرار هو تحديد وتقييم الموارد المائية المتوفرة كماً ونوعاً.

ج.طبوغرافية الإقليم:- حيث تساعد المعلومات الطبوغرافية في تحديد أساليب الري وتصريف مياه الأمطار والري بالإضافة إلى تحديد مدى ملائمة الموقع للزراعة ومدى تعرض أجزاء الموقع للعوامل الطبيعية (المناخية) من رياح وأشعة شمس وبالتالي تحديد الاحتمالات الممكنة في توقيع وتصميم المستقرات وعمارة أجزائها.

د.تركيب تربة الإقليم:-حيث تساعدنا المعلومات الدقيقة عن طبيعة مكونات تربة الإقليم (جفافها, محتوياتها, مساميتها) في تحديد أصناف النباتات الممكنة زراعتها في الإقليم للأغراض الاقتصادية أو في تحسين بيئة المستقرات فيه.

ه.عوامل المناخ:- من أمطار, رياح, درجات الحرارة, شدة الإشعاع, الرطوبة النسبية. حيث تلعب هذه العوامل دوراً مهماً في تصميم أجزاء المدينة وفي تخطيطها واختيار الموقع الملائم لها.

و.الموارد النباتية والحيوانية :- والتي تساعد في تحديد طبيعة الموارد الاقتصادية للمستقرات او تنميتها ضمن المنظومة الايكولوجية الكاملة.

- **اثر الخصائص الطبيعية في تخطيط وتصميم المستقرات الصحراوية**

سنتناول هنا ثلاثة من المكونات الايكويوجية هي العوامل المناخية والموارد المائية والموارد النباتية في توجيه الحلول التخطيطية والتصميمية الملائمة للأقاليم الصحراوية, قبل أن نتناول تفصيلياً الخصائص التخطيطية والتصميمية للمدن الصحراوية.

العوامل المناخية

حيث تلعب العوامل المناخية الرئيسة (الإشعاع الشمسي, الرياح, الرطوبة) دوراً مهماً في طبيعة المعالجات التخطيطية والتصميمية لمدن الصحراء والعامل الحاسم في ذلك هو السعي إلى تهيئة ما يسمى منطقة الراحة المناخية Comfort Zone من اشتراك تأثير العوامل الثلاثة أعلاه.

الإشعاع الشمسي

تعتبر الأشعة الشمسية هي المحرك الرئيسي لجميع المنظومات الطبيعية وأقوى العوامل المناخية تأثيرا. حيث يأتينا تأثيرها عن طريق أشعة موجية قصيرة (إشعاع حراري ضوئي) تأتينا من الشمس, من القبة السماتية ومن انعكاسات الأشعة الشمسية من الأرض, ويأتينا تأثيرها أيضا على شكل أشعة موجية طويلة (إشعاع حراري) عندما تشع من الأرض ومن العناصر المحيطة بنا ومن ذرات الجو.

وتلعب البيئة المبنية دورا ايجابياً أو سلبياً على عوامل البيئة المناخية من خلال ما نسميه المناخ المحلي للموقع " Site Micro-Climate " وبهدف جعل هذا التأثير ايجابياً (خفض درجات الحرارة) نعمل على الحد من تأثير الإشعاع الشمسي والحراري وعلى مستويين:-

الأول :تخطيطي على مستوى المدينة.

الثاني :تصميمي تفصيلي أو موضعي على مستوى الأبنية أو أجزاء المدينة.

ويتلخص هذا التوجه بالحد من تعرض الأوجه العمودية والأفقية لأشعة الشمس وتضليلها وتقارب الكتل البنائية وتقليل الفضاءات المفتوحة كما هو حاصل في البيئة الحضرية التقليدية وسنتناول ذلك تفصيليا في الفقرات القادمة.

الرياح

إن الرياح الحارة المتربة في الأقاليم الصحراوية تسبب أضرارا عديدة، فالرمال التي تحملها تلوث الهواء وتسبب التعرية لكل ما يواجهها، وكذلك تزيد من سرعة تبخر الماء وبالتالي استهلاك الموارد القليلة من الماء وتقلل من الفروق الحرارية بين المناطق المضللة وغير المضللة.

ويمكن السيطرة على الرياح بالتصدي لها وتبديل مجراها أو تقليل سرعتها بواسطة: المصدات النباتية, السواتر الترابية, العناصر المعمارية كالجدران والأبنية. غير إننا في كل الأحوال يجب المحافظة على انسيابية جريان طبقاتها وتفادي خلق جريان مضطرب دوامي والذي يصعب السيطرة عليه.

الرطوبة والأمطار

تتميز المناطق الصحراوية بالجفاف، أما الأمطار فقليلة إضافة إلى تباين منسوبها من سنة إلى أخرى مما يحثنا على الاستغلال الأقصى لما تجلبه من مياه عن طريق:-

-جمع مياه الأمطار "Rain Harvesting " بأساليب مناسبة.

-باستعمال المهاد "Mulch " للحد من كمية الماء المتبخرة من التربة.

-التوفيق بين صنف النبات المختار وبين الموقع المختار له ضمن المستقرات.

الموارد المائية

إن المصادر الرئيسة للموارد المائية للإقليم الصحراوي هي:مياه الأمطار, المياه السطحية, المياه الجوفية. ونظرا لندرة هذه المصادر في الأقاليم الصحراوية فإنها تعتبر من المحددات الأساسية لتطور تلك المناطق. ويكون ترشيد استغلالها على مستويين:-

أولاً. الابتعاد عن الاستعمال المكثف لها (المياه الجوفية) بمعدلات تفوق معدلات التجدد في الطبيعة.

ثانياً. عدم التبذير في مياه الأمطار دون الاستفادة القصوى منها ذلك إن التبذير يؤثر على التوازن الايكولوجي للإقليم.

أما فيما يخص مياه السيول (المياه السطحية الموسمية) فيتم استغلالها ببناء الخزانات لاحتواء مياه الأنهار الموسمية وتوزيع استغلالها على طول السنة وكذلك الحال بالنسبة لمياه الوديان الموسمية التي يمكن استغلالها بشكل جيد بطرق عديدة ومنها تغليف الأرض أو إنشاء سدود صغيرة

الموارد النباتية

إن الموارد النباتية من المكونات الأساسية للمنظومات الايكولوجية وتلعب الدور الأكبر في الحفاظ على التوازن في تلك المنظومات في الإقليم الصحراوي إذ تؤدي إزالتها تحويراً جذرياً في المكونات الايكولوجية للمنظومة. وإضافة إلى دورها هذا فان لها استعمالات أخرى عديدة منها اقتصادية بتوفير مصادر غذاء ووقود, ومناخية لما تلعبه من دور ايجابي في تحوير مناخ المستقرات الصحراوية ,الأقاليم المحيطة بها.

ويتم اختيار أنواع النباتات في مستقرات الإقليم الصحراوي على أساس مقاومتها للحرارة والجفاف ومقاومتها للرياح. كما تختلف في ضوء هذه العوامل حسب موقعها من الكتل البنائية في نسيج المستقرة الصحراوية.

استخدام الأشجار في تثبيت التربة

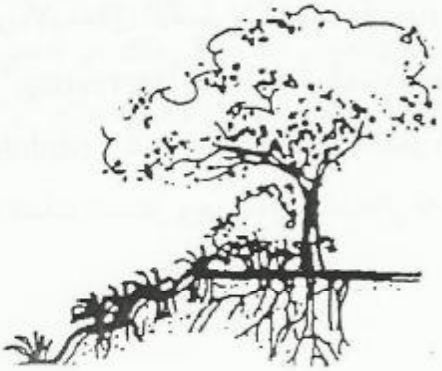

- أكاسيا سلجينا Acacia Saligna
- الخروع Ricinus Communis
- الأثل Tamarix Articuiata
- المبسكبت Prospis SP
- التين Ficus Canica

Source: Henry, Trees In urban Design,U.S.A,1993,P14.

6- المفاهيم الأساسية في تخطيط وتصميم المستقرات الصحراوية

سنتناول ألان أهم الأفكار أو الرؤى التخطيطية والتصميمية التي ميزت من الصحراء والتي جاءت كاستجابات بيئية غير إن عمقها يمتد إلى الخصائص الاجتماعية والحضارية التي ميزت كل مجتمع عن غيره لتشمل رؤاه العقائدية ونظرته إلى الكون والحياة.

مفهوم التضام Compactness

مفهوم التضام أو التنظيم المتراص وهو الميزة الأهم التي طالما ميزت النتاج الحضري التقليدي في المدينة العربية وغالبا ما عبر عن التماسك والوحدة في مجتمعات تلك المدن. ويمكن ملاحظة إن النسيج العمراني التراثي يتميز بتقارب كتله وضيق فضاءاته المفتوحة مقارنة بالنسيج العمراني المعاصر فتصل إلى 25% في النسيج التقليدي وترتفع في النسيج المعاصر إلى 75% وهكذا يعمل التوجه التقليدي إلى تقليل السطوح المعرضة لأشعة الشمس وزيادة نسبة التضليل على خلاف التوجه المعاصر.

ظاهرة التأثير الشبكي

MESH EFFECT

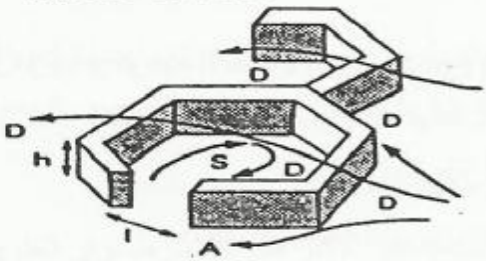

التأثير الشبكي
S المساحة
H الارتفاع
I عرض فتحة الدخول
$S/^2h < 20$

المصدر: محمد ثائر علي،"اثر العوامل المناخية في تخطيط وتصميم المستوطنات الحضرية في الناطق الصحراوية" ،رسالة ماجستير ،مقدمة إلى مركز التخطيط الحضري والإقليمي ،جامعة بغداد،1986،عن R.U.Cooke, architectural solutions for sand and dust, Urban geomorphology in dry lands P.P.270-2850

ويرى Gollany انه على الرغم من اختلاف أسباب تصميم المدن في الماضي, فقد حقق نظام التظام بيئة متوافقة مع الظروف المناخية الشديدة للبيئة الصحراوية. حيث قلل التشكيل المتظام من شدة الحرارة أثناء النهار والرياح الباردة أثناء الليل كما قلل من تأثير العواصف الترابية كما انه وفر شبكة ظلال كثيفة وفرت الهواء البارد في مسارات المشاة. ولتقوية وحدة التشكيل العمرانية "Physical Unity " في المدن ذات التشكيل المتظام لابد من تقوية العلاقات والأنساق الاجتماعية في مجموعات متجانسة وتوفير وحدات خدمية تتصل بوحدة الخدمات المركزية للتشكيل المتظام مما يقلل من أطوال شبكات البنية الاساسية واستهلاك الطاقة, وتحقيق إمكانية وصول عالية ووضوح صورة المدينة للأهالي.

الاحتواء والتوجه نحو الداخل

ويمكن إدراكه على مستوى المدينة بوصفها فضاءاً احتوائياً بواسطة المصدات الخارجية أو السور, حيث تنطلق من المركز شرايين الحركة أو على مستوى الوحدات البنائية أو السكنية حيث تشكل

الفناءات الداخلية Courtyards لخلايا الاحتواء (الأبنية) تتابعا احتوائيا مولدا النسيج العضوي من تلك الخلايا والذي تتخلله فضاءات تتسع وتضيق. تعمل الفناءات الداخلية كمنظمات مناخية في توفير بيئة محلية أو موضعية حيث تنفتح معظم فضاءات المعيشة على هذا الفضاء الوسطي.

غير انه يمكن لهذا الاحتواء أن يأخذ أبعادا حضارية ورمزية تتباين في المجتمعات المختلفة التي ظهر فيها حيث يمكن أن يعبر عن مبدأ الخصوصية وتأكيد مبدأ الحرمات في المجتمعات الإسلامية. أو احتواء الجسد للروح والمركز المحيط حيث تظهر هذه المعاني من جوانب أخرى غير البيئة الطبيعية.

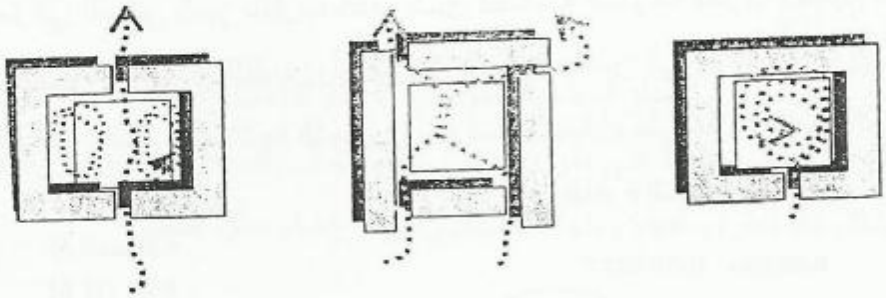

تأثير درجة و نوعية الأحتواء (Enclosure) على المناخ المصغر في الساحات
المصدر:حموش ،مصطفى،" استخراج المؤشرات المناخية الحضرية من المدن الصحراوية القديمة:دراسة مقارنة"كلية لهندسة،جامعة البحرين،2004،ص30.

التنظيم الفضائي والنسيج العضوي

حيث تميزت معظم مدن المناطق الحارة الجافة أو ذات المناخ القاري بنسيجها العضوي وشبكة تنظيمها الفضائي ذات الطرق والأزقة المتعرجة والتي ساهمت كثيرا ومن خلال آليات مختلفة في تكوين بيئة مناخية محلية مناسبة, فقللت من تأثير العواصف والرياح المتربة.

كما إن تعرج هذه الأزقة والكتل البنائية يخلق تتابعا من الضوء والظل الذي يعمل على تباين درجات الحرارة والضغط الموضعي مولداً تيارات هوائية محلية تعمل على تحسين المناخ المحلي.

وغالبا ما تكون شبكة الطرق الضيقة والمتعرجة مضللة وباردة أثناء النهار وتحافظ على درجات الرطوبة داخل فراغاتها وبالتالي تقل درجة حرارة الهواء المحيط أثناء اليوم وتقل سرعة الرياح نتيجة التأثير النفقي Tunneling Effect.

كما إن التدرج الهرمي في شبكة الحركة ومراعاة توجيه الشوارع طبقاً لدوران الشمس واتجاه الرياح وخط السماء وارتفاعات المباني يساعد على تحقيق النفاذية وإمكانية الوصول.

أثر نسبة الارتفاع إلى العرض (H/W) في المناخ المصغر للفراغات العامة

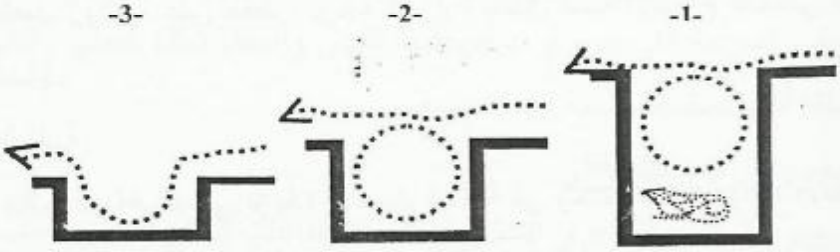

المصدر:خنكار،حسام بن إبراهيم واخزون،"التقرير النهائي للأداء الحراري للفضاءات المفتوحة"،معهد بحوث الطاقة،مدينة الملك عبد العزيز للعلوم والتقنية،،الرياض،2001،ص7 .

المصدات والأحزمة الخضراء

حيث إن المصدات تأخذ شكل مصدات ترابية أو أحزمة خضراء تحيط بالمدينة. ويفضل أن تصمم المصدات الترابية كجزء من عملية تخطيط المدينة ككل ويمكن ذلك من تحوير المنحدرات الطبيعية على سبيل المثال. أو أن تعمل الكتل البنائية على محيط المدينة على هذه الوظيفة.

غير إن استعمال مصدات الرياح النباتية هو الأكثر شيوعاً بشرط توفر الظروف الملائمة لنموها فالأشجار والشجيرات تزودنا بارتفاعات ومواصفات فيها الكثير من المرونة وهي في الوقت نفسه تعمل على تنقية الرياح من الرمال والأتربة.

العمارة المحمية

وهي من .الأنماط الجديدة في التصاميم المعمارية الذي يلائم البيئة الصحراوية هو ما يسمى العمارة المحمية بالأرض Earth Shelter وأساس هذه العمارة يتلخص بتغطية المبنى بالسواتر الترابية أو بدفنه كليا أو جزئيا تحت مستوى سطح الأرض فلا تتعرض أسطح المبنى أو جدرانه لأشعة الشمس وللاستفادة من خاصية العزل الحراري الذي توفره طبقات التراب.

7- الخصائص التخطيطية والتصميمية التفصيلية في المستقرات الصحراوية

سنحاول أن نستعرض هنا أهم الخصائص التخطيطية والتصميمية والتي يمكن أن تؤشر كمعايير أو ضوابط تخطيطية وتصميمية يمكن قياسها أو تفعيل آليات معينة في معالجة المشاكل المناخية للمستقرات الصحراوية:-

الخصائص التخطيطية

ومن أهم هذه الخصائص والتي ستتناول المدينة ككل:-

* **نسبة التغطية:**

والتي تعمل زيادتها على خفض درجة الحرارة بتقليل نسبة الإشعاع الشمسي الواصل وزيادة نسبة التضليل.

* **الأحجام البنائية:**

حيث يتأثر المناخ المحلي بزيادة الأحجام البنائية في وحدة المساحة (عدد الأمتار المكعبة في وحدة المساحة) والتي تؤدي إلى رفع درجة الحرارة للمناخ المحلي ولكنها تتناسب عكسيا مع نسبة التغطية.

* **نسبة الفضاءات الحركية الخارجية:**

حيث تؤثر زيادة نسبة هذه الفضاءات في ارتفاع درجة الحرارة حيث إن كل 1000م2 من الفضاءات المفتوحة هذه ترفع من درجة الحرارة الخارجية بمقدار °5م.

وتعتمد نسبة هذه الفضاءات على نمط الشوارع حيث يقدم النمط التجميعي "Clustering " أفضل أسلوب حيث انه يحقق 50% تقريبا من الطول اللازم قياسا ببقية الأنماط.

* **نسبة المساحة المبنية إلى مساحة قطعة الأرض التي تبنى عليها F.A.R :**

حيث تتناسب هذه النسبة عكسيا مع كمية الأشعة الواصلة ودرجة حرارة الموقع.

* **المقطع العمودي للمدينة:**

حيث ان تدرج ارتفاعات الابنية من الخارج الى المركز يعمل على توليد مناطق مضللة واخرى معرضة للشمس مما ينشأ عنه تباين في درجات الحرارة وتوليد تيارات هوائية افقية وعمودية وتخفيض درجة الحرارة المحلية.

الخصائص التصميمية

وهي الخصائص التي تتعلق بالوحدات البنائية والسكنية المفردة ويمكن إيجاز أهمها وتأثيراتها المناخية وكما يأتي:-

أ.تناسب أبعاد المسقط الأفقي للمبنى

حيث تؤثر أبعاد المسقط الأفقي على كمية الاكتساب والفقدان الحراري وتشير الدراسات إلى إن أفضل شكل للمبنى هو الشكل المستطيل بحيث تكون أضلاعه الطويلة مواجهة لمحور شمال –

جنوب وأفضل نسب للأبعاد هو 1:1.3 في المناخ الحار الجاف, كما أشار إلى ذلك اوليكاي "Olgyay" ويرتبط ذلك بالتوجيه.

ب.نسبة المساحة إلى الحجم

حيث يشير حجم المبنى إلى قابليته على خزن الحرارة أو ما يعرف "السعة الحرارية" في حين تشير المساحة السطحية إلى معدل الفقدان والاكتساب الحراري. وتعد نسبة الحجم إلى المساحة مؤشرا على السرعة التي يبرد أو يسخن فيها المبنى وأفضل شكل للمبنى بالتالي هو المكعب لكونه يحقق أدنى مساحة سطحية قياسا لحجمه.

ج.علاقة الحجم بشكل المسقط الأفقي

وحسب مفهوم المكعب الحراري السابق تختلف الارتفاعات المثلى للمبنى حسب شكل مسقطه الأفقي.

- **العلاقة بين كمية الأشعة الواصلة وزاوية توجيه السطوح**
- **العلاقة بين توجيه المبنى على درجة حرارة السطوح**

د.نسبة ارتفاع المبنى إلى عمقه H/D

فكلما زادت هذه النسبة تقل كمية الأشعة التي يستلمها المبنى صيفا وتزداد شتاءا بالعلاقة مع التوجيه.

ه.نسبة الفتحات (النوافذ)

حيث وجد إن درجة الحرارة العظمى الداخلية يمكن أن تتجاوز درجة الحرارة الخارجية العظمى ب(18%) في حالة كون الجدار كله عبارة عن فتحة زجاجية ثم تتصل تدريجيا لتنخفض عن درجة الحرارة الخارجية عندما تصبح نسبة النوافذ بحدود 20%.

و.التضليل

والذي يمكن أن يتم بواسطة الكتل البنائية أو كاسرات الشمس الأفقية والعمودية أو المركبة والتي تعطي نتائج مهمة في تخفيض درجة الحرارة وفي معدل استهلاك الطاقة.

ز.الخواص الحرارية لمواد البناء

والتي تؤثر كثيرا في بيئة المبنى الداخلية وخاصة المواد الإنشائية ذات المعامل الإجمالي لانتقال الحرارة عالي نسبيا كالطابوق والطين....وكذلك استخدام مواد العزل في الجدران الخارجية.

ح.الألوان المستخدمة

للألوان تأثير مهم في كمية ما تعكسه من أشعة الشمس الساقطة على السطوح فالألوان الفاتحة والأبيض خاصة له القابلية على عكس كل ما يسقط عليه أو معظمه وبذلك يمكن التوجه نحو هذه الألوان وتجنب الألوان الداكنة في الواجهات وسطوح المباني لأنها تمتص معظم ما يسقط عليها من أشعة وتنقلها إلى المبنى.

الاستنتاجات

لقد اشر البحث الى مجموعة من الاستنتاجات التفصيلية التي انتشرت في ثناياه ونكتفي هنا بالاشارة الى الاستنتاجات العامة:-

* ان المدخل او المقترب التخطيطي البيئي هو اهم المداخل في التعامل مع المجتمعات الصحراوية واساسا لصياغة استراتيجية التنمية الشاملة للصحراء, من خلال مفاهيم تحقيق الاكتفاء الذاتي والاستدامة والاستقلالية المحلية والرضا الاجتماعي.

* مع اعتماد مدخل التخطيط البيئي ينبغي ملاحظة ان اثر عناصر البيئة الطبيعية هو تعديلي وليس جوهري في عملية النتاج الحضري التي يمارس فيها الانسان تضمين خصائصه الحضارية العميقة.

* هناك العديد من المفاهيم التخطيطية Concepts التي تلاقي المتطلبات الايكولوجية والحضارية معاً مثل (التضام, الاحتواء والتوجه نحو الداخل, العمارة المحمية) والتي يمكن تمثيل خصائصها الدقيقة في بنيتها العميقة في نتاجات ظاهرية وحلول تخطيطية وتصميمية متنوعة ليس من الضروري الالتزام بالانماط الشكلية التقليدية التي ترافقت مع تلك المفاهيم.

* تبلور مجموعة من الخصائص التخطيطية للمستقرات الحضرية الصحراوية يمكن من خلالها تفعيل آليات كثيرة لمعالجة المشاكل المناخية لتلك المستقرات ويمكن توظيفها عبر توجهات تشريعية (ضوابط او معايير تخطيطية) لغرض تضمينها في التقنيات والاساليب التخطيطية. ومن هذه الخصائص: نسب التغطية, الاحجام البنائية, نسبة الفضاءات الخارجية...

* ينبغي تكامل المعالجات التخطيطية على المستوى الشمولي والموضعي للمستقرات مع المعالجات التصميمية التفصيلية للوحدات البنائية مثل: تناسب المسقط الافقي, نسب الاحجام الى تلك المساقط وارتفاع المباني والفتحات الخارجية والمواد البنائية والوانها.

التوصيات

* - استخدام التخطيط المتضام في تخطيط المستقرات الحضرية الصحراوية لتوفير اكبر قدر من الظلال التي تسقطها المباني على بعضها البعض والناتجة عن اختلاف الارتفاعات والبروزات في الجدران الخارجية بحيث لا يتعرض لاشعة الشمس سوى اقل مساحة من الواجهات والاسطح ومن ثم تكون الطاقة النافذة او المتسربة الى المباني في اضيق الحدود .

* - اتباع الطرق المثلى في البعد المناخي في تخطيط المستقرات الحضرية الصحراوية .

* - استخدام المصدات الترابية أو الاحزمة الخضراء التي تحيط بالمدينة كجزء من عملية تخطيط المستقرات الحضرية الصحراوية .

* - الاحتواء والتوجه نحو الداخل على مستوى المدينة بوصفها فضاءا احتوائيا بواسطة المصدات الخارجية أو السور ، حيث تنطلق من المركز شرايين الحركة او على مستوى الوحدات البنائية او السكنية حيث تشكل الفناءات الداخلية للأبنية تتابعا احتوائيا مولدا النسيج العضوي وتعمل الفناءات الداخلية كمنظمات مناخية في توفير بيئة محلية تنفتح معظم فضاءات المعيشة على هذا الفضاء الوسطي .

* - استخدام الطاقة الشمسية في توليد القوى الكهربائية للمستقرات الحضرية الصحراوية .

المصادر باللغة العربية

* الاشعب، خالص حسني و آخرون،**"الموارد الطبيعية و صيانتها"**،جامعة بغداد،دار الكتب للطباعة و النشر، 1988.

* الأمام,محمد وليد يوسف,**"البيت المتوافق مناخيا"**,رسالة ماجستير مقدمة إلى كلية الهندسة ,جامعة بغداد,1989.

* بشندي،سعاد يوسف ،**"مدخل التصميم العمراني المستدام:وتشكيل عمران المجتمعات الصحراوية ، دراسة مجتمعات الواحات التقليدية بصحراء مصر الغربية"**، كلية التخطيط الإقليمي والعمراني ، جامعة القاهرة ، 2005.

* الجوادي, مقداد وآخرون, 1989, **" تأثير الشكل الهندسي للفضاء الحضري على تضليله "**, بحوث المؤتمر العلمي الخامس, مجلس البحث العلمي, بغداد.

* حموش،مصطفى،**" استخراج المؤشرات المناخية الحضرية من المدن الصحراوية القديمة**، كلية الهندسة جامعة البحرين،2005

* خنكار، حسام بن إبراهيم و آخرون،**" التقرير النهائي للايداء الحراري للفناء الداخلي"**، معهد بحوث الطاقة،قسم الطاقة التقليدية، مدينة الملك عبد العزيز للعلوم و التقنية، الرياض،2001.

* الرحماني ، صباح فاضل ، **"موقع صدامية الثرثار في تخطيط مدن الصحراء"**،بحث منشور، 1999.

* فضيل, مدحت, 1972, "إنشاء السدود الترابية في وديان الصحراء الغربية في العراق" مؤتمر المهندسين العرب, القاهرة.

* كمونة، حيدر عبد الرزاق، "الفناء الداخلي و تصميم المسكن العربي التقليدي"، آفاق عربية،2001

* المخزومي, جالة محمد, 1988, " المكونات الايكولوجية في تصميم مستوطن الاقليم الصحراوي", مجلة بحوث البناء, بغداد.

* محمد، ثائر علي، "أثر العوامل المناخية في تخطيط وتصميم المستوطنات الحضرية في المناطق الصحراوية"،رسالة ماجستير، غير منشورة، مقدمة إلى مركز التخطيط الحضري والاقليمي،جامعة بغداد،1986.

* مجلد المؤتمر العلمي الخامس لمجلس البحث العلمي بغداد 1989.

المصادر باللغة الإنكليزية

* Gollany, Giedon, 1978, **"Urban Planning For Arid Zone"**, London.

* Gollany, Giedon, 1980, **"Housing in Arid Lands"**, London.

* Evans, Martin, 1980, **"Housing ,Climate and Comfort"**, London.

* Olgyay, Vietor, 1969, **"Design With Climate"**, Newyersty.

* Saini, Balwant Singh, **"Building in Hot Dry Climates"**, U.S.A., 1980

زوايا ظل الشمس المهندس المعماري

عبد السلام فرمان
جامعه بغداد /معهد التخطيط الحضري

خلاصة البحث

غالبا ما تمثل أشعة الشمس الداخلة عبر الشبابيك اكبر مصدر للكسب الحراري إلى داخل المبنى حيث تحتجز الحرارة في الداخل بسبب ظاهرة البيوت الزجاجية إن وقاية الشبابيك من أشعة الشمس تعتبر من أهم الطرق الفعالة بيد المهندس المعماري من اجل تقليل كمية الكسب الحراري هذا.

وان الحاجة للحماية كبيرة جدا في دولة الإمارات المتحدة ذات المناخ الصحراوي الساحلي الحار. ولكننا نجد عزوفا من جانب المهندسين المعماريين عن هذه الناحية البيئية في التصميم . ويعزى هذا أولا لعدم توفر البيانات المحلية بسهولة من جهة ولتعقيد الطرق المستخدمة من جهة أخرى ، وثانيا الانتشار المفهوم الخاطئ بان تكييف الهواء للمبنى يعني عدم الحاجة للوقاية من الشمس أو عدم أهمية ذلك.

إن هدف هذا البحث هو تبسيط الموضوع وتشجيع المهندسين على رعاية هذه الناحية المهمة من العملية التصميمية مع تهيئة البيانات المنشورة وغير المنشورة الخاصة بذلك.

بالاستناد على زوايا سقوط أشعة الشمس لخط عرض يمثل دولة الإمارات وحسب توقيتها المحلي الرسمي تم تهيئة العديد من الجداول المفيدة للمعماري المصمم أولها يحتوى على اتجاه وطول الظلال في كل ساعة ولكل شهر. وكذلك عددا من الجداول الخاصة بزوايا الضلال لمباني ذات توجيهات مختلفة في الإمارات. وبالاضافه لذلك واستناد على درجات الحرارة والرطوبة لكل ساعة ليوم يمثل كل شهر تم رسم شبكة درجات الحرارة المؤثرة للإمارات مع تحديد خط ضرورة الوقاية من الشمس . وأخيرا تثبيت هذه المعلومات على رسم مسارات الشمس حسب الساعة والشهر . وذلك لشرح مفهوم الفترة شديدة الحرارة بالنسبة للأمارات ولتسهيل استعمال منقلة الظلال معها مستقبلا عند الحاجة .

SUN SHADOW ANGLES FOR ARCHITECTCS With special reference to The UAE

BSTRACT

Often the greatest source of heat gain is the solar radiation entering through windows. Heat is then trapped in; because of the "greenhouse effect" shading the windows is one of the most effective method within the reach of the architect for reducing this heat gain. This is nowhere more necessary than in a country like the U.A.E. but we find the architects here often ignoring this important environmental aspect of design. This is partly due to the lack of relevant local meteorological data plus the complexity of the procedure involved ;and partly due to the misconception that such aspect looses much of its significance when the building is air conditioned .

The aim of this paper is to simplify the issue and promote greater attention to this aspect by architect designing for the U.A.E.

Based on the solar azimuth and altitude angles for the U.A.E. for the representative latitude related to local civil time, a number of useful tables to the architect have been prepared . One gives the hourly shadow angles and direction for each month. Then a set of tables to define the shadow angles for buildings of various possible orientations.

In addition effective temperature isopleth for the U.A.E. has been constructed, with the shading line definded on both the isopleths and the solar charts. This is done in order to give greater insight into the overheated period of the U.A.E., and facilitate future possible use of shadow protractor, when necessary.

المقدمة.

أهمية زوايا الظلال ، وأهداف البحث:

تقع دراسة حركة الشمس وإشعاعاتها على جانب كبير من الأهمية للمهندس المعماري حيث ان لها تأثيرات كبيرة على المباني وتصميمها بصورة عامة على وجه الخصوص في المناطق الصحراوية على سواحل البحار الحارة مثل منطقة الخليج العربي ذات الفصلين المناخين فقط الأول حارا صيفا والثاني حار باعتدال شتاء مع ارتفاع نسبة الرطوبة النسبية في كلا الفصلين . ويعتبر هذا النوع من أصعب أنواع المناخ في العالم بالنسبة للإنسان.

ان الإشعاع الشمسي يؤثر على المباني اما بدخوله إياها من الفتحات كالشبابيك مثلا بطريقة الإشعاع واما بتسرب الحرارة من الخارج الى الداخل عبر الغلاف الخارجي (وبضمنه زجاج الشبابيك) بطريقة التوصيل الحراري بالإضافة لما للحمل من الدور، ولكن بامكان المهندس المصمم ان يلعب دورا كبيرا في التأثير على هاتين الطريقتين ، حيث ان انتقال الحرارة عبر الشبابيك يتأثر بتوجيه المبنى بالنسبة للاتجاهات الاربعه وكذلك بمساحه الشباك ونوع الزجاج وطبقاته .بالإضافة الى

الحماية بواقيات الشمس . كما ان قدرة الواقية على الحماية من الشمس تتغير بتغير موضع الشمس بالنسبة لفتحة الشباك المطلوب حمايته عبر الفصول وعبر ساعات النهار . وعليه فمن المهم جدا ان يتمرس المهندس المعماري بكل ما يؤثر في ذلك لاجل تصميم الواقيات الملائمة خاصة للفترات الأشد حرارة.

ولا يضير هذه الأهداف في شيء اذا ماكان المبنى مكيف الهواء ام لا. حيث ان اي تخفيض في الكسب الحراري للمبنى سوف ينعكس حتما في تخفيض حمل التكييف مما يعني الاقتصاد بالوقود والحفاظ على الطاقة وفي اغلب الحالات تعتبر الشبابيك اكبر مدخل للحرارة لداخل المبنى ، لذا فان إيه حماية لها من إشعاع الشمس تعتبر احسن فرصه لتقليل الحرارة الداخلية للمبنى.

ان التظليل الامثل للشبابيك يمكن ان يتم بواسطة التصميم الصحيح للواقيات الشمسية . وهذا يتم اولا عن طريق تحديد زوايا الظلال الأفقية والعمودية للأشهر المختلفة من السنة وللساعات المختلفة من النهار. ولكن لأجل تحديد هذه الزوايا يجب علينا اولا معرفة زوايا سقوط أشعه الشمس بنوعيها الأفقية والعمودية خلال اشهر السنة وساعات النهار . وثانيا"يجب معرفة توجيه واجهات المبنى بالنسبة للجهات الأربع .

ان تحديد زوايا الظلال ليس مفيدا لتصميم الواقيات الملائمة للشبابيك الموجودة فعلا" فحسب بكل يمكن استغلال ذلك كأداة تصميم فعالة تؤثر في اختيار التوجيه الامثل للمبنى في ضوء الفرص المتاحة للمصمم ، وكذلك تهيىء للمصمم الخيارات المعمارية العديدة في تصميم الواجهات مع الاحتفاظ بدرجة الوقاية المطلوب للشبابيك.

هناك العديد من الطرق الحسابية او المرسومة التي تستخدم لتحديد زوايا الظلال للمباني ، ولكن غالبا" ما يجد المهندس المعماري صعوبة في الحصول على المصادر التي تساعده في تطبيق ذلك بالرغم من فهمة العام لهذا الجانب والمفترض فيه ان يعرفه. فهناك الكثير من المعلومات المناخية المحلية والمعرفة النظرية والعملية يحتاجها المهندس المصمم بسرعة ولكن كثرة انشغاله بجوانب التصاميم الأخرى العديدة تلهية عن الاهتمام بهذا الموضوع كما ان عدم وعي صاحب العمل لا تجعله يصر على المتابعه .ان أكثر الطرق شيوعا عادة هي الطرق المرسومة والتي تشمل الخطوات التالية مع ما يصحبها من سلبيات:

1- بعد تحديد خط العرض لمنطقة الموقع المطلوب يجب الحصول على رسم خطوط مسارات الشمس الخاصة بخط العرض هذا . واذا لم يوفر ذلك فعلينا اخذ الرسم الخاص باقرب خط عرض اخر للخط المطلوب.

ولذا فغالبا ما يضطر المصمم لاخذ رسم خطوط مسارات الشمس لخطوط عرض بعيدة عن الخط المقصود ، وكذلك غالبا" ما تكون مرسومة رسما صغيرا يؤدي الى ضرورة التقريب التقديري في عملية قراءة قيم زوايا سقوط أشعة الشمس الأفقية العامودية في الأشهر المختلفة والساعات المختلفة كذلك.

2- ان رسم خطوط مسارات الشمس لخط عرض معين يكون عادة موضوعا حسب التوقيت الظاهري للشمس* محليا وليس حسب التوقيت المحلي الرسمي او العادي للدولة وهو التوقيت المستعمل محليا". وقد يودي ذلك الى بعض الارتباك عند الحاجة لتحديد زاوية الظل لساعة معينة من النهار، حيث يستوجب ذلك تحويل التوقيت المحلي الى التوقيت الشمسي ويعتمد ذلك على تحديد خط الطول للمنطقة المقصودة ، والتوقيت المحلي العادي للبلاد وكذلك على قيمة ثابتة بالنسبة للشهر تدعى معادلة الوقت (المصدر :1 ص 36) وتختلف هذه القيمة باختلاف اشهر السنة.

3-في حالة استخدام الطريقة المرسومة لتحديد زوايا الظلال فيجب توفر المنقلة الخاصة بزوايا الظلال مرسومة على قطعة شفافة وبنفس حجم رسم خطوط مسارات الشمس المقصودة لاجل استعمالها معا بعد تطابق مركزيهما . وحتى بعد توفر هاتين الأداتين فلا بد من قراءة قيمة زوايا الظلال بشكل تقريبي وهذا بالإضافة الى ان التوقيت المستعمل يختلف عن التوقيت المحلي كما بينا ذلك أعلاه.

وبصورة عامة فان معظم السلبيات المذكورة أعلاه نابعة من كون الطريقة عامة تشمل كل المناطق بخطوط العرض المختلفة في العالم وقد أدى ذلك للتضحية بالبساطة والدقة وهذا ما لم يشجع على انتشار هذه الطريقة وبالتالي إهمال هذا الجانب البيئي المهم في العملية التصميمية بالرغم من أهميتها بالنسبة لدولة الأمارات العربية المتحدة مثلا".

ومن هذا المنطلق جاء الهدف من هذا البحث وهو تهيئة طريقة تطبيقية مبسطة بواسطة الجداول لتحديد زوايا الظلال من قبل المهندس المعماري للمباني بالاتجاهات المختلفة من دون التضحية بالدقة حيث يعتمد على المعلومات المناخية المحلية ومحسوبة خصيصا لهذا البلد ولا تدعى عمومية التطبيق بالرغم من أنها تشرح ذلك لمن يريد التطبيق في مناطق ومجالات أخرى عند الحاجة.

الاساس النظري لحركة الشمس الظاهرية بالنسبة للارض:

ان من اهم العوامل الي تحدد كميه أشعة الشمس التي تتلقاها نقطة ما على الأرض هو الموقع الظاهري للشمس بالنسبة للفصل وساعة النهار . كما ان موقع الشمس هذا في اي وقت يتحدد بزاويا

* التوقيت الظاهري للشمس هو التوقيت الزوالي أي ان الظهر يكون في الساعة الثانية عشر في ذلك الموقع الجغرافي.

سقوط أشعة الشمس على الأرض وهما : الزاوية الأفقية ونرمز لها بالحرف "ق" والزاوية العمودية ونرمز لها بالحرف "ع".

ان الزاوية "ق" هي الزاوية الأفقية التي تقاس من خط الشمال او الهاجرة اي منتصف النهار وباتجاه عقارب الساعة اما الزاوية "ع" فهي محصورة بين أشعة الشمس والمسطح الأفقي الذي يشمل دائرة الأفق.

ان هاتين الزاويتين لمنطقة محددة تتأثران بالتغيرات الموسمية لعلاقة الشمس بالكرة الأرضية . وهذا ناتج بصورة رئيسية عن كون محور دوران الأرض حول نفسها مائلا بشكل ثابت على مسطح مدار الأرض البيضوي حول الشمس بزاوية قدرها 66.5 درجة اي بـ 23.5 درجة عن العمودي (المصدر :1 ،ص 24و2و4).

وكنتيجة لهذا الوضع المائل نرى ان المنطقة التي تسقط عليها اشد أشعة شمسية وهي العمودية على سطح الأرض يختلف موقعها بين مدار السرطان شمالا ومدار الجدي جنوبا اي بين خطي عرض 23.5 شمالا وجنوبا وحسب الموسم . ويكون ذلك في 21 من الشهر السادس وهو أطول نهار في نصف الكرة الشمالي ، وفي 22 من الشهر الثاني عشر تكون الشمس عمودية على مدار الجدي وهو أطول نهار في نصف الكرة الجنوبي واقصرة في 21 من الشهر الثالث وثانية في 23 من الشهر التاسع وفي هذين اليومين بتساوي كل من الليل والنهار ومن هذا تظهر أهمية الأيام 21،22،23 من هذه الأشهر .

<u>اختيار خط العرض الذي يمثل دولة الأمارات العربية المتحدة :</u>

ان للبعد عن خط الاستواء اي لقيمة خط العرض تأثيرا على قيم الزوايا الأفقية والعمودية لسقوط أشعة الشمس ، لذا فلكل خط عرض معين زوايا مختلف للأشعة . وبما ان دولة الأمارات العربية المتحدة تقع بين الخطين 32.58 و26.00 درجة شمالا وذلك من أقصى الجنوب الى أقصى الشمال ماعدا بعض الجزر في الخليج ، لذا فان بالامكان تحديد خط عرض واحد ليمثل البلاد ككل وقد يكون ذلك هو المعدل اي خط 24.25 درجة شمالا . ولكن هناك عاملا" اخرا" يؤثر في تحديد هذا الخط وهو ان الخط المنتخب يجب ان يكون الأقرب للغالبية العامة لسكان المستوطنات البشرية لإمكانية الاستفادة القصوى من زوايا الظلال عند تصميم المباني .وبما ان جميع مدن الأمارات والغالبية العظمى لقراها تقع شمال خط عرض 24 درجة شمالا (المصدر :3 ، ص 166) . لذا

فان اغلب سكان الأمارات بمدنها وقراها وفعاليات البناء فيها تنحصر بين 24و26 درجة شمالا . ويشمل ذلك من خط جنوب خط مدينتي العين في ابو ظبي جنوبا" وحتى راس الخيمة شمالا" ، وتحتضن هذه المنطقة ما لا يقل عن 95% من سكان الأمارات*

وبما ان المطلوب هو اختيار خط عرض واحد يمثل الأمارات لغرض زوايا الظلال اذا" فهو خط 25 درجة شمالا وهذا يتطابق على وجه التقريب مع خط عرض مدينة دبي وهو 25.15 درجة شمالا" ولاحتمال توفر المعلومات المناخية المطلوبة لهذه المدينة لذا تم اختيار خط العرض هذا ممثلا للأمارات حيث لا تبعد عنه ايه مستوطنة بشرية ذات شأن أكثر من درجة واحده.

زوايا سقوط اشعة الشمس حسب الشهر والساعة في دولة الأمارات العربية المتحدة:

المطلوب الان تحديد زوايا سقوط أشعة الشمس الأفقية منها والعمودية لمدينة دبي اي خط عرض 25.15 درجة شمالا" . وهناك ثلاث طرق متاحة للحصول على ذلك:

أ- قراءة قيم الزوايا من الجداول المنشورة لبعض خطوط العرض (المصدر :4 ،ص:58-1) ولعدم توفر قيم الزوايا من الجدول المنشور لبعض خطوط العرض 25 درجة شمالا" لذا استوجب ذلك عملية استيفاء لتحديد القيمة المجهولة المحصورة بين قيمتين معروفتين وهذا يعني ان التقريب في القيم يلعب دورا" في العملية. هذا عدا كون التوقيت المستعمل في هذا الجداول هو التوقيت الظاهري للشمس وليس التوقيت المحلي.

ب-قراءة قيم الزوايا من رسم خطوط مسارات الشمس لأقرب خط عرض للخط 25 درجة شمالا" .ففي اغلب الحالات لا يكون المتوفر هو الرسم الخاص بـ25 درجة شمالا" (المصدر :1 ،ص: 85-2 ،ص: 98-5 ،ص:8) . وحتى في حالة توفر الرسم لخط العرض هذا (المصدر :6 ، ص: 27)فلا يزال هناك نوعا من التقديرات المقربة عند قراءة قيم الزوايا من الرسم نفسه بالإضافة لاستعمال التوقيت الشمسي وليس المحلي العادي كما سبق ذكر.

ج- القياس الفعلي لزوايا موقع الشمس عند كل ساعة من ساعات النهار ليوم يمثل كل شهر من اشهر السنة . وقد لجا الباحث لقسم الأنواء الجوية في مطار الشارقة الدولي لعدم توفرها في مطار دبي الدولي . وبذا فقد توفرت الزوايا المطلوبة ولكن حسب توقيت كرنتش .

وقد تم اختيار يوم 23 من الشهر كيوم ممثل لكل شهر وذلك نسبة لما لهذا التاريخ من أهمية كما ورد ذكره سابقا وقد تم تحويل توقيت كرنش الى التوقيت المحلي العادي (الجدول رقم 1)

* حسابات الباحث استنادا" على نتائج التعداد العام للسكان سنة 1981 م. الإدارة العامة للإحصاء -وزارة التخطيط- دولة الإمارات العربية المتحدة .

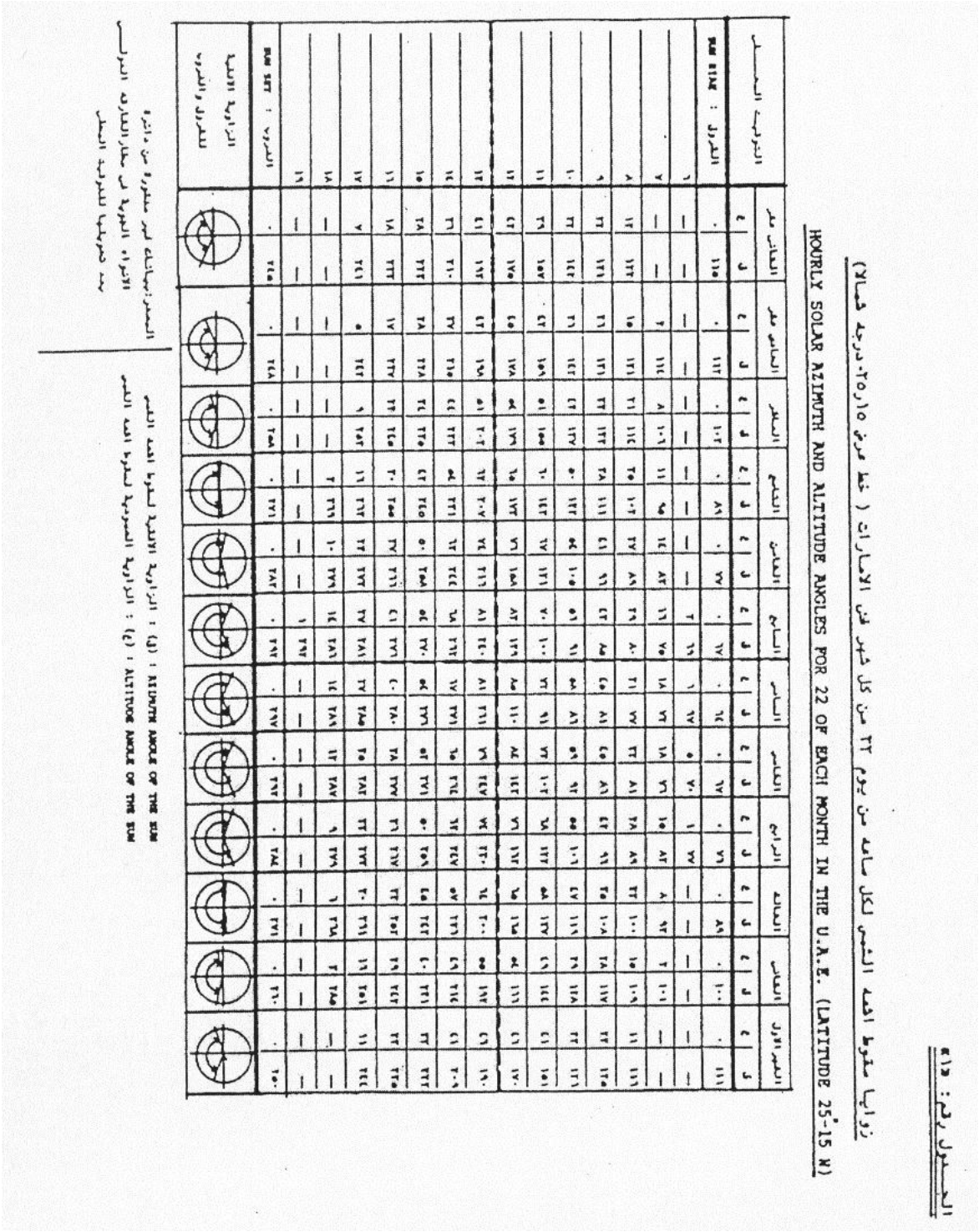

الجدول رقم: (1)

زوايا سقوط اشعة الشمس لكل ساعة من يوم ٢٢ من كل شهر في الامارات (خط عرض ٢٥ر١٥ درجة شمالا)

HOURLY SOLAR AZIMUTH AND ALTITUDE ANGLES FOR 22 OF EACH MONTH IN THE U.A.E. (LATITUDE 25°-15 N)

الشهر الاول		الثاني		الثالث		الرابع		الخامس		السادس		السابع		الثامن		التاسع		العاشر		الحادي عشر		الثاني عشر		الترتيب الساعي
ج	ع	ج	ع	ج	ع	ج	ع	ج	ع	ج	ع	ج	ع	ج	ع	ج	ع	ج	ع	ج	ع	ج	ع	
١١١	.	١٠٠	—	٨٩	.	٧٦	—	٦٤	—	٥٣	—	٤٣	—	٣٤	—	٢٧	—	٢٢	—	٢٠	—	٢٠	—	الشروق : 7 AM
١١١	—	١٠١	—	٩٢	—	٨٢	—	٧٣	—	٦٤	—	٥٦	—	٤٩	—	٤٤	—	٤٢	—	٤٤	—	٤٩	—	٨
١١٦	—	١٠٦	٢	١٠٥	٢	٩٥	٢	٨٥	٢	٧٦	٢	٦٨	٢	٦٢	٢	٦٠	٢	٦٢	٢	٦٨	٢	٧٦	٢	٩
١٢٥	٢٢	١١٧	٢٨	١٢٨	٢٦	١٢٦	٢٤	١٢٤	٢٢	١٢٢	٢٢	١٢١	٢٢	١٢١	٢٢	١٢٢	٢٤	١٢٤	٢٦	١٢٦	٢٨	١٢٥	٢٢	١٠
١٣١	٣٤	١٢٥	٤٢	١٣٦	٤٠	١٣٥	٣٨	١٣٣	٣٦	١٣٢	٣٦	١٣٢	٣٦	١٣٣	٣٨	١٣٥	٤٠	١٣٦	٤٢	١٣٥	٤٤	١٣١	٣٤	١١
١٤١	٥١	١٣٦	٥٢	١٤٢	٥٠	١٤١	٤٨	١٤٠	٤٦	١٤٠	٤٦	١٤٠	٤٦	١٤٠	٤٨	١٤١	٥٠	١٤٢	٥٢	١٤١	٥٠	١٤٠	٤٨	١٢
١٥٠	٦٣	١٤٥	٦٥	١٤٧	٦٣	١٤٦	٦١	١٤٥	٦٠	١٤٤	٦٠	١٤٤	٦٠	١٤٤	٦١	١٤٥	٦٣	١٤٦	٦٥	١٤٥	٦٣	١٤٥	٦٢	١٣
١٦٢	٧٥	١٥٣	٧٧	١٥٣	٧٥	١٥٢	٧٣	١٥١	٧٢	١٥١	٧٢	١٥١	٧٢	١٥١	٧٣	١٥٢	٧٥	١٥٣	٧٧	١٥٣	٧٥	١٥٣	٧٥	١٤
١٧٥	٩٠	١٦٣	٩٢	١٦٢	٩٠	١٦٢	٨٩	١٦١	٨٨	١٦١	٨٨	١٦١	٨٨	١٦١	٨٩	١٦٢	٩٠	١٦٢	٩٢	١٦٣	٩٠	١٦٢	٩٠	١٥
١٩٣	١٠٥	١٧٣	١٠٧	١٧٢	١٠٥	١٧٢	١٠٤	١٧١	١٠٣	١٧١	١٠٣	١٧١	١٠٣	١٧١	١٠٤	١٧٢	١٠٥	١٧٢	١٠٧	١٧٣	١٠٥	١٧٢	١٠٥	١٦
٢١٢	١١٧	١٨٣	١١٩	١٨٢	١١٧	١٨٢	١١٦	١٨١	١١٥	١٨١	١١٥	١٨١	١١٥	١٨١	١١٦	١٨٢	١١٧	١٨٢	١١٩	١٨٣	١١٧	١٨٢	١١٧	١٧
٢٣٢	١٢٧	١٩٣	١٢٩	١٩٢	١٢٧	١٩٢	١٢٦	١٩١	١٢٥	١٩١	١٢٥	١٩١	١٢٥	١٩١	١٢٦	١٩٢	١٢٧	١٩٢	١٢٩	١٩٣	١٢٧	١٩٢	١٢٧	١٨
٢٥٠	١٣٧	٢٠٣	١٣٩	٢٠٢	١٣٧	٢٠٢	١٣٦	٢٠١	١٣٥	٢٠١	١٣٥	٢٠١	١٣٥	٢٠١	١٣٦	٢٠٢	١٣٧	٢٠٢	١٣٩	٢٠٣	١٣٧	٢٠٢	١٣٧	١٩
٢٦٢	١٤٧	٢١٢	١٤٩	٢١٢	١٤٧	٢١٢	١٤٦	٢١١	١٤٥	٢١١	١٤٥	٢١١	١٤٥	٢١١	١٤٦	٢١٢	١٤٧	٢١٢	١٤٩	٢١٢	١٤٧	٢١٢	١٤٧	٢٠
٢٧٥	١٥٧	٢٢٢	١٥٩	٢٢٢	١٥٧	٢٢٢	١٥٦	٢٢١	١٥٥	٢٢١	١٥٥	٢٢١	١٥٥	٢٢١	١٥٦	٢٢٢	١٥٧	٢٢٢	١٥٩	٢٢٢	١٥٧	٢٢٢	١٥٧	٢١
٢٨٩	١٦٧	٢٣٢	١٦٩	٢٣٢	١٦٧	٢٣٢	١٦٦	٢٣١	١٦٥	٢٣١	١٦٥	٢٣١	١٦٥	٢٣١	١٦٦	٢٣٢	١٦٧	٢٣٢	١٦٩	٢٣٢	١٦٧	٢٣٢	١٦٧	٢٢
٣٠٠	١٧٧	٢٤٢	١٧٩	٢٤٢	١٧٧	٢٤٢	١٧٦	٢٤١	١٧٥	٢٤١	١٧٥	٢٤١	١٧٥	٢٤١	١٧٦	٢٤٢	١٧٧	٢٤٢	١٧٩	٢٤٢	١٧٧	٢٤٢	١٧٧	٢٣
٣١٠	١٨٧	٢٥٢	١٨٩	٢٥٢	١٨٧	٢٥٢	١٨٦	٢٥١	١٨٥	٢٥١	١٨٥	٢٥١	١٨٥	٢٥١	١٨٦	٢٥٢	١٨٧	٢٥٢	١٨٩	٢٥٢	١٨٧	٢٥٢	١٨٧	٢٤
٣٢٠	١٩٧	٢٦٢	١٩٩	٢٦٢	١٩٧	٢٦٢	١٩٦	٢٦١	١٩٥	٢٦١	١٩٥	٢٦١	١٩٥	٢٦١	١٩٦	٢٦٢	١٩٧	٢٦٢	١٩٩	٢٦٢	١٩٧	٢٦٢	١٩٧	٢٥
٣٣٠	٢٠٧	٢٧٢	٢٠٩	٢٧٢	٢٠٧	٢٧٢	٢٠٦	٢٧١	٢٠٥	٢٧١	٢٠٥	٢٧١	٢٠٥	٢٧١	٢٠٦	٢٧٢	٢٠٧	٢٧٢	٢٠٩	٢٧٢	٢٠٧	٢٧٢	٢٠٧	الغروب : PM SET

الترتيب الساعي للشروق والغروب

البسمر: نهاية فجر مستورة من دائرة الافق الموجودة في مجال الكاميرا الدولي بعد تحويلها للترتيب الساعي

الزاوية الافقية للشروق والغروب

(أ) : الزاوية الافقية لسقوط اشعة الشمس : AZIMUTH ANGLE OF THE SUN

(ع) : الزاوية العمودية لسقوط اشعة الشمس : ALTITUDE ANGLE OF THE SUN

اتجاه وطول الظلال في كل ساعة ولكل شهر على الأرض المستوية في دولة الامارات العربية المتحدة:

بعد تحديد زوايا سقوط الشمس الأفقية والعمودية لساعات اليوم الذي يمثل كل شهر في الأمارات العربية المتحدة (الجدول رقم 1) يصبح في الامكان تحديد الزاوية الأفقية لاتجاه الظل وكذلك طول ذلك الظل لكل ساعة ، ولإيجاد

ذلك نفترض ان هناك عصا عمودية على سطح الأرض المستوى طولها الوحدة مثل قدم واحد او متر واحد او غيرهما . وبذا يكون طول الظل بنفس وحدات القياس المستعملة لقياس ارتفاع العصا.

وقد تم احتساب الظلال في كل ساعة بالمعادلة التالية :

$$\text{طول الظلال} = \frac{1}{\text{ظل الزاويا العمودية لسقوط أشعة الشمس اي الزاوية (ع)}}$$

وبالنتيجة ظهر جدول بأطول الظلال لكل ساعة مع تحديد الاتجاه (الجدول رقم 2) . وكمثال على ذلك نأخذ عصا بارتفاع متر واحد فوق سطح الأرض المستوية فسوف يكون ظلها في الساعة الثامنة صباحا" حسب التوقيت المحلي للأمارات خمس أمتار في 23 من الشهر الأول من السنة و 3.5 في 23 من الشهر الثالث و1.6 مترا فقط في 22 من الشهر السادس وباتجاهات الزوايا 257،28،296 درجة على الوالي (الجدول رقم 2) اما اذا كان ارتفاع العصا او المبنى اكثر من ذلك فيكون طول الظلال مساويا لهذا الأطوال الموجودة في الجدول هذا مضروبة في ارتفاع المبنى .

اتجاه وطول الظلال في كل ساعة ولكل شهر على الأرض المستوية في دولة الامارات العربية المتحدة:

بعد تحديد زوايا سقوط الشمس الأفقية والعمودية لساعات اليوم الذي يمثل كل شهر في الأمارات العربية المتحدة (الجدول رقم 1) يصبح في الامكان تحديد الزواية الأفقية لاتجاه الظل وكذلك طول ذلك الظل لكل ساعة ، ولإيجاد ذلك نفترض ان هناك عصا عمودية على سطح الأرض المستوى طولها الوحدة مثل قدم واحد او متر واحد او غيرهما . وبذا يكون طول الظل بنفس وحدات القياس المستعملة لقياس ارتفاع العصا.

وقد تم احتساب الظلال في كل ساعة بالمعادلة التالية :

$$\text{طول الظلال} = \frac{1}{\text{ظل الزاويا العمودية لسقوط أشعة الشمس اي الزاوية (ع)}}$$

وبالنتيجة ظهر جدول بأطوال الظلال لكل ساعة مع تحديد الاتجاه (الجدول رقم 2) . وكمثال على ذلك نأخذ عصا بارتفاع متر واحد فوق سطح الأرض المستوية فسوف يكون ظلها في الساعة الثامنة

صباحا" حسب التوقيت المحلي للأمارات خمس أمتار في 23 من الشهر الأول من السنة و 3.5 في 23 من الشهر الثالث و1.6 مترا فقط في 22 من الشهر السادس وباتجاهات الزوايا 257،28،296 درجة على التوالي (الجدول رقم 2) اما اذا كان ارتفاع العصا او المبنى اكثر من ذلك فيكون طول الظلال مساويا لهذا الأطوال الموجودة في الجدول هذا مضروبة في ارتفاع المبنى .

بالاظافة لذلك فبالامكان الاستفادة من هذا الجدول في رسم ظلال اي مبنى على ارض مستويا لأيه ساعة من النهار ولكل شهر من اشهر السنة وبغض النظر عن توجيه المبنى كما هو مرسوم لكل من الشهرين السادس والثاني عشر ، كما ان بالا مكان رسم شكل دخول الشمس من الشباك لداخل المبنى اعتمادا على المعلومات الواردة في هذا الجدول رقم (2) .

المباديء الهندسية لزوايا الظلال على المبنى :

ان أداء واقيات الشمس يحدد بنوعين من الزاويا وهما زاوية الظل الأفقية ونرمز لها بالحرفين "فق" وزاوية الظل العمودية ونرمز لها بالحرفين "عم" . ويتم قياس كل منهما من الخط العمودي على الواجهة المطلوبة للمبنى عند قاعدتها . لذا فان هاتين الزاويتين لاتتاثران بزوايا سقوط أشعة الشمس الأفقية والعمودية في تلك الساعة من نهار ذلك الشهر لذلك الموقع فحسب ، بل تتاثران ايضا" في توجيه ذلك المبنى او واجهته المقصودة على وجه الخصوص . ان زوايا الظلال هذه تعني الحد الذي بعده تمنع ألواقيه مرور أشعة الشمس .

ان زواية الظلال الافقية "فق" توثر في تصميم الواقيات العمودية. وتمثل هذه الزاوية الفرق بين زواية سقوط اشعة الشمس الافقية في الساعة المطلوبة وزاوية اتجاه جدار المبنى المطلوب وان زواية اتجاه جدار المبنى هذه عبارة عن احدى زوايا الدائرة الـ 360 درجة التي يمر منها الخط العمودي على واجهة الجدار المطلوب ونرمز لها بالحرف "ك" (الشكل رقم 2).

اما زوايا الظلال العمودية "عم" فتوثر في تصميم الواقيات الافقية مثل المظلة الافقية للشباك وتقاس ضمن مسطح عمودي على الارض المستوية وكذلك على واجهة المبنى المطلوب.

وتجدر هنا الملاحظة بضرورة التمييز بين زاوي سقوط أشعة الشمس العمودية "عم" والتي تحدد ارتفاع الشمس على الأفق بالنسبة للمشاهد وبين زاوية الظل العمودية "عم" والتي تحدد مواصفات واقية الشمس . وقد تتطابق هاتين الزاويتين "ع" و "عم" في حالة واحدة هي عندما تكون الشمس مقابلة لواجهة المبنى تماما" اي عندما تتساوى زوايا سقوط أشعه الشمس الأفقية مع زاوية اتجاه جدار المبنى وبخلاف ذلك تكون زاوية الظلال العمودية اكبر من زاوية سقوط اشعة الشمس العمودية

.

اما العلاقة الرياضية بين هذه الزوايا "ع" و "عم" و"فق" فهي كما يلي :

ظا(عم)=ظا(ع) x قا(فق) (المصدر :7 ، ص 53).

وبذا يمكن إيجاد زاوية الظلال العمودية لاي مبنى بعد معرفة زوايا سقوط أشعة الشمس الأفقية والعمودية وبعد معرفة توجيه المبنى . وبما ان زوايا سقوط أشعة الشمس هي معروفة الان لخط عرض الأمارات 25.15 درجة شمالا" (الجدول رقم 1) فما علينا الا تحديد اتجاه المبنى بالنسبة للجهات الأربع . وبالامكان افتراض بعض الزوايا المحتملة.

<u>تحديد زوايا الظلال على المباني في دولة الامارات العربية المتحدة :</u>

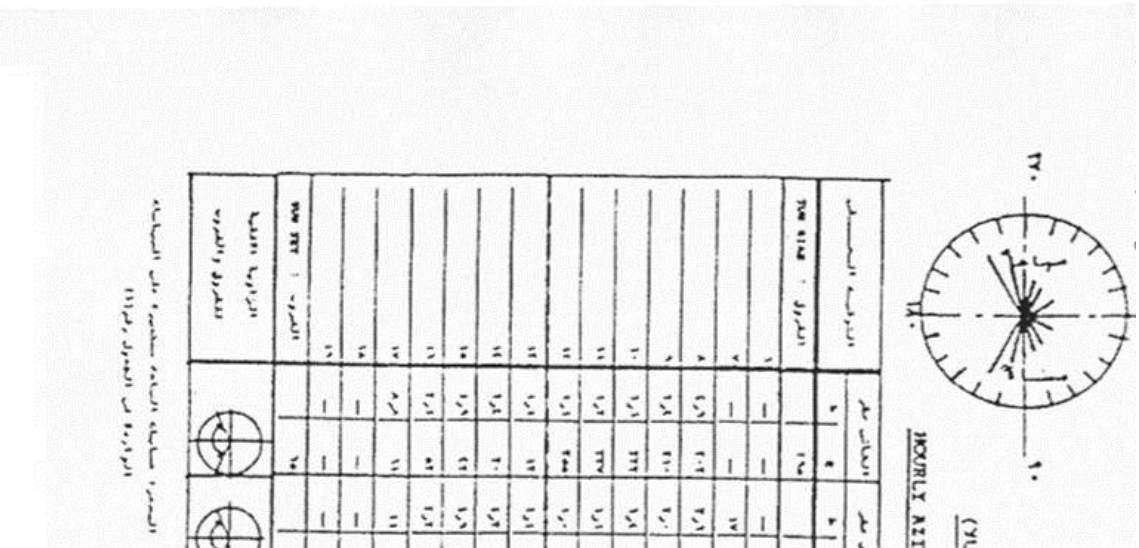

الجدول رقم: «٢»

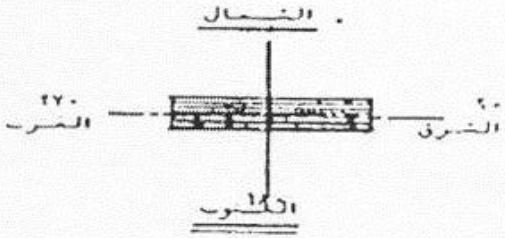

زوايا الظلال لكل ساعه من يوم ٢٢ من كل شهر في الامارات لمختلف بواجهة الشمال والجنوب

SHADOW ANGLES FOR EVERY HOUR OF 22 OF EACH MONTH IN THE U.A.E.

التوقيت المحلي	الواجهة المطلوبة	الثامن مساء		السابع مساء		السادس مساء		الخامس		الرابع		الثالث		الثاني		الأول	
		س	ش	س	ش	س	ش	س	ش	س	ش	س	ش	س	ش	س	ش
	الشرق																
الشروق : SUNRISE		٠	١٥	٠	٦٥	٠	٢٨	٠	٨٩	٠	٣٧	٠	١٧	٠	١٤	٠	٦٩
٦		—	—	—	—	—	—	—	—	١	٧٢	٨	١٦	١٥	١٧	١٤	٧٠
٧		—	—	—	٦١	٢٧	٢٦	١١	٨٥	١٤	٨٢	٤٨	٧٥	٤٩	٦٦	٥١	٦٦
٨		٢١	٥٥	٢٨	٥٦	٤٢	١١	١١	٧٥	٨٨	٨٦	٧٢	٨٠	٦٦	٧٧	٧٦	٨١
٩		٢٢	٤٩	٣٧	٤٦	٥٠	٥٧	٦٥	١٦	٨٢	٨٤	٨٥	٨٥	٨١	٨١	٨١	٨٦
١٠		٢٨	٢٨	٤٢	٣٧	٥٢	٤٢	٦٥	٥٢	٧٦	٧٥	٨٩	٨٩	٨٧	٨٦	٨٧	٨٦
١١		٤١	٣٢	٤٤	٢١	٥٤	٢٥	٦٥	٣٧	٧٨	٥٩	٨٦	٨٠	٨٩	٨٩	٨٩	٧٨
١٢	الجنوب	٤١	٥	٤٥	٢	٥٤	١	٦٥	٧	٧٧	٢٢	٨٥	٥١	٨٨	٣٠	٨٥	٣٧
١٣		٤١	١١٠	٤٤	١٨٠	٥٢	٣٢٠	٦٥	٣٧٠	٣٧	٣٦٠	٨٥	١٠	٨٩	٨١٠	٨٥	١٢٠
١٤		٤٠	٢٠٠	٤١	٢٥٠	٥١	٤٢٠	٦٥	٥١٠	٧٧	٦٤٠	٨٧	٨٢	٨٩	٨٩	٨٧	٨٤٠
١٥		٢١	٤٢٠	٢٨	٤٨٠	٥٠	٥٥٠	٦٥	٦٥٠	٨٠	٧٨٠	٨٩	٨٩	٨٩	٨٤	٨٩	٨٩
١٦		٢٨	٥٢٠	٢٠	٥٧٠	٤٤	٦٥٠	٦٥	٧٥٠	٨٥	٨٦٠	٨٢	٨١	٧٨	٨٠	٨١	٨١
١٧		١٢	٦١٠	١٢	٦٥٠	٢٨	٧٣٠	٦٥	٨٢٠	٨٥	٨٨	٧٦	٧٦	٥١	٧٥	٦١	٧٥
١٨		—	—	—	—	—	—	٣٠	٨٦٠	٥١	٨٤	٤٤	٧٤	٣٦	٧٠	٤٩	٧٦
١٩		—	—	—	—	—	—	—	—	—	—	٢	٦٨	—	—	—	—
الغروب : SUNSET		٠	١٥٠	٠	٦٥٠	٠	٢٨٠	٠	٨٩	٠	٣٢	٠	١٢	٠	١٤	٠	١٢
	الغرب																
الزاوية الأفقية للشروق والغروب																	

السهم : يشير الى مستوى على البيانات الواردة في الجدول رقم (١) وزاوية توجيه السهم

(ش) : زاوية الظل الأفقية (القيمة السالبة تعني أن القيم آتية من يسار المشاهد للواجهة)

(س) : زاوية الظل الرأسية VERTICA

(ش) : HORIZONTAL SHADOW ANGLE (NEGATIVE VALUES MEANT SUN COMING FROM THE LEFT WHEN FACING THE ELEVATION)

٢٦٠ ° الشمال

تحديد زوايا الظلال على المباني في دولة الأمارات العربية المتحدة:

وبالاستناد على المباديء الواردة أعلاه وكذلك على البيانات الواردة في الجدول رقم (1) تم احتساب زوايا الظلال الأفقية والعمودية لأربعة حالات بديلة فقط في التوجيهات المختلفة للمبنى وذلك لضيق المجال ، وهي كما يلي :

الجدول رقم 3 : زوايا الظلال للمبنى المواجه شمالا" وجنوبا".

الجدول رقم 4 : زوايا الظلال للمبنى المواجه لـ 30 درجة و 210 درجات.

الجدول رقم 5 : زوايا الظلال للمبنى المواجه شرقا وغربا".

الجدول رقم 6 : زوايا الظلال للمبنى المواجه لـ 165 درجة و245 درجة .

وهذا هو التوجيه الامثل في الامارات .

وتعطي هذه الجداول بصورة فورية زوايا الظلال العمودية والافقية لايه ساعة حسب التوقيت المحلي لليوم الذي يمثل الشهر المطلوب وحسب توجيه المبنى في ذلك الجدول . وكل جدول يحتوي على زوايا الظلال بالنسبة لجدارين متقابلين من المبنى ، وكذلك على زوايا الشروق والغروب مرسومة بالنسبة لتوجيهات المبنى والاختلافات الشهرية لهذه الزوايا .

وعند كون القيمة سالبة لزواية الظل الافقية فهذا يعني ان الشمس ساطعة من الجهة اليسرى للشخص المواجه للواجهة المطلوبة . كما ان هناك خطا" او اكثر في كل جدول يفصل الزوايا الخاصة بكل واجهة من الواجهات المطلوبة المتقابلة من المبنى .

وبذا يكمن للمهندس المصمم معرفة زوايا الظلال بسرعة في هذه الجداول الا اذا كان توجيه المبنى لا ينطبق على ايه حالة من هذه الحالات المذكورة وعندئذ بالامكان تقدير القيم بين تلك الموجوده في الجدولين المتقاربين بالتوجيه للتوجيه المطلوب او ان يتم حسابها من المباديء الاولية كما سبق شرحه . بعد تحديد زوايا الظلال هذه فبالامكان تصميم واقيات الشمس بالنسبة للساعة والتاريخ المطلوب فيهما لمنع دخول الشمس للمبنى .

الاساس النظري لتحديد اوقات الحماية من الشمس

بعد تحديد زوايا الظلال لكل ساعة من اليوم الذي يمثل كل شهر يبقى ان نعرف في اي ساعة من ساعات النهار واي شهر من اشهر السنة نحتاج الى وقاية الشباك من الشمس في حالة تعرضه لها.ان احسن طريقه لمعرفة ذلك هي التحديد الناتج من مفهوم الفترة شديدة الحرارة مرسومة على شبكة درجات الحرارة لكل ساعة لليوم الذي يمثل كل شهر (المصدر :2 ،ص 59- و63 و 115) وهذه تشمل التغيرات اليومية والموسمية لدرجات الحرارة .

اما درجات الحرارة هذه فهي على ثلاثة انواع (المصدر :2 ، ص 254) :

أ- درجة حرارة الهواء خارج المبنى ، ولكن هذه تهمل تاثير رطوبة الجو بالرغم من اهميتها كعامل مؤثر في مناخ الامارات العربية المتحدة.

ب-درجة الحرارة الشمسية لكل وجه جدار وحسب توجيهة بالنسبة للاتجاهات الاربعة وكل قيمة من ذلك تتاثر بشده الاشعاع الشمسي الساقط على الوجه بالاضافة الى درجة حرارة الهواء خارج المبنى وكذلك مقدرة الجدار على امتصاص الحرارة وتوصيلها للداخل . وعيب هذا المقياس هو عدم توفر البيانات الكافية خاصة في المرحلة الاولية من الدراسات وقبل تحديد مواد الجدار نفسه (المصدر :2 ، ص :74) .

ج-درجة الحرارة المؤثرة ،وهي تجمع بين عوامل درجة حرارة الهواء الخارجي ، ونسبة الرطوبة وكذلك احيانا مقدار حركة الهواء وخصائص الملابس المرتدية . وهناك درجة حرارة اخرى مقاربة وهي درجة الحرارة المؤثرة المتطورة وهذه تضيف عاملا" اخرا وهو تاثير الاشعاع الا انه قلما تتوفر كل هذه البيانات لاعطاء هذا المعامل الواحد (المصدر : 2 ، ص:50) . ولكن عند توفر بعض البيانات فقط فبالامكان تبسيط الامور عن طريق الاخذ بنظرالاعتبار بعض الافتراضات لغرض تكوين ورسم شبكة درجات الحرارة للساعات اليومية شهريا وهذه عبارة عن شبكة لمحاور متعامدة تمثل العمودية منها اشهر السنة وتمثل الافقية ساعات اليوم ، ومرسوم عليها مجموعة من المنحيات كل واحد منها يربط بين كل نقاط الوقت والتي تتساوى في درجة حرارتها . اي انها الخطوط "الكونتورية" لدرجات الحرارة المتساوية مرسومة على شبكة الوقت والشهر.وبعد رسم هذه المنحنيات على هذه الشبكة يجب تحديد خط الحرارة الذي يحدد منطقة الحرارة الشديدة وهذا الخط بدوره يحدد (خط درجة حرارة معينة) مواعيد ضرورة التظليل بالنسبة للساعة والشهر.

ولهذا الغرض يمكننا الاستفادة من مفهوم المنطقة المريحة ومفهوم الفترة شديدة الحرارة:

ان حدود المنطقة المريحة هي ما نتج عن اختبارات التجارب العلمية على اشخاص تحت ظروف

مختلفة من العوامل المناخية والتي يشعر تحتها بالراحة ما لايقل عن80% منهم وتعتمد هذه على القرار غير الموضوعي للشخص تحت التجربة . وقد اظهرت التجارب هناك اختلافات كبيرة بقيم درجات الحرارة الموثرة المقبولة كدرجة مريحة بين بلاد واخرى وبين الصيف والشتاء . ويعزى ذلك على تعود الجسم وتكيفه (المصدر : 1 – ص 20 و2 ، 57) فمثلا في الصيف تنحصر الفترة المريحة في الوالايات المتحدةالامريكية بين 18و24 درجة مئوية مؤثرة بينما تتراوح هذه الفترة في سنغافورة بين 24 و27 درجة(المصدر :2 ،ص 57) .

ويمكن نقل حدود المنطقة المريحة من رسم شبكة درجات الحرارة للساعات اليومية شهريا" الى رسم خطوط مسارات الشمس وذلك للاستفاده منها عند استعمال منقلة زوايا الظلال كما سياتي ذكره بالنسبة للامارات . وان درجة حرارة الحد الاعلى للمنطقة المريحة قد يمثل الحد الادنى للمنطقة شديدة الحرارة .

ومن رسم شبكة درجات الحرارة هذه يمكننا تحديد ساعة النهار والتاريخ الذي يستوجب التظليل ومن ثم تتبع طريقة الجداول السابقة (الجدول من 3–6).

تحديد اوقات الوقاية من الشمس في دولة الأمارات العربية المتحدة:

لاجل رسم شبكة درجات الحرارة المؤثرة المتطورة يجب معرفة درجة الحرارة والرطوبة والحرارة الاشعاعية وسرعة الهواء ليوم منوالي لكل شهر , ولكن بعض هذه البيانات غير متوفرة حتى لمدينة دبي اي خط عرض 25.15 درجة شمالا" . وعليه ينبغي الالتجاء الى بعض الافتراضات بالنسبة لبعض هذه المؤثرات.

أ– بالنسبة لدرجات حرارة الهواء ورطوبته لكل ساعة من ساعات النهار ، فلقد تم تحصيل هذه البيانات من دائرة الانواء الجوية في مطار دبي وهي معدلات درجة الحرارة المئوية بالمحرار الجاف لكل ساعة على حده لطول الشهر . وحيث ان ذلك متوفر لعدة سنوات فقد اخذ معدل قراءة الساعة المعنية على مدى هذه السنين . وكذلك فيما يخص درجات الحرارة حسب المحرار الرطب.

ب–بالنسبة لدرجات حرارة الاشعاع فانها لم تتوفر حيث ان دائرة الانواء لا تستخدم المحرار ذو الكرة المعدنية وعلى اي حال فلغرض دراسة الظروف الحرارية داخل المبنى يمكننا اهمال تاثير الاشعاع الشمسي . وهذا يعني ان درجة حرارة سطح الجدار او السقف نفترضها مساوية لدرجة حرارة الهواء (المصدر :2 ص 58و59). وقد جاء هذا الافتراض لتبسيط الامور .

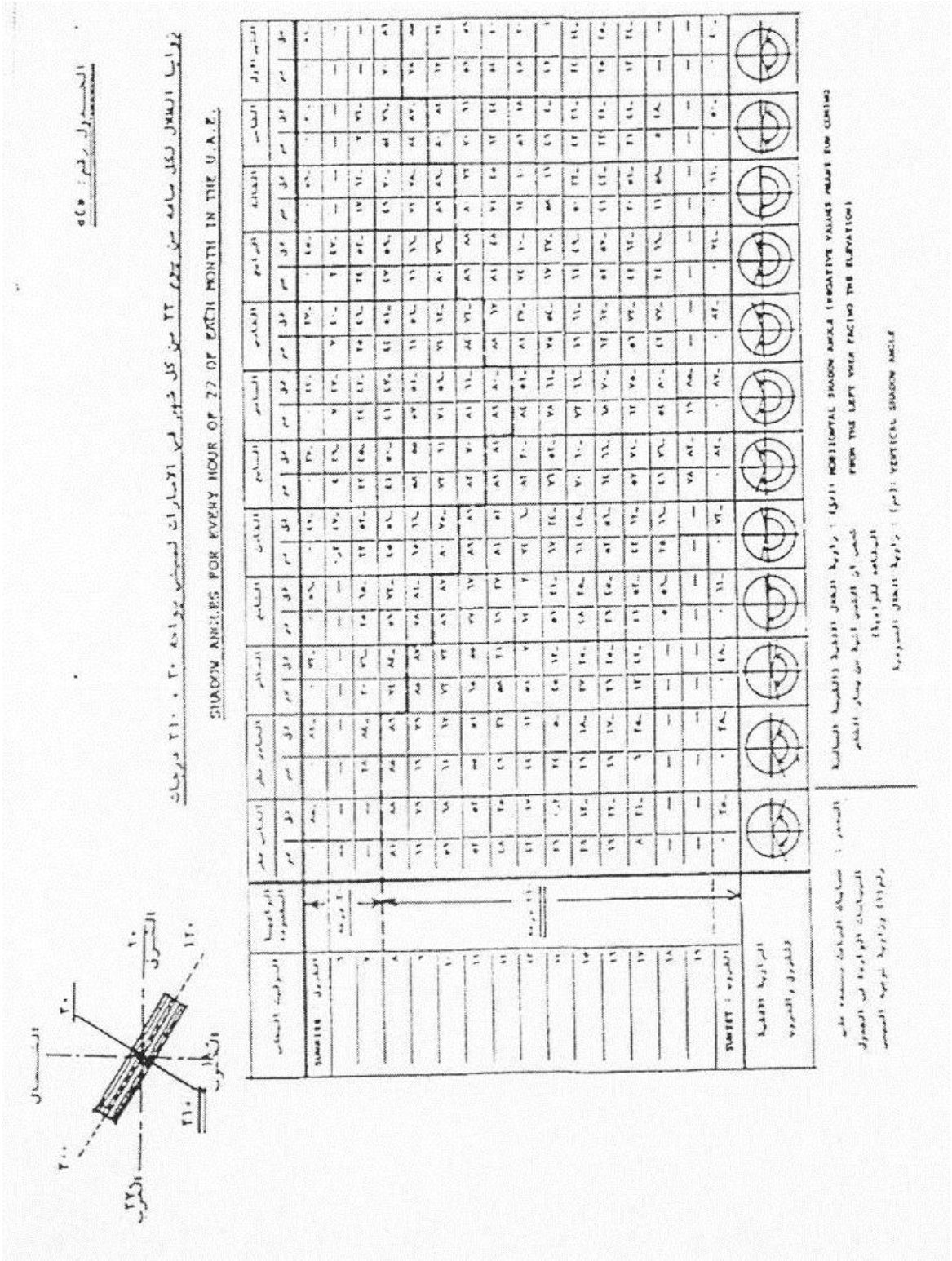

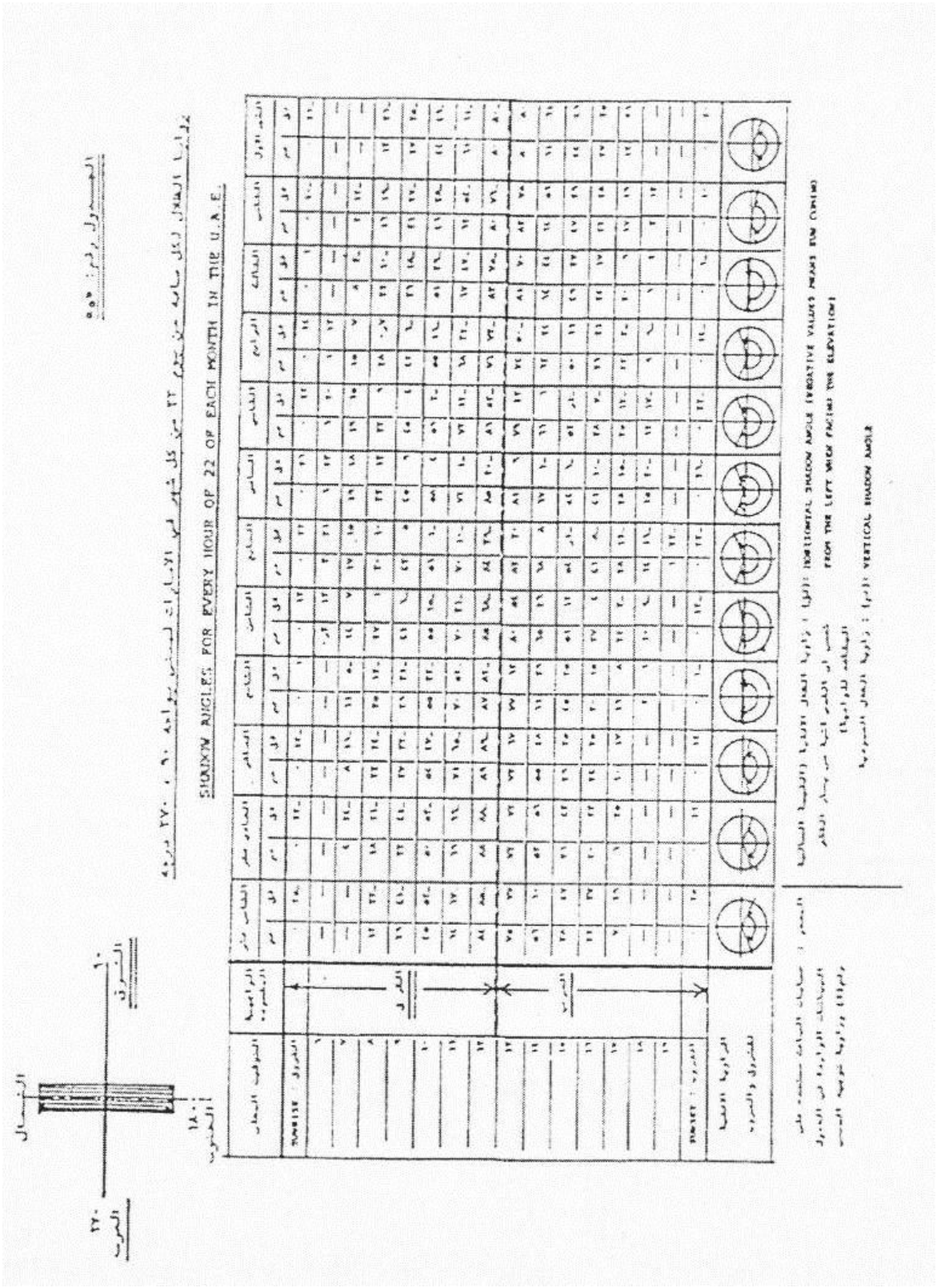

الجدول رقم: ٥٥٥

يوضح الظل لكل ساعة من كل يوم ٢٢ من كل شهر في الامارات لمستوى يواجه ٩٠ ، ٢٧٠ درجة

SHADOW ANGLES FOR EVERY HOUR OF 22 OF EACH MONTH IN THE U.A.E.

التاريخ	الساعة	الفجر		الشروق		الصباح		الضحى		الظهر		العصر		المغرب		العشاء		الفجر		الشروق	
		ظ	م	ظ	م	ظ	م	ظ	م	ظ	م	ظ	م	ظ	م	ظ	م	ظ	م	ظ	م
JANUARY	١	٢٤-	-	١٢-	-	٢-	-	١٢-	-	٢٠-	-	٢٤-	-	٢٤-	-	١٢-	-	٢٤-	-	١٢-	-
	٢	٢٤-	-	١٢-	-	٢-	-	١٢-	-	٢٠-	-	٢٤-	-	٢٤-	-	١٢-	-	٢٤-	-	١٢-	-
	٣	٢٤-	-	١٢-	-	٢-	-	١٢-	-	٢٠-	-	٢٤-	-	٢٤-	-	١٢-	-	٢٤-	-	١٢-	-
	٤	٢٤-	-	١٢-	-	٢-	-	١٢-	-	٢٠-	-	٢٤-	-	٢٤-	-	١٢-	-	٢٤-	-	١٢-	-
	٥	٢٤-	-	١٢-	-	٢-	-	١٢-	-	٢٠-	-	٢٤-	-	٢٤-	-	١٢-	-	٢٤-	-	١٢-	-
	٦	٢٤-	-	١٢-	-	٢-	-	١٢-	-	٢٠-	-	٢٤-	-	٢٤-	-	١٢-	-	٢٤-	-	١٢-	-
	٧	٢٤-	-	١٢-	-	٢-	-	١٢-	-	٢٠-	-	٢٤-	-	٢٤-	-	١٢-	-	٢٤-	-	١٢-	-
	٨	٢٤-	-	١٢-	-	٢-	-	١٢-	-	٢٠-	-	٢٤-	-	٢٤-	-	١٢-	-	٢٤-	-	١٢-	-
	٩	٢٤-	-	١٢-	-	٢-	-	١٢-	-	٢٠-	-	٢٤-	-	٢٤-	-	١٢-	-	٢٤-	-	١٢-	-
	١٠	٢٤-	-	١٢-	-	٢-	-	١٢-	-	٢٠-	-	٢٤-	-	٢٤-	-	١٢-	-	٢٤-	-	١٢-	-
	١١	٢٤-	-	١٢-	-	٢-	-	١٢-	-	٢٠-	-	٢٤-	-	٢٤-	-	١٢-	-	٢٤-	-	١٢-	-
	١٢	٢٤-	-	١٢-	-	٢-	-	١٢-	-	٢٠-	-	٢٤-	-	٢٤-	-	١٢-	-	٢٤-	-	١٢-	-
FEBRUARY	١	٢٤-	-	١٢-	-	٢-	-	١٢-	-	٢٠-	-	٢٤-	-	٢٤-	-	١٢-	-	٢٤-	-	١٢-	-
	٢	٢٤-	-	١٢-	-	٢-	-	١٢-	-	٢٠-	-	٢٤-	-	٢٤-	-	١٢-	-	٢٤-	-	١٢-	-
	٣	٢٤-	-	١٢-	-	٢-	-	١٢-	-	٢٠-	-	٢٤-	-	٢٤-	-	١٢-	-	٢٤-	-	١٢-	-
	٤	٢٤-	-	١٢-	-	٢-	-	١٢-	-	٢٠-	-	٢٤-	-	٢٤-	-	١٢-	-	٢٤-	-	١٢-	-
	٥	٢٤-	-	١٢-	-	٢-	-	١٢-	-	٢٠-	-	٢٤-	-	٢٤-	-	١٢-	-	٢٤-	-	١٢-	-
	٦	٢٤-	-	١٢-	-	٢-	-	١٢-	-	٢٠-	-	٢٤-	-	٢٤-	-	١٢-	-	٢٤-	-	١٢-	-
	٧	٢٤-	-	١٢-	-	٢-	-	١٢-	-	٢٠-	-	٢٤-	-	٢٤-	-	١٢-	-	٢٤-	-	١٢-	-
	٨	٢٤-	-	١٢-	-	٢-	-	١٢-	-	٢٠-	-	٢٤-	-	٢٤-	-	١٢-	-	٢٤-	-	١٢-	-
	٩	٢٤-	-	١٢-	-	٢-	-	١٢-	-	٢٠-	-	٢٤-	-	٢٤-	-	١٢-	-	٢٤-	-	١٢-	-
	١٠	٢٤-	-	١٢-	-	٢-	-	١٢-	-	٢٠-	-	٢٤-	-	٢٤-	-	١٢-	-	٢٤-	-	١٢-	-
	١١	٢٤-	-	١٢-	-	٢-	-	١٢-	-	٢٠-	-	٢٤-	-	٢٤-	-	١٢-	-	٢٤-	-	١٢-	-
	١٢	٢٤-	-	١٢-	-	٢-	-	١٢-	-	٢٠-	-	٢٤-	-	٢٤-	-	١٢-	-	٢٤-	-	١٢-	-

ج–ونظرا لعدم توفر سرعة الهاواء في كل ساعة ليوم منوالي من كل شهر ، فبالامكان افتراض كون الهاوء ساكنا" وهذا يمثل اسوأ الحلات من ناحية الحد المريح لدرجات الحرارة المؤثرة.

وباخذ درجات الحرارة بالمحرار الجاف وبالمحرار الرطب وباستعمال المخطط البياني بدرجات الحرارة المؤثرة (نوموجرام) (المصدر :2 ص 54) اصبح بالامكان استخراج درجات الحرارة المؤثرة لكل ساعة بالنسبة للهواء الساكن وملابس العمل العادية وذلك ليوم واحد من كل شهر. وبذا تم تركيب رسم شبكة درجات الحرارة المؤثرة

ولغرض تحديد المنطقة المريحة على هذا الرسم يقتضى تحديد درجاتها الحرارية ولعدم وجود تجربة علمية خاصة بدولة الامارات واستنادا على القيم التي سبق ذكرها بالنسبة للولايات المتحدة الامريكية وسنغافورة فلقد تم تحديد المنطقة المريحة تقديريا بين 22و27 درجة مئوية مؤثرة . فيتم تحديد ذلك على رسم شبكة درجات الحرارة ليتم تحديد المنطقة شديدة الحرارة عليه.

كما قد تم اختيار حد الظلال . نظريا ينطبق هذا الخط مع الحد الادنى لمنطقة الحرارة الشديدة اي خط 27 درجة مئوية مؤثرة . ولكن بما ان تاثير الاشعاع لا يمكن اهماله كاملا" في الحسابات لذا فمن المناسب تخفيض هذا الحد دون الـ27 درجة ولقد اعتبرنا خط الـ 25 درجة مئوية مؤثرة هو حد الظلال , ليتم رسم هذا الحد على مرسوم شبكة درجات الحرارة.

ان جميع المعلوامت المثبته على رسم شبكة درجات الحرارة للامارات العربية المتحدة قد يتم نقلها على مخططين لمسارات الشمس الاول من الشهر الاول للسادس والثاني من السابع للثاني عشر وذلك لاحتمال حاجة القاري لها ويتضح من دراسة الرسم البياني لشبكة درجات الحرارة هذه وحسب الافتراضات المذكروة سابقا" يلي :

– بالنسبة للشهر الاول والثاني والثالث من السنة لاضرورة للحماية من اشعة الشمس على الشباك

–بالنسبة للشهر الرابع ينبغي الحماية بين الساعة 11 و 17

– بالنسبة للشهر الخامس ينبغي الحماية بين الساعة 9 وساعة الغروب

–بالنسبة للشهرين السادس والتاسع ينبغي الحماية من الشروق وحتى الغروب

–بالنسبة للشهر العاشر ينبغي الحماية بين الساعة9 وساعة الغروب

–بالنسبة للشهرين الاخيرين فلا ضرورة للحماية

كما يظهر ايضا ان الفترة شديدة الحرارة خلال الشهر السابع تكاد تكون متواصلة طيلة الاربعة والعشرون ساعة يوميا اي ما عدا ساعة وبضع الساعة وقت الفجر .

الاستنتاجات والتوصيات:

1- ان الجدول رقم (1) الذي يحدد زوايا سقوط الشمس والجدول رقم (3) الذي يحدد زوايا الظلال الأفقية والعمودية لكل ساعة من ساعات النهار حسب التوقيت المحلي العادي ولكل شهر سوف تكون مفيده جدا" للمهندس المصمم لمعرفة موقع الشمس بالنسبة للمبنى واطوال الظلال الافقية لكل ساعة حسب التوقيت المحلي العادي مما يؤثر في استعمالات المسطحات الخارجية ومواعيد تظليلها ، ومن دون الحاجة للتحويلات من توقيت لاخر.

2- ان الشرح المبسط للعلاقات الهندسية لزوايا سقوط اشعة الشمس وزاوية توجيه المبنى وزوايا الظلال الناتجة لكل ساعة سوف يسهل قدره المهندس على حساب زوايا الظلال لاي توجيه يختاره للمبنى وحسب الوقت المحلي العادي والموسم المطلوب ، هذا في حالة ان توجيه المبنى المطلوب لا يتطابق مع احد التوجيهات العديدة المختارة في جداول زوايا الظلال (الجداول من 3–6) . ولولا ضيق المجال لتم تهيئة جداول اضافية تتناول زوايا توجيه اخرى لتسهيل مهمة المصمم.

3- اما في حالة كون التوجيه المطلوب للمبنى ينطبق مع التوجيه المذكور في احد هذه الجداول فما على المهندس المعماري الا اخذ قيمة الزوايا الافقية والعمودية للظلال من الجدول مباشرة.

كما ان التوجيهات المنتخبه لغرض الجداول تشمل التوجيهات المحتمله وبضمنها التوجيه الامثل بالنسبة للامارات العربية المتحدة (الجدول رقم 6) وهو المواجه للزاويا 345 درجة اي شرق الشمال الغربي والزاوية المقابل لها وهي 165 درجة ، حيث ان من المعروف ان هذا التوجيه هو الامثل بالنسبة لكل من اتجاه الشمس واتجاه الرياح السائدة وهي الرياح الشمالية الغربية بالنسبة لاشهر الحر في الامارات (المصدر :8 ص 91و92)

4- عند تحديد زوايا الظلال المطلوب عندها الوقاية من الشمس يستطيع المهندس المعماري توفير ذلك بانواع الواقيات الافقية والعامودية بنسب متفاوته وتشمل الواقيات الضيقه المتقاربة . كما يمكن تفادي الحلول باهضة التكاليف من خلال قبول دخول بعض اشعة الشمس باوقات قصيرة . ان تصميم الواقيات الشمسية هو جزء مكمل لمتطلبات التصميم الاخرى من شكل وجمالية وحركة الهواء والضوء. ويجب عدم تصميم الواقيات بمعزل عن

ذلك .

5- من الملاحظ ان الفترة الحارة في الامارات تكون على اشدها خلال الشهر السادس والسابع والثامن حيث تمتد طيلة 24 ساعة ما عدا ساعات الفجر الاولى وعلية فلا بد من الاعتماد على وسائل التكيف الميكانيكية . لذا فان وقاية الشبابيك من اشعة الشمس اثناء النهار غير كافية لوحدها لان وسائل العزل الحراري للجدران والسقوف هي ايظا ضرورية جدا " كما ان الواح الزجاج المزدوجة غير مجدية بدون وقاية من اشعة الشمس الداخلة بل على العكس فقد تزيد من ظاهرة البيوت الزجاجية من احتجاز الحرارة الداخلة للمبنى

6- ان بساطة وانسياب منحنيات درجات الحرارة المؤثرة للامارات (شكل رقم 4) وبضمنها حد ضرورة الحد من الشمس (اي خط 25 درجة مئوية مؤثرة) لا يستوجب استخدام حاجب طريقة الشمس واستعمال منقلة الظلال ورسم مسارات الشمس حيث ان لذلك ما يبرره عند كون منحنيات شبكة درجات الحرارة للساعة والشهر معقدة مثلا عندما تكون درجة الحرارة المؤثرة منخفضة صباحا ومساءا" وعالية حوالي منتصف النهار كما في بغداد والرياض مثلا. لذا فان استخدام الطريقة المبسطة هذه بشكل جداول لها مبرراتها بناء على طبيعة مناخ الامارات الخالي من الفترات محدودة الحرارة

المراجع

1- A.& V. Olgyay,"Solar control & Shading devices ". Princeton university press 1976

2- O.H> Koenigsberger & others , " Manual of tropical housing & building part 1- climatic design" , Longman ,1980

3- د. عبد الحميد ، عبد القادر غنيم –جامعة الامرات ، المستوطنات البشرية في دولة الامارات العربية المتحدة ، مكتبة الفلاح ، الكويت 1985 م

4- Carrier Air Conditioning Company . "Handbook of Air conditioning system Design" McGraw-Hill, 1982

5- R.T. Packard Ed., "Architectural Graphic Standards", Jone Wiley and Sons, 1980

6- E.P. Kukreja, " Tropical architecture " . Tata- McGraw hill, 1982

7- S.V Szokolay, " Solar energy and Building ". The Architectural Press 1975

8- د. عبد السلام فرمان – خبير الأمم المتحدة للإسكان في الامارات العربية المتحدة (1981م–1983) ، الإسكان والبيئة الحرارية في الامارات العربية المتحدة ، مركز الأمم المتحدة للمستوطنات البشرية (Habitat –Unchs) 1983 م

مقترح نظام اداري لقواعد اختيار اسلوب التنفيذ في مشاريع قطاع التشييد في العراق

د. حاتم خليفة بريسم العجيلي
مدرس / جامعة بغداد

الخلاصة

إن اكثر المشاكل التي واجهها الاسلوب الجديد هي إشاعة الأساليب القديمة والتعود عليها , وقد كان الاسلوب التقليدي (المقاول العام) وعقد جدول الكميات هما الأكثر شيوعا واستيعابا لدى الجهات الفنية والإدارية بمختلف مستوياتها ومواقعها وقد شاع استخدامهم خلال تطبيق اسلوب التنفيذ المتسارع بالرغم من عدم نجاحهم في تحقيق جميع متطلبات التنفيذ لاسلوب التنفيذ المتسارع , ولذا اصبح من الضروري البحث عن قواعد تعاقدية معينة يمكن استخدامها كبديل مفضل لجميع الحالات والظروف مع الاسلوب الجديد بعد استخلاص الدروس والعبر من تجارب القطر في حملات الأعمار .

يهدف البحث إلى تحليل موضوع اختصار عنصر الزمن وتطوير قواعد اختيار اسلوب التنفيذ المتسارع , مع مراعاة تاثير كل العوامل المؤثرة او التي تؤدي إلى زيادة الكلفة والوقت خلال التنفيذ .

لقد جرى اتباع منهجية علمية في الجانبين النظري والميداني من البحث . تضمن البحث اجراء التحليلات الاحصائية التفصيلية عن طريق إجراء الاستبيان الميداني لغرض تقويم العوامل المؤثرة بصورة مباشرة أو غير مباشرة على اسلوب التنفيذ المتسارع .

ABSTRACT

Among the most important problems which faced the new approach is the wide use of old approach , particularly the traditional approach (general contractor) and the bill of quantity contract, and this were commonly used in the course of the application of fast – track approach in spite of unfulfilling the execution requirements for the fast – track , so It became necessary to look for certain contract rules to be used as a substitute suited all conditions and cases after concluding lessons from the local experiments in rebuilding issues .

This research aims at analyzing the subject of shortening time factor taking in consideration the effect all the effective factors which leads to increase the cost and time

A scientific methodology was followed in both theoretical and practical phases of the study . A detailed statistical analysis of the study was incorporated using questionnaire and interview method to evaluate the effective factors directly or indirectly on fast – track approach.

* مقدمة :

تأخذ العملية التقليدية في المشاريع الكبيرة والمعقدة بخطواتها من الفكرة الى الاتفاق مع المعماري فالتصميم واعداد الوثائق ثم استدراج العطاءات والاحالة سنين , حتى اذا كان كل شئ يسير بسهولة بسبب تعاقب الفعاليات والانشطة وحجم المشروع . ان مجئ مبالغ العطاءات فوق مستوى الميزانية المحدد لصاحب العمل لايعتبر امرا غريبا الا انه يؤدي الى اعادة دورة المشروع اعتبارا من عملية التصميم او قبلها لغرض العمل على سلوك طريق باتجاه يتناسب مع حجم الميزانية المحددة . عليه يمكن ان تكون المدة بين التصميم والانشاء كبيرة جدا بالاضافة الى الوقت الحقيقي للانشاء نفسه . ولما كانت عقود التضخم لاوجود لاستخدامها في العراق فان على المقاول ان يعتبر تصاعد الكلفة المتضخم خلال فترة الانشاء مجازفة غير قابلة للتنبؤ يجب ان تنعكس على عطاءه (AL –Sedairy. , 1985)

ان اطالة مدة المشروع وتقلبات السوق وتاثير ذلك على الاسعار دفع المهندسون باتجاه تطوير اساليب التنفيذ والعمل على اتباع اساليب ادارية جديدة فكانت الادارة الانشائية والتنفيذ المتسارع حلول جيدة لتلك المشكلات من خلال تداخل الفعاليات والانشطة واختزال زمن المشروع .

* اسلوب التنفيذ المتسارع : (Fast Track)

ويسمى طريقة التداخل المرحلي او طريقة التصميم والتنفيذ المتوازي Phased Design /Construction (Merritt,1975) . يعرف اسلوب التنفيذ المتسارع بانه القدرة على البدء بالتنفيذ رغم استمرارية العمل بالتصميم وفور انتهاء التصاميم الاولية للمرافق حيث تتعاقب المهام والفعاليات والأعمال وتتراكب لاختصار زمن المشروع , وهو احد اساليب التنفيذ التي توفر الوقت لصاحب العمل من خلال التداخل بين عمليات التصميم والتنفيذ .

ان الاداة القانونية التي يتم التنفيذ فيها على هذا النحو هي وجود مدير انشاء يساعد على ترسية عدد من العقود بصورة مستقلة ومنفصلة تكون علاقتها مباشرة مع صاحب العمل (Ferry,1974) . ان التنفيذ المتسارع لايعطي صورة كاملة عن تكاليف المشروع لان اعمال التصميم تتتابع وتستمر مع التنفيذ بينما يحتفظ التصميم والانشاء بالوقت الحقيقي لكل منهما, ولكن المدة الكلية لتنفيذ المشروع يتم اختصارها نتيجة البدء بالتنفيذ قبل انتهاء التصميم الكلي (غولدهابر ,1982) .

يعتبر أسلوب التنفيذ المتسارع احد المنافع الاساسية لاسلوب الإدارة الإنشائية التي تجعل منه اسلوبا مفيدا وعمليا من اجل توفير الوقت وهو احد ثمارها . فالادارة الانشائية يتم الحاجة اليها في جميع المشاريع بينما التنفيذ المتسارع له متطلباته ويطبق في مشاريع محددة(Turner ,1989) اذا ما اردنا تطبيق الجدوى الاقتصادية للمشروع .

يتطلب نجاح تطبيق اسلوب التنفيذ المتسارع تقسيم المشروع الى مجموعة من المراحل والاجزاء والمقاولات مع زيادة حجم التنسيق والترابط في تنفيذ تلك المقاولات والتعامل معها كوحدة متكاملة . بالاضافة الى وجود مقاول ذو تجربة وخبرة في التنفيذ والتخطيط يشارك فريق ادارة مشروع قادر على جدولة العمل بالطريقة التي تضمن جودة الاداء على وفق الزمن والسعر المتفق عليه (AL–Sedairy, 1985) وتفهم كامل لعملية الإنشاء

المتوازية مع التصميم وتداخلاتها التي تتطلب تغذية عكسيةّ وسيطرة كلفة للمحافظة على ميزانية المشروع المقرة (Merritt,1975) بعد تجزئتها على العقود المتعددة . ان توفير الصلاحيات يعتبر احد اهم ادوات نجاح تطبيق اسلوب التنفيذ المتسارع (العجيلي, 2004)

يمتاز هذا الاسلوب بتشابك نشاطات التصميم والتنفيذ بطريقة مدروسة ومبرمجة مع استمرار عملية التنفيذ تحت رقابة شديدة , بالاضافة الى السماح بالبدء المبكر لتنفيذ المشروع في بعض اجزائه في نفس الوقت الذي يتم فيه استمرار التصميم لبقية الاقسام , والغاء دور المقاول العام لتصبح العلاقات مباشرة بين صاحب العمل والمقاولين المتعددين بعد ترسية عقود مختلفة عديدة (McNulty, 1982)

اما اهم الفوائد المتحققة من اتباع هذا المنهج تتمثل في تقليل الفترة الزمنية الكلية لانجاز المشروع (Fisk , 1982) مما يعني اختصار الكلفة وتخفيض حجم المجازفة على المقاولين لتقارب الاحالة من وقت التنفيذ وتقليل وتحجيم اثار التاخير الناجم في احد المراحل وعدم نقله الى المراحل الاخرى في التنفيذ وفسح المجال لعدد كبير من المقاولين وزيادة التنافس وتخفيض تأثير تضخم الكلفة (Merritt,1975)

إلا ان الاسلوب لايخلو من بعض العيوب التي تنحصر في عدم امتلاك صاحب العمل فكرة واضحة عن كلفة المشروع الكلية, بالاضافة الى الحاجة لادارة فريق حقلي كبير وزيادة حجم التنسيق بين المقاولين المتعددين (Fisk , 1982) وتحمل صاحب العمل لمجازفة كلفة اعلى من اسلوب التنفيذ التقليدي . كما يجب الانتباه الى تعرض المصمم لضغط كبير لاجل تسليم المشروع في اقل وقت (AL –Sedairy, 1985)

ان الصيغة التعاقدية الملائمة لتطبيق اسلوب التنفيذ المتسارع هي صيغة تسليم المفتاح او تعاقدات ادارة الانشاء لامكانية هذه الصيغ التعامل مع خواص الاسلوب **(Groton,1998)**

وفي الواقع لايوجد مشروع لايمكن اتباع هذا المنهج فيه ولكن الجدوى الاقتصادية والفنية تكون اكثر تحقيقا في المشاريع الكبيرة والمتعددة الابنية او الاقسام مثل المجمعات وفي المشاريع المتكررة والابنية العالية متعددة الطوابق والتي يمكن تشغيلها على مراحل مختلفة . (Turner ,1989) .

* العوامل المؤثرة على زمن التنفيذ :

تتعرض برمجة المشاريع للعديد من الاخفاقات الزمنية لاسباب عدة مثل سوء الادارة او ظهور قوة قاهرة او ظهور ظروف خارجية غير متوقعة تمنع المقاول تنفيذ احكام التعهد بصورة مطلقة او ظهور ظروف استثنائية جعلت التنفيذ مرهقا للمقاول (جعلوك ,1999)

يعتمد اختزال الزمن المطلوب في المشاريع المنفذة باسلوب التنفيذ المتسارع على عدة عوامل تختلف من مشروع لاخر مثل طبيعة التصميم وحجم الفعالية ونوعها وطبيعتها والامكانيات الاقتصادية المتوفرة والظروف المناخية المصاحبة لفترة التنفيذ وامكانية الالتزام بالبرمجة الزمنية ومدى توفر الخبرة للمنفذين والمشرفين ومدى احتمالية ظهور المشاكل . (العجيلي ,2004) . لذا تتوجب دراسة العوامل التي تساعد على تقليل مدة التنفيذ لامكانية

الاستفادة منها في تحقيق اهداف اسلوب التنفيذ المتسارع الاساسية ويمكن معالجة هذه العوامل من خلال التطوير باتجاهين هما : (العزي . 1992)

1- العوامل العامة التي تتعلق بدراسة ظروف التعاقد ومنها تطوير وتوفير وثائق وتصاميم المشروع وتحديد اسلوب التمويل المناسب وتهيئة موقع العمل والمواد الاولية وبقية الموارد المطلوبة

2- العوامل الخاصة المتعلقة بظروف التنفيذ المتمثلة بتهيئة القيادات الهندسية الموقعية ورفع الروح المعنوية للعاملين وتواجد الاستشاريين والقيادات العليا للعمليات التنفيذية في موقع العمل ومنح المكافئات والمحفزات المادية وايجاد البدائل الملائمة واعتماد مبدا المنافسة واستمرار الاشراف الهندسي والمتابعة طيلة زمن التنفيذ وصيانة واصلاح الاجهزة والمعدات ومضاعفة ساعات العمل

* الاجراءات للتخطيط السليم للتنفيذ المتسارع :

ان التخطيط السليم للمشروع هو مفتاح النجاح في تطبيق اسلوب التنفيذ المتسارع , وتكمن تفاصيل التخطيط السليم في القدرة على تحديد النظم الرئيسة والثانوية بحيث يرتبط كل منهما بالاخر وترتبط كلها بالاطار العام للمشروع , وهو مايعرف بهيكلية تجزئة المشروع التي يتم الحاجة اليها في تجزئة مراحل المشروع الى مراحل ثانوية ومجاميع صغيرة للسيطرة عليها , يتم احالتها إلى مقاولين متخصصين حال الانتهاء من تصميمها بعد استيفائها لإجراءات التعاقد المعمول بها كالإعلان عنها ودراسة العروض وتحليلها واختيارالعرض الأفضل وتكوين علاقة تعاقدية مباشرة بين المقاول وصاحب العمل .

تتطلب مشاريع التنفيذ المتسارع مدير انشاء يعمل دورا نشيطا في مراقبة ودعم جهد تطور التصميم , فحالما يبدا النشاط التنفيذي في الحقل تصبح عملية البرمجة واعداد الجدول الزمني مستعجلا جدا وملحا , ويجب ان يكون تسلسل توفير وثائق التصميم متتالية ليتجنب التأثير الكبير على تاخير وعرقلة نشاطات الحقل التنفيذية وليلغي أسلوب التتابع الذي تعتمد عليه كلفة المشروع الكفوء . (McNulty, 1982)

يتطلب التغيير الرئيسي في الإجراءات لمشاريع التنفيذ المتسارع زيادة الإنتباه إلى السيطرة المنظمة على الكلفة والوقت , كما يجب أن يحدد الجدول الزمني الأوقات المطلوبة للبرنامج وقرارات التصميم وتسليم الوثائق وهذه التواريخ يجب أن تكون متفق عليها . (McNulty, 1982)

معايير تطبيق اسلوب التنفيذ المتسارع :

يمكن استخدام معايير تطبيق اسلوب التنفيذ المتسارع لمعرفة مدى كفاءة وصحة تسمية الأسلوب المنفذ بالاسلوب المتسارع وهي (العجيلي ,2004) :

- القدرة على البدء بالتنفيذ رغم استمرارية العمل بالتصميم مع توفير الوقت لصاحب العمل عن طريق التداخل بين عمليات التصميم والتنفيذ .
- تداخل وتشابك نشاطات مرحلتي التصميم والتنفيذ بطريقة مدروسة ومبرمجة وبمستويات مختلفة.
- إنهاء بعض العناصر من عملية التصميم مبكرا لأعتماد العناصر المتاخرة من التّصميم عليها .

- ترسية عدد من العقود بصورة مستقلة بدلا من عقد واحد مع مقاول عام على ان تكون العقود المحالة كاملة الوثائق , وهذا يعني ان تقسيم العقود والمراحل يجب ان يعتمد على الاسبقية في التصميم والفعاليات الحرجة, ويجب ان تعرف الوثائق الشروط والمسؤوليات القانونية لكل مجموعة عقدية بوضوح .
- إلغاء دور المقاول العام وصنع علاقات مباشرة بين صاحب العمل والمقاولين المتعددين المختصين
- تتحرّك كل وسيلة في اسلوب التنفيذ المتسارع اسوة بالعملية التقليدية مرحلة مرحلة خلال كل عقد (البرمجة والتصميم واعداد وثائق العقد واستدراج العروض وتحليلها وترسيتها وتنفيذها الى قبول العمل)
- وجود فريق كفوء لإدارة المشروع لضمان برمجة العمل والاداء في الوقت المطلوب على وفق سعر العطاء المحدد
- تلائم عقود تسليم المفتاح أو عقد الإنشاء–التصميم أو تعاقدات إدارة الإنشاء او عقد الكلفة زائدا اسلوب التنفيذ المتسارع لامكانية هذه الصيغ التعامل مع مسؤوليات الاسلوب بواسطة مدير الإنشاء
- تزويد قاعدة صحيحة للتصميم قبل بداية الرسوم التفصيلية مع دليل كلفة . ان الاحالة والبداية المبكرة للأسس والانشاء بدون مثل هذه القاعدة والتزام الميزانية يمكن أن يقود إلى الحالة التي تتجاوز فيها الكلفة النهائية حيث يكون تأثيرها خطيرا على الميزانية الكليّة في وقت ما

* التنفيذ المتسارع والادارة الانشائية :

لمعرفة الفرق بين التنفيذ المتسارع والادارة الانشائية يجب ان نعرف ان ألاساليب التي تعتمد التعاقد لتنفيذ العمل هي : (العجيلي ,2004)

أ. تنفيذ العقد عن طريق المناقصات واختيار المقاول المنفرد (المقاول العام)

ب. التعاقد على اساس تسليم المفتاح أي التصميم والتنفيذ واحيانا التجهيز ايضا .

ت. اعتماد اسلوب الادارة الانشائية لتنفيذ المشروع ويتم على اساس المقاول العام او تعدد المقاولين حيث يستعان بمدير للمشروع يجري التعاقد معه بعقد اداري ليمثل صاحب العمل ويقوم بتنسيق الاعمال .

ث. اعتماد اسلوب التنفيذ المتسارع وهو احد ثمار الادارة الانشائية ونظام تعدد المقاولات مع امكانية التعاقد على اساس تصميم المشروع وتنفيذه او تنفيذه فقط, وتكون مسؤولية صاحب العمل التنسيق بين المصمم والمقاول للسيطرة على النوعية والوقت والميزانية.

* الاستبيان الميداني

تعتبر عملية المسح الميداني تسجيلا للوضع السائد لنظام معين لغرض التحليل والاستنتاج ضمن الوقت المحدد لغرض الحصول على معلومات كافية بهدف استنتاج قواعد تصلح للتطبيق في الأعمال المقبلة. ولغرض تقويم واقع العوامل المؤثرة على تطبيق اسلوب التنفيذ المتسارع المباشرة وغير المباشرة وأهميتها تم اللجوء إلى الاستبيان الميداني كوسيلة لإنجاز ذلك, وقد تم المسح الميداني لعينة مختارة كمصدر للمعلومات المطلوبة بعد تحديد حجم العينة ومواصفاتها. وقد بين الجدول (1) مواصفات أفراد العينة المنتخبة للبحث .

تمثل استمارة الاستبيان الميداني وسيلة لجمع المعلومات والحقائق من العينة بطريقة مجدولة ونظامية , وقد تم إعداد وتنظيم نموذج الاستمارة على وفق مدار الاستبيان المفتوح ومدار الاستبيان المغلق وعلى وفق محاور مختلفة تمثل كل ما يحتاجه البحث من بيانات وقد استوجبت عملية جمع وتحليل البيانات وجود معلومات شخصية عن أفراد العينة لتقويم إجابات أفراد العينة بموجبها . تم توزيع استمارات الاستبيان على جميع أفراد العينة المنتخبين بعناية والبالغ عددهم (50) فردا وقد تم اعتماد (38) استمارة من الاستمارات المستلمة بعد اهمال بعضها لعدم اكتمال اجاباتها وهو عدد مستوف لدقة الاستبيان بموجب نظرية النهاية المركزية , حيث يقترب توزيع العينة من التوزيع الطبيعي اذا كان حجم العينة اكبر او مساوي الى (30) , ويمكن تدقيق ذلك على وفق المواصفة (ASTM-E122-79) حيث تؤشر اعتماد حجم العينة على نوع التوزيع ومستوى الثقة المطلوبة .

جدول (1) المعلومات والبيانات الشخصية لافراد العينة

ت	اسم الدائرة	التحصيل العلمي		عدد سنوات الخدمة	المشاركة في التنفيذ المتسارع	الدور الحالي في فريق الانشاء						
		الشهادة	التخصص			مدير دائرة	مدير مشروع	رئيس قسم	مهندس مقيم	مهندس تخطيط	مهندس موقع	استشاري
1	جامعة بغداد /	ماجستير	مدني	35	*							*
2		ماجستير	ميكانيك	20	*	*						
3		ماجستير	مدني	35	*							*
4	الشؤون الهندسية	ماجستير	مدني	30	*							*
5		بكالوريوس	مدني	18	*				*			
6		بكالوريوس	مدني	38	*							*
7		بكالوريوس	معماري	29	*			*				
8		ماجستير	مدني	19								*
9	***وزارة الاسكان***	ماجستير	مدني	24	*			*				
10	المركز الوطني	ماجستير	مدني	23	*			*				
11	للاستشارات الهندسية	بكالوريوس	مدني	26	*							*
12		دبلوم عالي	مدني	20	*							*
13		بكالوريوس	معماري	29	*			*				
14		ماجستير	مدني	22								*
15		بكالوريوس	مدني	19	*							*
16	شركة المعتصم	ماجستير	مدني	25	*		*					
17	للمقاولات	دبلوم عالي	مدني	33	*		*					
18		بكالوريوس	مدني	31	*						*	
19		بكالوريوس	مدني	27	*						*	
20	شركة الرشيد	بكالوريوس	مدني	26	*			*				
21	للمقاولات	ماجستير	مدني	18	*		*					
22		بكالوريوس	مدني	21	*		*					
23	شركة رمضان	ماجستير	مدني	26	*		*					
24	شركة المنصور	بكالوريوس	مدني	28	*		*					

25	شركة اشور	ماجستير	مدني	25	*		*						
26	هيئة التصنيع الملغاة	ماجستير	مدني	32	*	*							
27		ماجستير	مدني	23	*		*						
28		بكالوريوس	مدني	24	*							*	
29		ماجستير	مدني	32	*		*						
30		دكتوراة	مدني	26	*				*				
31		بكالوريوس	مدني	22	*		*						
32	شركة الفاو الهندسية	ماجستير	مدني	22	*				*				
33		ماجستير	مدني	22	*		*						
34		بكالوريوس	مدني	19	*		*						
35		بكالوريوس	معماري	22	*				*				
36		دكتوراة	مدني	30	*								*
37	قطاع خاص	ماجستير	مدني	31	*								*
38		ماجستير	مدني	34	*								*

* محور اساليب التنفيذ والتنفيذ المتسارع :

وهو محور يتضمن الأسئلة الاستبيانية التي تهدف إلى تقويم اساليب التنفيذ ومجموعة العوامل المؤثرة على مدة التنفيذ والوسائل والاساليب التي تسيطر عليها والأسباب التي تعيق انتشار تطبيق اسلوب التنفيذ المتسارع بصورة مباشرة او غير مباشرة على وفق المعايير الموحدة المستخدمة في تحليلها . تتم الإجابة بموجب خمس درجات تقويمية هي (ضعيف ومتوسط وجيد وجيد جدا وممتاز) . ومن اجل الإبقاء على معيار موحد للمقارنة والقياس ولتحويل تلك المعلومات والدرجات التقويمية إلى أرقام يمكن التعامل معها تم اعتماد معايير رقمية لدرجات الأهمية فاعتبرت درجة (ضعيف) هي البداية وتعادل قيمة وزنية (1) وتغطي الفترة من (صفر) إلى (< 2) تتبعها بقية الدرجات التقويمية وكما موضحة في الجدول (2) .

الجدول (2) القيم الوزنية لدرجات الأهمية الواردة في إجابات العينة

ت	درجة التقويم في إجابات أفراد العينة	المجال أو (الفترة)	مركز المجال أو (القيمة الوزنية)
1	ضعيف	0 – < 2	1
2	متوسط	2 – < 4	3
3	جيد	4 – < 6	5
4	جيد جدا	6 – < 8	7
5	ممتاز	8 – < 10	9

وقد لوحظ اثناء عملية تحليل إجابات أفراد العينة للأساليب المبينة إن (65,8%) من حجم العينة قد منح اسلوب المقاول العام تقويم ممتاز ليحصل على معدل تكراري (7,89) يعادل تقويم (جيد جدا) . بينما حصل اسلوب

الإدارة الإنشائية على معدل تكراري (5,21) يعادل تقويم (جيد) وحصل اسلوب التنفيذ المتسارع على التقويم الثالث بمعدل تكراري (5,05) وهو يعادل تقويم (جيد) بعد أن منحه (26,3%) من العينة تقدير جيد و(23,7%) تقدير جيد جدا وفقط (15,8%) تقدير ممتاز وهو اكثر الأساليب التي تم الاختلاف في تقويمها لاسباب كثيرة منها عدم المعرفة التامة لأفراد العينة بأسس ومعايير تطبيق الاسلوب بصورة علمية صحيحة مع عدم التعود عليه وقلة استخدامه, وحصل اسلوب التصميم والإنشاء على التقويم الرابع بمعدل تكراري (4,82) يعادل تقويم (جيد) وكما موضح في الجدول (3) . مما يتضح إن اسلوب المقاول العام التقليدي قد حاز على الأغلبية ولكن موقع اسلوب التنفيذ المتسارع يعتبر جيدا إذا ماعرفنا حداثة الاسلوب وظهور العديد من المشكلات لدى الجهات الممارسة للأسلوب لأول مرة وعدم وجود جهات فنية ذات خبرة واسعة في مجال استخدام الاسلوب تعتبر كمرجع للجهات الراغبة في استخدامه .

جدول (3) تقويم اسلوب التنفيذ

ت	اسلوب التنفيذ	عدد الإجابات التكرارية بموجب درجات الأهمية مع النسب المئوية لمعدل تكرار الإجابات										% لمعدل تكرار الإجابات	التقويم
		ضعيف		متوسط		جيد		جيد جدا		ممتاز			
		العدد	%	العدد	%	العد	%	العدد	%	العدد	%		
1	المقاول العام	صفر	صفر	2	5,3	4	10,5	7	18,4	25	65,8	7,89	جيد جدا
2	الإدارة الإنشائية	1	2,6	8	21	15	39,5	14	36,9	صفر	صفر	5,21	جيد
3	التصميم والإنشاء	6	15,8	8	21	17	44,7	2	5,3	5	13,2	4,58	جيد
4	التنفيذ المتسارع	7	18,4	6	15,8	10	26,3	9	23,7	6	15,8	5,05	جيد

لتحديد حجم تأثير تلك العوامل المهمة في بناء النظام المقترح (حسب رأي العينة) فقد تم استخراج الوزن المعياري لها , وقد اعتمد التقويم (جيد جدا) كحد أدنى للقبول , واعتبرت العوامل المؤثرة ذات المعدل التكراري اقل من (6) غير مهمة في بناء النظام حسب رأي العينة .

- **العوامل المؤثرة في اختيار اسلوب التنفيذ :**

ت	العوامل المؤثرة في اختيار أسلوب التنفيذ المناسب	الوزن المعياري	الأهمية
1	مدى توفر وثائق التعهد من تصاميم هندسية وجداول كميات ومواصفات فنية	19,94	مهم
2	الخبرة المتوفرة لدى المقاول للأعمال المشابهة	16,8	مهم
3	مدى توفر الكوادر الهندسية والفنية والتنفيذية لدى صاحب العمل	16,19	مهم
4	مدى توفر الموارد من مواد وعمالة ومعدات لتنفيذ العمل وتخصصها وقربها من موقع العمل	16,11	مهم
5	حجم المشروع الهندسي وعدد الأبنية وحجم الأعمال المراد إحالتها بعهدة مقاولين ثانويين .	15,58	مهم
6	طبيعة المشروع وموقعه وعلاقته بالأبنية المجاورة مع تحديدات موقع العمل	15,38	مهم
7	درجة التعقيد في التصاميم الهندسية وشكل الابنية .		

8	مدى توفر المساحات المطلوبة لخزن المواد ونصب المعدات اللازمة للتشييد		
	مجموع الأوزان المعيارية للعوامل	100	

♦ الأسباب التي تعيق انتشار تطبيق اسلوب التنفيذ المتسارع :

ت	الأسباب	الوزن المعياري	الأهمية
1	احتمالية تحمل صاحب العمل لمجازفة عالية في الكلفة	22,21	مهم
2	عدم توفر الخبرة المطلوبة في فعاليات تنسيق الأعمال	20,73	مهم
3	تطلب تحمل صاحب العمل مسؤولية إدارية كبيرة	20,33	مهم
4	عدم وجود صلاحيات واسعة للإدارة للتعاقد مع مقاولين متخصصين متعددين	18,51	مهم
5	الإجراءات الروتينية السائدة	18,22	مهم
6	عدم وجود مقاولين ومعماريين ذوي خبرة في هذا الاسلوب		
7	عدم إمكانية تأسيس ميزانية واقعية حيث تبقى الكلفة مفتوحة النهايات		
8	اعتماد مبدأ الغرامات ألتاخيرية		
9	قلة المنفعة المالية المباشرة		
	مجموع الأوزان المعيارية للأسباب	100	

♦ الوسائل والأساليب التي تسيطر على مدة التنفيذ وتساعد على تقليص الفترة الزمنية :

ت	الوسائل والاساليب	الوزن المعياري	الأهمية
1	توفير إشراف هندسي موقعي واستشاري عالي وتوفير المتابعة في تحليل الانحرافات ومعالجتها	6,95	مهم
2	استخدام قيادات هندسية كفوءة في الموقع والمكتب الرئيس	6,63	مهم
3	توفير الخبرة والكفاءة لدى الكوادر الهندسية لجعل التصاميم اكثر انسيابية	6,5	مهم
4	توفير الكوادر الفنية المتخصصة الماهرة وغير الماهرة لإنجاز بعض الفقرات الخاصة في الوقت المحدد	6,37	مهم
5	توفير المخططات ووثائق التعهد في الوقت المطلوب	6,37	مهم
6	توفير المواد الأولية وفق الجدول الزمني المتفق عليه	6,16	مهم
7	تقليص حجم التغييرات في المخططات وتنفيذ الأعمال	6,15	مهم
8	فهم المشروع وإفهامه إلى المنفذين وعدم تعقيد التصاميم	6,14	مهم
9	رفع الروح المعنوية للعاملين من خلال منح الحوافز والمكافئات التشجيعية	6,11	مهم
10	منع الاختناقات والانقطاعات في العمل والالتزام بالجدول الزمني	5,89	مهم
11	التنسيق بين المقاولين والعمل على تداخل أعمالهم بدون التقاطع بينهم	5,83	مهم
12	تسهيل اسلوب التسديدات المالية وتوفير سيولة نقدية كافية	5,55	مهم
13	إيجاد البدائل لبعض الفقرات الإنشائية بسرعة	5,31	مهم
14	رفع الغموض والاختلاف عن الوثائق والمخططات	5,12	مهم
15	اعتماد مبدأ المنافسة بين القطاعات والمراحل	4,98	مهم

16	السيطرة على أعمال المقاولين الثانويين	4,97	مهم
17	مضاعفة ساعات العمل	4,97	مهم
18	اعتماد مبدأ الغرامات ألتاخيرية		
19	صيانة الأجهزة والمعدات وإصلاحها بسرعة		
20	السيطرة على الظروف الجوية من خلال تنسيق العمل في داخل وخارج المنشأ		
	مجموع الأوزان المعيارية للوسائل والأسباب	100	

* بناء النظام الإداري المقترح وتقويمه :

من خلال التحليل الدقيق للمحاولات النظمية المستخدمة في اختيار اسلوب التنفيذ المتسارع للمشاريع الانشائية , يمكن تحديد أهم المميزات لتلك المحاولات بالنقاط التالية :

- الاعتماد على الخبرة الشخصية لفريق الإنشاء بصورة رئيسة.
- كانت الرغبة في البدء المبكر بالتنفيذ من أهم العوامل المؤثرة في اختيار اسلوب التنفيذ المتسارع.
- كان لعدم توفر الوثائق اكبر تأثير في اختيار اسلوب التنفيذ .

اما اهم العيوب او نقاط الضعف المترافقة مع تلك المحاولات فهي :

- عدم الاستفادة من خبرة مقاولي القطاع الخاص في المقاولات الرئيسة .
- استخدام الإدارة الإنشائية لادارة المشاريع من خلال موظفين حكوميين يفتقرون إلى الخبرة والصلاحيات
- انخفاض مستوى التخطيط المستخدم .
- ضعف عملية التوثيق في المشاريع الإنشائية مما يضعف عملية التغذية العكسية للمعلومات .
- عدم وجود ضوابط معتمدة لاستخدام اسلوب التنفيذ المتسارع في المشاريع .

* إقتراح نظام إداري لقواعد اختيار أسلوب التنفيذ المتسارع في مشاريع قطاع التشييد :

يستند النظام المقترح بنائه لقواعد اختيار اسلوب التنفيذ المتسارع إلى واقع الحال بسبب الحاجة إلى ظهور هكذا نظام علمي واداري وعدم الاعتماد على الاراء الشخصية البحتة في اختيار اسلوب التنفيذ .

تنحصر المواصفات المؤمل أن يتمتع بها النظام المقترح والتي تضمن نجاحه في نوعين هما :

* **المواصفات العامة** : التي يجب أن يتمتع بها أي نظام مقترح وهي : (البياتي , 1992)

أ- التكامل : ويعني التنسيق بين الأنظمة الفرعية لغرض تحقيق الوحدة والترابط بينها .

ب- الاسلوب العلمي : ويعني استخدام الأساليب العلمية عند إنجاز هذه النظم بشكل كامل ومعقد .

ت- التكنولوجيا : ويعني استخدام التقنية الحديثة للمساعدة في تنفيذ النظام كالحاسوب .

***المواصفات الخاصة** : التي يجب ان يتمتع بها النظام المقترح بالذات وهي :

أ- تحقيق افضل فائدة مادية إلى صاحب العمل من خلال الاسلوب الأمثل لاختيار أسلوب التنفيذ المناسب

ب-إمكانية اختصار وقت العملية الإنشائية للمشروع إلى اقل وقت ممكن ابتداء من الفكرة

ت–توفير المرونة الكافية لصاحب العمل لاتخاذ القرارات المناسبة وفق التغييرات والمستجدات المستقبلية

ث–تحقيق الثقة بالنظام المقترح من خلال الدقة المطلوبة لعملية التنفيذ

* متطلبات استخدام النظام المقترح :

يعتمد نجاح أي نظام على ضرورة استحضار وتهيئة متطلباته في الوقت المناسب , وعليه يستوجب معرفة المتطلبات التي يحتاجها النظام الإداري المقترح في تطبيقه لكي يحقق مبتغاه , ويمكن أن نحدد المتطلبات التالية كضرورة فعلية لتطبيق النظام من خلال تحليل النظام المقترح :

- أن يكون المشروع كبيرا أو معقدا .
- تهيئة إدارة إنشائية للمشروع من داخل الهيكل التنظيمي لصاحب العمل أو من خارج تنظيمه .
- إعداد دراسة لجميع العوامل المؤثرة في تحديد الفترة الزمنية للتنفيذ أو المسببة لتأخير العمل في المشروع وإعداد وتهيئة وسائل اختزالها , وتهيئة درجة الأهمية النسبية لكل عامل من تلك العوامل .
- إعداد ودراسة الوسائل والأساليب التي تسيطر على مدة التنفيذ في المشاريع الانشائية وتساعد على تقليص الفترة الزمنية والتي يمكن استخدامها .
- دراسة العوامل المؤثرة في تحديد اسلوب التنفيذ , وتهيئة درجة الأهمية النسبية لتلك العوامل .
- معرفة العوامل المؤثرة على استخدام النظام المقترح من قبل مستخدم النظام .

* صياغة هيكلية النظام المقترح :

* المرحلة الأولى : تعريف المشكلة

يتم في هذه المرحلة تعريف وتحديد المشكلة قيد الدراسة ووضع صياغة واضحة ومحددة لابعادها ونطاقها , والتي تمحورت حول عدم وجود نظام اداري لقواعد اختيار أسلوب التنفيذ المتسارع الذي شاع استعماله أخيرا في القطاع العام في العراق لملائمته للمشاريع الكبيرة والمعقدة ولعدم استقرار السوق

* المرحلة الثانية : دراسة العوامل المؤثرة على العناصر الأساسية لأسلوب التنفيذ المتسارع

وفي هذه المرحلة يتم مايلي :

- تحديد العناصر الأساسية المكونة لفعالية تطبيق اسلوب التنفيذ المتسارع والمؤثرة عليها وهي العوامل المؤثرة في اختيار اسلوب التنفيذ الملائم للمشروع وسبب اللجوء إلى أسلوب التنفيذ المتسارع والاسباب المعيقة لانتشار تطبيق الاسلوب

- دراسة جميع المعايير والعوامل المؤثرة على تلك العناصر الأساسية كل على انفراد من اجل الوصول إلى جمع المعلومات الخاصة وتحديد الأهمية النسبية لتلك العوامل من خلال الدراسات والأبحاث النظرية والدراسة الميدانية لإعادة ترتيب تلك العوامل على وفق أهميتها وتأثيرها لتحديد :
  - معايير اختيار أسلوب التنفيذ .
  - معايير اختيار اسلوب التنفيذ المتسارع .
- حساب الوزن المعياري لتأثير كل عامل من هذه العوامل على حدة بعد استخدام معيار موحد لدرجات الأهمية حيث تم استخدام خمس درجات تقويمية هي (ضعيف ومقبول وجيد وجيد جدا وممتاز) وتوضح الجداول في هذه المرحلة الأهمية النسبية للعوامل ووزنها المعياري بعد تحويل تلك المعلومات والدرجات التقويمية إلى أرقام يمكن التعامل معها وفق معيار موحد للمقارنة .

* تحديد العوامل المؤثرة في اختيار اسلوب التنفيذ :

وقد تم جمع المعلومات الخاصة بالعوامل المؤثرة على اختيار أسلوب التنفيذ المناسب ومتطلبات ومعايير تطبيق أسلوب التنفيذ المتسارع والاسباب التي تعيق انتشار اسلوب التنفيذ المتسارع من خلال الدراسة النظرية والاستبيان الميداني حولها واعادة ترتيبها على وفق أهميتها وتأثيرها في ضوء الخبرة والواقع العملي وكما وردت في الفقرة (6−1)

أما متطلبات استخدام اسلوب التنفيذ المتسارع التي تم التوصل إليها فهي :

1) ضرورة إعداد الدراسات الأولية ودراسات الجدوى الفنية والمالية والاقتصادية لكل المشروع موحدة .
2) إجراء تخمين كلفة دقيق للحفاظ على ميزانية المشروع .
3) فهم كامل وشامل لتفاصيل عملية الإنشاء المتوازية للمشروع المتكامل .
4) تجزئة المشروع إلى مجموعة من المراحل والاجزاء والعناصر ألاساسية .
5) توفير الخبرة لدى صاحب العمل والاستشاري في مجال تجزئة الميزانية الكلية على العقود المتعددة والقيام بأعمال التصميم للمجاميع المتعددة والمساعدة في توفير برنامج سيطرة كلفة لبرنامج التصميم والإنشاء المتداخل بشكل فعّال من اجل المحافظة على ميزانية المشروع المقرة.
6) وجود فريق إدارة للمشروع محترف ومتمكن فنيا واداريا وقوي وقادر على برمجة العمل بصورة ممتازة بالتنسيق مع المقاولين المتعددين بالطريقة التي تضمن جودة الاداء على وفق الزمن والسعر المتفق عليه, وتهتم بتنسيق عمليات الإنشاء المختلفة للمجاميع المختلفة مع التغذية العكسية
7) توفير الصلاحيات لفريق ادارة المشروع والتي تعتبر أحد أهم أدوات نجاح تطبيق الاسلوب
8) زيادة حجم التنسيق والترابط في تنفيذ تلك المقاولات والتعامل معها كوحدة متكاملة

وقد تم تحديد معايير تطبيق اسلوب التنفيذ المتسارع كما ورد في الفقرة (5) .

* تحديد العوامل المؤثرة على المدة الزمنية للمشروع :

لما كان الهدف الأساسي لأسلوب التنفيذ المتسارع هو السيطرة الزمنية واختزال وتقليص مدة تنفيذ المشروع الكلية وتبيان انه الاسلوب التنفيذي الأسرع أو الأكثر اقتصادا بناءا على متطلبات المقاولة عليه يتوجب دراسة العوامل المؤثرة على المدة الزمنية لغرض التعامل معها بإيجابية في محاولة تحقيق الهدف الرئيسي لأسلوب التنفيذ , ولذلك يتوجب تبيان مايلي :

1) الاحتياجات من المواد الإنشائية وتواريخ استلامها .
2) مستوى استخدام الأيدي العاملة والمعدات والمكائن وأوقاتها .
3) تواريخ الحاجة إلى استخدام المقاولين الثانويين .
4) توفير طريقة سريعة لحساب الكلف والمصاريف المرافقة لتنفيذ فقرات المقاولة الإنشائية .

نظرا لوجود العديد من العوامل المؤثرة على عملية تخمين زمن التنفيذ الذي يعتبر العنصر المهم الذي يعمل على اختزاله, عليه يجب دراسة أهم المتطلبات لانجاح عملية تخمين المدة الزمنية والتي يجب تجهيزها قبل البدء بالمشروع أو خلاله بحيث لا تؤثر برمجتها على وقت إنجاز الفقرات المختلفة ولاتعرقل تنفيذها وهي :

أ- تقسيم المشروع إلى مراحل يكمل بعضها بعضا في حالة كبر حجمه , وتقسيم العمل في مراحل المشروع إلى مجاميع وقطاعات واجزاء محددة يتم إقرارها بناءا على الموقع أو الوظيفة أو الحاجة الآنية أو المهنة

ب-تجهيز جميع الوثائق لتلك المجاميع والأجزاء التي تم إقرارها بشكل واضح ومفهوم في وقت مناسب قبل المباشرة بالعمل لكل جزء أو مرحلة , وبرمجة تقديمها بحيث لا تؤثر على سرعة إنجاز العمل أو نوعيته أو التداخل مع بقية الأجزاء والمجاميع والمقاولين في حالة المباشرة بالتنفيذ قبل إكمال الوثائق .

ت-إعداد جدول زمني لتامين موارد المشروع الأساسية من الأيدي العاملة بالعدد والنوعية والموعد المحدد

ث-وضع جدول زمني لتوفير المكائن والمعدات والأجهزة المطلوبة في عملية تنفيذ المشروع الثابتة والمتحركة مع الأثاث والمدة اللازمة لبقائها في الموقع .

ج-وضع برنامج زمني لتوريد المواد الأولية وخزنها قبل المباشرة بالعمل , ومعرفة المواد المطلوبة ومصادرها ومدى قربها من موقع المشروع أو استيرادها من خارج القطر مسبقا .

ح-إعداد برنامج السيولة النقدية المطلوبة لتمويل المشروع .

خ-إعداد مخطط موقع العمل قبل المباشرة وتبيان مواقع الأبنية والمنشات الدائمية والمؤقتة الإدارية والخدمات والمخازن ومسارات نقل المواد وحركة العاملين .

د- تامين الحد الأدنى من وسائل الاتصالات بين موقع العمل والمستويات الإدارية المختلفة .

ذ- تنظيف الموقع من المعوقات الطبيعية والاصطناعية قبل المباشرة بالعمل , أو الاستمرار في عملية الإخلاء للموقع من الشواغل والمعوقات بحيث لا تؤثر برمجتها على برمجة العمل .

ر-تامين الخدمات الضرورية الدائمية والوقتية للعاملين في المشروع لجعل العمل في المشروع سهلا.

* المرحلة الثالثة : مرحلة حساب درجة الأهمية النسبية للعوامل المؤثرة :

بعد تحديد العوامل المؤثرة في تطبيق اسلوب التنفيذ المتسارع من خلال الدراسة النظرية والميدانية وكما ورد في المرحلة الثانية, يتم في هذه المرحلة تحديد المعدل التكراري لتلك العوامل بموجب الاستبيان الميداني وجدولتها بشكلها النهائي لغرض تقويم تأثير كل عامل من تلك العوامل المؤثرة , حيث يتم استخراج درجة الأهمية النسبية لتلك العوامل من خلال الاعتماد على المعدل التكراري للعوامل وتقويمها واعتبار العوامل الحاصلة على مستوى تقويم جيد جدا ذات درجة أهمية مهمة .

* المرحلة الرابعة/ بناء هيكلية النظام المقترح لدراسة إمكانية اعتماد الاسلوب المتسارع

إن الأساس في إمكانية اعتماد اسلوب التنفيذ المتسارع هو الموافقة على استخدام اسلوب التصميم والإنشاء أو اختيار نظام المقاولات المتعددة مع اسلوب الإدارة الإنشائية وكما موضح في الشكل (1), ولكنه قد يسمح بتوجيه اسلوب التنفيذ نحو غير ذلك , فهو قد يسمح باستخدام الإدارة الإنشائية بدون أسلوب التنفيذ المتسارع , مما يعني وجوب معرفة مدى توفر المتطلبات التي تسمح باستخدام التنفيذ المتسارع ومدى الحاجة إلى استخدامه على وفق مجموعة من الأسئلة تمثل معايير الاستخدام والتي تكون الإجابة عليها من خمس درجات تقويمية كما أشير إليها سابقا في الاستبيان, وكما موضح في الشكل (1)

أما الأسئلة المعيارية فهي :

1) هل المشروع كبير أو انه معقد التصميم ويحتاج إلى تقنية عالية متطورة ؟
2) هل هناك حاجة ملحة لتوفير الوقت والمباشرة بأعمال التنفيذ قبل إكمال التصاميم كوجود تضخم مالي أو حاجة آنية أو نية إلى استعمال المنشأ بصورة مبكرة أو عدم استقرار السوق ؟
3) هل تتوفر الإمكانية لدى ممثل صاحب العمل (الإدارة الإنشائية) او مقاول التصميم والإنشاء أو المصمم على تقسيم العمل في المشروع إلى مراحل تتعاقب في عناصرها التنفيذية إسوة بالعملية التنفيذية التقليدية (البرمجة , التصميم , تطوير التصميم , الوثائق , العطاء) ؟
4) هل تتوفر القدرة على الاستمرار بالتصميم والتنفيذ معا عن طريق تداخل نشاطات المرحلتين بنسب مختلفة تختلف من مشروع لآخر لدى الجهات المصممة والجهات المنفذة ؟
5) هل تتوفر الإمكانية لدى الجهة المسؤولة عن التصميم لإنهاء بعض عناصر التصميم مبكرا مثل تصميم الأسس سواء كانت تلك الجهة مقاول التصميم والإنشاء أو المصمم ؟
6) هل تتوفر القدرة على إدارة عدة عقود منفصلة في نفس الوقت ؟
7) هل يتمكن المسؤول عن العمل من التعاقد مباشرة مع المقاولين المتعددين سواء كان مقاول التصميم والإنشاء أو صاحب العمل ومن يخوله ؟

8) هل هناك إمكانية لوضع مرشد وقاعدة صحيحة للتصميم قبل بدء الرسوم التشغيلية مع دليل كلفة لضمان عدم تجاوز الميزانية الحدود المقررة لها ؟

ويتطلب الموافقة على استخدام اسلوب التنفيذ المتسارع عدة محددات هي :

أ- حصول المعيار الأول مع المعيار الثاني بصورة متكاملة على تقويم لايقل عن (50 %) إذ إن من الممكن أن يكون تقويم المعيار الأول ضعيفا والمعيار الثاني جيد جدا مثل كون المشروع غير معقد ولكنه يحتاج إلى توفير الوقت .

ب- الحصول على تقويم لكل معيار من المعايير الستة الأخيرة بصورة منفردة لايقل عن (50 %) .

ت- حصول التقويم العام للمعايير على معدل (70 %) كحد أدنى يمثل تطابق معايير استخدام اسلوب التنفيذ المتسارع مع اسلوب التصميم والإنشاء أو الإدارة الإنشائية مع التنفيذ المتسارع .

ث- في حالة عدم تحقيق ذلك وحصول التقويم العام على معدل ينحصر بين (50-70 %) فانه يعني عدم توافق أسلوب التنفيذ المتسارع مع أسلوب تنفيذ المشروع وعلينا اللجوء إلى أسلوب الإدارة الإنشائية منفردة أو مع استخدام اسلوب التصميم والإنشاء .

ج- في حالة حصول التقويم العام على معدل اقل من (50 %) يتم اللجوء إلى الأسلوب التقليدي (المقاول العام) او اسلوب التصميم والإنشاء بدون تسارع .

- تقويم النظام المقترح :

يهدف تقويم النظام المقترح إلى التأكد من مطابقته للحقائق وقبوله لدى الجهات الإنشائية التي تحتاجه, ومن اجل تقويم النظام المقترح وبيان أهميته وكفائته ودقته وسهولة استخدامه , فقد تم اعتماد التقويم على وفق التطبيق العملي للنظام على احد المشاريع التي تستخدم اسلوب التنفيذ المتسارع

تم اختيار مشروع مباني كلية العلوم / جامعة بغداد لغرض تطبيق النظام المقترح لكونه مازال في طور التنفيذ , ولكون صاحب العمل في ذلك المشروع جهة فنية وعلمية معروفة سبق ان تعاقدت وأنجزت الكثير من الأعمال والمشاريع وهي خبير يمتلك الدراية والخبرة لادارة مراحل العمل المختلفة كافة , ومن خلال متابعة كيفية تطبيق النظام المقترح على المشروع يمكن أن نوضح ان تقويم إجابات الأسئلة الثمانية هي :

1) التقويم الأول (جيدا) وهو يعادل (50%) لكون المشروع كبير ولكنه غير معقد التصميم ولايحتاج إلى تقنية متطورة .

2) التقويم الثاني (ممتازا) وهو يعادل (90%) للحاجة الملحة لتوفير الوقت والمباشرة قبل إكمال التصاميم لوجود تضخم مالي مع عدم استقرار السوق ووجود حاجة آنية إلى استعمال المنشأ بصورة مبكرة

3) التقويم الثالث (ممتازا) وهو يعادل (90%) لتوفر الإمكانية لدى الإدارة الإنشائية على تقسيم العمل الى مراحل واجزاء تتعاقب في عناصرها التنفيذية إسوة بالعملية التنفيذية التقليدية

4) التقويم الرابع (ممتازا) وهو يعادل (90%) لتوفر القدرة لدى الجهات المصممة والجهات المنفذة على الاستمرار بالتصميم والتنفيذ معا عن طريق تداخل نشاطات المرحلتين بنسب مختلفة
5) التقويم الخامس (ممتازا) وهو يعادل (90%) لتوفر الإمكانية لدى المصمم لإنهاء بعض عناصر التصميم مبكرا مثل تصميم الأسس
6) التقويم السادس (ممتازا) وهو يعادل (90%) لتوفر القدرة لدى الإدارة الإنشائية على إدارة عدة عقود منفصلة في نفس الوقت .
7) التقويم السابع (ممتاز) ويعادل (90%) لتمكن الإدارة الإنشائية من التعاقد مباشرة مع المقاولين المتعددين
8) التقويم الثامن (جيدا) وهو يعادل (50%) لتوفر إمكانية وضع مرشد وقاعدة صحيحة للتصميم قبل بدء الرسوم التشغيلية مع دليل كلفة لضمان عدم تجاوز الميزانية الحدود المقررة لها وبدرجة جيد .

وبموجب النظام المقترح فقد حصلت الموافقة على استخدام اسلوب التنفيذ المتسارع لتوفر المحددات التالية :

- حصول المعيار الأول مع المعيار الثاني بصورة متكاملة على تقويم (70 %) > (50%) .
- حصول كل معيار من المعايير الستة الأخيرة على تقويم > (50 %) .
- حصول التقويم العام للمعايير على معدل (80%) > (70 %)

وهذا يعني تطابق معايير استخدام الإدارة الإنشائية مع اسلوب التنفيذ المتسارع , مع إقرار نظام المقاولات المتعددة وهو الواقع الفعلي الذي تؤيده الادارة الانشائية لصاحب العمل

– الاستنتاجات :

في ضوء الدراسة النظرية ونتائج تحليل المسح الميداني لمجاميع العوامل المؤثرة في تطبيق اسلوب التنفيذ المتسارع فقد تم التوصل إلى مجموعة من الاستنتاجات الخاصة بإدارة المشاريع المتسارعة وكما يلي :

1- وجود ضعف واضح في مجال التخطيط للمقاولين من خلال الاعتماد على نوع واحد من أنواع التخطيط العام الذي يتعلق بالبرمجة الزمنية للفقرات ويسمى Bartchar , وإهمال مجالات التخطيط الأخرى المتعلقة بالاستخدام الأمثل للموارد البشرية أو الموارد الأخرى واستخدام البدائل وتحسين النوعية .
2- عدم فائدة تقسيم المشروع إلى أجزاء وعقود مادامت الجهة المنفذة التي تقوم بتنفيذ اغلب تلك العقود تعمل على برمجة نشاطاتها معا على الرغم من كونها عقودا مختلفة .
3- إحالة تنفيذ بعض الأعمال قبل إكمال تصاميمها ومخططاتها من خلال جدول كميات تقريبي في المراحل الأولى للتنفيذ ويعمل على تصحيحه لاحقا وتسميته تنفيذ متسارع هو اجراء خاطئ يسئ الى الاسلوب.
4- عدم إشراك القطاع الخاص في التنافس والاعتماد على القطاع العام فقط اضعف التنافس الفني والكلفوي وقلل من إمكانية استقدام مقاولين أو استشاريين أكفاء غير مرتبطين بالإجراءات الروتينية للقطاع العام .
5- من اجل نجاح تطبيق اسلوب التنفيذ المتسارع يجب توفير بعض المتطلبات الأساسية لذلك وهي :
   - إعداد الدراسات الأولية ودراسات الجدوى الفنية والمالية والاقتصادية لكل المشروع بصورة موحدة .

- تخمين كلفة العمل بأدق مايمكن من اجل الحفاظ على ميزانية المشروع .
- الفهم الكامل والشامل لتفاصيل عملية إنشاء المشروع المتكامل .
- تجزئة التصميم إلى مراحل وعناصر أساسية متوافقة مع هيكلية تجزئة العمل للمشروع .
- توفر الخبرة لدى صاحب العمل والمعمار في مجال تجزئة الميزانية الكلية على العقود المتعددة .
- ربط إدارة المشروع عمليات الإنشاء المختلفة للمراحل والقطاعات مع عملية التغذية العكسية .
- توفير الصلاحيات لإدارة المشروع لاعتبارها أحد أهم أدوات نجاح تطبيق اسلوب التنفيذ المتسارع

6- ضعف آلية تسعير الفقرات غير المدرجة في جدول الكميات الذي تتم إحالة الأعمال بموجبه , ادى الى ظهور الكثير من الخلافات حول اسلوب تحديد سعر تلك الفقرات واضعف اسلوب التنفيذ المتسارع

7- أوضح التقويم التطبيقي والاستبياني كفاءة النظام المقترح في البحث وأهميته في تجاوز حالة الضعف والقصور الظاهرة في المحاولات النظمية المعتمدة حاليا .

- التوصيات :

في ضوء النتائج المتحققة من البحث يوصي الباحث بما يلي :

1- ضرورة إعداد دورات تطويرية وإشراك المهندسين والفنيين بتلك الدورات لتطويرهم ورفع مستواهم العلمي والفني بما يتلائم مع التطور الحاصل في العلوم الهندسية وخاصة في مجال التخطيط والبرمجة والسيطرة بأشكالها ومنها استخدام اسلوب التنفيذ المتسارع .

2- الاهتمام بعملية التوثيق في المشاريع الإنشائية وتحقيق تغذية عكسية فعالة للمعلومات

3- الاهتمام بإدارات المشاريع وتأهيلهم كقيادات هندسية كفوءة في الموقع الحقلي والمركز ومنحهم الصلاحيات اللازمة لغرض تنفيذ العمل بنجاح متجاوزين المعوقات والإجراءات التقليدية والروتينية .

4- استخدام اسلوب الإدارة الإنشائية لإدارة عمليات المشروع التصميمية والتنفيذية سواء كان ذلك عن طريق خلق إدارة إنشائية تخصصية من القطاع العام مزودة بالصلاحيات المناسبة , أو من خلال اعتماد القطاع الخاص الخبير.

5- اعتماد نظام محفزات متكامل وكفوء يساعد في صرف الحوافز والمكافئات ويتناسب مع الحالة الاجتماعية والثقافية والمستوى المعاشي للأيدي العاملة لتشجيع العاملين والإسراع بعملية التنفيذ , ورفع روح الانتماء لدى المهندسين والفنيين ومتابعتهم للتنفيذ من خلال إشراكهم بالأرباح المتحققة من التوفير

6- البدء مبكرا بالاستخدام الامثل لعملية التخطيط من خلال مايلي :

- وضع خطة نهائية للمشروع متفق عليها تتلائم مع ظروف العمل والشروط العامة والخاصة المطلوبة ومع متطلبات صاحب العمل الزمنية وإمكانية المقاولين الثانويين في تنفيذها ضمن الوقت المحدد وتتلائم مع حجم الموارد والسيولة النقدية المتوفرة وتعتبر نهاية تخطيط الكلفة مع بدء التنفيذ

- وضع خطة محدودة الأمد مفصلة للعمليات التنفيذية الواجب القيام بها ترتبط زمنيا مع الخطة الزمنية ولا تخرج عنها وقد تكون لفترة زمنية محدودة أو لفقرة عمل محدود
- وضع خطة السيطرة الزمنية على وقت تنفيذ المشروع بالاعتماد على دراسة حجم العمل ومعدلات الاداء للعاملين والآليات بموجب متطلبات صاحب العمل ووضع برمجة زمنية رئيسية للمشروع ومفصلة للفقرات يتم تحديثها شهريا استنادا إلى المعلومات المتوفرة من المتابعة الميدانية للعمل.
- وضع خطة نظام ضبط الكلفة وسيطرة الكلفة لتسجيل وتقدير الالتزامات المالية والمصروفات ومقارنة التكاليف الناتجة مع الزيادات في تقديرات الكلفة وضبط التكاليف الفعلية مقابل الميزانية المخمنة والقيام بتقديم البدائل الفنية المقبولة في حالة انحراف مسارات الكلفة الحقيقية عن التخمينية.
- وضع خطة السيطرة النوعية وإجراء الفحوصات الفنية المتتابعة للنماذج كبرنامج متابعة للعمل ووضع خطة للسلامة المهنية للتأثيرات الكثيرة التي تسببها على الكلفة والزمن في حالة انحرافها, ووضع خطة لتشغيل المنشا وصيانته بعد إجراء عملية الاستلام تكون مكملة للخطط السابقة .

7- استخدام صيغة جديدة لإصدار أوامر التغيير تعتمد على مبدأ السرعة في العملية والتفاوض مع المقاول , واعتماد آلية جديدة لتسعير الفقرات غير المدرجة في جدول الكميات التي تظهر أثناء تنفيذ المشروع.

8- تقسيم العمل في المشروع إلى أجزاء ومراحل تتوافق مع البرمجة الزمنية الكلية للمشروع.

9- تجهيز جميع الوثائق لتلك المجاميع والأجزاء التي تم إقرارها بشكل واضح ومفهوم في وقت مناسب قبل المباشرة بالعمل لكل جزء أو مرحلة , وبرمجة تقديمها بحيث لا تؤثر على سرعة إنجاز العمل أو نوعيته أو التداخل مع بقية الأجزاء والمجاميع والمقاولين في حالة المباشرة بالتنفيذ قبل إكمال الوثائق .

- المصادر : (REFERENCES)

*** AL –Sedairy. Salman T. (LARGE – SCALE CONSTRUCTION PROJECTS)1st Published , Butlar & Tanner Ltd . , London , 1985 U.K.**

*** Ferry .D. J. (COST PLANNING OF BUILDING) Third Edition Gross By Lockwood &Sons ,Ltd , London 1974**

*** Fisk . Edward . R. (CONSTRUCTION PROJECT ADMINSTRATION) Second Edition , John Wiley & Sons , Inc , 1982 , U.S.A.**

*** McNulty, Alfred P. (Management of small Construction Projects) McGraw -Hill Book Co. , U.S.A. , 1982**

*** Merritt. F. S.(Building Construction Handbook) Third Edition , McGRAW-HILL BOOK COMPANY, u.s.a. , 1975**

*** Turner . Dennis F. (BUILDING CONTRACT DISPUTES ; THEIR AVOIDANCE AND RESOLUTION) Longman Scientific &Technical , Longman Group, U.K. Limited, U.K. ,1989**

*** Groton , (WEIGHTING THE OPTIONS) ASCE / JOURNAL OF MANAGEMENT IN ENGINEERING , V14 , N6 , 1998**

* البياتي , هلال عبود & محمد حسن , علاء عبد الرزاق (المدخل لنظم المعلومات الإدارية) الجامعة المستنصرية , وزارة التعليم العالي والبحث العلمي , بغداد , 1992

*العجيلي. حاتم خليفة (تطوير نظام إداري لقواعد اختيار اسلوب التنفيذ المتسارع في مشاريع قطاع المباني) أطروحة مقدمة إلى قسم هندسة البناء والإنشاءات في الجامعة التكنولوجية كجزء من متطلبات نيل درجة دكتوراه فلسفة في هندسة البناء والإنشاءات , بغداد 2004 .

*العزي . د. محمد ايوب صبري (مدة تنفيذ مشاريع اعادة الاعمار) منشورات وزارة الاسكان والتعمير ,(وقائع المؤتمر العلمي الثاني لوزارة الاسكان والتعمير). بحوث ادارة المشاريع , الموضوع 19 , بغداد . نيسان 1992

* جعلوك . د محمد علي (اعمال المقاولات) ط1 , دار الراتب الجامعية 1999 بيروت , لبنان

* غولدهابر ستانلي ,جها شاندراك ,ماسيدو مانويلي (النظم الإدارية لهندسة التشييد) ترجمة التنير د.أنيس عبد الله ,جمجوم د.محمد عمر منشورات دار جون وايلي وابنائه / انكلترا / ط1 / 1982.

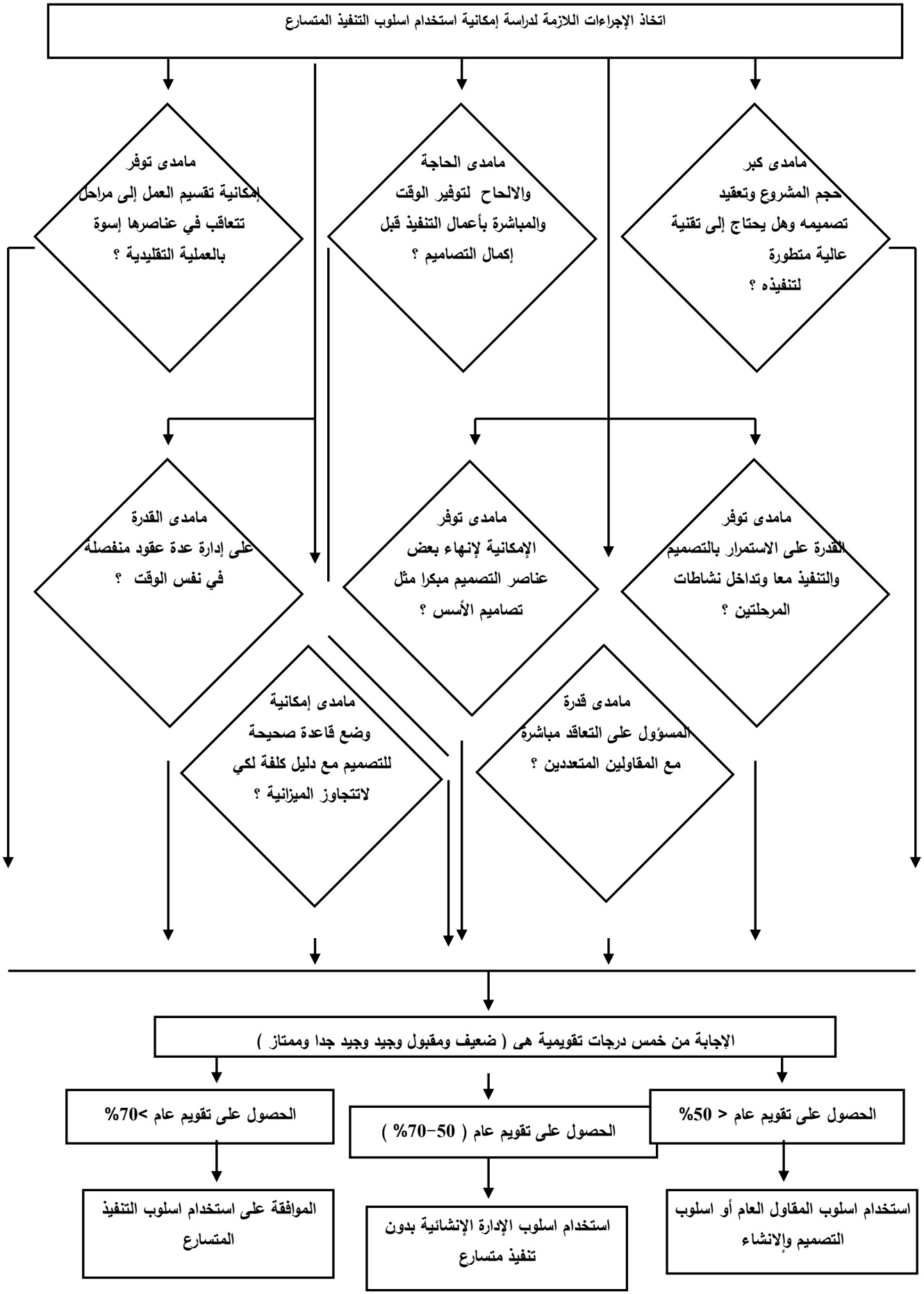

الشكل (1) مخطط انسيابية النظام الفرعي لدراسة إمكانية استخدام اسلوب التنفيذ المتسارع

طبقات العمارة المستدامة

عمار سالم
مدرس مساعد
جامعه بغداد – كلية الهندسة

الخلاصة:

يعتبر مفهوم العمارة المستدامة من أكثر المفاهيم المعمارية الحديثة تداولا بسبب أزمة الطاقة التي اعتلت حياة الإنسان وعانى منها كوكب الارض برمته,وحيث تعد العمارة احدى اكبر مجالات استنزاف الطاقة, لذلك كان الاهتمام بتقنين وترشيد استخدام الطاقة او امكانية توفيرها او حتى الاستغناء عنها في الابنية احدى اهم ما تسعى اليه العمارة الحديثة.وبسبب حداثة مفهوم العمارة المستدامة فقد اعتلى المفهوم الكثير من اللبس والغموض عندما عُمّم استخدامه,فاستخدم تارة للاشارة الى العمارة الخضراء واستخدم تارة اخرى للاشارة للعمارة الذكية, واستخدم مرة ثالثة للاشارة الى العمارة البيئية وهكذا,وامام هذا اللبس كان هدف هذا البحث الاول هو تحديد اهم ركائز مفهوم العمارة المستدامة التي تحددت بخفض الكلفة وتقليل التلوث البيئي والحفاظ على الطاقة,ثم كان هدف البحث الثاني هو وضع التعريف الاجرائي لمفهوم العمارة المستدامة عندما عرفها بانها العمارة التي تلبي حاجات الانسان المعمارية من حيث الجمال والوظيفية والمتانة مع قدرتها على توليد او تقليص استهلاكها للطاقة المطلوبة لتشغيلها وتقليل كلف الانتاج او الادامة قدر الامكان مع الحفاظ على كوكب الأرض وبيئته وموارده سليما معافى للأجيال القادمة.ثم انتقل البحث الى الهدف الثالث الا وهو تصنيف هذا المفهوم الى طبقات مختلفة تتخصص كل طبقة منها بحق معين من حقول العمارة,فكانت العمارة الذكية المستدامة هي العمارة التي تعتمد على التقنيات الحديثة لتحقيق مفهوم الاستدامة,فيما كانت العمارة الخضراء المستدامة هي العمارة التي تعتمد على النباتات والمناطق

الخضراء والأشجار لتحقيق مفهوم الاستدامة,وكانت العمارة البيئية المستدامة هي العمارة التي تعتمد على الخصائص البيئية لتحقيق الاستدامة ,وهكذا لباقي طبقات المفهوم.**فالبحث هو محاولة لفهم اوسع لمفهوم العمارة المستدامة وتمييزا لطبقات هذا المفهوم المتداخلة.**

SUSTAINABLE ARCHITECTURE LEVELS

ABSTRACT

Sustainable architecture has became one of the most important architectural concepts on earth today because of the energy crises. Architecture is concerned as the largest energy consuming field ,so that one of the main goals of modern architecture is to reduce energy consumption or reticence it from building if possible .

Sustainable architecture is a modern and new concept. It is used sometimes to refer to green ,intelligent and environmental architecture , and that make it confused term , therefore the main goals of this research is to clear the main important pillars of this architectural concept (reduce costs , reduce the environment pollution , reserve energy) as a first goal. Second goal establishing The Procedural definition for this architectural concept is sustainable architecture is Defined In This Paper As (The Architecture That Satisfies The architectural human needs) – beauty , function , structural needs , the ability to generate energy needed to operate the building or reduce the energy needs for it , reduce the costs of production & maintenance , consumption for environmental conservation purposes to preserve earth and its resources for the future generations.

This paper tried also to classify the concept to different levels each one dedicated to specified architectural field . Intelligent sustainable architecture is the one that depends on modern technologies for implement the sustainable concept .Green sustainable architecture is the architecture using plants and green areas ,environmental sustainable architecture is the one depending on environmental features to achieve sustainability. and so on for the rest of levels concepts .

As a summery this research is an attempt to understand the concept (sustainable architecture) and recognition for its interrelated levels.

المقدمة:

اشتهر مؤخرا مفهوم"العمارة المستدامة" خصوصا بعد ان تفاقمت مشاكل البيئة العالمية وارتفعت اسعار الطاقة وغدا كوكب الارض مهددا بشتى انواع الكوارث ليس اقلها ازمة الغذاء العالمي التي يتردد صداها هذه الايام حتى ارتفعت اسعار الخبز في كثير من دول العالم وخصوصا العالم الثالث.ورغم ان العمارة المستدامة هي جزء صغير من مفهوم اوسع نطاقا واكثر شمولا الا وهومفهوم "التنمية المستدامة" التي اعتنت بكل ما من شانه ان يحفظ هذا الكوكب سليما ومعافى قدر الامكان للاجيال القادمة الا اننا ما زلنا نشهد بعض اللبس والارتباك في استخدام مفهوم "العمارة المستدامة" وتبيان انواع هذه الاستدامة وطبقاتها.فقد اختلط الامر على الكثيرين فراحوا يتذبذبون بين استخدام مصطلح العمارة الخضراء وبين العمارة المستدامة وبين العمارة الذكية والعمارة البيئية والعمارة الاقتصادية وعمارة الفقراء. صُنفت عمارة "حسن فتحي" بانها من ضمن العمارة المستدامة رغم انها عمارة للفقراء تمتاز بقلة ما يصرف عليها, بينما نرى من جانب اخر ان الابنية الذكية تنتمي الى العمارة المستدامة مع ان كلف انتاجها تفوق أي عمارة اخرى!.

مشكلة البحث:ولهذا كانت مشكلة البحث هو وجود لبس وغموض في مفهوم العمارة المستدامة وغياب الاطار النظري الذي يمكن من خلاله تحديد اصناف العمارة المستدامة وطبقاتها.

هدف البحث:وهكذا كان هدف البحث هو تحديد الركائز التي يعتمد عليها مفهوم العمارة المستدامة,ثم وضع تعريف اجرائي لذلك المفهوم,واخيرا وضع الاطار النظري لطبقات مفهوم العمارة المستدامة يصنف من خلاله انواع هذه العمارة كل حسب تخصصها.

يتضمن البحث ما يلي:

- استعراض الدراسات السابقة التي تكلمت عن العمارة المستدامة.
- تحديد ركائز العمارة المستدامة.
- تعريف مفهوم العمارة المستدامة.
- تحديد الاطار النظري لطبقات العمارة المستدامة.

التنمية المستدامة:

كتب المعماري ""جون راسكن" : "ان الله أعارنا الأرض لنحيا عليها بعض الوقت فهي هبة ومنحة عظيمة، لكن ملكيتها تؤول لأبنائنا وأحفادنا أكثر مما تعود لنا، وليس لدينا أدنى حق في أن نتجاهلهم أو ان نشركهم في العقاب على جرائم لم يقترفوها ,أو أن نحرمهم من نعم وهبها الله لهم، ليس لنا أدنى حق في ذلك".(شديدي–2006).فيما يقول علماء تكنولوجيا السلوك الإنساني بان أي رفاهية كمالية يحققها الإنسان في العصر الحاضر هي على حساب الحاجات الأساسية لإنسان العصور القادمة(سكينر–1998).

أولت معظم دول العالم في العقد الأخير من القرن المنصرم عناية خاصة واهتماماً واسعاً بمواضيع حماية البيئة والتنمية المستدامة، ولم يولد هذا الاهتمام من فراغ فقد تعالت الأصوات البيئية المنادية بتقليل الآثار البيئية الناجمة عن الأنشطة البشرية المختلفة ونادت بخفض المخلفات والملوثات والحفاظ على قاعدة الموارد الطبيعية للأجيال القادمة. ونتيجة لذلك فإن القطاعات العمرانية في هذا العصر لم تعد بمعزل عن القضايا البيئية الملحة التي بدأت تهدد العالم وتم التنبه لها في السنوات القلائل الأخيرة، فهذه القطاعات من جهة تعتبر أحد المستهلكين الرئيسيين للموارد الطبيعية كالأرض والمواد والمياه والطاقة، ومن جهة أخرى فإن عمليات صناعة البناء والتشييد الكثيرة والمعقدة ينتج عنها كميات كبيرة من الضجيج والتلوث والمخلفات الصلبة. وتبقى مشكلة هدر الطاقة والمياه من أبرز المشاكل البيئية–الاقتصادية للمباني بسبب استمرارها وديمومتها طوال مدة تشغيل المبنى. ولهذه الأسباب وغيرها ونتيجة لتنامي الوعي العام تجاه الآثار البيئية المصاحبة لأنشطة البناء فقد نوه بعض المتخصصين أن التحدي الأساسي الذي يواجه القطاعات العمرانية في هذا الوقت إنما يتمثل في مقدرتها على الإيفاء بالتزاماتها وأداء دورها التنموي تجاه تحقيق مفاهيم التنمية المستدامة الشاملة، وأضاف آخرون بأن الإدارة والسيطرة البيئية على المشاريع العمرانية ستكون واحدة من أهم المعايير التنافسية الهامة في هذه القطاعات في القرن الواحد والعشرين(السواط–2006).

لقد بدأ العالم يعترف بالإرتباط الوثيق بين التنمية الاقتصادية والبيئة منذ انعقاد مؤتمر ستوكهولم في بداية السبعينات، وقد تنبه المتخصصون إلى أن الأشكال التقليدية للتنمية الاقتصادية تنحصر على الاستغلال الجائر للموارد الطبيعية وفي نفس الوقت تتسبب في إحداث ضغط كبير على البيئة نتيجة لما تفرزه من ملوثات ومخلفات ضارة. وقد شدد تقرير الأمم المتحدة المسمى "مستقبلنا المشترك" (Our Common Future) على أن هناك حاجة ماسة إلى أسلوب جديد يضمن استمرار التنمية الاقتصادية على المدى البعيد، ومن هنا ظهر مفهوم التنمية المستدامة (السواط–2006).

تعرف التنمية المستدامة (Sustainable Development) بانها: تلبية احتياجات الأجيال الحالية دون الإضرار بقدرة الأجيال القادمة على تلبية احتياجاتها)(السواط–2006).فيما عرفها "سعيد مرعي" بأنها قائمة على الإفتراض بأن القرارات الحالية يجب ألا تضعف من أمكأنية الحفاظ وتحسين مستوى الحياة بالمستقبل من خلال إدارة جيدة للنظم الاقتصادية التي تحقيق ربحية الموارد وصيانة الأصول الثابتة(مرعي –2006).

وقد شدد تقرير الأمم المتحدة عن البيئة والتنمية في العام 1987م على أهمية مشاركة جميع الحكومات والشعوب والقطاعات الصناعية بما فيها القطاعات العمرانية في الحفاظ على البيئة وصيانة الموارد الطبيعية، أيضاً شدد كل من مؤتمر قمة الأرض الأول (Earth Summit-I) الذي عقد في "ريو دي جانيرو" بالبرازيل في عام 1992م ومؤتمر قمة الأرض الثاني (Earth Summit-II) الذي عقد في "جوهانسبيرغ "بجنوب أفريقيا في عام 2002 على العمل بأسرع وقت ممكن للحد من فقدان الموارد الطبيعية التي أصبحت مهددة بالاضمحلال.(السواط–2006)

ومن هنا نعرف إن "التنمية المستدامة" هي المحاولات التي يبذلها الإنسان لأجل الحفاظ على سلامة الأرض مع تلبية ما يحتاجه منها,وحيث تعتبر "العمارة" من اهم متطلبات الانسان على هذه الأرض,وحيث ان العمارة تعد من اكبر ملوثات الأرض واهم عناصر تخريب البيئة,حيث أشار "جيمس واينز" (James Wines) إلى أن المباني تستهلك سُدس إمدادات الماء العذب في العالم، وربع انتاج الخشب، وخُمسين الوقود والمواد المصنعة. وفي نفس الوقت تنتج نصف غازات البيت

الزجاجي الضارة(ظاهرة البيت الزجاجي او ما يسمى بالاحتباس الحراري او الدفيئة الارضية هو ظاهرة ارتفاع درجة الحرارة نتيجة لتغير في سيلان الحرارة من البيئة واليها)(ويكيبيديا–2008).ثم يضيف بأن مساحة البيئة المشيدة (built environment) في العالم ستتضاعف خلال مدة وجيزة جداً تتراوح بين 20–40 سنة قادمة(السواط–2006). وهذه الحقائق تجعل من عمليات إنشاء وتشغيل المباني العمرانية واحدة من أكثر الصناعات استهلاكاً للطاقة والموارد في العالم. كما أن التلوث الناتج عن عدم كفاءة المباني والمخلفات الصادرة عنها هي في الأصل ناتجة عن التصميم السيء للمباني، فالملوثات والمخلفات التي تلحق أضراراً كبيرة بالبيئة ليست سوى نواتج عرضية (by-products) لطريقة تصميم مبانينا وتشييدها وتشغيلها وصيانتها، وعندما تصبح الأنظمة الحيوية (bio-systems) غير صحية نتيجة لهذه الملوثات فإن ذلك يعني وجود بيئة غير آمنة للمستخدمين(السواط–2006). اشارت الدراسات بان المباني المعمارية في امريكا تستهلك لوحدها 65% من اجمالي استهلاك الطاقة وتتسبب في 30% من ظاهرة البيت الزجاجي(السواط–2006),فيما اوضحت دراسات مصرية بان التلوث الناتج عن اصدار غاز ثاني اوكسيد الكاربون من استهلاك الصناعة للطاقة هو27 % بينما التلوث الناتج عن الابنية السكنية والتجارية يبلغ 10% من 94 مليون طن من غاز ثاني اوكسيد الكاربون المستخدم لاستهلاك الطاقة البترولية(عبدة–2005) .وهكذا نجد ان الميل نحو "العمارة المستدامة" ليس بذخا او ترفا طبقيا ,كما انه لا يمكن ان يكون نزعة ذاتية امام ما تسببه العمارة السيئة من مخاطر تتعدى الذات لتشمل كوكب الارض باجمعه.

تعريف العمارة المستدامة:

لم يجري تحديد تعريف شامل للعمارة المستدامة ,فقد اختلفت المصادر في تعريف هذه العمارة من خلال دمج كل طبقاتها في المفهوم .فقد قال "علي بن محمد السواط" ان:

التصميم المستدام .. العمارة الخضراء .. الإنشاءات المستدامة .. البناء الأخضر .. كل هذه المفاهيم جميعها ما هي إلا طرق وأساليب جديدة للتصميم والتشييد تستحضر التحديات البيئية والاقتصادية التي ألقت بظلالها على مختلف القطاعات في هذا العصر، فالمباني الجديدة يتم

تصميمها وتنفيذها وتشغيلها بأساليب وتقنيات متطورة تسهم في تقليل الأثر البيئي، وفي نفس الوقت تقود إلى خفض التكاليف وعلى وجه الخصوص تكاليف التشغيل والصيانة (Running Costs)، كما أنها تسهم في توفير بيئة عمرانية آمنة ومريحة. وهكذا فإن بواعث تبني مفهوم الاستدامة في القطاع العمراني لا تختلف عن البواعث التي أدت إلى ظهور وتبني مفهوم التنمية المستدامة (Sustainable Development) بأبعادها البيئية والاقتصادية والاجتماعية المتداخلة)(السواط-2006).

فيما قال عنها "رشيد اكرم شلهوب"بانها: العمارة التي تعتمد أساسا على المواد الطبيعية في الإنشاء والانهاء والتي تتلائم مع البيئة المحيطة, فلا ينتج عنها عناصر ذات آثار ضارة على صحة مستعمليها ,كما تعتمد على التصميم الذي يراعي احتياجات هؤلاء السكان سواء كانوا كبارا أم شبابا نساء أو أطفال أصحاء أو مرضى، فتكون هذه العمارة متوافقة مع متطلبات و توجهات من يستعملونها(شلهوب-2007).

فيما يرى المعماري "وليام ريد": ان المباني الخضراء (ويقصد بذلك العمارة المستدامة)ما هي الا مباني تصمم وتنفذ وتتم إدارتها بأسلوب يضع البيئة في اعتبارة وهو يري ايضا ان احد اهتمامات المباني الخضراء يظهر في تقليل تأثير المبنى السلبي على البيئة إلى جانب تقليل تكاليف إنشائه وتشغيله(حسام-2006).

اما المعماري "كين يانج": فلقد ناقش مفهوم العمارة الخضراء من وجهة نظر بيئية ,فهو منزعج من تاثير المباني علي الانظمة الطبيعية وهو يري ان العمارة الخضراء او العمارة المستدامة يجب ان تقابل احتياجات الحاضر دون اغفال حق الاجيال القادمة لمقابلة احتياجاتهم ايضا فالقرارات التصميمية لاتنحصر تاثيرها علي البيئة فقط ولكن يمتد تاثيرها للاجيال القادمة ايضا(حسام-2006).

فيما قال المعماري "ايان مشارج": ان مشكلة الانسان مع الطبيعة تتجلي في ضرورة اعطاء الطبيعة صفة الاستمرارية بكفاءة كمصدر للحياة ,كما انه ينظر للمشكلة من وجهة نظر بيئية تدعو للتفكر في العالم والتعلم منه(حسام-2006).

وعرّفها "سعيد مرعي" بقوله:أنها ممارسات البناء التي تسعى إلى الجودة المتكاملة (الإقتصادية – الإجتماعية – البيئية) بطريقة واضحة ، فالاستخدام المنطقى للموارد الطبيعية والإدارة الملائمة للمبانى يسهم في إنقاذ الموارد النادرة وتقليل إستهلاك الطاقة وتحسين البيئة مع الأخذ في الاعتبار دورة حياة المبنى كاملة وكذلك الجودة البيئية ، الوظيفيه ، الجماليه و القيم المستقبليه((مرعي-2006).

مميزات العمارة المستدامة:

تمتاز العمارة المستدامة حسب "كولدهام "(coldham-2001) بانها:

1- توفر احتياجات مستعمليها من الطاقة.

2- تؤدي الى الحفاظ على صحتهم.

3-تزيد شعورهم بالرضى .

4-وتعمل على زيادة انتاجيتهم.

5- واشباع الحاجات الروحية (coldham-2001).

فيما وضع ميزاتها "سعيد مرعي"بانها:

1-الحد من إستهلاك الموارد غير القابلة للتجديد .

2- تجميل البيئة الطبيعية .

3- إزالة أو الحد من إستخدام المواد السامة .

تطبيق هذة المبادىء يقلل التأثير السلبى على البيئة الطبيعية والمشيدة من حيث المباني ومحيطها المباشر والإقليمي والعالمى(مرعي-2006).

فيما توسع "صفاء عبدة" فذكر ميزاتها بانها:

1- توفير البيئة الصحية الداخلية لضمان عدم اصدار مواد البناء او الانظمة الانشائية أي غازات سامة كما يتعين العمل على تجديد الهواء في الداخل وتنقيته بواسطة المزروعات والمرشحات.

2- كفاءة استخدام الطاقة فيجب مراعات الاجراءات التي تضمن ان يستخدم المبنى اقل طاقة ممكنة في عملية التبريد والتدفئة والاضاءة وذلك باستخدام الوسائل الفنية والمنتجات التي تحافظ على الطاقة المتوفرة وتحول دون سوء استخدامها.

3- الاعتماد على المواد ذات التأثير الحميد على البيئة, حيث يجب مراعاة استخدام مواد البناء والمنتجات التي تؤدي لخفض تدمير البيئة عالميا.فيمكن اختيار الخشب شريطة الا يدمر الغابات كما تؤخذ في الاعتبار المواد الاخرى على اساس عدم سمية العناصر التي تنتجها.

4- التشكيل المرتبط بالبيئة المحيطة فيجب مراعات ضرورة ربط التشكيل والتصميم بالموقع المقام عليه وبالمنطقة وبطقس تلك المنطقة من حيث درجة الحرارة وحركة الرياح.هذا مع توفر وسائل اعادة تدوير المخلفات waste recycling ومراعاة تجانس العلاقة بين شكل المبنى وقاطنيه والطبيعة المحيطة.

5- توخي التصميم الجيد, فيجب مراعاة الحصول على تصميم يحقق كفاءة في العلاقة بين المساحات المستخدمة ومسارات الحركة وتشكيل المبنى والنظم الميكانيكية وتكنلوجيا البناء كما يعبر عن تاريخ المنطقة والارض وكذلك القيم والمباديء الروحية التي يجب دراستها حتى يصبح المبنى متميزا بسهولة الاستعمال وجودة البناء وجمال الشكل(عبدة-2005).

التصميم المستدام:

لقد تعدى مفهوم العمارة المستدامة مجرد تلبية متطلبات تصميم العمارة المستدامة إلى ان اصبح "فلسفة تصميمية".ولهذا ظهرت نزعة تسمى بالتصميم المستدام والتي عرفها البعض بانها: التداخل بين العمارة والهندسة الكهربائية والميكانيكية والإنشائية فضلا عن الاهتمام بالجماليات التقليدية للحجم والنسب والمقياس والملمس وغيرها.فان فريق تصميم المبنى يجب ان يهتم بالتكاليف طويلة المدى بيئيا واقتصاديا وبشريا(عبدة-2005).وقد حدد معهد "روكي ماونتن" خمسة عناصر للتصميم المستدام(عبدة-2005) وهي:

1- شمولية التخطيط والتصميم اذ ان لها اكبر الاثر في كفاءة استخدام الطاقة.
2- اعتبار التصميم المستدام فلسفة بناء اكثر من كونه طراز مقترح للبناء,فالابنية التي تبنى بهذا الفكر غير محدودة الشكل والطابع.
3- لا يتعين زيادة تكلفة المباني المستدامة عن المباني التقليدية كما انها لا تختلف عنها من حيث البساطة وعدم التعقيد.
4- تكامل التصميم باعتبار إن كل عنصر من العناصر جزء من الكل وضروري لنجاح هذا التصميم.
5- اعتبار خفض استهلاك الطاقة والحفاظ على صحة الافراد وتحسنها من المباديء المنظمة للتصميم المستدام(عبدة-2005).

التخطيط العمراني المستدام:

لقد توسع مفهوم الاستدامة في العمارة ليشمل الاستدامة على مستوى التخطيط العمراني مشاريع انشاء المدن وخاصة في المناطق النائية والصحراوية(عبدة-2005).ولهذا ظهر مفهوم مصفوفة التخطيط العمراني المستدام sustainable urban matrix التي يُعنى التخطيط العمراني المستدام فيها بالتشكيلات العمرانية والفراغية المؤثرة في التنمية العمرانية والتي تحقق التوافق المستمر

للاحتياجات المتغيرة ونظم العمران.وقد طرح كل من frey و williamse وpunter اسس التخطيط العمراني المستدام من خلال ثلاث عناصر اساسية تؤثر في تركيب المدينة (بشندي-2005) وهي:

1-إمكانية الوصول accessibility.

2-التقارب proximity.

3- اندماج الوظائف function mix .

والتي تتوافق مع احتياجات الانسان وفق ما حددها ماسلو في مقياسه وكالتالي:

1-توفير الاحتياجات العمرانيةphysical needs .

2-توفير الامن والامان والحماية safety,security and protection.

3-توفير الانتماء والتواصل الاجتماعي a conducive social.

4- تحقيق الاكتفاء الذاتي self sufficiency.

5- احتمالية الابداع a chance to creative .

6 تحقيق البيئة الجمالية an aesthetically pleasing environment (بشندي-2005).

فيما حدد barton مباديء التخطيط العمراني المستدام (بشندي-2005)من خلال:

1- الاكتفاء الذاتي.

2- تصميم المجاورة السكنية.

3- تلبية احتياجات الانسان وتحقيق الاهداف الاجتماعية والبيئية.

4- تشكيل العمران الطاقة المفتوحة.

5- تخطيط الشوارع .

6- تصميم شبكة الفراغات المفتوحة .

7- ستراتيجية استخدام الطاقة.

8- استراتيجية استخدام المياه(بشندي-2005).

العمارة الذكية والاستدامة:

بدأ المعماريون في إعادة تعريف كلمة العمارة الخضراء بالعمارة الذكية لإقناع المستخدمين بمزاياها وقدرتها على الوفاء بالحاجات الوظيفية للمنشآت(نورالدين-2006)،وقد تم تعريف المبانى الذكية على أنها المبانى التى توفر بيئة سريعة الإستجابة ، وفاعلة ، وداعمة من أجل تحقيق آداء أفضل لمستخدمى المبانى (احمد-2005). وعلى الرغم من التقنية العالية المستخدمة في الابنية الذكية إلا أن تلك التقنية ينظر اليها من وجهة نظر العمارة المستدامة على أنها داعم ومحرك فحسب وليست هدفاً او غاية,فالتقنية وسيلة لتحقيق الاستدامة في العمارة .

لقد تم إستخدام مصطلح المبانى الذكية فى الولايات المتحدة فى بداية الثمانينات من القرن المنصرم. وعرفت المبانى الذكية آنذاك بواسطة معهد المبانى الذكية على أنها مبانى يتم فيها دمج أنظمة متعددة بكفاءة عالية لإدارة الموراد والإمكانيات من أجل تعظيم الآداء الفنى، وزيادة العائد ، وترشيد تكلفة التشغيل ، وتحقيق المرونة(احمد-2005).

وعرفت المبانى الذكية أيضاً على أنها مبانى تتميز بفاعلية وتغير مستمرين ، وكذلك تستجيب لإحتياجات الأفراد وتساعد على رفع كفاءة الإنتاج ، وترشيد الإنفاق ، ومتوافقة بيئياً وذلك من خلال التفاعل المتواصل بين المكونات الرئيسية للمبانى الذكية وهى البناء ، والعمليات ، والمستخدمين ، والإدارة ،وكذا العلاقات المتبادلة بينهم(احمد-2005).

إن المبانى الذكية تتطلب ذكاءاً يجب أن يتم تطبيقه خلال مراحل التفكير فى تصميم المبنى ، اثناء إنشائه ، وعند تشغيله وصيانته ويجسد فى أنظمة المبانى ومكوناتها وسبل تفعيلها وطرق تفاعلها مع المستعملين ومع بعضها البعض. ويتفاوت التركيز على مفهوم المبانى الذكية من مكان

إلى آخر ففى المعهد البريطانى للمبانى الذكية يتم التركيز على الإستجابة لمتطلبات الأفراد، اما فى المعهد الأمريكى للمبانى الذكية فيتم التركيز على التقدم التقنى ، ومن جانب ثالث نجد أن تركيز المعهد الأسيوى للمبانى الذكية هو وحدات الكفاءة البيئية فضلا عن متطلبات وظيفية وتقنية لفراغات المبانى(احمد-2005).

وإذا نظرنا إلى تطور فكر المبانى الذكية سنجد أنه فى الماضى كان هو توظيف تقنيات الحاسب الآلى ووسائل الإتصال والمعرفة فى دمج أنظمة المبنى والتنسيق بينها من أجل رفع كفاءة إدارة موارد المبنى وترشيد تكلفة الإستخدام والصيانة مع تحقيق ديناميكية وتفاعلية أنظمة المبنى لتحقق الراحة لمستعملية مع تحسين إنتاجيتهم. أما هذه الأيام فقد تطور مفهوم وفكر المبانى الذكية لتعدى المقدرة على الإستجابة ورد الفعل إلى القدرة على التعلم وتعديل الآداء بناءاً على أنماط الأستخدام وظروف الزمان والمكان(احمد-2005).إن التطورات الحديثة فى تقنيات المبانى الذكية تشير إلى دور هام لها فى دعم بناء مدن المعرفة, حيث أنها تنحى بها إلى مفهوم التحكم عن بعد عبر الشبكة العنكوبيته لتدعم مفهوم الشراكة المعرفية والتى هى أهم دعائم مدن المعرفة .

تيار الايكوتيك EcoTech والاستدامة:

الايكوتيك هو مصطلح يطلق على العمارة التي تهتم بمجالات البيئة والتقنيات الحديثة في العمارة.والمصطلح مكون من اختصار لكلمتين: Ecology=Eco وهي تعني علوم البيئة و Tech = Technology وتعني التقنية(الشايع-2007).

يُعرّف النظام الايكولوجي Ecosystem بانه العلاقة التفاعلية بين المكونات الفيزياوية physical components وبين المكونات البايولوجية Biological components في مكان محدد(فجال-2004).فالنظام الايكولوجي هو وحدة بيئية متكاملة تتكون من مكونات حية واخرى غير حية في مكان محدد يتفاعل بعضها مع البعض الاخر وفق نظام دقيق ومتوازن في ديناميكية ذاتية لتستمر في اداء دورها في الحياة.القيمة الاساسية في فهم النظام الايكولوجي تتمثل في دراسة

التغيرات البيئية المعقدة كما يعتبر القاعدة العلمية الاساسية للتعرف على ابعاد العلاقات الوظيفية المتكاملة بين عناصر البيئة السليمة والتخطيط البيئي الجيد.دراسة تاثير وانعكاس الظروف البيئية والمناخ على التصميم جزء من المقدمة البيئية لتطوير عملية البناء والتي تسمى بالتصميم الايكولوجي المستدام Ecological Sustainable Design(ESD)(فجال-2004).

واهتمامات هذا المجال تصب فيما يتعلق بمجال:"العمارة المستدامة والتقنية المتقدمة "Sustainable Architecture and High Technology".رواد المجال هم من أسسه وتبنى المنهج حتى أصبح تيارا معماريا بحد ذاته,من ضمن المعماريين الذين اشتهروا به هم:رنزو بيانو,رتشارد روجرز , نورمان فوستر.

السمات العامة لهذا التيار هي:

1- ان الغرض الرئيسي من هذا التيار في مجال استخدام التقنية المتقدمة في المباني هوالحفاظ على الطاقة.
2- الاهتمام بالأداء الإنساني والبيئي من العوامل المهمة في نجاح أي مبنى.
3- تخفيض الإنبعاثات لغاز ثاني اكسيد الكربون الناتجة عن المباني وإعادة تدوير المخلفات.
4- استعمال الطاقة ذات الكلفة الطويلة المدى للمباني.

6- استخدام مواد بناء ذات مصدر طبيعي قدر الإمكان(الشايع-2007).

7- استخدام المواد المتجددة والقابلة للتدوير(فجال-2004).

ومن سمات هذا التيار نلاحظ انها تصب مباشرة في مفهوم العمارة المستدامة الذي نبحث فيه, مع تركيزها على استخدام التقنية العالية,وبالتالي تكون هي والابنية الذكية مشتركتان في هذا المجال تحديدا.

التيار الطبيعي (اوعمارة الفقراء) والاستدامة:

"عندما ابتعث الرائد المعماري "حسن فتحي" نمط بيوت النوبة المبنية بالطين والمسقفة بالقبب والأقبية في بداية الأربعينيات لم يكن يخترع شيئًا من عدم، ولم يكن يبتعثه أيضًا كفلكلور يبغي منه أن يحوز إعجاب الأثرياء والأجانب لما يجدون فيه من غرابة وطرافة، إنما كان هذا نابعًا من مسئوليته كمهندس معماري يقوم بدور رائد وهو إحياء التراث المعماري المحلي للعمارة الشعبية المصرية؛ إذ وجد فيه الحل المناسب إن لم يكن الأمثل لمشكلة شديدة الإلحاح وهي توفير بيت لكل فلاح فقير في الريف المصري، بتكلفة اقتصادية منخفضة تناسب دخل هذا الفلاح، على ألا تنتقص هذه التكلفة المنخفضة من حق هذا الفلاح في أن يكون له بيت متين وواسع ومريح وجميل"(نور الدين– 2006).يطلق على عمارة "حسن فتحي" بانها "عمارة الفقراء", فقد امتازت بميلها لاستخدام المواد الطبيعية ووسائل البناء التقليدية لتكوينها,وبالتالي كانت كلف انتاج تلك العمارة قليلة جدا لتقف في الضد من العمارة الذكية او عمارة الايكوتيك من حيث الكلفة .وحسن فتحي احد رواد تيار ما يسمى بالـ"naturalists " والذي كان يعمد الى استخدام المواد الطبيعية والتصاميم التقليدية في انشاء المباني,فالعزل الحراري يتم من خلال تصميم نسيج المبنى والتجميع حول الفناء الداخلي, تطبيقا لمباديء الحفاظ على الطاقة والتهوية والطبيعة المناسبة(عبدة–2005).

ان الاستدامة الموجودة في العمارة الطبيعية او "عمارة الفقراء" تكون من خلال التخلي عن التقنية الحديثة التي تعتمد في تشغيلها على الطاقة,وبالتالي فان نقيضها مع العمارة الذكية انها بدلا من الاعتماد على البناء في توليد الطاقة التي يحتاجها المبنى,فانها تعمد الى الاستغناء قدر الامكان عن الاجهزة او التقنيات التي تحتاج الى تلك الطاقة, وحيث يتم الاعتماد على التخطيط الحضري الناجح والتصميم المعماري الجيد والمواد البنائية المناسبة وطرق البناء المقدور عليها لتحقيق اقل كلفة وافضل انتاج واحسن اداء بيئي للعمارة.اي ان ضم عمارة الفقراء الى مفهوم الاستدامة جاء من خلال قلة تكاليف الانتاج والادامة والحفاظ على ما موجود من طاقة ,وليس اعتمادا على مبداء توليد الطاقة كما في الابنية الذكية.

ان البيوت المبنية بالطوب واللبن والمسقفة بالقبب والأقبية لحسن فتحي حازت الجدارة ليس لما فيها من جماليات معمارية فقط، بل ولنتائجها الاقتصادية الجيدة حين تم إخضاعها للحسابات الاقتصادية في التكلفة، والحسابات العلمية والهندسية في المتانة وتصميمات البناء، فضلا عن تناسبها وتجاوبها مع البيئة المحيطة، فخامة الطين التي تُعَدّ مادة البناء الأساسية في هذه البيوت خامة موجودة ومتوفرة في البيئة الريفية ومن هنا تنعدم تكلفتها تقريبًا، وقد أثبتت البحوث العلمية التي أجراها حسن فتحي نفسه على هذا النمط من البناء مدى قوة خاماته وتناسب تصاميمه(نورالدين-2006),وبالتالي كانت الكلفة الاقتصادية لتشييد العمارة معيارا ناجعا في تحقيق الاستدامة لعمارة حسن فتحي خصوصا ولاسلوب عمارة "الفقراء" عموما.

العمارة الخضراء والاستدامة:

العمارة الخضراء هي مدخل لتصميم مباني ايكولوجية عالية الكفاءة تتعامل مع محيطها الحيوي بأقل الأضرار الجانبية بالبحث الدائم عن البدائل التصميمية لحلول اقتصادية تتوافق مع البيئة(فجال-2004).إن التكلفة العالية للطاقة والمخاوف البيئية والقلق العام حول ظاهرة "المباني المريضة" المقترنة بالمباني الصندوقية المغلقة في فترة السبعينات، جميعها ساعدت على إحداث قفزة البداية لحركة العمارة المستدامة الخضراء. أما في الوقت الحاضر فإن "الاقتصاد" هو الباعث الرئيس على التحول والتوجه نحو التصاميم والمباني الأكثر خضرة(السواط-2006).

المؤيدون للعمارة المستدامة الخضراء يراهنون على المنافع والفوائد الكثيرة لهذا الإتجاه. في حالة مبنى إداري كبير – على سبيل المثال – فإن إدماج أساليب التصميم الخضراء (Green Design Techniques) والتقنيات الذكية (Clever Technology) في المبنى لا يعمل فقط على خفض إستهلاك الطاقة وتقليل الأثر البيئي، ولكنه أيضاً يقلل من تكاليف الإنشاء وتكاليف الصيانة، ويخلق بيئة عمل سارة ومريحة، ويحسّن من صحة المستخدمين ويرفع من معدلات انتاجيتهم، كما أنه يرفع من قيمة ملكية المبنى وعائدات الإيجار.

رغم ان فوائد المباني الخضراء ليست مقصورة فقط على الجوانب البيئية والاقتصادية المباشرة، فإستعمال ضوء النهار الطبيعي في عمارات المكاتب – على سبيل المثال – فضلا عن أنه يقلل من تكاليف الطاقة التشغيلية فهو أيضاً يجعل العاملين أكثر إنتاجاً وراحة، فقد وجدت الدراسة التي أجراها المتخصصان في علم النفس البيئي بجامعة ميتشيغان (Rachel and Stephen Kaplan) أن الموظفين الذين تتوفر لهم اطلالة على مناطق طبيعية من مكاتبهم أظهروا رضى أكبر تجاه العمل، وكانوا أقل اجهاداً وتعرضهم للأمراض كان أقل. وعلى نفس المنوال، فإن استعمال ضوء النهار الطبيعي في مراكز التسوق يؤدي إلى رفع حجم المبيعات، فالمجموعة الإستشارية المتخصصة في تقنيات المباني ذات الكفاءة في الطاقة (Heschong Mahone) ومقرها كاليفورنيا، وجدت أن المبيعات كانت أعلى بنسبة (40%) في المخازن التسويقية التي تمت اضاءتها من خلال فتحات السقف (Skylights). وقد وجدت المجموعة أيضاً أن أداء الطلاب في قاعات الدرس المضاءة طبيعياً أفضل بنسبة (20%)(السواط–2006).

احد اهم ركائز العمارة الخضراء هو الاعتماد على النباتات والمساحات الخضراء,حيث ان معظم الدراسات التي تناولت تأثير المساحات الخضراء على الظروف الحرارية للفراغ الخارجي قد ركزت بشكل أساسي على المساحات الخضراء الواسعة, اما استخدام المزروعات في الساحات الصغيرة كالساحات العمرانية و الشوارع فهو أقل بكثير, لكنه رغم ذلك يبقى فعالا في التاثير على البيئة الموضعية(شديدي–2006).

تاثير المناطق الخضراء يتم من خلال تخفيض حدة الإشعاع الشمسي عن طريق تظليل الأبنية بواسطة النباتات.حيث إن الطاقة الشمسية الساقطة على الكتلة الخضراء ينعكس قسم منها فيما يتشتت قسم اخر في الجو على شكل حرارة كامنة واخر قسم يمتص ليستخدم في النباتات في عملية التحويل الغذائي من خلال عملية التركيب الضوئي .تحويل النباتات للطاقة الشمسية وخصوصا الاشعة المرئية التي هي الاشد حرارة يعتبر العنصر الاكثر فعالية في تاثير النبات على البيئة المحيطة(شديدي–2006).

نوع النباتات المستخدمة وشكل الاوراق والاغصان وفيما اذا كانت نفضية او دائمية وقربها من الابنية كل ذلك يؤثر في درجة تظليل النباتات للابنية او تاثيرها في البيئة المحيطة. ظل الكساء الأخضر يساهم بأكثر من طريق في تبريد المباني فهو يستطيع تخفيض الحرارة الداخلية لها ودرجة الحرارة العظمى المحيطة من خلال استعماله على جوانب الأبنية اوتعديل تبادل الإشعاع الشمسي و الموجات الطويلة بين السطح و البيئة الخارجية.بالاضافة الى ان الغطاء الأخضر يصدر اشعة تحت الحمراء أقل مما تصدره الأرض الجرداء أوالمواد الصناعية وبهذا يخفض من معدل الأشعاع الحراري للبيئة هذا بالاضافة الى ان الأبنية التي تواجه المسطحات الخضراء تواجه كمية أقل من الحرارة الأشعاعية العالية بالنسبة للأبنية المطلة على ابنية اخرى.

ان ستراتيجية استخدام النبات تكون فعالة لانه لا يستخدم طاقة لاجل تقليل اثر طاقة الحراة كما نفعل نحن اليوم حيث نستخدم الطاقة الكهربائية لاجل تقليل حدة الطاقة الحرارية الشمسية,حيث تعمل النباتات على امتصاص الطاقة الشمسية وتحويلها الى غذاء ومواد نافعة وذلك افضل حل للتخلص من الطاقة الفائضة.

العمارة البيئية والاستدامة:

وهو ذلك العلم الناتج عن أندماج العمارة كفن وهندسة مع البيئة وقد ظهر هذا التخصص منذ بداية الخمسينيات كرد فعل طبيعي للمشاكل البيئية التي أصبحت علي درجة كبيرة من التشعب والتعقيد وذلك بهدف وضع سياسات عامة وبرامج شامله متنوعة وجذرية تحقق اسهاما في مجال الحفاظ علي البيئة وتحسن نوعيتها سواء في المدن الحالية او المدن الجديدة والمستقبلية , وبالتالي تحقيق أسهام له وزنه في انتماء المواطن لبيئته.(مرعي– 2006).فيما اطلق "عباس الزعفراني" على العمارة البيئية اسم العمارة المناخية وعرفها بانها جانب من تصميم البيئة المبنية يهتم بتوفير الظروف المناخية الامنة والمريحة للانسان باقل قدر من التكاليف(الزعفراني–2007).

فالعمارة البيئية هي ثمرة التفاعل الكامل والوثيق بين المواطن والعوامل البيئية من حوله وفريق التصميم البيئي بقيادة المهندس المعماري , وهي تلك العمارة التي تحقق للانسان الحد الكافي من

متطلباتة البيئية والحد الادني من التلوث البيئي والحد المقبول من الشروط الصحية اللازمة لمعيشتة وهو ما ينعكس بدورة علي نوعية وكفاءة البيئة الحضرية ومدي أنتماء الانسان لتلك البيئة والتزامه ووعيه بالمحافظة عليها (مرعي– 2006).

العمارة صديقة البيئة:

لقد ظهر مؤخرا مصطلح"صديق البيئة" واعتبر احد مقاييس الانتاج في الشركات التقنية العالمية,وهو يعني باختصار نوع العلاقة بين المنتج والبيئة,فان كان العلاقة بين الاثنين واحد الى واحد هذا يعني ان تاثير المنتج على البيئة صفرا,فان كانت اقل من واحد فهذا يعني ان المنتج ضار بالبيئة وان كان اكثر من واحد فهذا يعني انه يعمل على تنقية البيئة.ووفق هذا المقياس وضعت شركة "باناسونيك"هدفا لها ان تكون صداقة منتجاتها للبيئة واحد الى واحد ثم بعد ان حققت هذه النسبة فقد طورت هدفها لتصبح منتجاتها القادمة محققة لنسبة اثنان الى واحد وهذا يعني ان منتجاتها سوف تكون منقية للبيئة وليس فقط غير ضارة للبيئة.(جبران–2007).

ركائز العمارة المستدامة:

من خلال ما سبق ,يلخص البحث ركائز مفهوم العمارة المستدامة بثلاث نقاط رئيسة وهي:

1– التركيز على تقليص استخدام الطاقة او من خلال توليدها داخل العمارة.
2– التركيز على الجانب الاقتصادي وتقليل الكلفة قدر الامكان,وتقليل تلك الكلفة يحسب اما بتقليل كلفة الانتاج او من خلال تقليل كلف التشغيل والادامة المستمرة مع عمر البناء.
3– الحفاظ على بيئة الكرة الارضية من خلال تقليل مخلفاتها الضارة عن طريق اختيار المواد المناسبة في البناء وتقليل التلوث والتخلص او تنقية الفضلات باستخدام المرشحات المنقية للبيئة الطبيعية مثل النباتات او باستخدام التقنيات الحديثة.

وبهذا تكون كل عمارة محققة لاحد هذه المرتكزات الثلاثة او اكثر هي عمارة مستدامة ,وتتنافس قيم العمارة ونجاحها في اعتماد الاستدامة على كفاءتها في تحقيق ما يلي:

1- اكثر عدد من تلك الركائز.

2- كفاءته في تنفيذ أي من تلك الركائز.

تعريف البحث الاجرائي للعمارة المستدامة:

من خلال ما تم ذكره فان التعريف الاجرائي الذي يمكن للبحث ان يضعه بالنسبة للعمارة المستدامة وبعد ان يتم الربط بين متطلبات العمارة وركائز الاستدامة الثلاث وبين التنمية المستدامة هو كما يلي:

العمارة المستدامة: هي العمارة التي تلبي حاجات الانسان المعمارية من حيث الجمال والوظيفية والمتانة مع قدرتها على توليد او تقليص استهلاكها للطاقة المطلوبة لتشغيلها وتقليل كلف الانتاج و الادامة قدر الامكان مع الحفاظ على كوكب الارض وبيئته وموارده سليما معافى للاجيال القادمة.

النتائج:

ان نتائج هذا البحث تتلخص في تحديد ركائز مفهوم العمارة المستدامة اولا,ثم وضع التعريف الاجرائي لهذا المفهوم ثانيا ,ثم وضع الاطار النظري لمفهوم العمارة المستدامة باعتباره هدف البحث الرئيسي ثالثا,وحيث ذكرنا قبل قليل ركائز العمارة المستدامة وقدمنا تعريف البحث الاجرائي لهذا المفهوم ,فان الاطار النظري الذي سيضعه البحث سيتمثل في تحديد مستويات استخدام هذا المفهوم وتمييزه وفق طبقات كل حسب تخصصها ,حتى يتم ازالة اللبس الذي يعتلي بعض استخدامات هذا المصطلح.

حيث اننا سنعمد حاليا الى تقسيم مفهوم العمارة المستدامة الى مجموعة طبقات ,كل طبقة تتخصص في مجال من المجالات التي تعتمدها العمارة كاسلوب تصميمي او كطراز او كمنهج,وعند ذلك سوف لا يتم اطلاق مفهوم العمارة المستدامة الا مقروننا بمجال تخصصه وكما يلي:

العمارة الخضراء المستدامة:وهي العمارة التي تستخدم النباتات والمناطق الخضراء والاشجار لتحقيق مفهوم العمارة المستدامة.

العمارة الذكية المستدامة:وهي العمارة التي تستخدم التقنيات الحديثة لاجل تحقيق مفهوم العمارة المستدامة.

العمارة صديقة البيئة المستدامة: هي العمارة التي تقاس نسبة استدامتها نسبتة الى مقدار صداقتها للبيئة والتي يجب ان تساوي واحد او اكثر .

العمارة البيئية المستدامة:هي العمارة التي تهتم بتحقيق العمارة المستدامة عن طريق استخدام العمارة البيئية.

عمارة الفقراء المستدامة:هي العمارة التي تحقق مفهوم العمارة المستدامة عن طريق استخدام طرق البناء التقليدية والمواد المتوفرة طبيعيا والتي تكون كلف انتاجها وديمومتها قليلة قدر الامكان.

ان هذا الاطار النظري مفتوحا لتقبل المزيد من المجالات والحقول المعمارية ,حيث يمكن ادراج اي تخصص معماري اخر واعتباره طبقة من طبقات العمارة المستدامة في حالة تحقيقه لأي من ركائز العمارة المستدامة التي سبق ذكرها,وبالتالي يمكن زيادة عدد طبقات مفهوم العمارة المستدامة او تقليلها اذا افتقرت اي من تلك الحقول لشروط مفهوم الاستدامة.

التوصيات:

1- ضرورة الاهتمام بمفهوم الاستدامة وتفعيله تطبيقيا على ارض الواقع وعدم الاكتفاء بالتنظير.ويتم ذلك من خلال التركيز على اعتماد ركائز العمارة المستدامة الواردة في البحث من حيث توفير الطاقة وتخفيض كلف الانتاج وتقليل نسبة التلوث قدر الامكان.

2- ضرورة ادخال ركائز العمارة المستدامة ضمن معايير تقييم اي مشروع معماري,فتكون معايير تقييم اي مشروع بالاضافة الى جودته التصميمية والوظيفية, جودته من حيث تقليل كلف الانتاج ونسبة صداقته للبيئة ومدى توفيره للطاقة او توليده لها,ومن شان دخول معايير العمارة المستدامة هذه ان تخلق منهجا تصميميا يستطيع ان يرتقي بالهندسة المعمارية وينقلها من حقل الفن الذي اصطبغت به مؤخرا الى حقل الهندسة.

3- ضرورة تدريس مفاهيم العمارة المستدامة وطبقاتها الواردة في البحث ضمن المواد التدريسية في اقسام الهندسة المعمارية لزيادة وعي المهندسين الشباب بها.

4- يوصي البحث بضرورة زيادة البحوث والدراسات التي تعنى بالاستدامة لما لها من اثر كبير في التصدي للمشاكل التي تواجه عصرنا الحالي والمتمثلة بالتلوث البيئي ونقصان الطاقة.

المراجع:

1- coldhamarch .coldham,b.,(2001),"what is green arch " .

www.coldhamarch.com/green/what.html . last visit at 22-9-2008.

2- احمد, ربيع محمد رفعت(2005)" تقنيات المبانى الذكية ودورها فى تدعيم بناء مدن المعرفة".جامعة الملك فهد للبترول والمعادن.السعودية.

3- السواط ,علي بن محمد(2006)."التخطيط المستدام و العمارة البيئية ".امانة مدينة الدمام.

4- الشايع,محمد فوزان(2007)"العمارة المستدامة والتكنولوجيا المتقدمة"جامعة الملك سعود.السعودية.

5- Egypt Architecture.الزعفراني,عباس محمود(2007)"التصميم المناخي للابنية".
http://www.egyptarch.com/abbasphd1,3/main.htm .اخر زيارة في 22-9-2008.

6- بشندي, سعاد يوسف حسنين(2005)"مدخل التصميم العمراني المستدام وتشكيل عمران المجتمعات الصحراوية,دراسة مجتمعات الواحات التقليدية بصحراء مصر الغربية".مصر.

7- الحرة. جبران,توفيق(2007) "برنامج آي تك". قناة الحرة. زيارة الى شركة باناسونيك اليابانية.
http://www.alhurra.com/ProgramDetailsAr.aspx?ID=1813655&CID=1 ,اخر زيارة 22-8-2008.

8- شبكة العمارة للجميع.حسام,محمد(2006)"مبادي العمارة الخضراء".
http://www.arch4all.net/vb/showthread.php?t=2021&highlight=%C7%E1%DA%E3%C7%D1%C9+%C7%E1%E3%D3%CA%CF%C7%E3%C9 ,اخر زيارة في 22-9-2008.

9- سكينر,ف.ب(1998)"تكنلوجيا السلوك الانساني" ترجمة عبد القادر يوسف.عالم المعرفة,الكويت.

10- منتديات الهندسة نت.شديدي,منال(2006)"العمارة المستديمة"
http://www.alhandasa.net/forum/printthread.php?t=83893, .اخر زيارة في 22-9-2008.

11- صفحة اكرم شلهوب.شلهوب,رشيد اكرم. السنة(2007)"العمارة الخضراء".http://www.sendian.org/a13/a13s6.htm ,اخر زيارة في 21-7-2008.

12- عبدة,صفاء محمود عيسى(2005)"التشريعات والعمارة المستدامة,اهم ركائز بيئة جاذبة للسكان في المدن الصحراوية"جامعة المنوفية.مصر.

13- فجال,خالد سليم(2004)"العمارة البيئية المعاصرة".مؤتمر الازهر الهندسي الدولي الثامن.

14- Architecture Engeenering,مرعي,سعيد(2006)"مفهوم البيئة ومكوناتها".
http://arch-sustainable.blogspot.com/2006/04/blog-post.html ,اخر زيارة في 22-9-2008.

15- ملتقى المهندسين العرب,نورالدين,محمود(2006):"العمارة البيئية"الجزءالاول.
http://www.arab-eng.org/vb/t12530.html ,اخر زيارة في 22-9-2008.

16- ويكبيديا,الموسوعة الحرة.2008"الاحتباس الحراري,
http://ar.wikipedia.org/wiki/%D8%A7%D8%AD%D8%AA%D8%A8%D8%A7%D8%B3_%D8%AD%D8%B1%D8%A7%D8%B1%D9%8A
,اخر زيارة في 22-9-2008.